

AD-A183 158

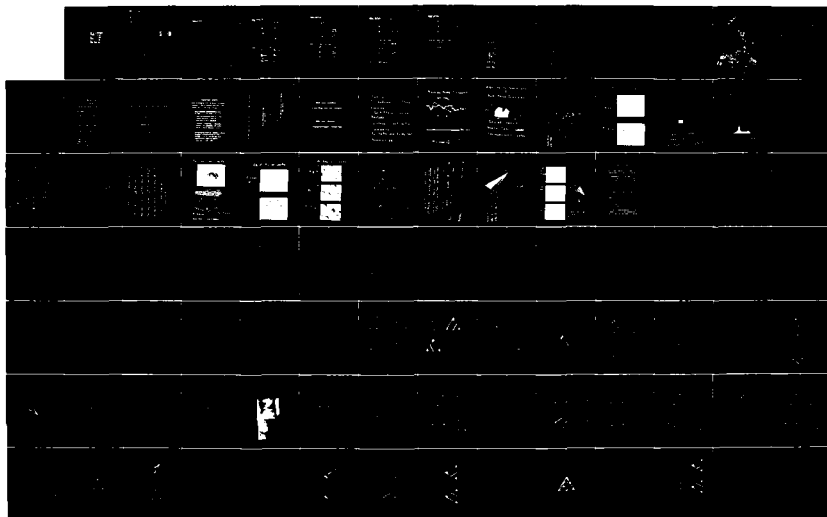
A WORKSHOP ON 3-5 SEMICONDUCTOR: METAL INTERFACIAL  
CHEMISTRY AND ITS EFFECTS (U) STANFORD UNIV CA  
W E SPICER ET AL. 05 NOV 86 N00014-87-G-0038

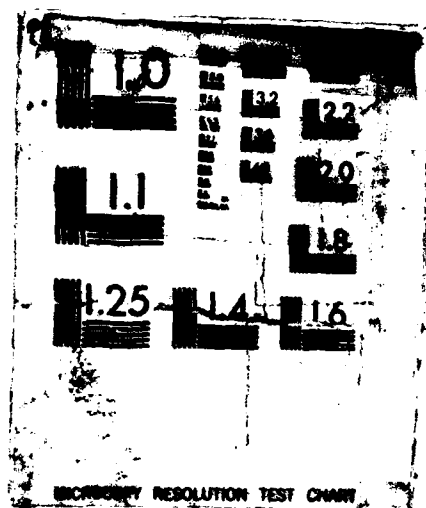
1/7

UNCLASSIFIED

PAG 20/12

NL





RESOLUTION TEST CHART

DTIC FILE COPY



AD-A183 158

A Workshop on 3-5 Semiconductor: Metal Interfacial  
Chemistry and Its Effect on Electrical Properties

Sponsored by  
Stanford University  
and  
ONR

November 3-5, 1986

W. E. Spicer  
Larry Cooper

Contract N00014-87-G-0038

DTIC  
ELECTE  
JUL 30 1987  
S D

**DISTRIBUTION STATEMENT A**  
Approved for public release  
Distribution Unlimited

87 7 14 084

## Program

A Workshop on 3-5 Semiconductor: Metal Interfacial Chemistry and Its Effect on Electrical Properties

Monday, November 3rd

Chairman: W. E. Spicer - Stanford University

↓  
This workshop discusses

8:00 - 8:30	Continental breakfast	
8:30 - 8:35	Introduction - Chairman	
8:35 - 9:05	R. Stanley Williams UCLA	"The Thermodynamics of Bulk Metal: III-V Systems Related to Interfacial Chemistry"
9:05 - 9:10	Questions	
9:10 - 9:30	Ki Bum Kim Stanford University	"Thermodynamic Considerations of Metal-GaAs Reactions plus TEM Results"
9:30 - 9:35	Questions	
9:35 - 9:55	M. Kniffin/C. Robert Helms Stanford University	"Chemistry of Ti:GaAs Interfaces"
9:55 - 10:00	Questions	
10:00 - 10:20	General discussion of all papers in session	
10:20 - 10:35	Coffee	
<u>Chairman: Thomas C. McGill, CALTECH</u>		
10:35 - 10:55	William E. Spicer Stanford University	"Questions Concerning Interfacial Chemistry, Equilibrium, and Electrical Properties"
10:55 - 11:00	Questions	
11:00 - 11:25	John Weaver University of Minnesota	"The Chemistry and Morphology of Metal/ III-V Semiconductor Interfaces"
11:25 - 11:30	Questions	
11:30 - 11:50	Tomasz Kendelewicz Stanford University	"Schottky Barriers on InP(110); Comparison to GaAs(110) Interface"
11:50 - 11:55	Questions	
11:55 - 12:20	Discussion of all preceding papers in Workshop	
12:20 - 1:40	Luncheon - Durand 450	



1  
Approved for Public Release. Distribution Unlimited.  
Per Dr. Larry Cooper, ONR/Code 1114

over →

per phonecon

Distribution /	
Availability Codes	
Dist	Avail and/or Special
A-1	



**Monday, November 3rd**  
**Chairman: Dr. Larry Cooper. ONR**

1:40 - 2:00      Tim Sands  
Bell Communications  
Research

"Stable Phases at Reactive Metal/Compound  
Semiconductor Interfaces"

2:00 - 2:05      Questions

2:05 - 2:25      Masanori Murakami  
IBM Yorktown Heights

"Thermally Stable Ohmic Contact to n-type  
GaAs"

2:25 - 2:30      Questions

2:30 - 2:50      Thomas McGill  
CALTECH

"Effects in Ohmic Contacts"

2:50 - 2:55      Questions

2:55 - 3:15      S. S. Lau  
UC - San Diego

"Non-Alloyed Ohmic Contacts by Solid State  
Reactions"

3:15 - 3:20      Questions

3:20 - 3:40      Discussion of all papers in session

3:40 - 3:55      Coffee

**Chairman: Jack Dew, Notre Dame University**

3:55 - 4:15      James Waldrop  
Rockwell International

"Large Variations of GaAs Schottky Barrier  
Height by Interface Layers"

4:15 - 4:20      Questions

4:20 - 4:40      Edgar Krut  
Rockwell International/  
Walter Harrison, Stanford

"Effects on Schottky Barriers of Metal  
Substitution in Semiconductors"

4:40 - 4:45      Questions

4:45 - 5:05      Giorgio Margaritondo  
University of Wisconsin

"III-V Interfaces: Schottky Barriers vs.  
Heterojunctions"

5:05 - 5:10      Questions

5:10 - 5:40      General discussion - including all material presented this day

**Tuesday, November 4th**  
**Chairman, Pierre Petroff - U.C. Santa Barbara**

8:00 - 8:30 Continental Breakfast

8:30 - 8:50

Chris Palmström  
Rutgers University  
and Bell Labs

"A Comparison between Conventional and *in-situ* UHV Processing for Ge/GaAs and Co/GaAs Structures"

8:50 - 8:55

Questions

8:55 - 9:20

Nathan Newman  
Stanford University

"Electrical Study of Schottky Barriers on Atomically Clean 3-5(110) Surfaces; A Comparison to the Results of Studies Using Surface Sensitive Techniques and Au-GaAs Ohmic Contacts"

9:20 - 9:25

Questions

9:25 - 9:55

Z. Liliental-Weber  
UC-Berkeley

"The Structure of Au/GaAs and Al/GaAs Interfaces"

9:55 - 10:00

Questions

10:00 - 10:35

Discussion of three papers of this session

10:35 - 10:50

Coffee

**Chairman: Paul Ho, IBM, Yorktown Heights**

10:50 - 11:10

Thomas Jackson  
IBM-Yorktown Heights

"Refractory Silicide Contacts for Self-Aligned GaAs MESFETs"

11:10 - 11:15

Questions

11:15 - 11:35

Tom Knech  
IBM - Yorktown Heights

"Heterojunction Growth and Impurity Incorporation During Vapor Growth of Compound Semiconductors"

11:35 - 11:40

Questions

11:40 - 12:00

Bruce Bunker  
Notre Dame University

"Reflection EXAFS Studies of Semiconductor-Metal Interfaces"

12:00 - 12:05

Questions

12:05 - 12:30

General discussion of preceding papers

12:30 - 1:30

Luncheon, Demand 450

**Tuesday, November 4th**

**Chairman: Ron Grant, Rockwell International**

1:30 - 1:50	Harry Wieder UC-San Diego	"Composition Dependence of Metal $\text{In}_x\text{Al}_{1-x}\text{As}$ Barrier Height and Its Applications"
1:50 - 1:55	Questions	
1:55 - 2:15	Steven Wright IBM-Yorktown Heights	" <i>In-situ</i> Contacts to GaAs Based on InAs"
2:15 - 2:20	Questions	
2:20 - 2:40	Jerry Tersoff IBM-Yorktown Heights	"Intrinsic Mechanisms for Fermi-level Pinning at Surfaces and Interfaces"
2:40 - 2:45	Questions	
2:45 - 3:10	General discussion of preceding papers	
3:10 - 3:30	Coffee	

**Chairman: Ingrid Linden, Stanford University**

3:30 - 3:50	Leonard J. Brillson Xerox Corporation	"Recent Photoemission and Cathodoluminescence Spectroscopy Studies of III-V Semiconductor- Metal Interfaces"
3:50 - 3:55	Questions	
3:55 - 4:15	Jack Dow Notre Dame University	"Antisite Defects and Schottky Barriers"
4:15 - 4:20	Questions	
4:20 - 4:40	Paul Ho IBM-Yorktown Heights	"Direct Measurements of Electronic States at Metal/GaAs Interfaces"
4:40 - 4:45	Questions	
4:45 - 5:05	Discussion of preceding papers	
5:05 - 5:45	General discussion of all papers presented at meeting	
6:00 - 7:00	Stanford Faculty Club - no host cocktail party	
7:00	Dinner - Stanford Faculty Club	

**Wednesday, November 5th**  
**Chairman, Harry Wieder, U.C. San Diego**

8:00 - 8:30	Continental breakfast	
8:30 - 8:50	Rudolf Ludeke IBM-Yorktown Heights	"The Role of Transition Metal Impurity States in Schottky Barrier Formation"
8:50 - 8:55	Questions	
8:55 - 9:15	Walter Harrison Stanford University	"Effects of Coverages, Relaxation, and Screening at Interfaces"
9:15 - 9:20	Questions	
9:20 - 9:40	Jerry M. Woodall IBM-Yorktown Heights	"Unpinned GaAs Surfaces by Photochemistry"
9:40 - 9:45	Questions	
9:45 - 10:05	Discussion of preceding papers	
10:05 - 10:25	Coffee	

**Chairman, Piero Pianetta, Stanford University**

10:25 - 10:45	Antoine Kahn Princeton University	"Kinetics of Schottky Barrier Formation: Metals on Low Temperature GaAs (110)"
10:45 - 10:50	Questions	
10:50 - 11:10	Seb Doniach Stanford	"Microscopic Metal Clusters and Schottky Barrier Formation"
11:10 - 11:15	Questions	
11:15 - 11:35	Discussion of papers of this day	
11:35 - 12:15	General discussion of workshop	

### Workshop attendees

Ludeke, Dr. Rudolf  
IBM Thomas J. Watson Research Center  
P.O. Box 218  
Yorktown Heights, NY 10598  
(914) 945-2591

Woodall, Dr. Jerry  
IBM Thomas J. Watson Research Center  
P.O. Box 218  
Yorktown Heights, NY 10598  
(914) 945-1568

Lau, Dr. S. S.  
University of California-San Diego  
P.O. Box 109  
LaJolla, CA 92037  
(619) 534-6940

Wieder, Dr. Harry  
University of California-San Diego  
Department of Electrical Engineering  
P.O. Box 109  
LaJolla, CA 92037  
(619) 534-3546

Liliental-Weber, Dr. Zuzanna  
University of California  
Lawrence Berkeley Laboratory  
1 Cyclotron Road 622-203  
Berkeley, CA 94720  
(415) 486-6276

Weber, Dr. Eicke  
University of California  
Hearst Mining Building  
Berkeley, CA 94720  
(415) 624-3801

Weaver, Prof. John  
University of Minnesota  
Department of Chemical Engineering  
and Materials Science  
151 Washington S.E.  
Amundson Hall 421  
Minneapolis, MN 55455  
(612) 625-6548

Dow, Dr. Jack  
University of Notre Dame  
Department of Physics  
Notre Dame, IN 46556  
(219) 239-6407  
(219) 239-6386

Bunker, Dr. Bruce  
University of Notre Dame  
Department of Physics  
Notre Dame, IN 46556  
(219) 239-7219  
(219) 239-6386

McGill, Dr. Thomas C. (818) 356-4849  
CALTECH  
Department of Applied Physics  
Mail Code 128-95  
Pasadena, CA 91125

Ho, Dr. Paul (914) 945-2007  
IBM Thomas J. Watson Research Center  
P.O. Box 218  
Yorktown Heights, NY 10598

Lindau, Dr. Ingolf (415) 723-1052  
Stanford Electronics Laboratories  
McCullough Building, Rm. 336  
Stanford, CA 94305

Helms, Dr. C. Robert (415) 723-0406  
Stanford Electronics Laboratories  
McCullough Building, Rm. 342  
Stanford, CA 94305

Harrison, Dr. Walter (415) 723-4224  
Department of Applied Physics  
Stanford University  
Stanford, CA 94305

Kim, Mr. Ki Bum (415) 725-2648  
Department of Materials Science  
Stanford University  
Stanford, CA 94305

Deal, Dr. Mike (415) 725-0209  
Department of Electrical Engineering  
McCullough Building Rm. 118  
Stanford, CA 94305

Sands, Dr. Tim (415) 486-6254  
Bell Communications Laboratories  
331 Newman Springs Road  
Redbank, NJ 07701

Margaritondo, Dr. Giorgio (608) 873-6651  
Department of Physics  
Synchrotron Radiation Center  
University of Wisconsin-Madison  
3275 Schneider Drive  
Stoughton, WI 53589-3098

Dr. Larry Cooper (202) 696-4214  
Electronic and Solid State Departments  
Office of Naval Research, Code 414  
800 N. Quincy Avenue  
Arlington, VA 22217

Brillson, Dr. Leonard  
Xerox Corporation  
800 Phillips Road  
Webster, NY 14580

(716) 422-6468

Petroff, Dr. Pierre  
Department of Materials Science and  
Electrical Engineering  
University of California-Santa Barbara  
Goleta, CA 93106

(805) 961-8256

Williams, Dr. R. Stanley  
University of California-Los Angeles  
Department of Chemistry  
Los Angeles, CA 90024

(213) 825-8818

Grant, Dr. Ronald W.  
Rockwell International Science Center  
1046 Camino Dos Rios  
P.O. Box 1085  
Thousand Oaks, CA 91360

(805) 373-4219

Waldrop, Dr. James  
Rockwell International Science Center  
1046 Camino Dos Rios  
P.O. Box 1085  
Thousand Oaks, CA 91360

(805) 373-4249

Kraut, Dr. Edgar  
Rockwell International Science Center  
1046 Camino Dos Rios  
P.O. Box 1085  
Thousand Oaks, CA 91360

(805) 373-4186

Kahn, Dr. Antoine  
Department of Electrical Engineering  
Princeton University  
Princeton, NJ 08540

(609) 452-4642

Dr. Masano Murakami  
IBM Thomas J. Watson Research Center  
P.O. Box 218  
Yorktown Heights, NY 10598

(914) 945-1865

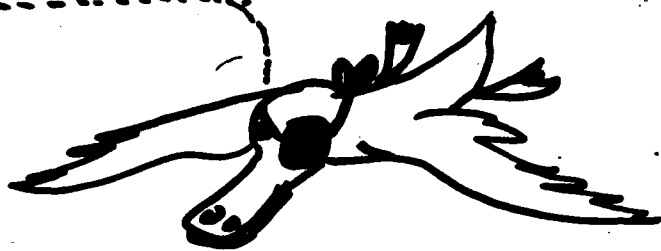
Dr. Thomas Jackson  
IBM Thomas J. Watson Research Center  
P.O. Box 218  
Yorktown Heights, NY 10598

(914) 945-1947

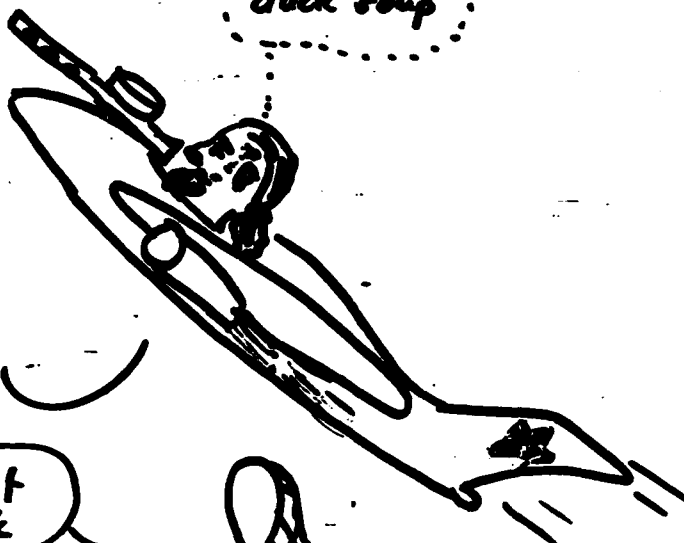
Dr. Tom Kuech IBM Thomas J. Watson Research Center P.O. Box 218 Yorktown Heights, NY 10598	(914) 945-1644
Dr. Chris Palmstrøm Department of Physics SERIN Lab at Rutgers University P.O. Box 849 Piscataway, NJ 08854	(201) 699-2221
Tersoff, Dr. Jerry IBM Thomas J. Watson Research Center P.O. Box 218 Yorktown Heights, NY 10598	(914) 945-3128
Kim, Ki Bum Department of Materials Science Stanford University Stanford, CA 94305	(415) 725-2648
Beyers, Dr. Robert K-32-801 IBM Almaden Research Center 650 Harry Road San Jose, CA 95120-6099	(408) 927-2383
Wright, Dr. Steven IBM Thomas J. Watson Research Center P.O. Box 218 Yorktown Heights, NY 10598	(914) 945-3000
Spicer, Dr. William E. Department of Electrical Engineering/ Stanford Electronics Laboratories McCullough 238 Stanford, CA 94305	(415) 723-4639
Pianetta, Dr. Piero Stanford Electronics Laboratories McCullough 232 Stanford, CA 94305	(415) 723-1083
Doniach, Dr. Sebastian Department of Applied Physics Stanford University Stanford, CA 94305	(415) 723-4786



if it quacks...



duck soup



just a bit more junk



I thought I saw a quack



antisite?!



Uniformly Defective Missile

**The Thermodynamics of Bulk  
Metal-III-V Systems  
Related to Interfacial Chemistry**

**R. Stanley Williams**

**Department of Chemistry and Biochemistry  
and  
Solid State Science Center  
UCLA**

**11**

**for the Workshop on III-V Semiconductor: Metal  
Interfacial Chemistry and Its Effect on  
Electrical Properties**

## **ACKNOWLEDGMENTS**

**Dr. Jeffrey R. Lince**

**C. Thomas Tsai**

**John H. Pugh**

**and**

**Office of Naval Research**

**California MICRO**

**Hughes Aircraft Corporation**

# **Relevance of Bulk Thermodynamics to the Chemistry of Metal/Compound-Semiconductor Interfaces**

## **1) BOUNDARY CONDITIONS**

**An interface cannot be stable if the bulk phases that are joined can react to form more stable products.**

## **2) PHASE STABILITY**

**Determine the conditions under which two phases are stable with respect to one another.**

## **3) REACTION SEQUENCES**

**Predict the equilibrium phases and the intermediate products that can form during a reaction.**

## **4) STABLE INTERFACES**

**Deposit metals that are at chemical equilibrium under the conditions that the interface will experience.**

**Hasn't all of this been done already?**

**Hasn't it been shown that  
thermodynamic predictions  
fail for thin metal films on  
compound semiconductors ?**

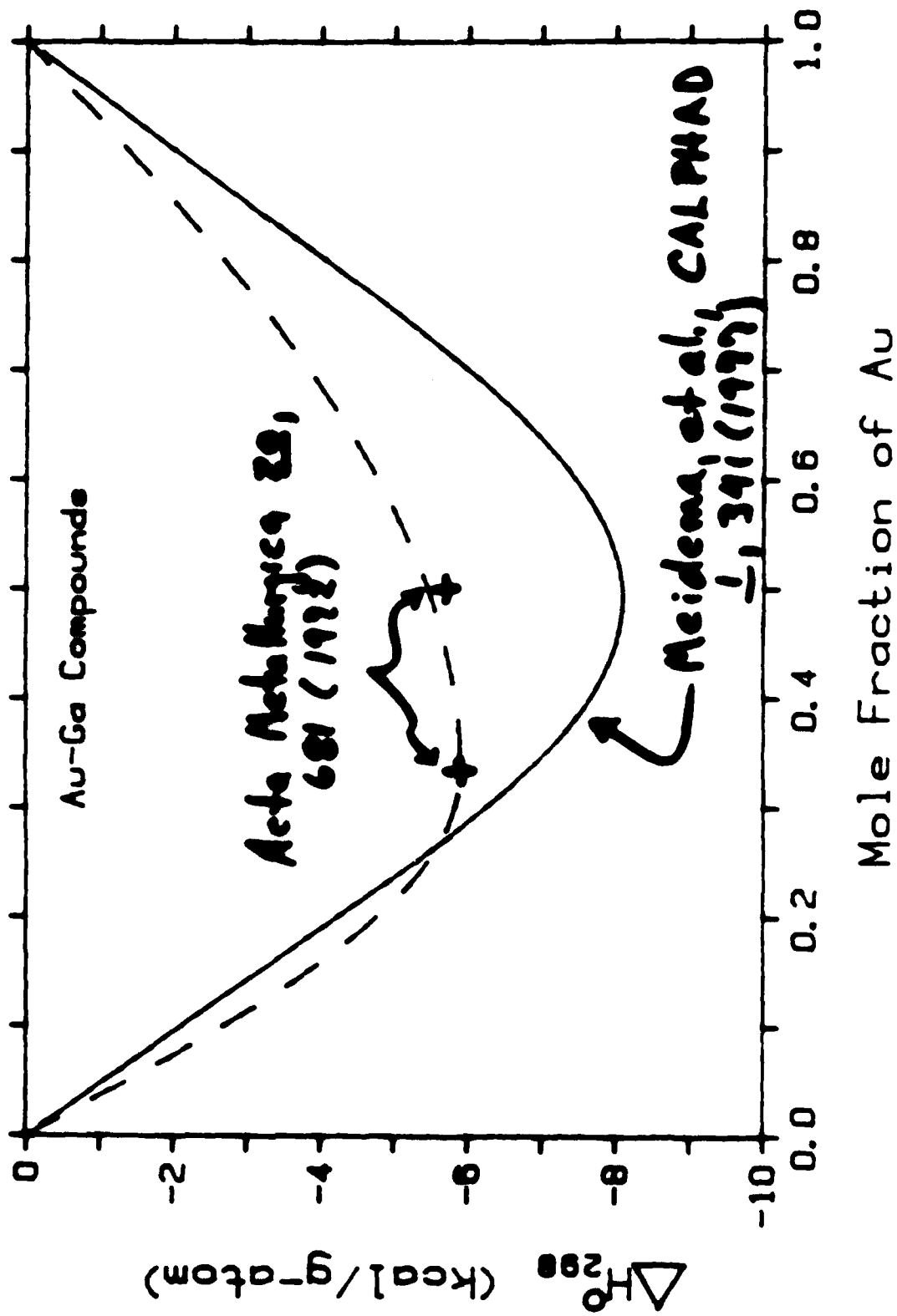
**N O !**

## **PREVIOUS WORK**

Many investigators have calculated the change in *enthalpy* ( $\Delta H_p$ ) for possible reactions. These studies have had two basic problems:

- 1) Use of incorrect thermochemical data from Meidema et al., CALPHAD 1, 341 (1977).
  - a) Often the enthalpies were for mixing of liquids, which have little relation to the formation of solid compounds.
  - b) Meidema's predictions of enthalpies of formation for compounds with group III elements contain systematic errors
- 2) The equilibrium state of a system at constant pressure is determined by the Gibbs Free Energy,  $G = H - TS$ . The entropy is not negligible and cannot be ignored.  
J.Mats.Res. 1, 343 (1966).

# Enthalpy of formation vs. Au mole fraction



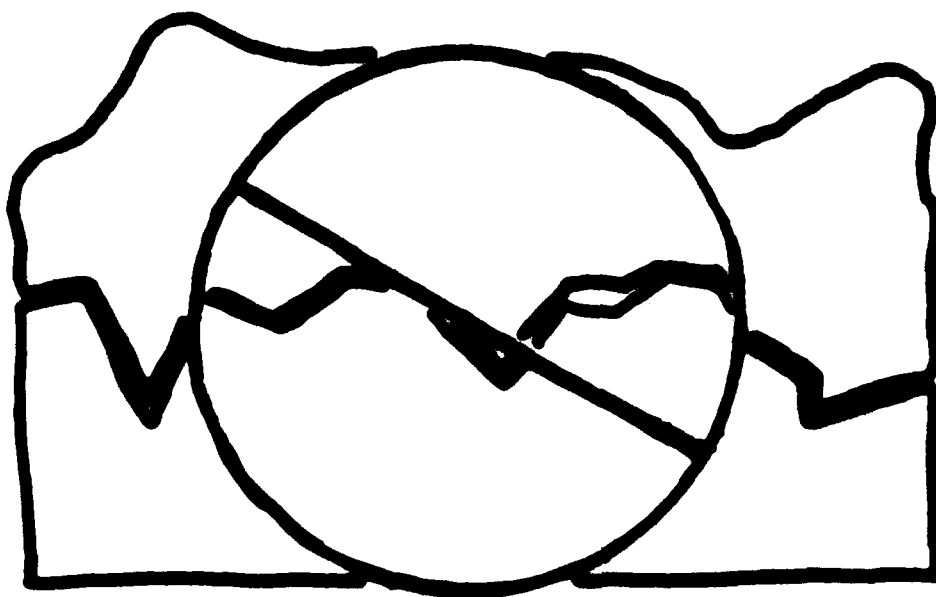
**Will not explain - -**  
**Schottky barrier heights.**

**Will not discuss - -**  
**Submonolayer coverages.**

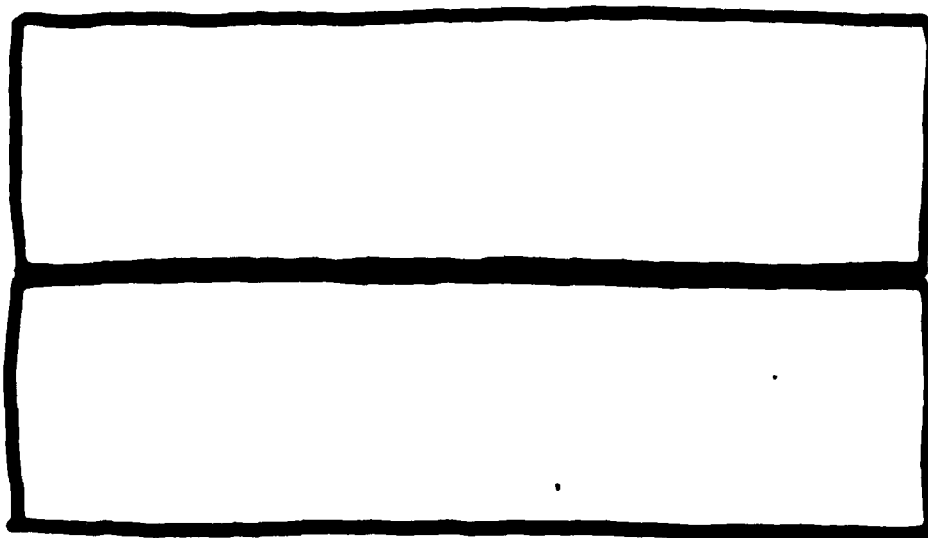


- Define  
"Thermodynamically Stable"
- Examine  
Bulk Phase Diagrams
- Analyze  
Entropic Contributions
- Compare  
Au/GaAs and AuGa<sub>2</sub>/GaAs
- Summarize

Minimize Mass Transport



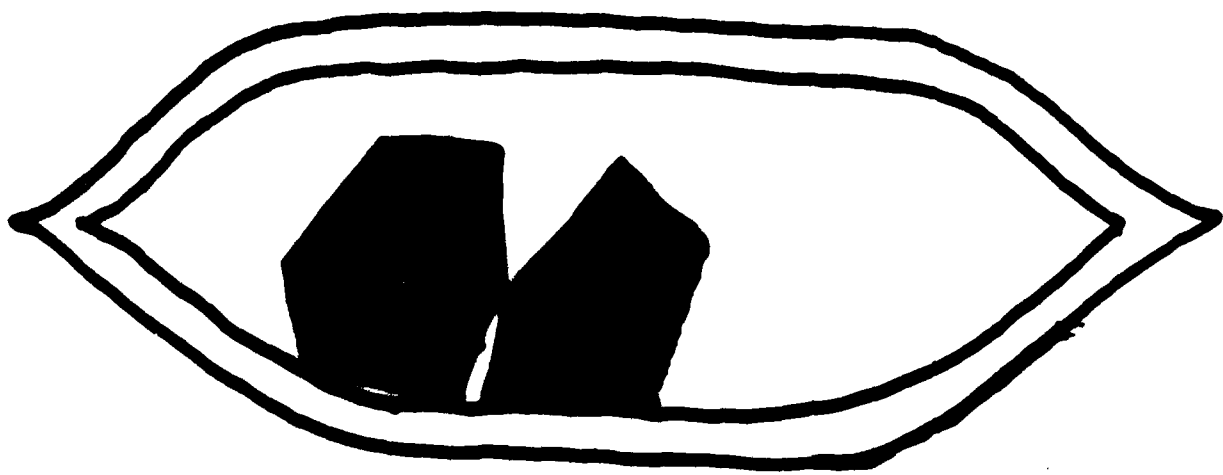
Rough



Abrupt

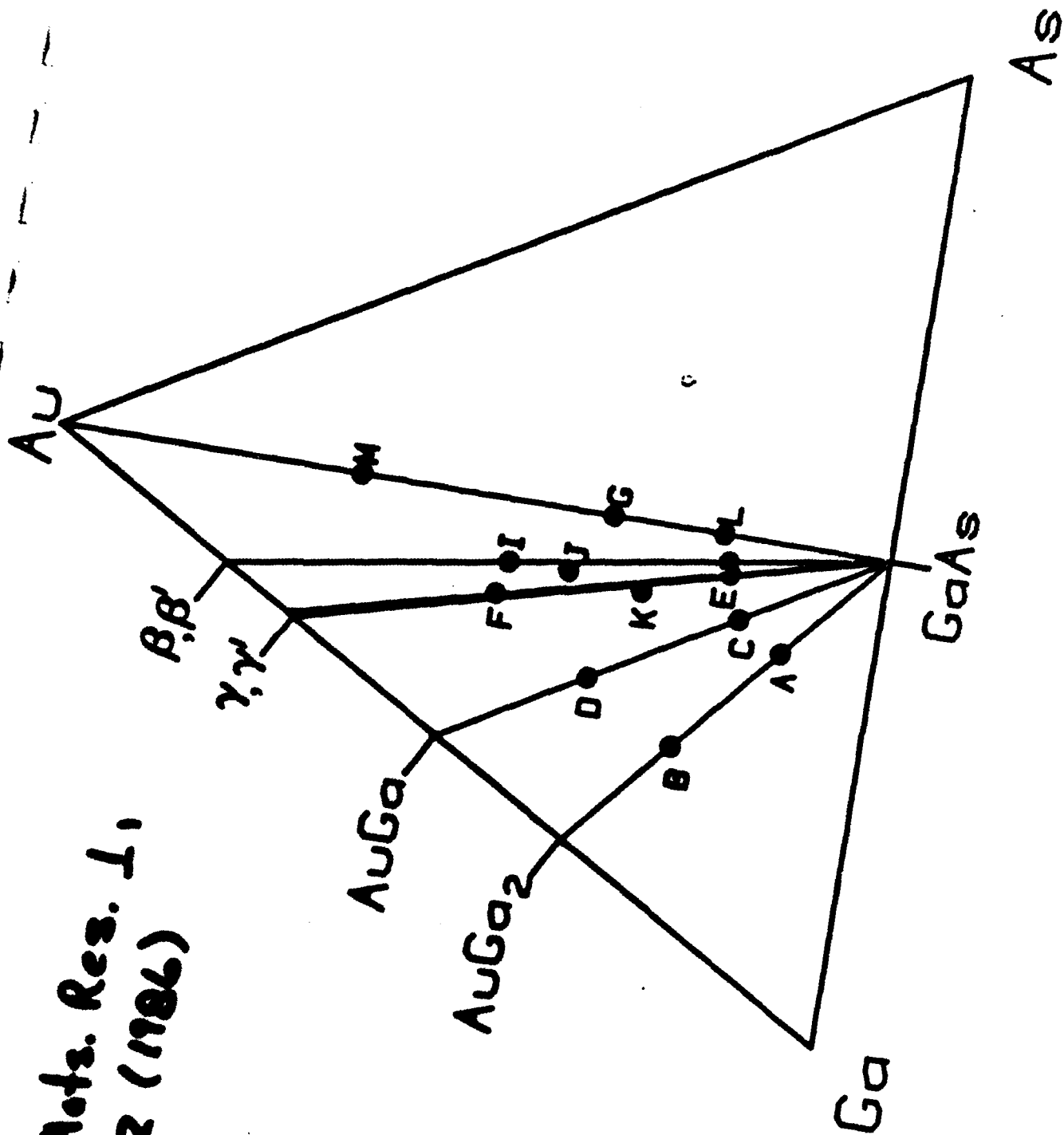
Minimize  $G$

# Experimental Determination of Bulk Phase Diagrams



Sealed Capsule  
(Nearly Ideal Closed  
Thermodynamic System)

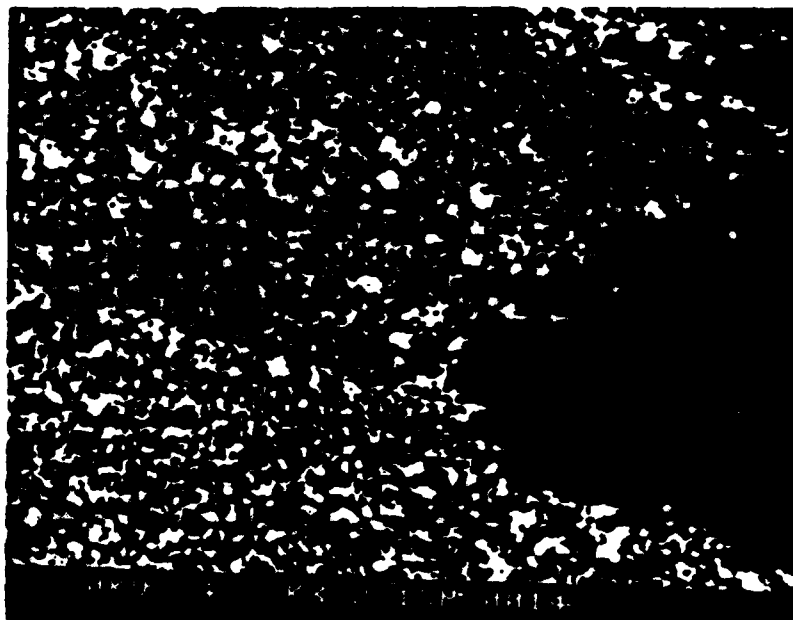
J. Appl. Res. 1,  
352 (1986)



# Au on GaAs

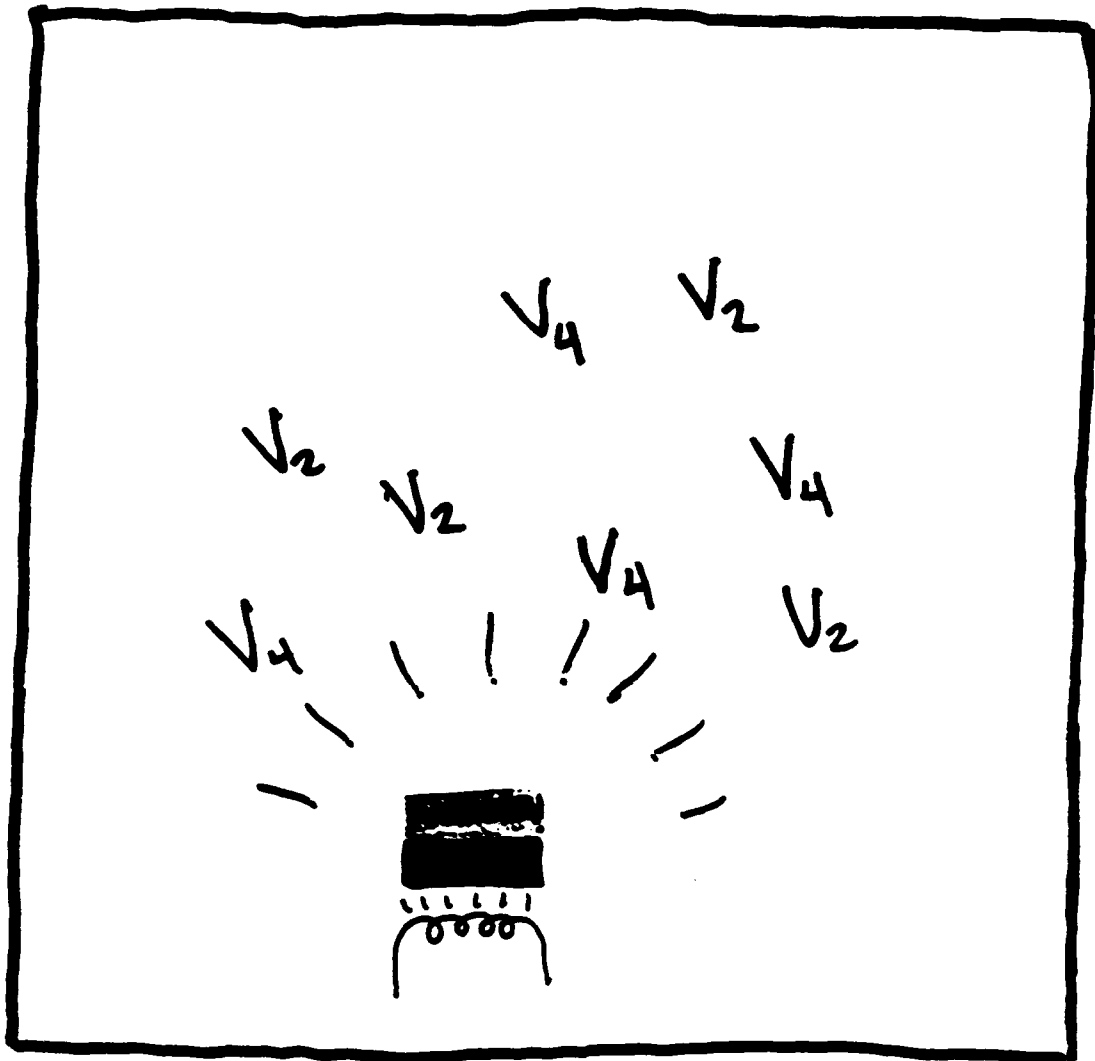
---

Room  
Temp.



500°C





Open System:  
ie. mass is not  
necessarily constant

# Solid State Electronics

## 22 (1979) 517.

### DISSOCIATION OF GaAs AND Ga<sub>0.7</sub>Al<sub>0.3</sub>As DURING ALLOYING OF GOLD CONTACT FILMS

E. KINSEBORN, P. K. GALLAGHER and A. T. ENGLISH  
Bell Laboratories, Murray Hill, NJ 07974, U.S.A.

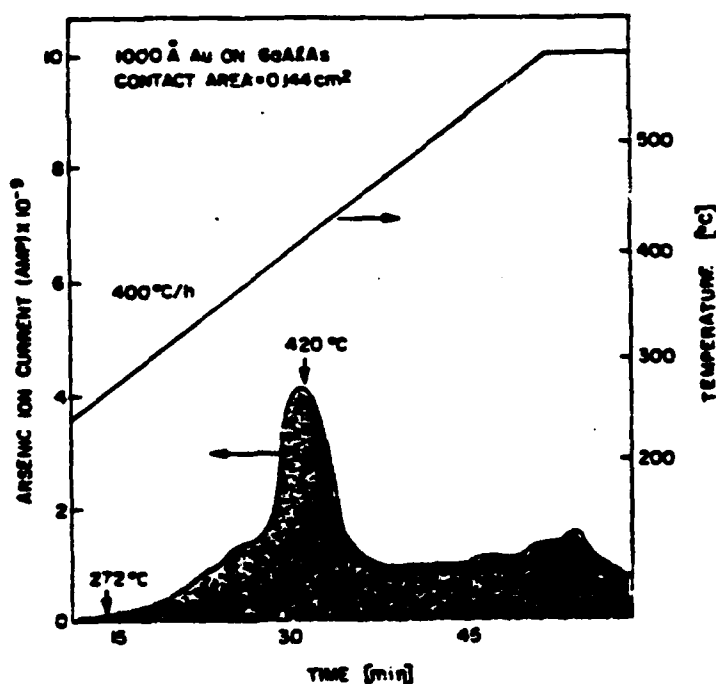
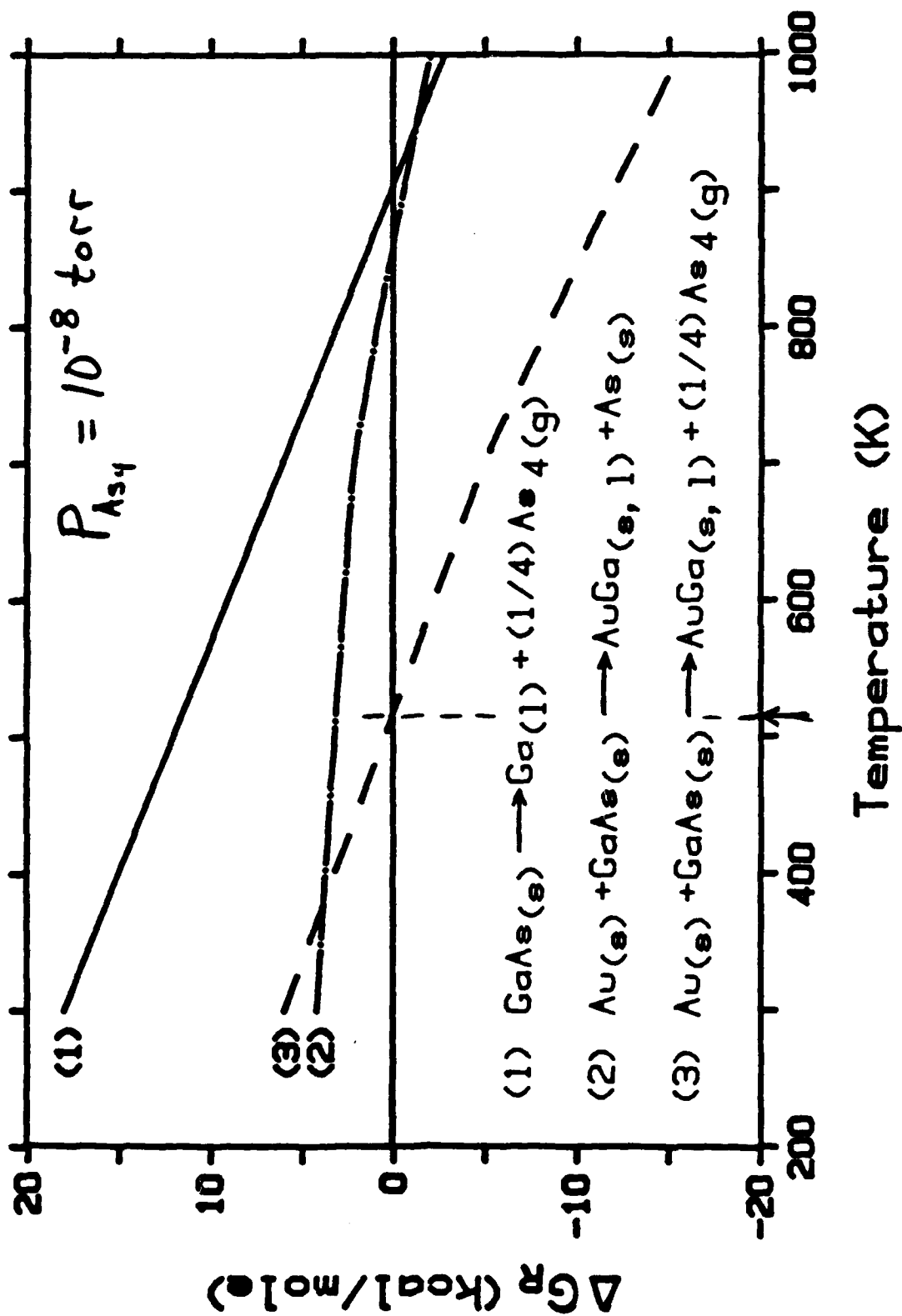


Fig. 1. The mass spectrometer output for a repeated scan through a short range around the As a.m.u. As starts to appear at  $-230^\circ\text{C}$  and reaches a maximum rate of evolution at  $420^\circ\text{C}$ . Unreacted GaAs starts to decompose at  $-620^\circ\text{C}$ .

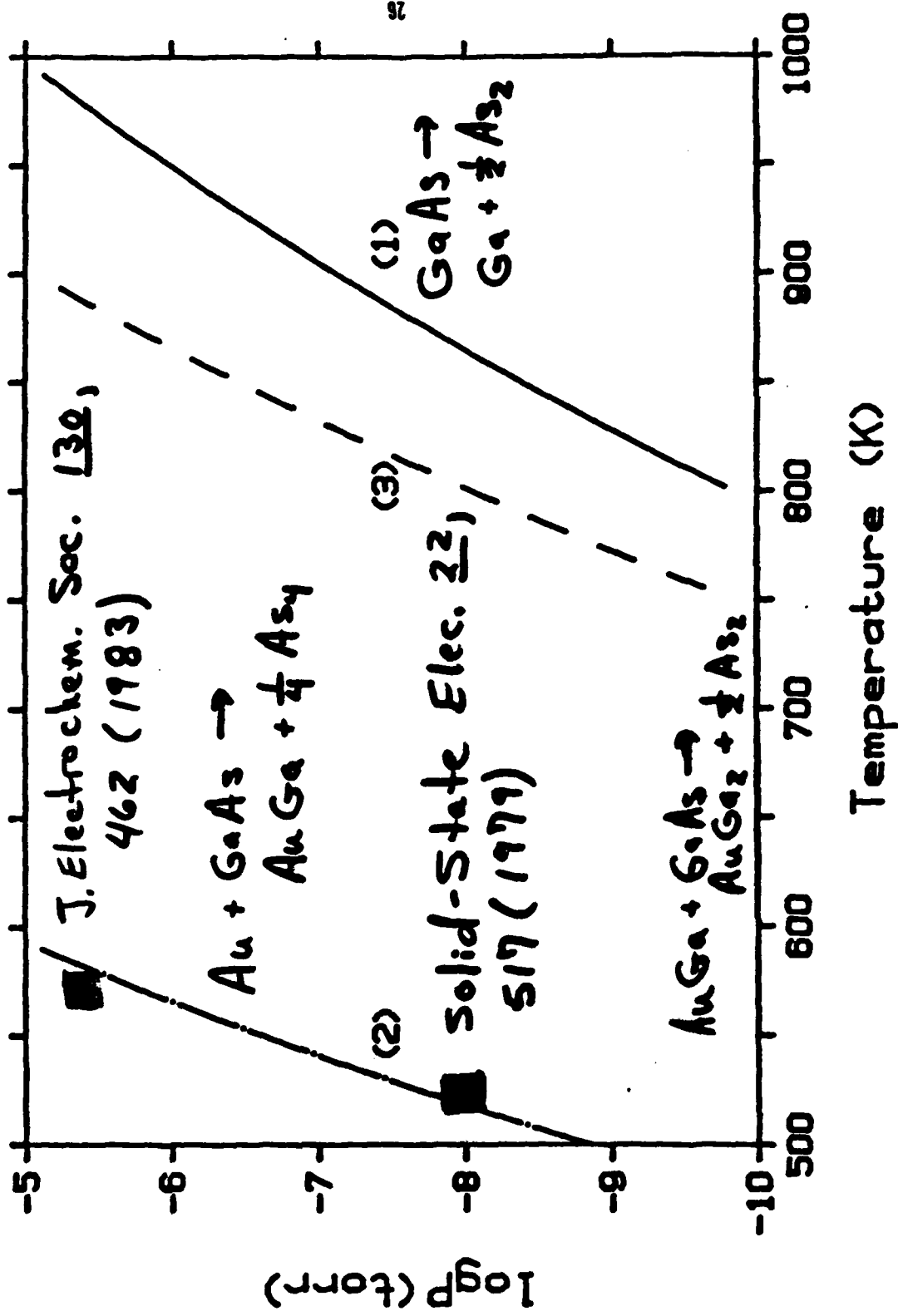
# Gibbs Free Energy of Reaction

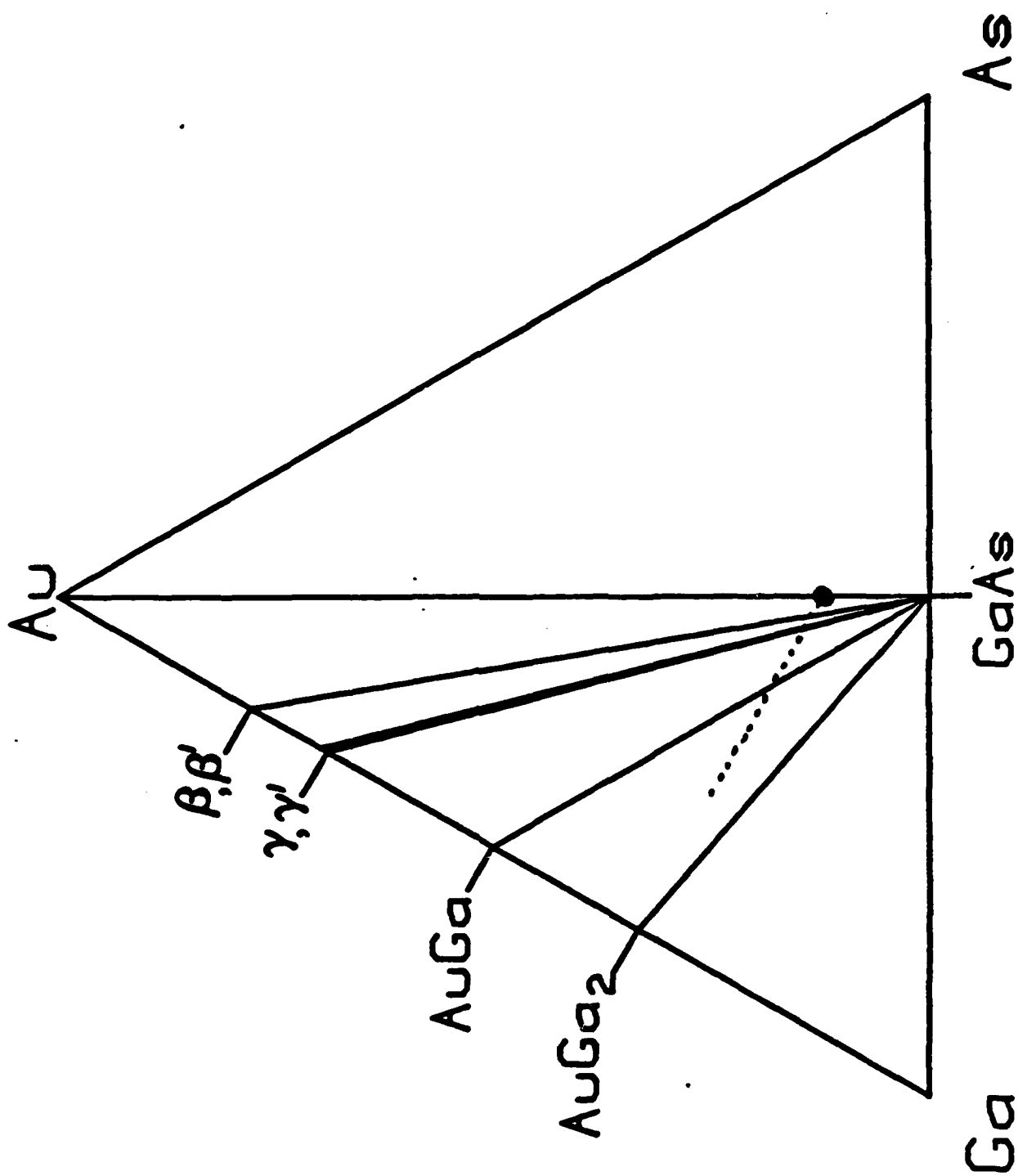


J. Mats. Res. L, 343 (1986)



As partial pressure vs temp.





## Reaction Sequence



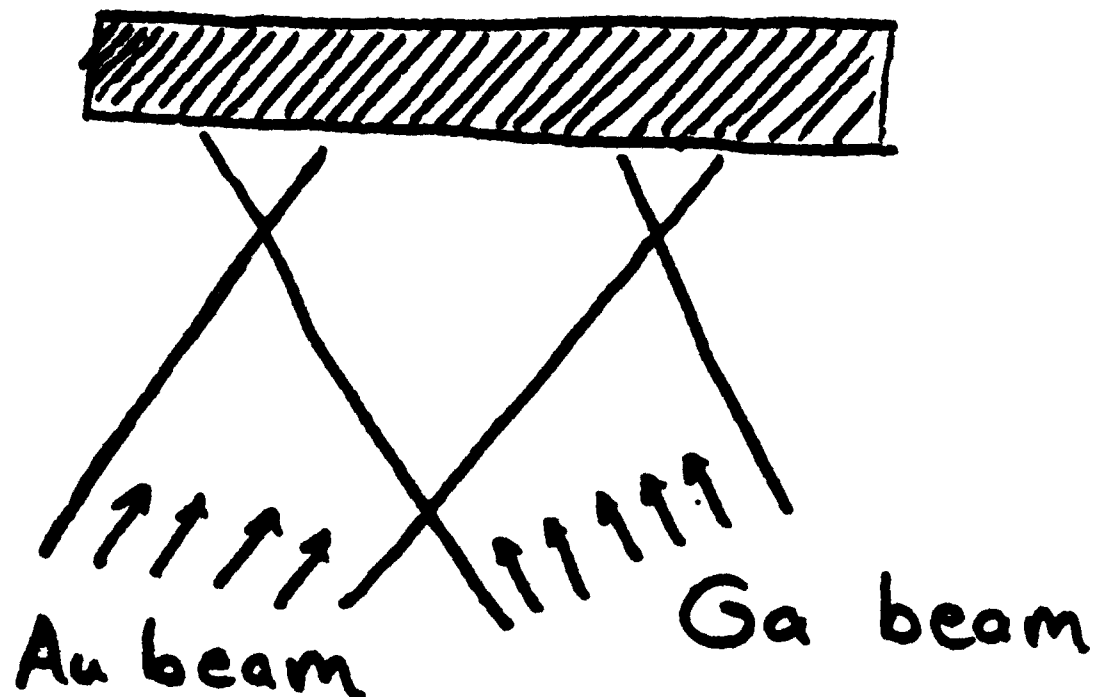
for all reactions,  $\Delta H > 0$

but  $\Delta G < 0$ !

Au + Ga on GaAs



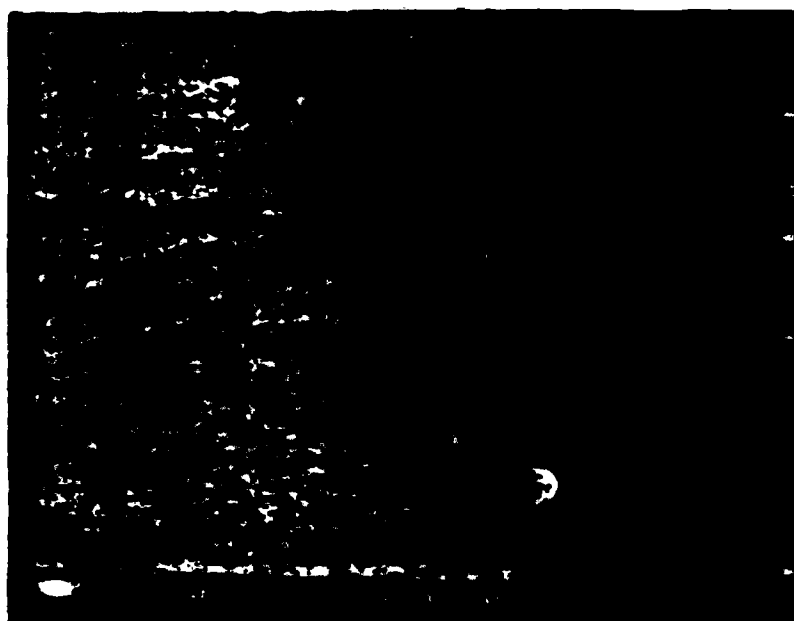
GaAs Substrate



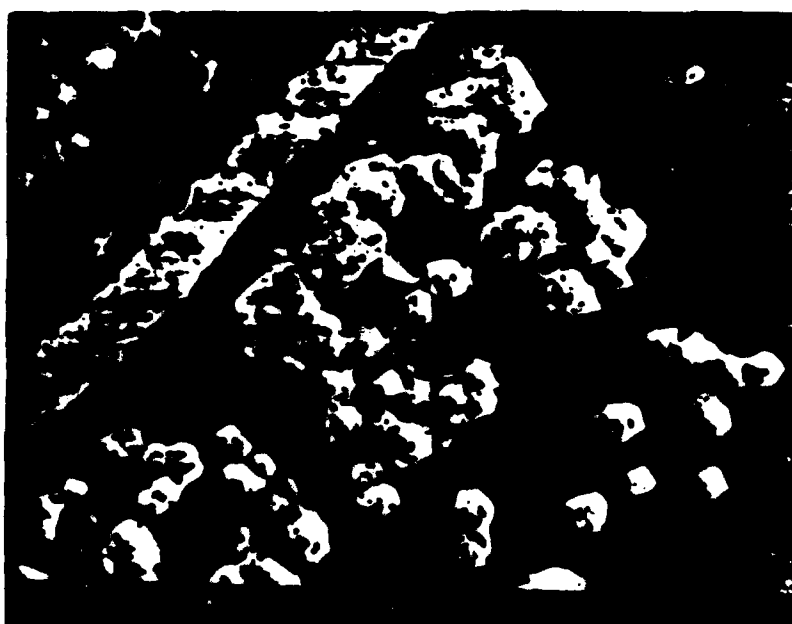
J. Appl. Phys. 61, 537 (1986)

# 2000Å Au on GaAs

Room  
Temp.



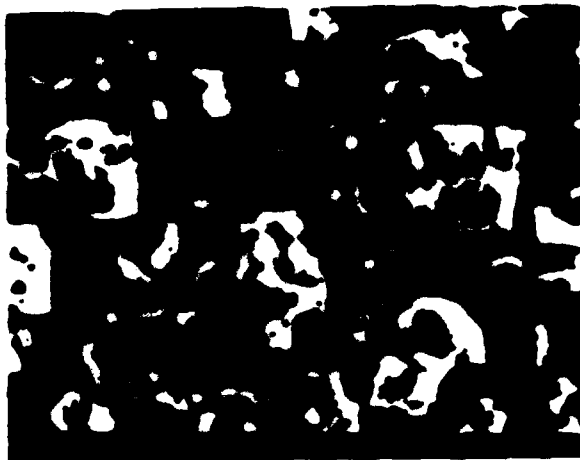
500°C



# $\text{AuGa}_2$ on GaAs

a)

$300^\circ\text{C}$

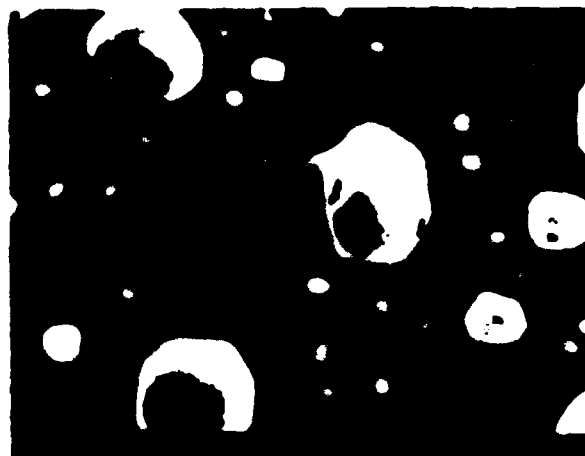


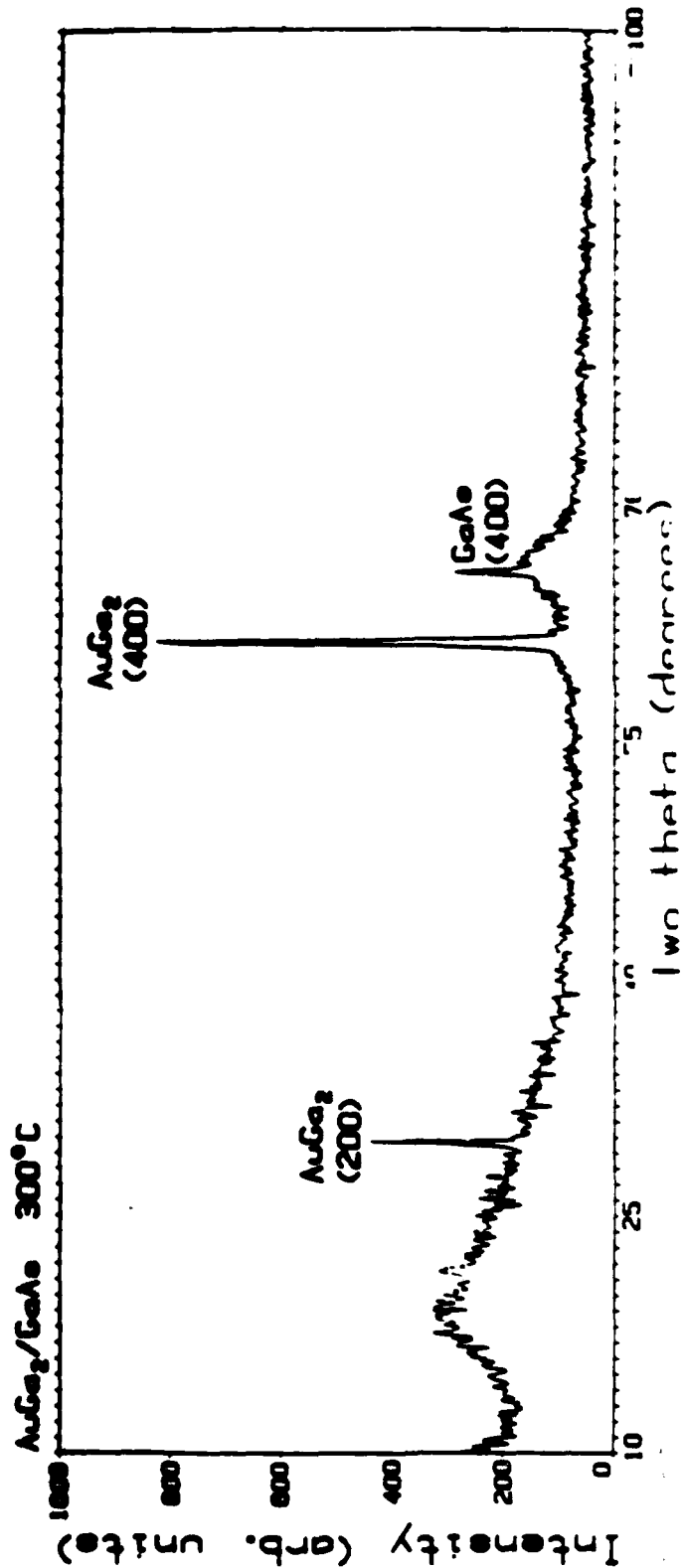
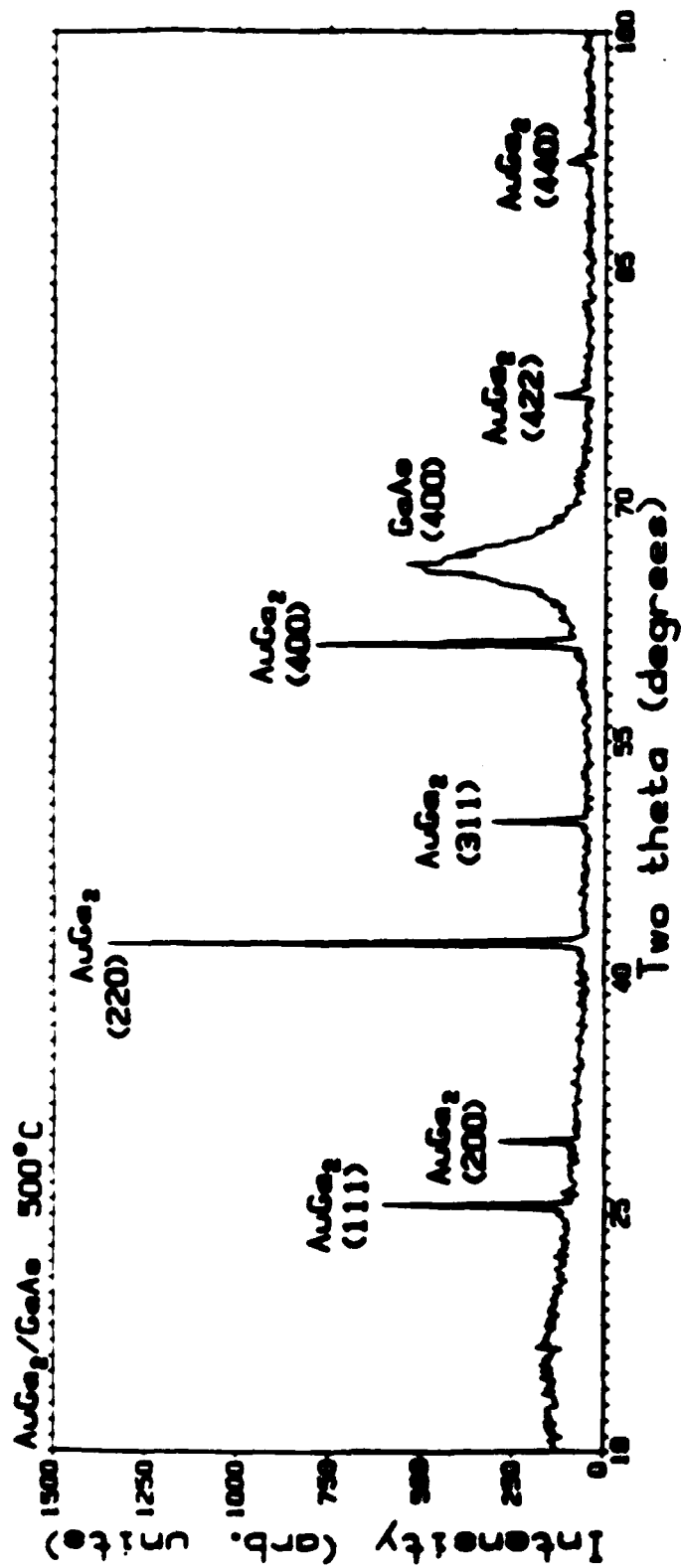
b)

$480^\circ\text{C}$



$500^\circ\text{C}$  c)





# Electrical Properties of Metal Contacts on GaAs

Leung, Yoshie, Bauer, and Milnes

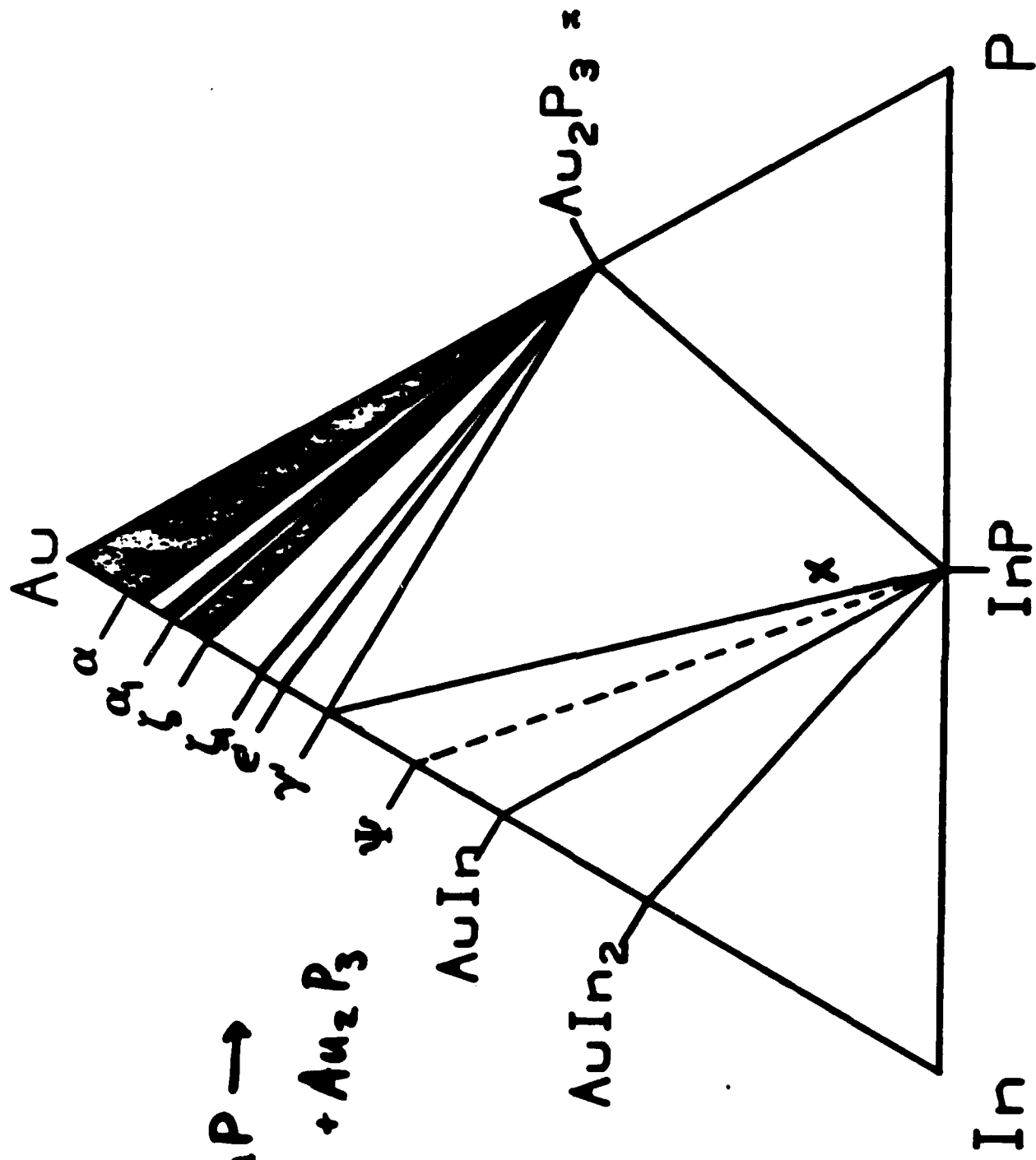
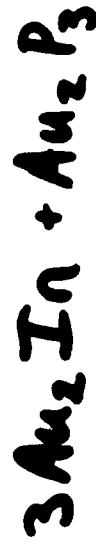
J. Electrochem. Soc. 133, 898 (1985)

	As deposited	350°C Anneal				
	$\phi$ (eV)	$n$	$V_B$ (volts)	$\phi$	$n$	$V_B^R$
Au	0.95	1.05	33	-	ohmic -	

AuGa <sub>2</sub>	0.68	1.05	21	0.74	1.04	18
-------------------	------	------	----	------	------	----



# Predict



1

1

**1 a)**

**I.R.T.**

**35 days**

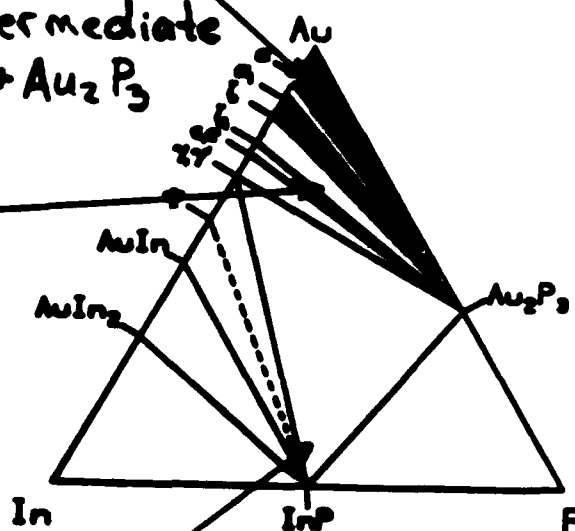
initial reaction stage  
continuous film  
2 phase

**b)**

1365c

100 min

intermediate  
 $\text{I}_2 + \text{Au}_2\text{P}_3$



**c)**

510°C

40 min

closed system equil.  
islands

$$\gamma + Au_2P_3$$

## **CONCLUSIONS**

- 1) Bulk phase diagrams are guides to the understanding of interfacial chemistry.**
- 2) Thermochemistry can be used to predict the end products of a chemical reaction, and provide information on the intermediates.**
- 3) Entropy must be considered explicitly in reactions that can produce volatile group V products.**
- 4) Thermodynamics cannot be used to predict how fast a reaction will proceed.**
- 5) Chemically stable interfaces are also electrically stable.**
- 6) Phase diagrams should be consulted before a metal/compound-semiconductor is designed.**
- 7) The current thermochemical data base is inadequate for a broad understanding of metal/compound-semiconductor systems.**

**Phase Equilibria in Metal-Gallium-Arsenic Systems:  
Thermodynamic Considerations for Metallization Materials**

**Robert Beyers\*, Ki Bum Kim, and Robert Sinclair**  
**Department of Materials Science and Engineering**  
**Stanford University, Stanford, California 94305**

**Journal of Applied Physics ( in press )**

### **Abstract**

We propose a classification scheme for phase equilibria in elemental metal-gallium-arsenic systems. Using available data we assign as many metals as possible to seven generic types of ternary phase diagrams. We describe how the phase diagrams can provide a framework for interpreting previous studies of metal reactions with GaAs substrates and for identifying stable materials for GaAs metallizations.

## I. Introduction

One of the most challenging problems in GaAs integrated circuit fabrication is the formation of reliable metal contacts. This problem has resulted in numerous studies of metal reactions with GaAs substrates, which typically attempt to relate changes in the electrical properties of the contact to interdiffusion and reaction at the metal-semiconductor interface. Clearly, as device dimensions decrease in GaAs integrated circuits, it will become increasingly important to form uniform contact layers to GaAs with minimal substrate interaction.<sup>1-3</sup>

While there have been many investigations of metal-GaAs chemistry, the results of these studies have been explained largely with empirical correlations, such as comparing the electronegativities of the elements involved<sup>4</sup> or the heats of formation of the compounds involved.<sup>5, 6</sup> Unfortunately, these correlations provide little or no framework for understanding actual processing problems or for choosing stable metallization materials because they disregard classical thermodynamic considerations, most notably the implications of the Gibbs phase rule. In contrast, metal-gallium-arsenic (M-Ga-As) ternary phase diagrams should provide just such a framework.<sup>7</sup>

Indeed, ternary diagrams have already been used to understand other aspects of GaAs processing. For instance, to assist in studies of dopant diffusion in GaAs and solution growth of doped GaAs crystals, Panish<sup>8-16</sup> determined the liquidus and solidus data for numerous dopant-Ga-As diagrams. Similarly, Deal<sup>17, 18</sup> recently determined the Cr-Ga-As diagram and resolved many ambiguities in previous studies of chromium solubility and diffusivity in GaAs. Moreover, Thurmond *et al.*<sup>19</sup> used the Ga-As-O diagram to explain the phases formed during GaAs oxidation. However, the use of ternary phase equilibria to explain metallization processing problems in GaAs has only just begun, with the recent work by Williams *et al.*<sup>20,21</sup> being the most notable example.

The purpose of the present article, then, is to describe how M-Ga-As phase diagrams can provide a framework for interpreting previous results and for identifying suitable materials for

stable contacts. We begin by outlining the seven generic M-Ga-As diagrams that are possible. For the four simplest types, we show how they can be identified in principle by a single experiment, and we point out which metal-containing phases will be stable contacts. Next, based on previously published studies, we identify metals that belong to each type. Finally, we describe how the phase diagrams can be used to search systematically for stable metallization materials.

## **II. CLASSIFICATION SCHEME**

Because the thin-film reactions to be discussed involve three elements distributed in various phases, they should be described using ternary phase diagrams. At fixed temperature and pressure, the Gibbs phase rule predicts a maximum of three phases in equilibrium in any portion of the phase diagram. Regions of three-phase equilibrium form triangles in isothermal sections of the ternary phase diagram. The phases at the corners of a given triangle are thermodynamically stable in contact with each other. For metal-gallium-arsenic systems, this means that the chemical potential of the metal is the same in all three phases, and similarly for the gallium and the arsenic. If free energy data are available for all the phases, then the regions of three-phase equilibrium can be found by determining the stable two-phase tie-lines, which in turn are established by straightforward free energy calculations.<sup>22</sup> Alternatively, the stable tie-lines and three-phase regions can be found experimentally by reacting various M-Ga-As compositions in closed, inert containers and identifying the phases formed. Through judicious use of the phase rule, the number of compositions that must be evaluated to determine the stable tie-lines and three-phase regions can be quite small. In particular, for some simple cases, the metal-containing phases with stable tie-lines to GaAs can be determined by a single experiment.

For understanding M-Ga-As chemistry, it is useful to classify the diagrams according to their key features, i.e., the disposition of their stable tie-lines. In practice, other aspects of the diagrams (solubility ranges, solidus and liquidus data) will be important for interpreting particular problems. Thus, we begin by classifying the diagrams according to their general features and then consider in

turn subtler factors that may be important for interpreting M-Ga-As thin-film reactions.

#### A. Simplest cases

For the moment, let us make the following assumptions and simplifications:

- (1) Assume just one  $\text{MGa}_x$  and one  $\text{MAs}_y$  binary compound exist.
- (2) Assume no  $\text{MGa}_x\text{As}_y$  ternary phases exist.
- (3) Neglect the homogeneity range of each phase.
- (4) Neglect the formation of liquid phases.
- (5) Neglect arsenic sublimation.
- (6) Assume equilibrium between the solid phases is reached during processing.

(The converse of each of these simplifications will be considered in the next section.)

Given these simplifications, there are four possible types of M-Ga-As diagrams (Fig. 1a-d):

Type I: GaAs dominant. The most important feature of this diagram is the GaAs-M tie-line (Fig. 1a), which indicates that GaAs is stable in contact with the elemental metal. This is the only type of diagram in which the elemental metal can be in thermodynamic equilibrium with the semiconductor. In all other cases, heating the M-GaAs couple will result in a chemical reaction and the production of new phases. The simplest way to verify such a diagram is to heat a mixture of the elemental metal and GaAs in a closed, inert container. While some interdiffusion between the two phases will take place, no new phases will form. To further check this result, a  $y:x$  mixture of  $\text{MGa}_x\text{-MAs}_y$  can be heated in a closed, inert container. A solid-state reaction will occur, producing a mixture of the elemental metal and GaAs. For this type of diagram,  $\text{MGa}_x$ ,  $\text{MAs}_y$ , and M are all stable with respect to new compound formation when in contact with GaAs.

Type II:  $\text{MGa}_x$  dominant. The key feature of this diagram is the  $\text{MGa}_x\text{-As}$  tie-line (Fig. 1b). From the Gibbs phase rule, the presence of the  $\text{MGa}_x\text{-As}$  tie-line precludes the existence of a GaAs-M tie-line. The elemental metal, therefore, cannot be stable in contact with GaAs. The simplest way to verify such a diagram is to heat a mixture of the elemental metal and a large excess



of GaAs in a closed, inert container. At equilibrium, the container will hold a mixture of  $\text{MGa}_x$ , elemental arsenic, and the excess GaAs. These phases can normally be identified by X-ray or electron diffraction techniques. For this type of diagram,  $\text{MGa}_x$  is the only metal-containing phase that is stable in contact with GaAs.

Type III:  $\text{MAS}_y$  dominant. This diagram is the complement of the Type II diagram. Its key feature is the  $\text{MAS}_y$ -Ga tie-line (Fig. 1c). As before, the simplest way to verify such a diagram is to heat a mixture of the elemental metal and a large excess of GaAs in a closed, inert container. At equilibrium, the container will hold a mixture of  $\text{MAS}_y$ , elemental gallium, and the excess GaAs. For this type of diagram,  $\text{MAS}_y$  is the only metal-containing phase that is stable in contact with GaAs.

Type IV: No phase dominant. The most important feature of this diagram is the lack of any tie-lines between a binary compound and the remaining third element (Fig. 1d). Once again, the simplest way to verify such a diagram is to heat a mixture of the elemental metal and a large excess of GaAs in a closed, inert container. At equilibrium, the container will hold a mixture of  $\text{MGa}_x$ ,  $\text{MAS}_y$ , and the excess GaAs. For this type of diagram, both  $\text{MGa}_x$  and  $\text{MAS}_y$  are stable in contact with GaAs, but the elemental metal is not.

### B. Complicating factors

In this section, we consider in turn the converse of each of the aforementioned simplifications.

(1) More than one  $\text{MGa}_x$  or  $\text{MAS}_y$  binary compound exists. Many metals have more than one  $\text{MGa}_x$  or  $\text{MAS}_y$  binary compound. This complication, however, does not change the two key ideas presented in the previous section. First, the reaction of the elemental metal with excess GaAs in a closed, inert container can still be used to determine to which type of diagram the metal belongs. Additional binary compounds may result in more intermediate phases forming in a M-GaAs ternary diffusion couple, but the end phases will remain the same (See Fig. 2.). Second,

for the purpose of materials selection, only the phases with tie-lines to GaAs warrant further study because only these phases can form thermodynamically stable contacts to GaAs (We are not considering materials stable by virtue of kinetic barriers in this analysis, even though they may be useful in practice.). Note that some metals do not form stable  $\text{MGa}_x$  or  $\text{MAs}_y$  binary compounds, thereby simplifying the phase diagram determination for these metals. Because our classification scheme is based on the presence of certain key tie-lines, no new categories are introduced by the existence of more than one  $\text{MGa}_x$  or  $\text{MAs}_y$  binary compound.

(2)  $\text{MGa}_x\text{As}_y$  ternary phases exist. If ternary phases exist, then additional experiments will be required to determine the stable tie-lines in the diagram. The basic approach, however, remains the same: through judicious use of the phase rule, a small number of experiments can be performed to determine the stable tie-lines in the M-Ga-As diagram, and only those ternary phases with stable tie-lines to GaAs deserve further study as potential metallization materials. Fortunately, there appear to be few  $\text{MGa}_x\text{As}_y$  ternary phases.

The presence of a ternary phase creates another category, which we have designated Type V. Although many new tie-line configurations become possible if ternary phases are present, further subclassification of these configurations is unwarranted for our purposes. In Fig. 1e, we have drawn the Type V diagram with a  $\text{M}_2\text{GaAs}$  ternary phase, since this is the most common type of ternary phase observed in M-GaAs reactions. The existence of a  $\text{M}_2\text{GaAs}$  phase implies that the elemental metal cannot be stable in contact with GaAs, i.e., there is no direct GaAs-M tie-line. Moreover, the  $\text{M}_2\text{GaAs}$  phase itself will be stable in contact with GaAs only if no  $\text{MGa}_x$ - $\text{MAs}_y$  tie-line intervenes (Type IV).

(3) Each phase has a homogeneity range. Most  $\text{M}(\text{Ga})$  solid solutions and some  $\text{MGa}_x$  and  $\text{MAs}_y$  phases have substantial homogeneity ranges. Thus, a pure, stoichiometric metal-containing phase cannot be at complete equilibrium with the GaAs substrate, even if there is a stable tie-line between the metal-containing phase and the GaAs. Metal atoms will diffuse from the pure phase into the GaAs until the solubility limit is reached, and similarly gallium and arsenic will diffuse into

the pure phase. Moreover, differences in the gallium and arsenic solubilities in the metal-containing phase can cause a third phase to form. If arsenic is less soluble than gallium in the metal-containing phase, then the excess arsenic will react to form the arsenic-rich phase adjacent in the M-Ga-As diagram to the metal-containing phase (See Fig. 3.). Conversely, if gallium is less soluble, then the gallium-rich phase adjacent to the metal-containing phase will form.

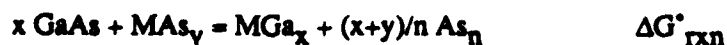
To minimize the net exchange of material between the metal-containing phase and the GaAs substrate, the metal-containing phase should be deposited with the maximum solubility of gallium and arsenic already incorporated in it, if this is feasible. Indeed, several researchers have found that codepositing (M + Ga) improved the contact stability of GaAs metallizations during subsequent high-temperature processing.<sup>23-26</sup> Such a saturated film should also be a stable, more reproducible metal diffusion source for the GaAs substrate.

Lastly, note that some Group III-As and Ga-Group V compounds form a complete series of solid solutions with GaAs, thereby producing the final two categories of M-Ga-As phase diagrams, Types VI and VII (Figs. 1f, g).

(4) Liquid phase formation cannot be neglected. "Alloying" is commonly used to make ohmic contacts to GaAs.<sup>1, 27</sup> The alloying process involves melting and resolidifying the metallization layer. While this process has been used successfully in low-density circuits, the morphological changes brought on by melting and resolidification will become unacceptable as device dimensions continue to shrink. Because liquid phase formation needs to be avoided, solidus data for the phases with stable tie-lines to GaAs need to be determined. This information can be readily obtained from differential thermal analysis experiments. Furthermore, since gallium melts at low temperatures, the composition of the thin film-substrate system must remain outside the three-phase region containing elemental gallium during processing. If liquid phase formation cannot be avoided, then both solidus and liquidus data will be required to explain the liquid and solid compositions and the resolidification path.

(5) Arsenic sublimation cannot be neglected. Because processing is typically done in an open system, there may be substantial arsenic loss to the gas phase as the M-Ga-As system continually tries to establish the equilibrium arsenic pressure.<sup>28, 29</sup> This arsenic loss will result in varying proportions of the condensed phases in mutual equilibrium (if the overall composition remains in one three-phase region of the diagram) or a sequence of increasingly gallium-rich phases (if tie-lines are crossed). In this instance, the heat-treatment time and temperature are clearly critical to the observed products. Several methods are commonly used to minimize or eliminate arsenic loss to the vapor: an arsenic overpressure can be maintained in the annealing furnace,<sup>30</sup> an inert capping layer can be deposited over the wafer,<sup>31</sup> or rapid thermal annealing can replace conventional furnace annealing.<sup>32, 33</sup>

In addition, since arsenic must diffuse through the metallization layer prior to sublimation and since equilibrium between the metallization layer and the GaAs substrate fixes the equilibrium arsenic vapor pressure, the metallization material chosen will also affect the rate of arsenic loss. From the Gibbs phase rule, the equilibrium arsenic pressure is fixed in each three-phase region of the ternary diagram, being largest in the three-phase region containing elemental arsenic. If the free energy data are available, then the equilibrium arsenic pressure can be calculated. The partial pressure of each arsenic gas specie ( $As$ ,  $As_2$ , and  $As_4$ ) in a particular three-phase region is determined by writing an equilibrium reaction between the arsenic gas specie and the condensed phases comprising the three-phase region.<sup>34</sup> For example, for the  $MGa_x$ - $MAs_y$ -GaAs three-phase region in Fig. 1d, the reaction is



the  $As_n$  partial pressure is given by

$$P_{As_n} = \exp[-\Delta G^\circ_{rxn} / n(x+y)RT]$$

and the total arsenic pressure is the sum of the partial pressures. A similar analysis applies to the equilibrium vapor pressures of both gallium and the metal, but these pressures are typically much less than the arsenic pressure and will not be considered here.

If the most gallium-rich  $\text{MGa}_x$  phase having a stable tie-line to GaAs is chosen as the metallization material, then it will also have the lowest equilibrium arsenic vapor pressure and potentially lower arsenic losses.<sup>20</sup> Note, however, that arsenic sublimation from the GaAs substrate through this phase would result in the undesirable formation of liquid gallium.

(6) Equilibrium between the solid phases is not reached during processing. The time-temperature combinations used in processing may not be sufficient to reach equilibrium. In particular, metastable intermediates in M-GaAs ternary diffusion couples may form. This possibility can be checked by determining whether the same phases in a possible three-phase region are produced by different combinations of starting materials.

Thus, while many complicating factors can and do arise, the use of ternary diagrams to explain M-Ga-As thin-film reactions need not be abandoned. Quite the contrary, the ternary diagrams provide the simplest, most logical framework in which to explain the complications.

### III. Specific systems

In this section, we attempt to assign as many metals as possible to the seven categories described in the preceding section. If a M-Ga-As diagram has been previously determined experimentally, then making this assignment is a simple matter. Similarly, if free energy data are available for all the phases in a particular M-Ga-As system, then the diagram can be easily calculated<sup>22</sup> and classified. Unfortunately, for many metals, neither of these situations exist. Instead, the only information available for many metals are published studies of metal thin-film reactions with GaAs substrates. For these metals, we try to infer the stable tie-lines (and thus classify the diagram) from the reported reaction products. This method has been quite useful in

explaining ternary reactions involving silicon metallizations.<sup>35,36</sup> For GaAs metallizations, however, arsenic volatilization can lead to incorrect conclusions using this method. Moreover, for many metal-GaAs thin-film reactions, the product phases have not been identified unambiguously using diffraction methods. For both of these reasons, the diagrams for such metals must be considered only tentative. If anything, this section points out the need to complement thin-film investigations of metal-GaAs reactions with bulk studies in closed systems.

The simplified diagrams in Figs. 4-9 show the equilibria between solid phases at typical processing temperatures. The diagrams are "pseudoisothermal" sections, meaning that changes in the tie-line configurations due to solid-state transformations (eutectoids, peritectoids, melting, etc.) with changing temperature are not explicitly shown.

#### **A. Type I**

Metals such as gold, silver, and tungsten have a Type I diagram.

Tsai and Williams<sup>21</sup> recently determined the Au-Ga-As diagram. The fact that gold has long been employed in GaAs metallizations is consistent with its simplified diagram (Fig. 4a). The many technological problems associated with the use of gold, however, can be appreciated immediately from the exact Au-Ga-As diagram. Gold dissolves a substantial amount of gallium (~10%) and some arsenic (<1%) at a processing temperature of 300°C.<sup>37</sup> The metal composition in equilibrium with GaAs is a saturated ternary solid solution, whose composition changes with annealing temperature. Thus, when pure gold is annealed on GaAs, the substrate locally disintegrates, a ternary solid solution forms, and the excess arsenic crystallizes or sublimes. Several researchers have shown that this interdiffusion dramatically alters the microstructure and resulting electrical properties of the metal-semiconductor interface.<sup>26,38-40</sup> From a thermodynamic perspective, the problem can be minimized either by depositing an alloy of suitable composition (or even one supersaturated with gallium and arsenic) or by substituting a Au-Ga compound for pure gold, as demonstrated by Guha *et al.*<sup>26</sup> and Williams *et al.*<sup>20</sup> respectively.

The simplified Ag-Ga-As diagram shown in Fig. 4b can be derived from Panish's work.<sup>13</sup> The  $\epsilon$  phase is stable only in the temperature range 446-582°C.<sup>41</sup>

Tungsten forms two compounds with arsenic<sup>42</sup> —  $W_2As_3$  and  $WAs_2$  — but none with gallium. From available thermochemical data,<sup>43</sup> it can be shown that the W-GaAs tie-line is favored over the Ga- $W_2As_3$  tie-line and that therefore the former exists. Thus, we believe the W-Ga-As diagram is as shown in Fig. 4c. At first glance, a recent study<sup>44</sup> of  $SiO_2$ -encapsulated W-GaAs diffusion couples would appear to contradict the existence of the W-GaAs tie-line. This study found that no new phases formed after annealing at 750°C, but a reaction producing  $W_2As_3$  occurred at 900°C. However, greater gallium solubility in tungsten at higher temperatures and selective gallium loss through the  $SiO_2$  encapsulant can explain this high-temperature instability. Thus, during high-temperature annealing, the composition of the system moved from the W-GaAs two-phase region to the W- $W_2As_3$ -GaAs three-phase region.

For completeness, we note that the semiconductors silicon, germanium, and tin also have Type I diagrams, as determined by Panish.<sup>8,11</sup> Simplified diagrams for silicon and germanium are shown in Figs. 4d and 4e. Like tungsten, silicon and germanium have two arsenides, but no gallium-based phases. The mutual equilibrium of silicon and germanium with GaAs is expected from chemical considerations and is quite important technologically for heteroepitaxial growth of GaAs films on silicon substrates, and vice versa. Moreover, Kavanaugh *et al.*<sup>45</sup> have recently investigated the formation of thermally stable, degenerately doped polycrystalline silicon contacts to GaAs.

### B. Types II and III.

Few metals have these types of diagrams since it is unusual for either elemental arsenic (Type II) or elemental gallium (Type III) to be in equilibrium with a complementary binary compound. Lahav and Eizenberg<sup>46</sup> reported that a thin film of tantalum reacts with GaAs at 650°C and produces TaAs and liquid gallium. Tantalum thus appears to have a Type III diagram. In

addition, x-ray photoemission spectroscopy has identified metal arsenides and "metallic" gallium as products of GaAs reactions with Re, Ir, Tb, Dy, and Er monolayers.<sup>47, 48</sup> If "metallic" gallium corresponds to elemental gallium, then these metals also have  $MA_s$  dominant Type III diagrams. On the other hand, if "metallic" gallium corresponds to  $MGa_x$  compounds, then these metals belong to the no phase dominant Type IV category. Note that diffraction studies of thicker films would be simpler to perform, easier to interpret, and more representative of thin-film behavior in actual metallizations than spectroscopic studies of monolayer films. Based on published results of numerous M-GaAs thin-film reactions, there do not appear to be any metals which have Type II diagrams. However, studies of GaAs oxidation by Thurmond *et al.*<sup>19</sup> have shown that the Ga-As-O diagram is basically of this type (Fig. 5).

### C. Types IV and V.

The most commonly found M-Ga-As diagram is Type IV, no phase dominant. Copper, chromium, and platinum can definitely be assigned to this category, as can palladium, nickel, and cobalt at high temperatures. In Fig. 6, the copper diagram is established by Panish's work,<sup>13</sup> the chromium diagram from an X-ray analysis by Deal,<sup>17</sup> and the platinum diagram from thin film studies.<sup>49-52</sup>

The Pd-Ga-As diagram determined by El-Boragy and Schubert<sup>53</sup> (Fig. 7) can be used to explain several recent studies of Pd-GaAs thin-film diffusion couples.<sup>54-58</sup> Their diagram predicts that the final products of a reaction between a thin film of palladium and a GaAs substrate should be a mixture of PdGa, PdAs<sub>2</sub>, and excess GaAs. Moreover, their diagram predicts that several palladium-rich phases, including two ternary phases, may precede the formation of the final equilibrium products. In the thin-film studies, a ternary phase, designated "Phase I" by Sands *et al.*,<sup>57</sup> formed in the temperature range 25-250°C; Phase I was followed by a second ternary phase, designated "Phase II", between 250-500°C; and finally, a mixture of PdGa and PdAs<sub>2</sub> formed at 600°C.<sup>58</sup> The crystal structure, lattice parameters, and stoichiometry of Phase I



— hexagonal,  $a_0 \sim 0.67$  nm and  $c_0 \sim 0.37$  nm,  $\sim \text{Pd}_{2.4}\text{GaAs}$  — match those of the ternary phase designated  $\text{Pd}_2\text{Ga}_N\text{As}_{1-N}$  by El-Boragy and Schubert.<sup>59</sup> Similarly, Phase II — hexagonal,  $a_0 \sim 0.9$  nm and  $c_0 \sim 0.34$  nm,  $\sim \text{Pd}_{3.3}\text{Ga}_{1.2}\text{As}_{0.8}$  — matches the phase designated  $\text{Pd}_{12}\text{Ga}_5\text{As}_2$  by El-Boragy and Schubert.<sup>53</sup>

Type V diagrams that have a ternary phase with the stoichiometry  $\text{M}_2\text{GaAs}$  might be regarded as a subset of Type IV since the ternary phase usually transforms to a mixture of  $\text{MGa}_x$  and  $\text{MAs}_y$  after high-temperature annealing. Whether these ternary phases are metastable intermediates in M-GaAs diffusion couples or are stable, low-temperature phases with tie-lines to GaAs remains to be determined. Metals in this category include nickel<sup>60, 61</sup> and perhaps cobalt<sup>62</sup>. The diagrams for these metals are drawn with dashed tie-lines to the ternary phase because of the present uncertainty about the stability of the ternary phase (Fig. 8).

#### D. Types VI and VII.

These diagrams exist for elements that can readily substitute for gallium or arsenic in the GaAs crystal structure, thereby forming ternary semiconductor compounds. Thus, aluminum and indium belong to Type VI, and phosphorus belongs to Type VII. While technological interest centers on their optical properties, one of the ternary semiconductors —  $\text{In}_x\text{Ga}_{1-x}\text{As}$  — has also been suggested for use in graded heterojunction ohmic contacts.<sup>63, 64</sup>

Photoemission studies of aluminum monolayer reactions with GaAs substrates are consistent with aluminum having a Type VI diagram. These studies<sup>65-68</sup> have found that aluminum replaces gallium in the top layers of the GaAs substrate and that free gallium forms on the surface. For thicker aluminum films, the observed extent of reaction depends on the time-temperature combinations used and the amount of oxygen contamination present.<sup>69-72</sup>

#### **IV. APPLICATIONS**

The ideal metallization is a material that does almost nothing. It does not react with the substrate. It does not interdiffuse with the substrate. It does not react with other solids and gases with which it comes in contact. It does not melt during processing. Essentially all it does is conduct electricity well. Of course, actual metallization materials cannot satisfy all of these criteria, and compromises have to be made. Note, however, that ternary diagrams provide the basis for evaluating many of these criteria. The tie-lines in a ternary diagram indicate which phases will be stable in contact with GaAs. The solubility data show the maximum extent of interdiffusion as a function of temperature. The solidus data reveal the temperature at which melting begins for particular solid compositions.

Most materials comprising an integrated circuit are inherently in a metastable state. Short-time, low-temperature processing is used to prevent the materials from reaching a complete equilibrium state (and the undesirable properties associated with that state). For metallization materials, however, we suggest that a complementary approach may be useful: if the metallization is deposited with a composition that is already near equilibrium with the GaAs substrate, then minimal interaction between the metallization and the substrate will occur during subsequent processing. Thus, besides rapid thermal annealing, the composition of the as-deposited metallization layer can also be used to prevent solid-state reactions, to minimize interdiffusion, and to reduce arsenic sublimation.

If such an approach is adopted, then the following steps should be taken to identify optimal metallization materials. First, for a particular metal, the metal-containing phases with stable tie-lines to GaAs need to be determined. As shown in Section IIA, most of these phases can be deduced from the results of reacting the metal with excess GaAs in a closed, inert container. Second, the electrical properties of the stable phases have to be evaluated. Stable phases with high resistivities need not be examined further for use as metallizations. Third, for those stable phases with suitable electrical properties, the solubility and solidus data need to be measured to ascertain

the optimum as-deposited composition and the maximum allowable processing temperature. In addition to the thermodynamic and electrical data, kinetic and microstructural data also must be determined. The time-temperature combinations required to crystallize the as-deposited film, the crystallization path (i.e., the intermediate phases formed from the as-deposited film), and the resulting film morphology all must be established. Moreover, the diffusion of the metal into the substrate has to be quantified, as this diffusion will alter the electrical properties of the contact. Note also that the amount of metal diffusion will depend on which phase is used as the metal source.

The search for stable, low-resistivity GaAs metallizations need not be limited to  $M$ ,  $MGa_x$ , and  $MAs_y$  phases: other phases can also be considered. Indeed, based on their low resistivity and high thermal stability on silicon, metal silicides are already being considered.<sup>73-77</sup> It has been found that the silicide used on GaAs need not be the most silicon-rich silicide.<sup>75</sup> This result should not be considered surprising. While only the most silicon-rich silicide has a stable tie-line to silicon, several silicides can have stable tie-lines to GaAs. A partial thermodynamic analysis of the stability of silicides on GaAs has appeared recently.<sup>78</sup> However, a complete analysis requires determination of the stable tie-lines in the  $M$ -Si-Ga-As quaternary diagram. For example, using the Gibbs phase rule, it is straightforward to show that both  $WSi_2$  and  $W_5Si_3$  have stable tie-lines to GaAs in the  $W$ -Si-Ga-As diagram. Because tungsten and silicon also have stable tie-lines to GaAs, the relevant phase equilibria can be represented by a pseudoternary section of the isothermal quaternary diagram (See Fig.9.).

Finally, we note that the analysis outlined here can be applied to metallizations for any compound semiconductor. Our choice of a particular compound semiconductor, GaAs, was for illustrative purposes only.

## **V. CONCLUSIONS**

We have proposed a classification scheme for phase equilibria in M-Ga-As systems. Through judicious use of the phase rule, a small number of experiments can be used to determine to which type of diagram a particular metal belongs. Moreover, phases that are stable in contact with GaAs can be rapidly identified. This approach may enable a more systematic search for stable metallizations. Using previously published phase diagrams, available free energy data, and reported products of metal thin film reactions with GaAs substrates, we have assigned as many elements as possible to the seven generic types. Many M-Ga-As diagrams, however, remain unknown, and some of the present ones cannot be regarded as definitive. Further studies in this area will aid in the production of reproducible and reliable GaAs metallizations.

### **Acknowledgements**

Partial financial support from the NSF-MRL Program through the Center for Materials Research at Stanford University is gratefully acknowledged.

## References

1. N. Braslau, J. Vac. Sci. Technol. **19**, 803 (1981).
2. N. Braslau, Thin Solid Films **104**, 391 (1983).
3. A. Piotrowska, A. Guivarc'h, and G. Pelous, Solid-State Electron. **26**, 179 (1983).
4. A.K. Sinha and J.M. Poate, in *Thin Films — Interdiffusion and Reactions*, edited by J.M. Poate, K.N. Tu, and J.W. Mayer (Wiley-Interscience, New York, 1978), p. 407.
5. L.J. Brillson, Phys. Rev. Lett. **40**, 260 (1978).
6. L.J. Brillson, Thin Solid Films **89**, 461 (1982).
7. For an overview, see F.N. Rhines, *Phase Diagrams in Metallurgy*, McGraw-Hill, New York (1956).
8. M.B. Panish, J. Less-Common Metals **10**, 416 (1966).
9. M.B. Panish, J. Phys. Chem. Solids **27**, 291 (1966).
10. M.B. Panish, J. Electrochem. Soc. **113**, 861 (1966).
11. M.B. Panish, J. Electrochem. Soc. **113**, 1226 (1966).
12. M.B. Panish, J. Electrochem. Soc. **114**, 91 (1967).
13. M.B. Panish, J. Electrochem. Soc. **114**, 516 (1967).
14. M.B. Panish, J. Phys. Chem. Solids **30**, 129 (1969).
15. M.B. Panish, J. Electrochem. Soc. **117**, 1202 (1970).
16. M.B. Panish and M. Ilegems, Prog. in Solid State Chem. **7**, 39 (1972).
17. M.D. Deal, Ph.D. Thesis, Stanford University (1983).
18. M.D. Deal and D.A. Stevenson, J. Electrochem. Soc. **131**, 2343 (1984).
19. C.D. Thurmond, G.P. Schwartz, G.W. Kammlott, and B. Schwartz, J. Electrochem. Soc. **127**, 1366 (1980).
20. R.S. Williams, J.R. Lince, T.C. Tsai, and J.H. Pugh, Mat. Res. Soc. Symp. Proc., 1986 (in press).
21. C.T. Tsai and R.S. Williams, J. Mater. Res. **1**, 352 (1986).
22. R. Beyers, J. Appl. Phys. **56**, 147 (1984).

23. T. Sebestyen, H.L. Hartnagel, and L.H. Herron, *IEEE Trans. Electron Devices* ED-22, 1073 (1975).
24. T. Sebestyen, I. Mojzes, and D. Szigethy, *Electronics Lett.* 16, 504 (1980).
25. I. Mojzes, T. Sebestyen, P.B. Barna, G. Gergely, and D. Szigethy, *Thin Solid Films* 61, 27 (1979).
26. S. Guha, B.M. Arora, and V.P. Salvi, *Solid-State Electron.* 20, 431 (1977).
27. N. Braslau, J.B. Gunn, and J.L. Staples, *Solid-State Electron.* 10, 381 (1967).
28. E. Kinsbron, P.K. Gallagher, and A.T. English, *Solid-State Electron.* 22, 517 (1979).
29. I. Mojzes, T. Sebestyen, and D. Szigethy, *Solid-State Electron.* 25, 449 (1982).
30. C.T. Lee, *Appl. Phys. Lett.* 46, 554 (1985).
31. A.A. Lakhani, L.C. Oliver, E.F. Dvorsky, and E.U. Hempfling, *IEEE Electron Device Lett.* EDL-6, 586 (1985).
32. S.J. Pearton, K.D. Cummings, and G.P. Vella-Coleiro, *J. Electrochem. Soc.* 132, 2743 (1985).
33. M. Kuzuhara, T. Nozaki, and H. Kohzu, *J. Appl. Phys.* 58, 1204 (1985).
34. N.A. Godshall, I.D. Raistrick, and R.A. Huggins, *J. Electrochem. Soc.* 131, 543 (1984).
35. R. Beyers, R. Sinclair, and M.E. Thomas, *J. Vac. Sci. Technol. B* 2, 781 (1984).
36. R. Beyers, *Mat. Res. Soc. Symp. Proc.* 47, 143 (1985).
37. C.J. Cooke and W. Hume-Rothery, *J. Less-Common Metals* 10, 42 (1966).
38. J. Gyulai, J.W. Mayer, V. Rodriguez, A.Y.C. Yu, and H.J. Gopen, *J. Appl. Phys.* 42, 3578 (1971).
39. K. Kumar, *Jap. J. Appl. Phys.* 18, 713 (1979).
40. W.G. Petro, I.A. Babalola, T. Kendelewicz, I. Lindau, and W.E. Spicer, *J. Vac. Sci. Technol. A* 1, 1181 (1983).
41. R.P. Elliott, *Constitution of Binary Alloys, First Supplement* (McGraw-Hill, New York, 1965), p. 2.
42. J.B. Taylor, L.D. Calvert, and M.R. Hunt, *Can. J. Chem.* 43, 3045 (1965).
43. J.J. Murray, P.L. Mart, and J.B. Taylor, *J. Less-Common Metals* 64, 45 (1979).

44. S.K. Cheung, K.-M. Yu, T. Sands, N.W. Cheung, J.M. Jaklevic, and E.E. Haller, *Mat. Res. Soc. Symp. Proc., Compound Semiconductor Materials, Spring Meeting, 1986* (in press).
45. K.L. Kavanagh, J.W. Mayer, C.W. Magee, J. Sheets, J. Tong, P.D. Kirchner, J.M. Woodall, and I. Haller, *J. Electrochem. Soc.* **133**, 1176 (1986).
46. A. Lahav and M. Eizenberg, *Appl. Phys. Lett.* **46**, 430 (1985).
47. J.R. Waldrop, S.P. Kowalczyk, and R.W. Grant, *J. Vac. Sci. Technol.* **21**, 607 (1982).
48. J.R. Waldrop, *Appl. Phys. Lett.* **46**, 864 (1985).
49. V. Kumar, *J. Phys. Chem. Solids* **36**, 535 (1975).
50. S.P. Murarka, *Solid-State Electron.* **17**, 869 (1974).
51. A.K. Sinha, *Appl. Phys. Lett.* **26**, 171 (1975).
52. C. Fontaine, T. Okumura, and K.N. Tu, *J. Appl. Phys.* **54**, 1404 (1983).
53. M. El-Boragy and K. Schubert, *Z. Metallkde.* **72**, 279 (1981).
54. P. Oelhafen, J.L. Freeouf, T.S. Kuan, T.N. Jackson, and P.E. Batson, *J. Vac. Sci. Technol. B* **1**, 588 (1983).
55. T.S. Kuan, J.L. Freeouf, P.E. Batson, and E.L. Wilkie, *J. Appl. Phys.* **58**, 1519 (1985).
56. T. Sands, V.G. Keramidas, R. Gronsky, and J. Washburn, *Materials Lett.* **3**, 409 (1985).
57. T. Sands, V.G. Keramidas, A.J. Yu, K.-M. Yu, R. Gronsky, and J. Washburn, *J. Mater. Res.*, 1986 (in press).
58. K.-M. Yu, J.M. Jaklevic, and E.E. Haller, *Mat. Res. Soc. Symp. Proc., Materials Characterization, Spring Meeting, 1986* (in press).
59. M. El-Boragy and K. Schubert, *Z. Metallkde.* **61**, 579 (1970).
60. M. Ogawa, *Thin Solid Films* **70**, 181 (1980).
61. T. Sands, V.G. Keramidas, J. Washburn, and R. Gronsky, *Appl. Phys. Lett.* **48**, 402 (1986).
62. A.J. Yu, G.J. Galvin, C.J. Palmstrom, and J.W. Mayer, *Appl. Phys. Lett.* **47**, 934 (1985).
63. A.A. Lakhani, *J. Appl. Phys.* **56**, 1888 (1984).
64. D.C. Marvin, N.A. Ives, and M.S. Leung, *J. Appl. Phys.* **58**, 2659 (1985).

65. R.Z. Bachrach, J. Vac. Sci. Technol. **15**, 1340 (1978).
66. L.J. Brillson, R.Z. Bachrach, R.S. Bauer, and J. McMnamin, Phys. Rev.Lett. **42**, 397 (1979).
67. P. Skeath, I. Lindau, P. Pianetta, P.W. Chye, C.Y. Su, and W.E. Spicer, J. Elect. Spectr. Relat. Phenom. **17**, 259 (1979).
68. A. Khan, L.J. Brillson, A.D. Katnani, and G. Margaritondo, Solid State Comm. **38**, 1269 (1981).
69. N.M. Johnson, T.J. Magee, and J. Peng, J. Vac. Sci. Technol. **13**, 838 (1976).
70. A. Christou and H.M. Day, J. Appl. Phys. **47**, 4217 (1976).
71. A. Christou, J.E. Davey, H.M. Day, and A.C. Macpherson, J. Appl. Phys. **50**, 1139 (1979).
72. A.K. Srivastava and B.M. Arora, Solid-State Electron. **24**, 1049 (1981).
73. N. Yokoyama, T. Ohnishi, K. Odani, H. Onodera, and M. Abe, IEEE Trans. Electron Devices **ED-29**, 1541 (1982).
74. W.F. Tseng, B. Zhang, D. Scott, S.S. Lau, A. Christou, and B.R. Wilkins, IEEE Electron Device Lett. **EDL-4**, 207 (1983).
75. T. Ohnishi, N. Yokoyama, H. Onodera, S. Suzuki, and A. Shibatomi, Appl. Phys. Lett. **43**, 600 (1983).
76. J.K. Truman and P.H. Holloway, J. Vac. Sci. Technol. A **3**, 992 (1985).
77. S.S. Gill, G.J. Pryce, and J. Woodward, Physica **129B**, 430 (1985).
78. S.S. Lau, W.X. Chen, E.D. Marshall, and C.S. Pai, Appl. Phys. Lett. **47**, 1298 (1985).

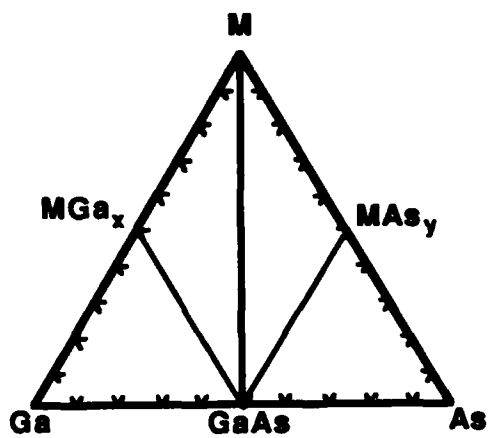


### Figure Captions

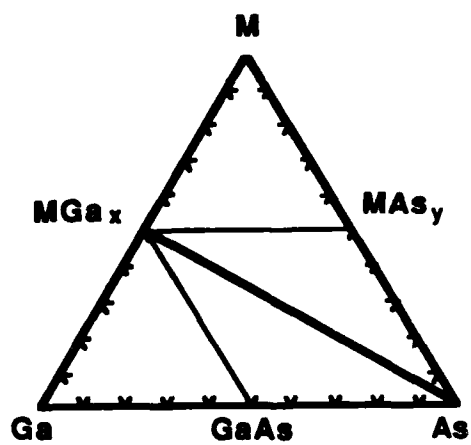
1. The seven basic types of M-Ga-As phase diagrams. Key tie-lines in the diagrams are emboldened. In (f) and (g), the one-phase and two-phase regions have been expanded for clarity.
2. Interpretation of the M-excess GaAs reaction when more than one  $\text{MGa}_x$  and/or  $\text{MAs}_y$  compound exists. "X" marks the three-phase region the system will be in when equilibrium is reached. "⊗" denotes the phases that will be stable with respect to new compound formation when in contact with GaAs.
3. Interpretation of the Type I M-GaAs diffusion couple when the metal has a large gallium solubility, but little arsenic solubility. The arsenic-rich phase (elemental arsenic in this example) adjacent to the metal-containing phase (elemental metal in this example) forms, and the system composition lies in the M(Ga)-As-GaAs three-phase region at equilibrium.
4. Pseudoisothermal sections of elements with Type I diagrams: (a) gold, (b) silver, (c) tungsten, (d) silicon, and (e) germanium.
5. A schematic of the Ga-As-O diagram of Thurmond *et al.*<sup>19</sup>

6. Pseudoisothermal sections of metals with Type IV diagrams: (a) copper, (b) chromium, and (c) platinum. In the copper diagram, Panish's work<sup>13</sup> indicates that the  $\text{Cu}_3\text{As}$ - $\text{Cu}_9\text{Ga}_4$  tie-line exists at  $\sim 600^\circ\text{C}$ , but the  $\text{Cu}_8\text{As}$ - $\text{GaAs}$  tie-line may exist at lower temperatures ( $\sim 400^\circ\text{C}$ ). To account for this possibility, both of these tie-lines are drawn with dashes.
7. A schematic of the Pd-Ga-As diagram of El-Boragy and Schubert.<sup>53</sup>  $T = 600^\circ\text{C}$ .
8. Pseudoisothermal sections for (a) nickel and (b) cobalt. The diagrams for these metals are drawn with dashed tie-lines to the ternary phase because of the present uncertainty about the stability of the ternary phase.
9. (a) Quaternary and (b) pseudoternary representations of silicide equilibria with GaAs in the W-Si-Ga-As system.

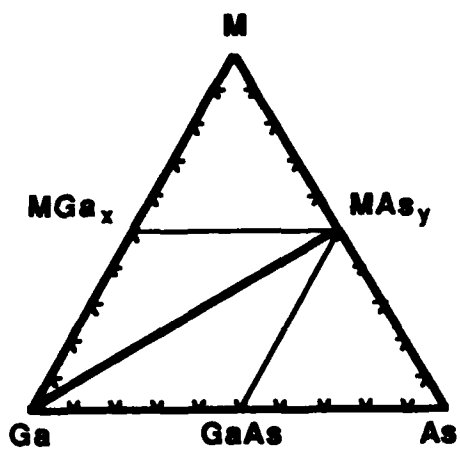
(a)



(b)



(c)



(d)

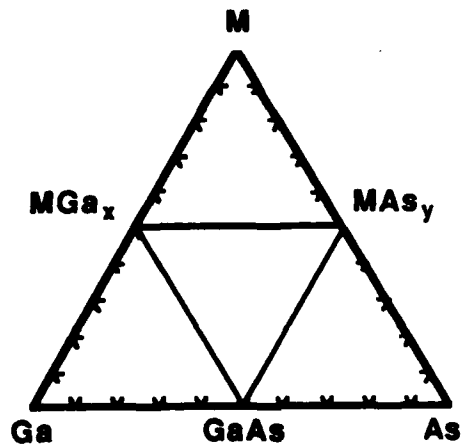
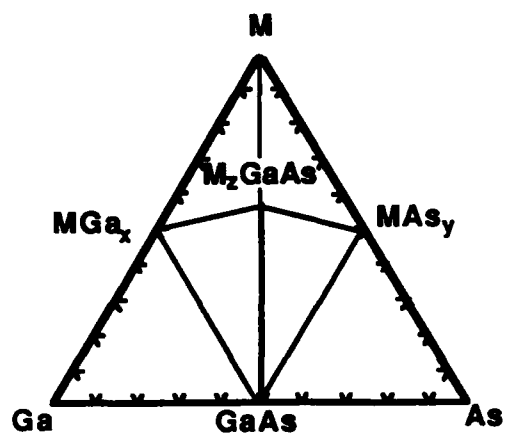
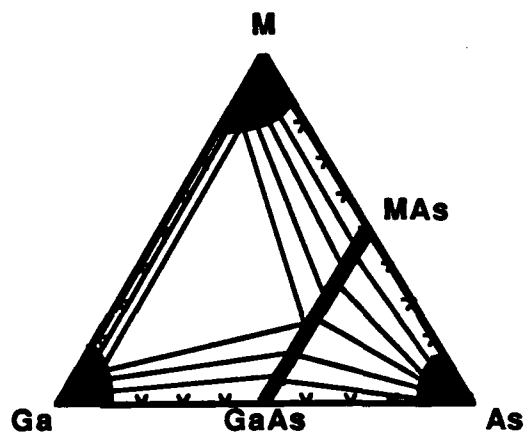


Fig. 1

(e)



(f)



(g)

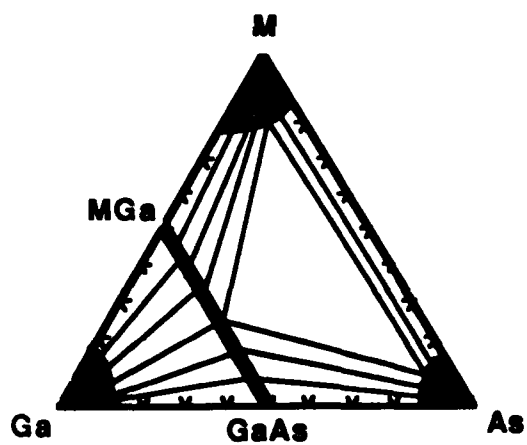


Fig. 1

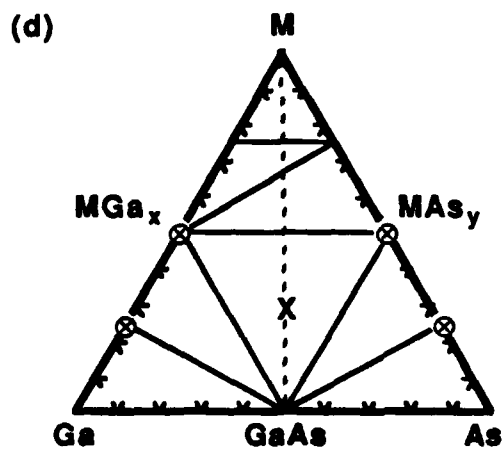
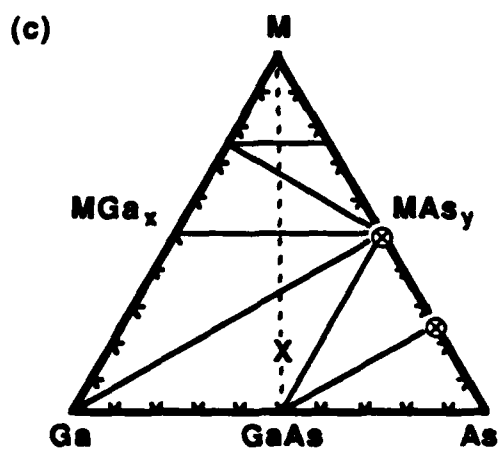
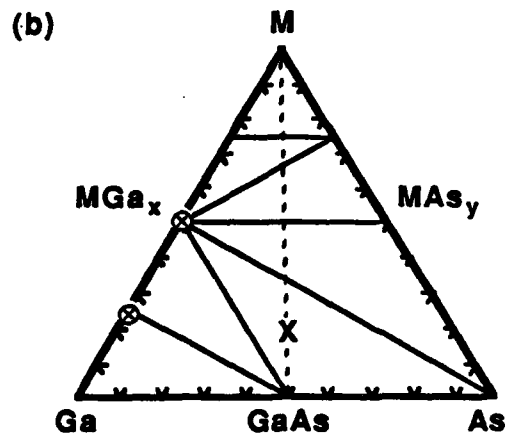
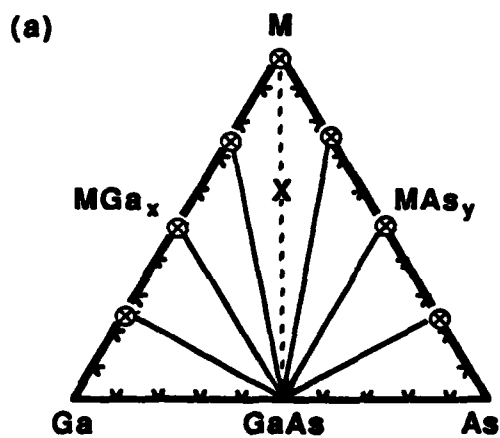


Fig. 2

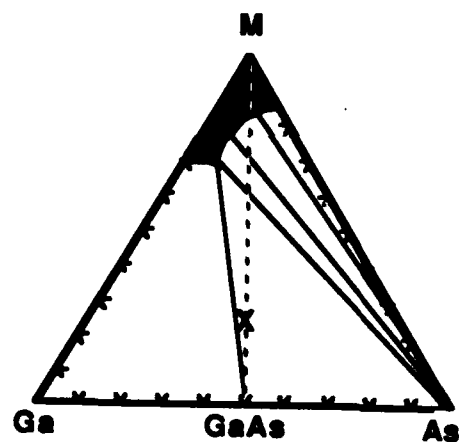
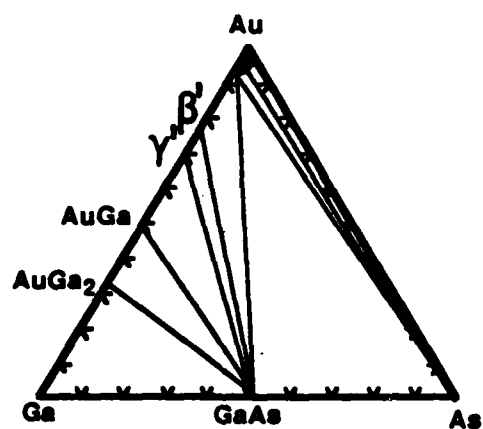
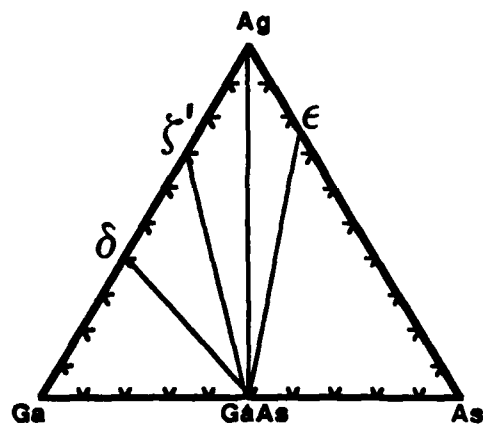


Fig. 3 11

(a)



(b)



(c)

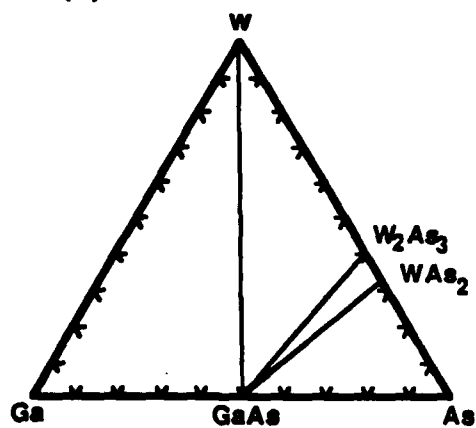
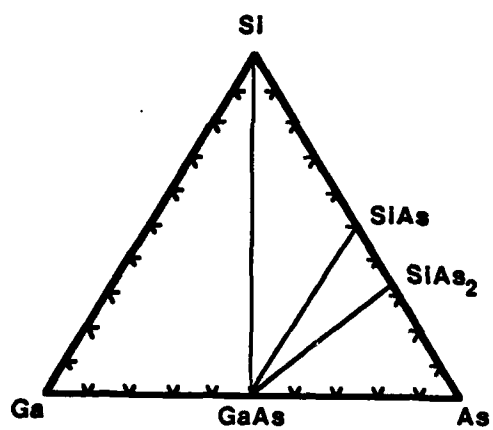


Fig. 4

(d)



(e)

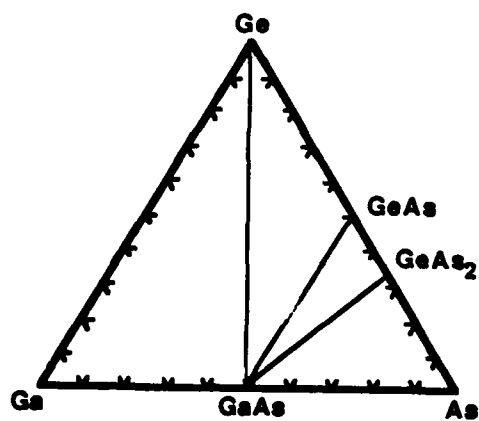


Fig. 4



Type II

Ga-As-O

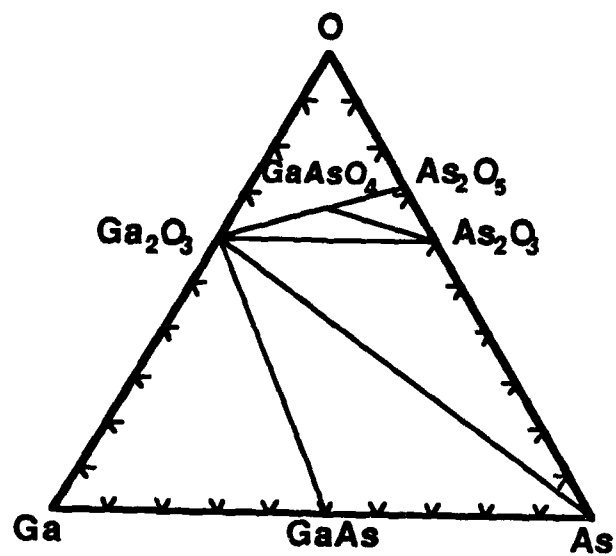
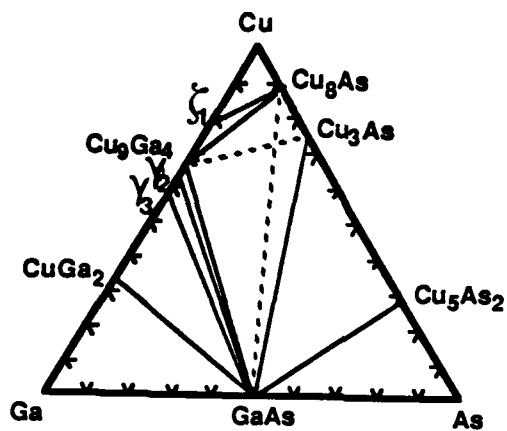
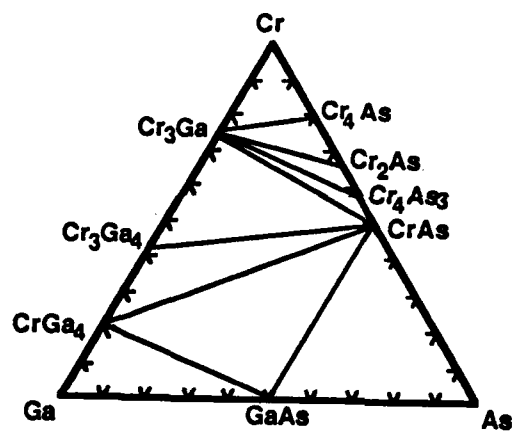


Fig. 5

(a)



(b)



(c)

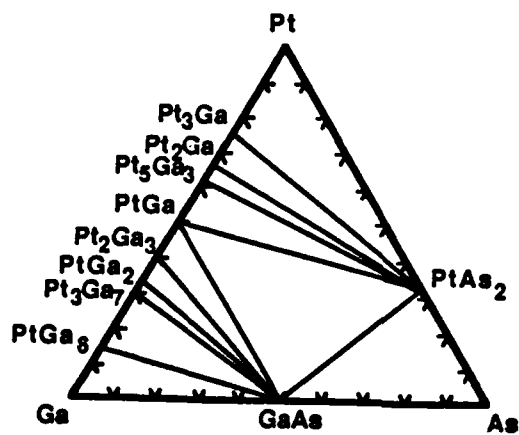


Fig. 6

Pd-Ga-As

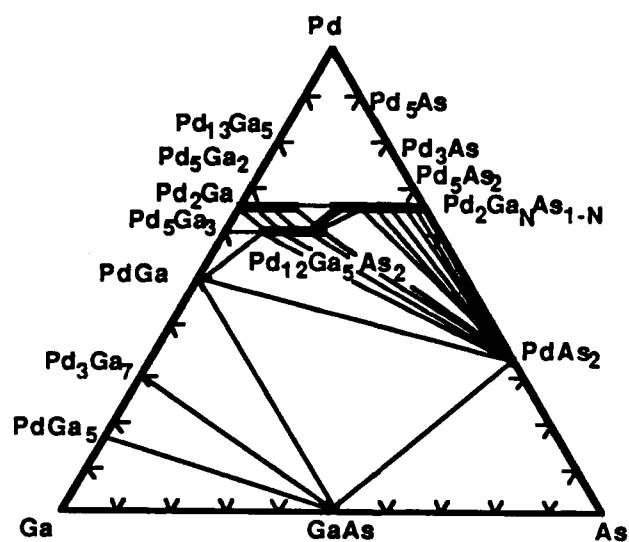
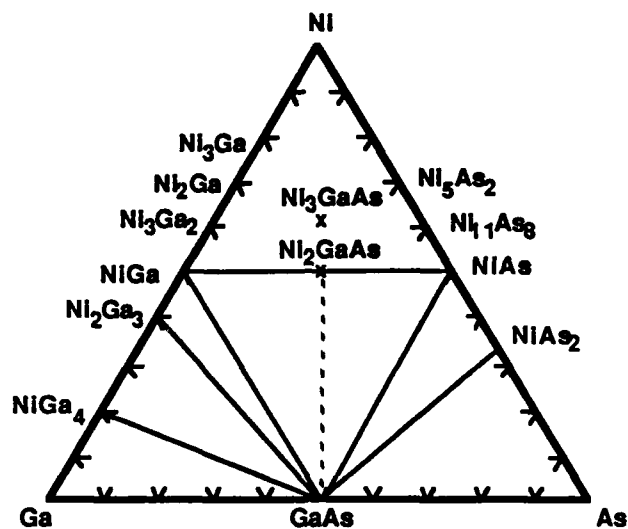


Fig. 7 . 68

# Ni-Ga-As



# Co-Ga-As

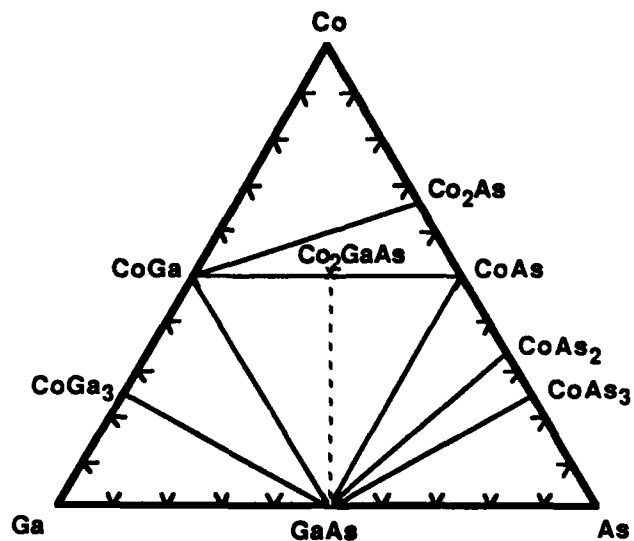
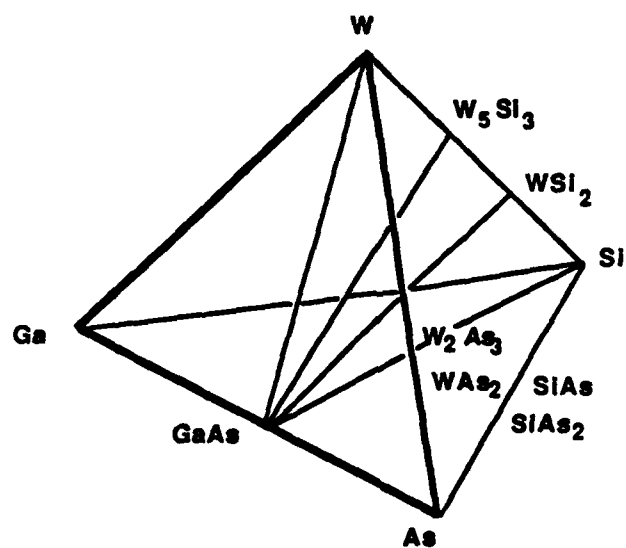


Fig. 8

W-Si-Ga-As



W-Si-GaAs

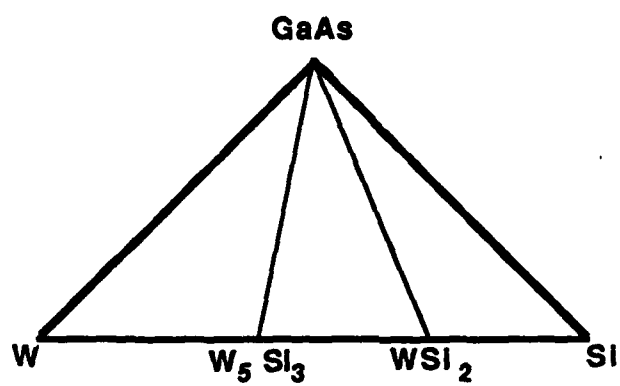


Fig. 9 70

**slide #1**

**Phase Equilibria in Metal-Gallium-Arsenic Systems:  
Thermodynamic Considerations for Metallization Materials**

**KI Bum Kim, Robert Beyers\* and Robert Sinclair  
Department of Materials Science and Engineering  
Stanford University, Stanford**

**\*present address: IBM Almaden Research Center**



**slide #2**

**Outline**

**Thermodynamics**

**Simplest Cases - Idealized systems**

**Complicating Factors - real systems**

**Applications**

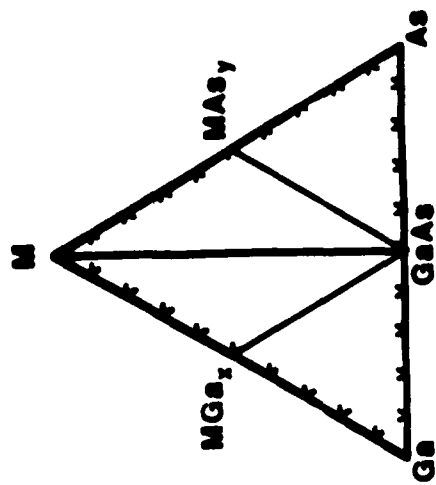
**Conclusions**



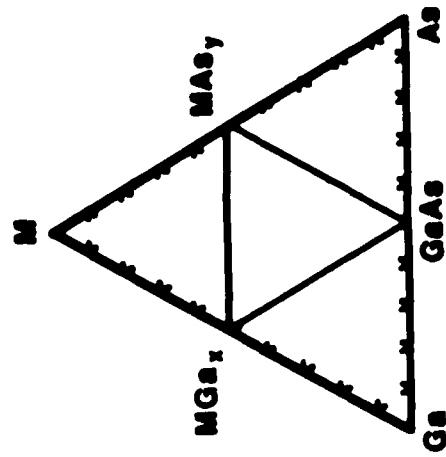
**slide #3**

## **Simplest Cases**

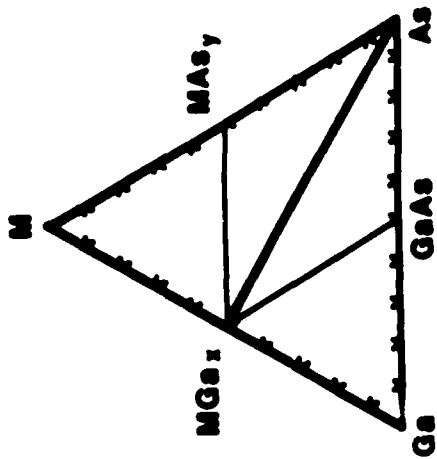
Type I: GaAs dominant



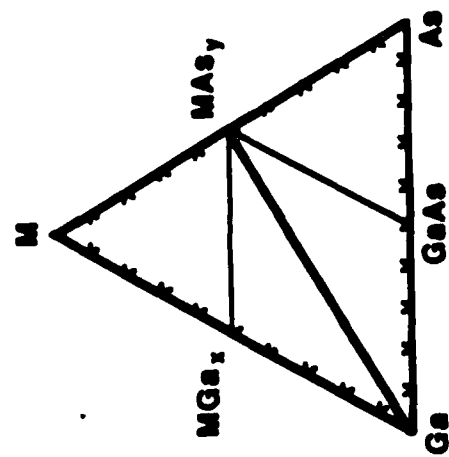
Type IV: no phase dominant



Type II: MGax dominant



Type III: MASy dominant

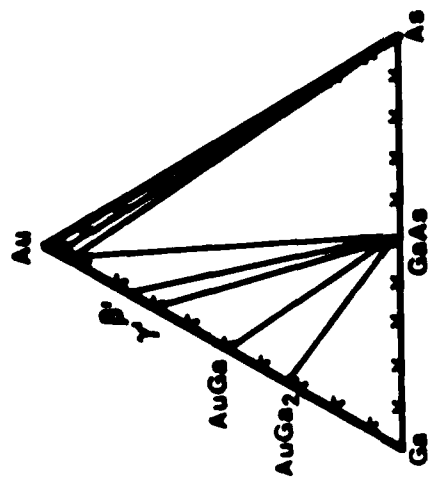


**slide #4**

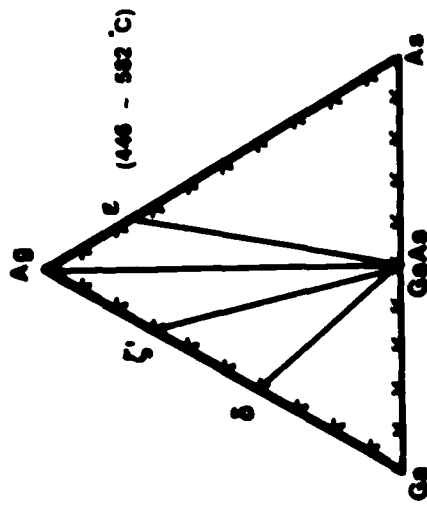
## **Complicating Factors**

**Type I**

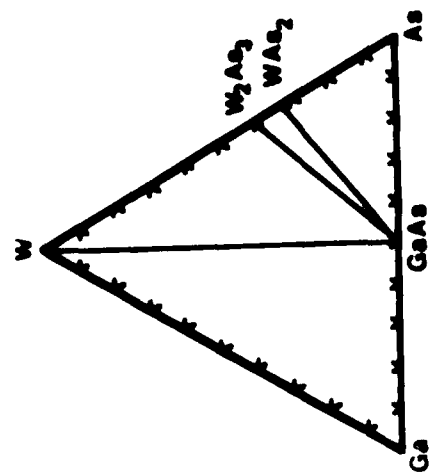
**Au-Ga-As**



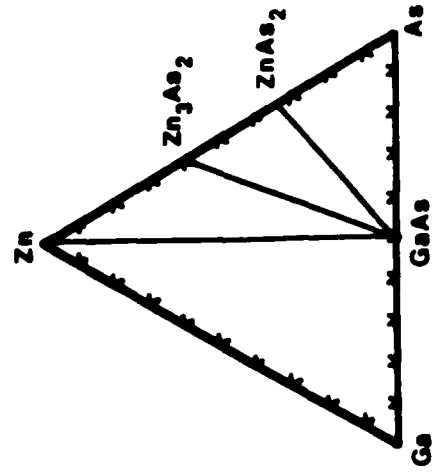
**Ag-Ga-As**



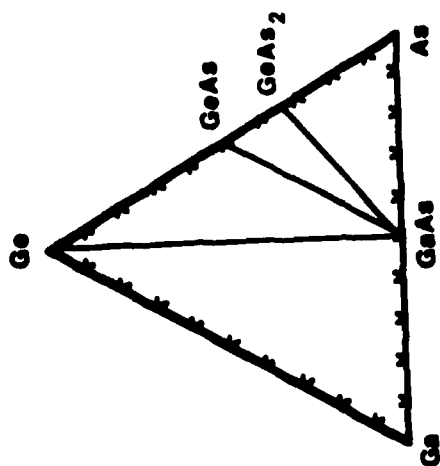
**W-Ga-As**



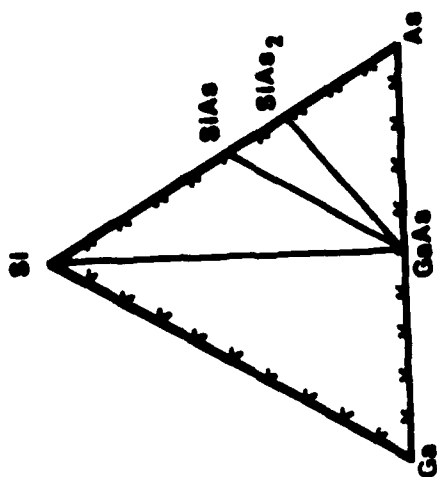
**Zn-Ga-As**



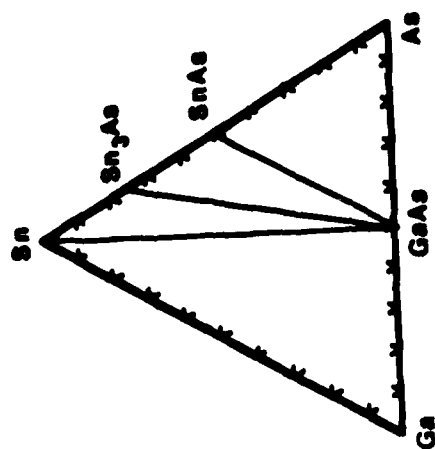
Ge-Ga-As



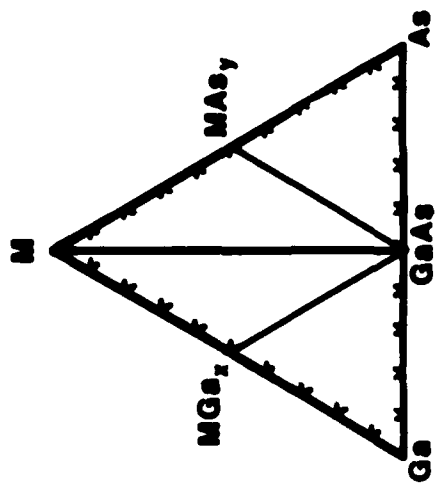
Si-Ga-As



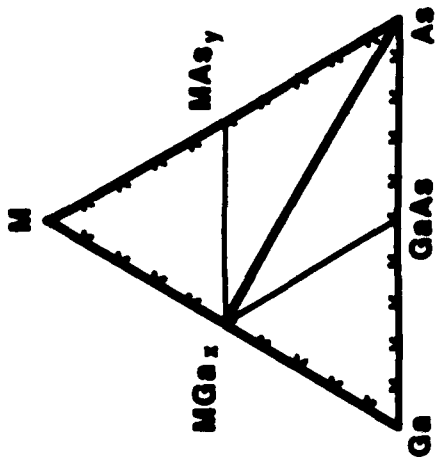
Sn-Ga-As



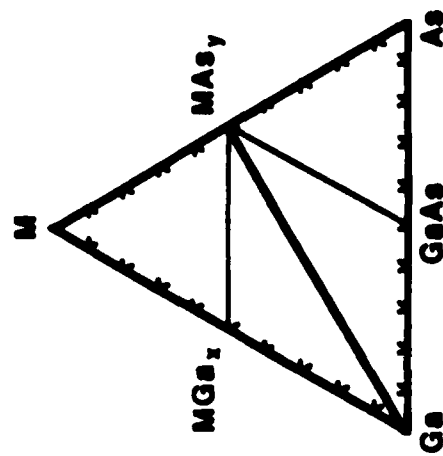
Type I: GaAs dominant



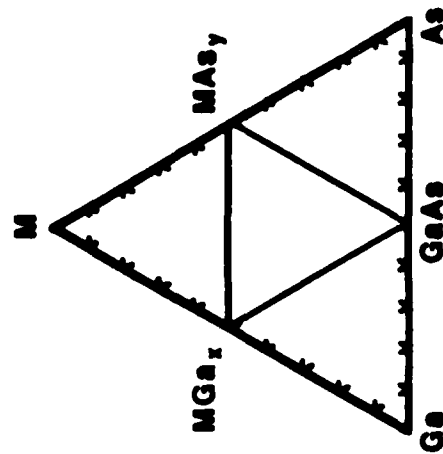
Type II: MGa\_z dominant



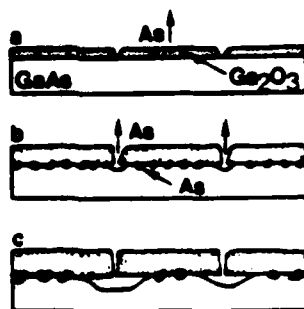
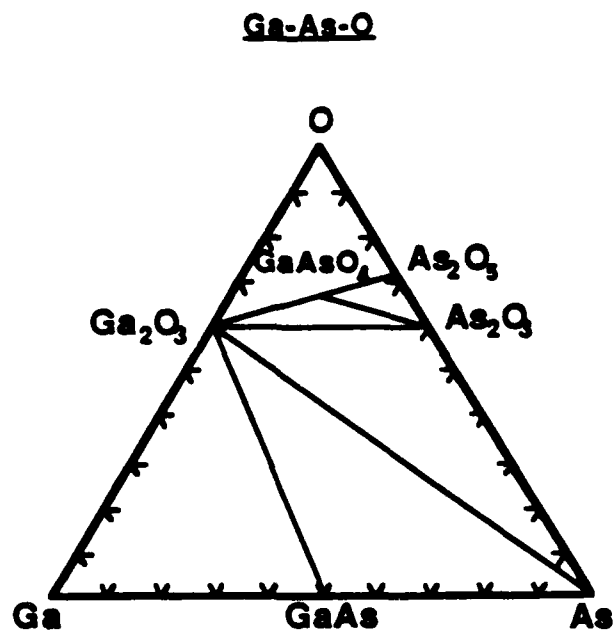
Type III: MAS\_y dominant



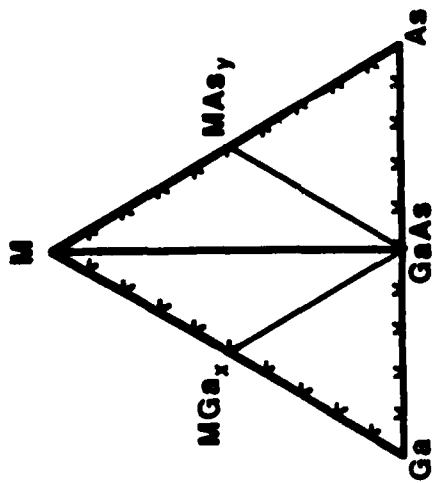
Type IV: no phase dominant



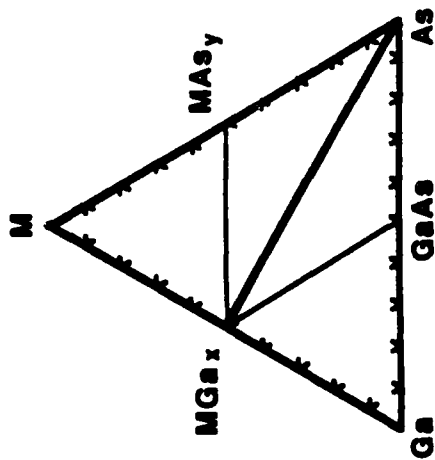
Type II



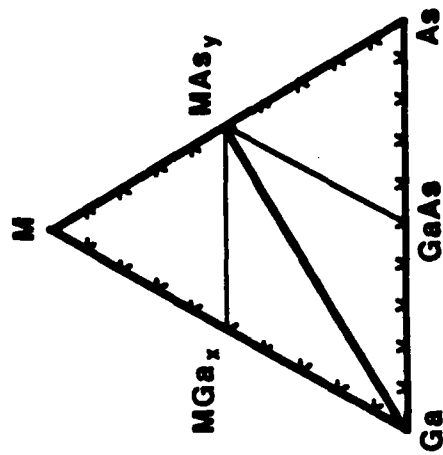
Type I: GaAs dominant



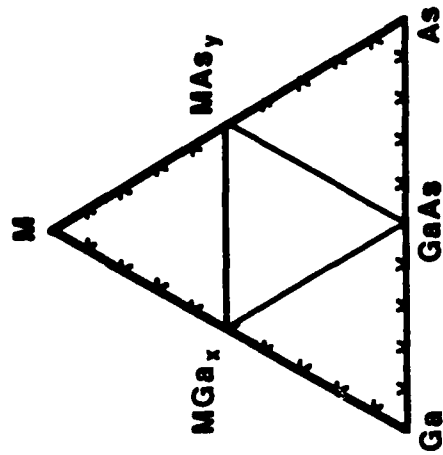
Type II:  $MGa_x$  dominant



Type III:  $MAs_y$  dominant



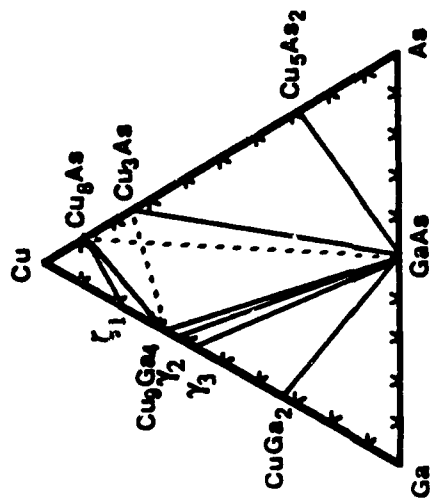
Type IV: no phase dominant



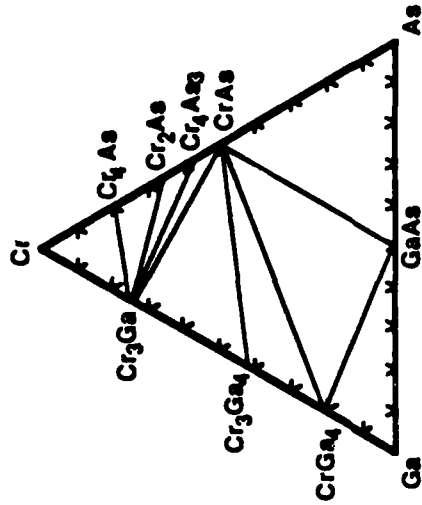


Type IV:

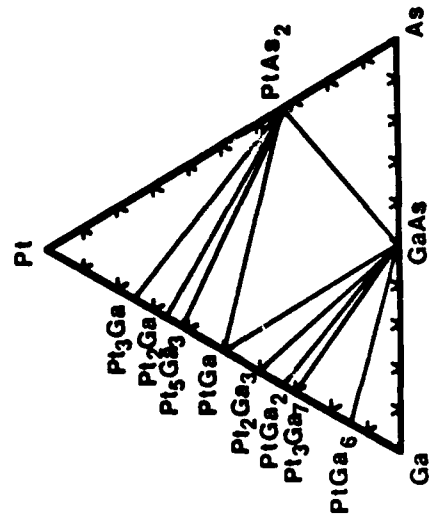
Cu-Ga-As

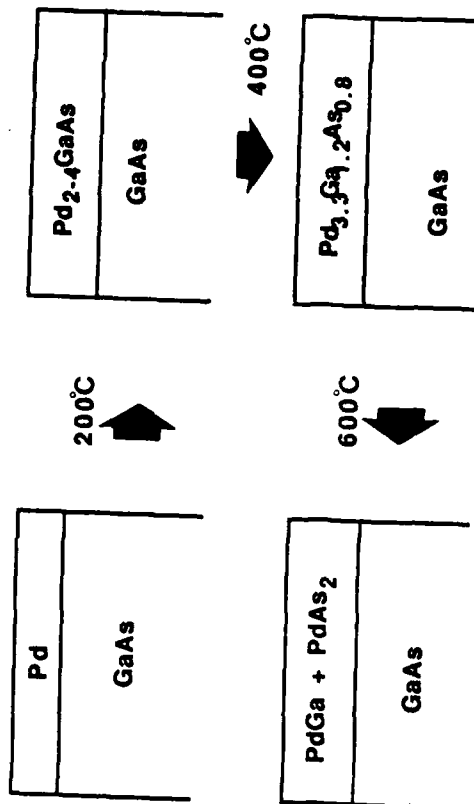


Cr-Ga-As

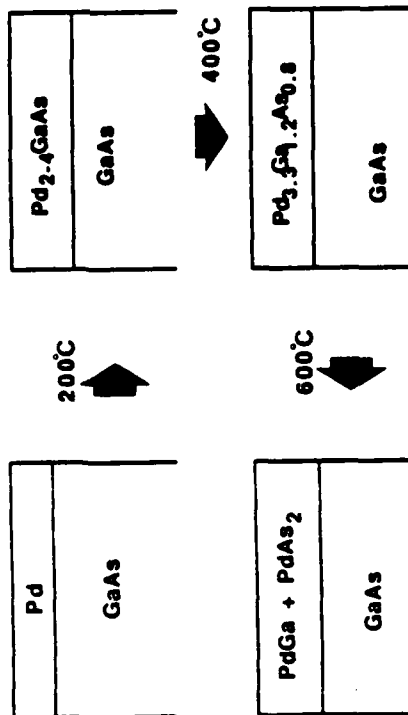
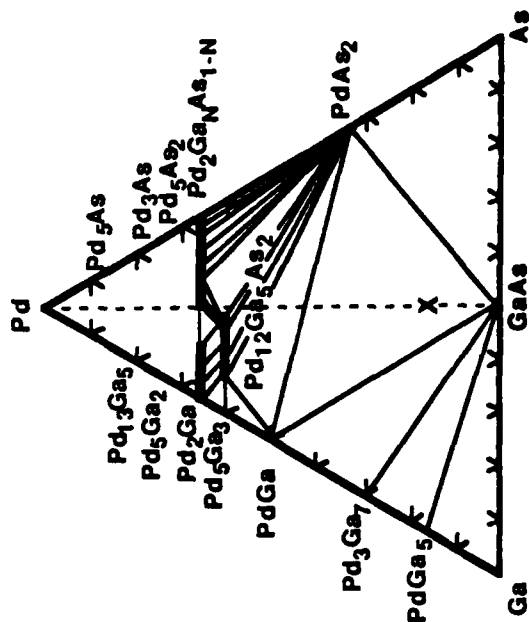


Pt-Ga-As

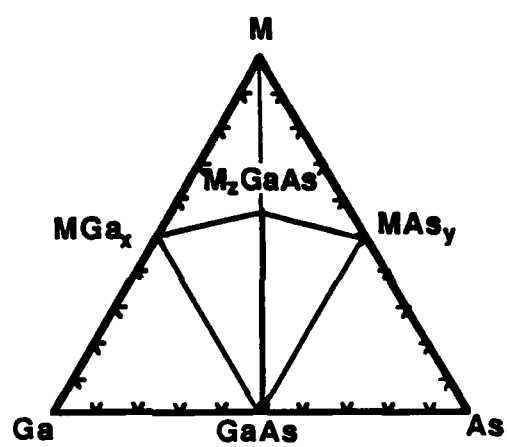




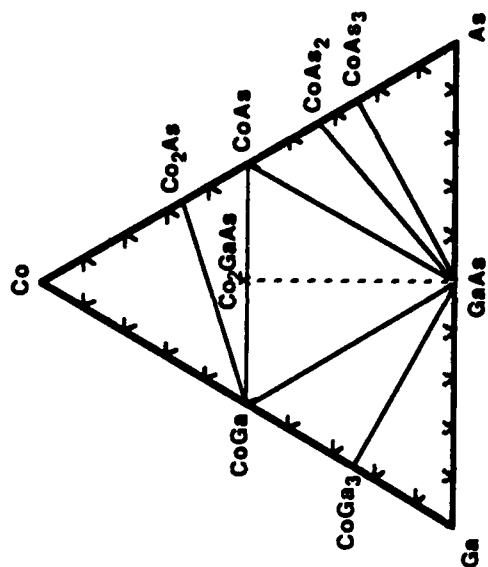
# Pd-Ga-As



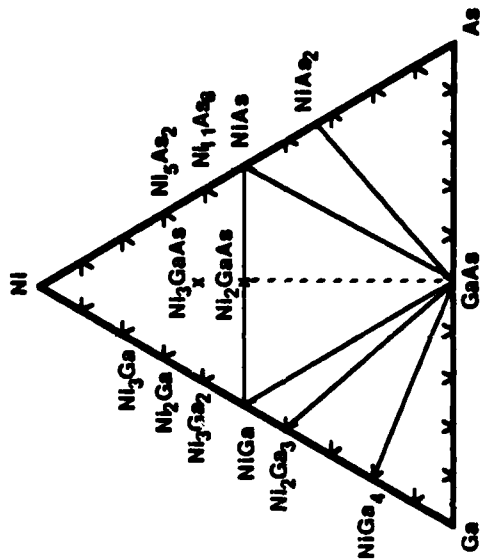
Type V: Ternary phase

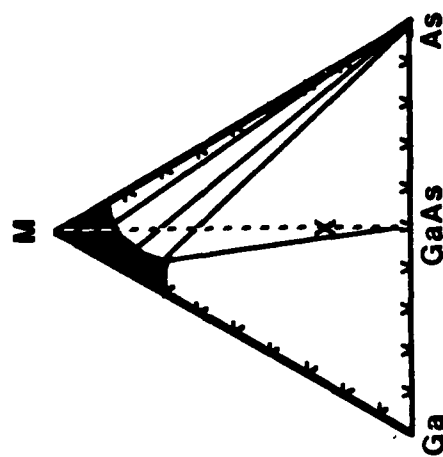
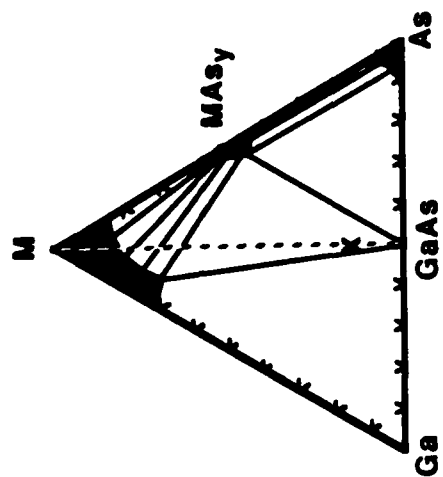


**Co-Ga-As**

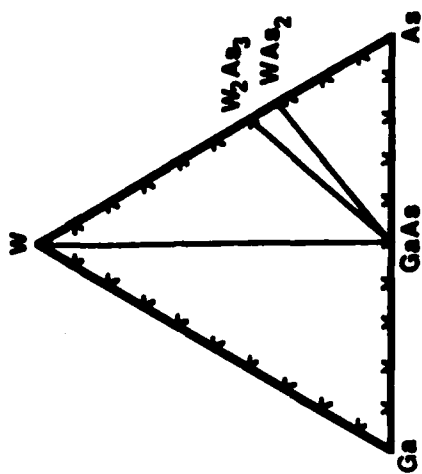


**Ni-Ga-As**

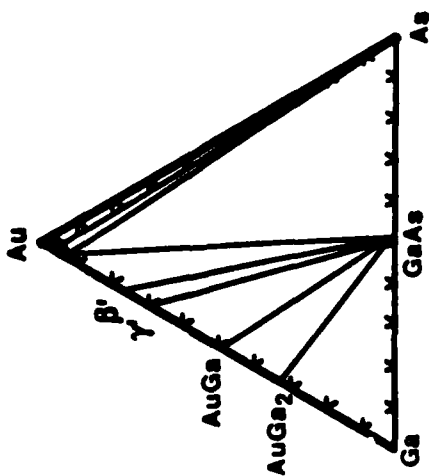




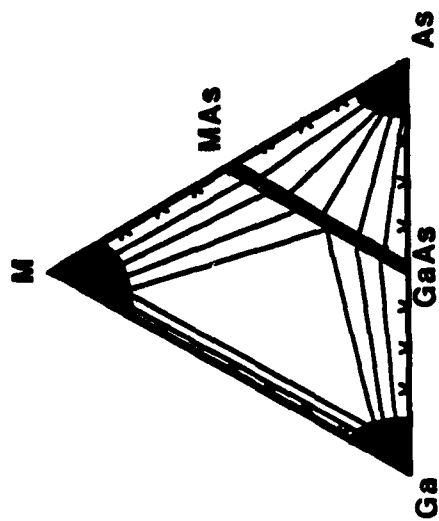
W-Ga-As



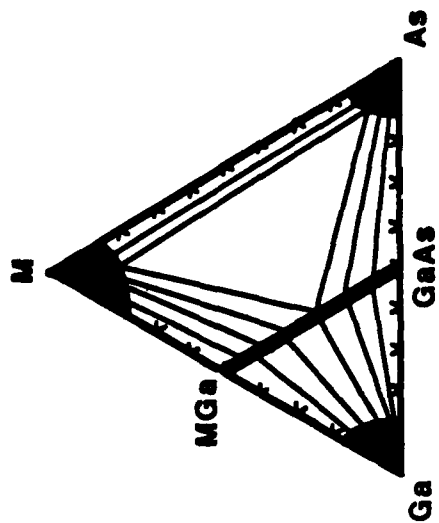
Au-Ga-As



Type VI: Solid Solubility



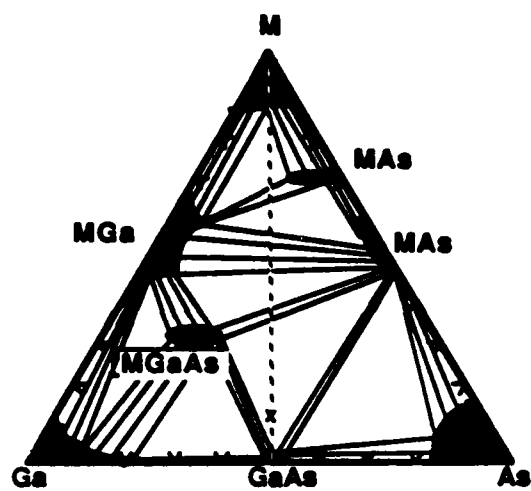
Type VII: Solid Solubility



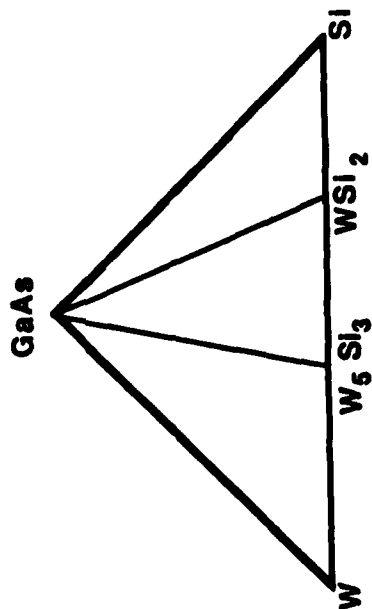


**slide #5**

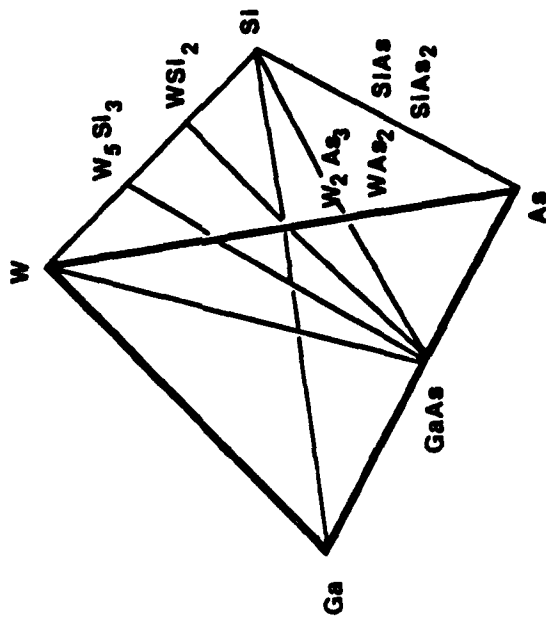
## **Applications**



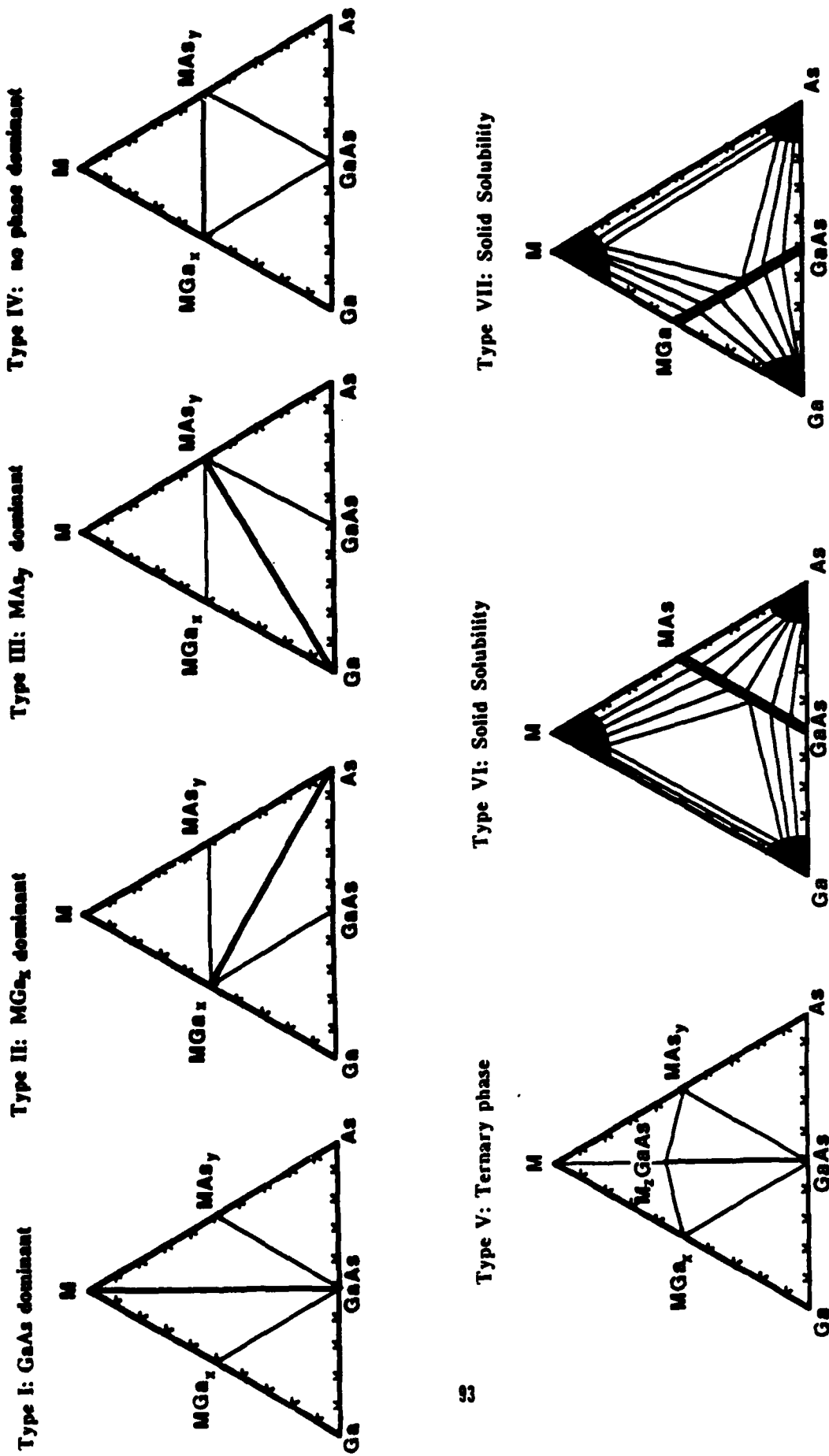
W-Si-GaAs



W-Si-Ga-As



## Conclusions



## **CHEMISTRY OF Ti:GaAs INTERFACES**

**M. KNIFFIN, C. R. HELMS**

**K. B. KIM, R. L. SINCLAIR**

### **BACKGROUND - Ti:Si SYSTEM**

### **GaAs SURFACE PREPARATION EFFECTS**

### **EFFECT OF ANNEALING ON CHEMISTRY/ BARRIER HEIGHT**

### **MODEL FOR KINETICS OF Ti:GaAs REACTIONS**

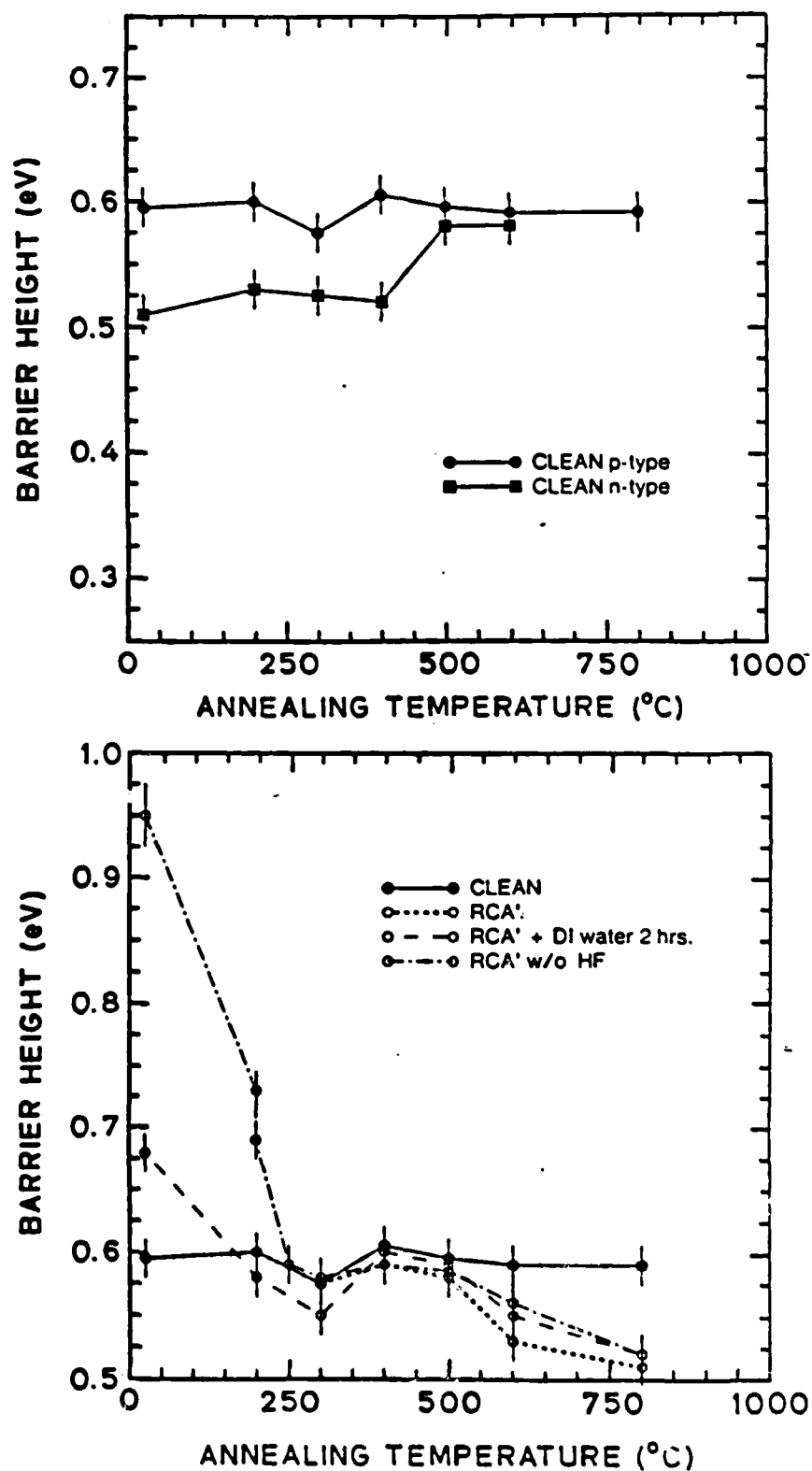


Figure 5.10: Barrier height as a function of annealing temperature for a variety of chemical procedures on *p*-Si. Procedures: Clean, RCA', RCA' + 2 hours in DI water, RCA' w/o HF. The RCA' w/o HF sample was reannealed for 10 min at 200°C.

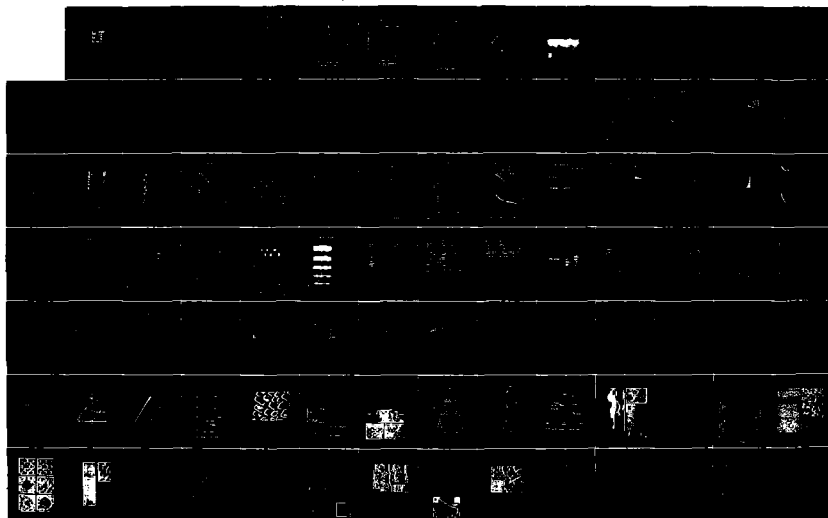
AD-A183 158

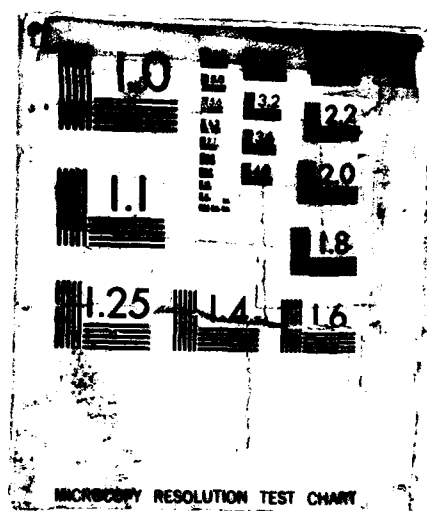
A WORKSHOP ON 3-5 SEMICONDUCTOR: METAL INTERFACIAL  
CHEMISTRY AND ITS LIFE (U) STANFORD UNIV CA  
W E SPICER ET AL. 85 NOV 86 N00014-87-G-0038

2/7

UNCLASSIFIED

F/G 20/12 NL







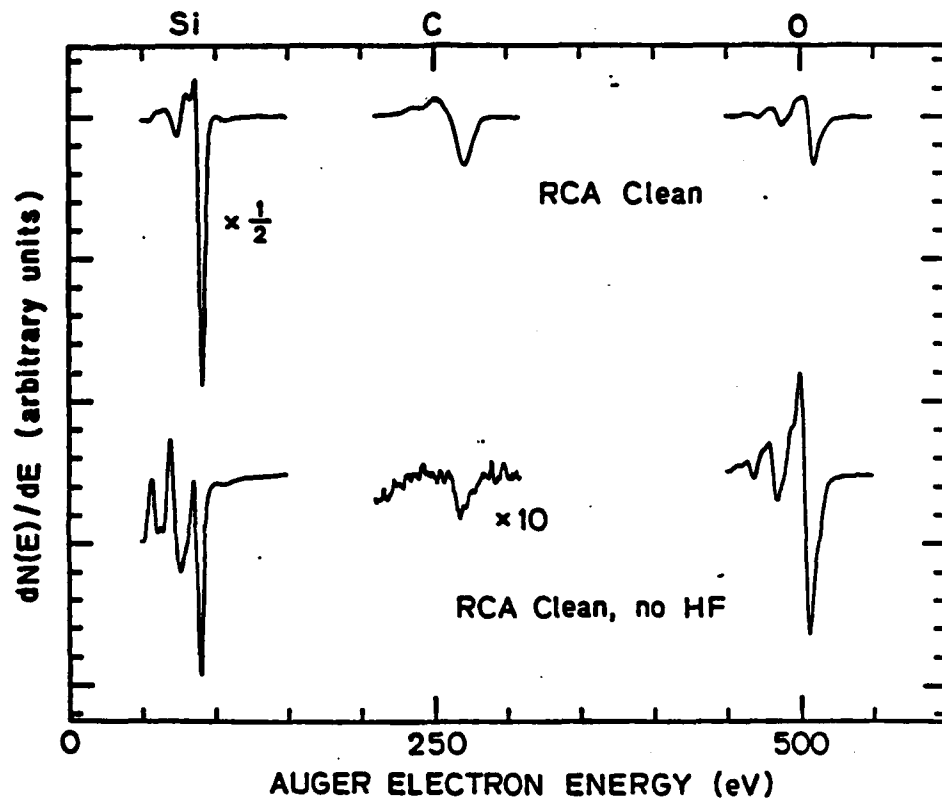


Figure 3.1: AES spectra of two chemical cleaning procedures: RCA' and RCA' w/o HF.

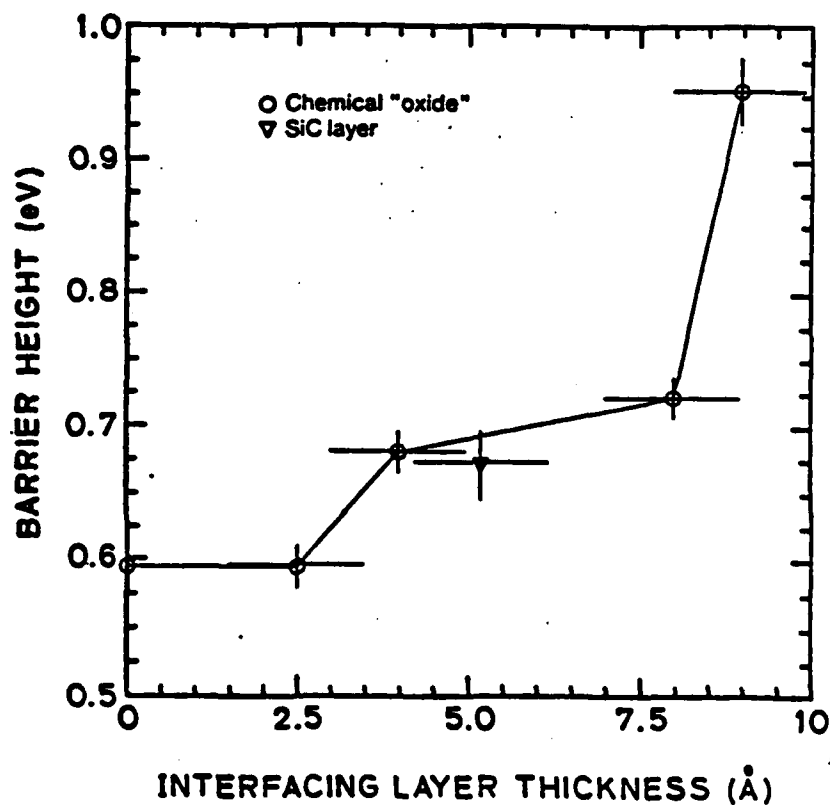


Figure 5.9: Schottky barrier height as a function of interfacial layer thickness for p-Si. Preparations used in order of increasing thickness: sputter/annealed, RCA', RCA' + 2 hours DI water, RCA' w/o HF\*, RCA' w/o HF. Also shown is one point for the SiC layer.

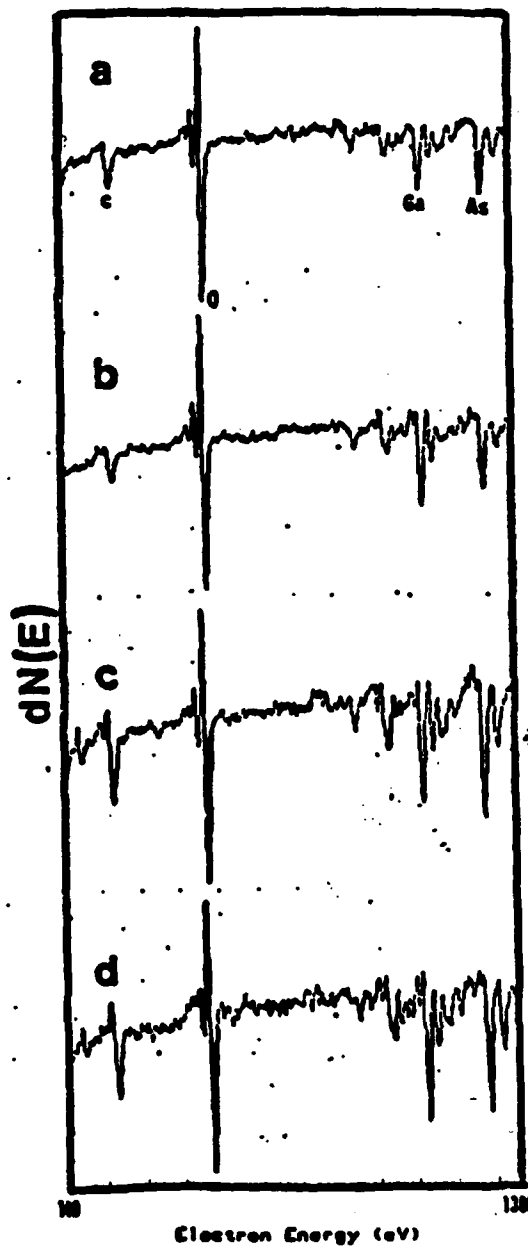
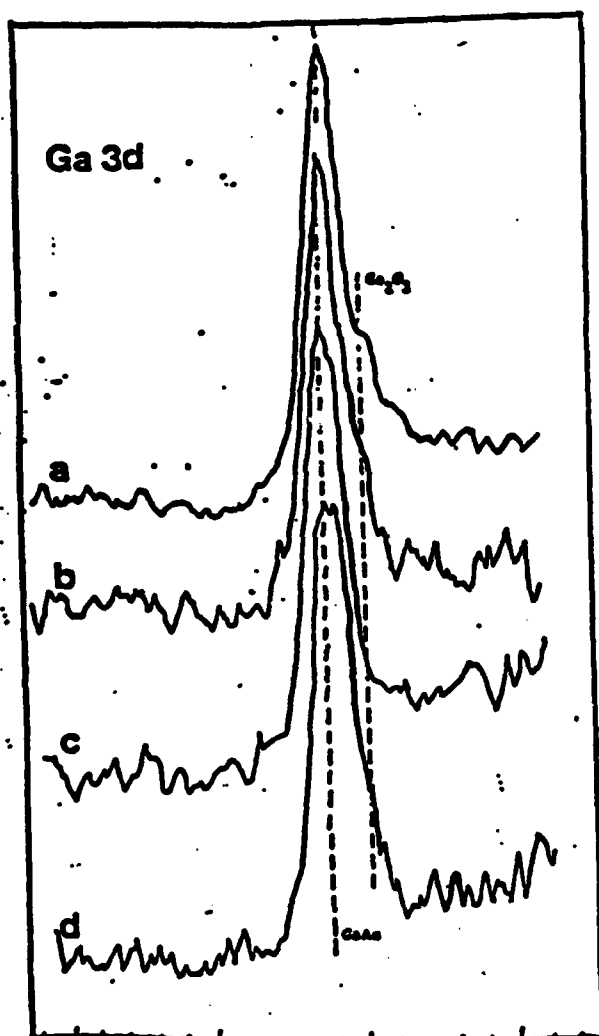


FIGURE 1.1: AES SPECTRA OF GAAS SURFACE FOR FOUR CLEANING PROCEDURES:

- (A)  $\text{H}_2\text{SO}_4:\text{H}_2\text{O}_2:\text{H}_2\text{O}(5:1:1)$
- (B)  $\text{NH}_4\text{OH}:\text{H}_2\text{O}_2:\text{H}_2\text{O}(1:1:10)$
- (c)  $\text{HCl}:\text{H}_2\text{O}(1:1)$
- (c)  $\text{NH}_4\text{OH}:\text{H}_2\text{O}(1:10)$



B.E. [eV]

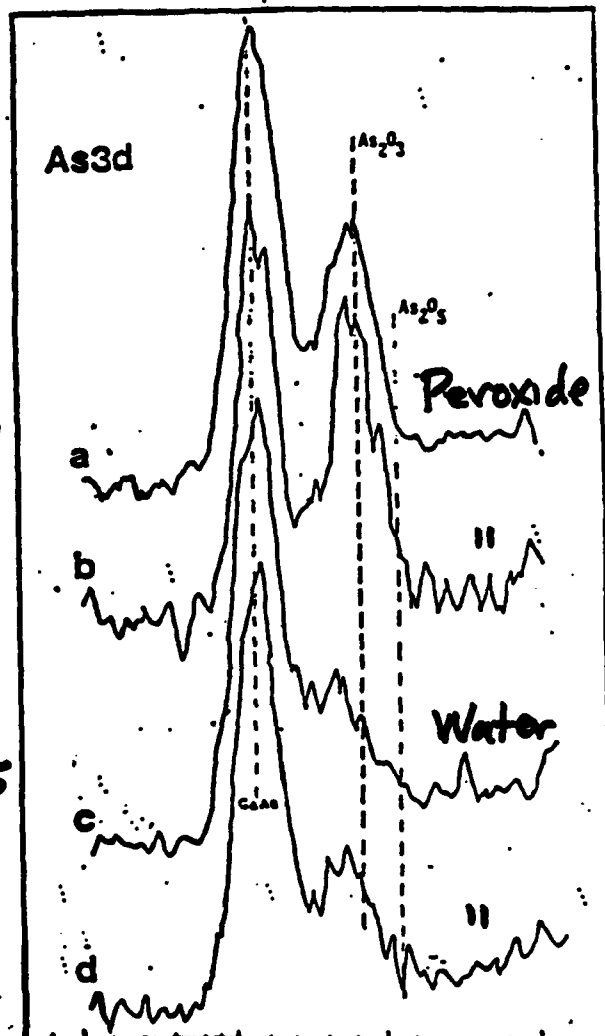
$\Phi_B$ :

.71 eV

.69

.725

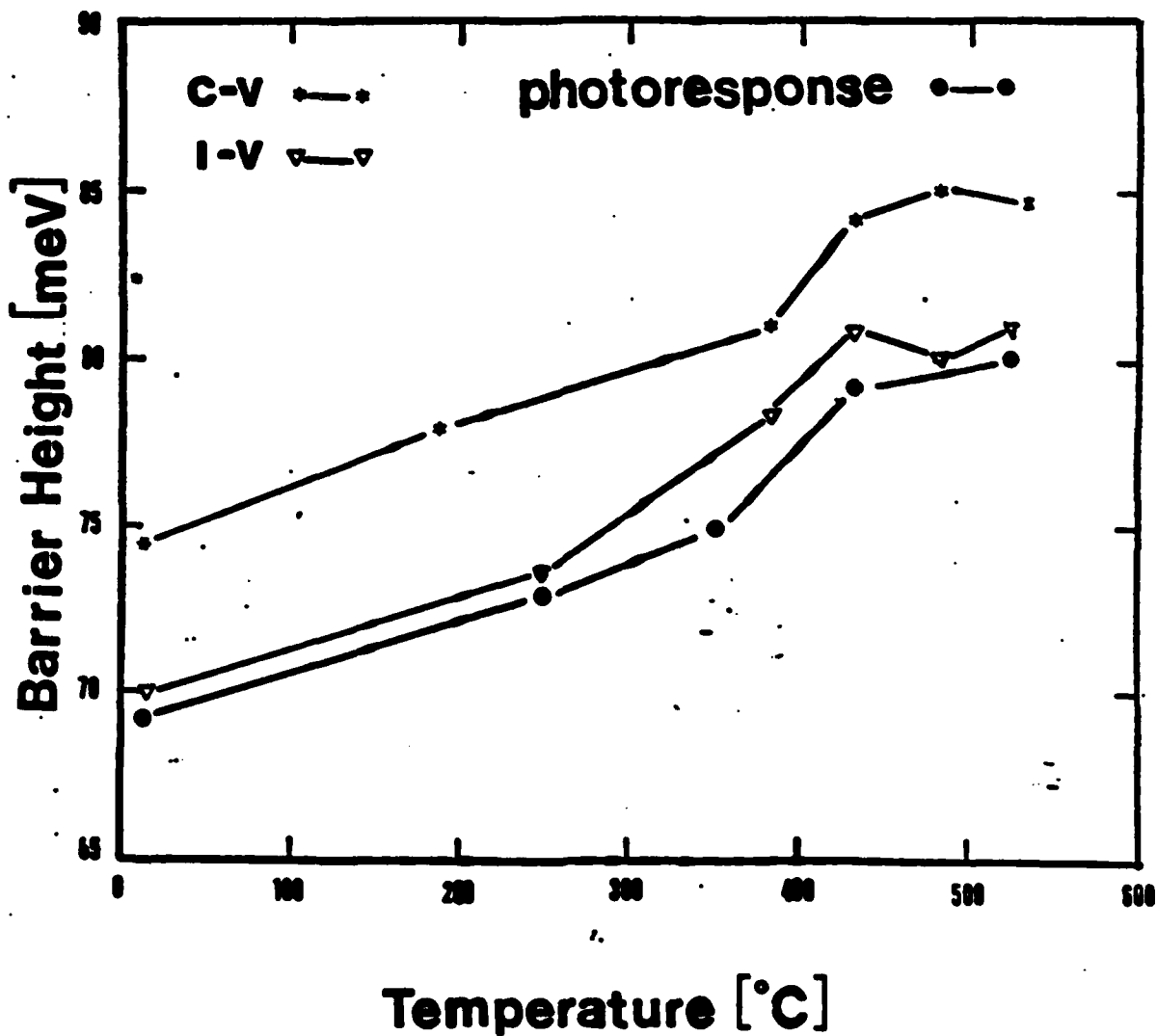
.69



B.E. [eV]

Effect of Surface Clean on  
Ga As Surface

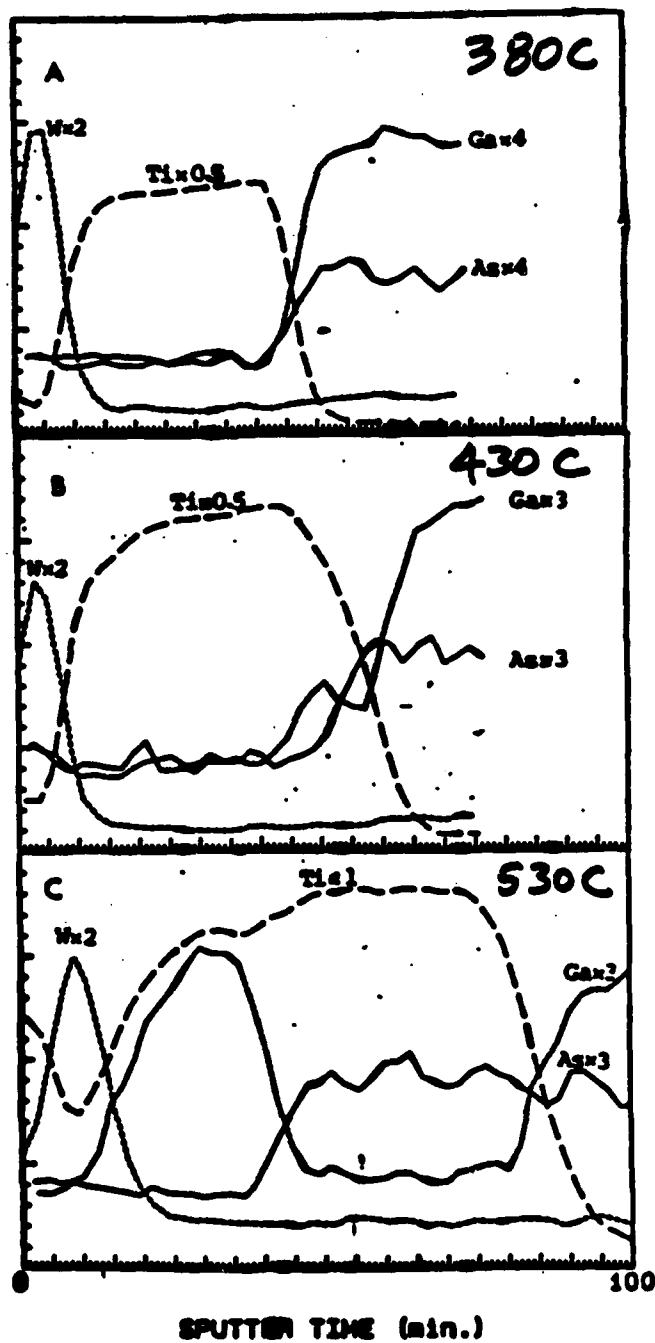
# **SCHOTTKY BARRIER HEIGHT OF Ti: GaAs INTERFACES VERSUS ANNEALING TEMPERATURE\***



\*MEASUREMENTS DONE IN SPICER/HELMS ELECTRICAL CHARACTERIZATION FACILITIES

# EFFECT OF ANNEALING ON W:Ti:GaAs LAYERED STRUCTURE\*

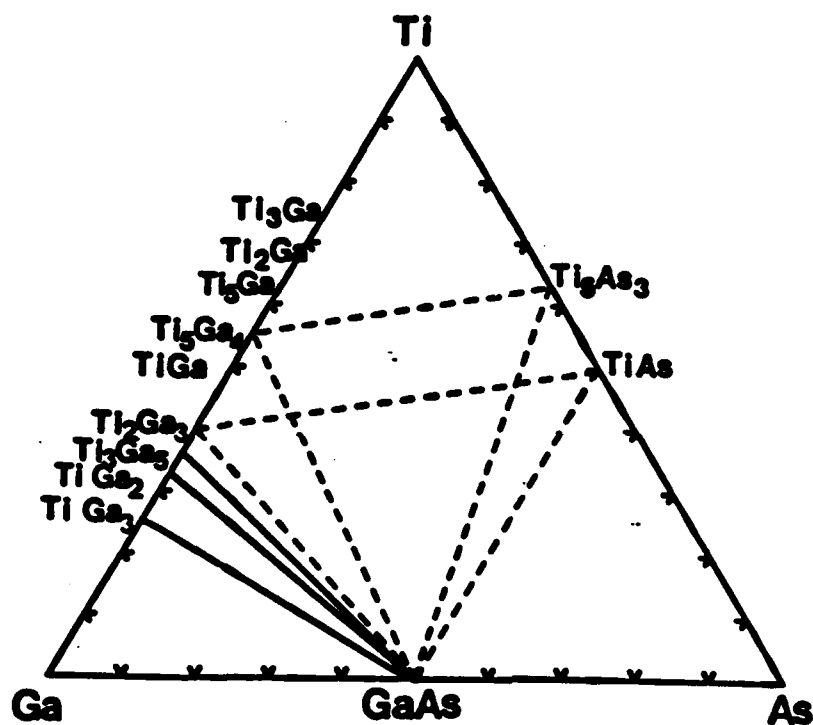
AUGER P-P SIGNAL (arb. units)

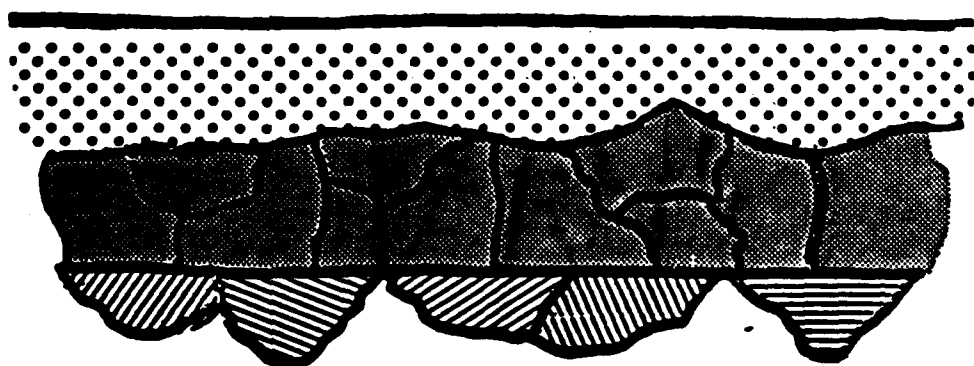


\*AUGER SPUTTER PROFILING PERFORMED IN SYSTEM  
PARTIALLY OBTAINED WITH CMR FUNDS

# PRELIMINARY Ti-Ga-As PHASE DIAGRAM

(KIM, SINCLAIR)





GaAs

-  Ti:O
-  Ti:As
-  Ti:Ga



W. E. Spicer

"Questions Concerning Interfacial Chemistry, Equilibrium, and Electrical Properties"

Outline

1. PES examination of chemistry near interface due to deposition of metal
  - What is Chemistry?
  - Is Chemistry governed by bulk thermodynamics?
  - Is Chemistry the dominant factor in determining electrical properties of Schottky barrier
2. Study of Annealing Au on GaAs (N. Newman)
  - Decrease of Schottky barrier height (SBH) under Au dot (0.9 --> 0.8 eV)
  - Ohmic at perimeter - morphology
3. Study of Annealing Al on GaAs (N. Newman)
  - $\text{Al} + \text{GaAs} \rightarrow \text{Al}_x\text{Ga}_{1-x}\text{As} + \text{Ga}_y\text{Al}$
  - SBH increases 0.8 --> 0.89 eV

Study (PES) Annealing In on GaAs (K. Chin)

  - Melting point of In, InAs formed
  - Correlates with ohmic contact
4. Conclusions

1  
Is "Chemistry" on deposition of metals in agreement with bulk thermodynamics?

Or is it controlled by kinetics of <sup>s</sup> Surface or <sup>t</sup> Interface Thermodynamics?

~~No ideal way to examine experimentally~~

However, <sup>p</sup> photoemission spectroscopy (PES) using synchrotron radiation gives a method for examining early stages of metal:3-5 interactions *due to metal deposition*

Characteristics of PES used here

1. Examine core states

For example	As-3d
	Ga-3d
	Au-4f

As deposited metal (e.g. Au) on clean semiconductor (e.g. GaAs) surface formed by cleaving. In situ - diodes for electrical measurements made in the same way.

2. <sup>^</sup>Measure

- Binding Energy (B.E.) of core levels  
Gives "Chemical Environment" of Atoms
- Intensity of Cores  
Gives Chemical Composition of Layer Studied

Key to understanding this PES:

Sampling Depth is 5 to 10 Å, i.e. 2 to 10 Atomic Layers

Thus:

Thus, <sup>1) F</sup> form clean GaAs surface (usually by cleaving in UHV)

2) <sup>→</sup> Examine spectrum of core levels after metals deposition

- Up to formation of metal layer several Å thick - look principally at substrate, i.e. GaAs
- With increasing metal coverage examine metal plus any Ga and As involved in " reactions"

By Core B.E. Shifts and

Relative Intensity Changes ( e.g. does Ga to As intensity ratio change from that of GaAs)

— A look at changes in detail, can give insight into any new chemical species formed.

### POSSIBLE COMPLICATIONS:

Metal may not deposit on GaAs in uniform way, layer by layer. Rather metal "islands" of various types may form.

But using both core shifts this complicates the analysis and intensities the effects can be sorted out

e.g.:

If large islands of metal formed leaving some GaAs exposed with no metal on it,

Would see GaAs after enough Au was deposited to completely cover GaAs if metal went down uniformly.

However, Ga and As

- Intensity ratio would be same as for GaAs
- Core level binding energies would be same as for GaAs

Thus, we see

1. Change in Ga to As intensity ratio and/or
2. New core shifts (particularly different As and Ga core shifts)

Have Strong Evidence that Chemical Reaction Has Taken Place

Now Illustrate with Data From Au on GaAs

NOTE:

1. For coverages greater than  $8.7\text{\AA}$ , intensity of As becomes increasingly larger than that of Ga
2. For coverages greater than  $1.3\text{\AA}$  have:
  - Ga shift to lower B.E.
  - No shift in As peak but changes in shape at higher binding energies

Clear evidence that GaAs is being disassociated with Ga and As moving into new environment:

A shift suggests at least two new As configurations present possibilities:

- Elemental As, perhaps surface segregated
- As in or reacted with Au

Ga shift can be explained by alloying with Au

Calculation of Ga3d shift due to alloying with deposited metal  
(also done for In 4d - InP case)

1. A recent article describes method to predict core shifts with respect to Ga metal, then can relate to the shift in GaAs. ↩

Based on: P. Steiner and S. Hufner, Act. Metall. 29, 1885 (1981) and B. Johansson and N. Martensson, Phys. Rev. B 21, 4427 (1980).

(J. Nogami, T. Kendelewicz, I. Lindau, and W. E. Spicer, Phys. Rev. B 34, 669 (1986).

$$\Delta E_A(x) = E(A; A_x B_{1-x}) - E(A+1; A_x B_{1-x}) + E(A+1; A)$$

Take dilute limit, i.e.  $\Delta E_A(x)$  as  $x \rightarrow 0$

Compare to experimental shift with lowest Ga intensity (e.g. large coverages)

$E(A;M)$  is partial heat of solution of A in M: A+1 denotes element to right of A in periodic table

$\Delta E_A(x)$  positive - increase in B.E. with respect to Ga in Ga metal

(6)

$\Delta E = G = S_{\text{u}} - E$  Due to Alloying  
 $\Delta E$  with respect to  $G$  in  $G = \text{As}$

Metal	$\Delta E^{\text{exp}}$ (eV)	$\Delta E^{\text{cal}}$ (eV)	PES <del>evapor</del> of evaluation Chemistry
Au	-0.4	-0.38	Strong disruption of GaAs As surface segregation?
Cu	-0.8	-0.83	Strong disruption of GaAs
Ag	----	-0.79	No GaAs disruption No <u>alloying</u> No reaction
Ni	-0.7	-0.60	Strong disruption of GaAs As outdiffusion Ni/Ga/As phase?
Pd	-0.7	-0.30	B.E. still decreasing at 50Å Pd As surface segregation, arsenide formation
Cr	-1.25	-1.05	Strong disruption of GaAs, Strong As out-diffusion
Ti	-1.8	-1.43	Strong disruption of GaAs

Overall Conclusions: on deposit of metal on GaAs (or InP) at room temperature reactions can take place which are not predicted by bulk thermodynamics

Suggest these due to:

Non-equilibrium conditions; i.e. kinetic process

Consider, e.g., heat released due to condensation of metal on GaAs

Annealing will take interface toward thermodynamic equilibrium

(Another possibility to consider, interfacial or surface thermodynamics)

For annealing:

- If reactions go to completion

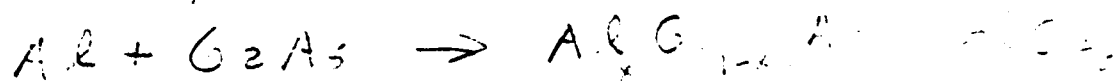
For example:



So that all Au converted uniformly to GaAu<sub>x</sub>  
Bulk Thermodynamics seems to predict

- However, many interfacial reactions approach to be kinetically or diffusion limited

For example:



Al<sub>x</sub>Ga<sub>1-x</sub>As where can't go to completion



See "Chemistry" of various types, using PES.

9

What effect on Electrical Properties:

1) Seen via PES (Very Thin Films) - (0.1 to ~10 Å)

2) Seen via electrical measurements on "thick" (~1000 Å) films ~~PES and IV and/or~~

CV  
3) *in general, PES and electrical measurements agree*  
For example,

Have different chemistry on deposition for Au, <sup>Au</sup>Co, and Pd on GaAs - but all give similar Schottky barrier heights:  
~0.9 on n-type

Variation from Metal to Metal correlates more strongly with electronegativity than other criteria including chemical activity

High electronegativity: higher barrier height on n-type GaAs

*However, Chemistry can be important  
on annealing*

Chemistry doesn't seem to be the key to understanding Schottky barrier height *metal deposition*

Much more likely to be important for:

Changes on order of 0.1 eV of the Schottky barrier height on annealing at moderate temperatures

Complete Loss of Schottky barrier on annealing at very high temperatures

Look at two studies at Stanford and Berkeley (Newman, et al; Liliental-Weber, et al.)

Au and Al

Examine Au and then Al and In

### Au + GaAs - Annealed

Can explain in terms of  $\text{AuGa}_x$  formed at the interface

Decreased electronegativity - thus decrease Schottky barrier height

#### Questions:

1. Model predicts p-type barrier must increase by amount n-decreases must check -
2. Need direct evidence of significant Ga concentration in Au at interface. Difficult to determine if very near interface. Evidence to date is not conclusive.
3. What happens to As if Ga builds up?

---

#### Examine TEM lattice image (Liliental-Weber)

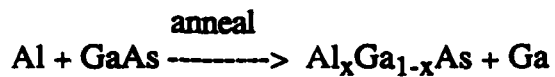
1. 5/6 Lattice mismatch (affect Schottky barrier height (SBH)?)
2. Defects in GaAs beneath the interface

#### Other Liliental-Weber Electronic Microscopic Studies

1. GaAs near ( $\sim 25\text{-}50\text{\AA}$ ) interface As rich
2. Au-Ga + As; more Ga but measurements at limits of technique  
Al:GaAs for comparison

#### Tentative Conclusion:

Defects and "impurities" (Ga in Au or excess As in GaAs) at interface may be important  
Finally: Effect of Oxidation TEM



show PES results

SBH increases 0.8  $\longrightarrow$  0.89 eV on annealing to 360°

stable to 565°

(Think loss of rectification at higher temperatures due to Al melting and/or GaAs dissociating - more study necessary)

Thought explanation of increase of Schottky barrier heights was alloy formation with larger  $E_g$  - But would predict that sum of (SBH) Schottky barrier heights on annealed n- and p-type would be greater than  $E_g$

Newman's experiments to date don't agree - find  $\Sigma$  Schottky barrier heights =  $E_g$

Suggestion of Eicke Weber: small fraction Al on As sides - doping p-type changes would be in the right direction.

**Conclusions:**

1. On deposition of the metal on to GaAs or InP, chemical reactions which are not predicted by bulk thermodynamics occur.
2. There does not seem to be a strong relationship between the type or extent of chemical reaction and the Schottky barrier height (SBH) on as deposited samples. (SBH correlates most strongly with electronegativity.)
3. "Chemistry" may be a key in determining changes in SBH due to annealing *but other factors important - must look at whole system.*
4. Much more to be done.

In on GaAs - gives Schottky barrier  
 room temperature SBH = 0.76 eV

Anneal, etc - "ohmic"  
 In + GaAs ----->  $\text{In}_x\text{GaAs}_{1-x} + x\text{Ga}$

PES - Room Temperature see In metal  
 anneal above melting point of In (see In in InGaAs)

Fermi level unchanged

Consistent with "ohmic" behavior due to InGaAs alloy

Problem - only Ga in GaAs detected using photoemission

not metallic Ga (little metallic In)

could be due to island formation but have not conclusively established this

The Chemistry and Morphology  
of  
Metal / III-V Semiconductor Interfaces

J. H. Weaver

Dept. Chem. Eng. + Materials Science

Univ. Minnesota

Coworkers

M. Grioni  
J. J. Joyce  
M. del Giudice  
M. Ruckman  
S. A. Chambers  
F. Boscherini  
Xu Fang

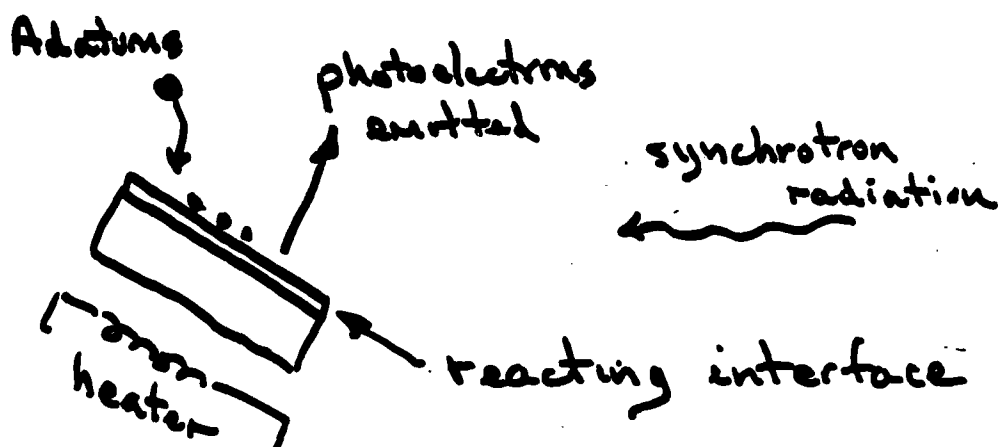
Support

ONR  
Minnesota Microelectronics Center

# Metal / Semiconductor interface formation

Goal: to understand the chemistry & physics of interfaces

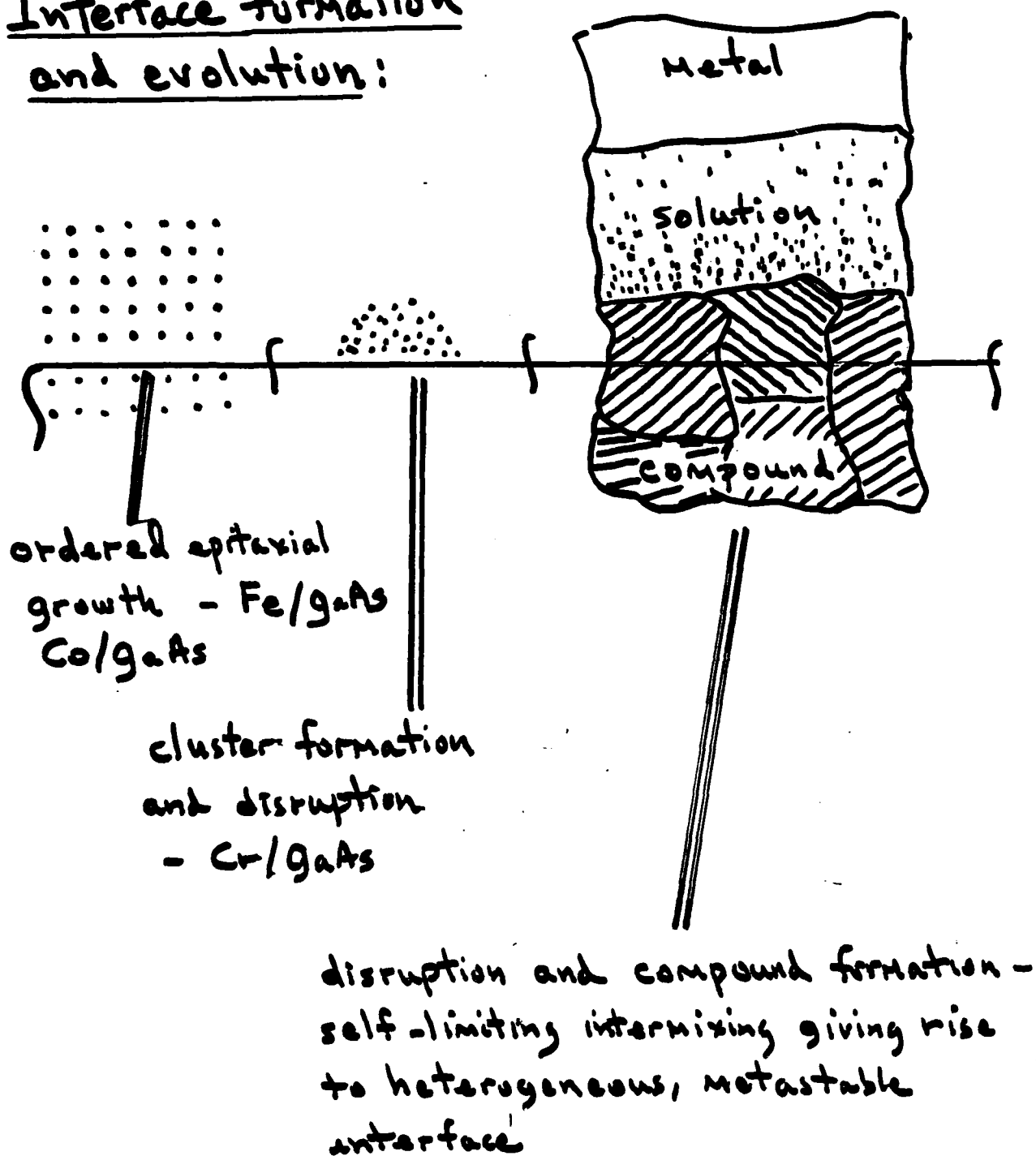
- dimensional constraints
- metastable
- local chemistry

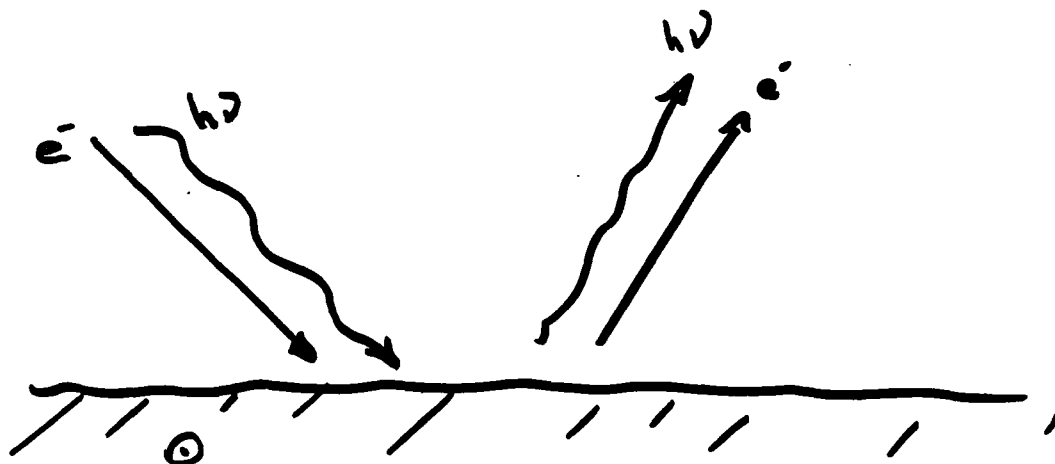


1. What products form? Are they distinct in terms of stoichiometry? stability?
2. Role of kinetics
3. Role of reaction barriers & diffusion barriers
4. Role of clusters



## Interface formation and evolution:





Photoemission : photons in, electrons out

Auger : electrons in, electrons out

LEED : electrons in, spots

Inverse photoemission : electrons in, photons out

(STM)

Co/GaAs > Excellent lattice  
Fe/GaAs match

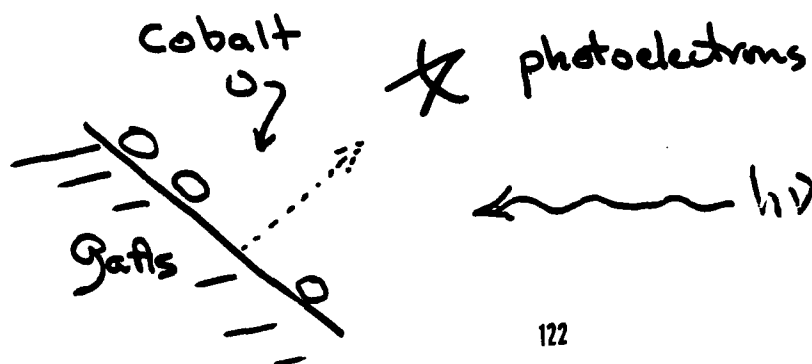
Q: can epitaxial layers be grown?

Yes. Prinz et al. NRL

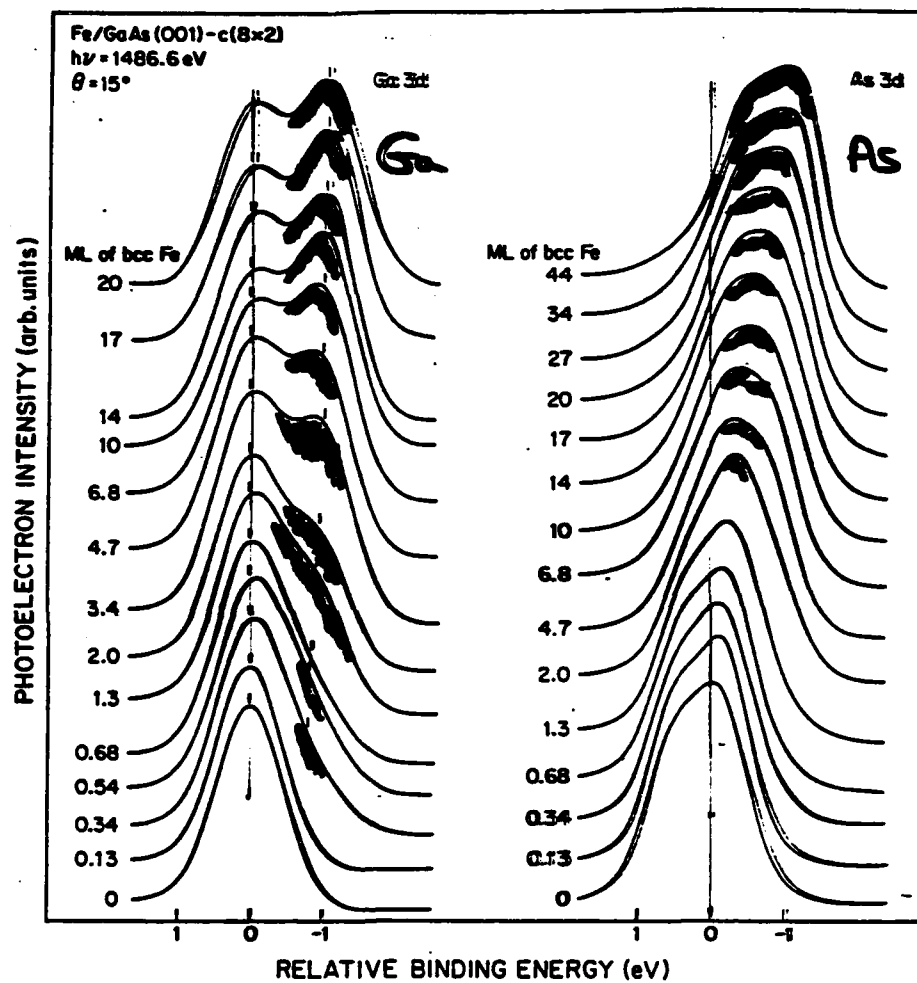
Q: Why? (Most metals induce disruption - will there be disruption?)

Q: Can we use these systems to gain insight into more complex interfaces?

e.g. epi. vs. disruption.  
atom profiles



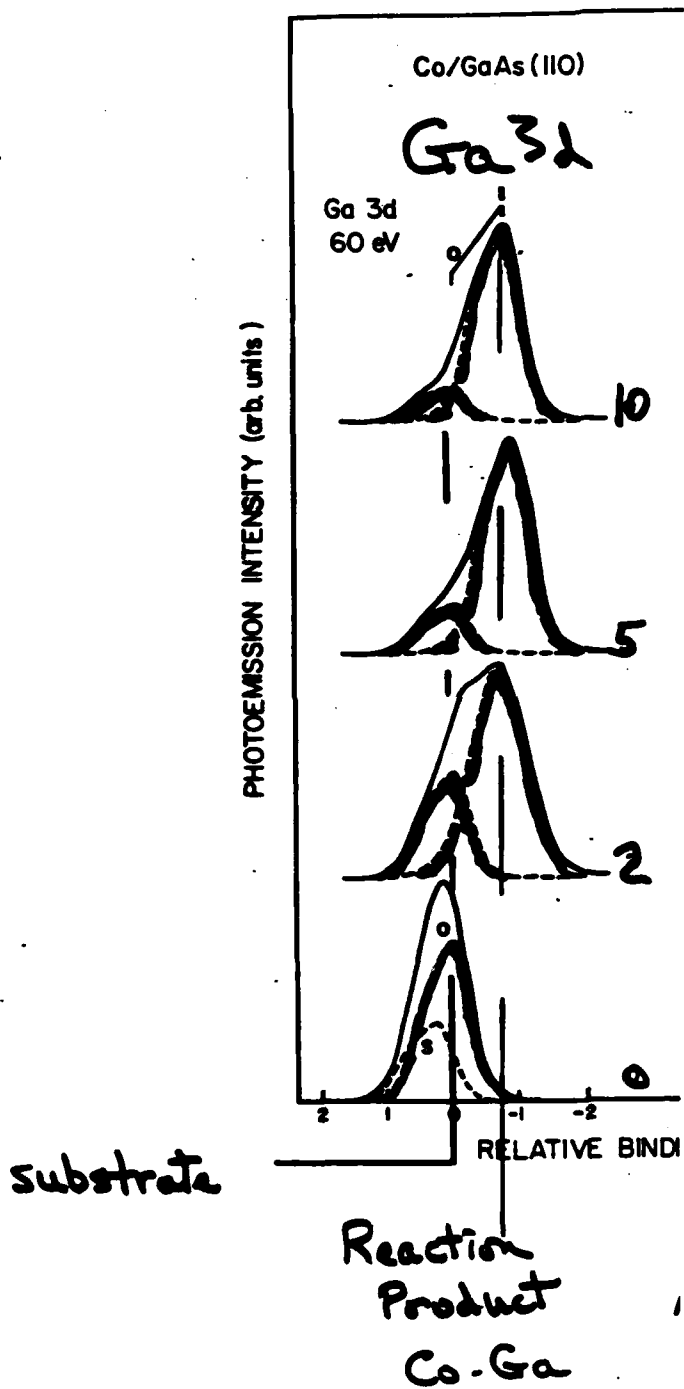
XPS Fe/GaAs(100)  
 $h\nu = 1486.6 \text{ eV}$  Modest resolution



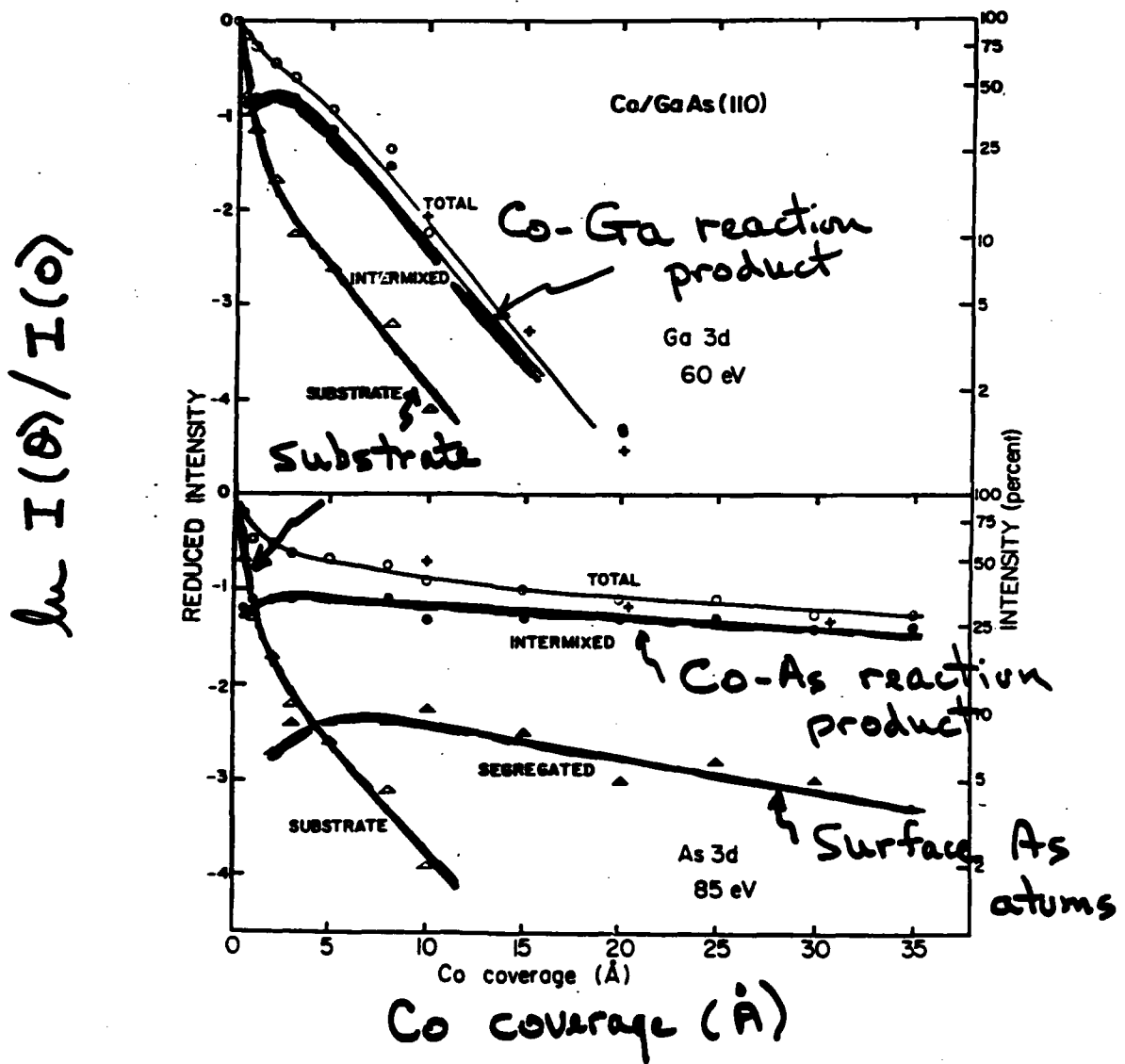
↑ reaction products  
 ↑ substrate

Fig. 6

# Co/GaAs (110)



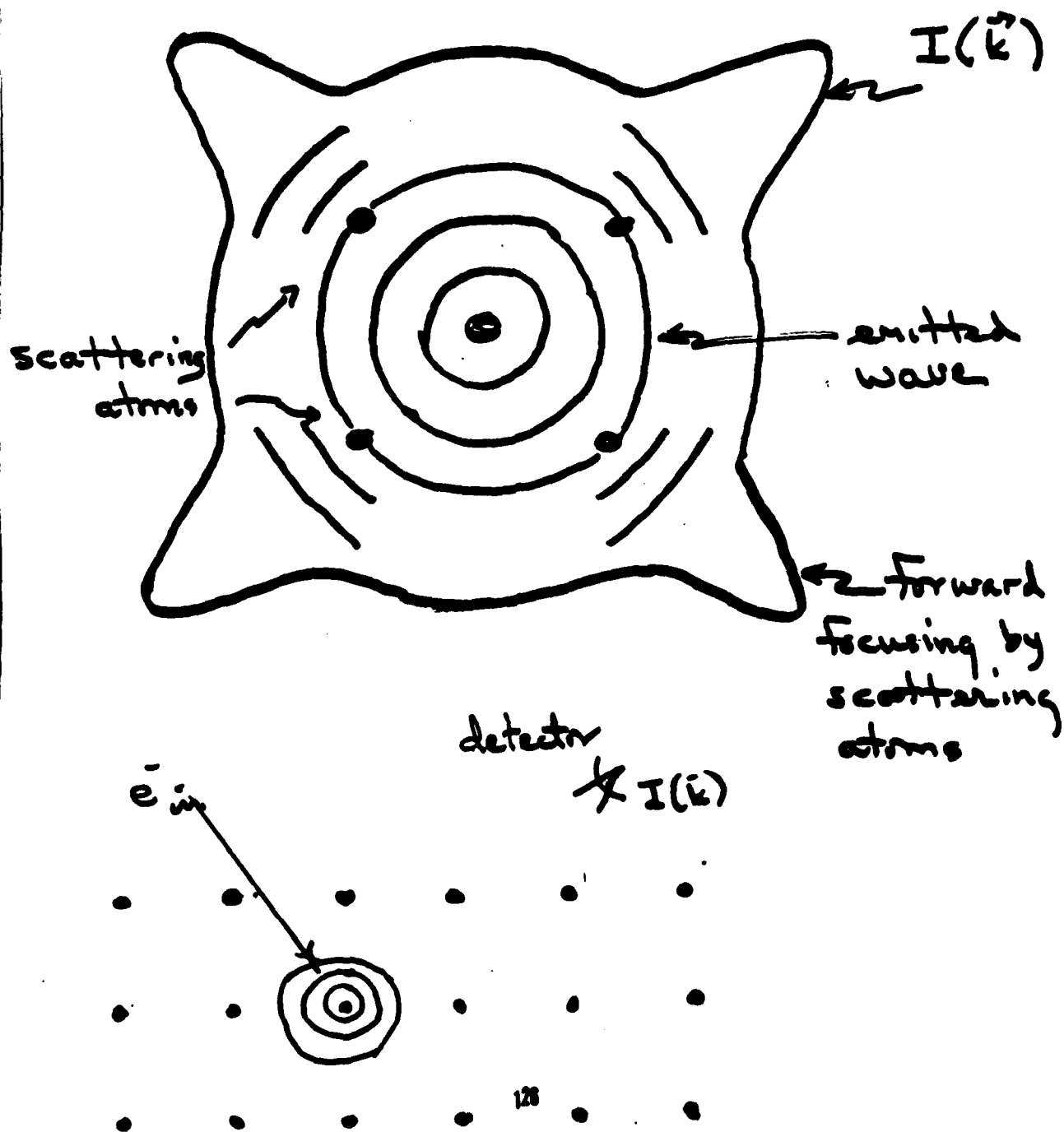
# Co/GaAs (110)



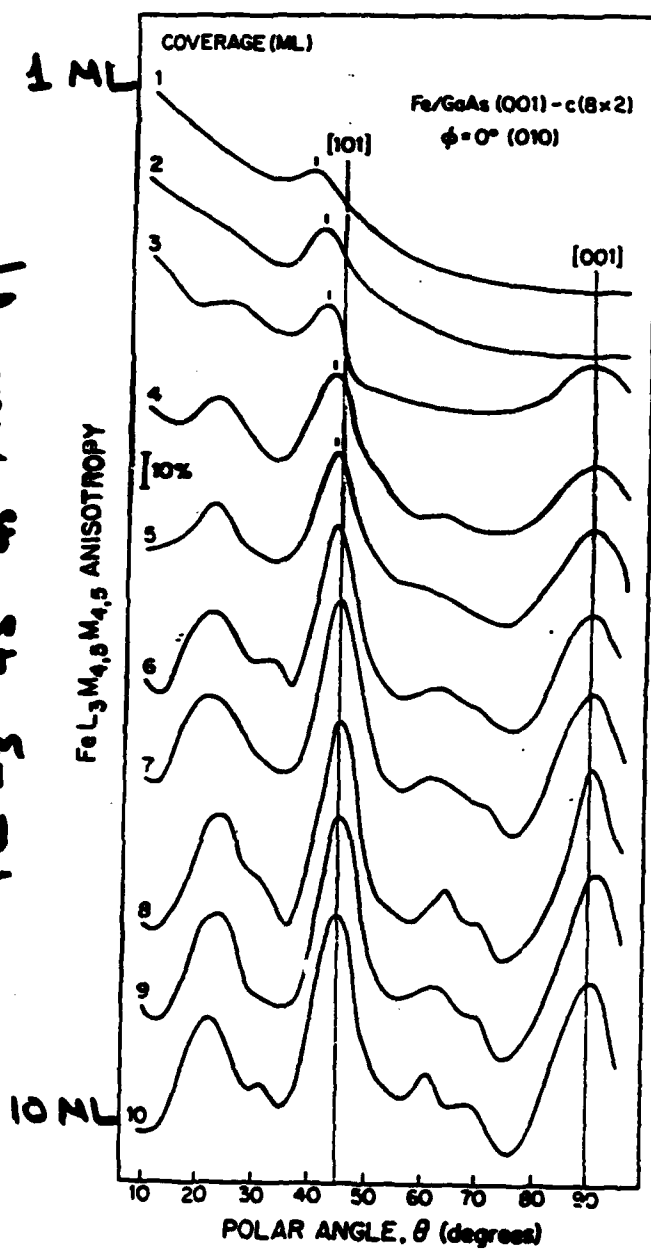
Conclusion: there is reaction and intermixing

Q: Is there epitaxy?

Angle-resolved Auger electron diffraction:  
(Structural probe)



Fe L<sub>3</sub> M<sub>4,5</sub> Anisotropy



evolving epitaxial  
bcc Fe on GaAs (100)

Fig. 2

Conclusion: Excellent epitaxy.

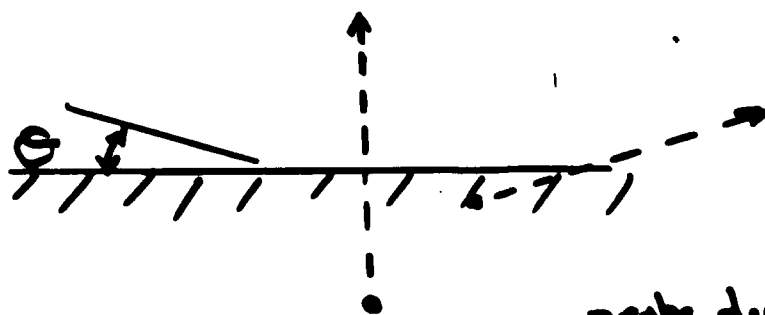


So far:

1. Surface sensitive photoemission shows copious amounts of As at and near vacuum surface  $\Rightarrow$  disruption of GaAs by Co
2. Auger diffraction shows nearly perfect epitaxy, starting at low coverage

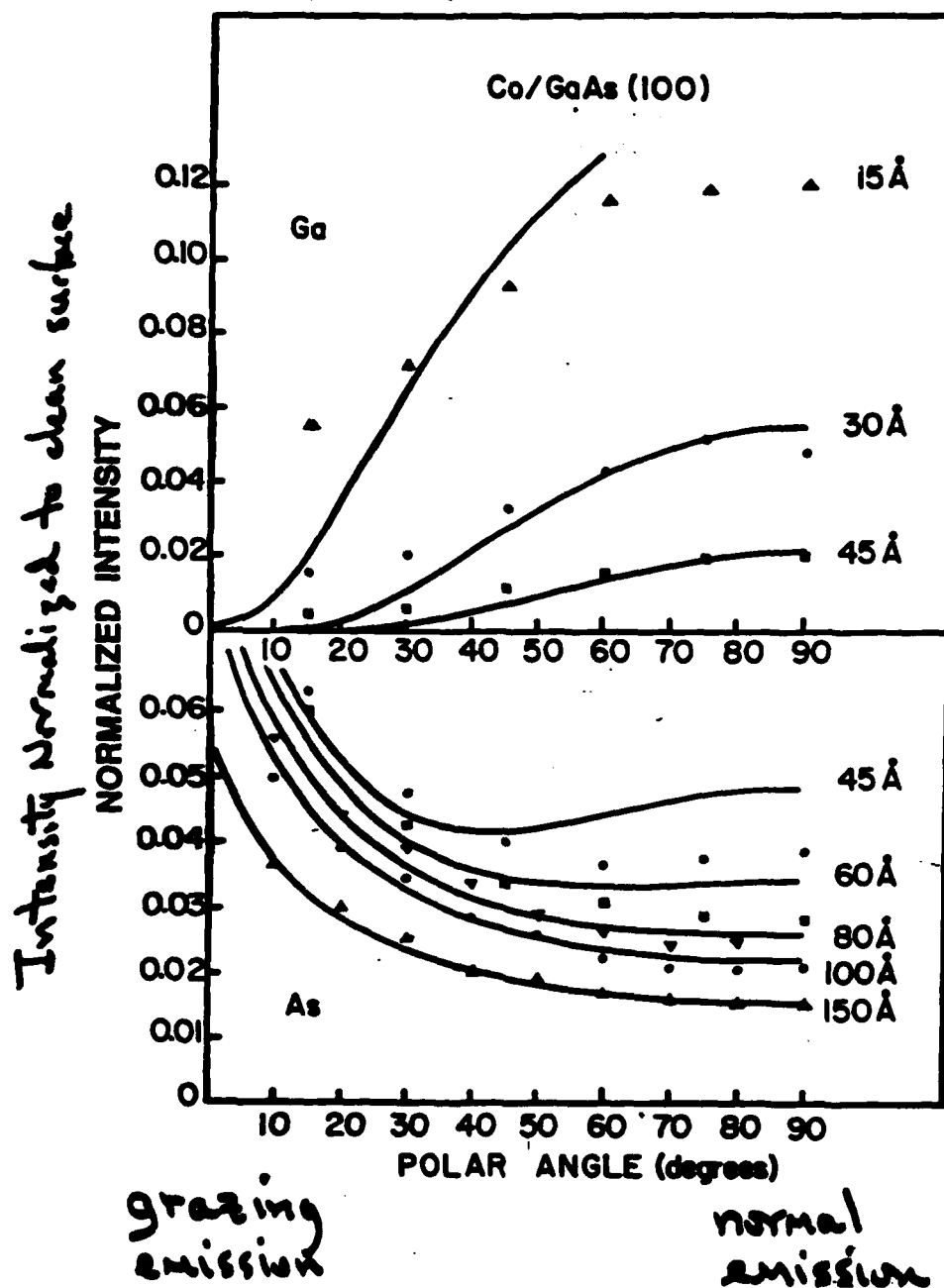
Q: What is the distribution of Ga and As in the overlayer?

$\Rightarrow$  Nondestructive depth profiling with polar-angle-dependent XPS



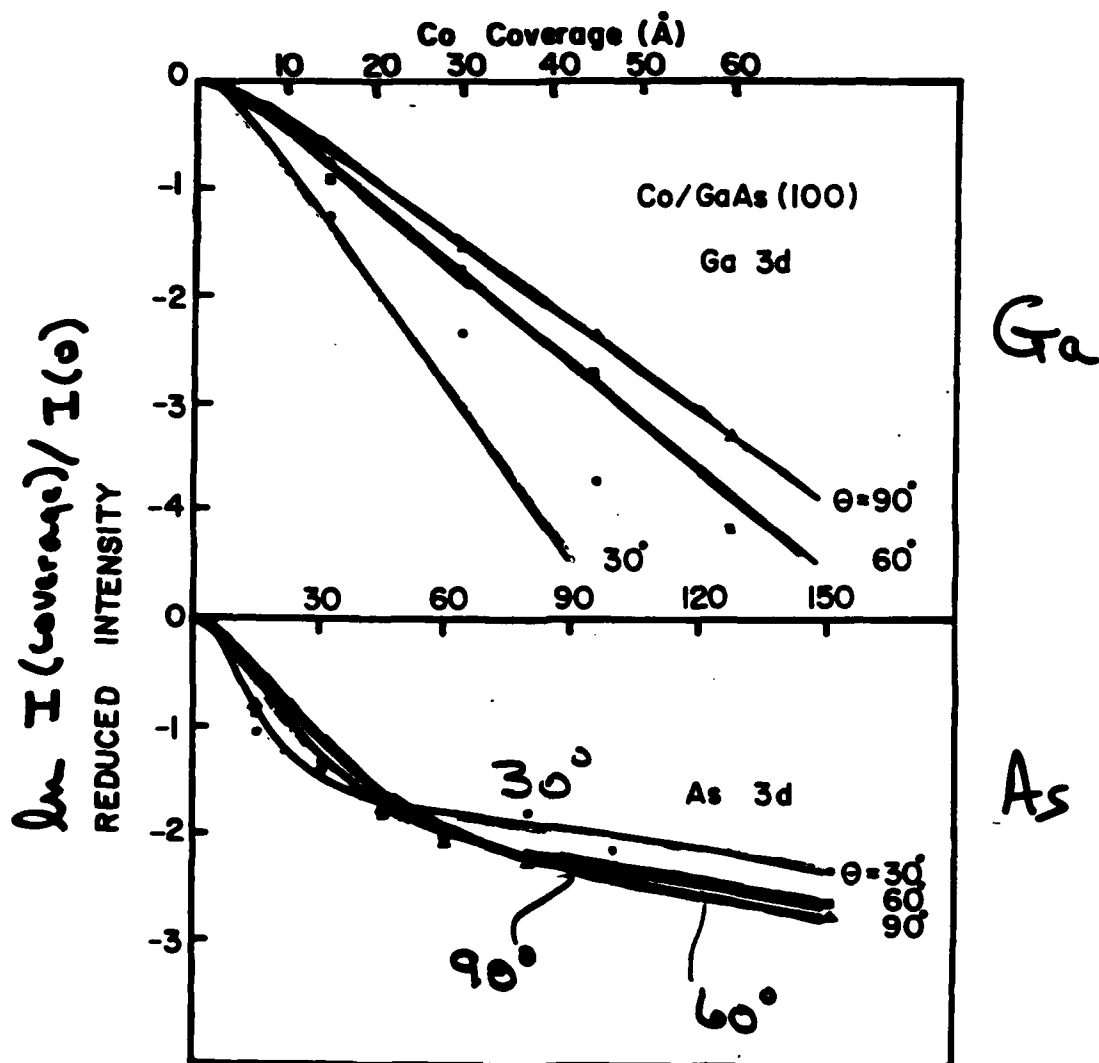
probe depth  $\sim \lambda \sin \theta$

# Polar-angle-dependent XPS Co / GaAs (100)



⇒ As segregation! (on a reactive metal surface)

Attenuation Curves:  
polar-angle-dependent xPS  
Co/GaAs(100)

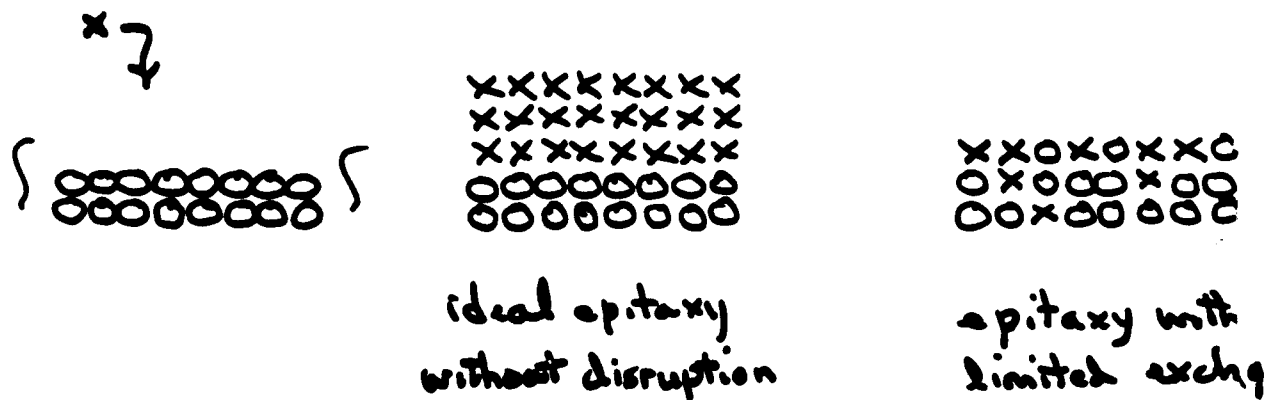


Conclusion: significant segregation to surface  
and near-surface

Why does interface develop in this fashion?

What are the important parameters?

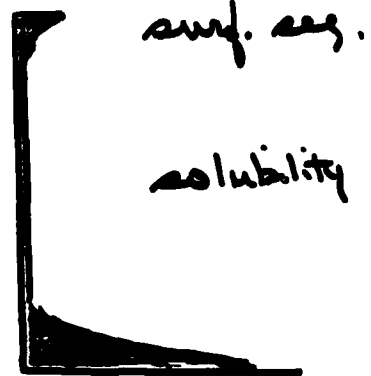
Evolution: Generic M/SC Interface



What if solubility is very low?



thin overlayer



thick overlayer

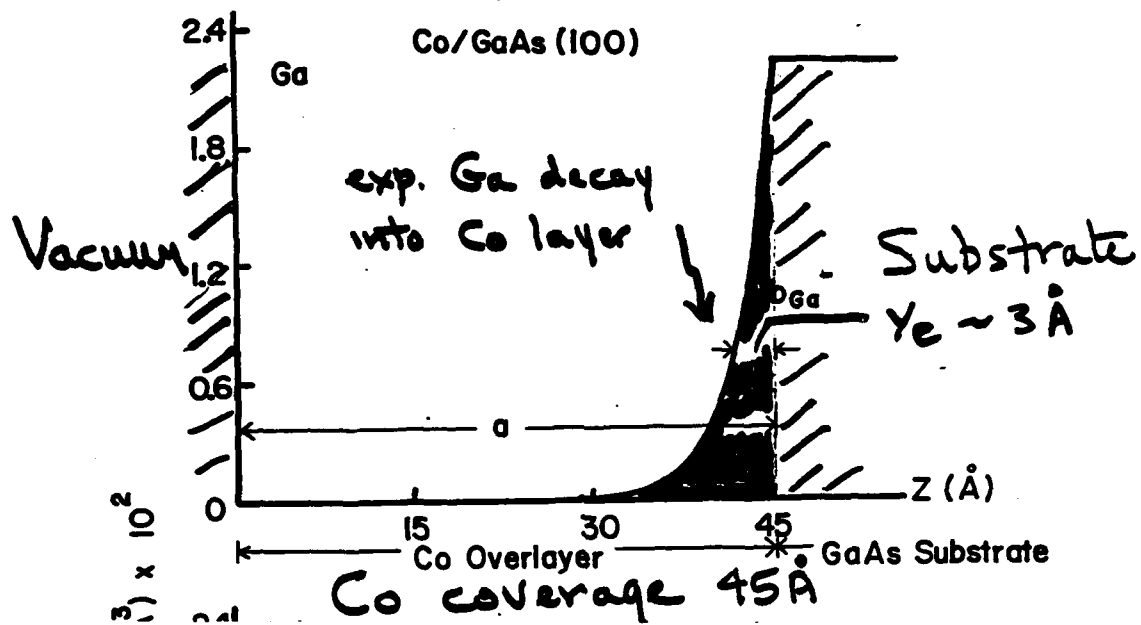
Photoemission intensity of element A detected  
at an angle  $\theta$  wrt surface is

$$I_A(\theta) = \underbrace{\sigma_A}_{\text{photoemission cross section}} \underbrace{I_0(\theta)}_{\text{clean surface}} \underbrace{S}_{\text{spot size}} \int_0^{\infty} \underbrace{\rho_A(z)}_{\text{density } f^{\text{A}} \text{ of element A}} e^{-\frac{z}{\lambda \sin \theta}} dz$$

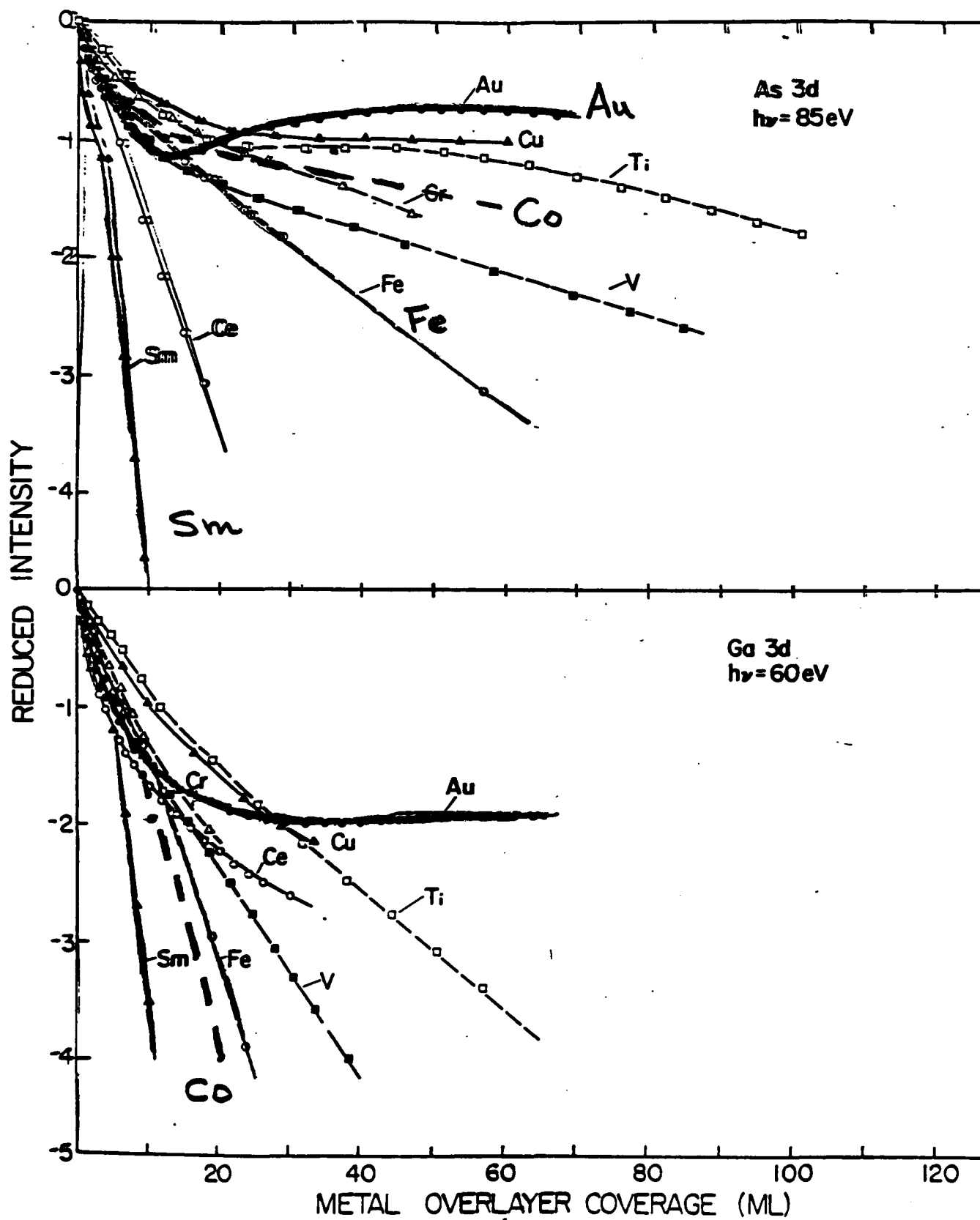
Unknown

# Atom Profiles :

## Co / GaAs (100)



How abrupt are interfaces?





Similar picture for Au/GaAs

$\frac{1}{e}$  values  $\sim 3 \text{ \AA}$

$\rho^{\text{sol}} \sim 0.2 \text{ at. \%}$

Segregated Ga and As (amount depends  
on surface)

For GaAs (100),  $\sim 2 \text{ ML}$  of disruption.

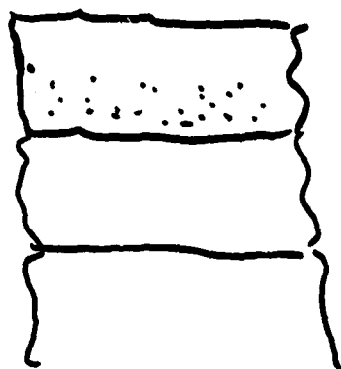
then  $\sim \text{Au layer}$

For GaAs (110), As signal rises for

coverages  $\geq 10 \text{ ML}$ , then decreases

very slowly

What if compound formation occurs  
during early stages of reaction?



Metal overlayer with solution

reaction product(s)  $\leftrightarrow xM + yS \rightarrow M_xS_y$

substrate

Example Ti / Si

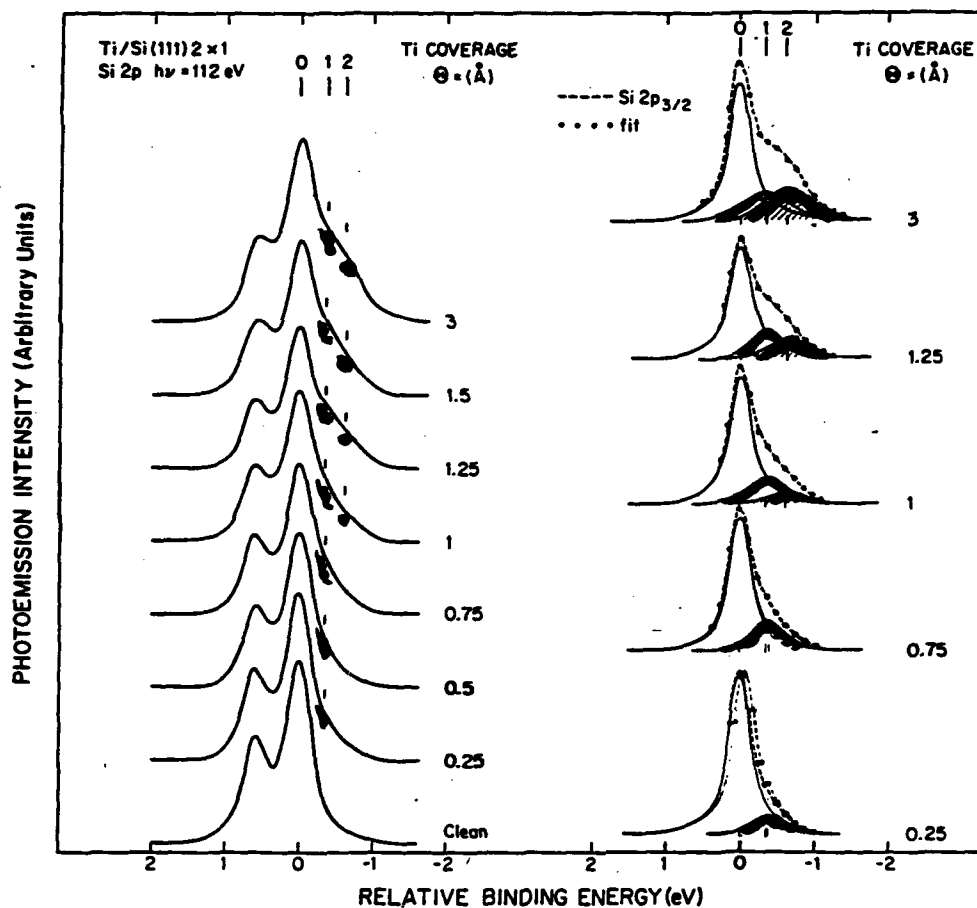
Ti / GaAs

Ce / GaAs

V / Ge

⋮

Ti/Si(111)  $h\nu = 112\text{ eV}$



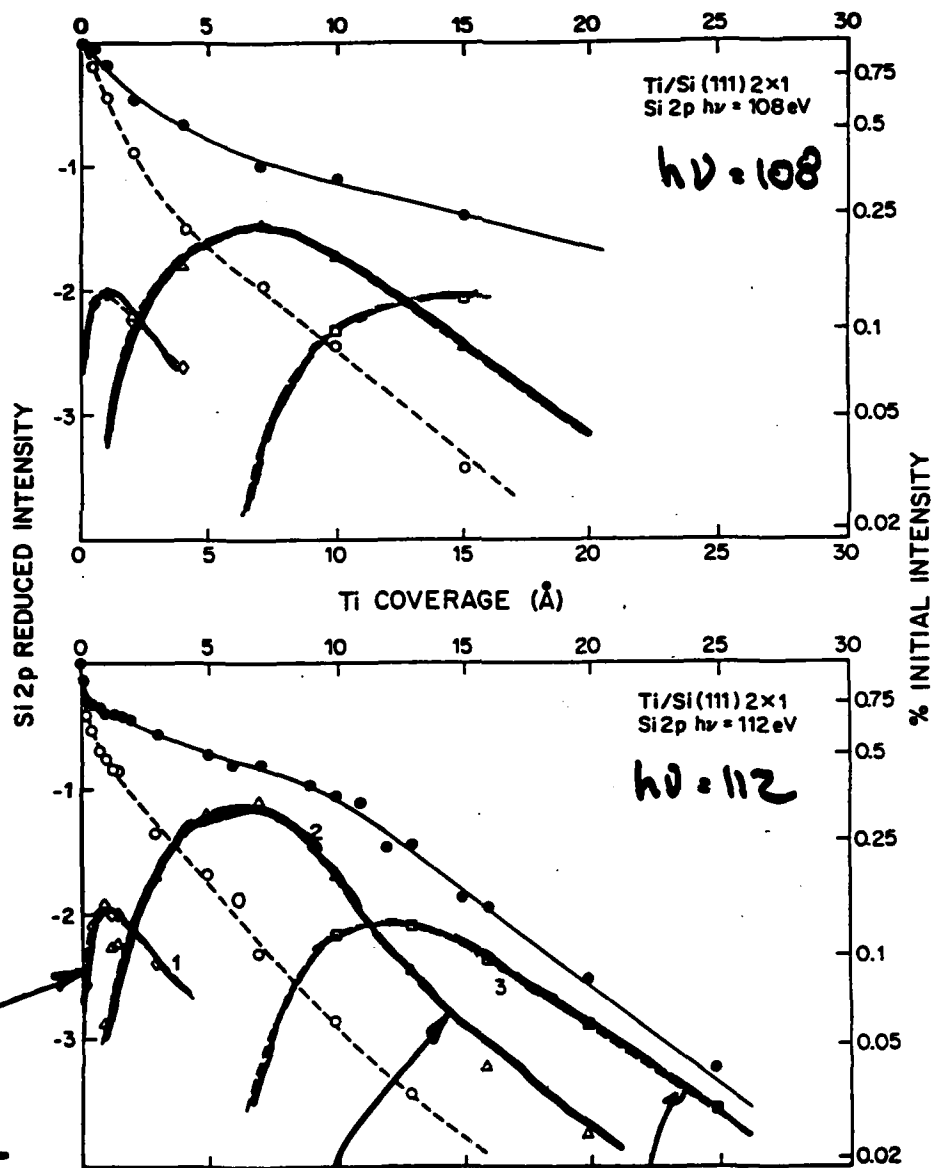
Si-2p<sub>1/2,3/2</sub>

2p<sub>3/2</sub>

→ complex reaction products

Fig. 3

# Ti/Si(111)

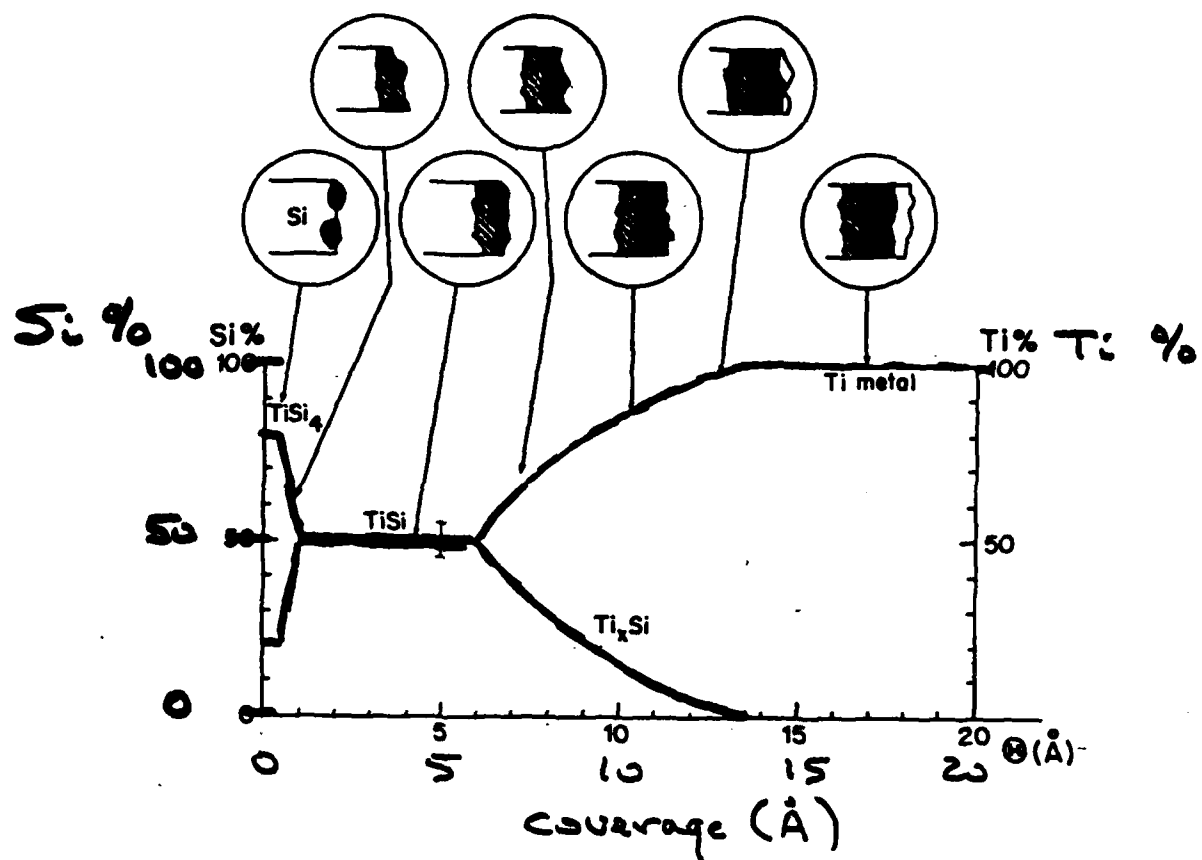


ultra thin  
'transition  
region

Ti-Si  
reaction product

Si in solution  
in Ti

Fig. 5



Metastable Ti/Si interface Fig. 6

Ti-Si acts to regulate its own growth through kinetics

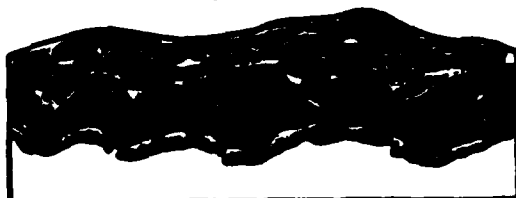
Modeling gives stoichiometry. Temp dependences give  $D_0$  and activation energy

# Interface Evolution

Convergence  
to metal  
overlayer



5. Metal overlayer growth on a complex, multiphase system

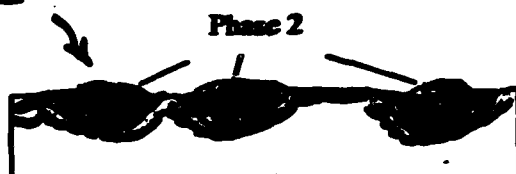


4. Complete coverage by final reaction product



3. Both reaction products grow as overlayer thickness increases

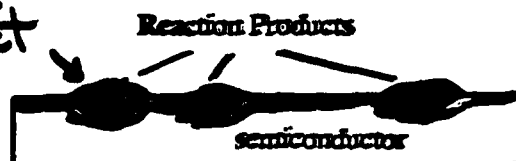
Phase 2



2. Onset of mixed phase growth

Reaction product

substrate



1. Heterogeneous formation of reaction products (islands)

Schematic of evolving metal/semiconductor interfaces showing heterogeneous, metastable growth with spatial dimensions approaching atomic scale. Modifying the physics and chemistry of bulk solids to be applicable to these dimensionally-constrained systems is a major challenge.

# **Room Temperature Chemical Reactions and Schottky Barrier Formation at the Metal/InP(110) Interfaces : Comparison to Si and GaAs Interfaces.**

**T. Kendelewicz, SEL, Stanford University,**

**K. A. Bertness  
K. K. Chin  
R. S. List  
P. H. Mahowald  
C. E. McCants  
N. Newman  
M. D. Williams**

**I. Lindau  
W. E. Spicer**

## **Outline:**

- 1. Introduction and experimental approach**
- 2. Systematics of chemical reactions at the M/InP interfaces**
- 3. Submonolayer band bending vs band bending for thick interfaces. Is there a correlation between barrier height and chemistry?**
- 4. Implications on models of Schottky barrier formation**

## **Experimental approach**

**Use high resolution surface sensitive core level photoemission spectroscopy to study metal/InP interfaces built in a layer by layer fashion in UHV.**

**Get information on:**

- 1. Evolution of the band bending with metal thickness.  
(from shifts of the substrate components of the core levels)**
- 2. Chemical reactions between the substrate and the overlayer  
(from the chemically shifted peaks).**
- 3. Overlayer growth mode (from intensities).**

XX

**Studies were performed in UHV on clean cleaved InP(110) surfaces exposed to controlled amounts of metals deposited by resistive heating from in situ cleaned sources (deposition rates of about 1Å/min, pressure during evaporations about  $10^{-10}$  Torr).**



**Advantage of the technique:**

- 1. Surface sensitivity- allows one to study the very beginning of the chemical reactions and initial band bending.**
- 2. Photon energy tunability - allows modeling of interfaces.**
- 3. Atomic specificity - possibility to independently study the reactions of all the species building the interface.**
- 4. Control of contamination- possibility to detect contaminants (O, C etc.)**

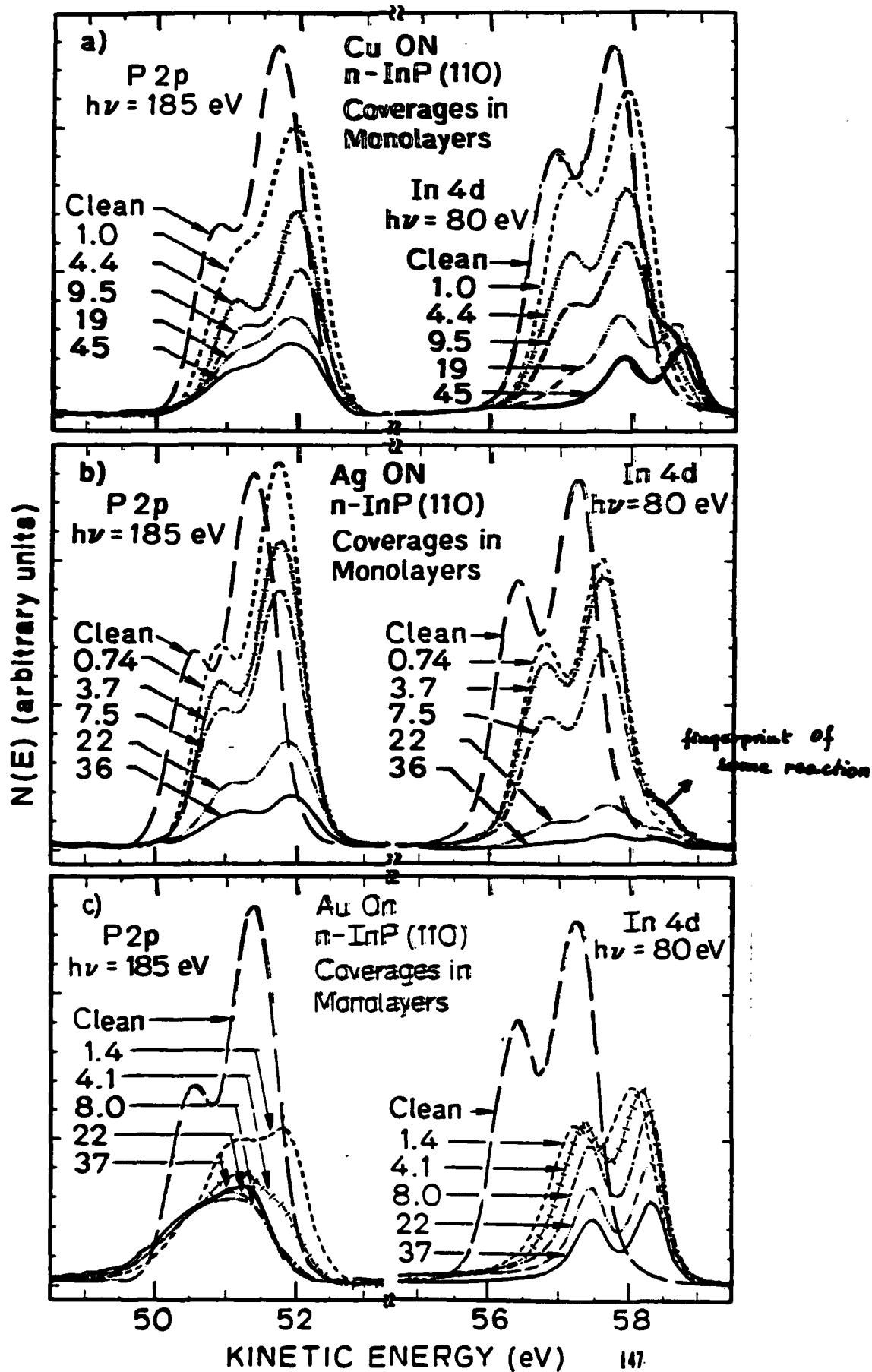
**Limitation of PES:**

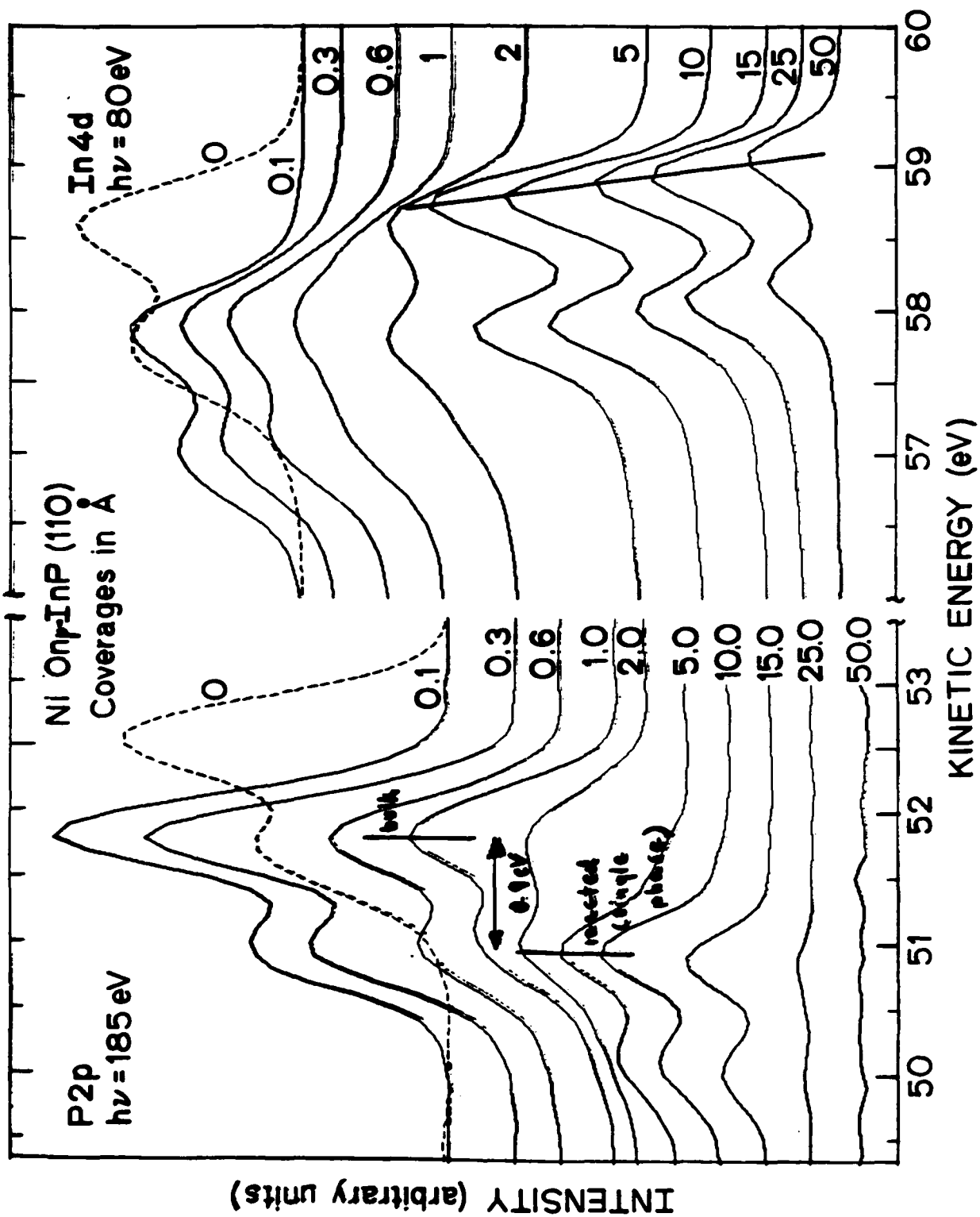
- 1. Does not provide information on buried interfaces**
- 2. Has to be combined with other techniques (ex I-V or C-V) to compare submonolayer band bending with thick devices barrier heights**
- 3. Often requires computer fitting of the data to separate band bending (error bar 0.1 eV) and model chemistry**

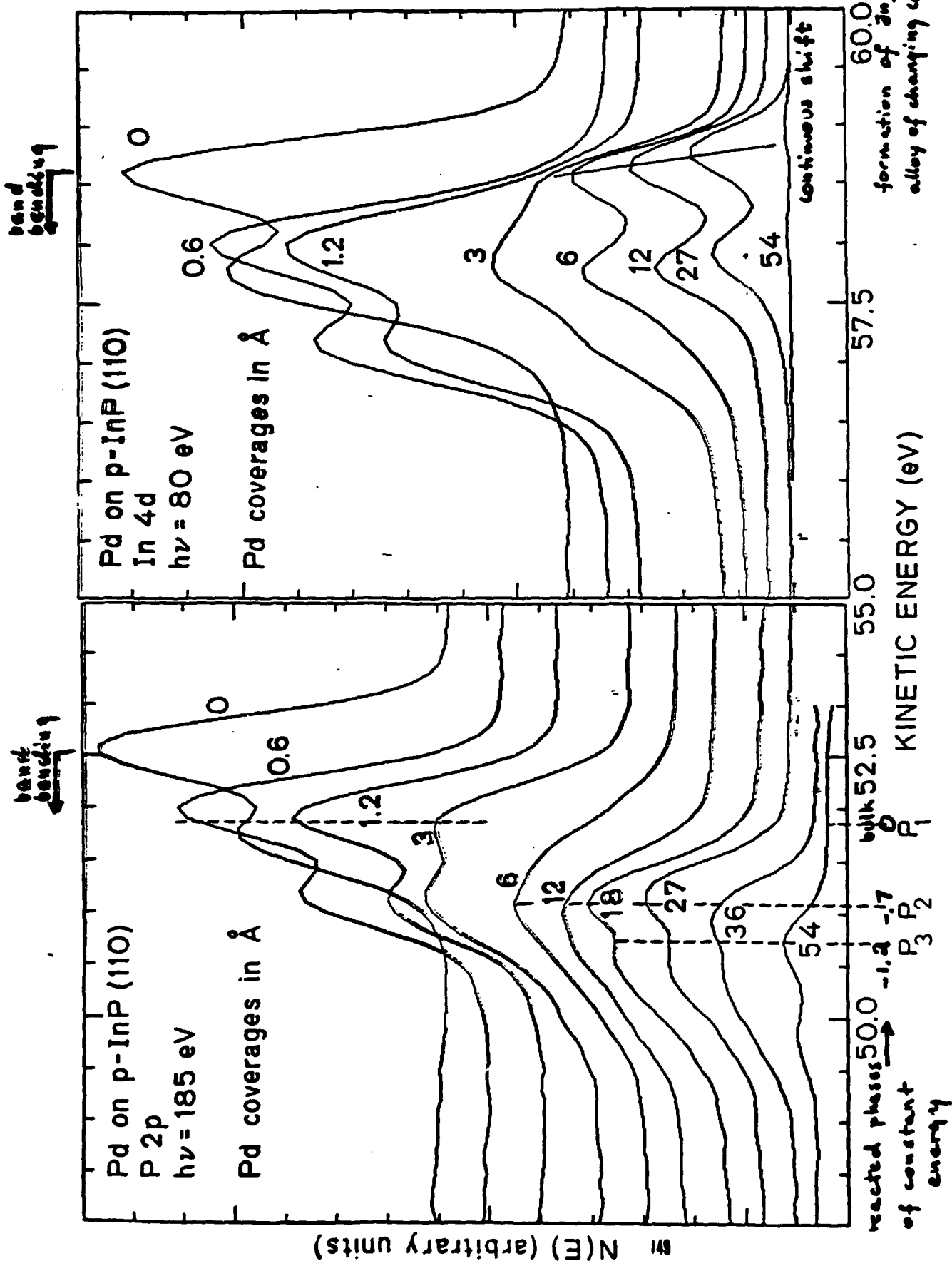
1 27 H																	2 He																										
3 24 B	4 39 K																	10 Ne																									
5 10 B	6 12 Mg																	18 Ar																									
7 17 Cl	8 19 K	9 20 Ca	11 23 V	12 24 Cr	13 25 Mn	14 26 Fe	15 27 Co	16 28 Ni	17 29 Cu	18 30 Zn	19 31 Ga	20 32 Ge	21 33 As	22 34 Se	23 35 Br	24 36 Kr	36 Xe																										
11 23 Na	12 24 Mg	13 25 Al	14 26 Si	15 27 P	16 28 S	17 29 Cl	18 30 Ar	19 31 K	20 32 Ca	21 33 Sc	22 34 Ti	23 35 V	24 36 Cr	25 37 Mn	26 38 Fe	27 39 Co	28 40 Ni	29 41 Cu	30 42 Zn	31 43 Ga	32 44 Ge	33 45 As	34 46 Se	35 47 Br	36 48 Kr	37 49 Rb	38 50 Sr	39 51 Y	40 52 Zr	41 53 Nb	42 54 Mo	43 55 Tc	44 56 Ru	45 57 Rh	46 58 Pd	47 59 Ag	48 60 Cd	49 61 In	50 62 Sn	51 63 Sb	52 64 Te	53 65 I	54 66 Xe
15 31 P	16 32 S	17 33 Cl	18 34 Ar	19 35 K	20 36 Ca	21 37 Sc	22 38 Ti	23 39 V	24 40 Cr	25 41 Mn	26 42 Fe	27 43 Co	28 44 Ni	29 45 Cu	30 46 Zn	31 47 Ga	32 48 Ge	33 49 As	34 50 Se	35 51 Br	36 52 Kr	37 53 Rb	38 54 Sr	39 55 Y	40 56 Zr	41 57 Nb	42 58 Mo	43 59 Tc	44 60 Ru	45 61 Rh	46 62 Pd	47 63 Ag	48 64 Cd	49 65 In	50 66 Sn	51 67 Sb	52 68 Te	53 69 I	54 70 Xe				
19 39 K	20 40 Ca	21 41 Sc	22 42 Ti	23 43 V	24 44 Cr	25 45 Mn	26 46 Fe	27 47 Co	28 48 Ni	29 49 Cu	30 50 Zn	31 51 Ga	32 52 Ge	33 53 As	34 54 Se	35 55 Br	36 56 Kr	37 57 Rb	38 58 Sr	39 59 Y	40 60 Zr	41 61 Nb	42 62 Mo	43 63 Tc	44 64 Ru	45 65 Rh	46 66 Pd	47 67 Ag	48 68 Cd	49 69 In	50 70 Sn	51 71 Sb	52 72 Te	53 73 I	54 74 Xe								
23 47 K	24 48 Ca	25 49 Sc	26 50 Ti	27 51 V	28 52 Cr	29 53 Mn	30 54 Fe	31 55 Co	32 56 Ni	33 57 Cu	34 58 Zn	35 59 Ga	36 60 Ge	37 61 As	38 62 Se	39 63 Br	40 64 Kr	41 65 Rb	42 66 Sr	43 67 Y	44 68 Zr	45 69 Nb	46 70 Mo	47 71 Tc	48 72 Ru	49 73 Rh	50 74 Pd	51 75 Ag	52 76 Cd	53 77 In	54 78 Sn	55 79 Sb	56 80 Te	57 81 I	58 82 Xe								
27 55 Rb	28 56 Sr	29 57 Y	30 58 Zr	31 59 Nb	32 60 Mo	33 61 Tc	34 62 Ru	35 63 Rh	36 64 Pd	37 65 Ag	38 66 Cd	39 67 In	40 68 Sn	41 69 Sb	42 70 Te	43 71 I	44 72 Xe	45 73 Rb	46 74 Sr	47 75 Y	48 76 Zr	49 77 Nb	50 78 Mo	51 79 Tc	52 80 Ru	53 81 Rh	54 82 Pd	55 83 Ag	56 84 Cd	57 85 In	58 86 Sn	59 87 Sb	60 88 Te	61 89 I	62 90 Xe								
31 63 K	32 64 Ca	33 65 Sc	34 66 Ti	35 67 V	36 68 Cr	37 69 Mn	38 70 Fe	39 71 Co	40 72 Ni	41 73 Cu	42 74 Zn	43 75 Ga	44 76 Ge	45 77 As	46 78 Se	47 79 Br	48 80 Kr	49 81 Rb	50 82 Sr	51 83 Y	52 84 Zr	53 85 Nb	54 86 Mo	55 87 Tc	56 88 Ru	57 89 Rh	58 90 Pd	59 91 Ag	60 92 Cd	61 93 In	62 94 Sn	63 95 Sb	64 96 Te	65 97 I	66 98 Xe								
35 79 K	36 80 Ca	37 81 Sc	38 82 Ti	39 83 V	40 84 Cr	41 85 Mn	42 86 Fe	43 87 Co	44 88 Ni	45 89 Cu	46 90 Zn	47 91 Ga	48 92 Ge	49 93 As	50 94 Se	51 95 Br	52 96 Kr	53 97 Rb	54 98 Sr	55 99 Y	56 100 Zr	57 101 Nb	58 102 Mo	59 103 Tc	60 104 Ru	61 105 Rh	62 106 Pd	63 107 Ag	64 108 Cd	65 109 In	66 110 Sn	67 111 Sb	68 112 Te	69 113 I	70 114 Xe								
39 87 K	40 88 Ca	41 89 Sc	42 90 Ti	43 91 V	44 92 Cr	45 93 Mn	46 94 Fe	47 95 Co	48 96 Ni	49 97 Cu	50 98 Zn	51 99 Ga	52 100 Ge	53 101 As	54 102 Se	55 103 Br	56 104 Kr	57 105 Rb	58 106 Sr	59 107 Y	60 108 Zr	61 109 Nb	62 110 Mo	63 111 Tc	64 112 Ru	65 113 Rh	66 114 Pd	67 115 Ag	68 116 Cd	69 117 In	70 118 Sn	71 119 Sb	72 120 Te	73 121 I	74 122 Xe								
43 93 K	44 94 Ca	45 95 Sc	46 96 Ti	47 97 V	48 98 Cr	49 99 Mn	50 100 Fe	51 101 Co	52 102 Ni	53 103 Cu	54 104 Zn	55 105 Ga	56 106 Ge	57 107 As	58 108 Se	59 109 Br	60 110 Kr	61 111 Rb	62 112 Sr	63 113 Y	64 114 Zr	65 115 Nb	66 116 Mo	67 117 Tc	68 118 Ru	69 119 Rh	70 120 Pd	71 121 Ag	72 122 Cd	73 123 In	74 124 Sn	75 125 Sb	76 126 Te	77 127 I	78 128 Xe								
47 99 K	48 100 Ca	49 101 Sc	50 102 Ti	51 103 V	52 104 Cr	53 105 Mn	54 106 Fe	55 107 Co	56 108 Ni	57 109 Cu	58 110 Zn	59 111 Ga	60 112 Ge	61 113 As	62 114 Se	63 115 Br	64 116 Kr	65 117 Rb	66 118 Sr	67 119 Y	68 120 Zr	69 121 Nb	70 122 Mo	71 123 Tc	72 124 Ru	73 125 Rh	74 126 Pd	75 127 Ag	76 128 Cd	77 129 In	78 130 Sn	79 131 Sb	80 132 Te	81 133 I	82 134 Xe								
51 105 K	52 106 Ca	53 107 Sc	54 108 Ti	55 109 V	56 110 Cr	57 111 Mn	58 112 Fe	59 113 Co	60 114 Ni	61 115 Cu	62 116 Zn	63 117 Ga	64 118 Ge	65 119 As	66 120 Se	67 121 Br	68 122 Kr	69 123 Rb	70 124 Sr	71 125 Y	72 126 Zr	73 127 Nb	74 128 Mo	75 129 Tc	76 130 Ru	77 131 Rh	78 132 Pd	79 133 Ag	80 134 Cd	81 135 In	82 136 Sn	83 137 Sb	84 138 Te	85 139 I	86 140 Xe								
55 111 K	56 112 Ca	57 113 Sc	58 114 Ti	59 115 V	60 116 Cr	61 117 Mn	62 118 Fe	63 119 Co	64 120 Ni	65 121 Cu	66 122 Zn	67 123 Ga	68 124 Ge	69 125 As	70 126 Se	71 127 Br	72 128 Kr	73 129 Rb	74 130 Sr	75 131 Y	76 132 Zr	77 133 Nb	78 134 Mo	79 135 Tc	80 136 Ru	81 137 Rh	82 138 Pd	83 139 Ag	84 140 Cd	85 141 In	86 142 Sn	87 143 Sb	88 144 Te	89 145 I	90 146 Xe								
59 117 K	60 118 Ca	61 119 Sc	62 120 Ti	63 121 V	64 122 Cr	65 123 Mn	66 124 Fe	67 125 Co	68 126 Ni	69 127 Cu	70 128 Zn	71 129 Ga	72 130 Ge	73 131 As	74 132 Se	75 133 Br	76 134 Kr	77 135 Rb	78 136 Sr	79 137 Y	80 138 Zr	81 139 Nb	82 140 Mo	83 141 Tc	84 142 Ru	85 143 Rh	86 144 Pd	87 145 Ag	88 146 Cd	89 147 In	90 148 Sn	91 149 Sb	92 150 Te	93 151 I	94 152 Xe								
63 123 K	64 124 Ca	65 125 Sc	66 126 Ti	67 127 V	68 128 Cr	69 129 Mn	70 130 Fe	71 131 Co	72 132 Ni	73 133 Cu	74 134 Zn	75 135 Ga	76 136 Ge	77 137 As	78 138 Se	79 139 Br	80 140 Kr	81 141 Rb	82 142 Sr	83 143 Y	84 144 Zr	85 145 Nb	86 146 Mo	87 147 Tc	88 148 Ru	89 149 Rh	90 150 Pd	91 151 Ag	92 152 Cd	93 153 In	94 154 Sn	95 155 Sb	96 156 Te	97 157 I	98 158 Xe								
67 129 K	68 130 Ca	69 131 Sc	70 132 Ti	71 133 V	72 134 Cr	73 135 Mn	74 136 Fe	75 137 Co	76 138 Ni	77 139 Cu	78 140 Zn	79 141 Ga	80 142 Ge	81 143 As	82 144 Se	83 145 Br	84 146 Kr	85 147 Rb	86 148 Sr	87 149 Y	88 150 Zr	89 151 Nb	90 152 Mo	91 153 Tc	92 154 Ru	93 155 Rh	94 156 Pd	95 157 Ag	96 158 Cd	97 159 In	98 160 Sn	99 161 Sb	100 162 Te	101 163 I	102 164 Xe								
71 135 K	72 136 Ca	73 137 Sc	74 138 Ti	75 139 V	76 140 Cr	77 141 Mn	78 142 Fe	79 143 Co	80 144 Ni	81 145 Cu	82 146 Zn	83 147 Ga	84 148 Ge	85 149 As	86 150 Se	87 151 Br	88 152 Kr	89 153 Rb	90 154 Sr	91 155 Y	92 156 Zr	93 157 Nb	94 158 Mo	95 159 Tc	96 160 Ru	97 161 Rh	98 162 Pd	99 163 Ag	100 164 Cd	101 165 In	102 166 Sn	103 167 Sb	104 168 Te	105 169 I	106 170 Xe								
75 141 K	76 142 Ca	77 143 Sc	78 144 Ti	79 145 V	80 146 Cr	81 147 Mn	82 148 Fe	83 149 Co	84 150 Ni	85 151 Cu	86 152 Zn	87 153 Ga	88 154 Ge	89 155 As	90 156 Se	91 157 Br	92 158 Kr	93 159 Rb	94 160 Sr	95 161 Y	96 162 Zr	97 163 Nb	98 164 Mo	99 165 Tc	100 166 Ru	101 167 Rh	102 168 Pd	103 169 Ag	104 170 Cd	105 171 In	106 172 Sn	107 173 Sb	108 174 Te	109 175 I	110 176 Xe								
79 147 K	80 148 Ca	81 149 Sc	82 150 Ti	83 151 V	84 152 Cr	85 153 Mn	86 154 Fe	87 155 Co	88 156 Ni	89 157 Cu	90 158 Zn	91 159 Ga	92 160 Ge	93 161 As	94 162 Se	95 163 Br	96 164 Kr	97 165 Rb	98 166 Sr	99 167 Y	100 168 Zr	101 169 Nb	102 170 Mo	103 171 Tc	104 172 Ru	105 173 Rh	106 174 Pd	107 175 Ag	108 176 Cd	109 177 In	110 178 Sn	111 179 Sb	112 180 Te	113 181 I	114 182 Xe								
83 153 K	84 154 Ca	85 155 Sc	86 156 Ti	87 157 V	88 158 Cr	89 159 Mn	90 160 Fe	91 161 Co	92 162 Ni	93 163 Cu	94 164 Zn	95 165 Ga	96 166 Ge	97 167 As	98 168 Se	99 169 Br	100 170 Kr	101 171 Rb	102 172 Sr	103 173 Y	104 174 Zr	105 175 Nb	106 176 Mo	107 177 Tc	108 178 Ru	109 179 Rh	110 180 Pd	111 181 Ag	112 182 Cd	113 183 In	114 184 Sn	115 185 Sb	116 186 Te	117 187 I	118 188 Xe								
87 159 K	88 160 Ca	89 161 Sc	90 162 Ti	91 163 V	92 164 Cr	93 165 Mn	94 166 Fe	95 167 Co	96 168 Ni	97 169 Cu	98 170 Zn	99 171 Ga	100 172 Ge	101 173 As	102 174 Se	103 175 Br	104 176 Kr	105 177 Rb	106 178 Sr	107 179 Y	108 180 Zr	109 181 Nb	110 182 Mo	111 183 Tc	112 184 Ru	113 185 Rh	114 186 Pd	115 187 Ag	116 188 Cd	117 189 In	118 190 Sn	119 191 Sb	120 192 Te	121 193 I	122 194 Xe								
91 165 K	92 166 Ca	93 167 Sc	94 168 Ti	95 169 V	96 170 Cr	97 171 Mn	98 172 Fe	99 173 Co	100 174 Ni	101 175 Cu	102 176 Zn	103 177 Ga	104 178 Ge	105 179 As	106 180 Se	107 181 Br	108 182 Kr	109 183 Rb	110 184 Sr	111 185 Y	112 186 Zr	113 187 Nb	114 188 Mo	115 189 Tc	116 190 Ru	117 191 Rh	118 192 Pd	119 193 Ag	120 194 Cd	121 195 In	122 196 Sn	123 197 Sb	124 198 Te	125 199 I	126 200 Xe								
95 171 K	96 172 Ca	97 173 Sc	98 174 Ti	99 175 V	100 176 Cr	101 177 Mn	102 178 Fe	103 179 Co	104 180 Ni	105 181 Cu	106 182 Zn	107 183 Ga	108 184 Ge	109 185 As	110 186 Se	111 187 Br	112 188 Kr	113 189 Rb	114 190 Sr	115 191 Y	116 192 Zr	117 193 Nb	118 194 Mo	119 195 Tc	120 196 Ru	121 197 Rh	122 198 Pd	123 199 Ag	124 200 Cd	125 201 In	126 202 Sn	127 203 Sb	128 204 Te	129 205 I	130 206 Xe								
99 177 K	100 178 Ca	101 179 Sc	102 180 Ti	103 181 V	104 182 Cr	105 183 Mn	106 184 Fe	107 185 Co	108 186 Ni	109 187 Cu	110 188 Zn	111 189 Ga	112 190 Ge	113 191 As	114 192 Se	115 193 Br	116 194 Kr	117 195 Rb	118 196 Sr	119 197 Y	120 198 Zr	121 199 Nb	122 200 Mo	123 201 Tc	124 202 Ru	125 203 Rh	126 204 Pd	127 205 Ag	128 206 Cd	129 207 In	130 208 Sn	131 209 Sb	132 210 Te	133 211 I	134 212 Xe								
103 183 K	104 184 Ca	105 185 Sc	106 186 Ti	107 187 V	108 188 Cr	109 189 Mn	110 190 Fe	111 191 Co	112 192 Ni	113 193 Cu	114 194 Zn	115 195 Ga	116 196 Ge	117 197 As	118 198 Se	119 199 Br	120 200 Kr	121 201 Rb	122 202 Sr	123 203 Y	124 204 Zr	125 205 Nb	126 206 Mo	127 207 Tc	128 208 Ru	129 209 Rh	130 210 Pd	131 211 Ag	132 212 Cd	133 213 In	134 214 Sn	135 215 Sb	136 216 Te	137 217 I	138 218 Xe								
107 189 K	108 190 Ca	109 191 Sc	110 192 Ti	111 193 V	112 194 Cr																																						

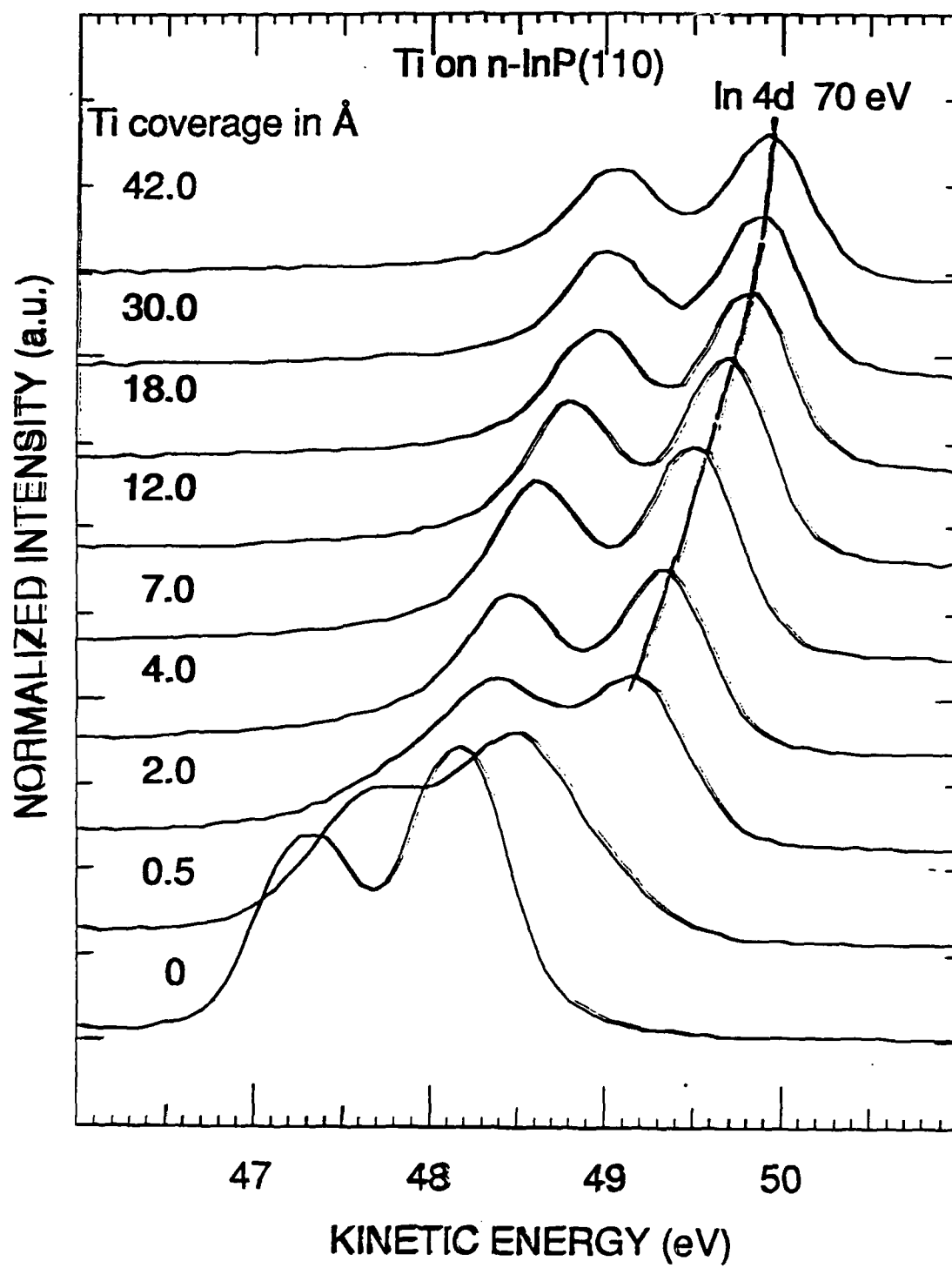
## **Description of chemical reactions at the M/InP interfaces**

- 1. 3d transition metals (Ti, V, Cr, Mn, Co, Ni)- strongly reactive, multiphase reactions, uniform overlayers (no clustering).**
- 2. Near noble metals (Ni, Pd, Pt)- strength of the reaction decreases in the sequence Ni-Pd-Pt, clustering for Pt.**
- 3. Noble metals - much less reactive than transition metals. Reaction switches from mostly M-P for Cu to mostly M-In for Au. Ag- one of the least reactive metals.**
- 4. Column III simple metals (Al, Ga, In, Tl)- Limited exchange reaction for Al and Ga, with exception of Tl tendency to cluster.**
- 5. Column IV elements (Si, Ge, Sn)- Considerably less reactive than transition metals or Al. However, some outdiffusion of substrate species clearly observed. Typically form uniform overlayers (no clustering).**









## **General trends in reactivity (comparison with GaAs and Si)**

1. All metals studied react with the InP surface. A truly nonreactive and sharp interface was not found. Ag closest to ideal.

### **2. In reactions**

In is diluted into the overlayer. The changing stoichiometry of the alloy is reflected in the binding energy shifts of the In 4d core level. Trends in data understood in terms of the model calculations using Born-Haber cycle and heats of solution from Miedema.

Similar behavior as for M/GaAs interfaces.

### **3. P reactions**

P is involved in single (Ni) or multiphase (Pd,Ti) reactions. Binding energies of these phases are constant through the interface evolution indicating well defined reaction products.

Similar behavior as for M/GaAs interfaces.

4. There seems to be no indication for ternary reaction products.

5. For strongly reactive interfaces P containing phases are trapped at the interface and In strongly outdiffuses (In signal often detected for overlayers thicker than 100Å).

Opposite trend observed for M/GaAs interfaces. The differences may be related to larger heats of compound formation for phosphides.

6. Trends in reactions are remarkably similar to those detected for M/Si interfaces with P playing the role of Si in the reaction



products and In segregating out. This observation seems to be true (to some extent) for M/GaAs interfaces.

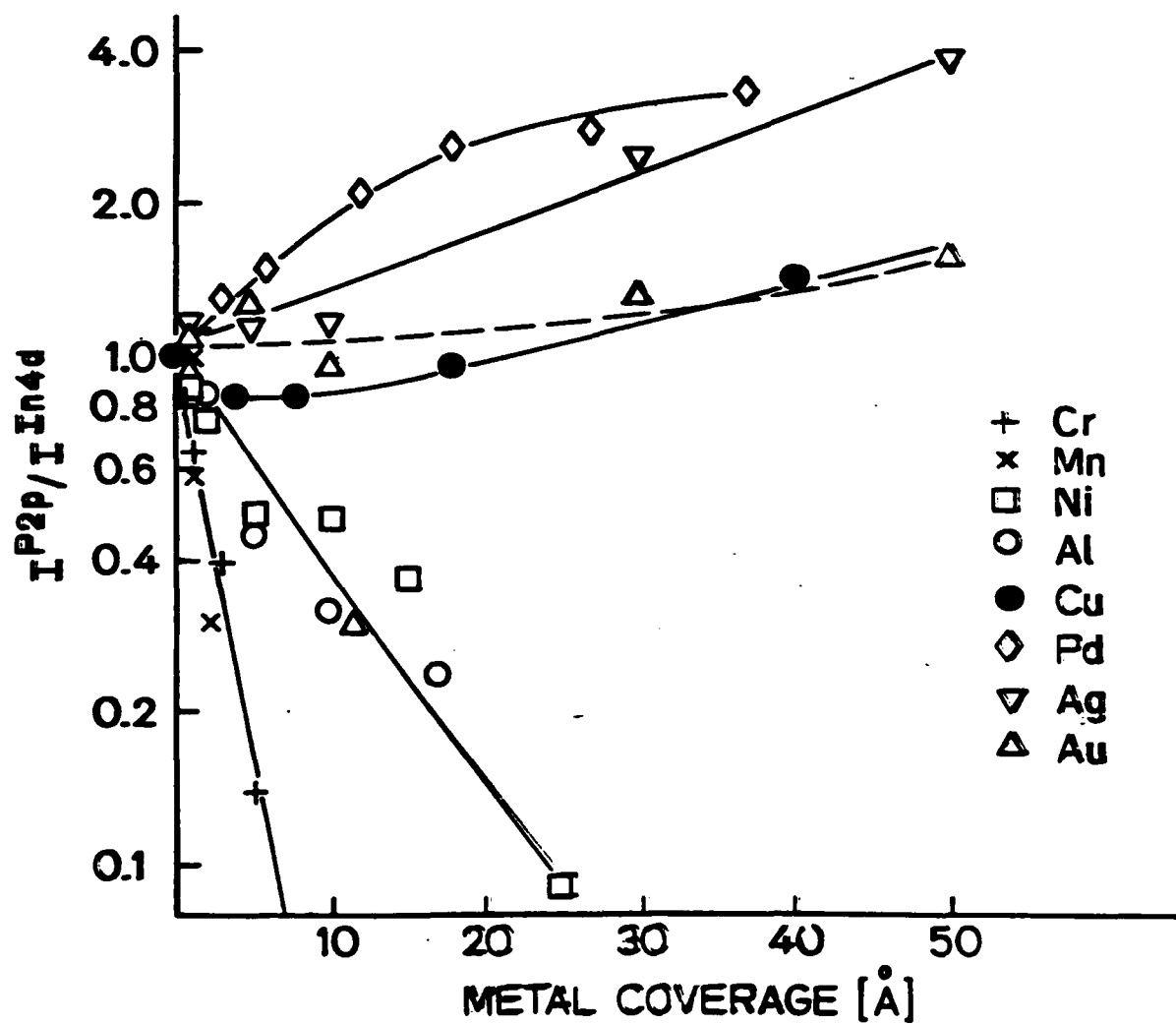
7. The data pin point the important role played by unfilled d shells in the interfacial reactions. The metals with unfilled d-shells react particularly strongly with InP (p-d hybridization).

8. Bulk thermodynamics is quite useful in predicting or accounting for interfacial reactions. However, at RT the interfaces are not in equilibrium and kinetics has to be considered.

# INTIMATE SCHOTTKY BARRIERS ON CLEAVED n-InP(110)

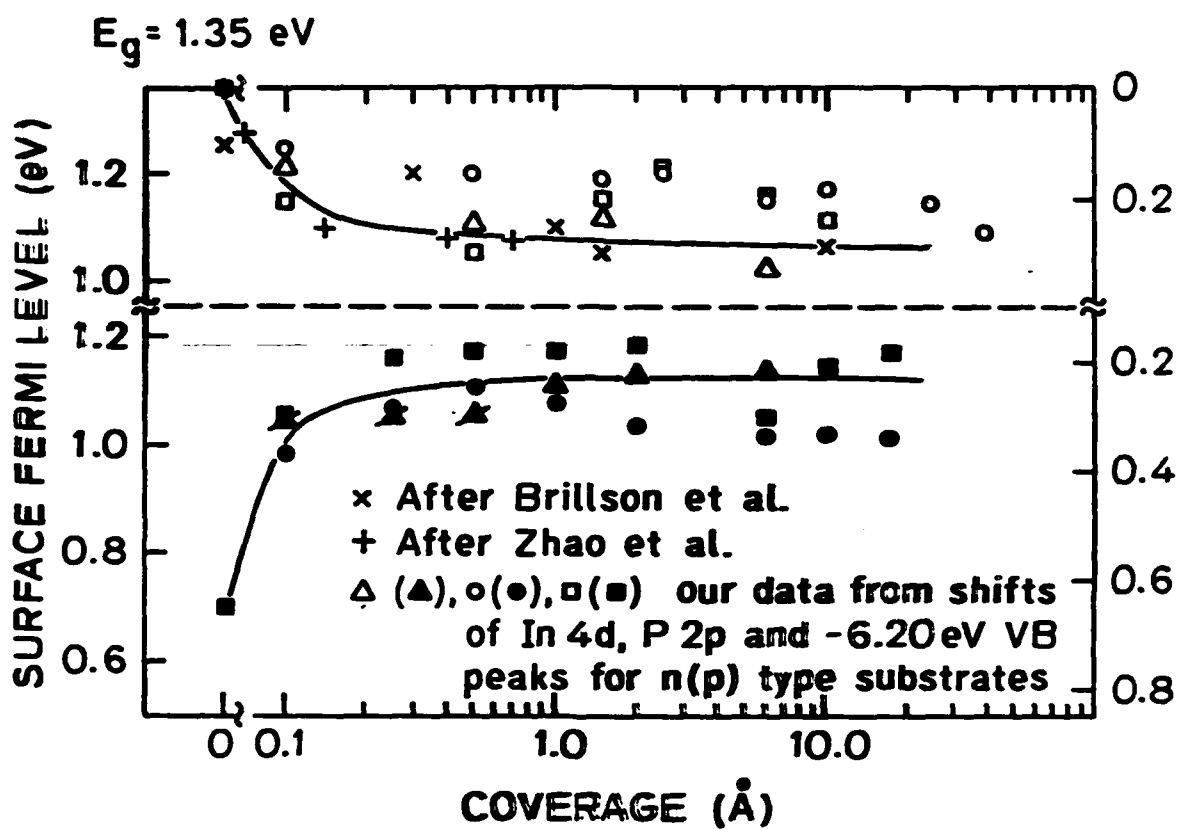
Metal	I-V Measurements		Fermi Level Pinning from PES*	
	Our Data Barrier Height (eV)	Ideality Factor	Our Data $\pm 0.1\text{eV}$	Brillson et al.
Ag	0.54	$1.02 \pm 0.02$	0.45	0.45
Cr	0.45	$1.10 \pm 0.10$	$> 0.40$	-
Cu	0.42	$1.03 \pm 0.05$	0.65	0.70
Au	0.42	$1.03 \pm 0.03$	0.40	0.40
Pd	0.41	$1.03 \pm 0.07$	0.40	0.30
Mn	0.35	$1.1 \pm 0.3$	0.40	-
Sn	0.35	$1.04 \pm 0.15$	0.30	-
Al	0.33	$1.0 \pm 0.4$	0.30	0.30
Ni	0.32	$1.0 \pm 0.3$	0.30	0.20

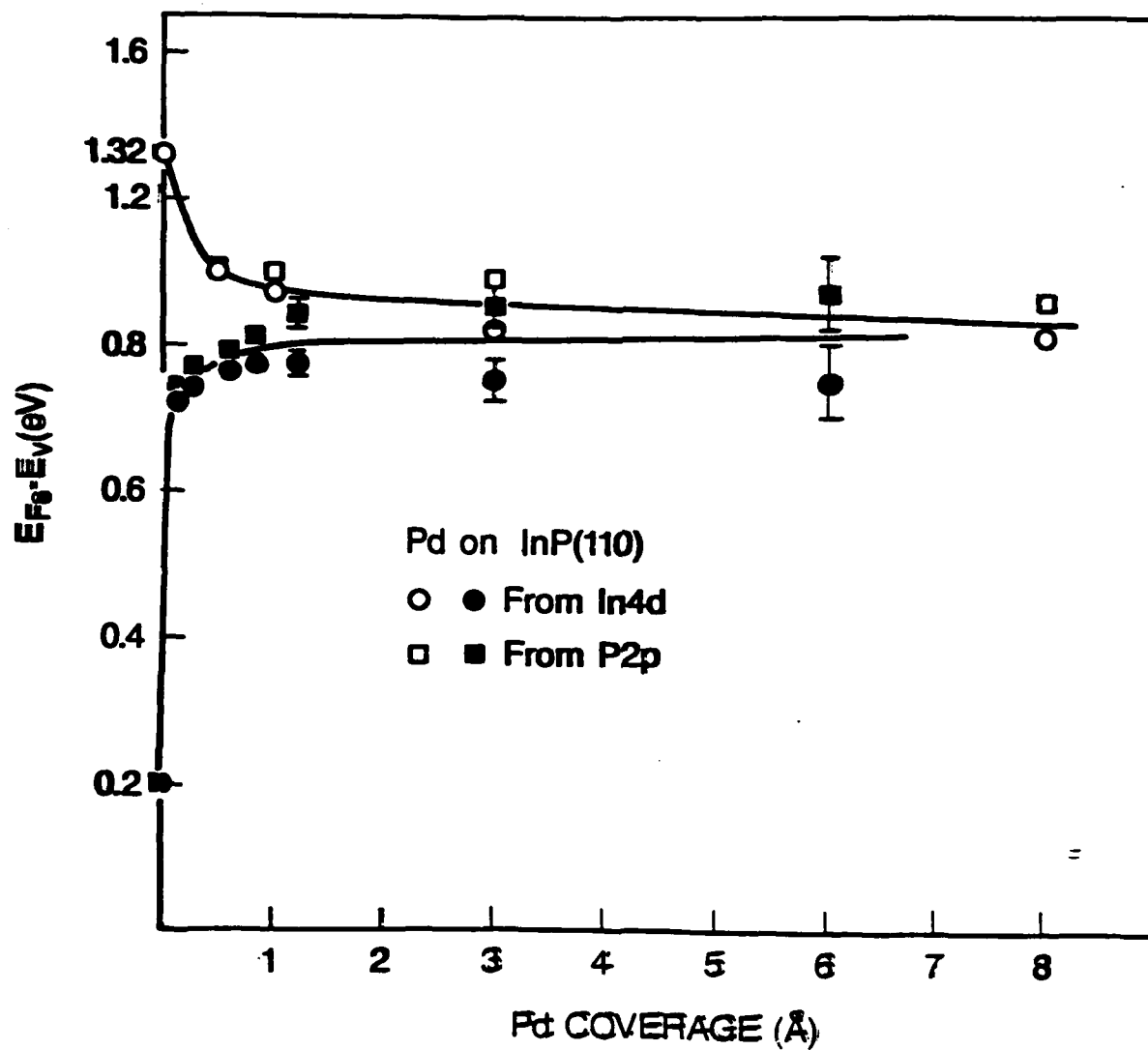
\*Pinning established from original data for coverages below  $10\text{\AA}$



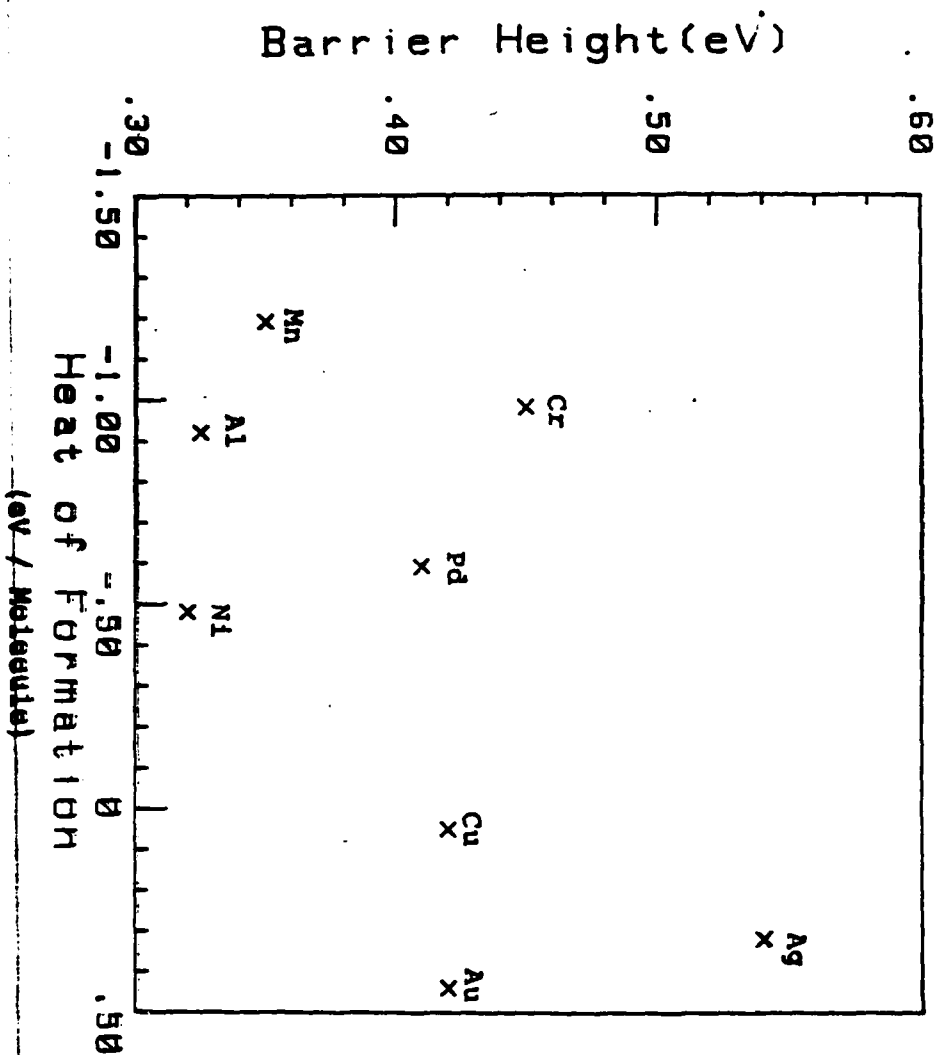
## **Band bending**

- 1. Fermi level is pinned very rapidly. In the extreme case of transition metals, only a small fraction of a monolayer is necessary to complete the band bending.**
- 2. Pinning level is independent on the type of doping (including ex. Al overlayers).**
- 3. Pinning in the submonolayer coverage range agrees very well with barrier heights for diodes measured with I-V.**
- 4. Barrier heights for all metals studied are between 0.3 and 0.6 eV (n-type) and certainly DO NOT correlate with chemistry. There seems to be some dependence on electronegativity (work function). This point is in disagreement with older studies which suggested possible correlation with reactivity.**
- 5. Trends for InP and GaAs are very similar which indicates similar basic mechanisms.**





# INP I-V



**STABLE PHASES AT** **REACTIVE METAL**  
-----  
**COMPOUND SEMICONDUCTOR** **INTERFACES**

**T. Sands**  
**Bell Communications Research, Inc.**

**Contributors:**

**V. G. Keramidas and C. C. Chang**  
**Bellcore**

**J. Ding, K-M. Yu, J. Washburn, K. Krishnan and R. Gronsky**  
**LBL**

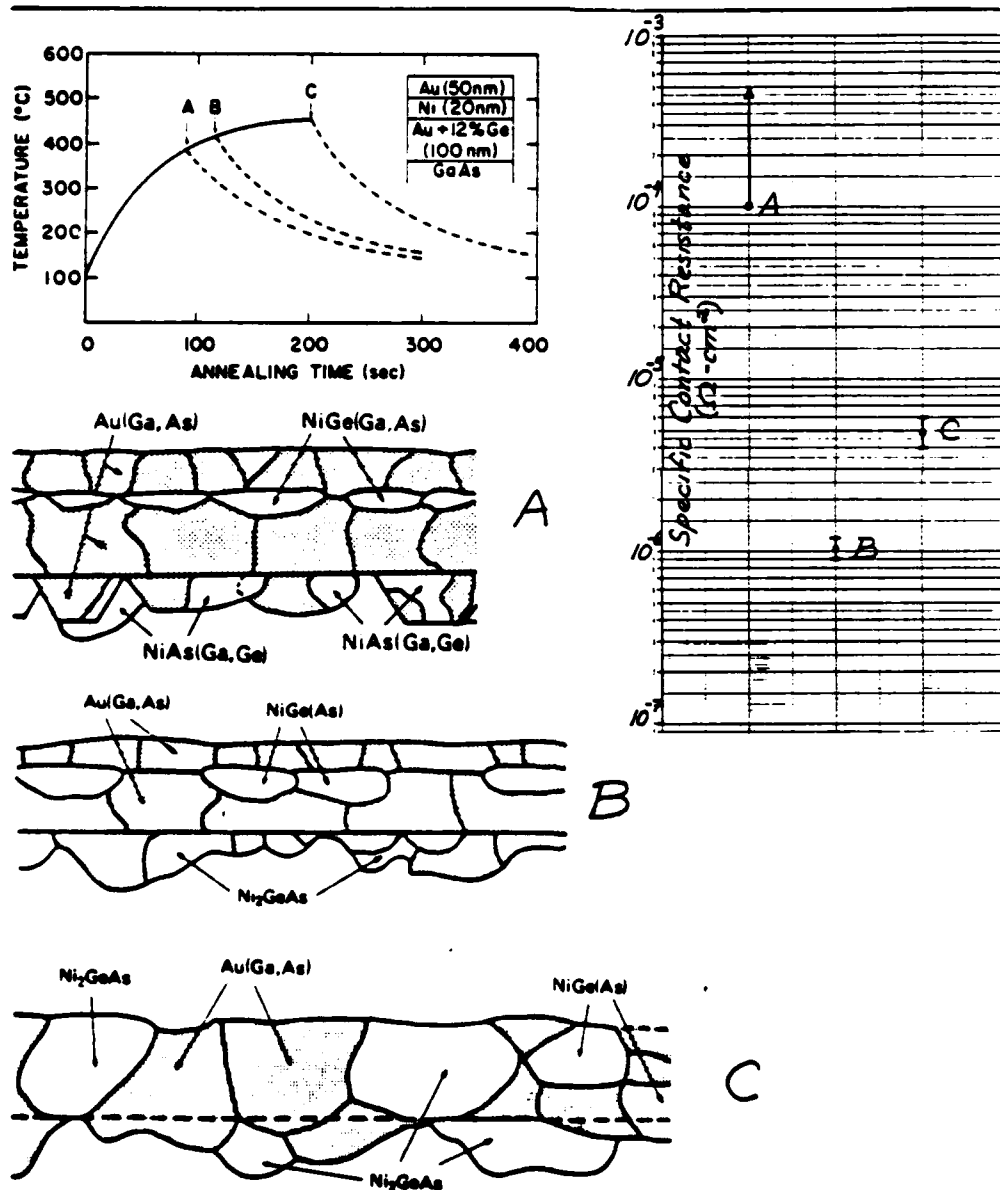
**A. J. Yu**  
**Cornell**



- o **Motivation for M/AB studies**
- o **Application of bulk equilibrium M-A-B phase diagrams to M/AB reactions:**
  - o **In/GaAs, a "success"**
  - o **Pd/GaAs, a "failure"**
- o **An example of uncharted territory:  
the Ni/InP reaction**
- o **Conclusions**

# Electron microscope studies of an alloyed Au/Ni/Au-Ge ohmic contact to GaAs JAP 54 (1983) 6952

T. S. Kuan, P. E. Batson, T. N. Jackson, H. Rupprecht, and E. L. Wilkie  
IBM Thomas J. Watson Research Center, Yorktown Heights, New York 10598



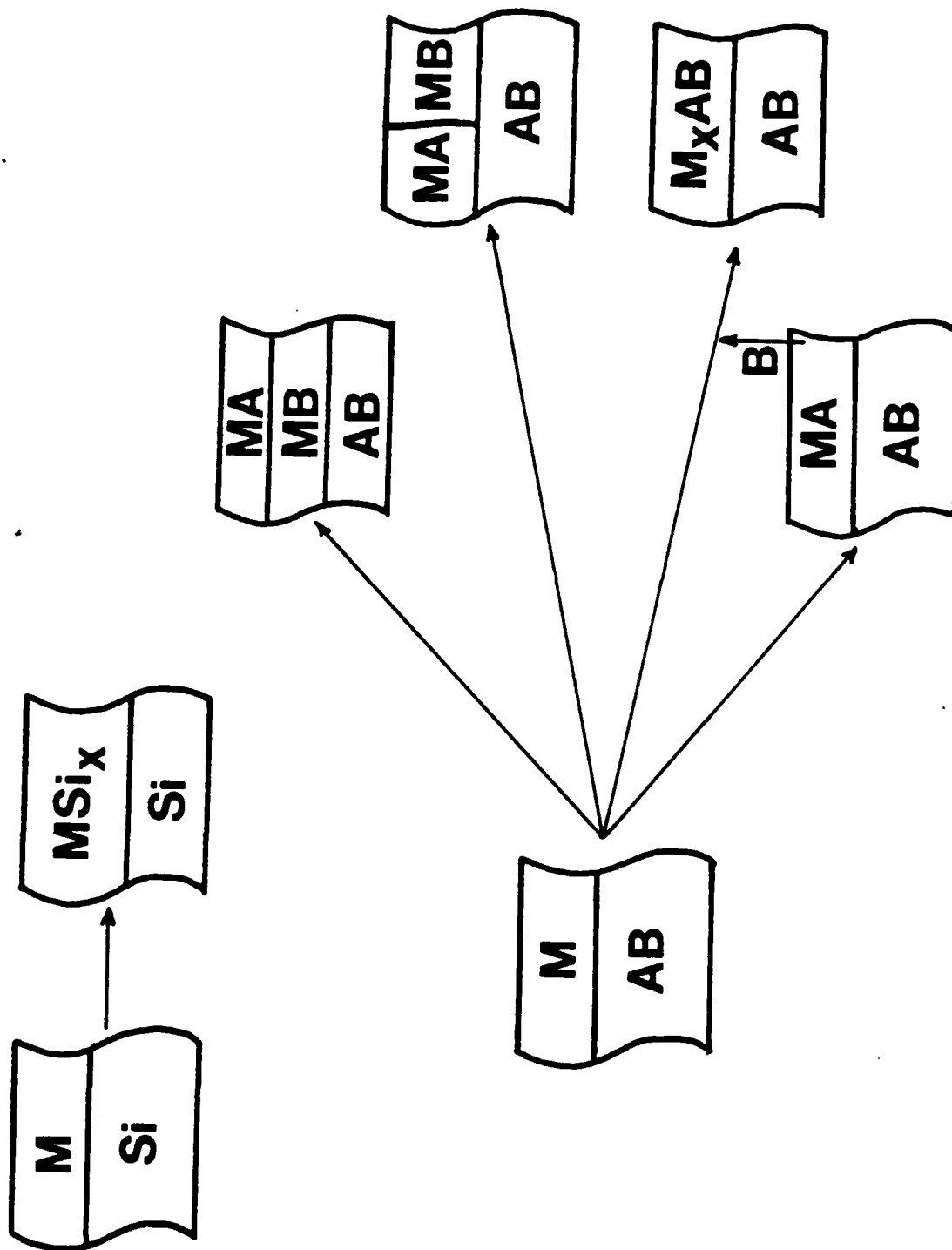
### **Why study M/AB reactions?**

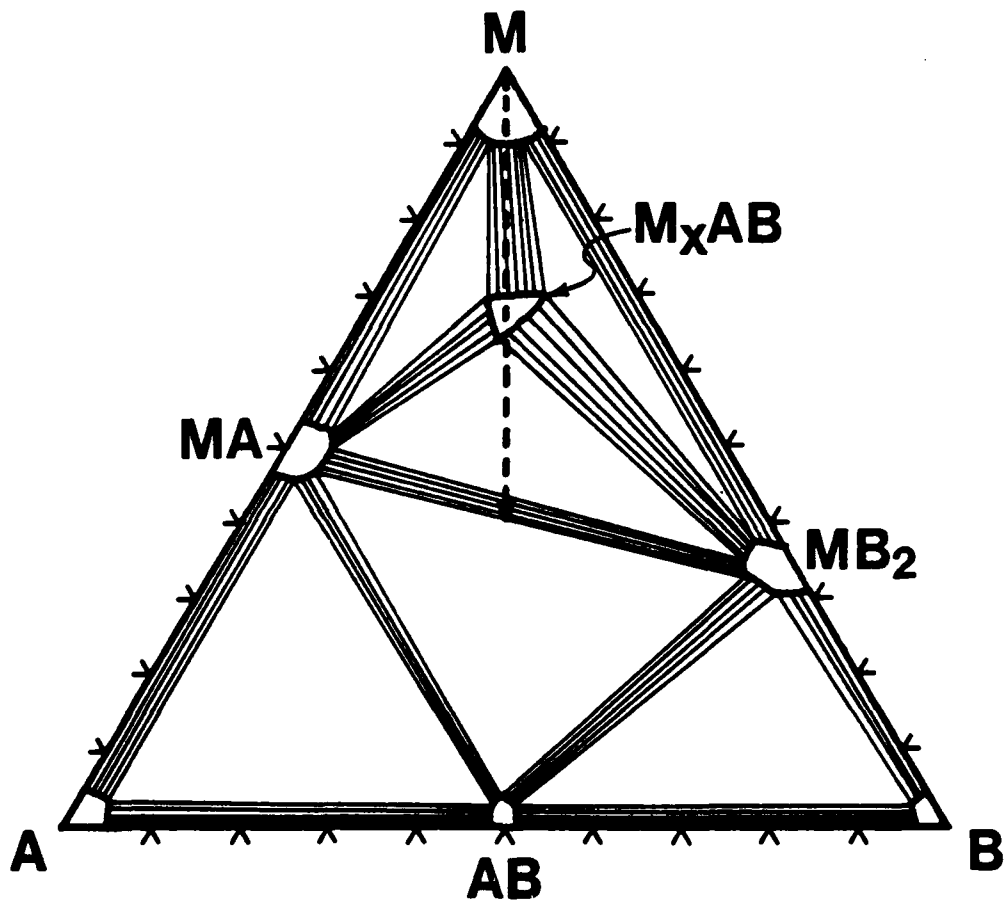
- Au-Ni-Ge/n-GaAs:**
- o low  $r_c$  but**
  - o difficult to reproduce**
  - o not stable at moderate T**
  - o lacks submicron lateral uniformity**

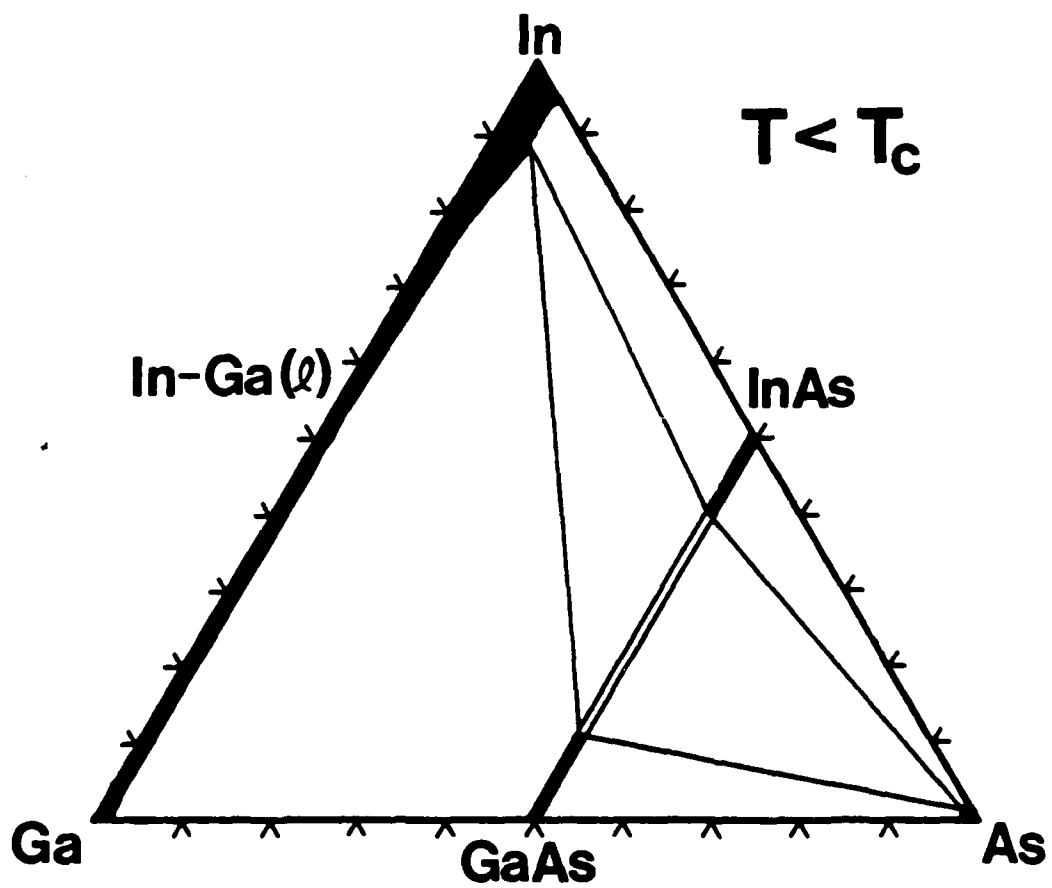
**Design of contact metallizations which are compatible with future device requirements will require at least a rudimentary understanding of phase stability in M-A-B systems.**

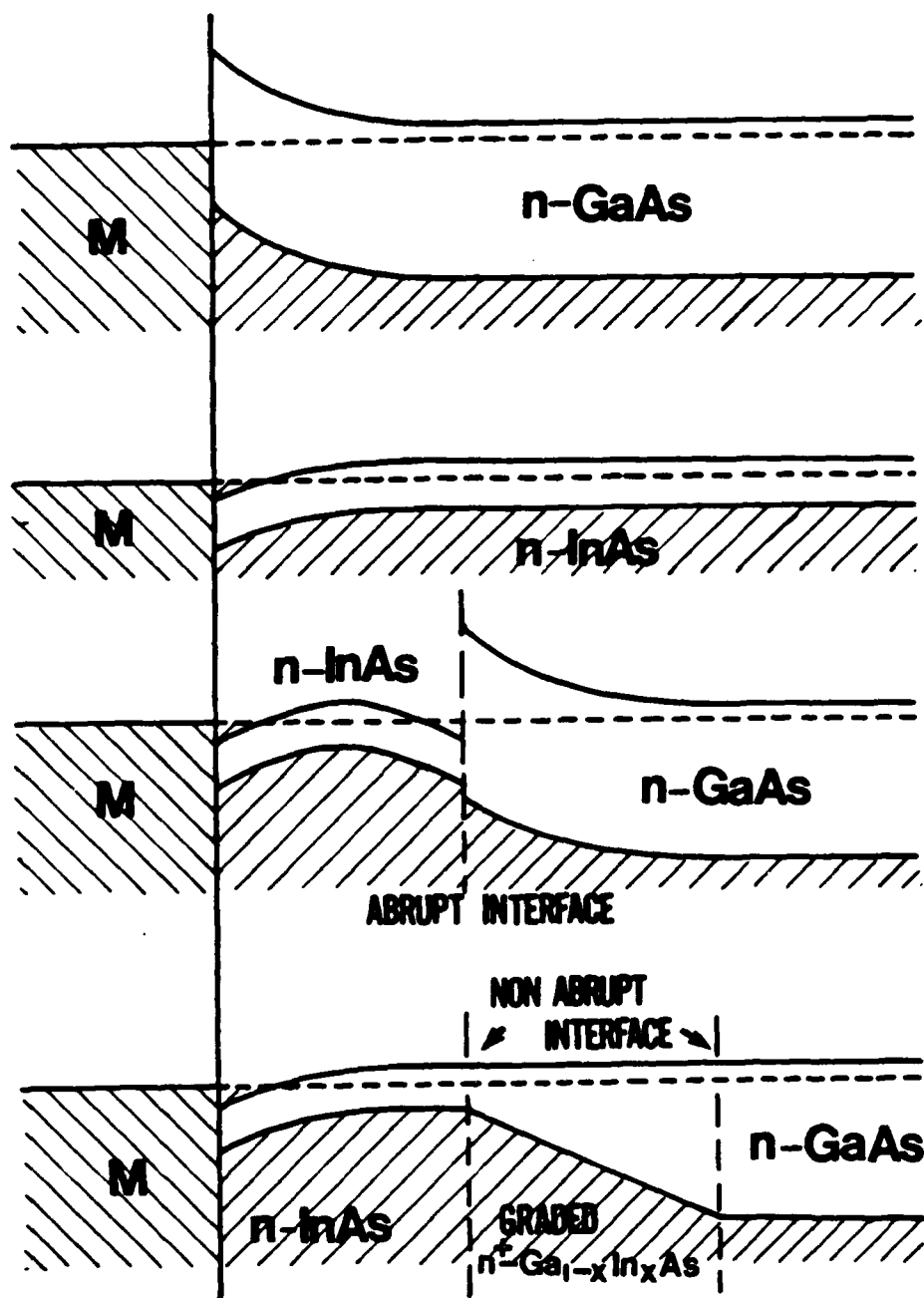
**"If it ain't broke don't fix it ..."**

**... but if you know it's gonna break tomorrow, you better have your tools in your back pocket.**





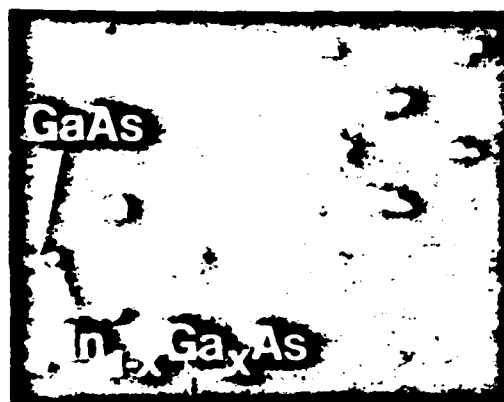
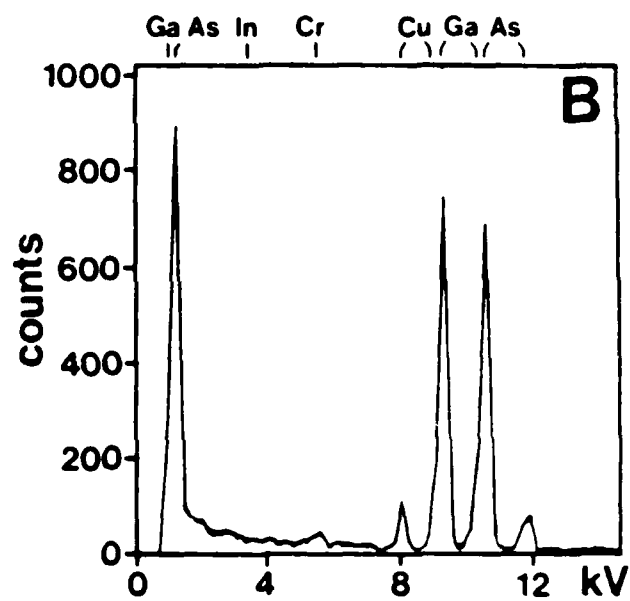
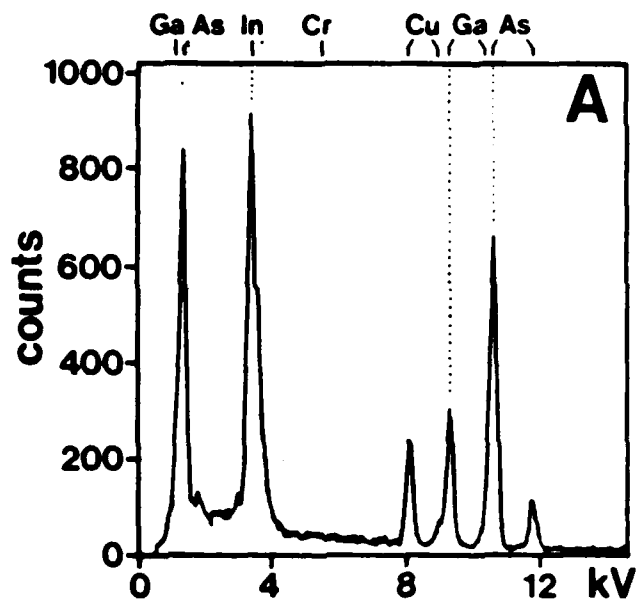




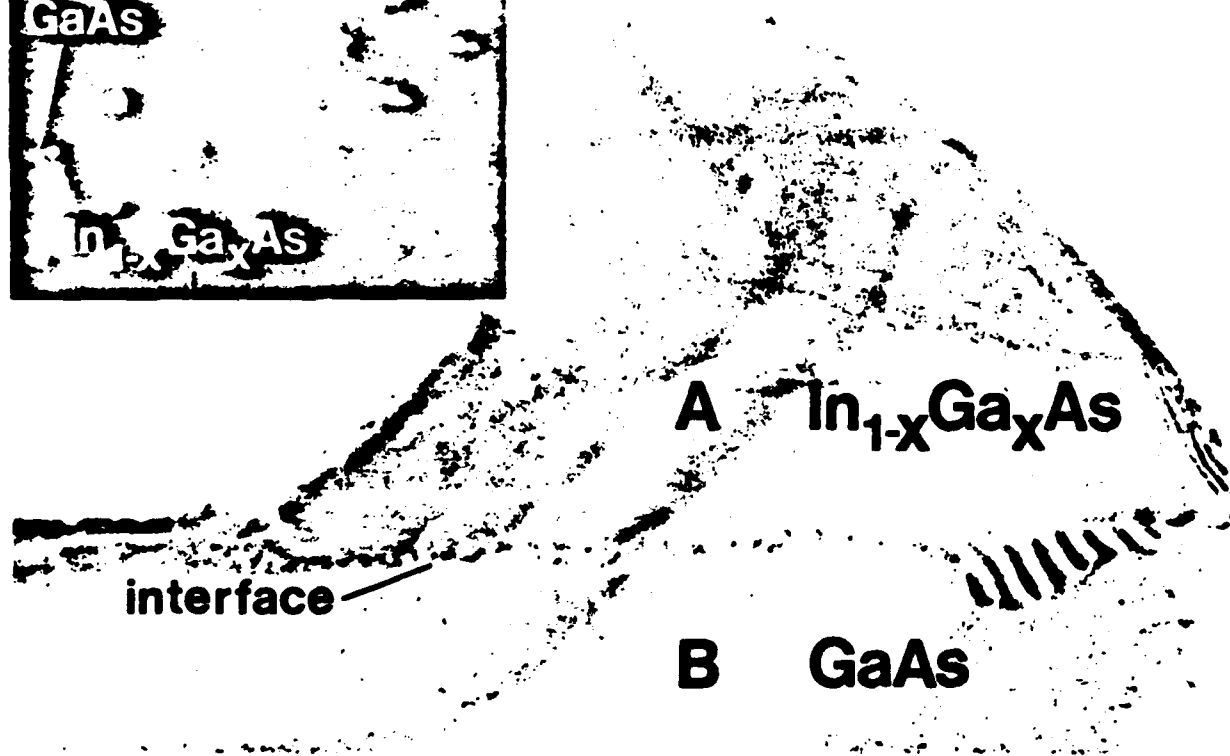
Woodall et al. JVST 1981 XBL 864-1319

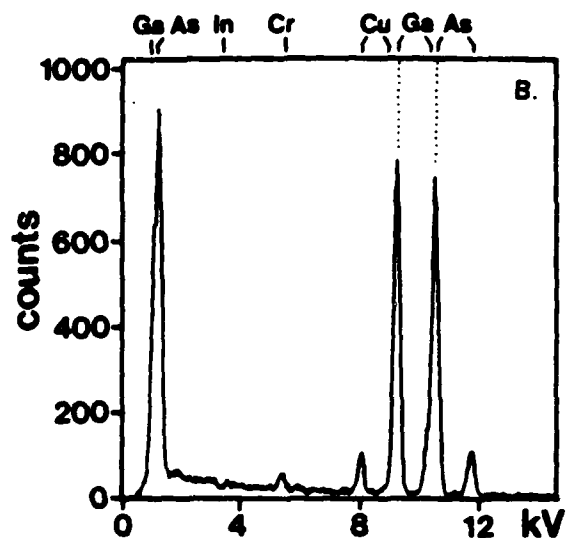
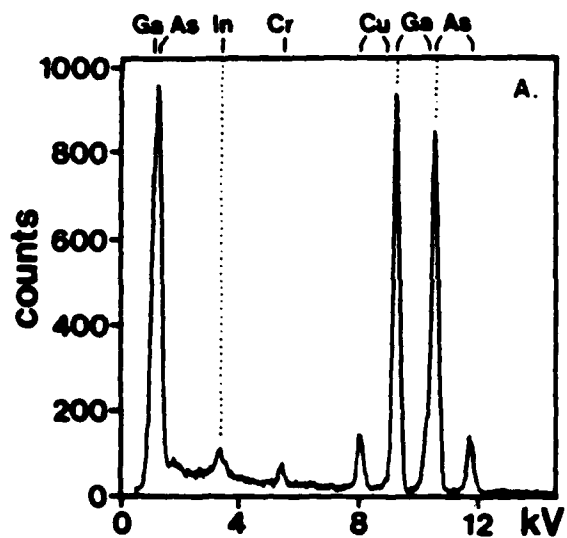




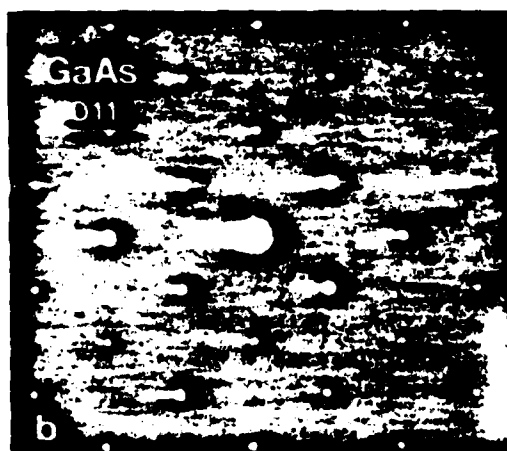


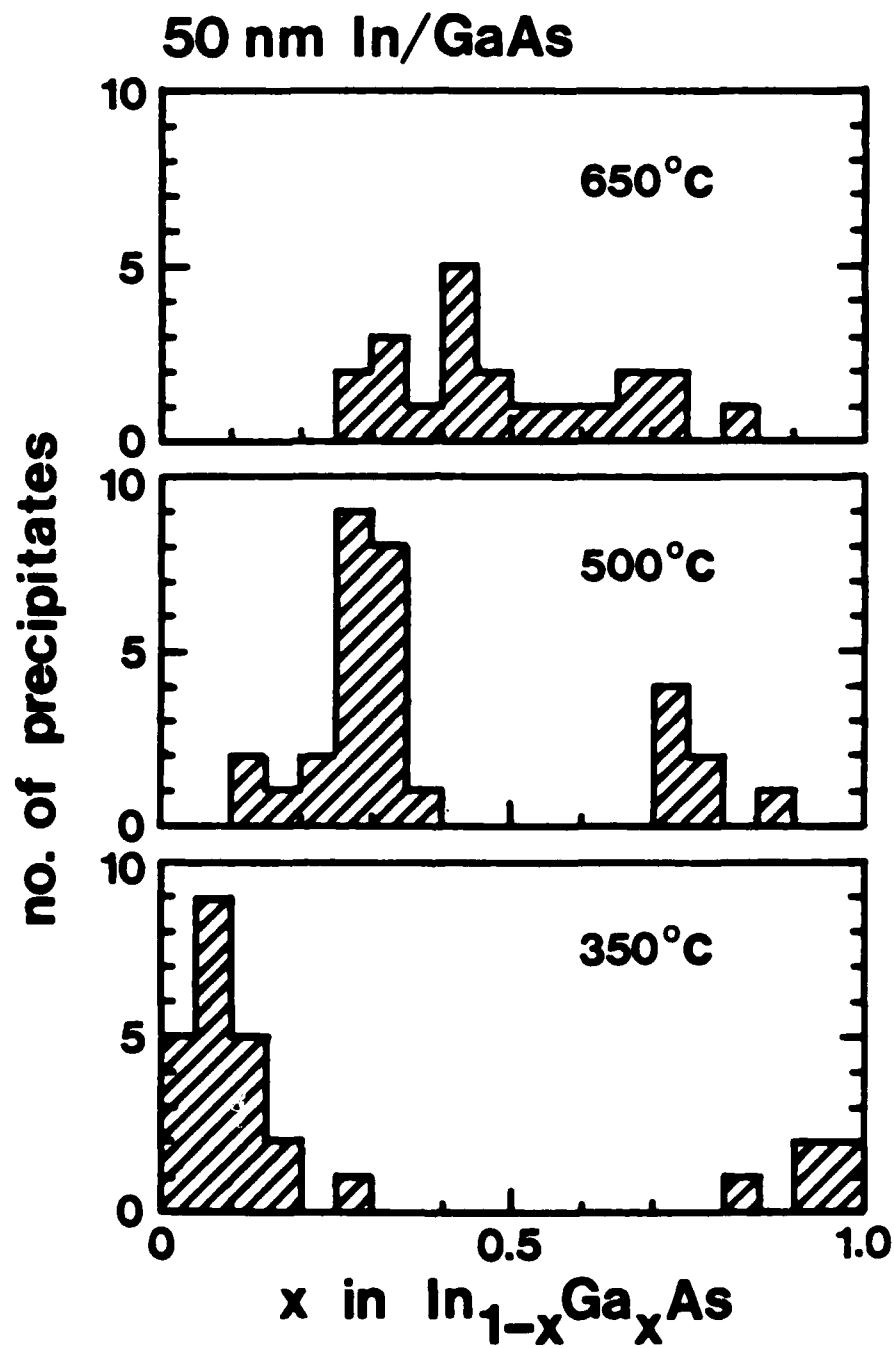
50 nm



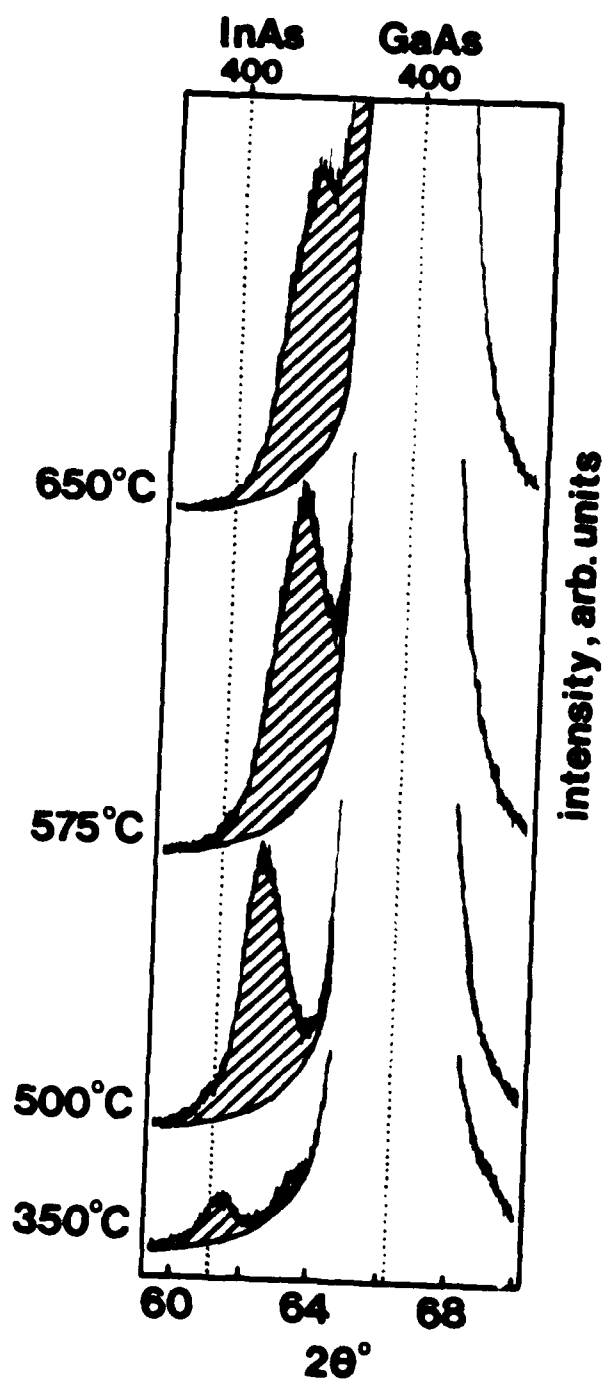


NO/A

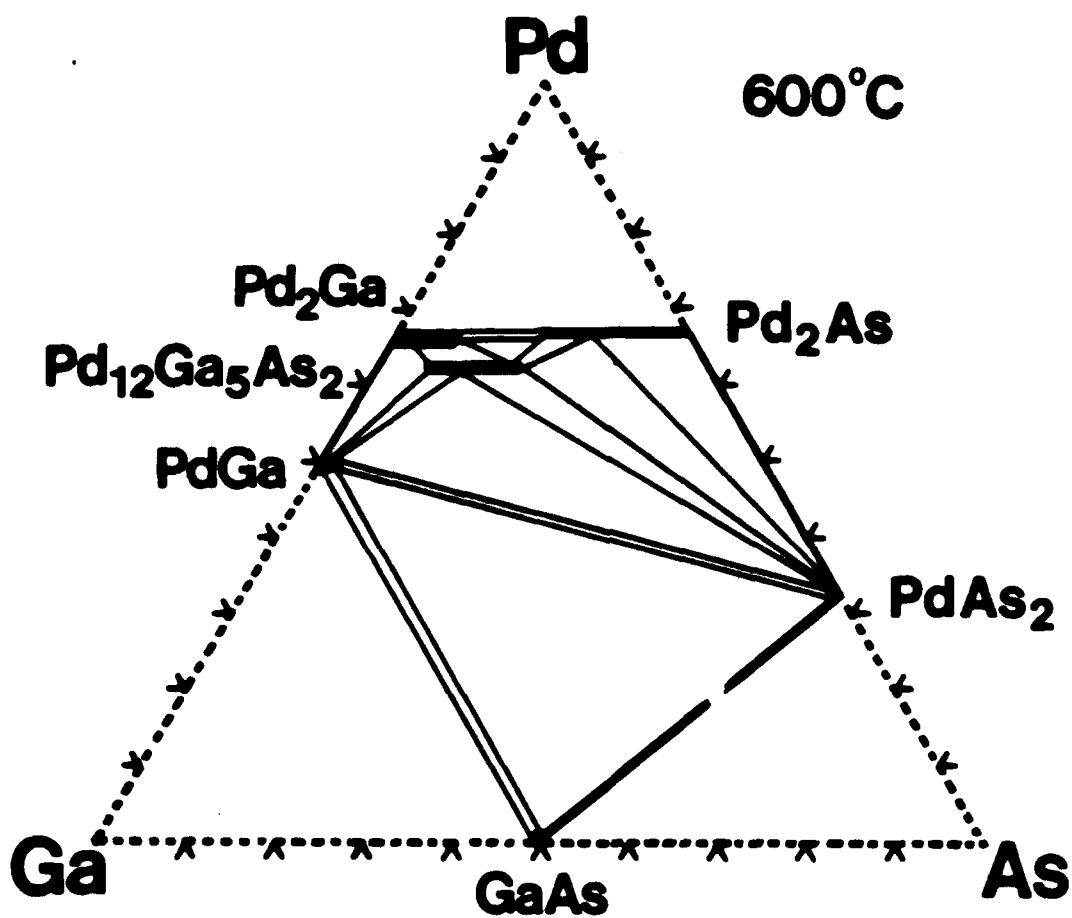




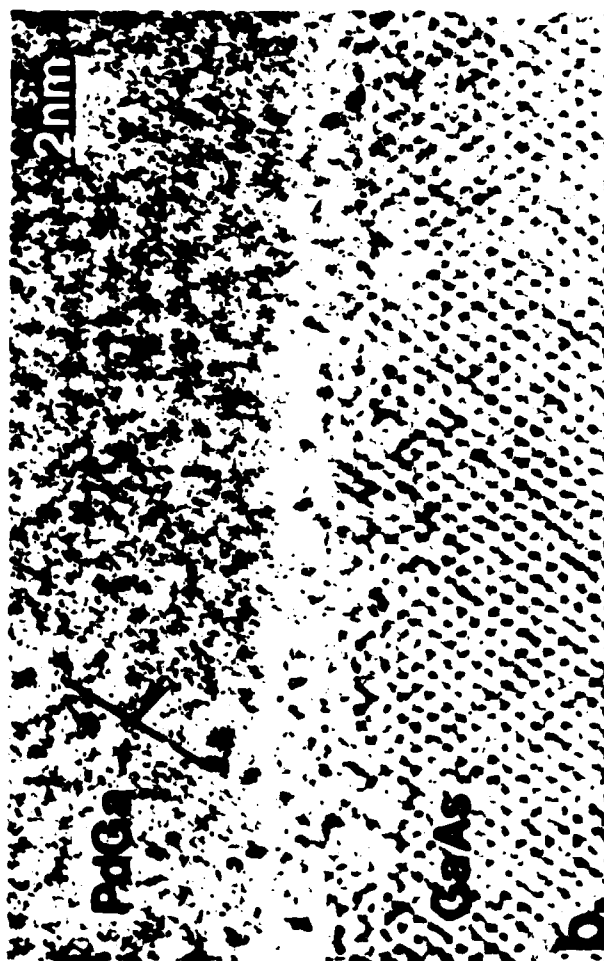
XBL 868-3109

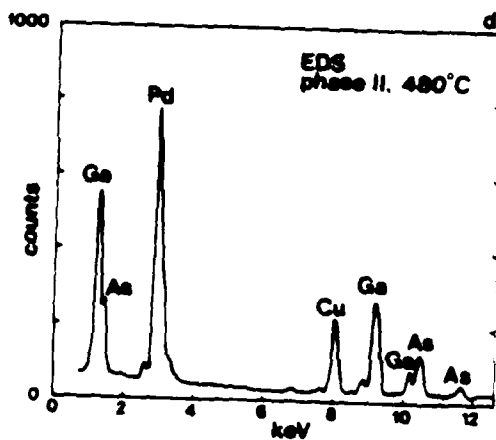
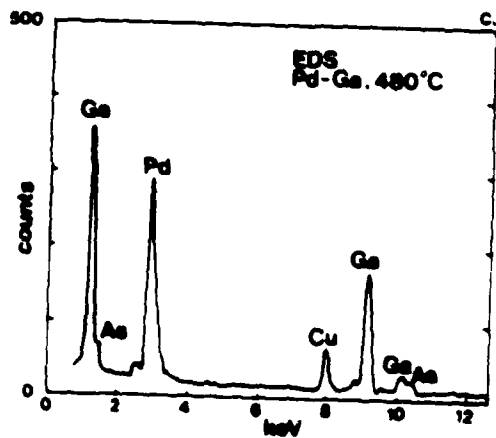
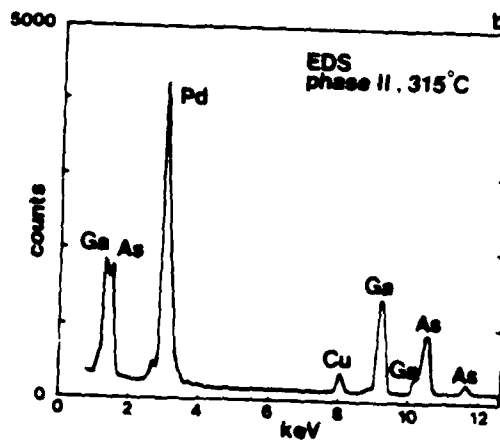
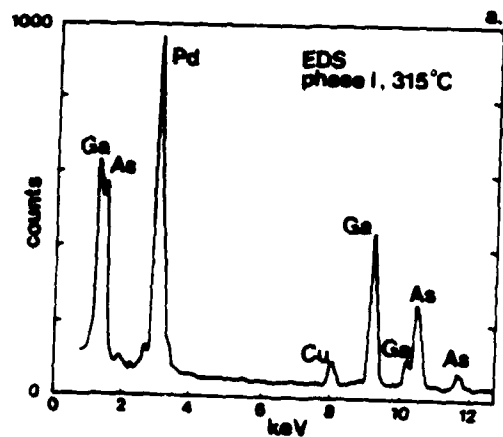


XBL 869-3272



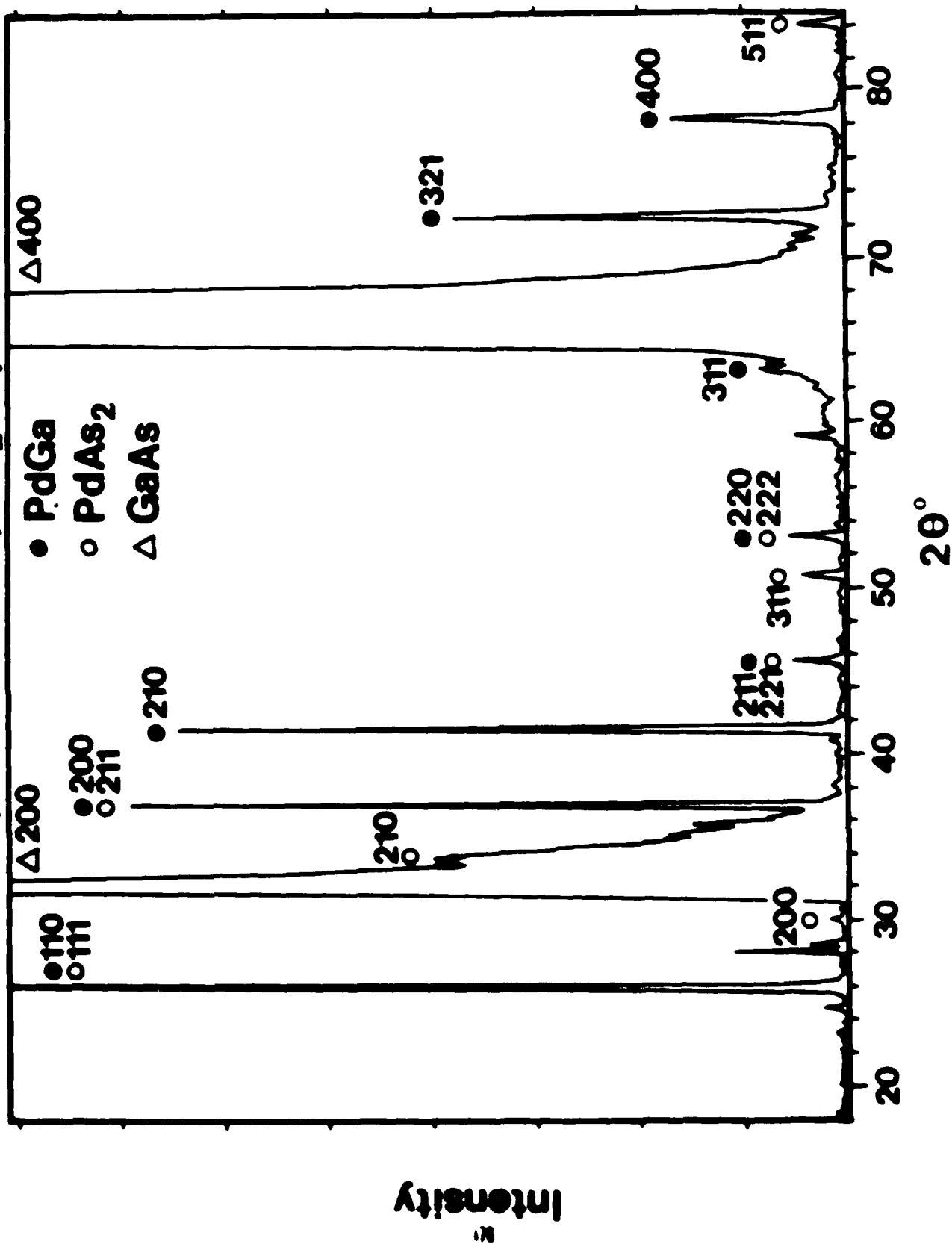
El-Boragy & Schubert, Z.Metall., 1981

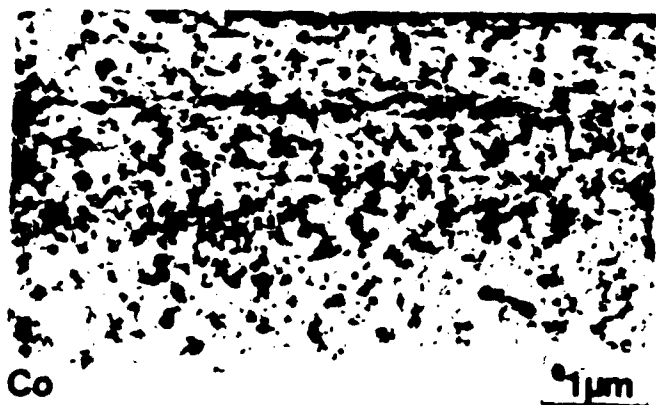




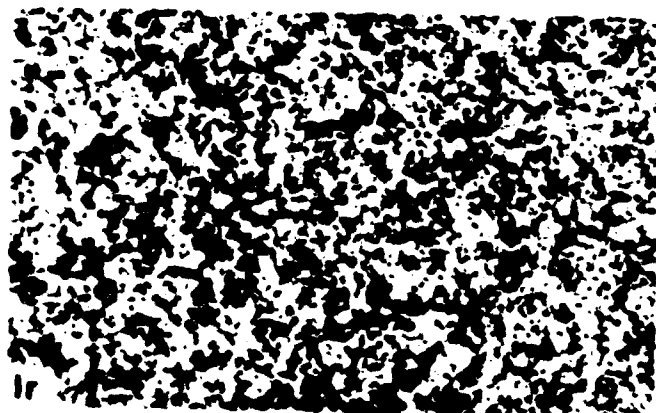
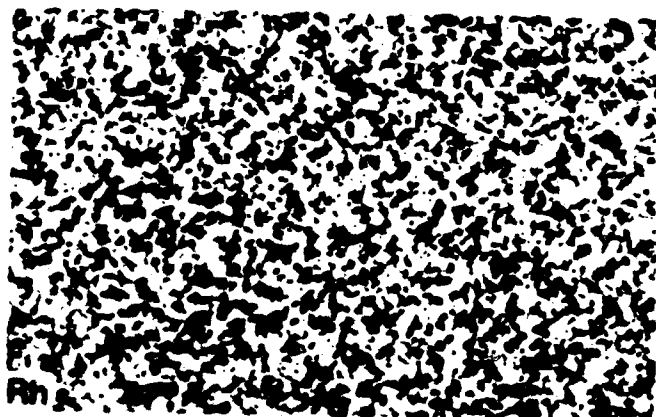
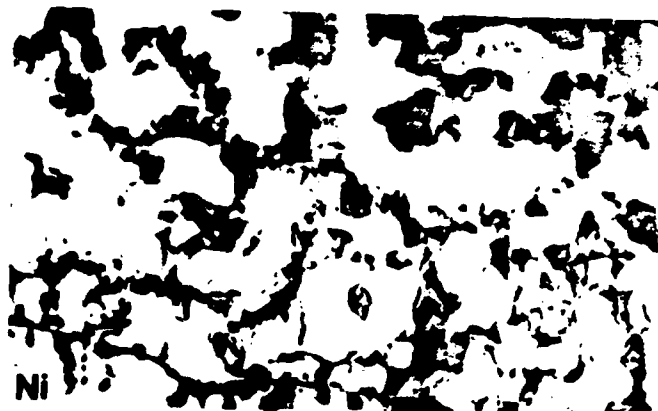


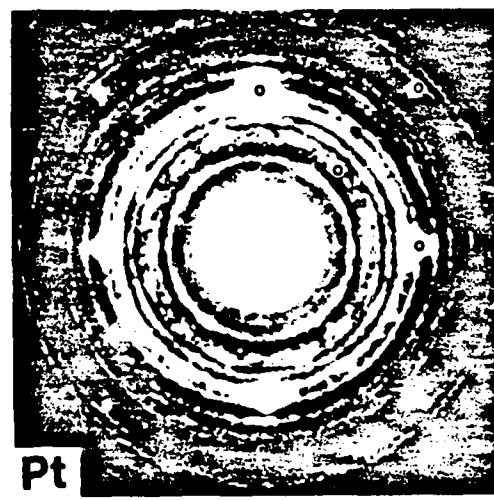
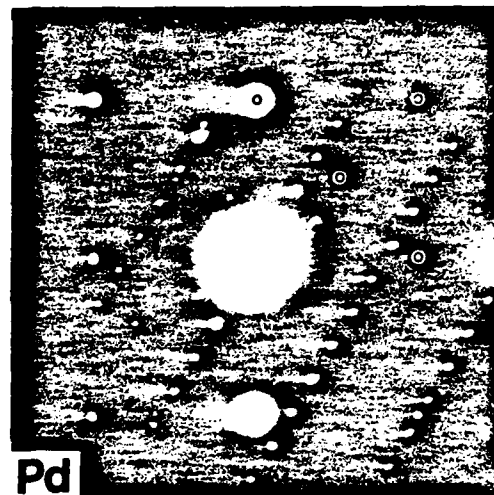
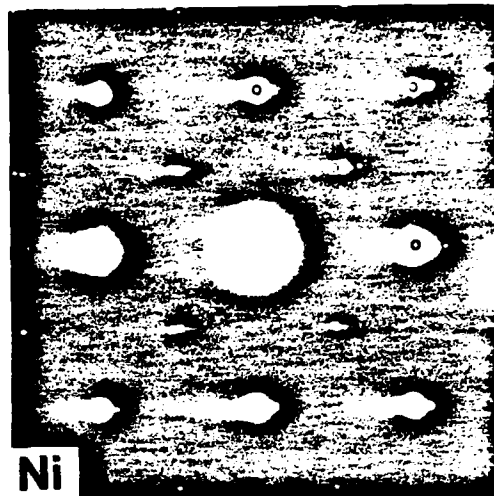
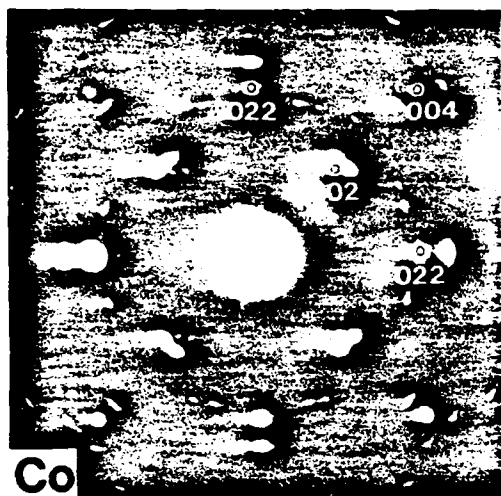
# 60 nm Pd/GaAs, 500°C, 10 min, SiO<sub>2</sub> cap

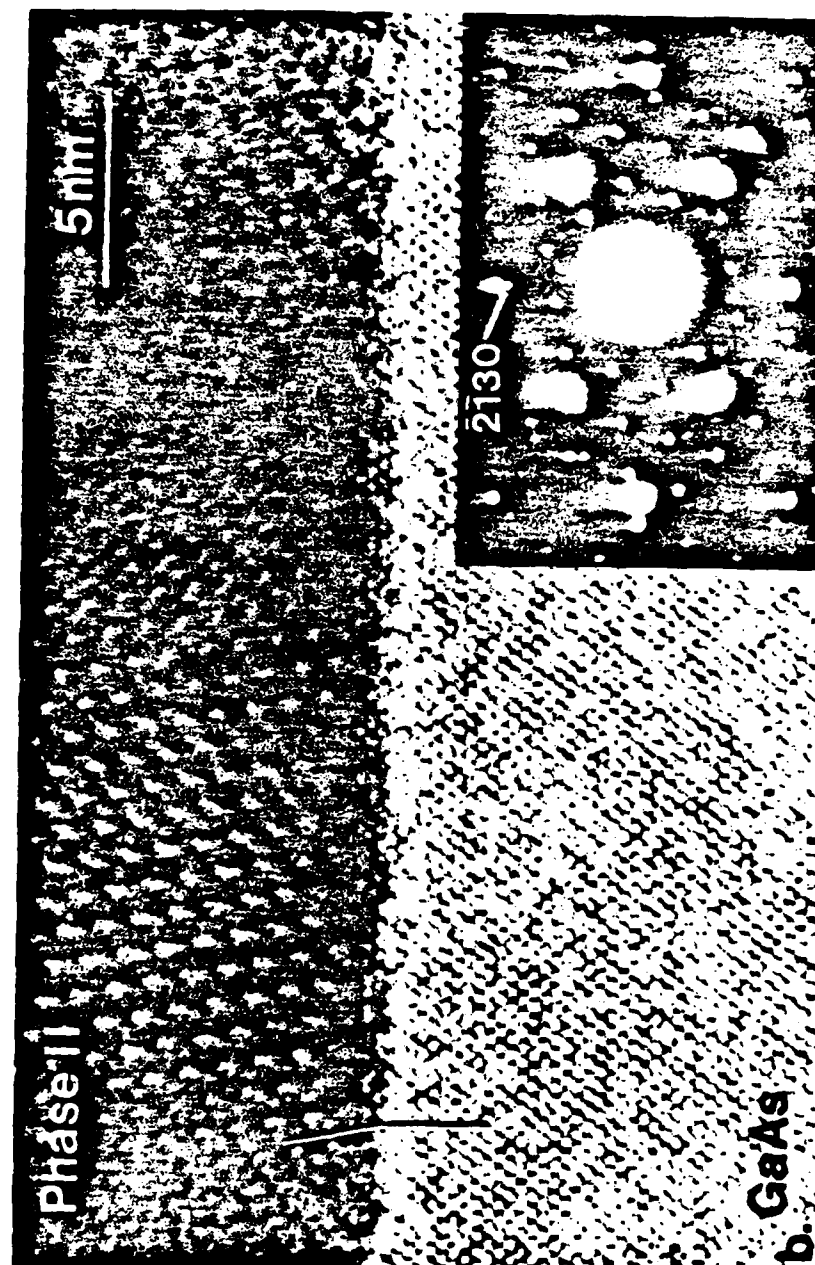


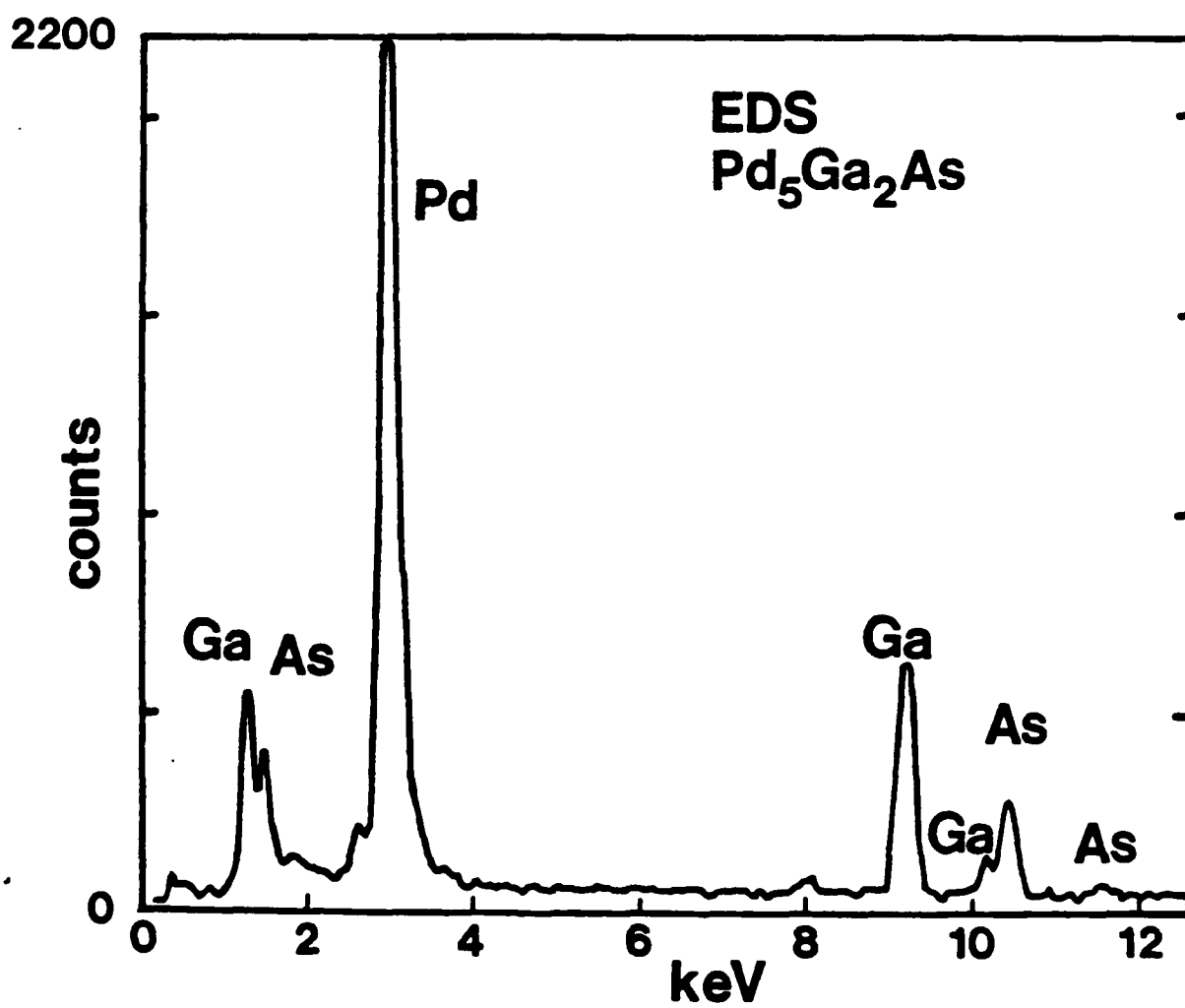


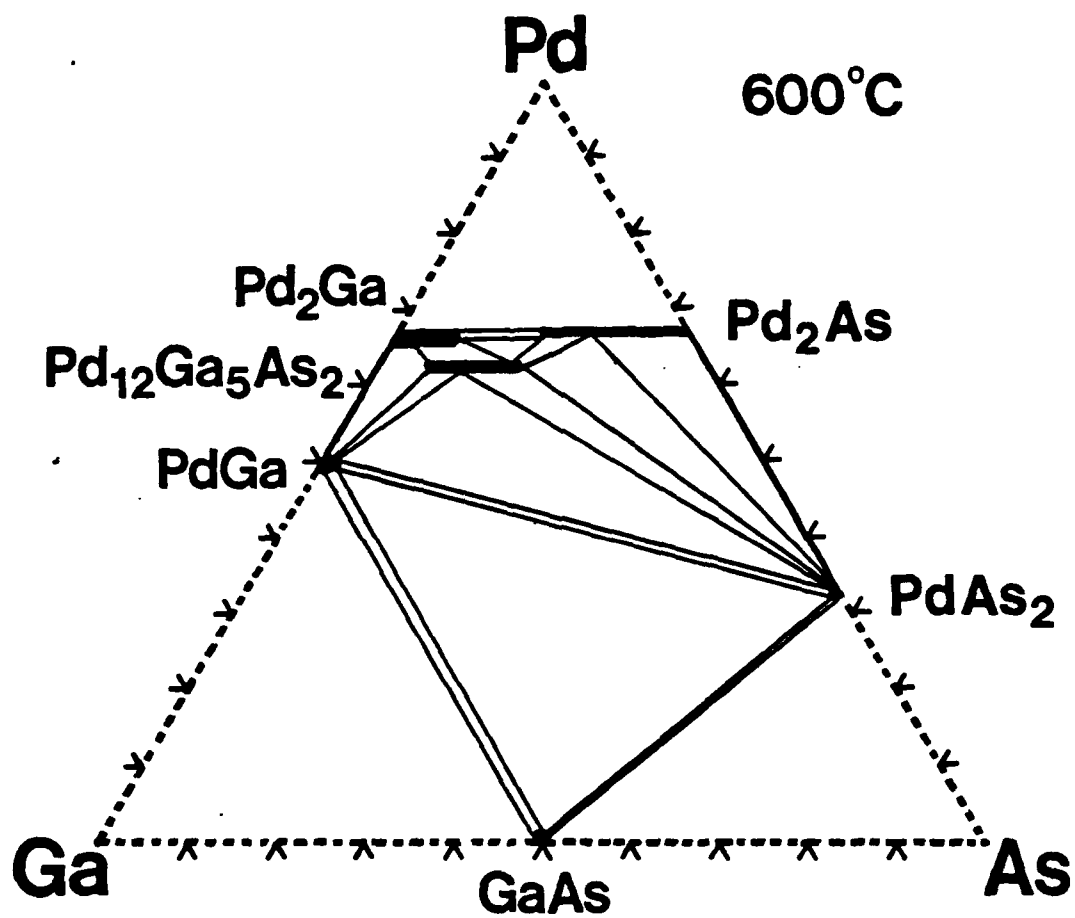
1μm



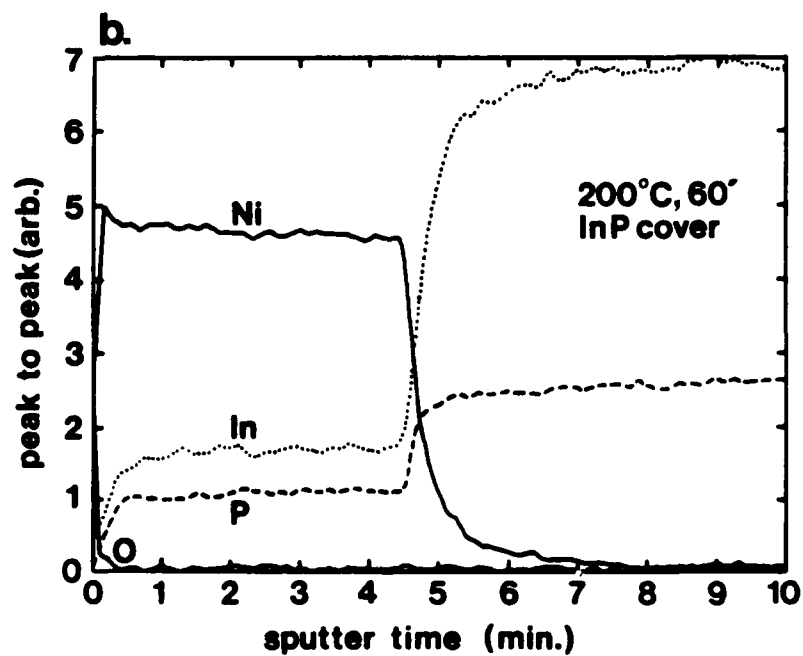
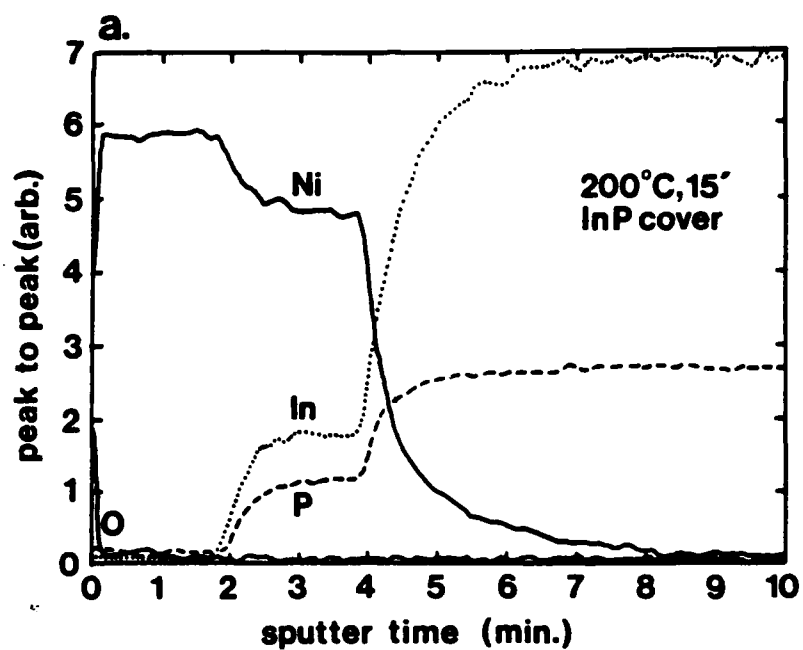




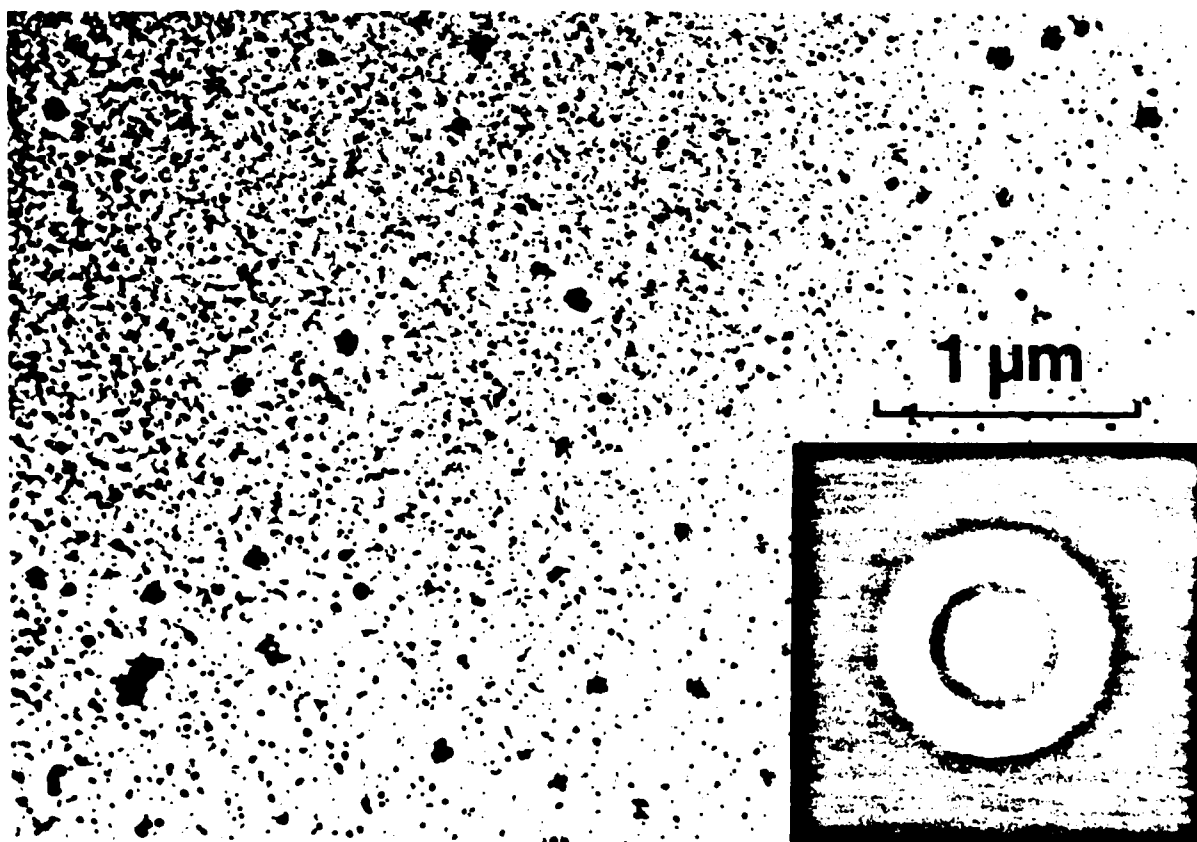
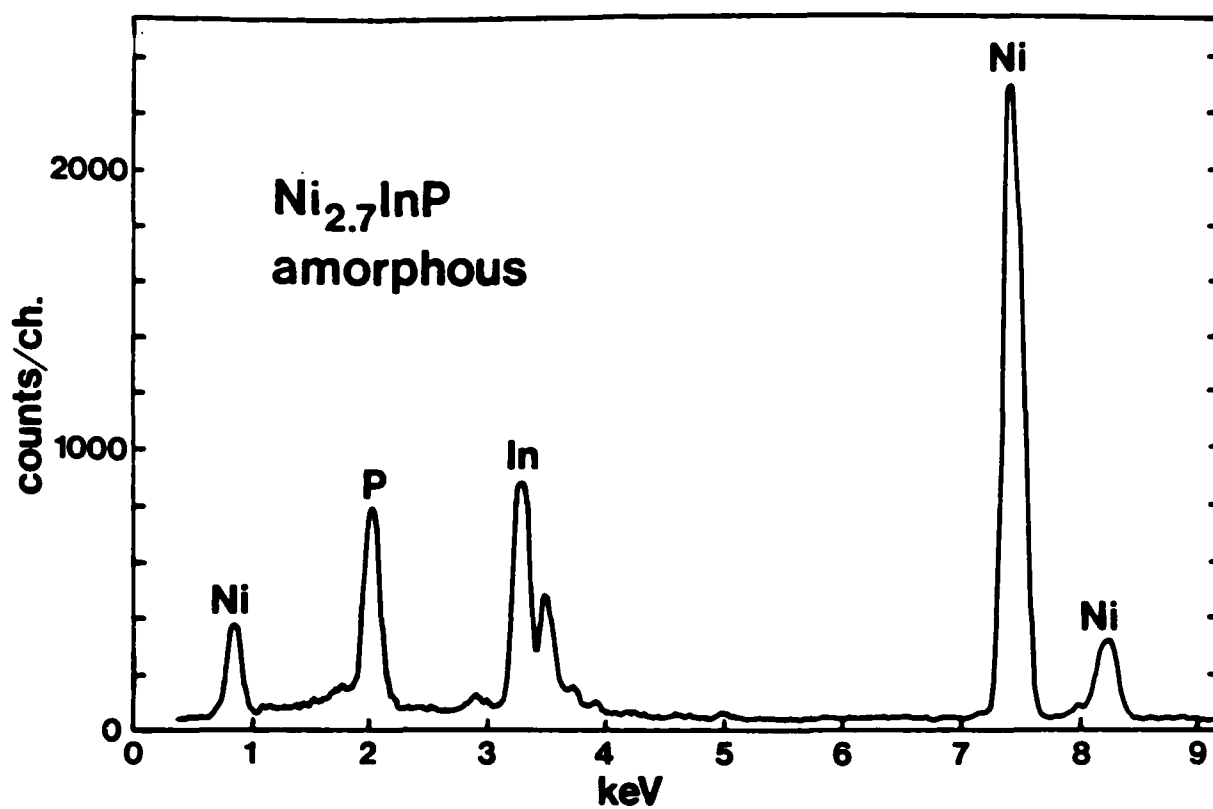




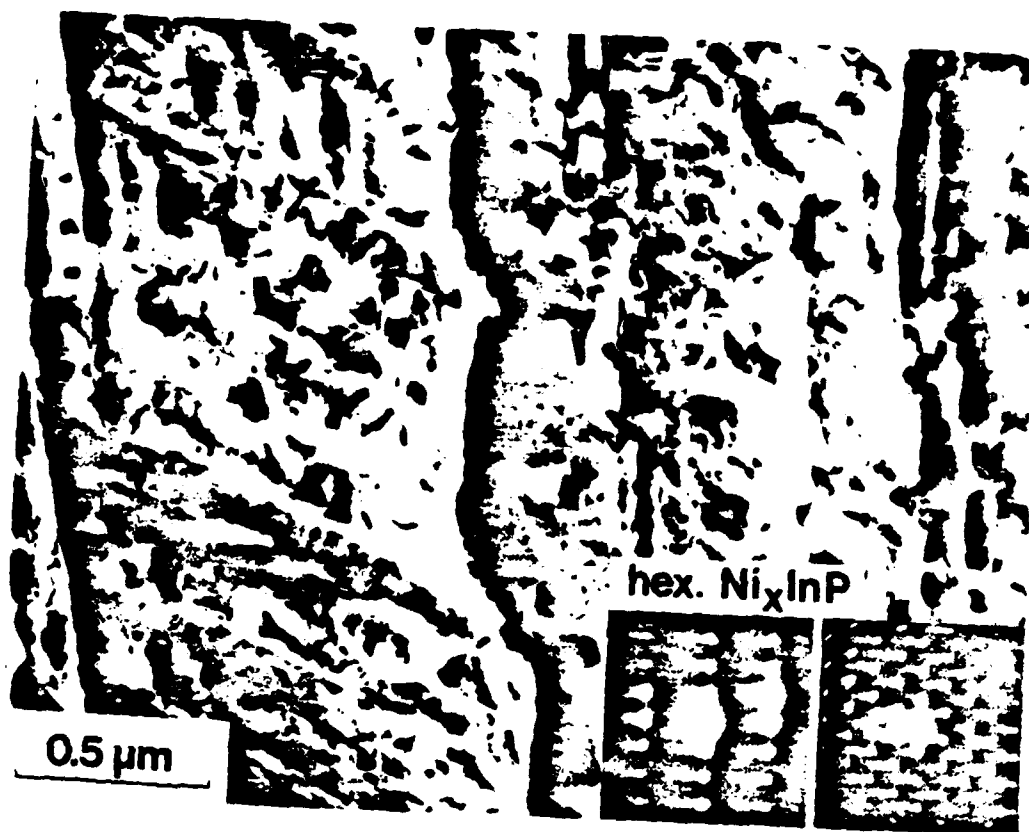
El-Boragy & Schubert, Z.Metall., 1981

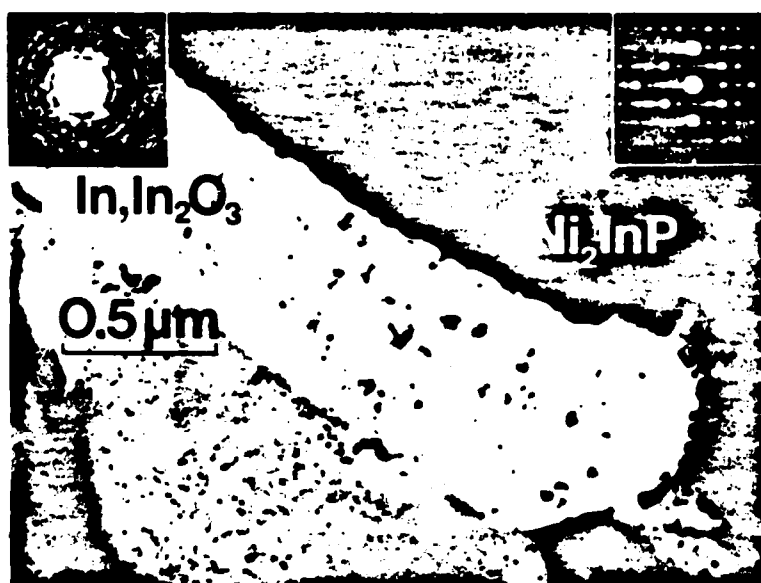
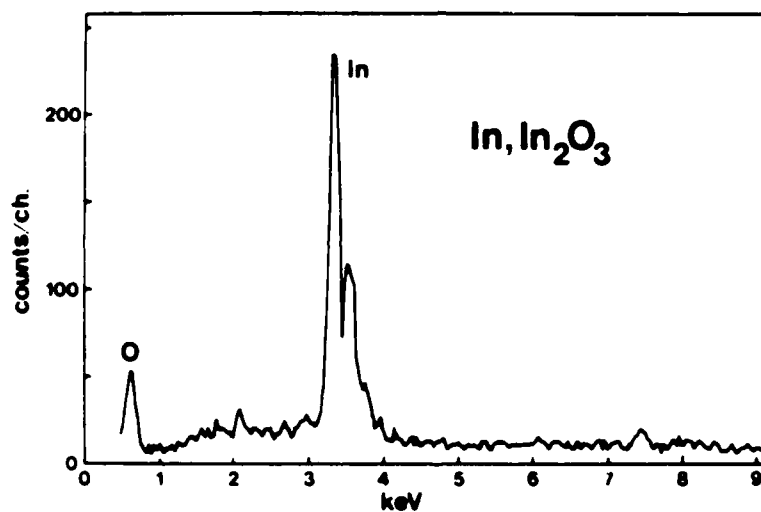
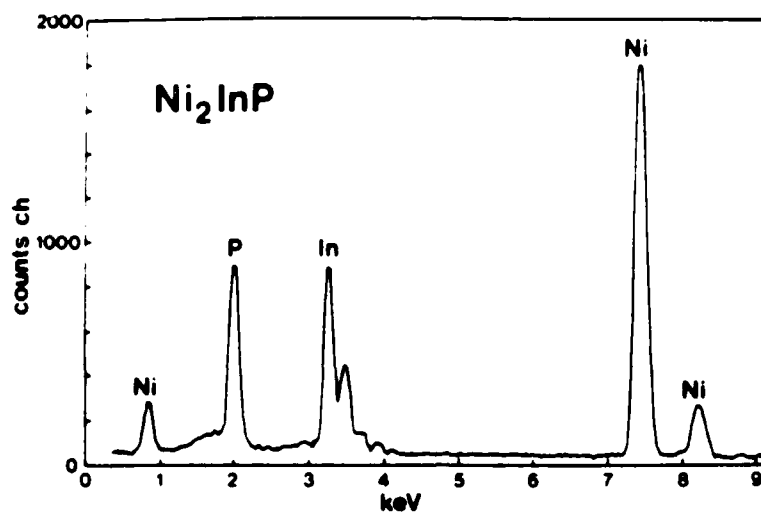


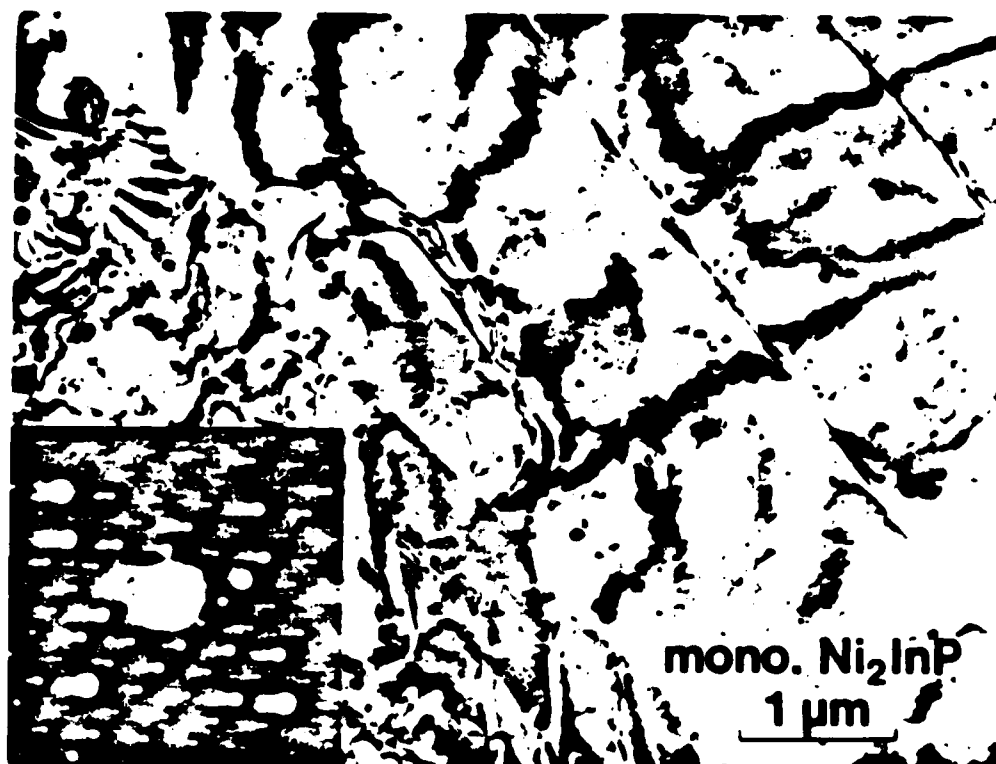
XBL 869-3271











## **Conclusion**

- o **Bulk equilibrium M-A-B phase diagrams, if available, can be used to predict the stable phases resulting from an M/AB reaction with the following caveats:**
  - o **surface and interface contributions to the free energy may be significant (e.g. Pd/GaAs)**
  - o **An M/AB system cannot be assumed to be a closed system (e.g. Pd/GaAs, Ni/InP, ...)**
- o **Bulk equilibrium M-A-B phase diagrams are not available for most systems of interest**
  - > more experimental data is needed**

### Intermediate and Stable Phases in Selected M/AB Systems

<u>System</u>	<u>Intermediate</u>	<u>Stable*</u>
Co/GaAs	Co <sub>2</sub> GaAs ?	CoGa, CoAs
Rh/GaAs	RhAs	RhGa, RhAs <sub>2</sub>
Ir/GaAs	IrGa	Ir <sub>3</sub> Ga <sub>5</sub> , IrAs <sub>2</sub>
Ni/GaAs	Ni <sub>3</sub> GaAs	NiGa, NiAs
Pd/GaAs (60nm)	Pd <sub>x</sub> GaAs (I and II) Pd <sub>2</sub> Ga, Pd <sub>2</sub> As	PdGa, PdAs <sub>2</sub>
Pd/GaAs (12nm)	Pd <sub>x</sub> GaAs (I)	Pd <sub>5</sub> Ga <sub>2</sub> As (II)
Pt/GaAs	Pt <sub>3</sub> Ga	PtGa, PtAs <sub>2</sub>
Ni/InP	Ni <sub>2-7</sub> InP (amor.) Ni <sub>x</sub> InP (hex.)	Ni <sub>2</sub> InP (mono.)

\*e-gun deposited on (100) GaAs, capped with SiO<sub>2</sub>. Stable phases are final product phases after annealing at 500°C < T < 700°C

## **Thermally Stable Ohmic Contacts to n-type GaAs**

**M. Murakami, N. Braslau, Y. C. Shih and W. H. Price**

**November 3, 1986**

### **Outline**

- I. Concern for AuNiGe Ohmic Contacts**
- II. Thermally Stable Ohmic Contacts**
  - MoGeW System**
  - MoGeInW System**
- III. Summary**

## **I. AuNiGe Ohmic Contacts**

### **Advantages:**

- (a) Low contact resistance
- (b) Extensive history (invented by N. Braslau in 1967)
- (c) Excellent run-to-run reproducibility
- (d) Prepared by standard evaporation and annealing techniques

### **Disadvantages:**

- (a) Thermally unstable (process requirement— 400°C, 2 hrs)
- (b) Require a barrier layer between Al-Cu wiring and contact metal

### **Focus of the Present Research for AuNiGe Contact Metals:**

- Explore the possibility to improve thermal stability

### **Approach:**

- Identify compounds or phases which produce low  $R_c$
- Investigate thermal stability of these compounds

## AuNiGe Ohmic Contacts

typical as-deposited sample

Au	50 nm
Ni	30 nm
Au-Ge	100 nm
Ni	5 nm

GeAs

Si peak doping:  $1 \times 10^{18} / \text{cm}^3$

- Annealed in Ar/H<sub>2</sub> atmosphere
- $R_c$  measurement ..... transmission line method
- Microstructural analysis ..... X-ray diffraction, TEM, AES

"Correlate microstructures with low or high  $R_c$ "

"Low Contact Resistance"

"High Contact Resistance"



AD-A183 158

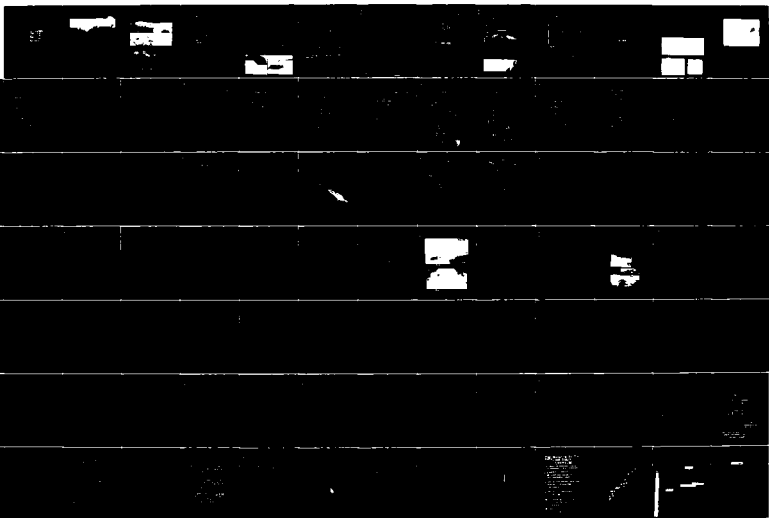
A WORKSHOP ON 3-5 SEMICONDUCTOR: METAL INTERFACIAL  
CHEMISTRY AND ITS EFFECTS (U) STANFORD UNIV CA  
W E SPICER ET AL. 05 NOV 86 N00014-87-G-0038

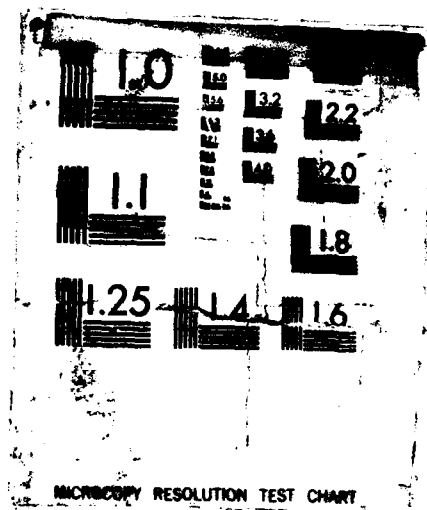
3/7

UNCLASSIFIED

F/G 20/12

NL

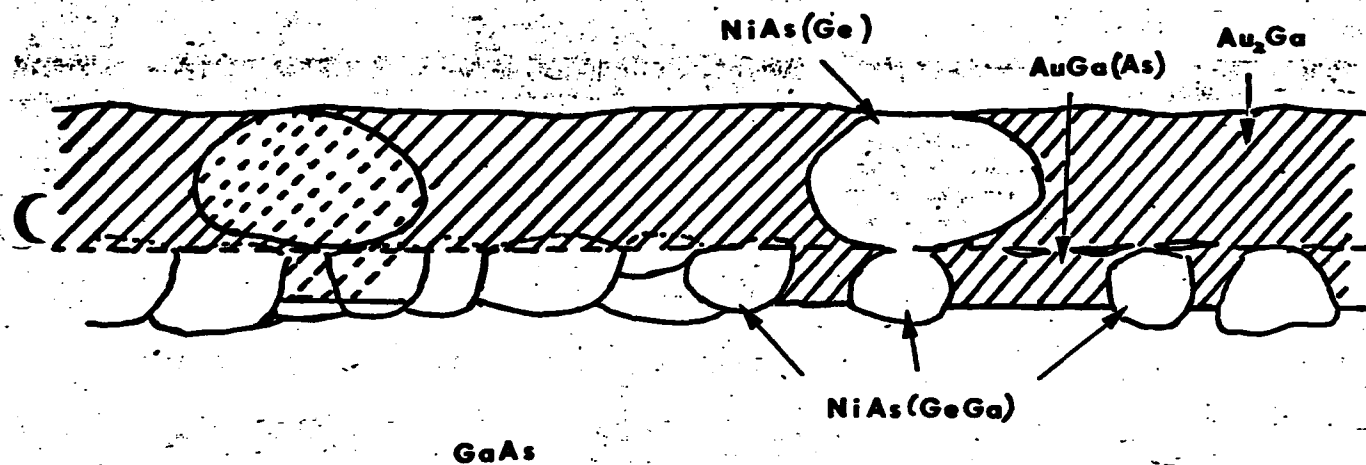




5 Ni 1st layer-contact after annealing at 440°C for 2 min.

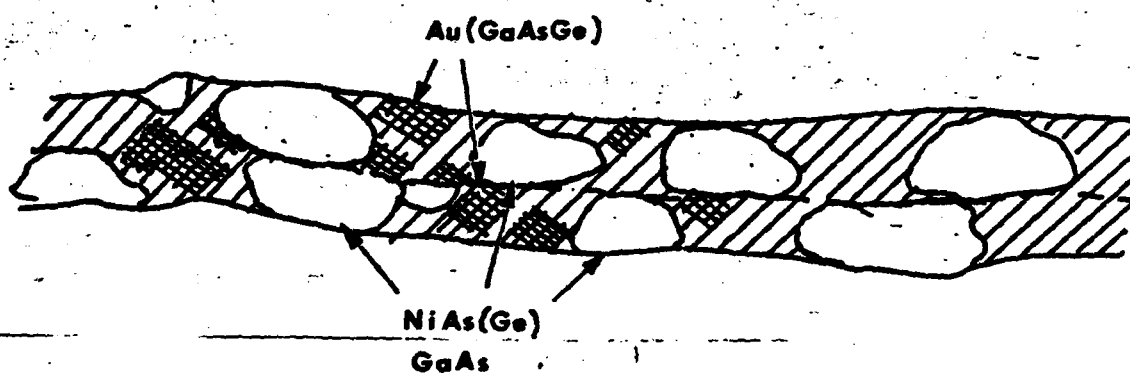


0.1 μm



"Low Contact Resistance"

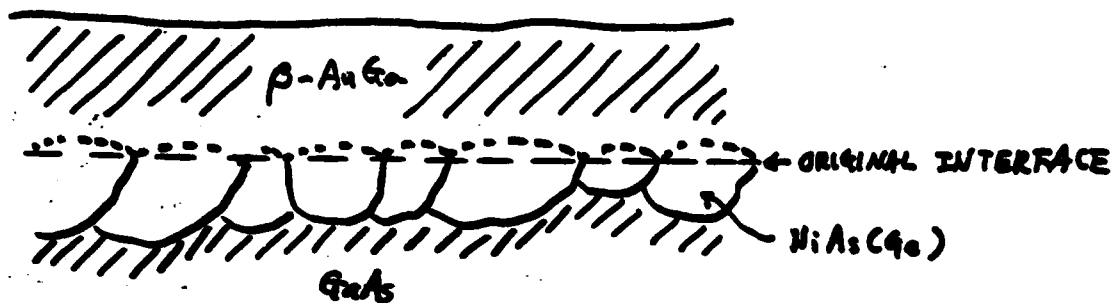
10 Ni 1st layer contact after annealing at 440°C for 2 min.



"High Contact Resistance"

## Microstructure Which Produces Low Contact Resistance

—Cross-sectional TEM, X-ray Diffraction, AES



- $\text{NiAs(Ge)}$  compounds in contact with the  $\text{GaAs}$  substrate
- $\beta\text{-AuGa}$  phase ( $T_m = 360^\circ\text{C}$ ) close to the top surface

## Concern for Device Application

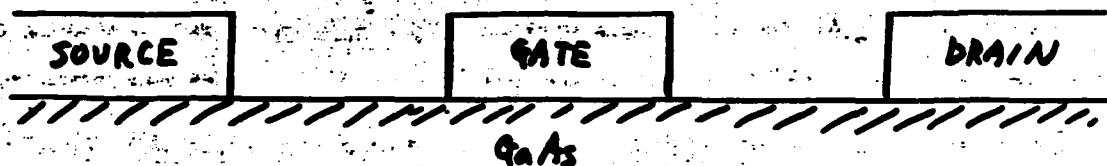
1. Profile at contact edges would deteriorate after contact formation
2. The microstructure would be unstable at  $400^\circ\text{C}$  annealing

## Deterioration of Edge Profile After Formation of Contact

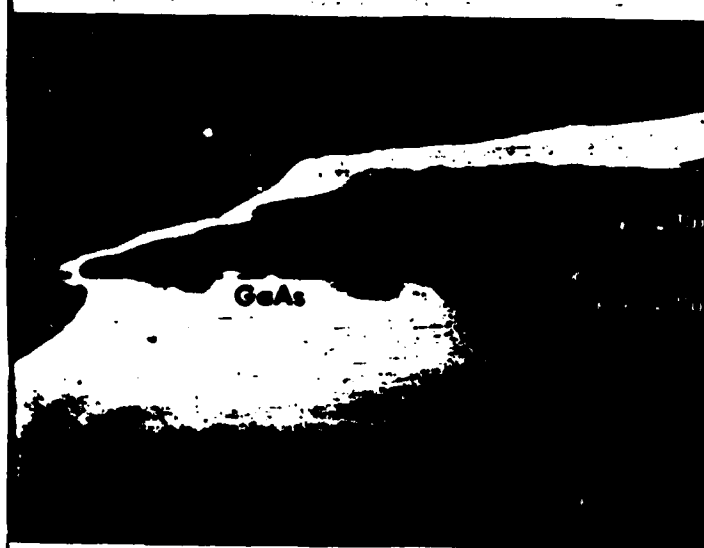
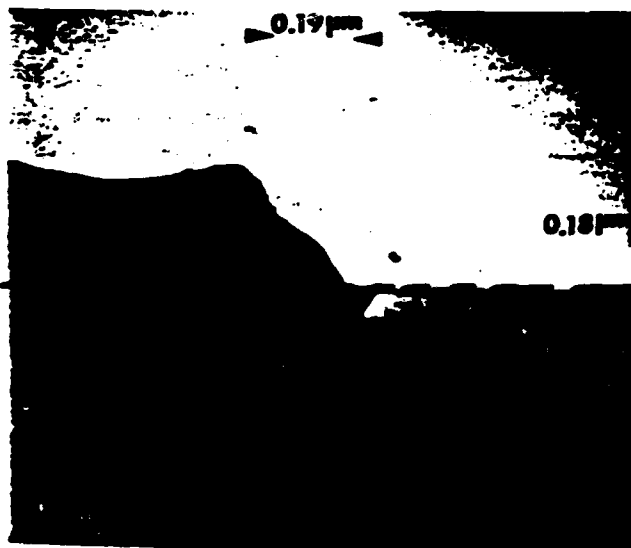
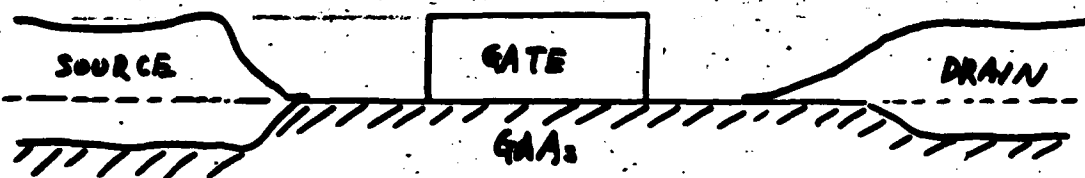
Melting point (360°C) of  $\beta$ -AuGa < Contact formation temp (440°C)

### Deterioration of Edge Profile

Before annealing

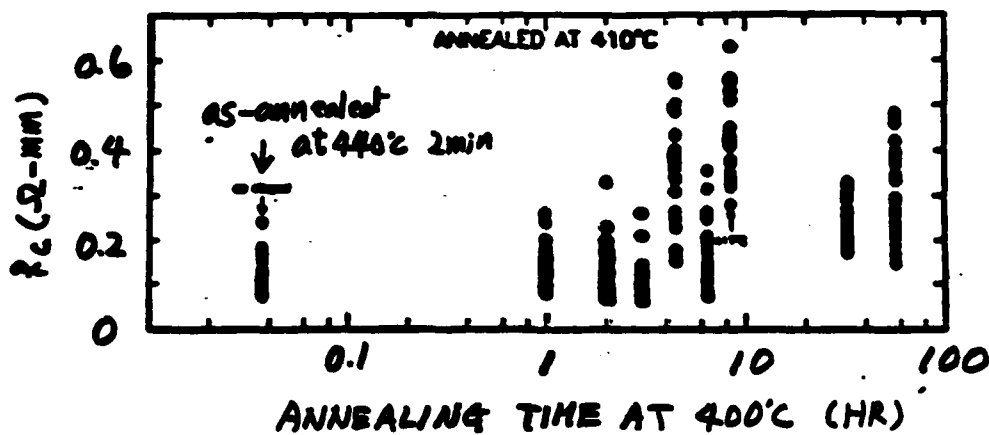


After 440°C 2min annealing



(b) Thermal stability at 400°C annealing

• Electrical resistance measurement



Grain growth and phase transformation of  $\beta\text{-AuGa}$  at 400°C



## II. MoGeW Ohmic Contacts

### Why MoGeW Contact Metal?

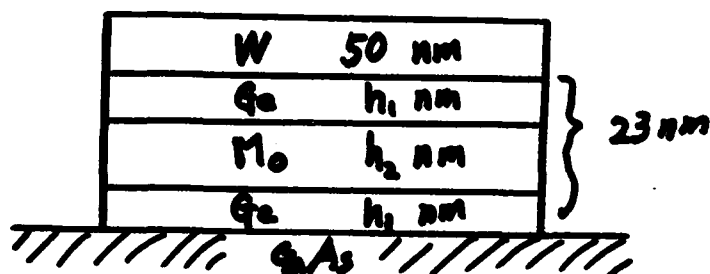
- First ohmic contact to n-type GaAs formed using refractory metals (Tiwari, Kuan and Tierney, 1983)
- Formed by annealing at  $\sim 800^{\circ}\text{C}$
- Expected to be thermally stable at  $400^{\circ}\text{C}$  after contact formation

### Focus of Present Research

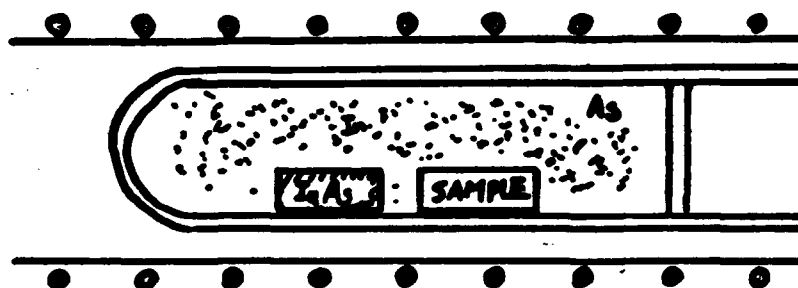
- (a) Search process (composition-temperature) window to form  $R_c < 0.5 \Omega\text{-mm}$
- (b) Investigate thermal stability at  $400^{\circ}\text{C}$  annealing
- (c) Further reduction of  $R_c$  — understand the carrier transport mechanism



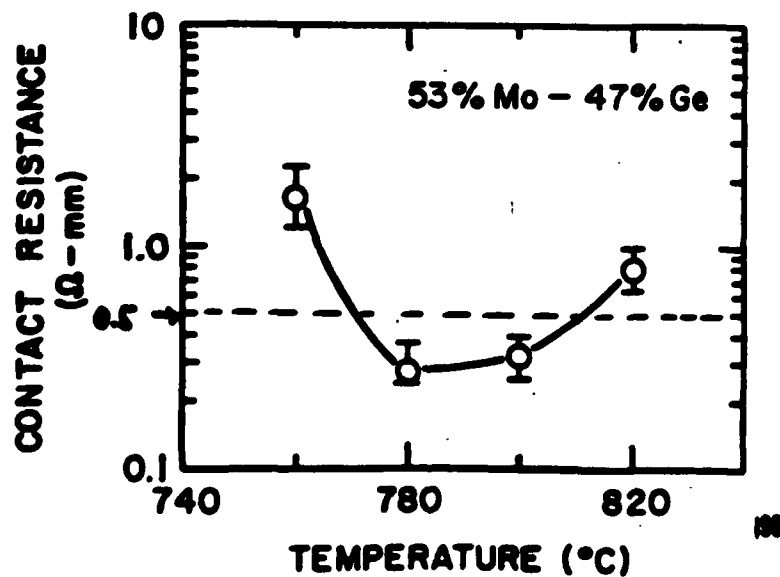
# MoGeW Contacts Annealed in InAs Overpressure Atmosphere



- Annealed in InAs overpressure atmosphere



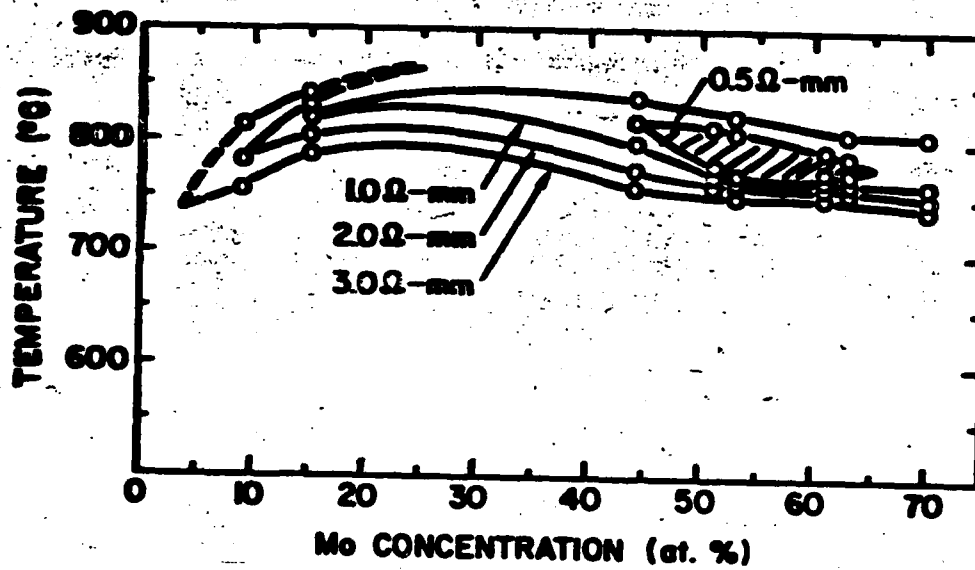
Contact Resistance



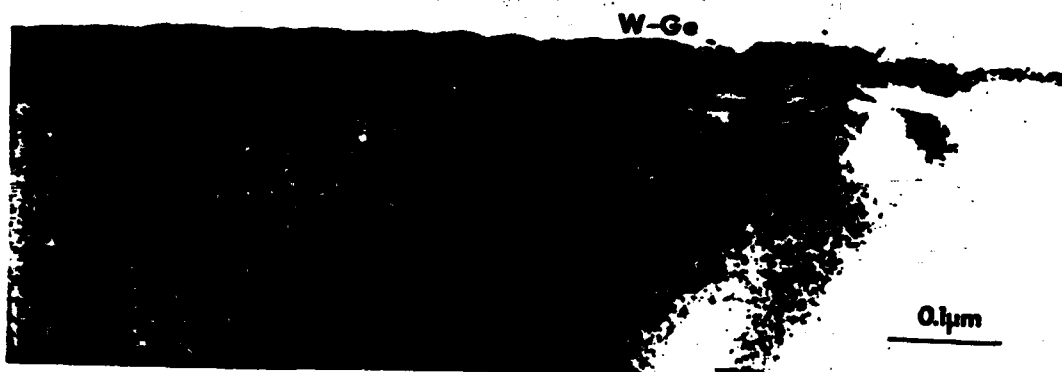
### Search Process Window for $R_c < 0.5 \Omega\text{-mm}$

variables — • Mo/Ge composition ratio, • annealing temperature

### Contact Resistance

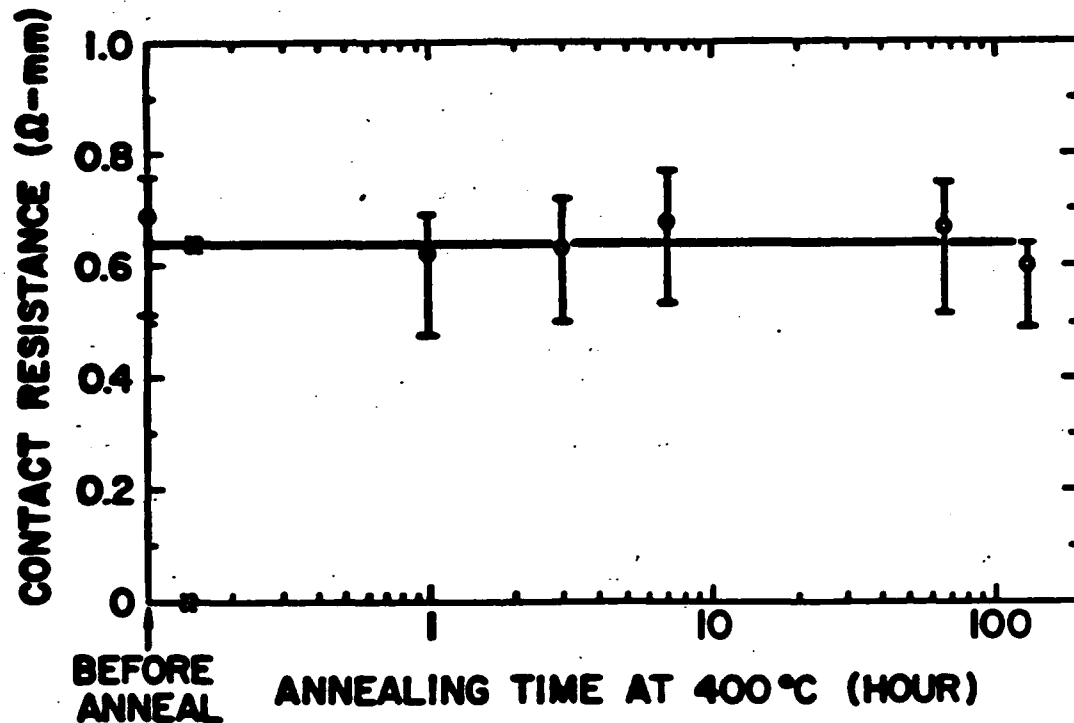


### Morphology at Metal/GaAs Interface



### Thermal Stability at 400°C After Formation of Ohmic Contact

Isothermal annealing at 400°C for ohmic contact formed at 800°C



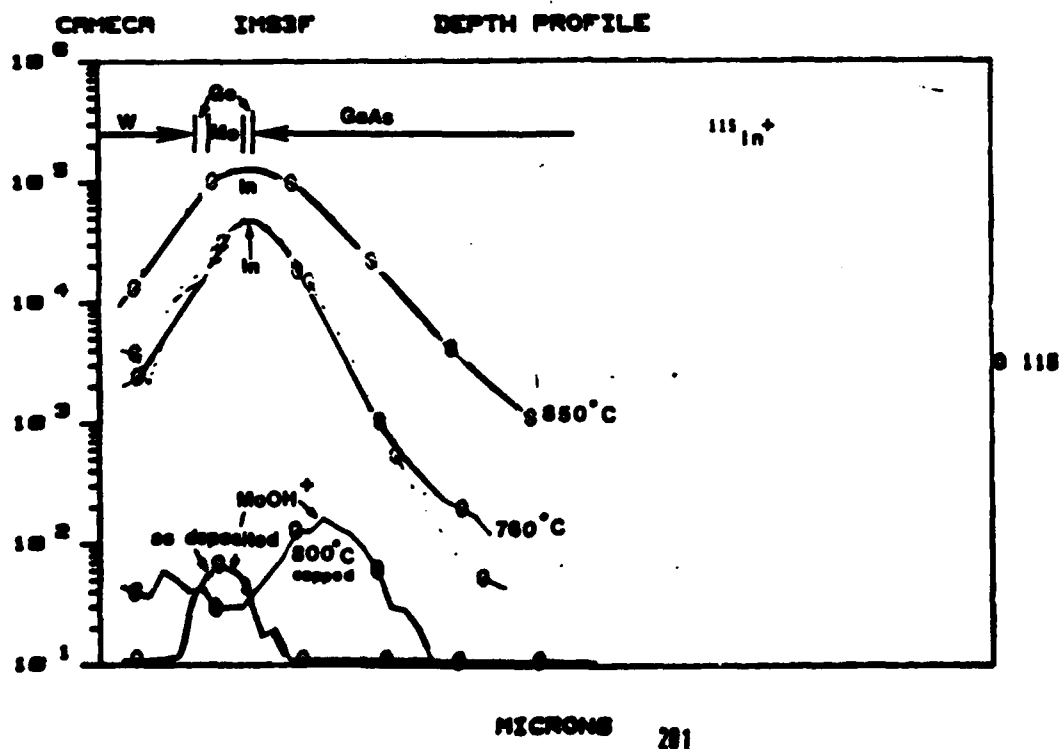
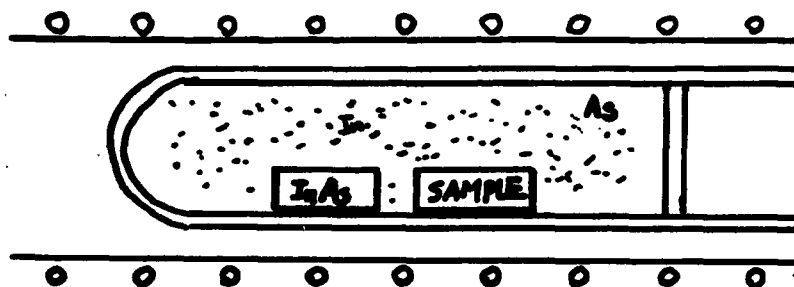
### Concern for MoGeW Ohmic Contact

1. Narrow (composition-temperature) process window
2. Further reduction in the  $R_c$  values

Understand the carrier transport mechanism

## 13

- Annealed in InAs over pressure atmosphere



# (1) Direct Deposition of Indium

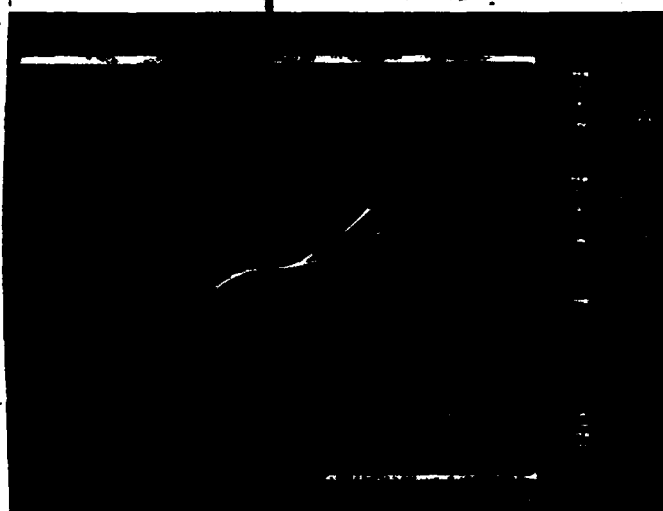
W	50 nm
Mo	13 nm
Ge	10 nm

/// GeAs ///

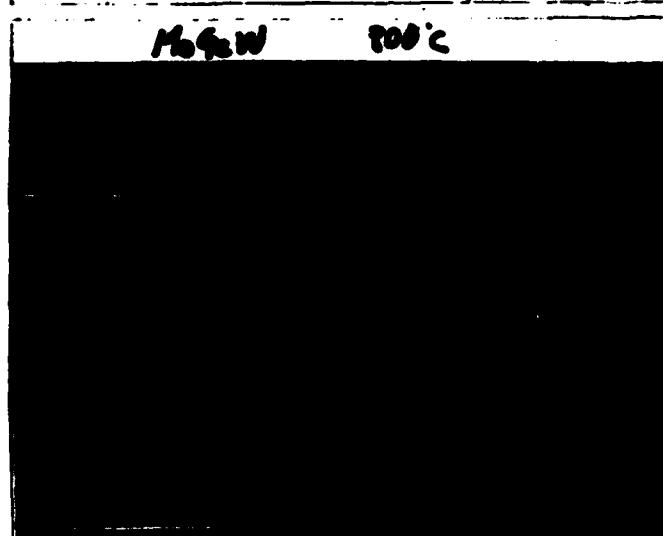
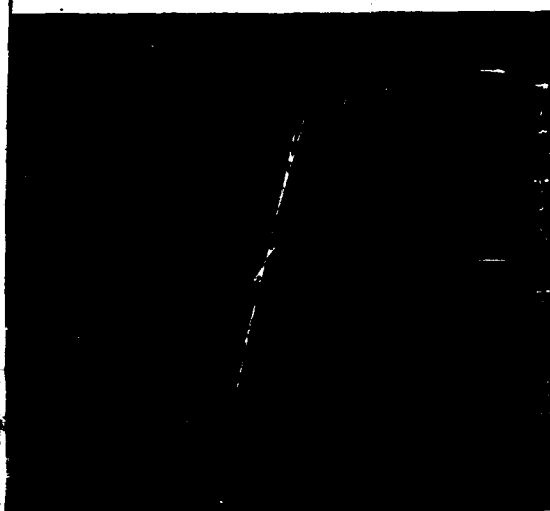
W	50 nm
Mo	13 nm
In	2-6 nm
Ge	10 nm

/// GeAs ///

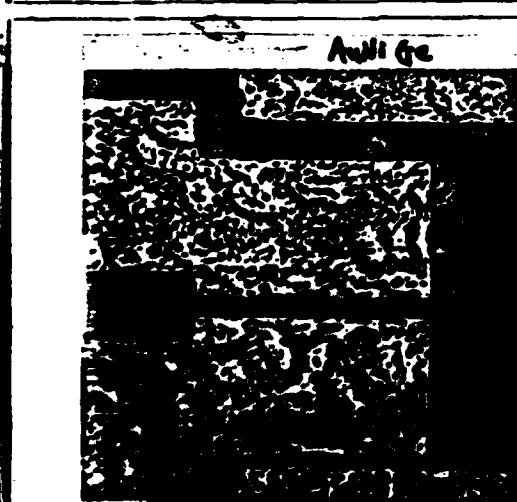
capped by 100nm thick  $\text{Si}_3\text{N}_4$  layer  
annealed at  $800^\circ\text{C}$  for 10 min in Ar/ $\text{H}_2$  gas



RL44  $800^\circ\text{C}$  10 min  $\text{Si}_3\text{N}_4$  capped



MoGeW  $800^\circ\text{C}$



Anti Ge

# Microstructure Which Produces Low Contact Resistance



Before Anneal

W	40 nm
Mo	12 nm
In	4 nm
Ge	10 nm
GaAs	

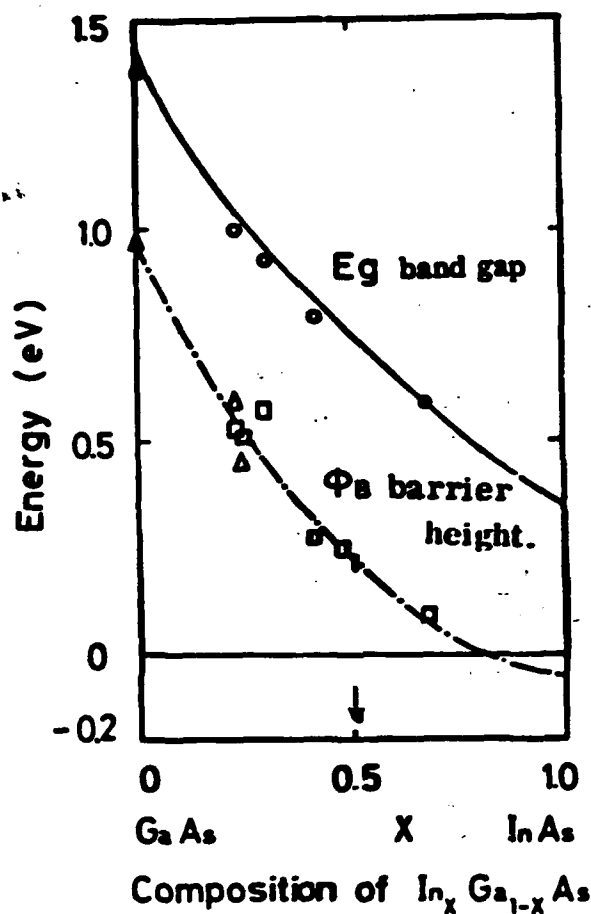


750°C Anneal

W, Ge	40 nm
Mo <sub>5</sub> As <sub>4</sub>	25 nm
(Mo <sub>2</sub> Ge <sub>3</sub> )	
In GaAs	10 nm
GaAs	

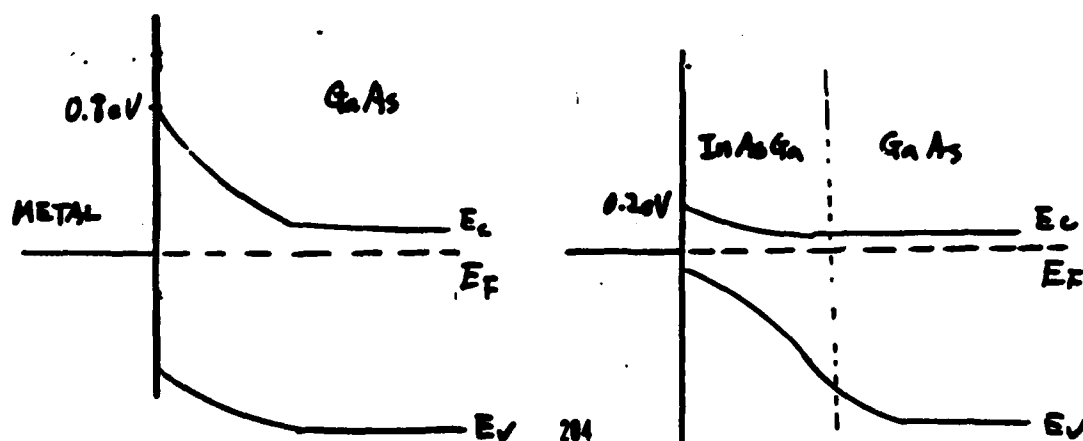
# (c) Present Understanding

InGaAs layer could contribute the barrier height reduction



(Kajiyama, 1973)

$In_{0.5} Ga_{0.5} As$



## Summary

### I. AuNiGe ohmic contacts

- Low contact resistance ( $\sim 0.2 \Omega\text{-mm}$ )
- Deterioration of edge profiles
- Thermally unstable at  $400^\circ\text{C}$

### II. MoGeW ohmic contacts (InAs overpressure annealing)

- Thermally stable at  $400^\circ\text{C}$
- $R_c \sim 0.3 \Omega\text{-mm}$
- Poor run-to-run reproducibility

### III. MoGeInW ohmic contact

- Good reproducibility
- No visible morphological change
- Wide application (short diffusion distance)
- $R_c \sim 0.8 \Omega\text{-mm}$

Focus of Future Study for MoGeInW Ohmic Contacts:

"Reduction of  $R_c < 0.2 \Omega\text{-mm}$ "



# OHMIC CONTACTS

by

T.C. McGill + W.J. Boudville

California Institute

of

Technology

The LORD created so-called ohmic contacts to give solid-state types (especially theorists) an opportunity to make fools of themselves.

H. Kroemer (October 1984).

# REQUIREMENTS

FOR

## OHMIC CONTACTS

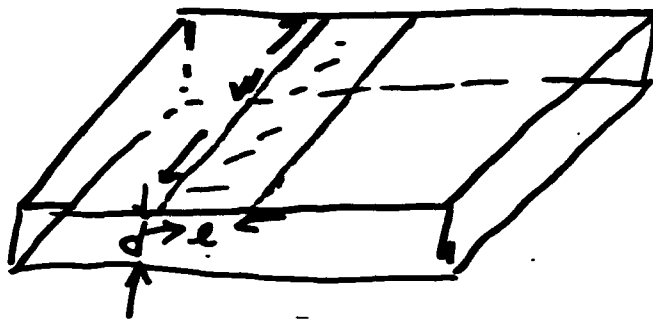
A. CONTACT RESISTANCE

SMALL COMPARED TO

SOURCE-DRAIN RESISTANCE

B. FLUCTUATIONS IN CONTACT  
RESISTANCE SMALL

# SIMPLE CONSIDERATIONS FOR OHMIC CONTACT



$\rho_c$  = specific contact resistance  $\Omega$ -Area.

$$R_c \equiv \text{Contact Resistance} \approx \frac{\rho_c}{dw}$$

$R_{SD} \equiv$  Source-Drain Resistance

$$\approx \frac{l}{wd} \rho_{\text{Bulk-channel}}$$

Condition for neglecting

$$R_{SD} > R_c$$

or

$$\left\{ \rho_c < l \rho_{\text{Bulk-channel}} \right\} \quad 200$$

## Numerical Considerations

$$\rho_{\text{Bulk}} \approx 4 \times 10^{-2} \Omega\text{-cm.}$$

$$l \sim 1 \mu\text{m.}$$

$$\rho_c < 4 \times 10^{-6} \Omega\text{-cm}^2$$

Future

$$\rho_c < 4 \times 10^{-6} \Omega\text{-cm}^2 \left( \frac{l}{1 \mu\text{m}} \right)$$

## OUTLINE

- A. SIMPLE MODEL OF OHMIC CONTACT
- B. FLUCTUATIONS IN POTENTIAL  $\Rightarrow$  FLUCTUATIONS IN CONDUCTANCE
- C. POSSIBLE WAYS OF SUPPRESSING FLUCTUATIONS
- D. SUMMARY
- E. FUTURE

## SIMPLE CONTINUUM MODEL

### I. FIRST THEORY CHANG, FANG, AND SEE, SSE (1971).

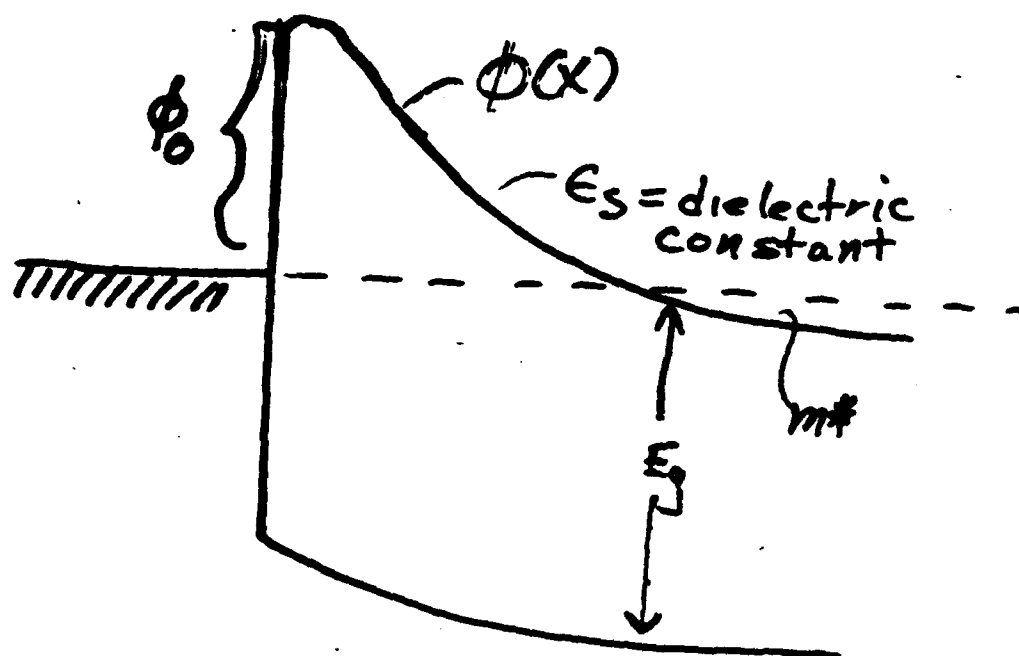
- VERY SIMPLE MODEL OF SCHOTTKY BARRIER

- $K_i(E) \sim \sqrt{\frac{2m_e^* E}{\hbar^2}}$

### II. IMPROVED THEORY

- USE TWO BAND MODEL OF COMPLEX BAND STRUCTURE

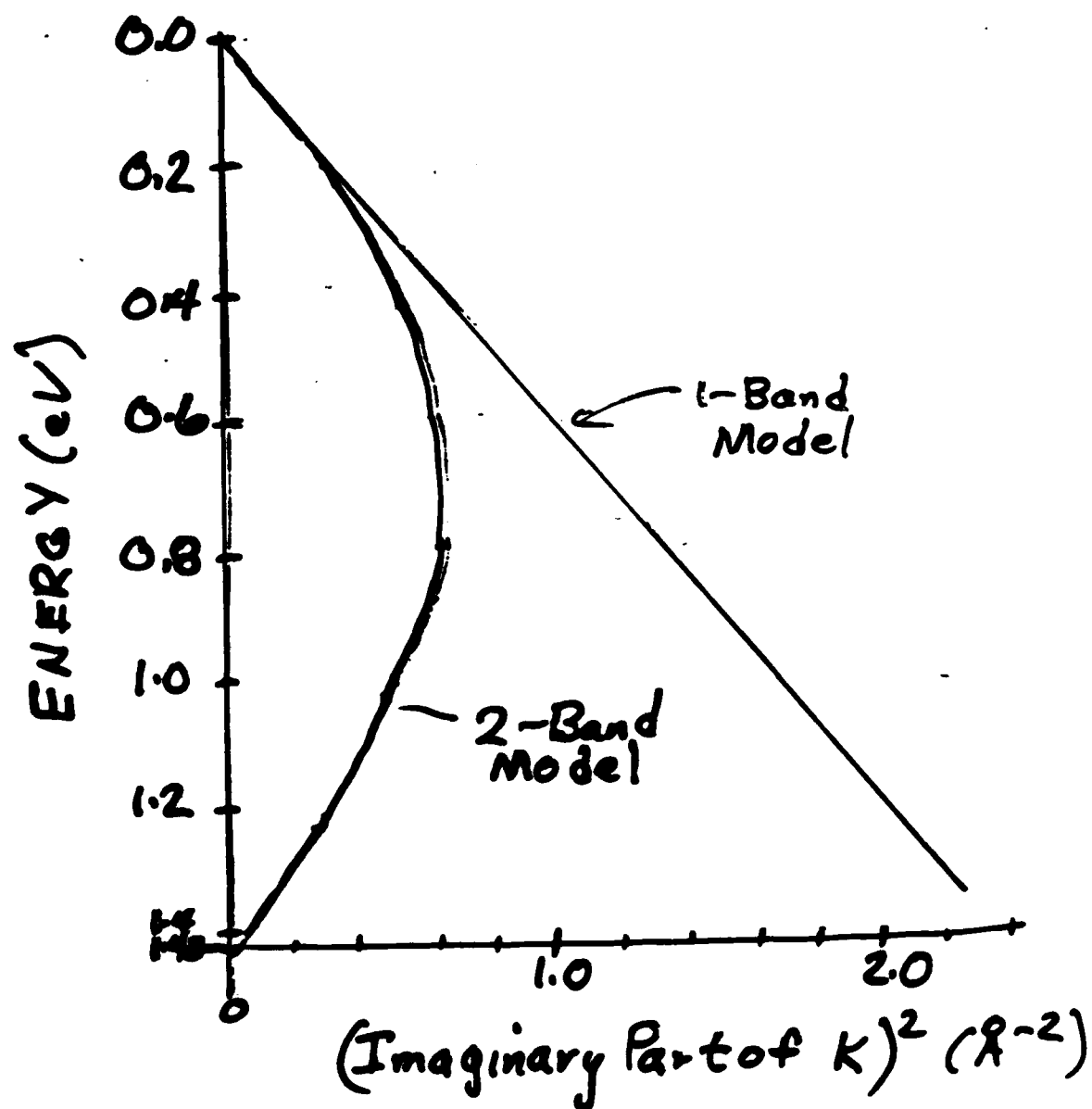
# BARRIER MODEL



$$\phi(x) = \phi_0 + \frac{N_D e^2}{2\epsilon_0 \epsilon_s} (x^2 - 2x_0 x) - \frac{e^2}{8\pi\epsilon_0 \epsilon_s x} - \frac{N_A e^2 d}{\epsilon_0 \epsilon_s} e^{-x/d}$$

$$x_0 = \sqrt{\frac{2\epsilon_0 \epsilon_s}{N_D e^2} [\phi_0 + V_A - V_D]}$$

# TWO BAND VS ONE BAND MODEL





# CURRENT

$$J_{NET} = J_{L \rightarrow R} - J_{R \rightarrow L}$$

$$= 2e \int \frac{d^2 k_{\parallel}}{(2\pi)^2} \int_0^{\infty} \frac{dk_{\perp}}{2\pi} \frac{\hbar k_{\perp}}{m^*} T(E_{\perp}) [f_L(E) - f_R(E)]$$

$T(E_{\perp})$  = Transmission coefficient

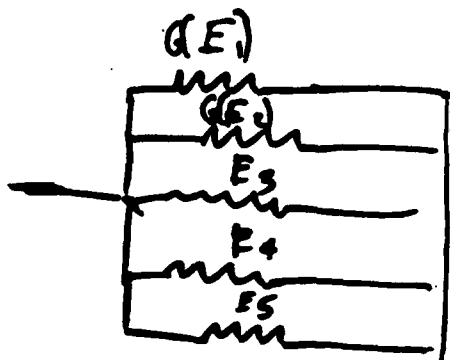
$$= \exp \left[ -2.0 \int_{\text{over barrier}} k_{im}(x) dx \right]$$

$f_L(E), f_R(E)$  = Fermi functions.

# CONDUCTANCE AND RESISTANCE.

$$G \text{ (S/m}^2\text{)} = \frac{1}{R \text{ (}\Omega\text{m}^2\text{)}} = \left( \frac{\partial J}{\partial V} \right)_{V=0}$$

$$G = \frac{1}{R} = \frac{m^* e^2}{2\pi^2 \hbar^3} \int dE_{\perp} \frac{T(E_{\perp})}{e^{(E_{\perp} - E_F)/kT} + 1}$$



$$G(E) = \frac{m^* e^2}{2\pi^2 \hbar^3} \frac{T(E_{\perp})}{e^{(E_{\perp} - E_F)/kT} + 1}$$

## CALCULATIONS

$$\phi_0 = 0.80 \text{ eV}$$

$$E_{\text{gap}} = 1.43 \text{ eV}$$

$$\epsilon_s = 13.18$$

$$m_r^* = 0.065 m_e$$

$$T = 300^\circ \text{K}$$

$$E_{\text{r-L}} = 0.28 \text{ eV}$$

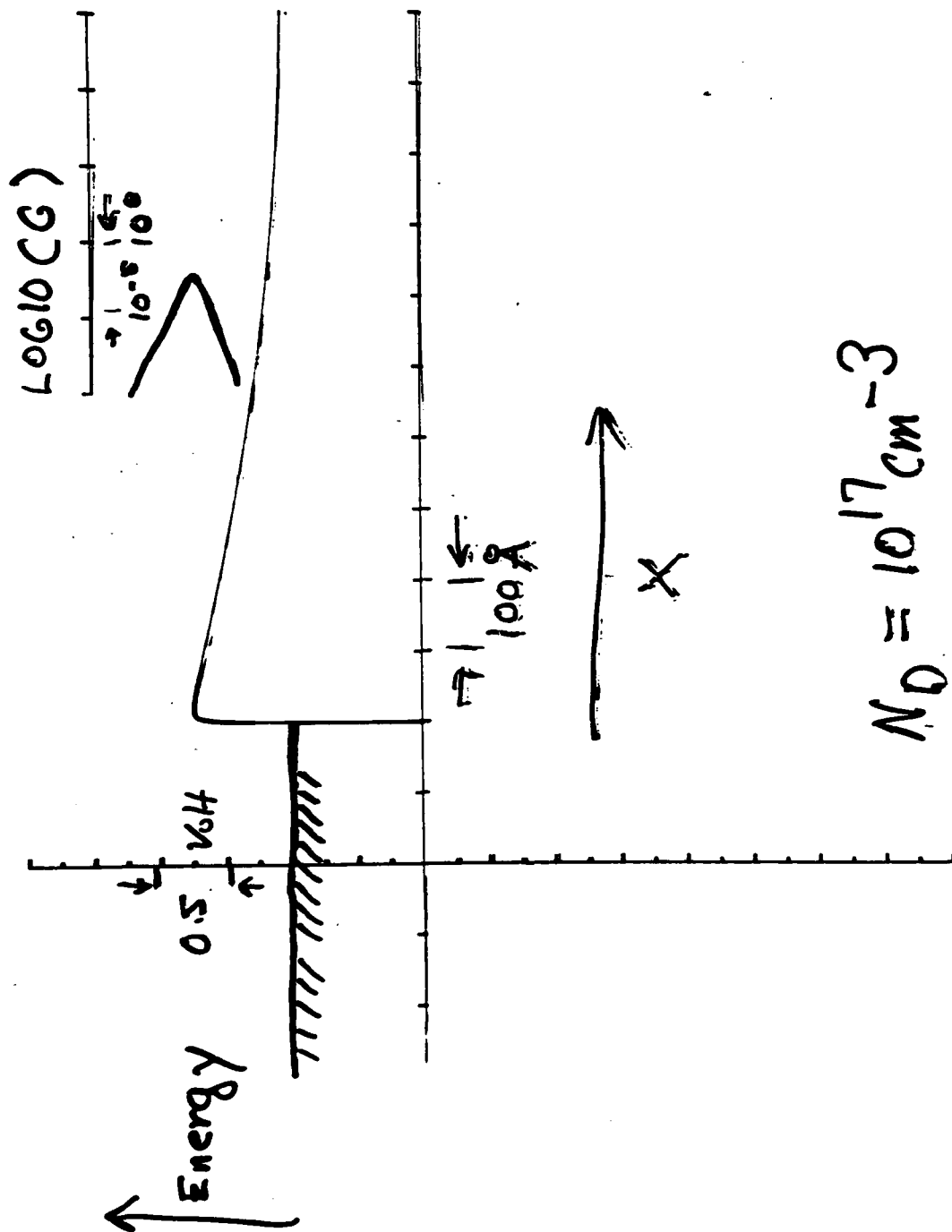
$$m_L^* = 0.55 m_e$$

$$N_s = 3 \times 10^{14} \text{ cm}^{-2}$$

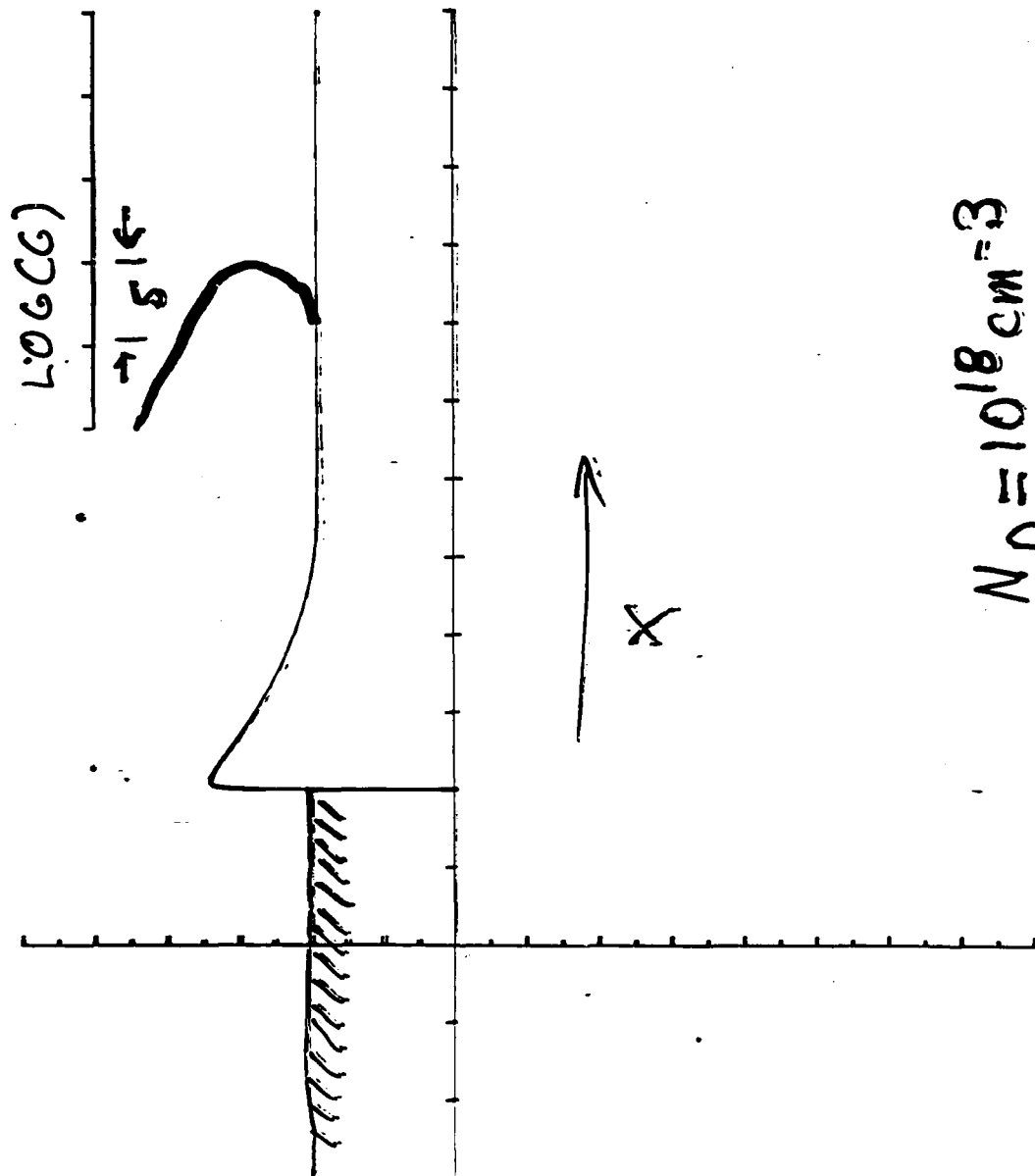
$$d = 5 \text{ \AA}$$

$$\text{DOPING} = ?$$

# DISTRIBUTION OF CONDUCTANCE

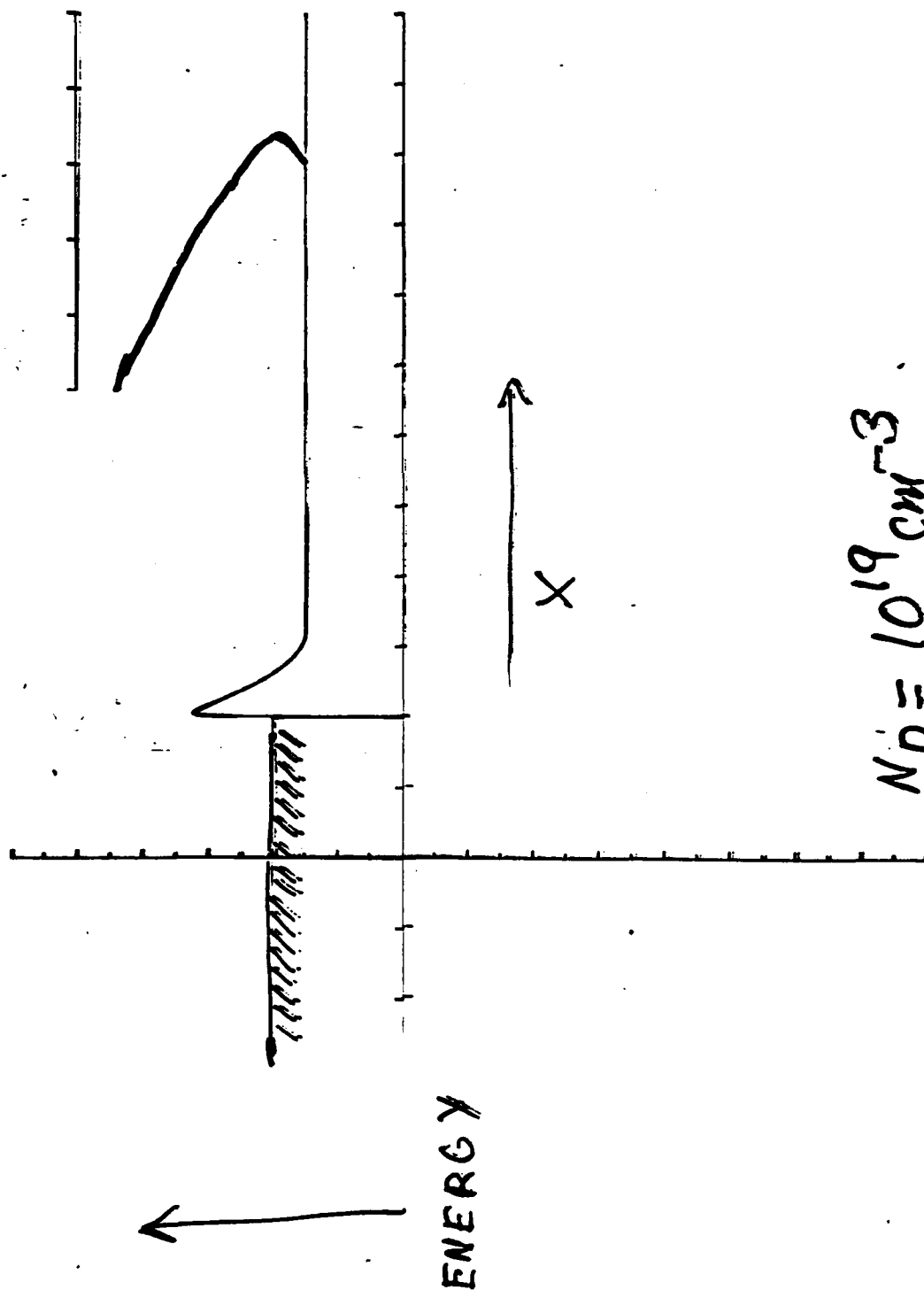


# DISTRIBUTION OF CONDUCTANCE



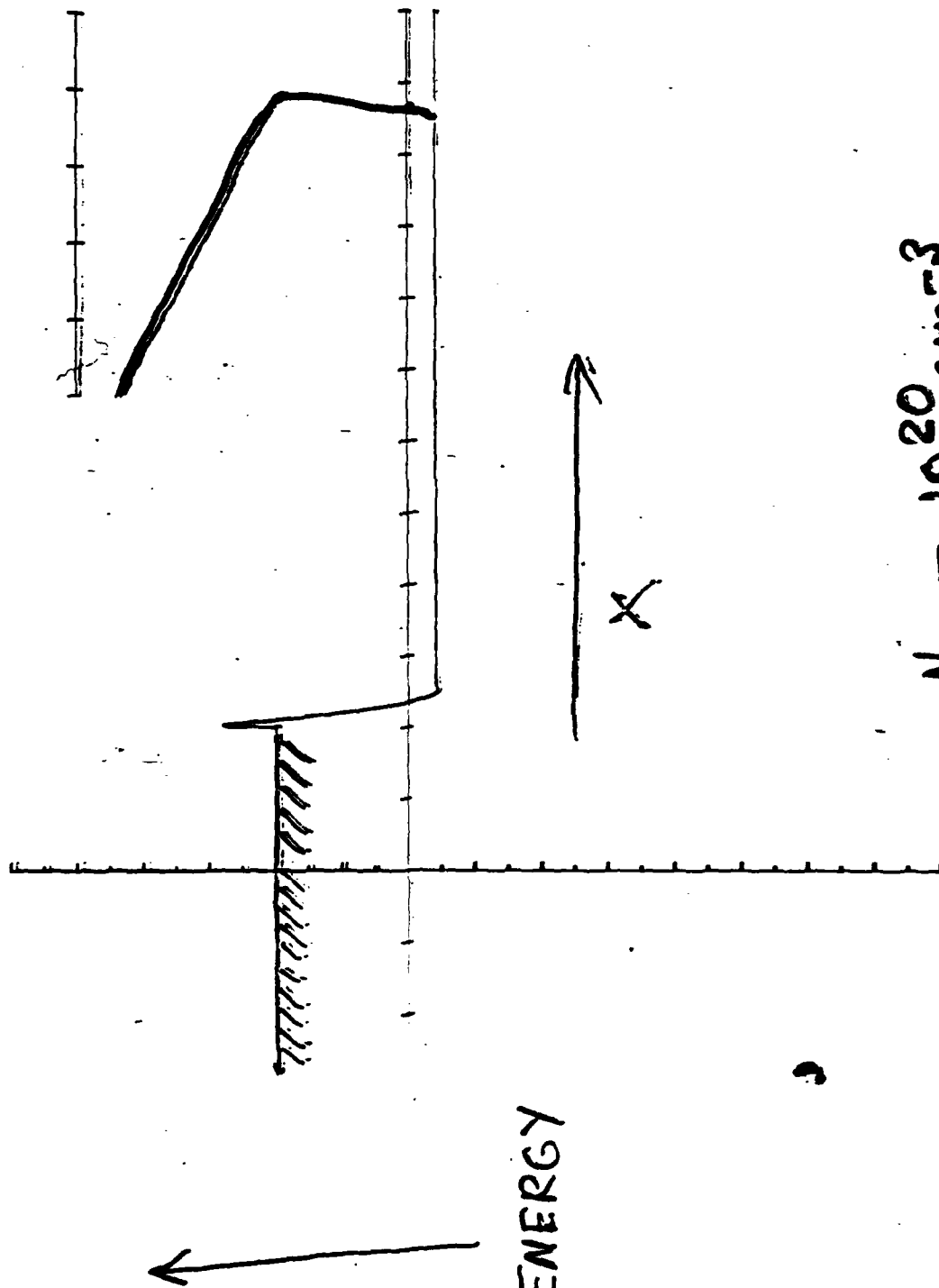
$$N_D = 10^{18} \text{ cm}^{-3}$$

# DISTRIBUTION OF CONDUCTANCE

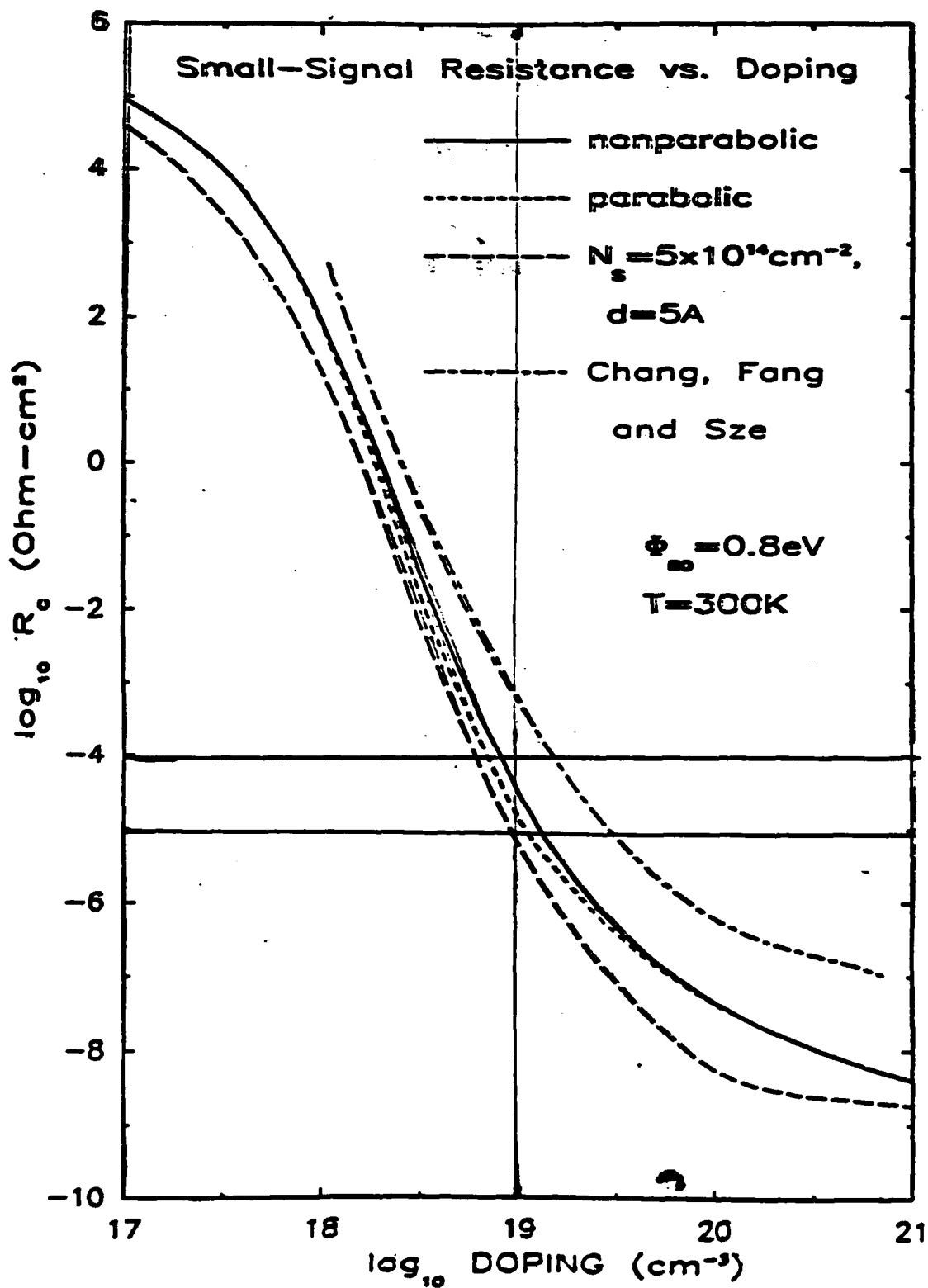


$$N_D = 10^{19} \text{ cm}^{-3}$$

# DISTRIBUTION OF CONDUCTANCE

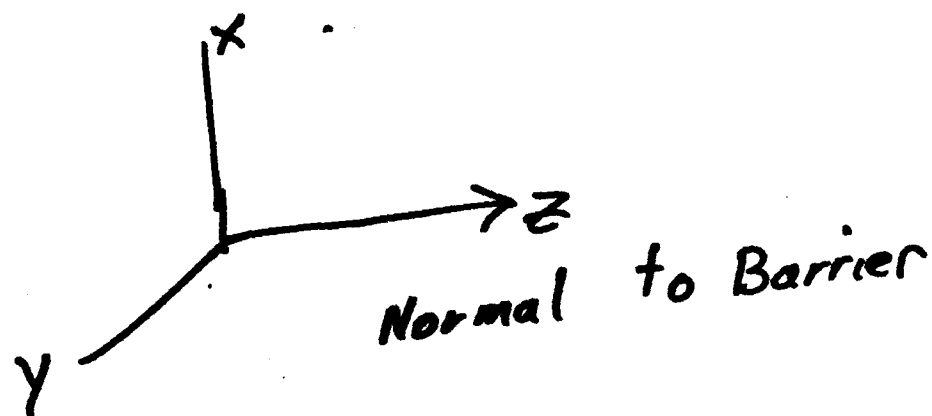


$$N_D = 10^{20} \text{ cm}^{-3}$$





## INHOMOGENEOUS MODEL



$$G = \int G(x, y) dx dy = \langle g \rangle (\text{Area})$$

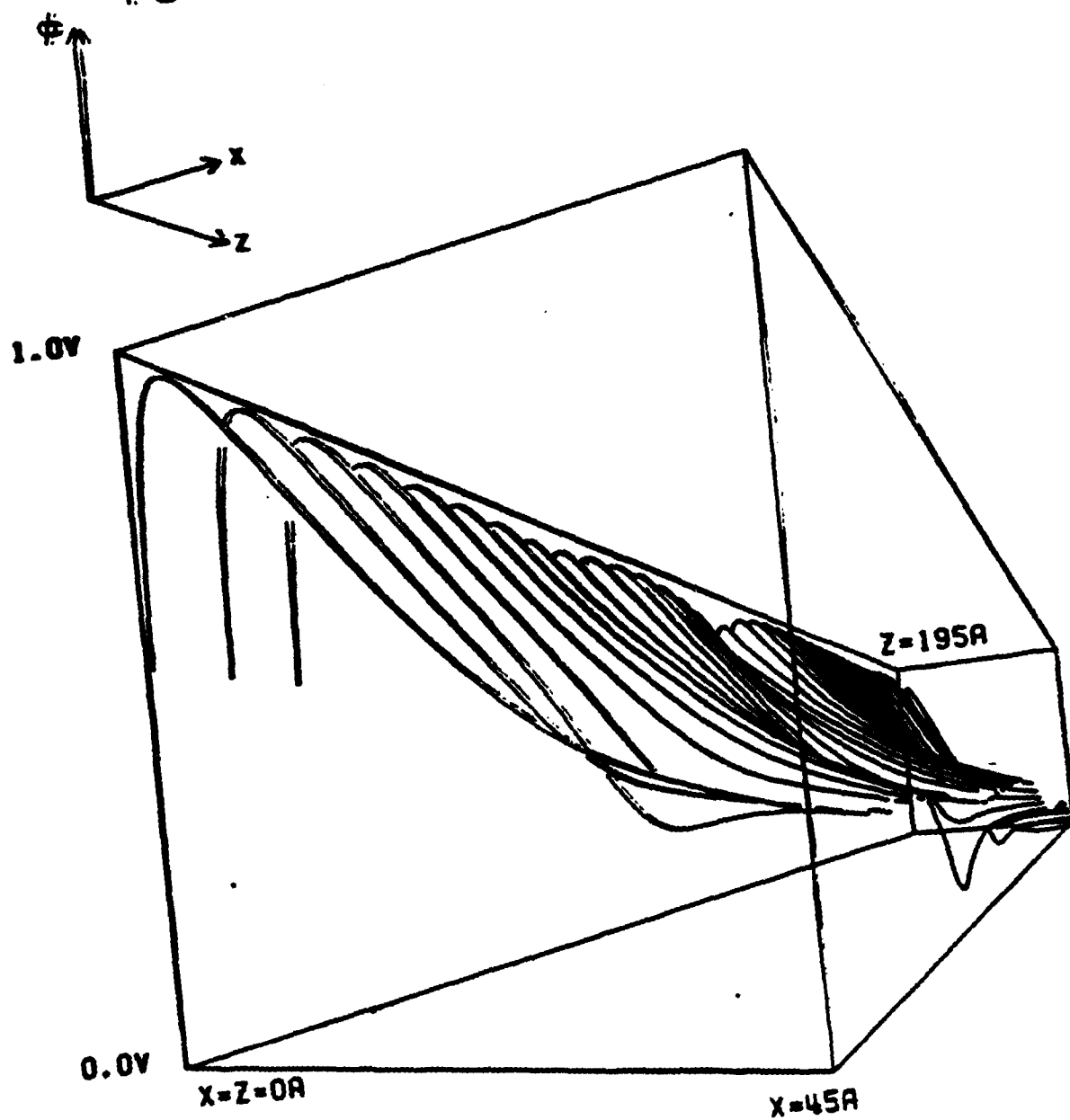
where  $G(x, y)$  = conductance/area  
at  $(x, y)$ .

- REGIONS OF HIGH  $G$   
DOMINATE

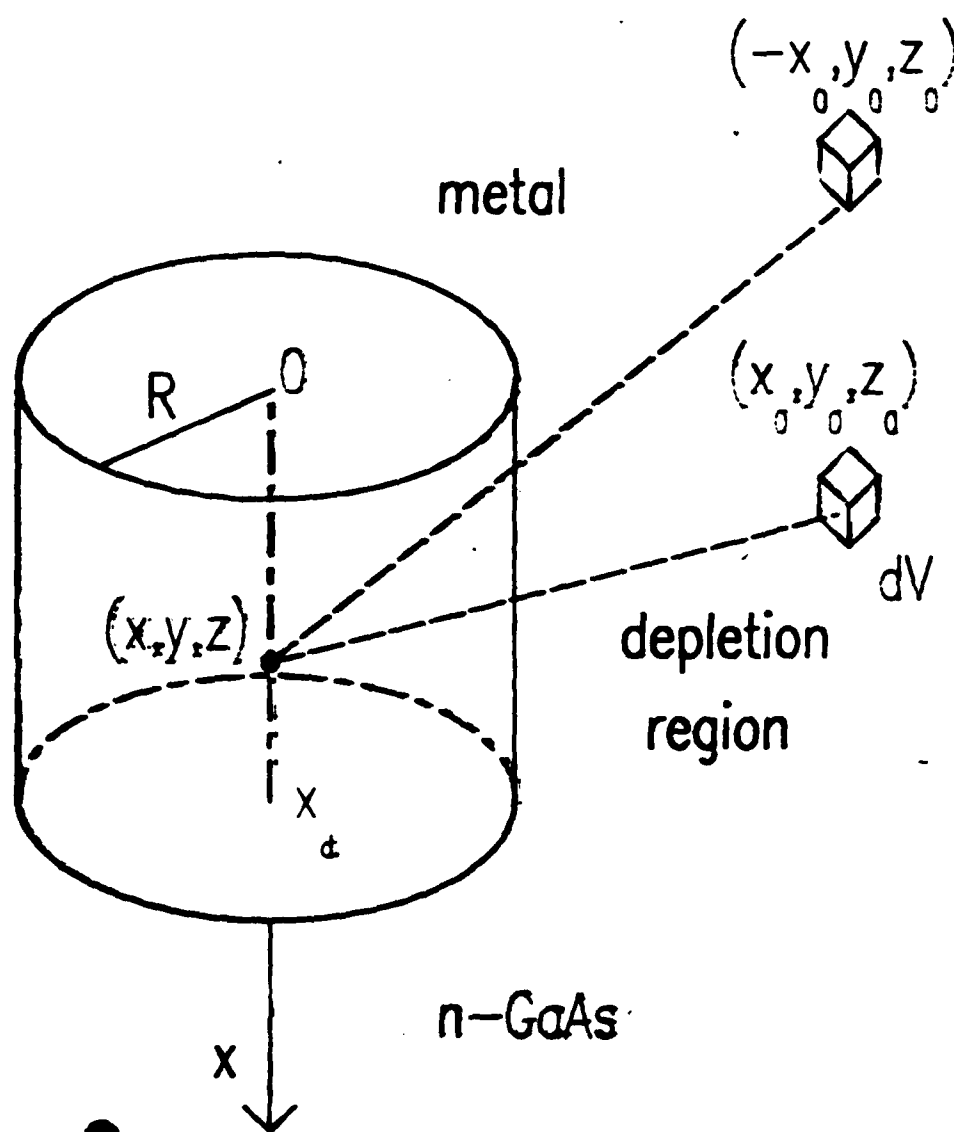
SPATIAL INHOMOGENEITY  
DUE  
TO DISCRETE DOPANTS.

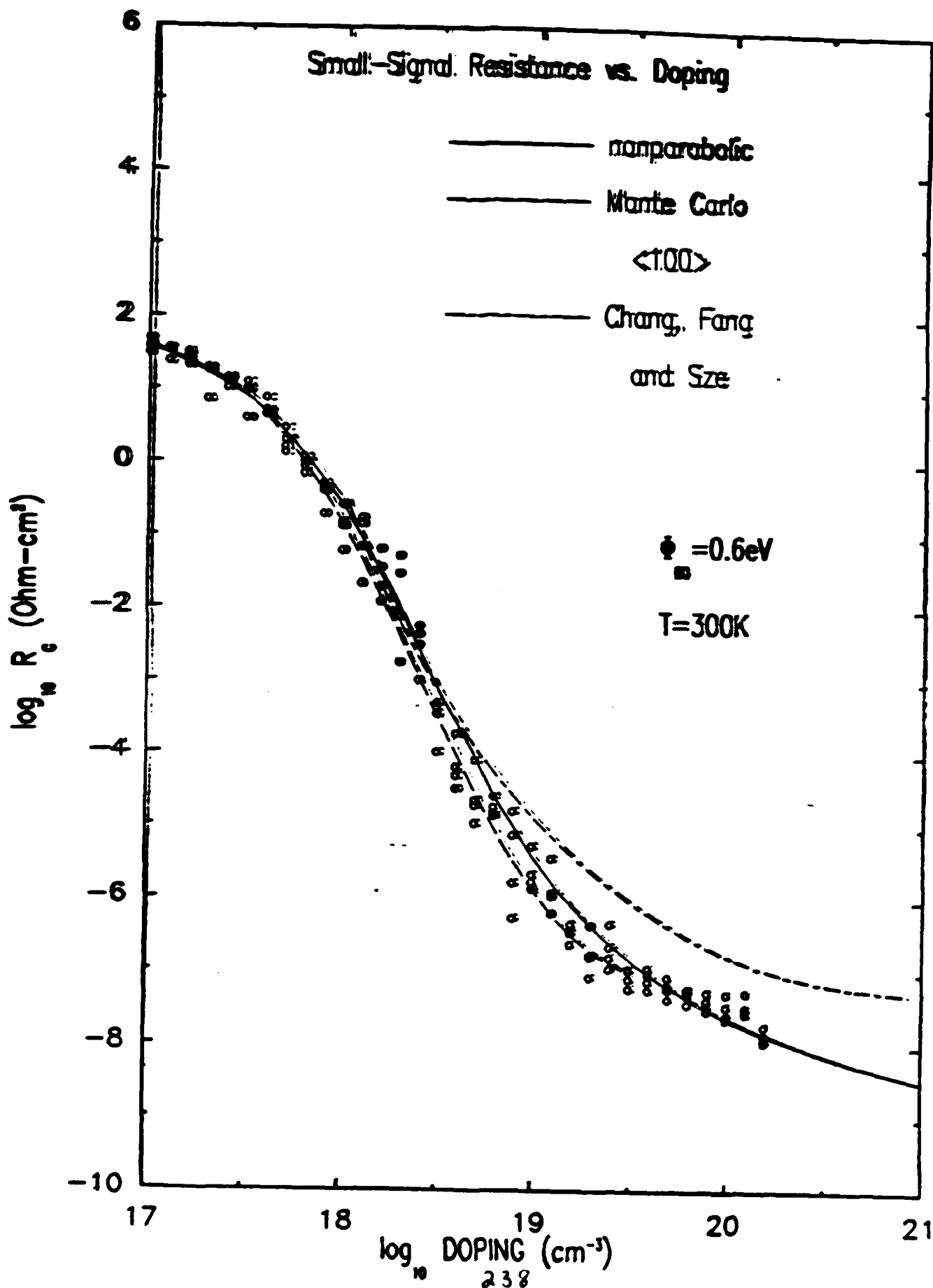
- DOPANT ATOMS DISCRETE.  
⇒ POTENTIAL INHOMOGENEOUS
- USE "RENO" TECHNIQUES  
TO SIMULATE EFFECT.

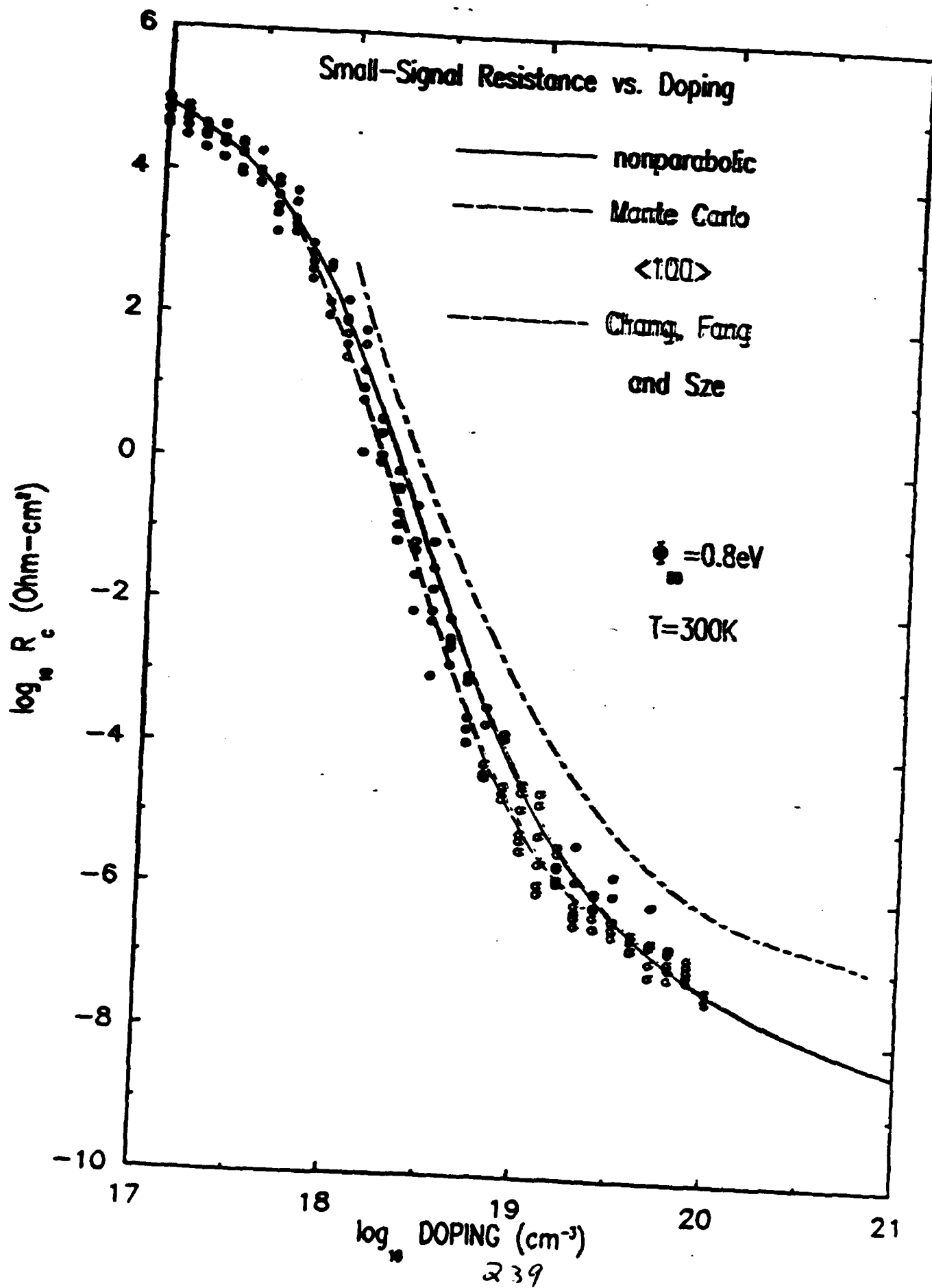
# POTENTIAL IN DEPLETION REGION

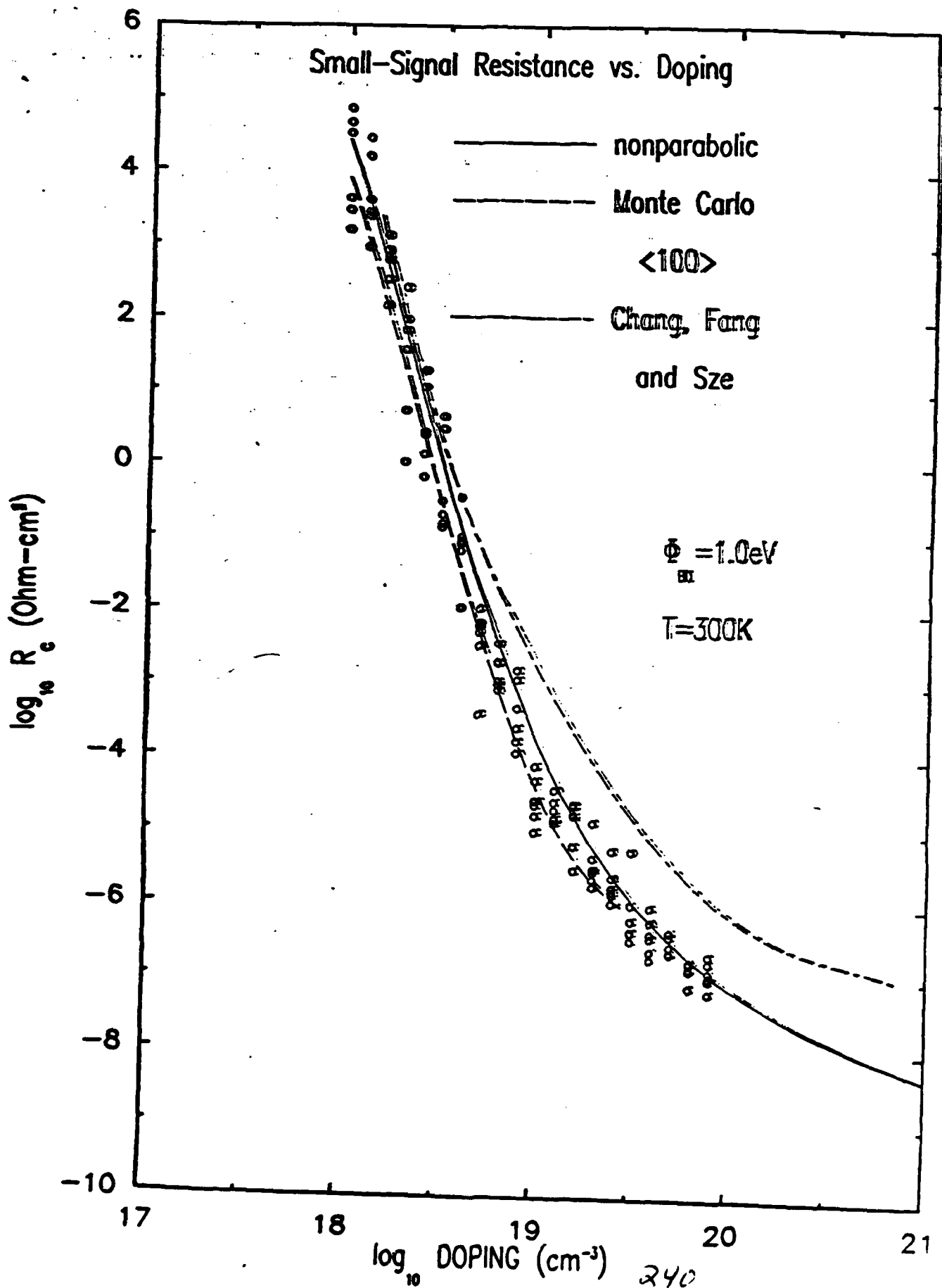


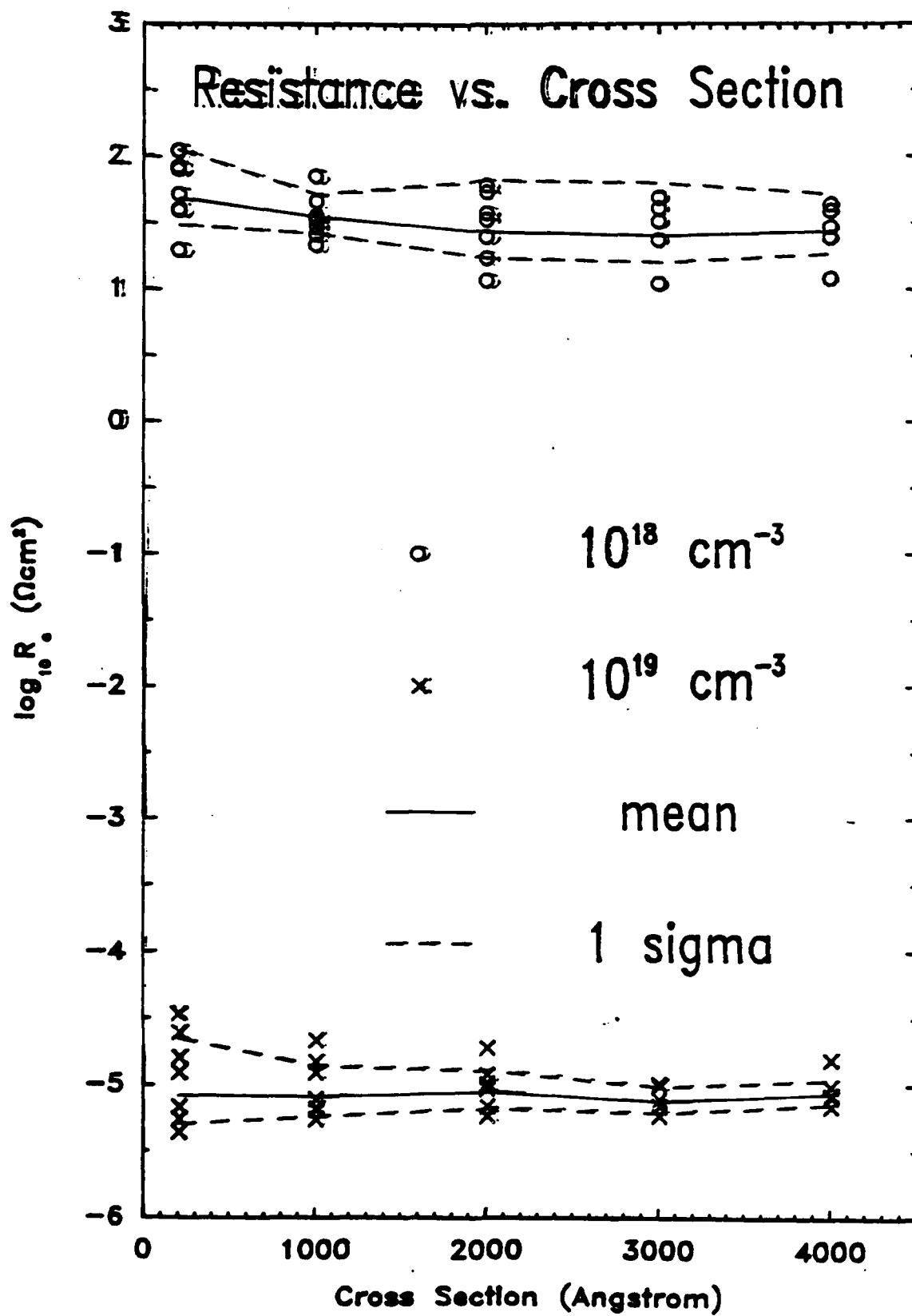
## Contributions to the Potential



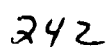


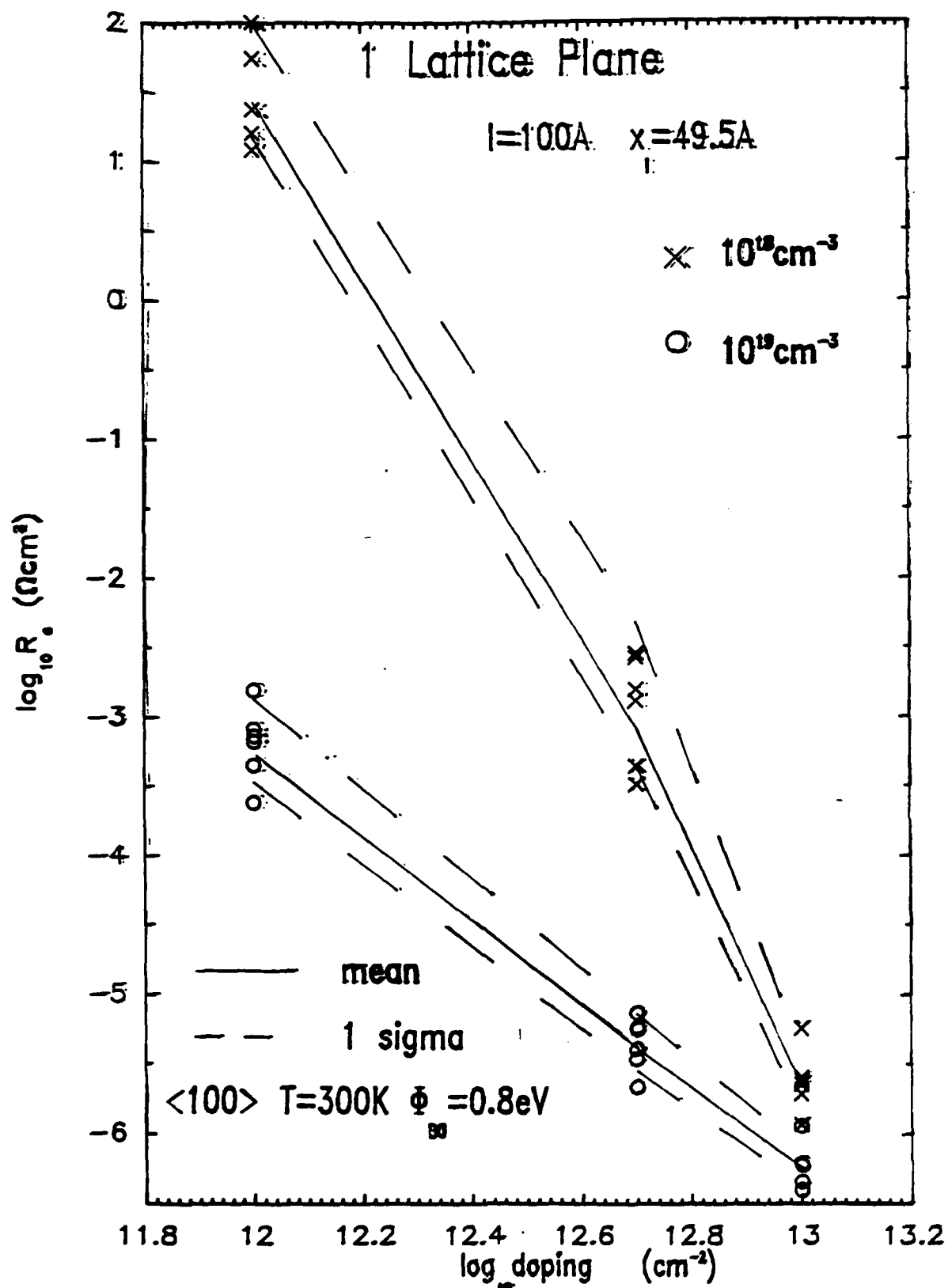


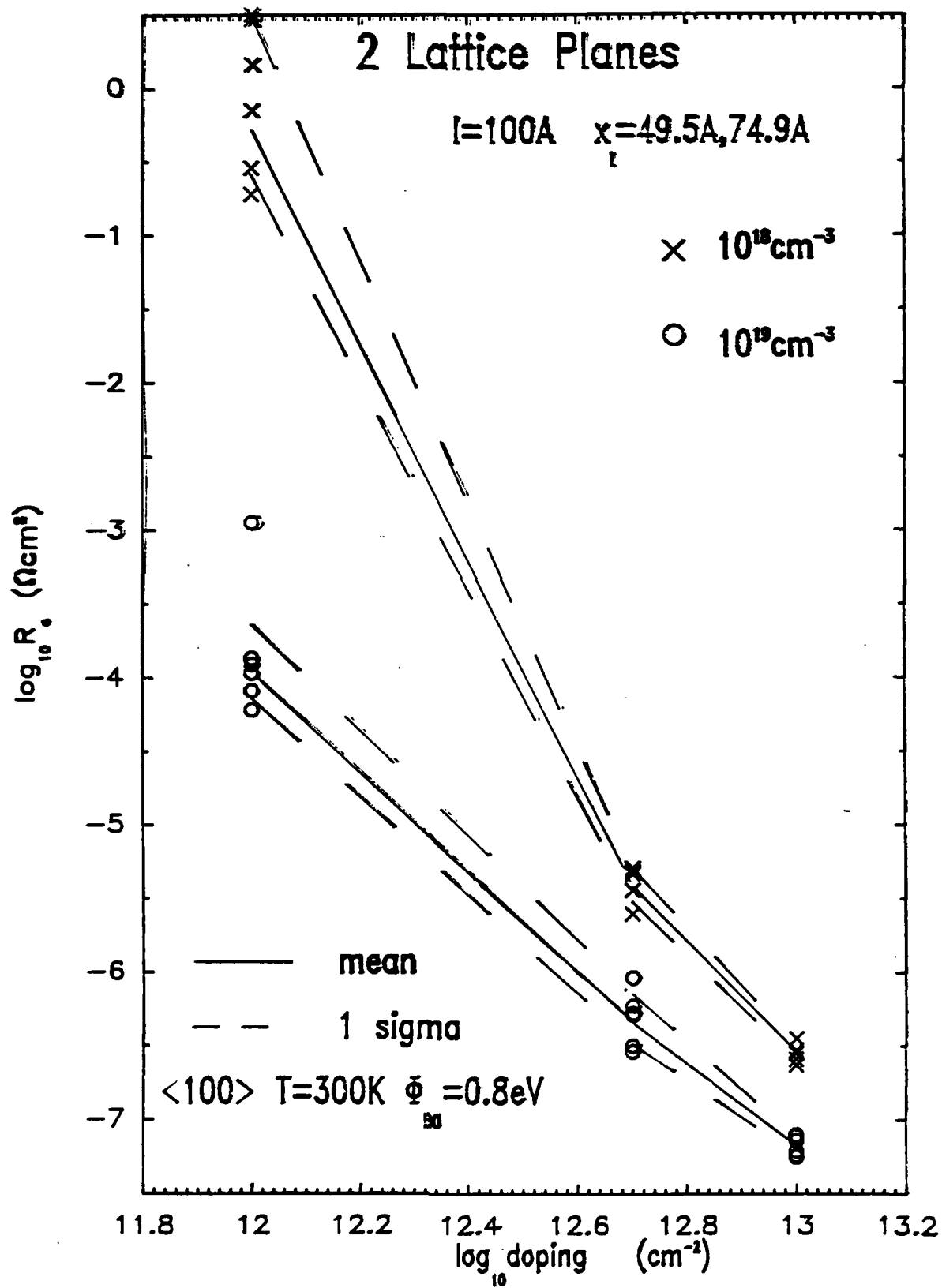












## SUMMARY

- A. OHMIC CONTACTS COULD  
LIMIT SMALL DEVICES
- B. FLUCTUATIONS ARE  
INHERENT DUE TO  
DISCRETE DOPING
- C. DELTA-DOPING ALLOWS  
SUPPRESSION OF FLUCTUATIONS

## FUTURE

- A. WHAT IS MINIMUM  
VALUE OF  $\rho_c$  ?
- B. HOW DOES  $\rho_c$  DEPEND  
ON METAL?
- C. CAN FLUCTUATIONS BE  
SUPPRESSED?
- D. WHAT ARE THE NOISE  
PROPERTIES OF OHMIC  
CONTACTS?
- E. WHAT IS THE DISTRIBUTION  
OF ELECTRONS EMITTED BY  
"OHMIC" CONTACT UNDER LARGE  
BIAS ?

S. S. Lau

**Non-alloyed ohmic contact by  
Solid State Reactions**

U.C.S.D.

IBM

Cornell

Eric Marshall  
Bei Zhang  
L. C. Wang  
S. S. Lau

T. F. Kuech

K. Kavanagh

We concentrate on:

Ge/Pd/n - GaAs

and

Si/Pd/n - GaAs

The use of Ge-Pd on n-GaAs is not new:

A. K. Sinha et al 1975

H. R. Grinolds and G. Y. Robinson 1980.

n-GaAs	Ge	Pd
$1.2 \times 10^{16}$	500 Å	500 Å

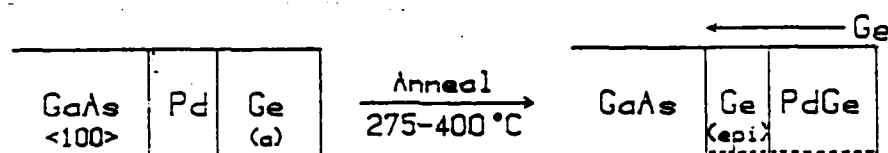
500 - 600°C

$3 - 4 \times 10^{-7} \Omega \text{cm}^2$

Surface very rough

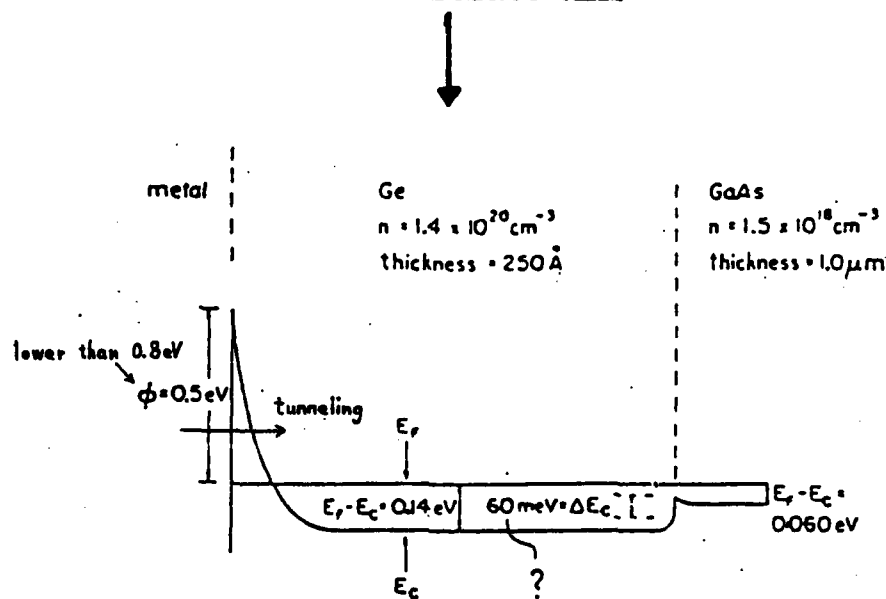
The contact deposition scheme is inverted in our case →  
appears to make a big difference

Solid State Reactions:  
Configuration(schematic):



Thickness: 500 Å 1150 Å  
 Atomic Ratio: 1 : 1.5

The idea is to simulate this

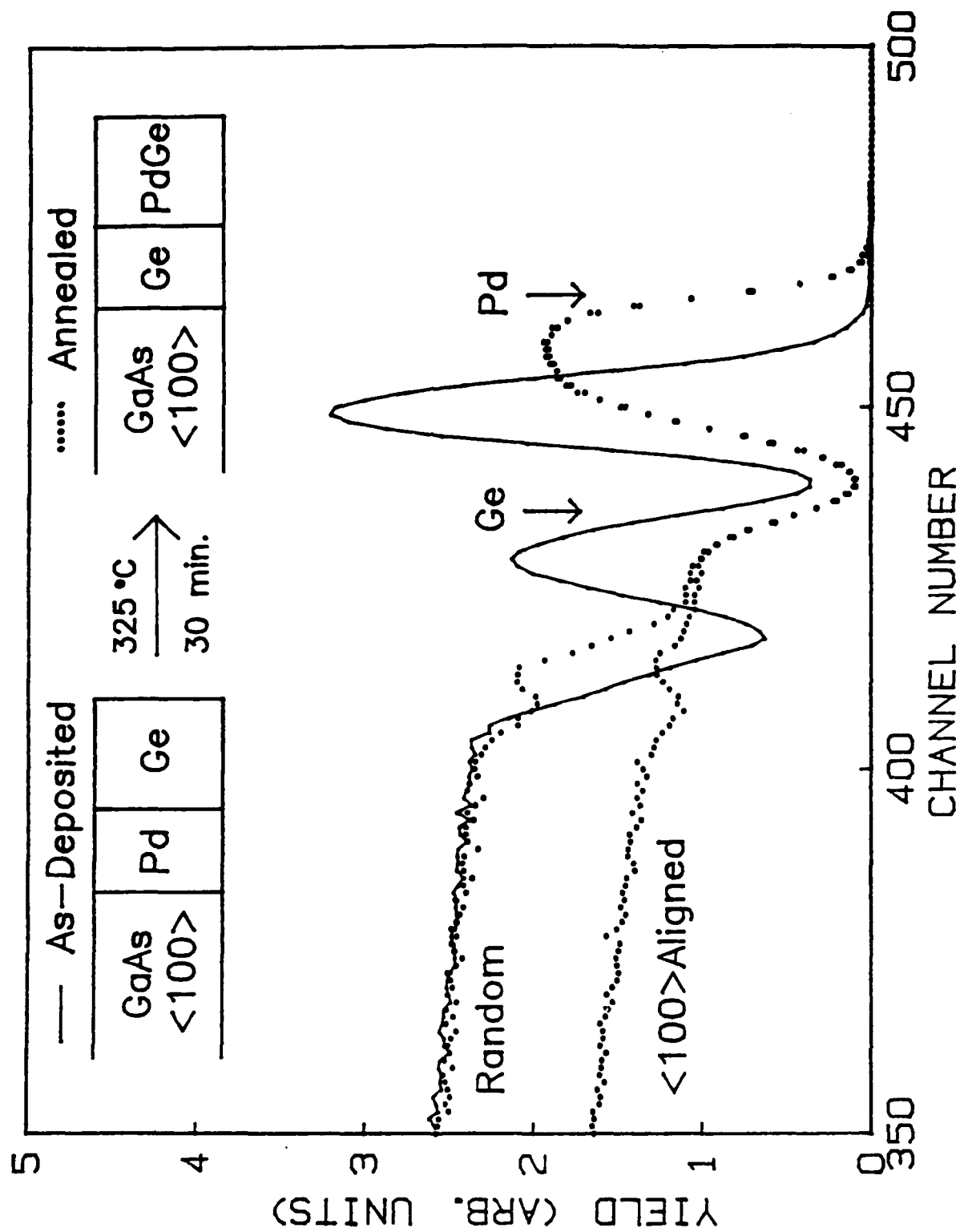


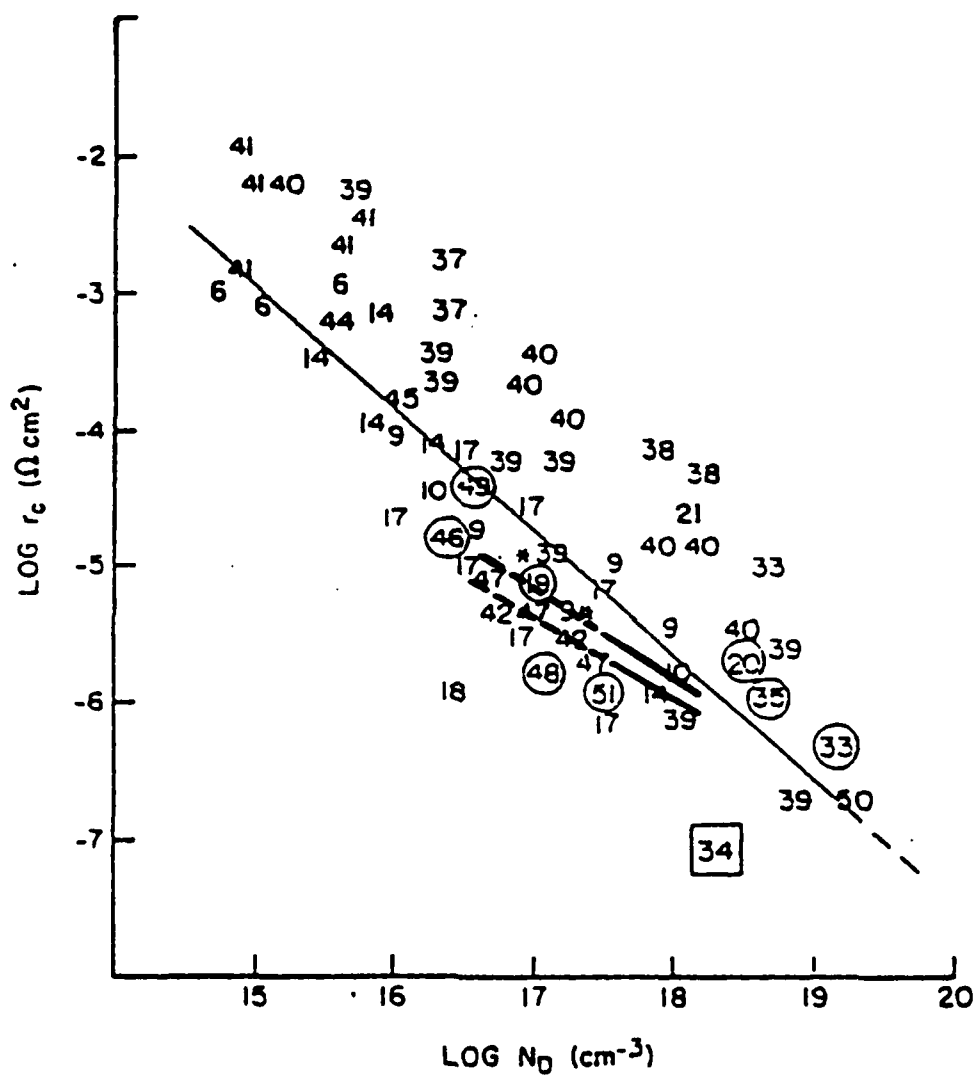
R. Stall, C.E.C. Yeod, K. Board, and L.F. Eesteen,  
 Electronics Letters, 15, 888 (1979).

$$R_c \sim 10^{-7} \Omega \text{ cm}^2 \text{ or less}$$

249







Observed contact resistance a function of n-GaAs doping.



a) — 50nm



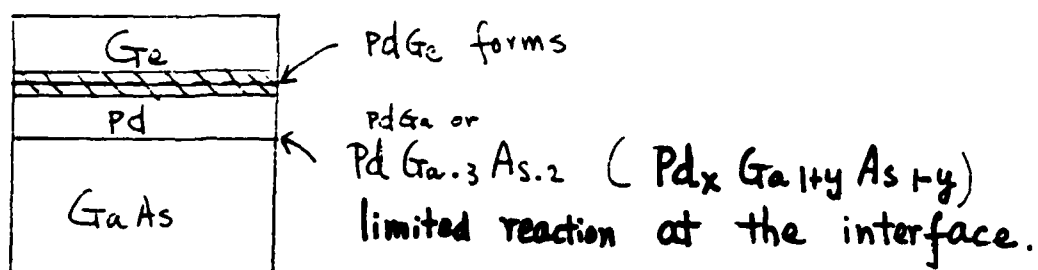
b) — 5nm

Conditions for ohmic behavior:

- (1) Pd must be in contact with GaAs initially  
(Ge/Pd/GaAs  $\rightarrow$  low  $\rho_c$ ; Pd/Ge/GaAs  $\rightarrow$  high  $\rho_c$ )
- (2) Ge is necessary  
(Pd/n-GaAs  $\rightarrow$  high  $\rho_c$  or non- $\Omega$ .)
- (3) Complete transport of Ge generally leads to  
lower  $\rho_c$  and better thermal stability.

How does the Ge/Pd system work?

It is proposed:



Formation of PdGa (or PdGa<sub>3</sub>As<sub>2</sub>) → Excess  
Ga vacant sites → Ge occupies these sites, surface →  
 $n^+$

If this replacement mechanism works for n type  
GaAs, the same mechanism should not yield low  $\rho_c$   
for p type GaAs!

a) ——— 40nm

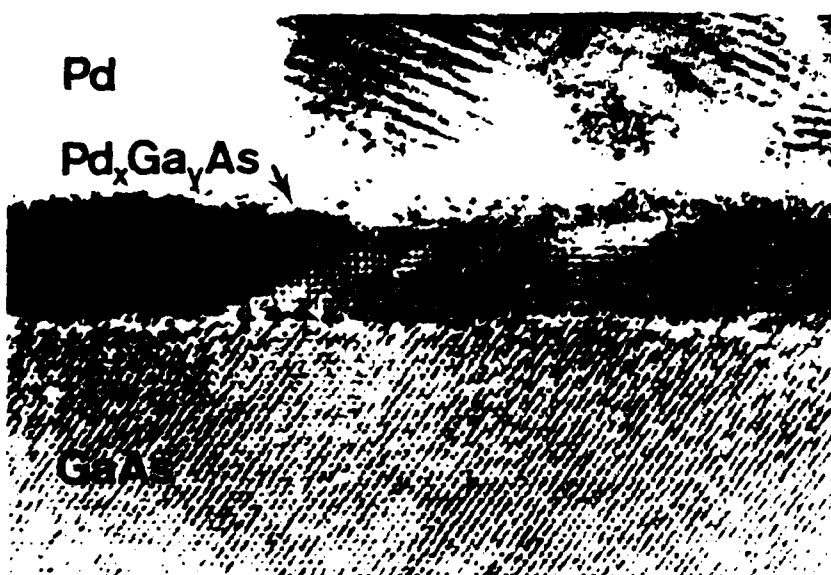
Ge



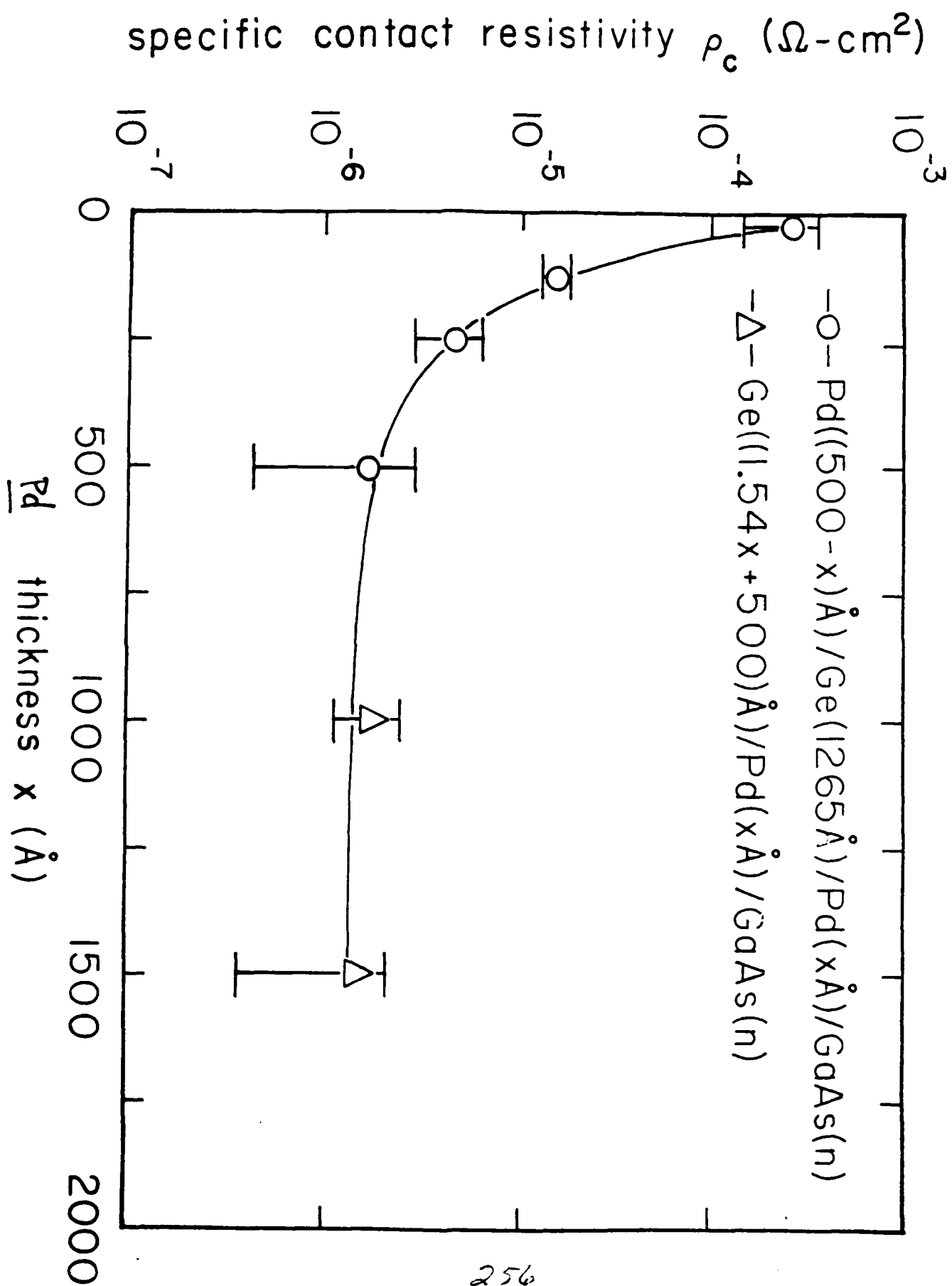
Pd

← Pd<sub>x</sub>Ga<sub>y</sub>As

GaAs



b) ——— 4nm



Experimentally:

(1) For n-type GaAs.

Ge/Pd yields low  $\rho_c$  from  $4 \times 10^{16}$  to  $2 \times 10^{18}/\text{cm}^3$   
( $N_c = 4.7 \times 10^{17}$ )

Pd alone does not work well.

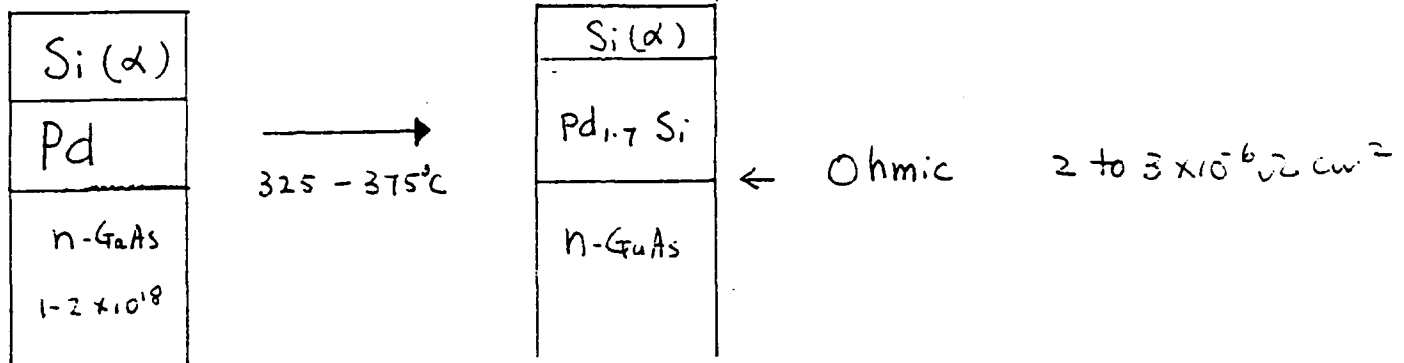
(2) For p-type GaAs,

Ge/Pd yields low  $\rho_c$  from  $> 1 \times 10^{19}/\text{cm}^3$   
( $N_v = 7 \times 10^{18}/\text{cm}^3$ ). For lower concentrations, Pd  
alone works better. To dope p type surface  
selectively, a metal which form mAs should be  
used.



Is the Ge/GaAs heterojunction important in this Ohmic contact scheme?

The evidence we have so far seems to say no.



Note:

- (1) the temperature is low – no macroscopic Si transport (from Backscattering measurement)
- (2) even if there is some microscopic Si transport – the lattice match is poor - should not result in good epitaxy.

Heterojunction does seem to play an important role in ohmic contact formation.

## SUMMARY

- (1) For this ohmic contact scheme to work:
  - (i) Pd must be in contact with GaAs initially.
  - (ii) Ge is necessary.
- (2) The replacement mechanism seems to be applicable.
- (3) The interface is structurally abrupt to atomic dimensions.
- (4) Thermal stability - good at  $\sim 400^{\circ}\text{C}$  for hours (still in the  $10^{-6}$  range) - appear to be related to the uniformity of the transport.
- (5) Applicable to n, p GaAs, n, p InGaAs n, p InGaAsP and n - InP.

## Large Variations of GaAs Schottky Barrier Height by Interface Layers

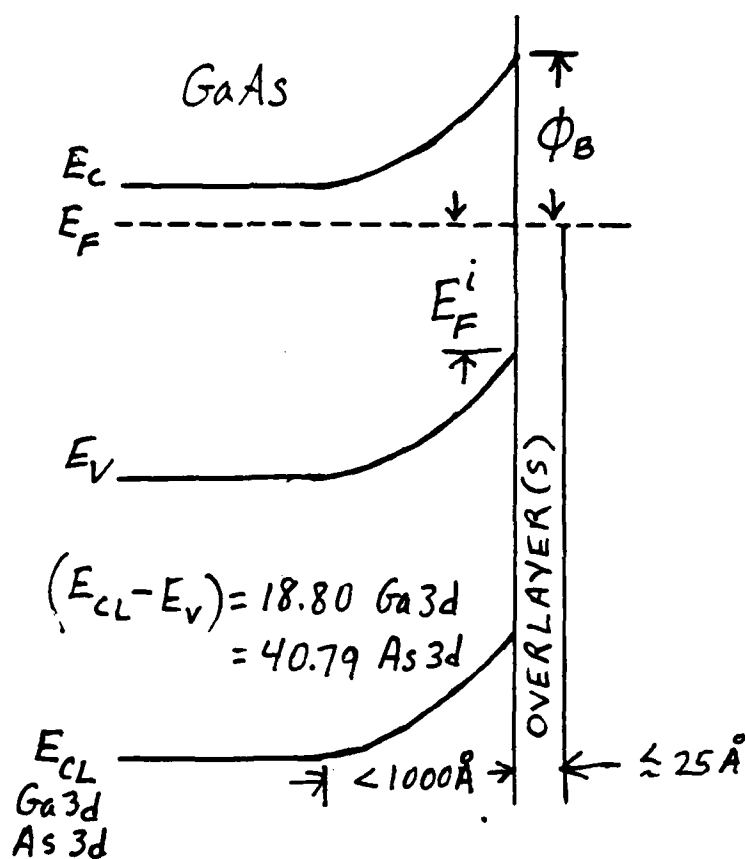
J. R. Waldrop  
Rockwell International

Three examples of interface Fermi energy  $E_F^i$  varying by  
more than 0.6 eV at n-type GaAs (100) interfaces

- a) oxides + Au
- b) metals + chalcogens (S, Se, Te)
- c) model AuGeNi contacts for ohmic contact  
applications

## EXPERIMENTAL TECHNIQUES:

- XPS FOR INTERFACE FERMİ ENERGY  $E_F^i$  AND CHEMISTRY
- I-V AND C-V ELECTRICAL MEASUREMENTS FOR  $\phi_B$



$E_{CL}$  MEASURED AT INTERFACE

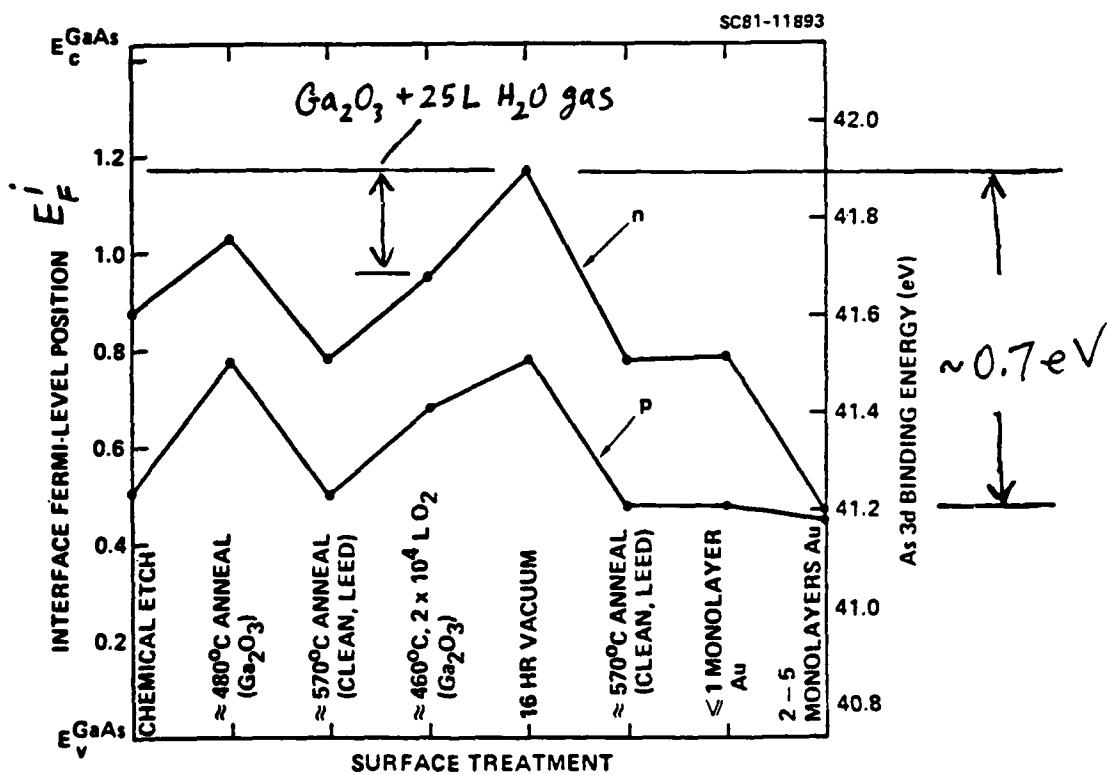
$$E_F^i = E_{CL} - (E_{CL} - E_V) \text{ eV}$$

$$\Delta E_F^i = \Delta E_{CL} \quad 262$$

$$\phi_B = 1.43 - E_F^i \text{ eV}$$


CHANGE IN  $E_F^i$  FOR OXIDE AND METAL SURFACE TREATMENTS (GRANT et al JVST 19, 477 (1981))

GaAs (100)

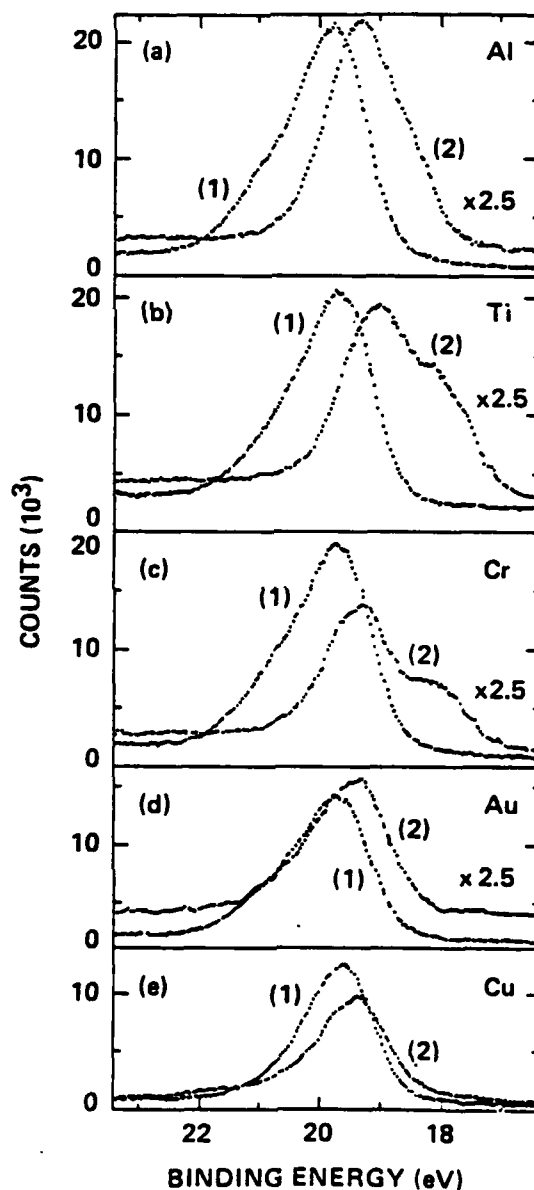


(SAME BASIC BEHAVIOR ON 110 SURFACE)

# DEPOSITION OF METALS ON $\text{Ga}_2\text{O}_3$ SURFACE

$$\Delta E_{\text{Ga}3d} = \Delta E_F^i$$


KOWALCZYK, et al  
Appl Phys Lett 38, 167 (1981)



Ga 3d core level

(1) INITIAL  $\text{Ga}_2\text{O}_3$  SURFACE (LOW BAND BENDING)

(2) AFTER DEPOSITION OF SEVERAL MONOLAYERS METAL

INCREASE IN  $\text{Ga}3d$  B.E. IN EACH CASE INDICATES  
INCREASE OF  $E_F^i$  WITH METAL DEPOSITION

- low band bending,  $E_F^i \sim 1.2$  eV, observed for  $\text{Ga}_2\text{O}_3$  ( $\text{H}_2\text{O}$ ) covered 100 surfaces
- results of Offsey et al (Appl Phys Lett 48, 475 (1986)) indicate low band bending on oxide surfaces after treatment with water and laser irradiation
- low band bending condition eliminated after metal deposition onto  $\text{Ga}_2\text{O}_3$
- up to  $\sim 0.7$  eV shift in  $E_F^i$  occurs with sequential oxide and metal surface treatments



### metal-chalcogen (S, Se, Te)-GaAs interfaces

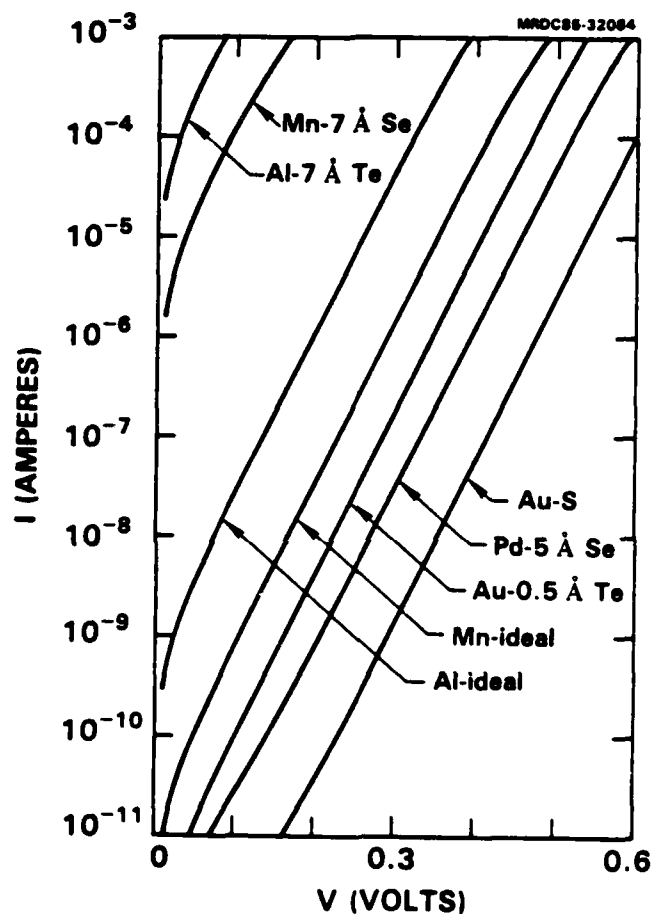
Waldrop, JVST B3, 1197 (1985)

APL 47, 1301 (1985)

- H<sub>2</sub>S exposure (~425°C) of clean GaAs prior to R.T. Al deposition gives I-V measured  $\phi_B$  of ~0.4 eV (Massies, et al, APL 38, 693 (1981))

### Summary of XPS results

- exposure of clean R.T (100) surfaces to elemental S, Se, or Te increases  $E_F^i$  ~0.15 eV to  $E_F(\text{chalcogen}) = \sim 0.85$  eV. Chalcogen exposure alone does not account for low  $\phi_B$
- S and Se form ~5Å reacted region, Te is nonreactive
- Additional  $E_F^i$  shift occurs with metal deposition onto chalcogenide surface
- reactive metals (Al, Mn) increase  $E_F^i$  upon metal-chalcogen reaction; nonreactive metals (Au, Ag, Pd) decrease  $E_F^i$
- Final  $E_F^i$  is after metal deposition
- XPS observed range in  $E_F^i$  is >0.5 eV



REPRESENTATIVE I-V DATA FOR A SELECTION  
OF GaAs SCHOTTKY BARRIER CONTACTS  
AREA =  $5.07 \times 10^{-4} \text{ cm}^2$

I-V DATA CONSISTENT WITH XPS  $E_F^i$  OBSERVATIONS  
NONREACTIVE METAL-CHALCOGEN CONTACTS HAVE  
HIGHER  $\phi_B$  THAN REACTIVE METAL-CHALCOGEN  
CONTACTS 267

Table I  
Influence of Interface S, Se and Te on the Schottky Barrier  
Height of Various Metal Contacts to GaAs

Metal	Interface	n	$\phi_B^{IV}$ (eV)	$\phi_B^{CV}$ (eV)
Al	S	1.05	0.52	0.45
	1.5 Å Se	1.03	0.53	0.52
	4 Å Se	--	~ 0.35	--
	21 Å Se	1.19	0.48	0.39
	3 Å Te	1.04	0.51	0.53
	7 Å Te	1.06	0.44	0.40
	22 Å Te	1.06	0.52	0.50
	ideal	1.04	0.74	0.75
	ideal <sup>a</sup>	1.07	0.85	0.84
Mn	7 Å Se	1.08	0.51	0.61
	ideal	1.03	0.82	0.82
Ti	11 Å Te	1.02	0.72	0.72
	ideal <sup>a</sup>	1.03	0.83	0.83
Au	S <sup>b</sup>	1.03	1.00	1.02
	20 Å Se <sup>b</sup>	1.08	0.97	0.96
	0.5 Å Te	1.03	0.89	0.87
	10 Å Te	1.03	0.83	0.81
	~ 100 Å Te	1.02	0.79	0.78
	ideal <sup>a,b</sup>	1.03	0.89	0.89
Ag	S <sup>b</sup>	1.05	0.96	0.99
	3 Å Te	1.04	0.84	0.84
	ideal, <sup>a,b</sup>	1.03	0.90	0.89
Pd	5 Å Se	1.04	0.93	0.94
	ideal <sup>a</sup>	1.03	0.91	0.93

I-V      C-V

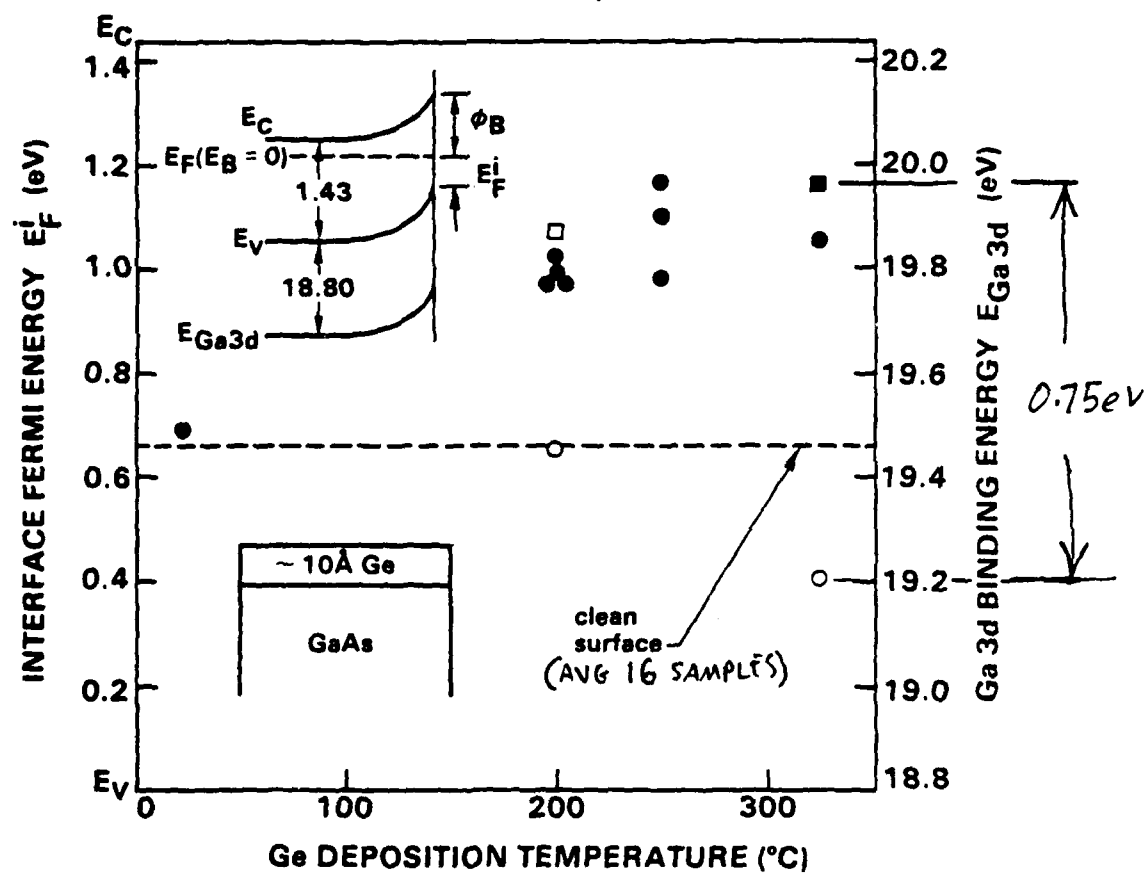
$\phi_B$  RANGE IS ~0.35 eV TO 1.0 eV  
268 (~0.65 eV VARIATION)

### Model AuGeNi contacts to GaAs

Waldrop and Grant, submitted to APL

- nonalloyed contacts consisting of Au, Ni, Ge, NiAs, and Te layers
- correlation of interface composition and  $\phi_B$
- XPS for  $E_F^i$  measurement and composition analysis
- $\phi_B$  measured on thick contacts by I-V (XPS characterized interfaces)
- high temperature nonalloyed ohmic contact applications

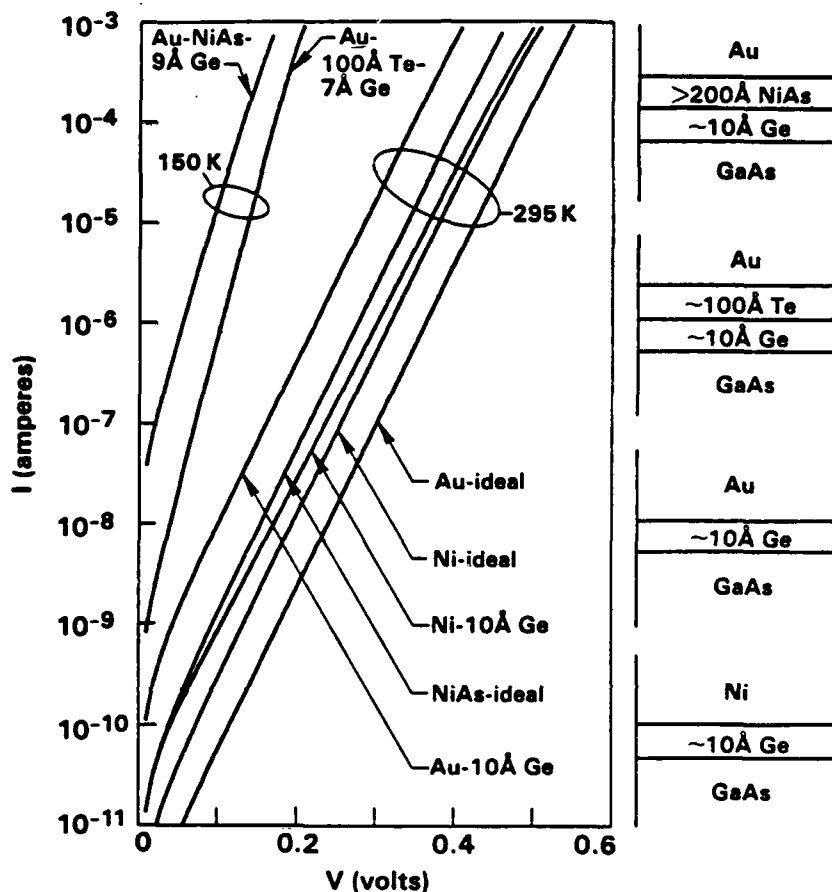
- $10^{-7}$  Torr As DURING Ge DEPOSITION
- $10^{-6}$  Torr As " "
- VACUUM CLEANED / VACUUM Ge DEPOSITION
- CLEANED IN  $10^{-6}$  Torr As / VACUUM Ge DEPOSITION



$E_F^i$  FOR THIN ( $\sim 10\text{\AA}$ ) Ge OVERLAYER ON  
CLEAN GaAs (100)

MAX  $E_F^i$  VARIATION IS  $0.75\text{ eV}$

MAXIMUM  $E_F^i$  IS  $\sim 1.2\text{ eV}$   
270



Representative I-V data for a selection of contacts that have a variety of structures (area =  $5.07 \times 10^{-4} \text{ cm}^2$ )

Multilayered contacts are shown on right

For contacts with Ge interlayer,  $E_F^i = 1.0 - 1.2 \text{ eV}$  before subsequent depositions

XPS  $E_F^i$  measurements for deposition on Ge overlayer consistent with I-V measurements

- low  $\phi_B$  obtained when Ge layers are deposited under certain conditions and Ge-GaAs interface is separated from metal by intervening layer
- intervening layer was NiAs or Te
- for all contact structures  $\phi_B$  ranged from 0.23 to 0.89 eV (~0.65 eV range)

### Summary

- $E_F^i$  of  $\sim 1.0 - 1.2$  eV can be obtained with  $\text{Ga}_2\text{O}_3(\text{H}_2\text{O})$  overlayers,  $\text{Ge}(\text{As})$  overlayers, and metal-chalcogen reactions
- $\phi_B$  ( $E_F^i$ ) variations  $> 0.6$  eV can occur with interfaces that have a wide variety of compositions
- $E_F^i$  is not restricted to a narrow range for all GaAs interfaces



Effects on Schottky Barriers of  
Metal Substitution in Semiconductors\*

E. A. Kraut and W. A. Harrison\*\*

Rockwell International Science Center  
Thousand Oaks, California 91360

ABSTRACT

The question of what effects transport of metal atoms into the semiconductor at a Schottky barrier may have on the barrier properties is examined using tight-binding theory based on universal parameters. For example, the total change in energy associated with an interchange of aluminum and gallium atoms across an interface between metallic aluminum and gallium arsenide is calculated and is found to favor the interchange in agreement with the experimental results of Bachrach and others. Since aluminum and gallium have the same valence this interchange does not transfer charge nor generate appreciable dipoles. However, we take the Schottky barrier height to be determined by the position of the bands relative to the average hybrid energy of the compound, which is expected to match the Fermi-energy of the metal, as suggested by Harrison and Tersoff (PCSI, 1986), who find the energy to the valence band maximum (relative to the average hybrid energy) differs by 0.12 eV between GaAs and AlAs, the latter lying lower. Thus, for example, if 25% of the first layer of Ga atoms are replaced by Al, the Schottky barrier for holes in a junction with p-type material would be increased by 0.03 eV. The shift for n-type barriers can be similarly estimated using the experimental band gaps and is larger. The corresponding calculation for any other system is just as easily obtained using our recent tables of energies of substitution to determine if substitution is expected and the tables of band-lineups to estimate the sign and magnitude of the effect.

\*Supported, in part, by ONR Contract No. N00014-85-C-0135

\*\* Permanent address: Applied Physics Department, Stanford University, Stanford California 94305.

Effects on Schottky Barriers  
of Metal Substitution in  
Semiconductors

E. A. Kraut<sup>1</sup> and W. A. Harrison<sup>2</sup>

Rockwell International  
Science Center <sup>1</sup>

Thousand Oaks, CA 91360  
and

Applied Physics Department  
Stanford University<sup>2</sup>  
Stanford, CA 94305

Work supported, in part, by ONR  
Contract # N00014-85-C-0135

When a metal/semiconductor junction is formed some of the metal atoms may become incorporated into the semiconductor lattice.

A good example is the incorporation of Al atoms into the GaAs lattice at an Al/GaAs interface.

We have used Harrison's tight-binding theory with universal parameters to:

- 1.) calculate the energetics of this interchange and to
- 2.) determine the resulting shift in Schottky barrier height

## INTERFACE BETWEEN METALLIC ALUMINUM & GALLIUM ARSENIDE

Total Change in Energy To  
Substitute an Al atom for a bulk  
Ga atom in GaAs:

- 1.) Energy to remove an Al atom  
from bulk Al (cohesive energy)  
3.39 eV/atom (exp val from Kittel)
- 2.) Energy gained by replacing a Ga  
atom in GaAs by an Al atom  
-1.03 eV (Our calculations)
- 3.) Energy to add the released Ga  
atom to a clump of metallic Ga  
-2.81 eV/atom (coh.energy-Kittel)
- 4.) Net energy gain by replacement:  
 $3.39 - 1.03 - 2.81 = -0.45$  eV/atom

Conclusion: Substitution will occur  
for high enough temperature given  
long enough time 278

## Effect on Schottky Barrier Height

1.) Al and Ga have the same valence so, to first order, there is no charge transfer nor appreciable dipole generation.

2.) The Schottky barrier height is determined by the position of the bands relative to the average hybrid energy of the compound which is expected to match the Fermi energy of the metal (Harrison and Tersoff, 1986).

3.) Relative to the average hybrid energy, the valence-band maximum of AlAs is 0.12 eV lower than the VBM in GaAs. Thus if 25% of the first layer of Ga atoms are replaced by Al atoms, the Schottky barrier for holes in a junction with p-type GaAs would be increased by 0.03 eV.

Tin on Germanium: Also Homopolar  
Energy cost to remove a tin atom  
from the metal =  $3.14 \text{ eV/atom}$

Energy cost to replace a Ge atom  
in bulk Ge by a tin atom =  $1.12 \text{ eV}$

Energy gained by returning the Ge  
atom to bulk Ge =  $3.85 \text{ eV}$

There is now a net energy cost for  
the exchange:  $3.14 + 1.12 - 3.85 = 0.41$   
The two are not very soluble  
largely because of the misfit  
energy which dominates the  $1.12$   
 $\text{eV/atom}$  it costs to substitute tin  
in Ge. So little mixing is expected  
and the effect of what little  
mixing occurs is readily estimated.

## Aluminum on Germanium

### Heterovalent Substitution

Energy cost to remove an Al atom  
from the metal = 3.39 eV/atom

Energy cost to replace a Ge atom  
in bulk Ge by an Al atom = 2.34 eV

Energy gained by returning the Ge  
atom to bulk Ge = 3.85 eV

Net energy cost =  $3.39 + 2.34 - 3.85 =$   
1.88 eV/atom

Because the Al only brings 3  
valence electrons with it, we  
supply the missing electron from  
the Ge valence band, leaving a hole.  
If we started with intrinsic Ge the  
Al substitution dopes Ge p-type  
If the starting Ge is n-type, an  
electron at the Fermi energy near  
the CB edge could drop to the hole,  
gaining a few tenths of an eV and  
reducing the substitution energy  
by this amount. 281

In any case, the actual energy cost to substitute Al for Ge is large. Doping in general is energetically expensive. The energy cost is primarily associated with the rearrangement of bond polarity. We conclude that doping effects, charge shifts, and Schottky barrier variations associated with heterovalent metal substitution into a semiconductor must be associated primarily with nonequilibrium processes i.e. they will not be observed even at high temperatures over long time intervals. These observations may have a bearing on the stability of various types of metal/semiconductor contacts.



## Summary

- Appreciable atomic transfer can occur in special cases-homopolar substitution or compensating doping
- Where large effects can occur-the heteropolar case-the amount of substitution in equilibrium is too small to allow appreciable effects.
- These calculations for other systems are just as easily done using our recent tables of energies of substitution<sup>1-3</sup> and the recent Harrison-Tersoff tables of band lineups.<sup>4</sup>

1.) E.A. Kraut and W. A. Harrison, J. Vac. Sci. Technol. B 3(4), 1267(1985)

2.) E. A. Kraut and W.A. Harrison, J. Vac. Sci. Technol. B 2(3), 409 (1984) 3.) E. A. Kraut

and W. A. Harrison, to be published

4.) W. A. Harrison and J. Tersoff, J. Vac. Sci. Technol. B 4(4), 1058(1986)

III-V Interfaces: Schottky Barriers vs.  
Heterojunctions

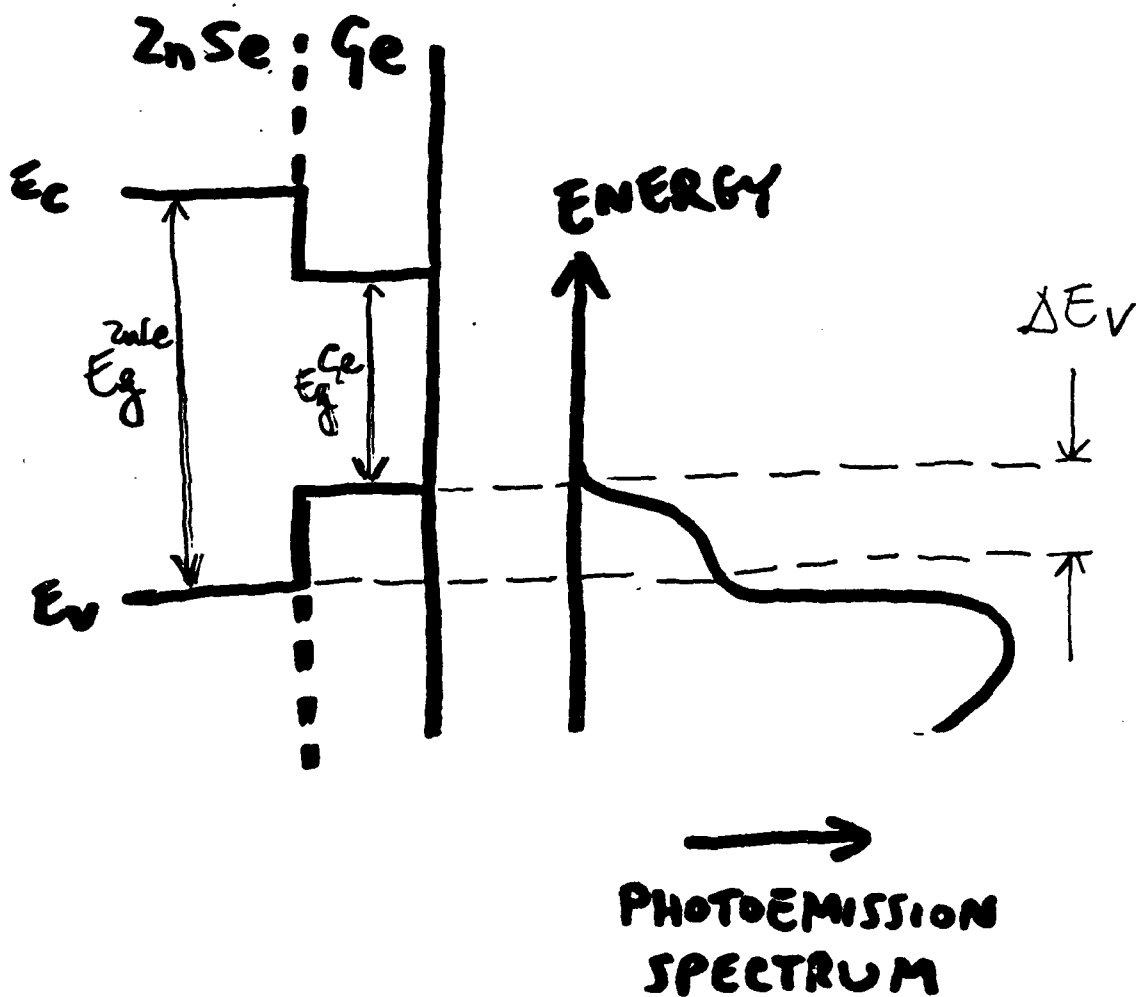
Giorgio Margaritondo

University of Wisconsin

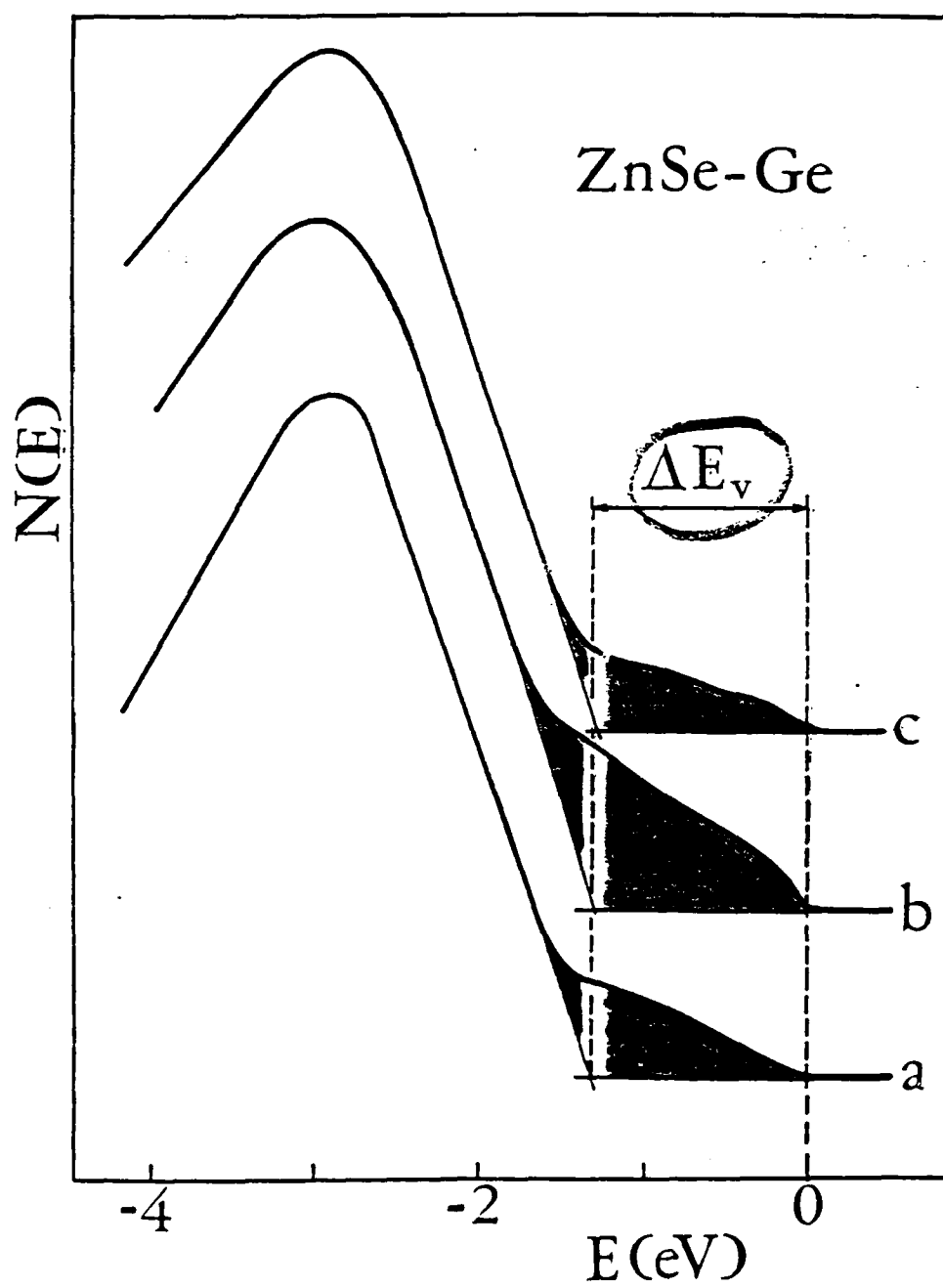
MARGARITON

HETEROJUNCTION BAND LINEUPS  
VS.  
SCHOTTKY BARRIER HEIGHTS

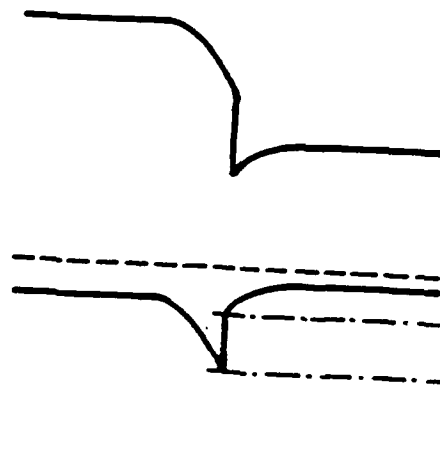
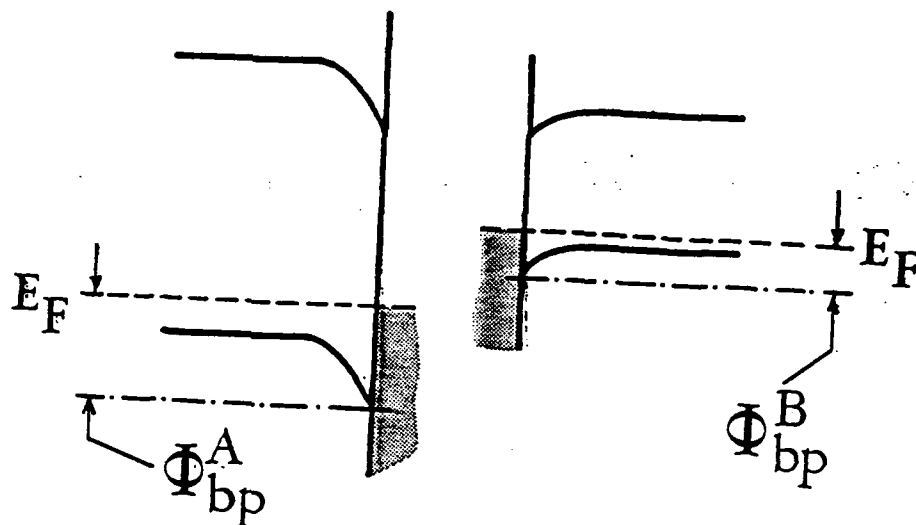
What can we learn from their  
correlation?



**PHOTOEMISSION  
MEASUREMENTS OF  
BAND LINEUPS**



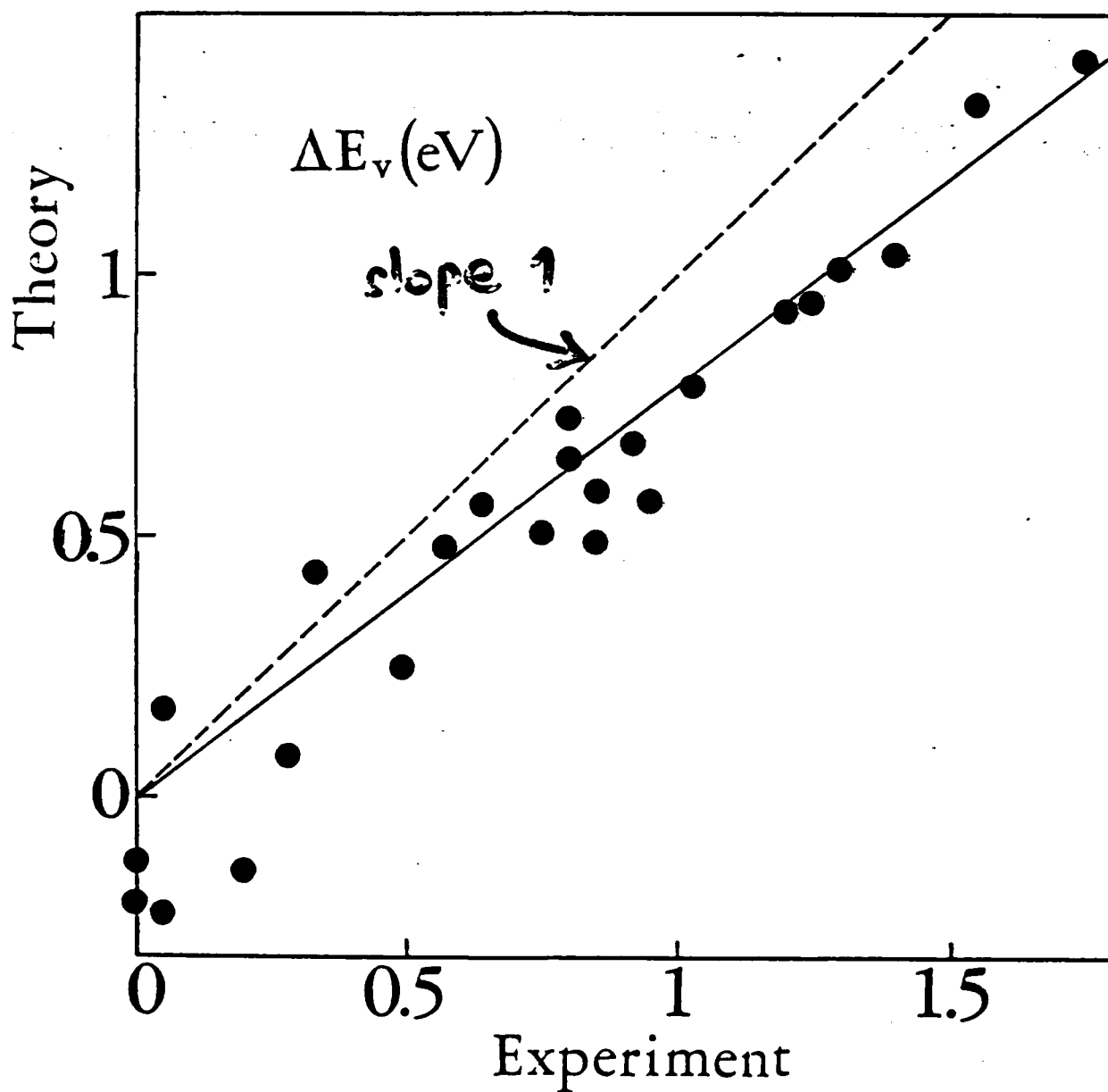
# CORRELATION BETWEEN SCHOTTKY BARRIERS AND HETEROJUNCTION BAND DISCONTINUITIES



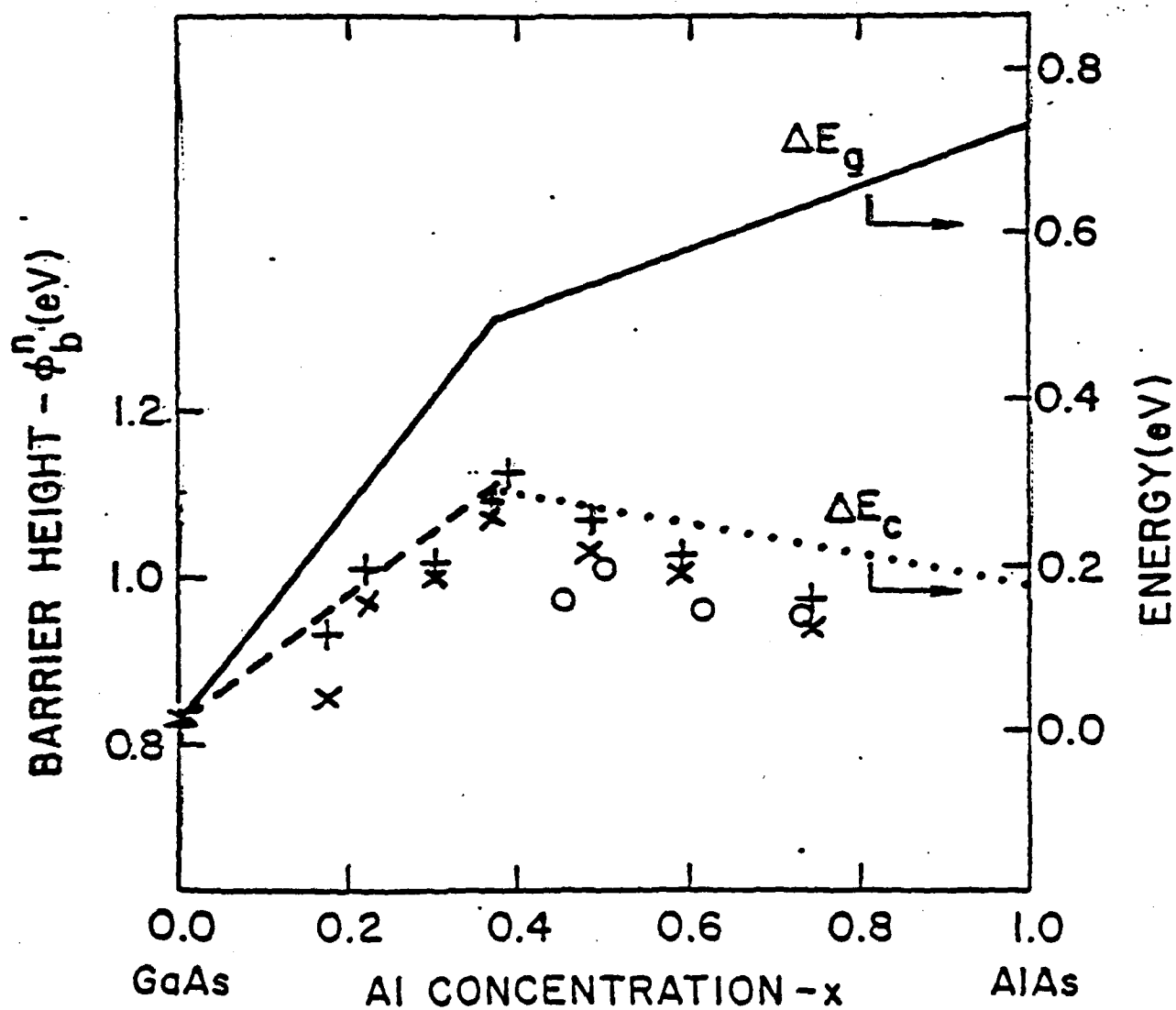
$$\Delta E_v = \Phi_{bp}^A - \Phi_{bp}^B = \Delta \Phi_{bp}$$

(A NAÏVE PICTURE !!!)

# \* CORRELATION BETWEEN SCHOTTKY BARRIERS & HETEROJUNCTION BAND DISCONTINUITIES



CORRELATION BETWEEN  
HETEROJUNCTION BAND LINEUPS  
& SCHOTTKY BARRIER HEIGHTS  
(EIZENBERG, HEIBLUM, NATHAN & BRESLAU)

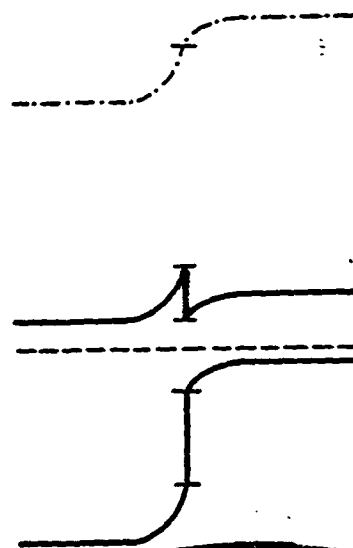
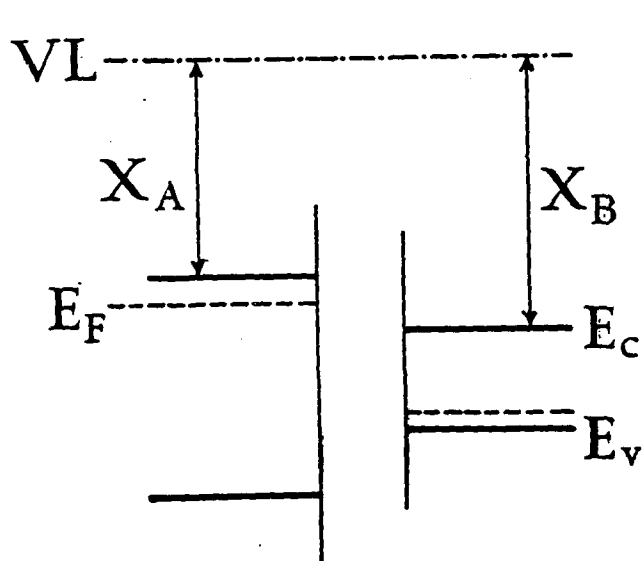




THE CORRELATION BETWEEN  
SCHOTTKY BARRIER HEIGHTS  
AND HETEROJUNCTION BAND  
DISCONTINUITIES IS  
PREDICTED BY:

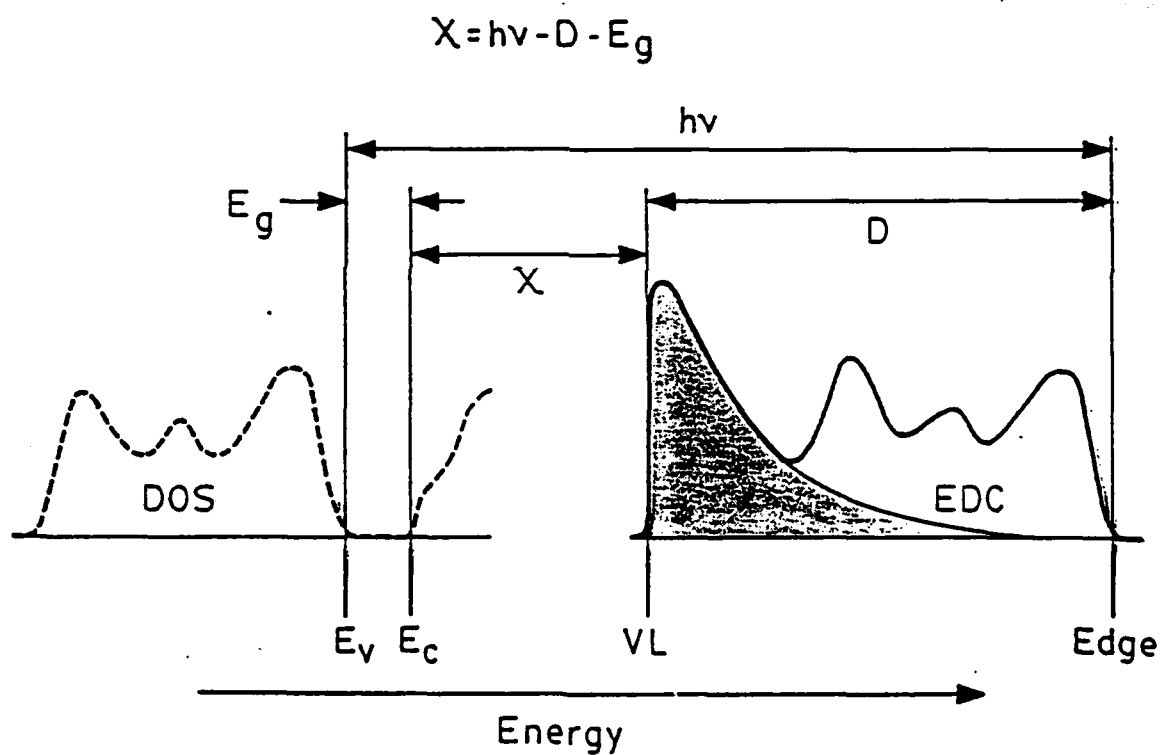
1. Schottky Model for M-S  
Interfaces, plus Electron  
Affinity Rule for S-S  
Interfaces
2. Midgap-Energy (or Charge-  
Neutrality-Point) Theory  
for both M-S and S-S  
Interfaces (Tersoff,  
Flores and coworkers)

# \* ELECTRON AFFINITY RULE



$$\Delta E_C = X_B - X_A$$

# \* PHOTOEMISSION TEST OF THE ELECTRON AFFINITY RULE



## **BREAKDOWN OF THE ELECTRON AFFINITY RULE**

**The Rule Predicts:**

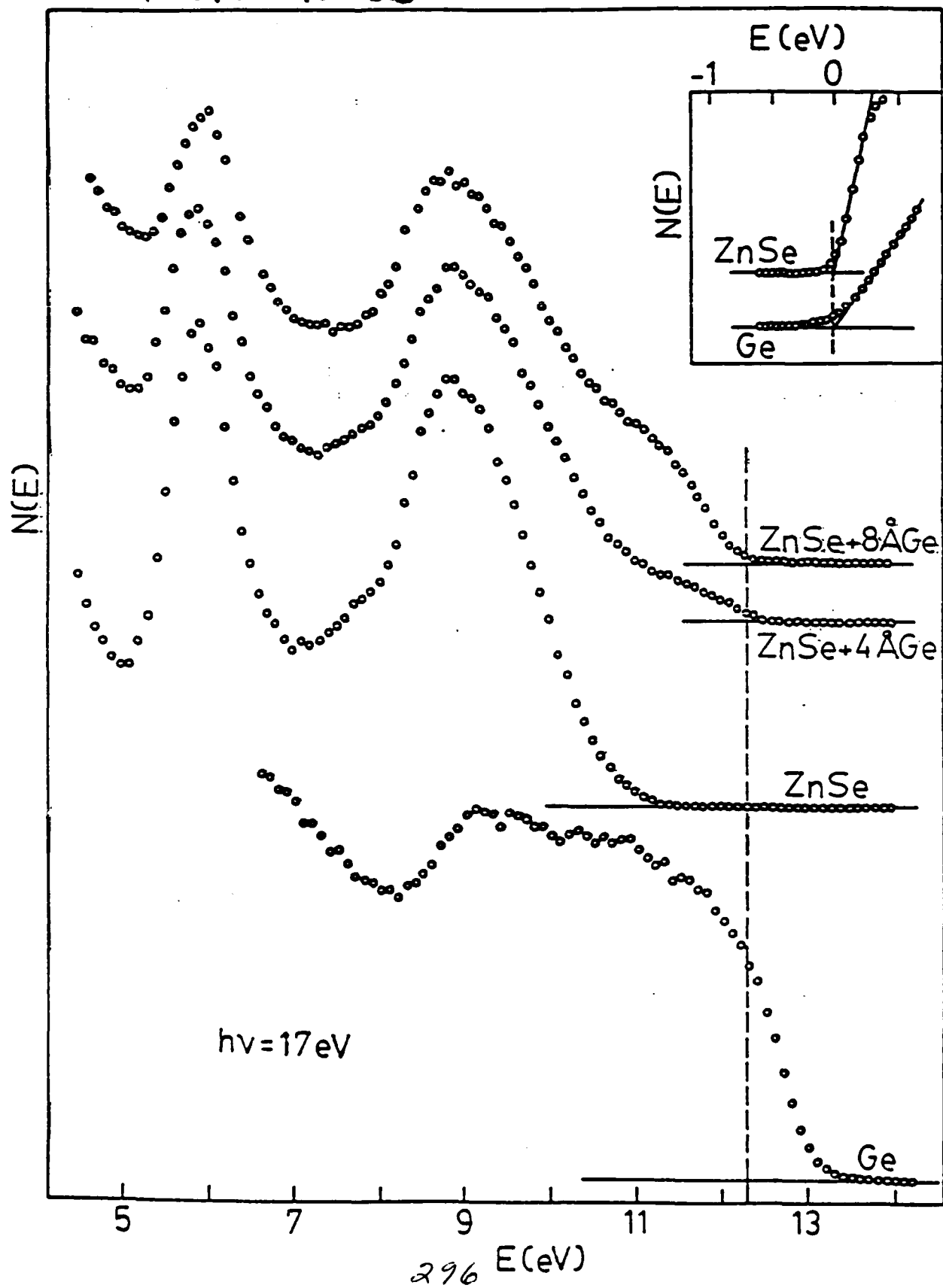
$$\Delta E_v = D_1 - D_2$$

**Experimental Reality  
(ZnSe-Ge):**

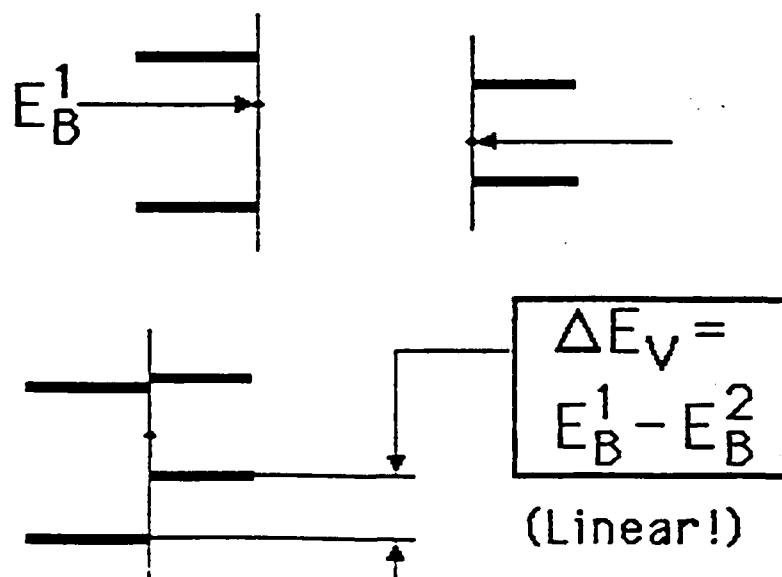
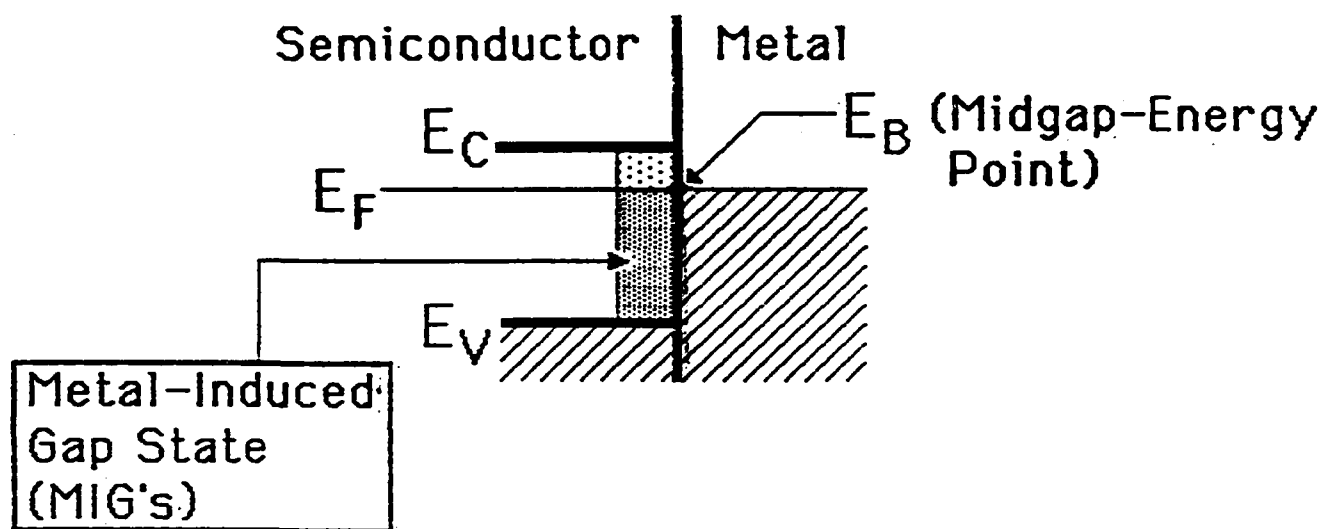
$$D_1 - D_2 = 2.21 \pm 0.46 \text{ eV}$$

$$\Delta E_v = 1.44^{+0.08}_{-0.15} \text{ eV}$$

# \* STANDARD OF THE ELECTRON AFFINITY RULE



# \* Midgap-Energy Approach (J. Tersoff)



## HIGH-RESOLUTION ELECTRON ENERGY LOSS RESULTS:

### Si(111)7x7 - Al

(M. KELLY, G. MARGARITONAS,  
J. FRANKEL, G.J. LAPEYRÉ)

→ Si(111)7x7 is metallic; first  
Al adatoms make it  
non-metallic (GAP WIDENS)

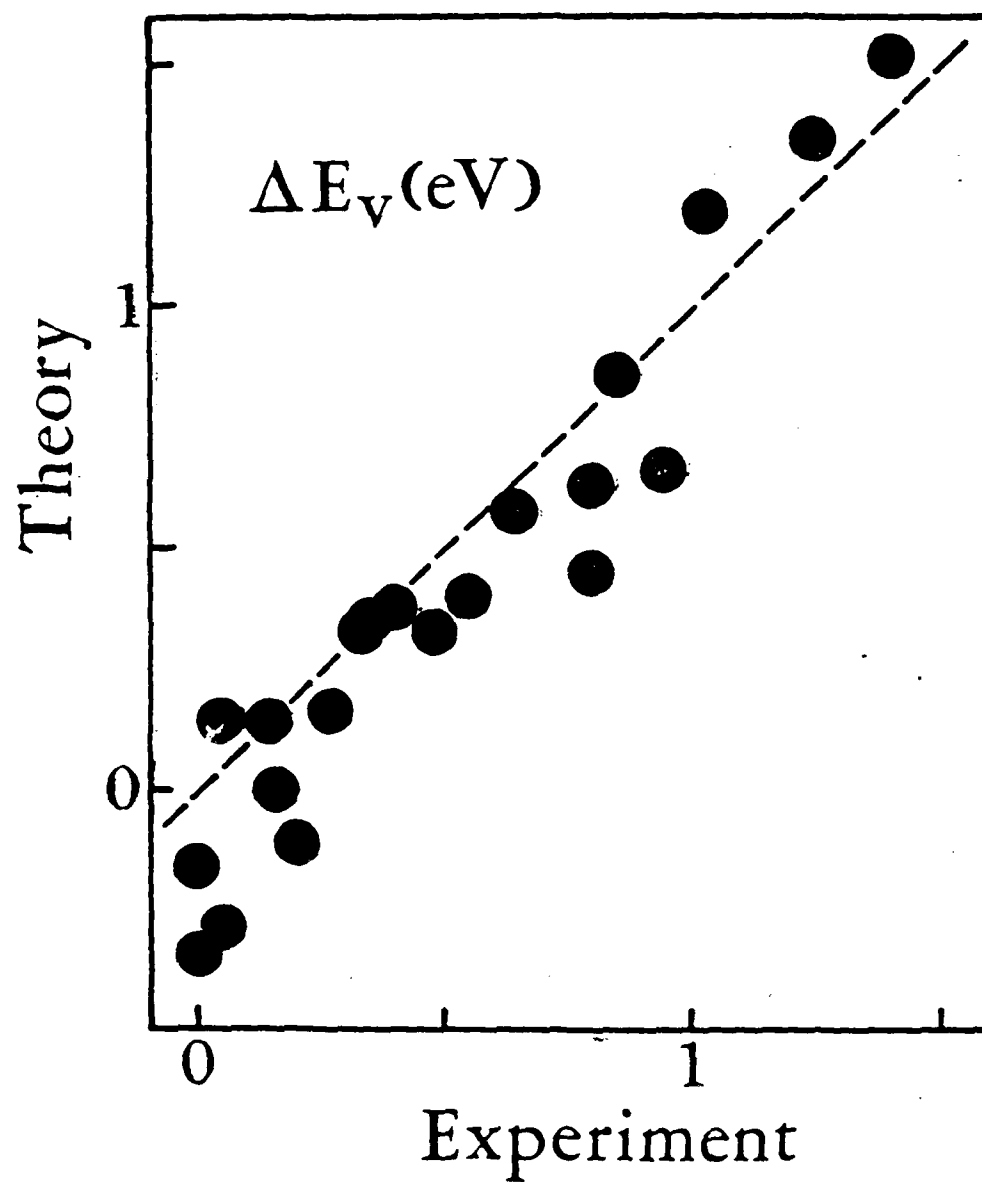
→ At  $\approx$  monolayer coverage,  
metallic character  
reappears

→ At  $\approx$  1.5 monolayer  
coverage:

\*  $E_F$  movement saturates  
(Schottky Barrier is  
formed)

\* Metallic character  
is strong

# ~~X~~ MIDGAP - ENERGY - THEORY VS. EXPERIMENT ( $\Delta E_v$ )





## DEFINITION OF "LINEAR" MODELS:

Band Discontinuity =  $T_1 - T_2$

$T_i$  depends on semiconductor  $i$

### Examples:

- o ELECTRON AFFINITY RULE  
(Anderson, Duke-Mailhiot, Flores et al., etc.)
- o MIDGAP-ENERGY APPROACH  
( )
- o TIGHT-BINDING  
(Harrison)
- o PSEUDOPOTENTIAL  
(Frensley-Kroemer)
- o DEEP-IMPURITY APPROACH  
(Zunger et al., Langer-Heinrich)

General Optimization: Katnani-Margaritond

ALL THE GENERAL-PURPOSE HETEROJUNCTION DISCONTINUITY MODELS ARE

**LINEAR MODELS:**

$$\Delta E_v^{1,2} = T_1 - T_2$$

(WHERE THE TERMS  $T_1$ ,  $T_2$  ARE DETERMINED BY THE TWO COMPONENTS OF THE HETEROJUNCTION)

(EXAMPLES: HARRISON, FRENSLEY-KROEMER, TERSOFF, ANDERSON ETC.)

CONSEQUENCES OF THE LINEARITY THAT CAN BE TESTED WITH OUR DATA BASE:

1. TRANSITIVITY:  $\Delta E_v^{1,2} + \Delta E_v^{2,3} + \Delta E_v^{3,1} =$
2. THE DISCONTINUITIES ARE INDEPENDENT OF THE MICROSCOPIC INTERFACE PROPERTIES

GENERAL RESULT OF TESTS:

ALL LINEAR MODELS HAVE AN UNDERLYING ACCURACY LIMIT. THEIR AVERAGE ACCURACY IN PREDICTING THE BAND DISCONTINUITIES CANNOT EXCEED 0.15 eV.

AD-A183 158

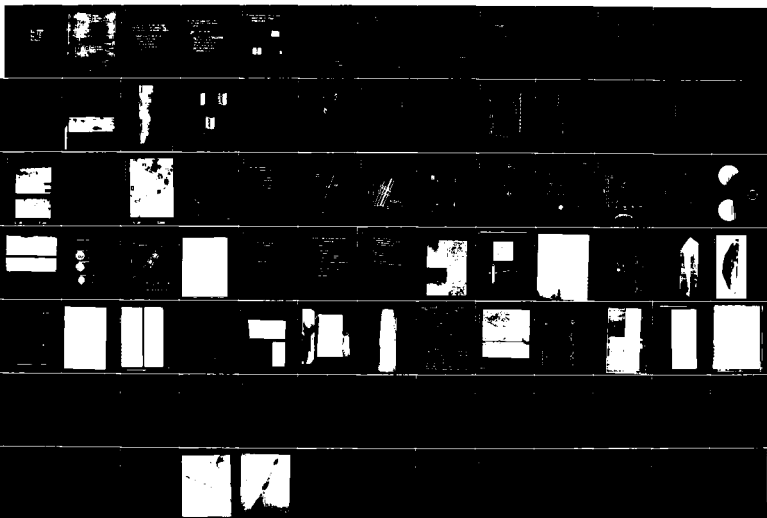
A WORKSHOP ON 3-5 SEMICONDUCTOR: METAL INTERFACIAL  
CHEMISTRY AND ITS EFFECTS (U) STANFORD UNIV CA  
W E SPICER ET AL. 05 NOV 86 N00014-87-G-0038

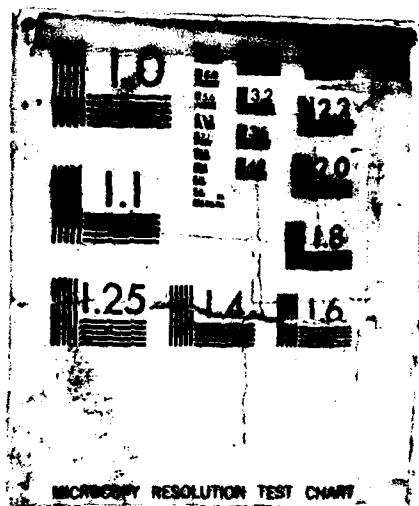
4/7

UNCLASSIFIED

F/G 20/12

NL

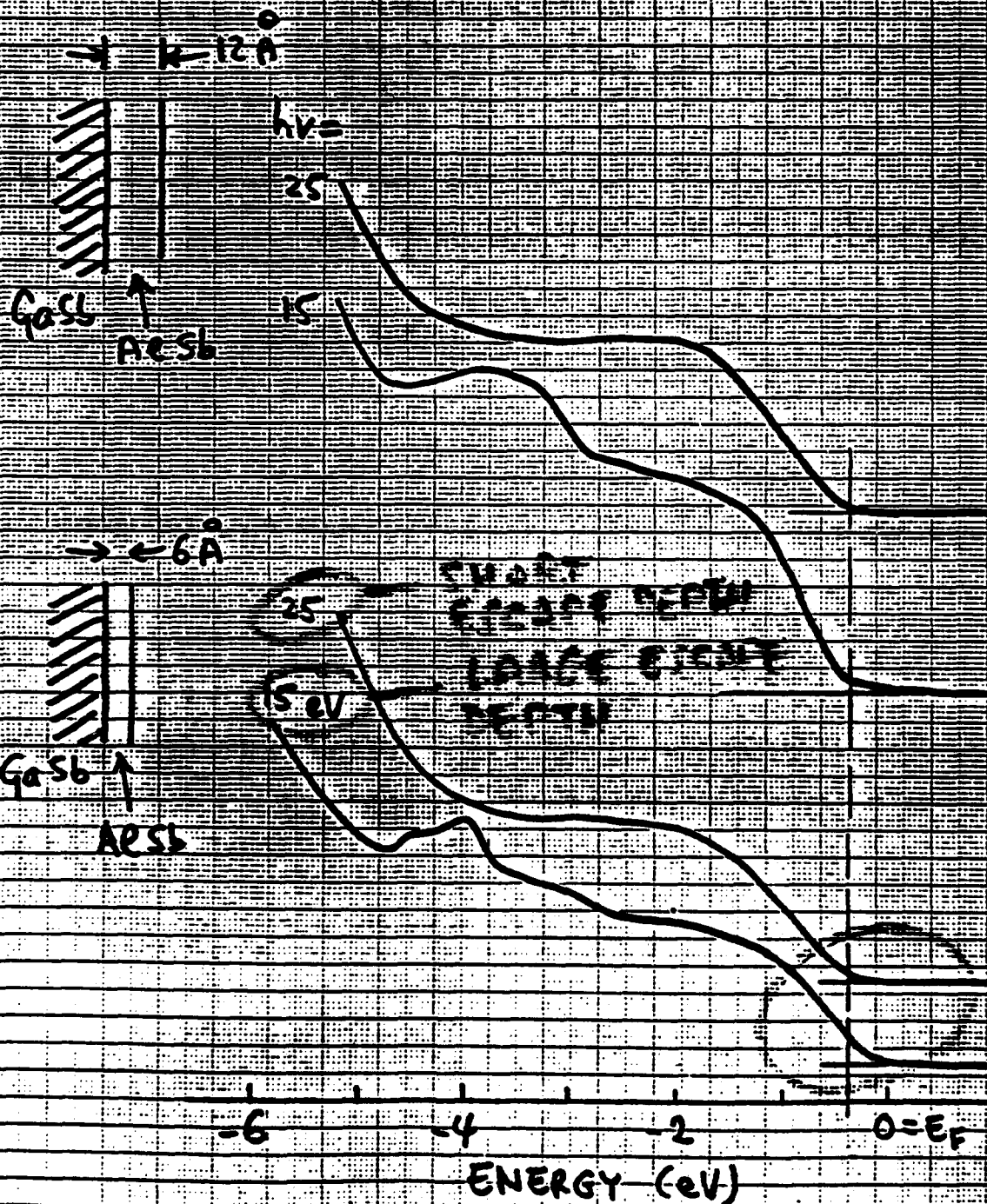




(INTERFACES -  
PHOTODEMISSION

G. GUALTIERI, G. P. SCHWARTZ,  
R. G. NUZZO, W. A. SUNDER

D. NILES, BARRY LAI, G. WEUS,  
J. MCKINLEY, F. GERHARD,  
G. HARRINGTON]



**\* LOCAL FACTORS WHICH CAN**  
**POTENTIALLY INFLUENCE THE**  
**HETEROJUNCTION BAND LINEUP:**

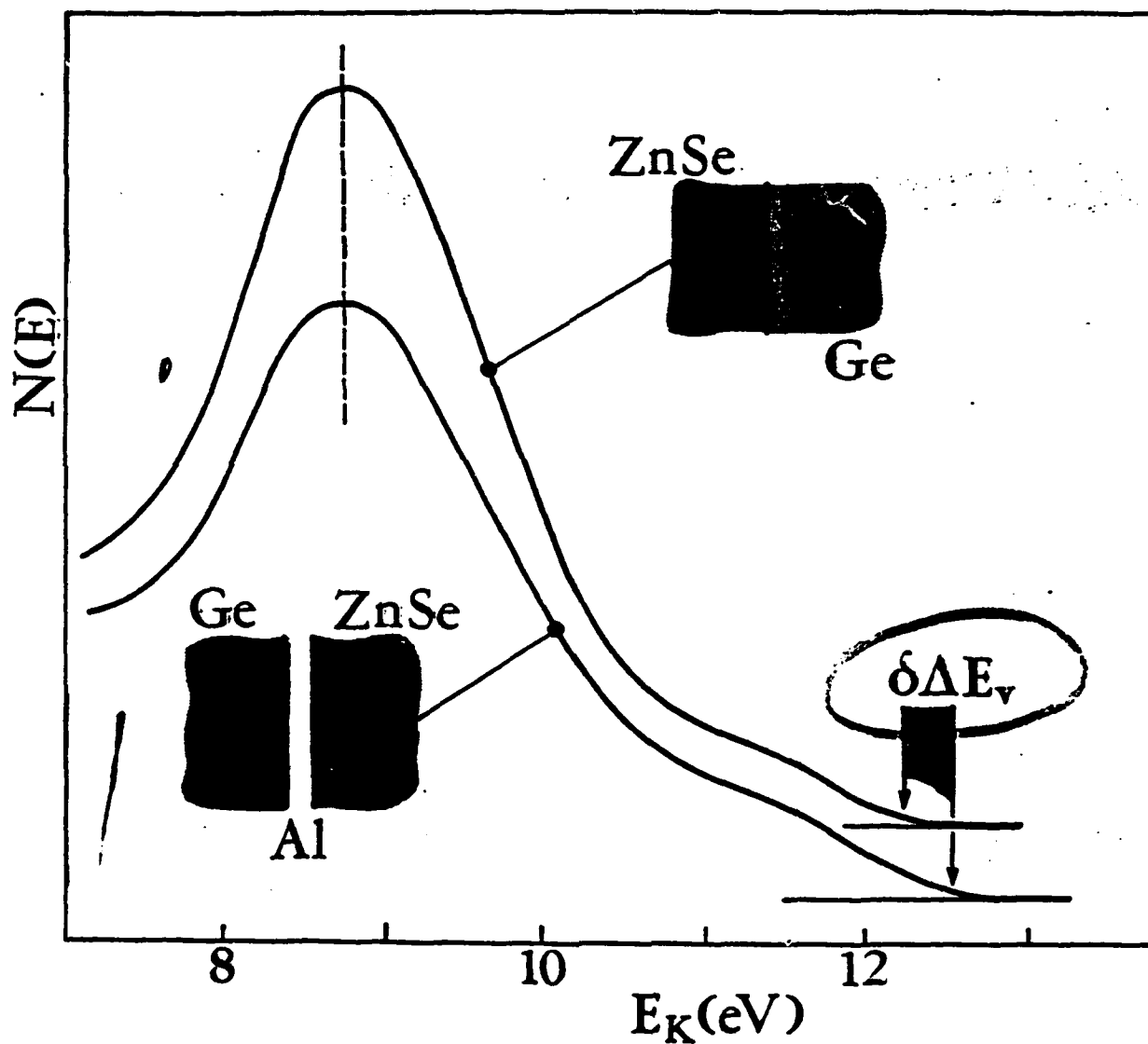
- \* 1. Substrate Orientation**
- \* 2. Local Morphology**
- \* 3. Microdiffusion**
- \* 4. Interface Bonds**
- \* 5. Interface Defects**
- ... etc.**

● **CAN WE CONTROL THE  
HETEROJUNCTION BAND  
LINEUP?**

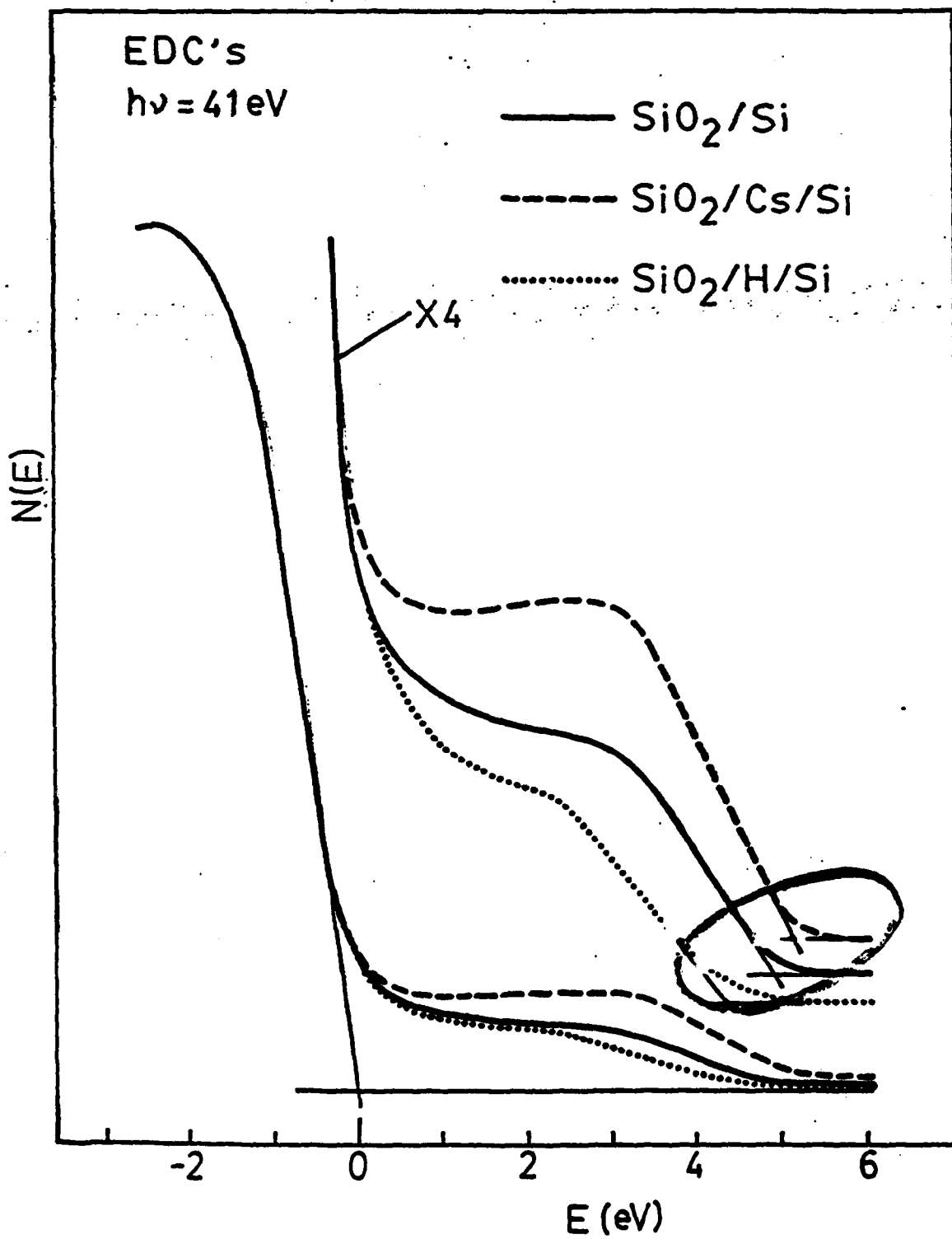
**YES -- BY USING:**

- **1. ULTRATHIN INTRALAYERS**  
(Perfetti et al.,  
Margaritondo et al.,  
Grunthaner et al.)
- **2. DOPING PROFILES**  
(Capasso et al.)

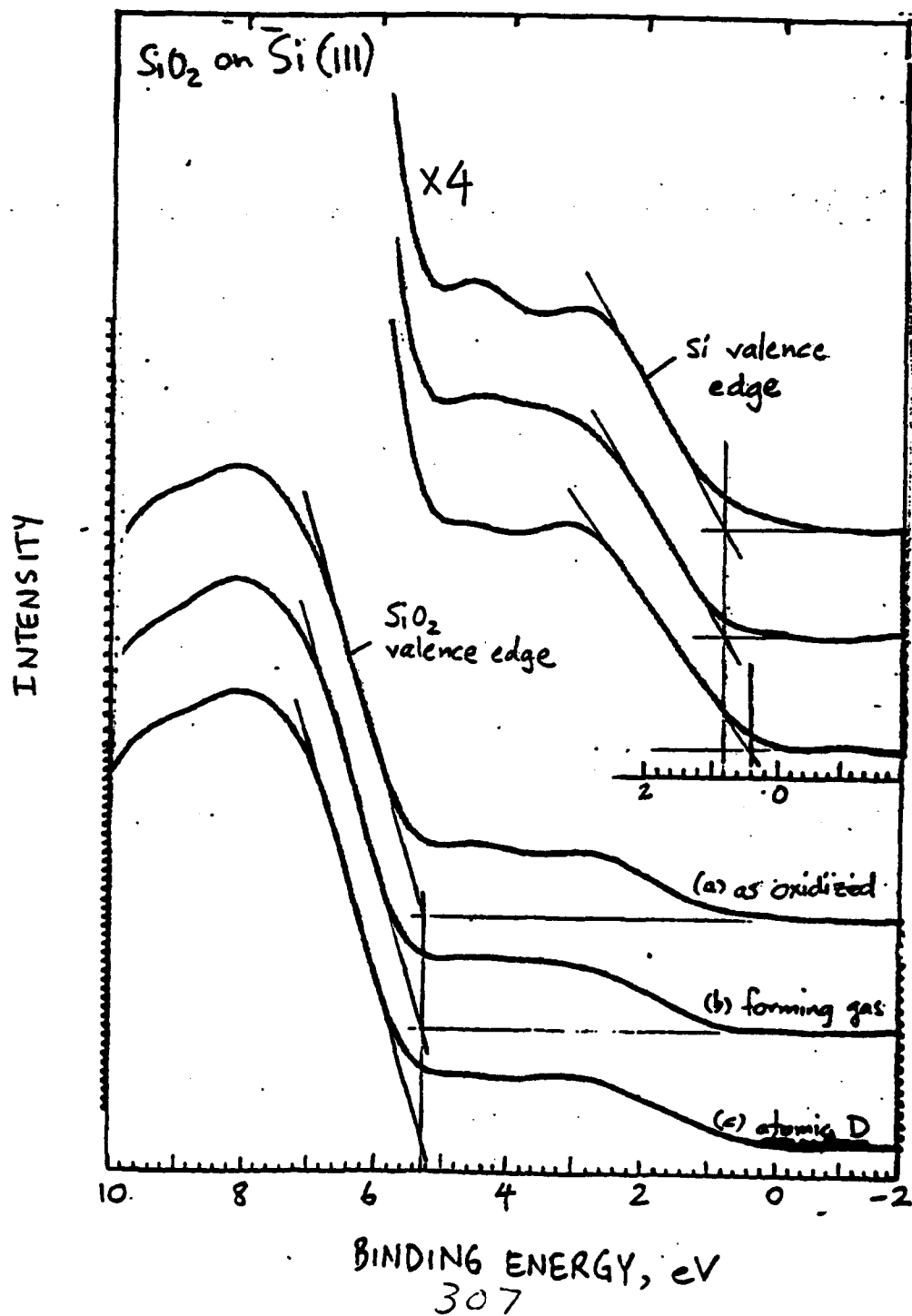
# \* MODIFICATION OF A BAND LINEUP BY A THIN INTRALAYER







[GRUNTHANER, P. & F.J.,  
et al.]



***A theoretical calculation for a ZnSe-Ge(110)  
heterojunction with an ultrathin intralayer***

by

J.C. Durán\*, A. Muñoz and F. Flores

Departamento de Física del Estado Sólido

Universidad Autónoma de Madrid, Cantoblanco, 28049 Madrid, Spain.

***Abstract***

We present a consistent tight-binding calculation of the ZnSe-Ge(110) heterojunction with an Al-monolayer between the two semiconductors. Our results are in reasonable agreement with the experimental evidence found by Niles et al, showing that an ideal interface is an adequate model to explain the interface behaviour. The shift in the valence band offset due to the Al-intralayer is interpreted as a shift in the difference between the charge neutrality levels of both semiconductors, induced by the deposited intralayer.

PACS numbers: 73.40.-c , 73.40.-Lq , 73.40.-Vz .

A comparison between conventional and in-situ  
UHV processing for Co/GaAs structures

**C.J.Palmstrøm, E.W. Chase,**

**Bell Communications Research  
Serin Physics Lab  
Rutgers University  
Box 849  
Piscataway  
N.J. 08854**

**J.P. Harbison, C.C. Chang, A.S. Kaplan, D.-M. Hwang,**

**Bell Communications Research  
Navesink Research and Engineering Center  
Box 7020  
331 Newman Springs Rd.  
Red Bank  
N.J. 07701**

**A.Yu, G.J. Galvin and J.W. Mayer**

**Materials Science and Engineering  
Bard Hall  
Cornell University  
Ithaca  
N.Y. 14850**

K.-N. Tu and J. Cuomo

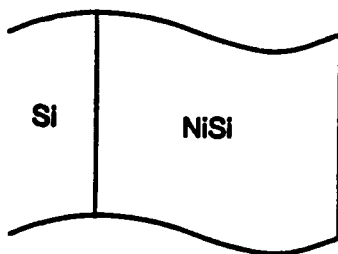
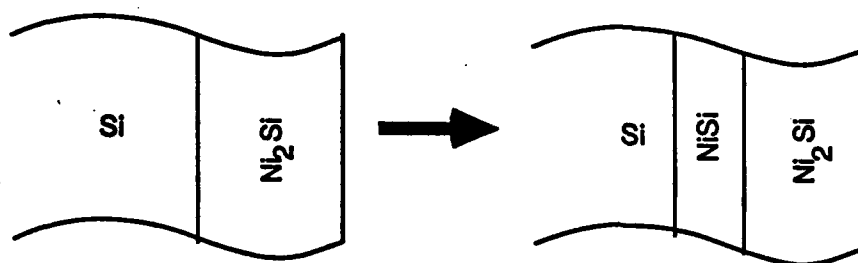
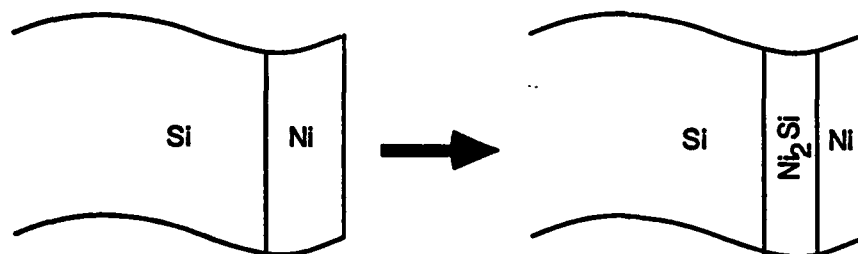
IBM YORKTOWN

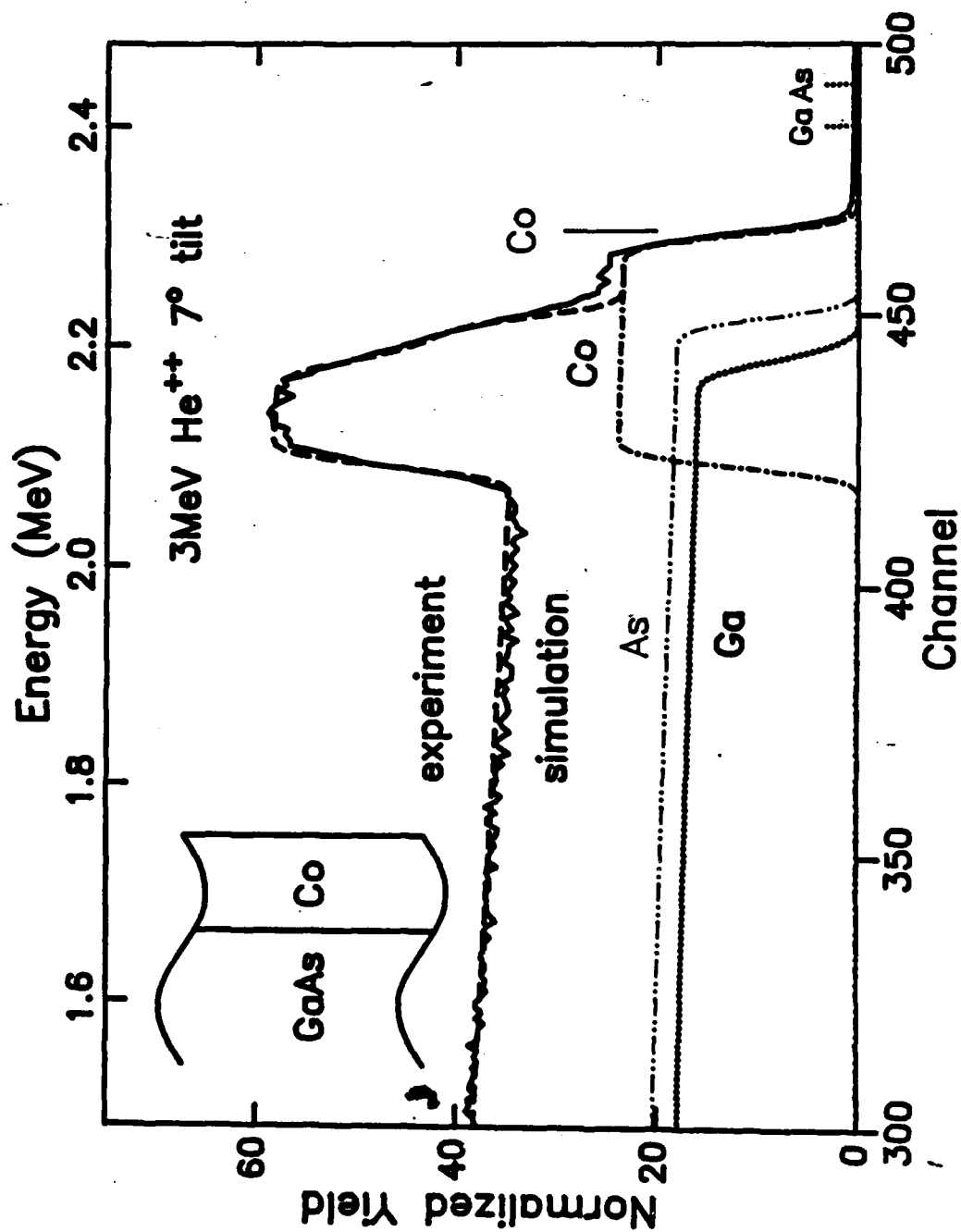
} Thick samples

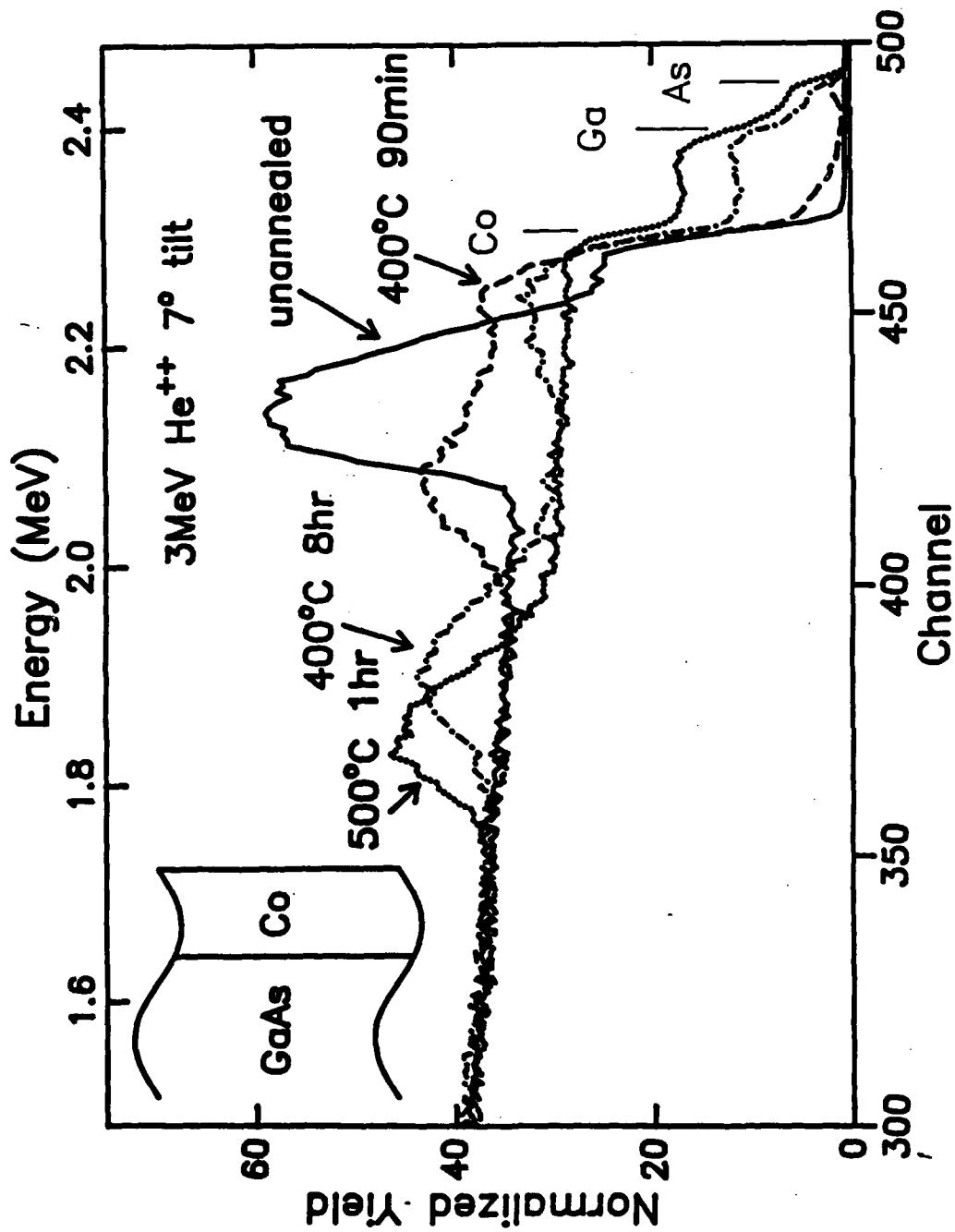
L. Doolittle & M. Thompson  
Cornell.

'RUMP' RBS  
analysis program

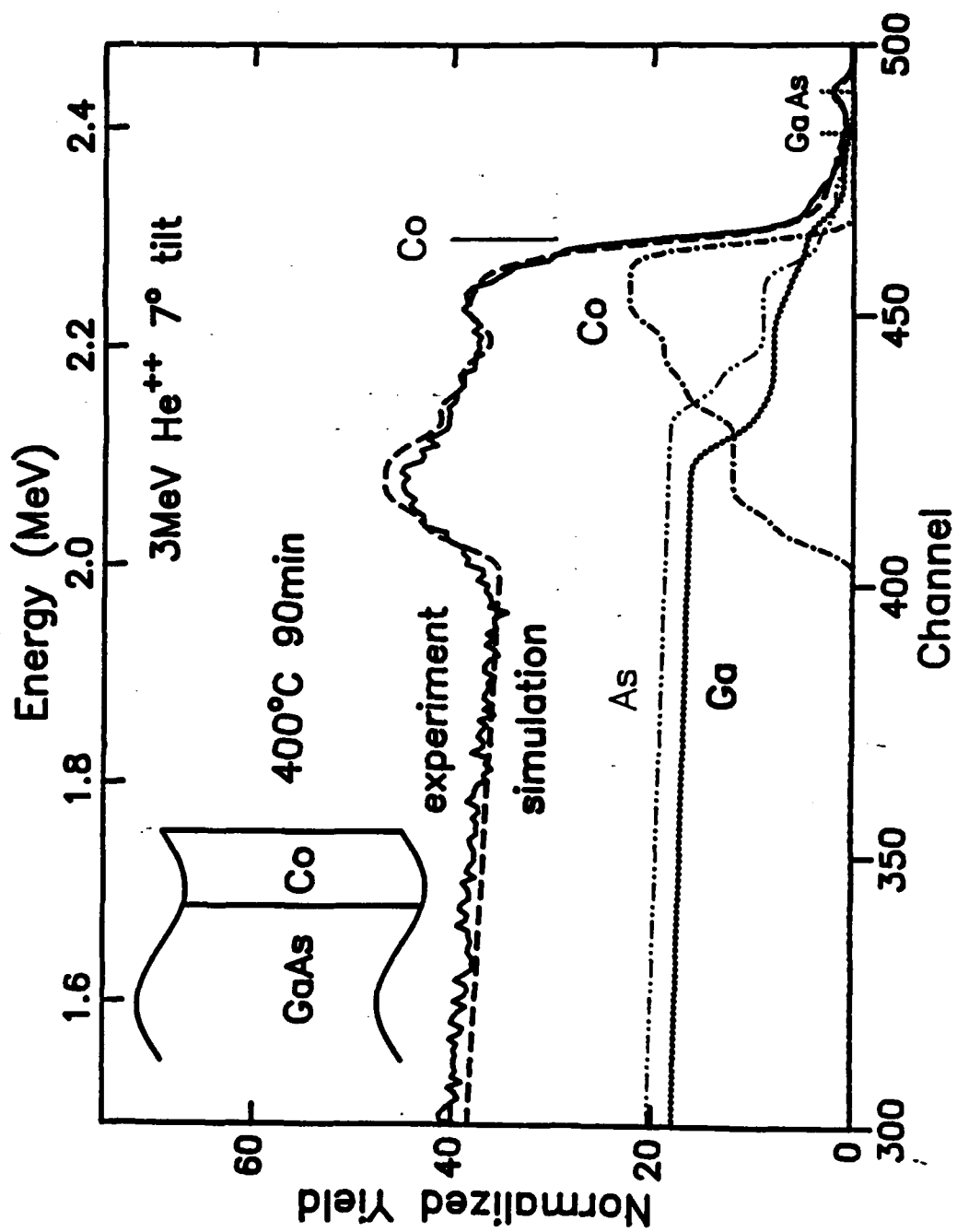
# Metal/Si reactions

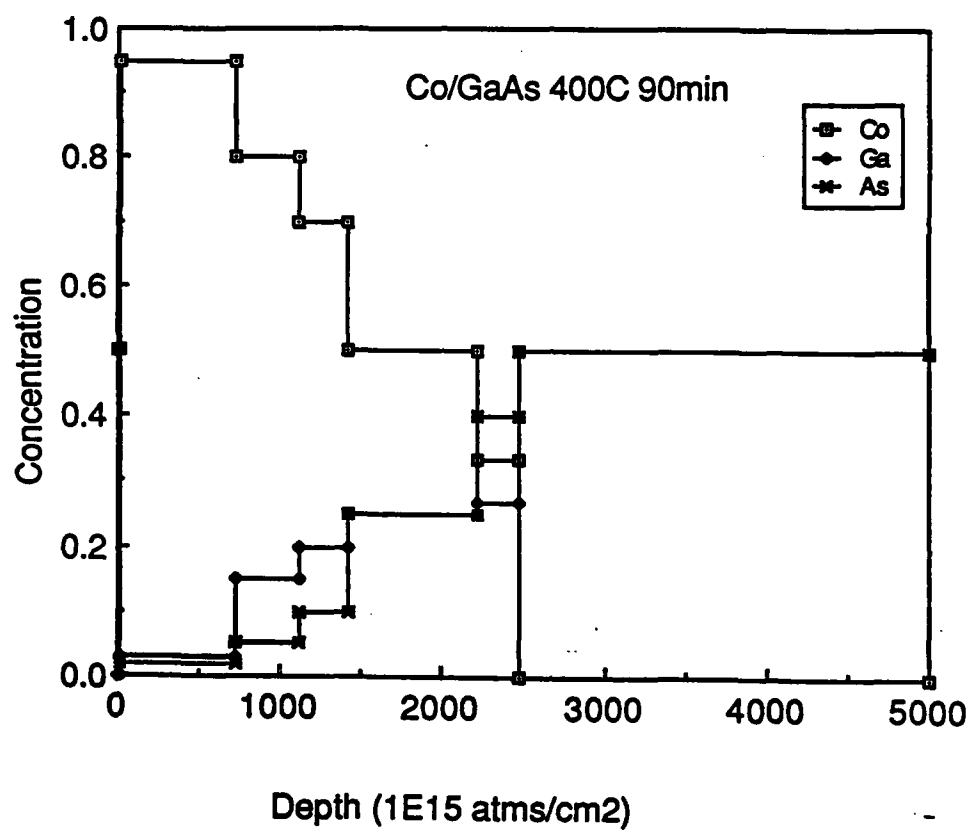




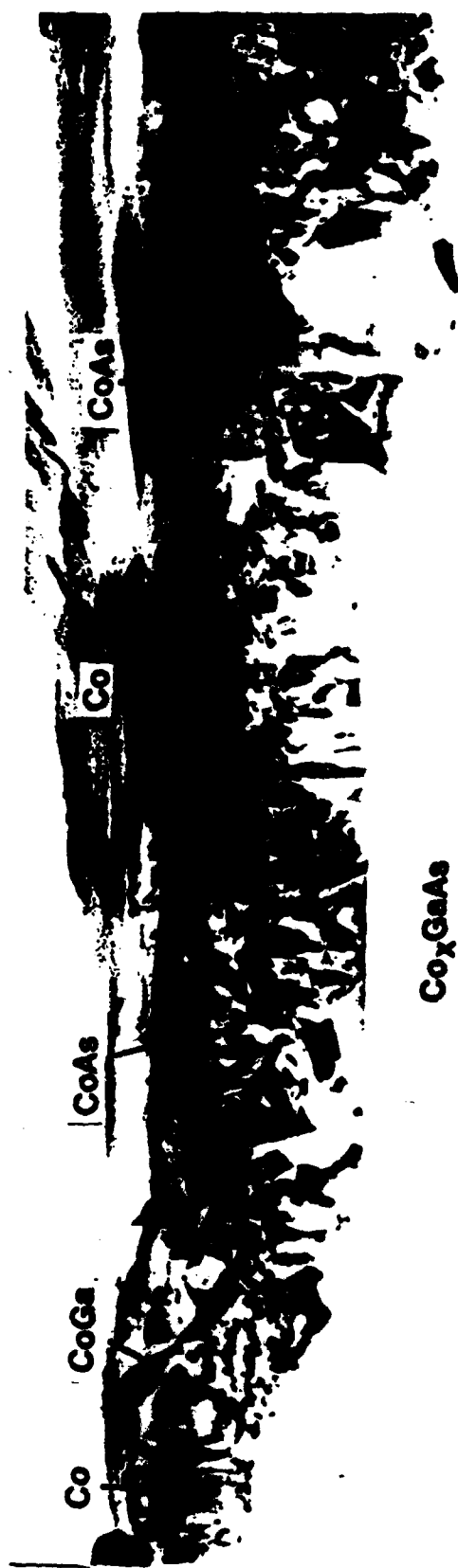








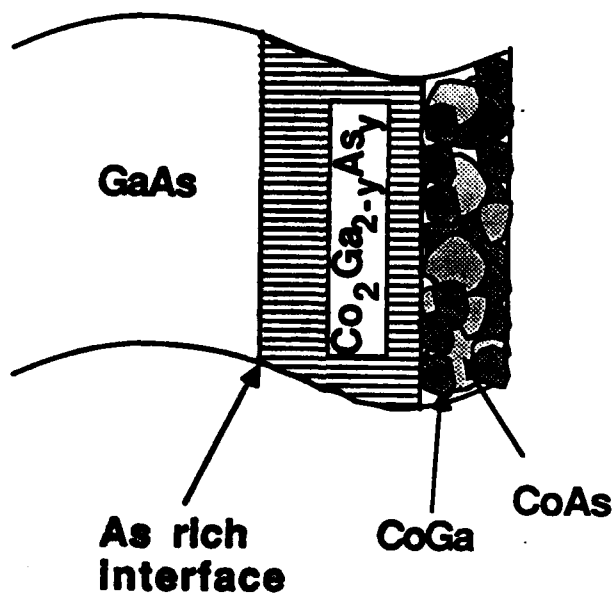
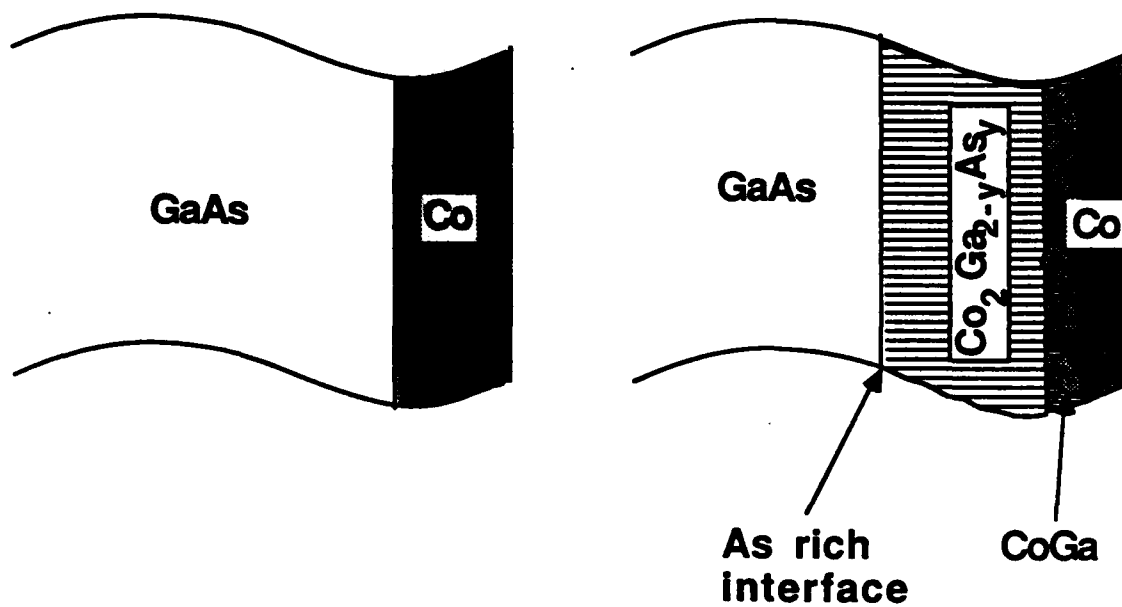




$\text{Co}_x\text{GaAs}$

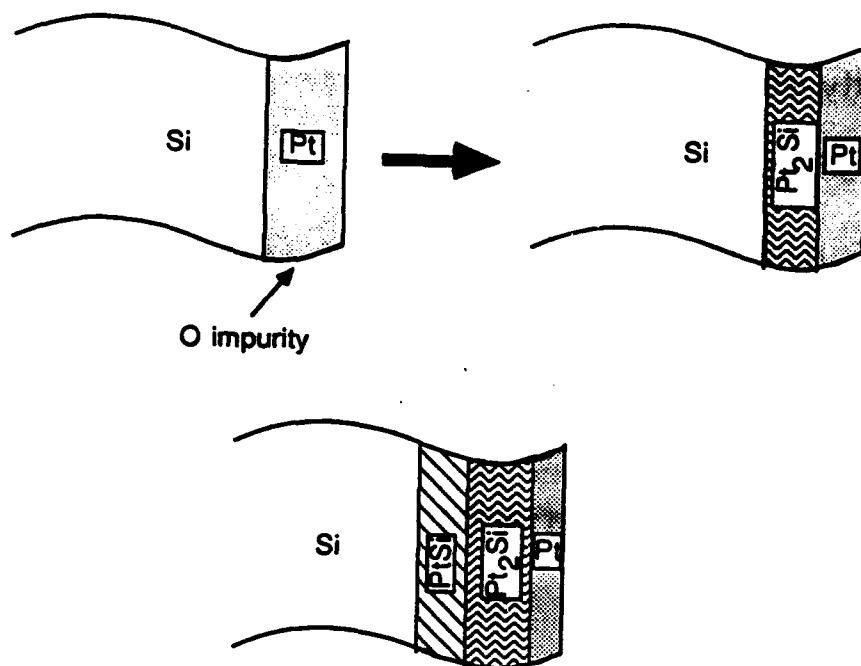
100nm

317

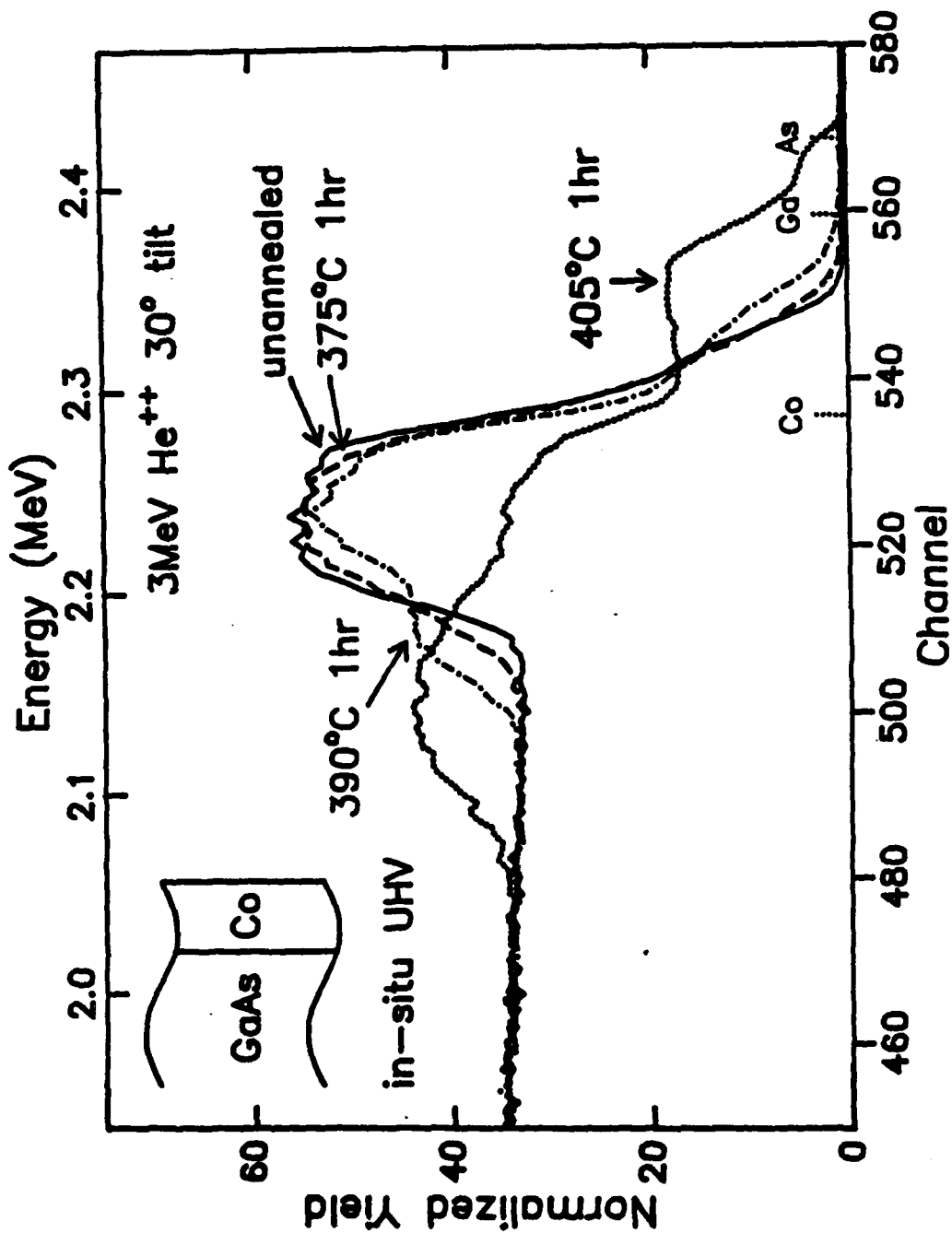


**Why are there two distinct regions**

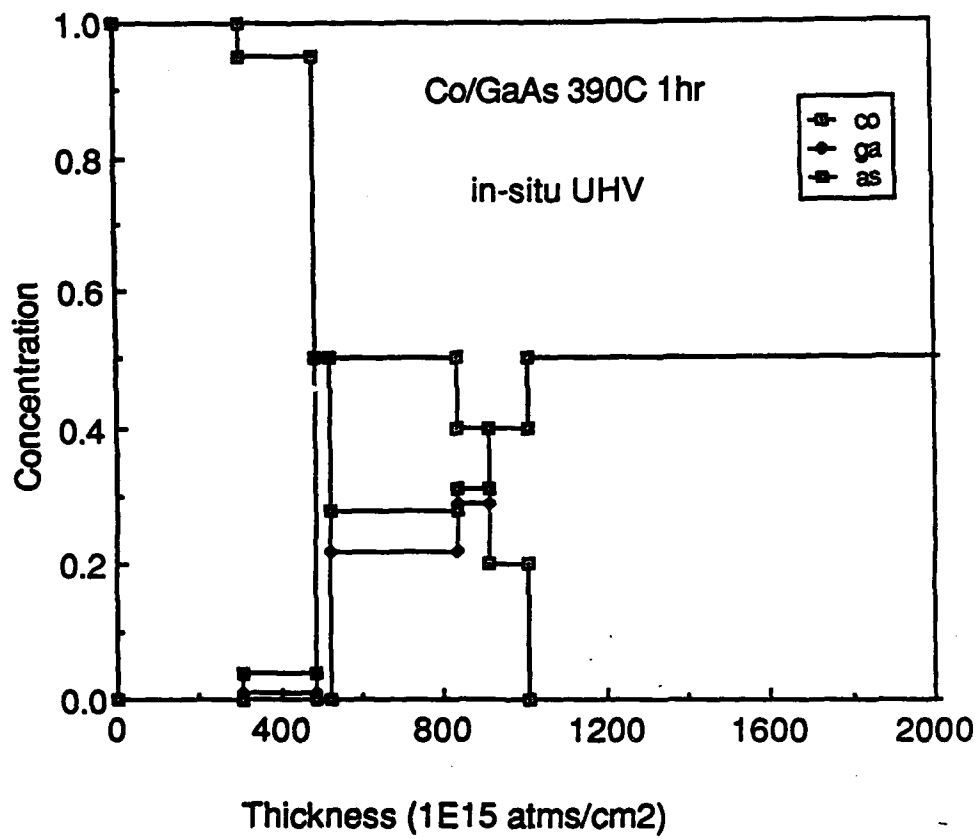
- 1) Impurity effect**
- 2) Competing reactions**
  - a) Ternary phase formation ( $\text{Co}_x\text{Ga}_{2-y}\text{As}_y$ )**
  - b) Ternary phase decomposition (Metastable)**
  - c) Binary phase formation ( $\text{CoGa} + \text{CoAs}$ )**
  - d) Evaporation of arsenic**

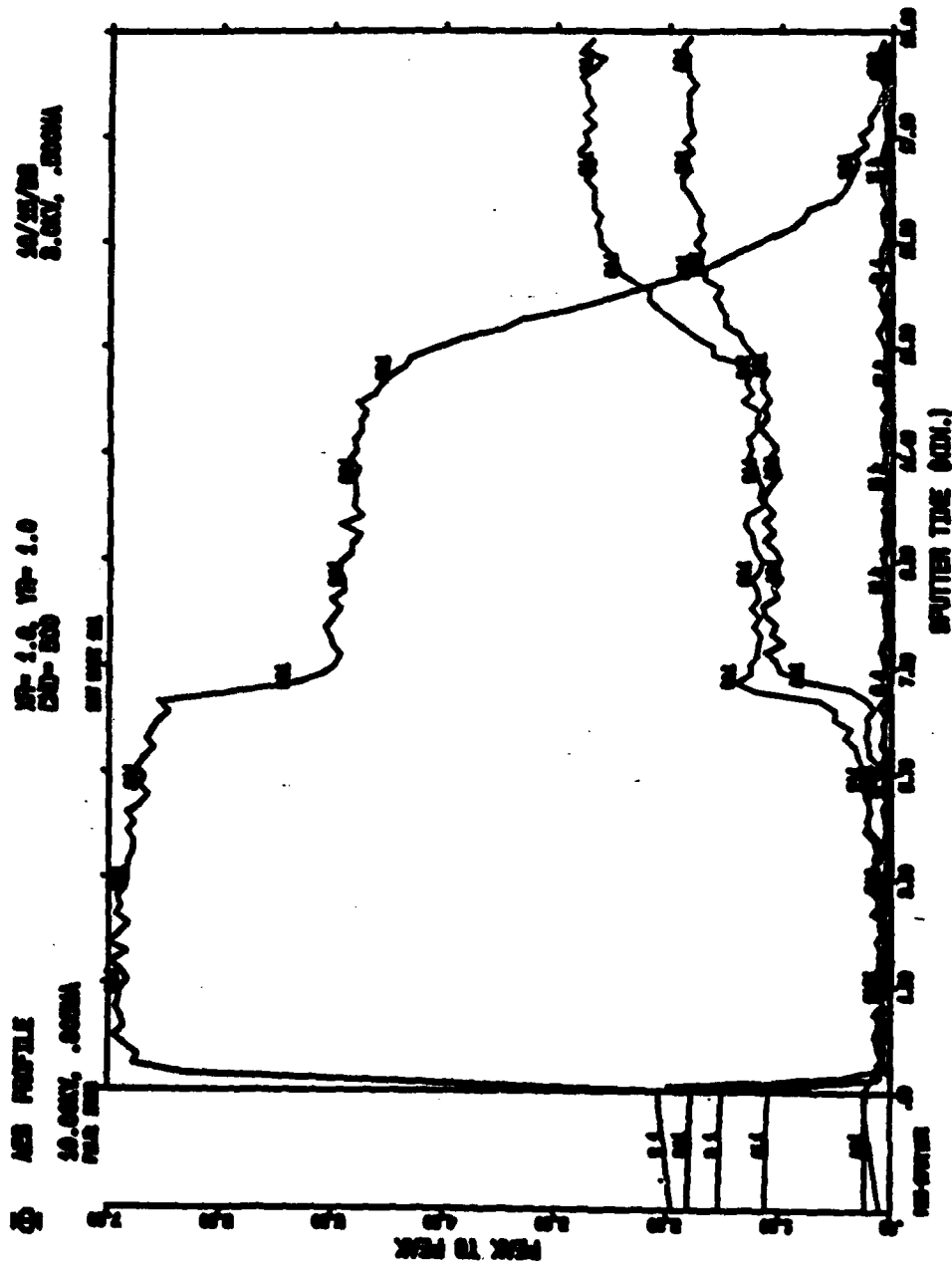


C.A. Crider et. al. JAP (1981)

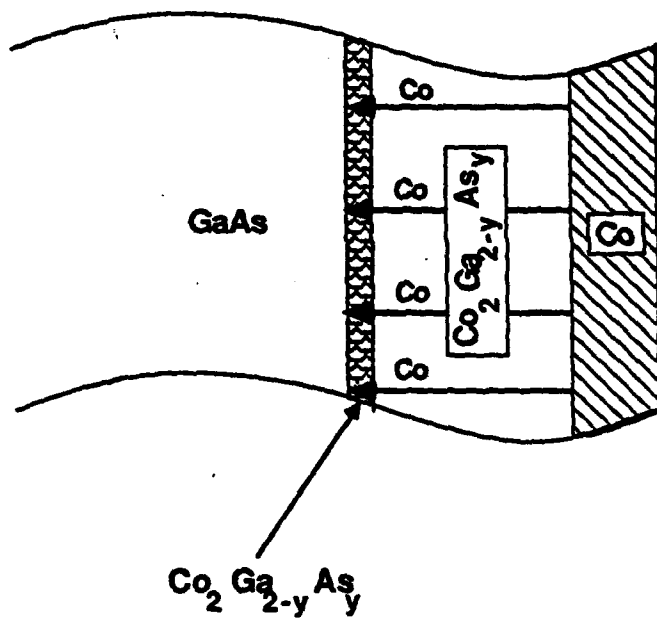




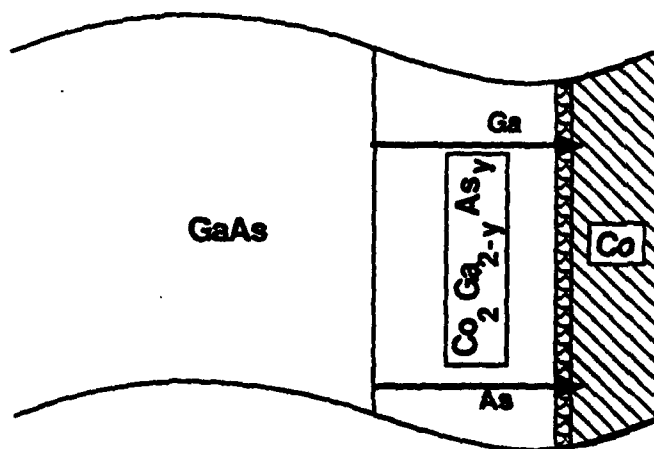


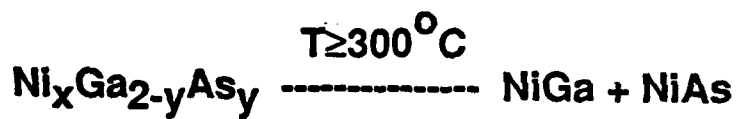
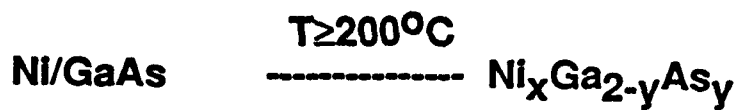


### Co dominant diffusing species



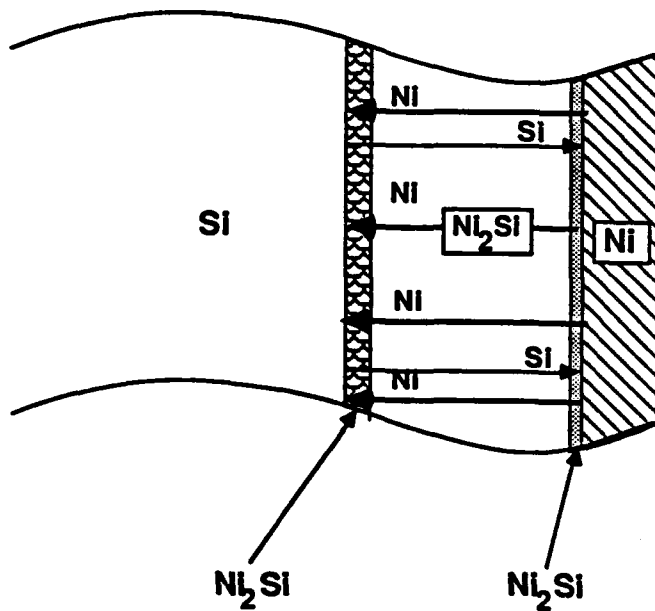
### Ga and As dominant diffusing species

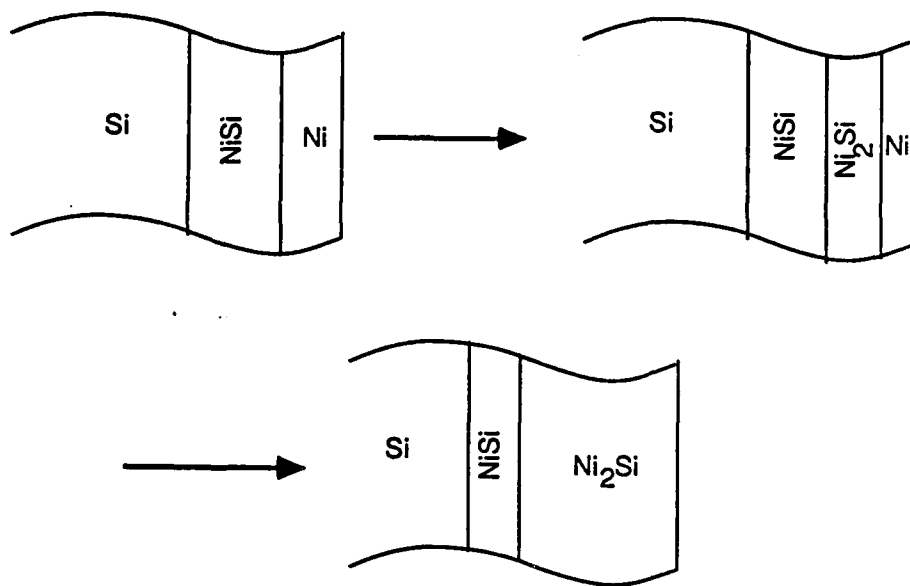


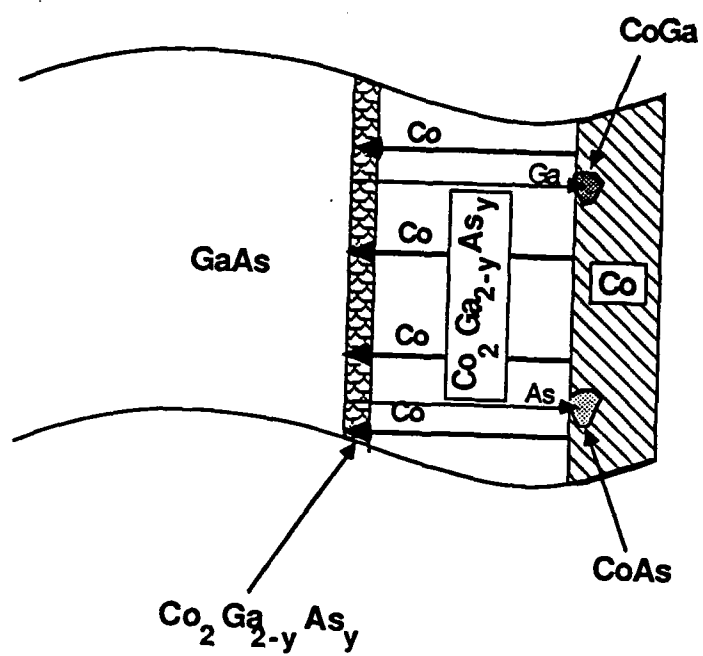


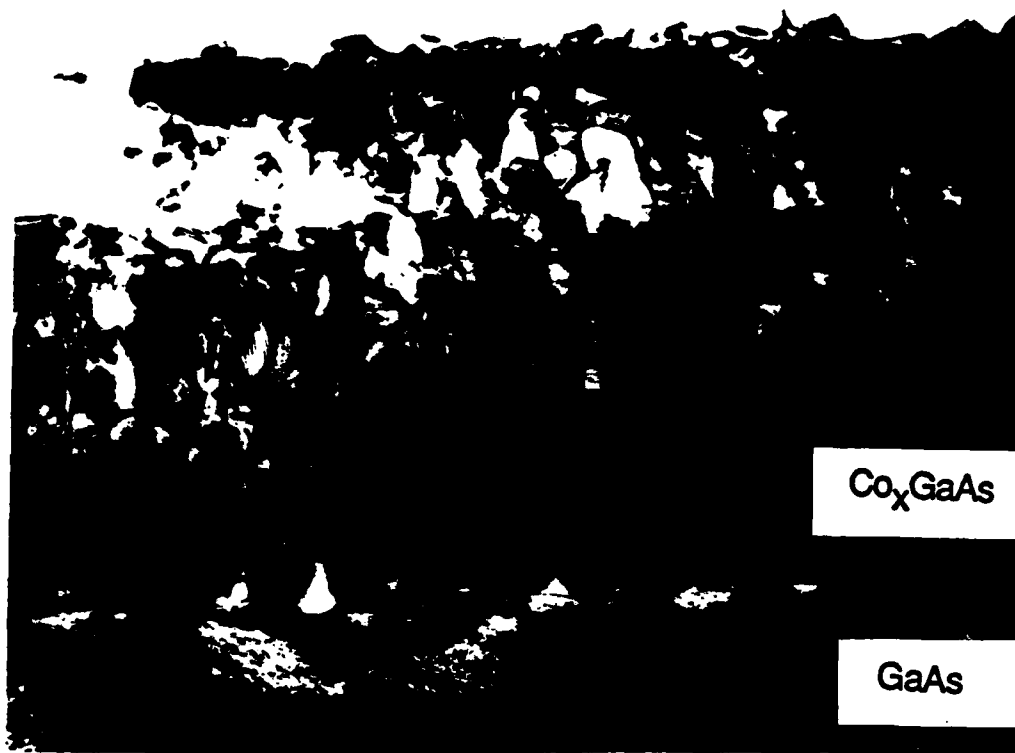
$$y \approx 1$$

Lahav et al (1984, 85, 86)  
 Chen et al (1985)  
 T. Sands (1986)

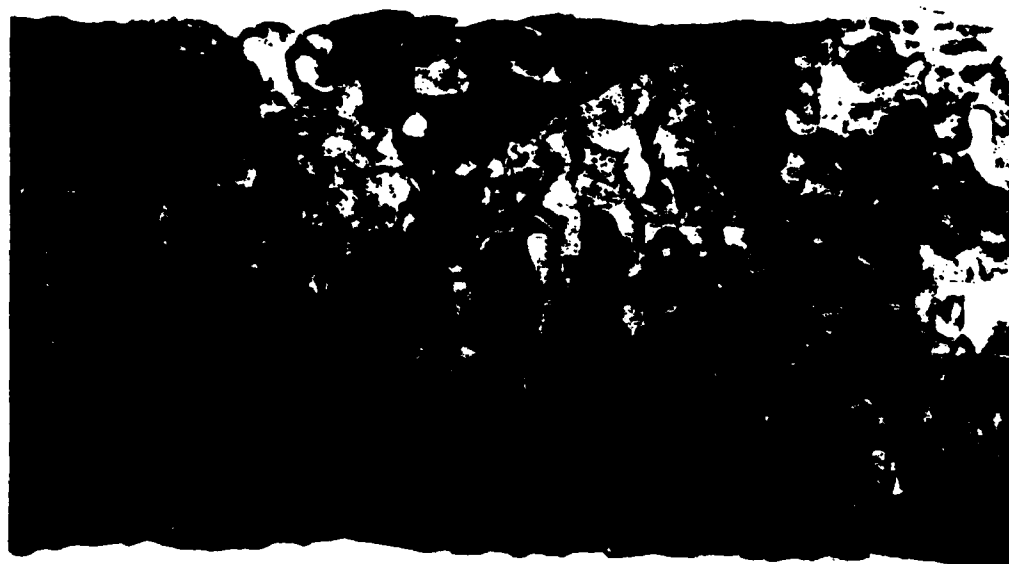






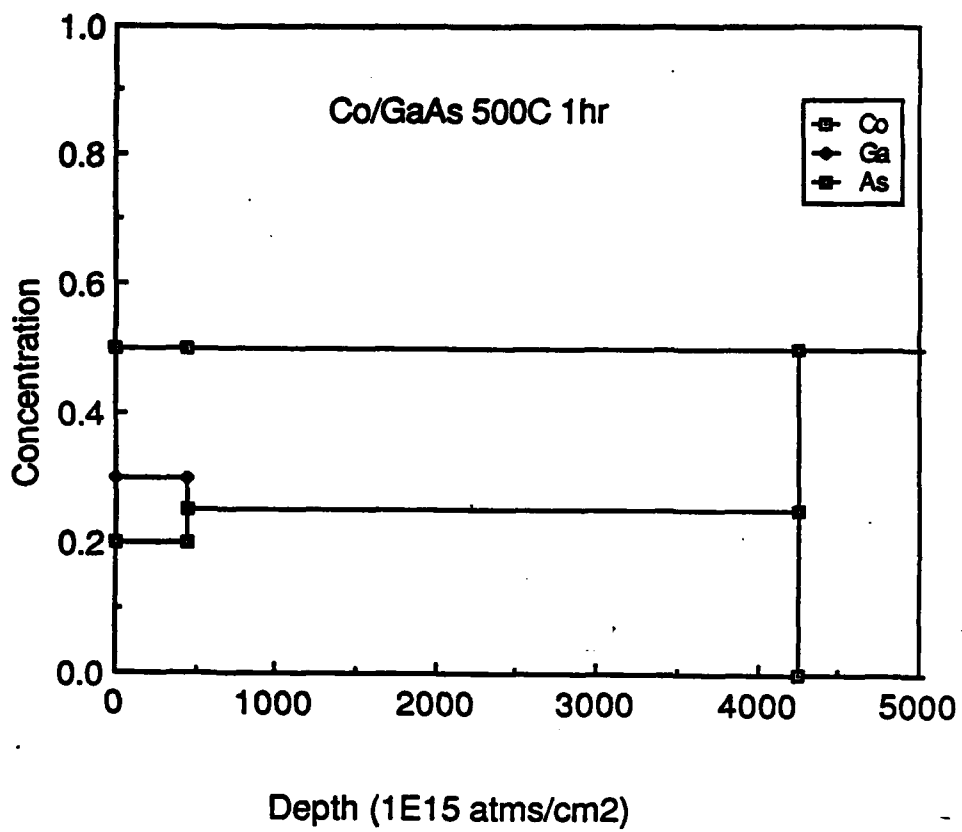


100nm



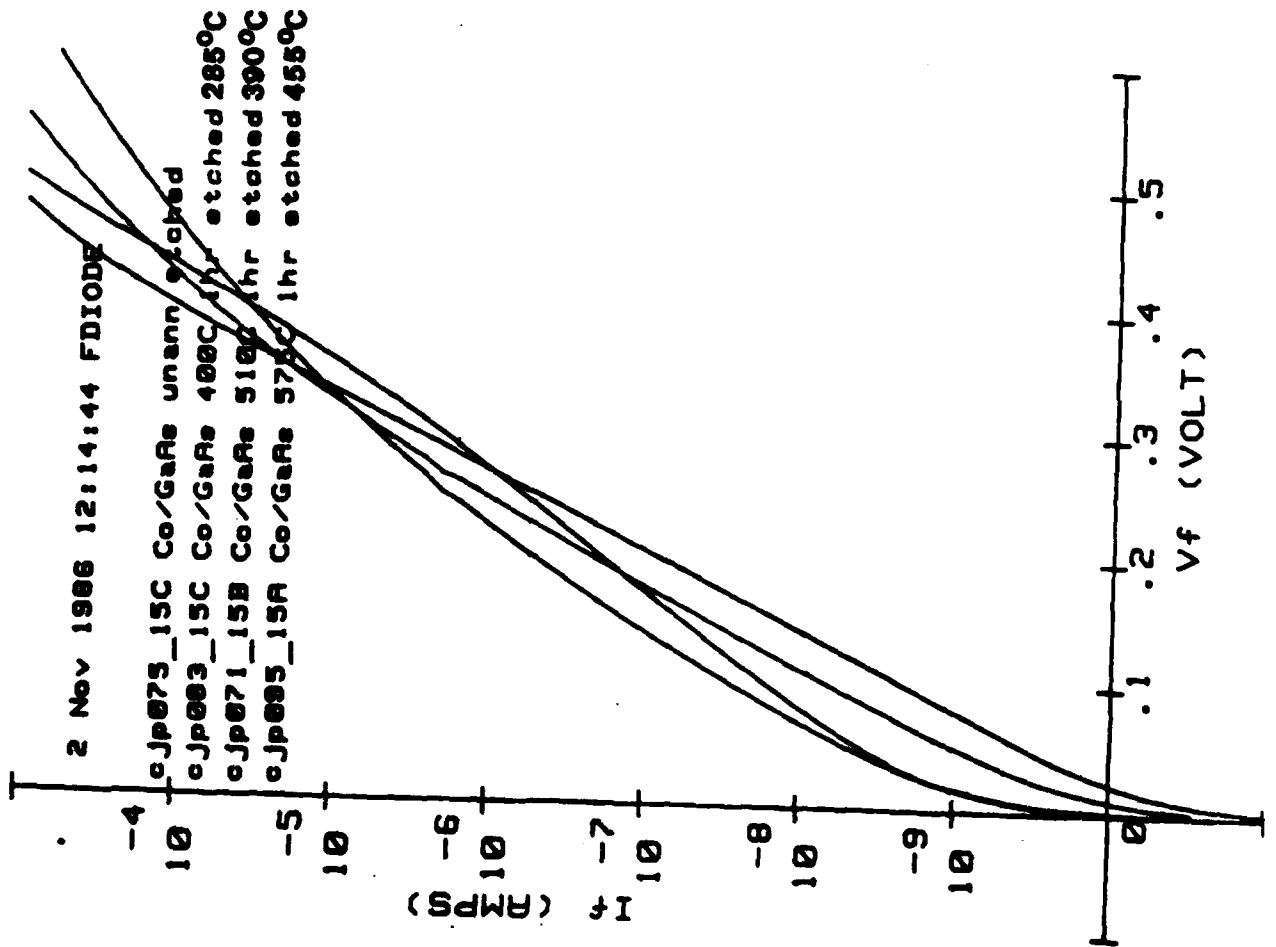
329







331



332

**Electrical study of Schottky diodes formed on clean cleaved III-V surfaces:**

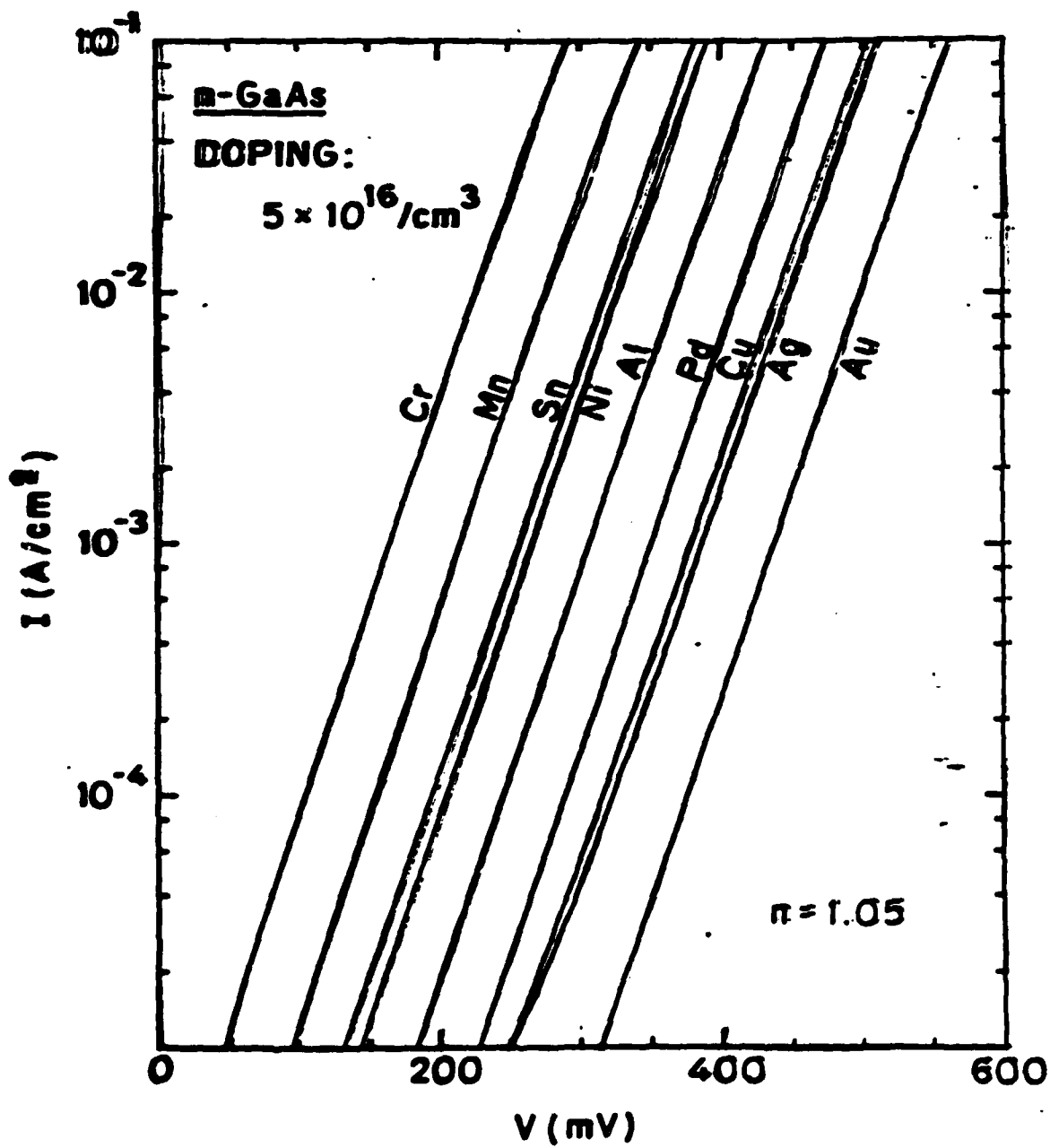
**Implications to Theoretical Models**

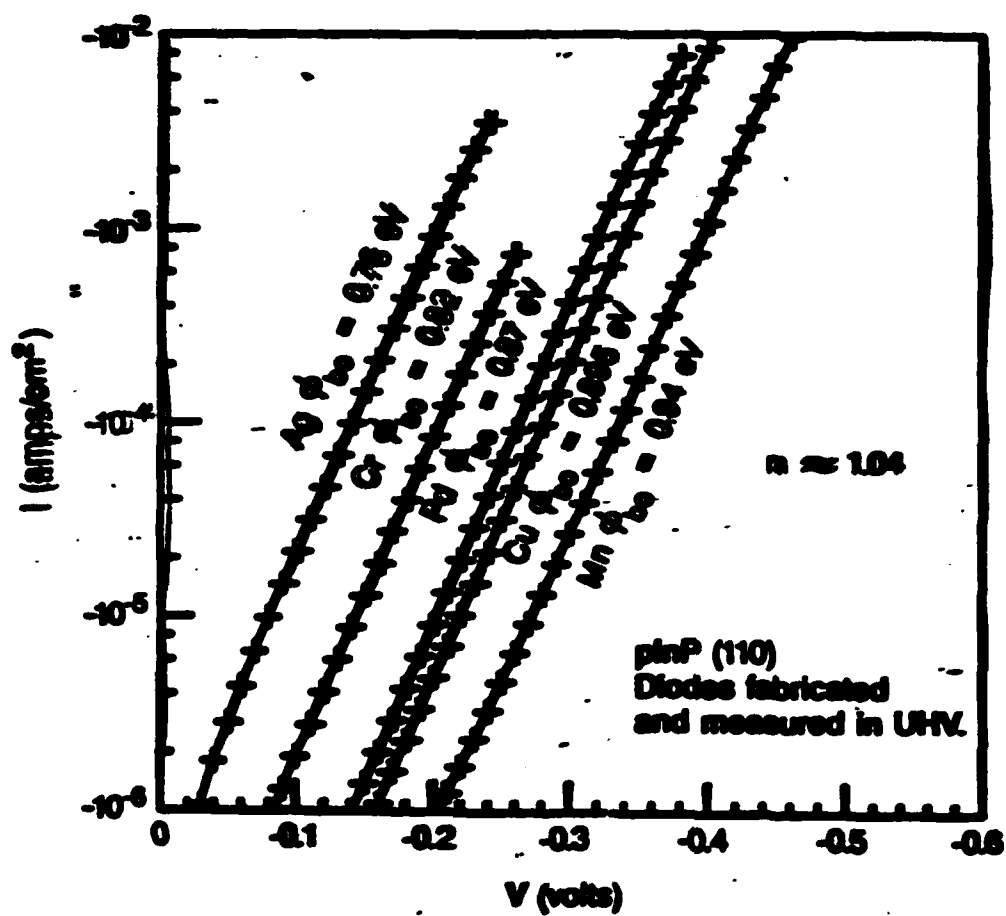
**N. Newman, M. van Schilfsgaede, and W. E. Spicer**

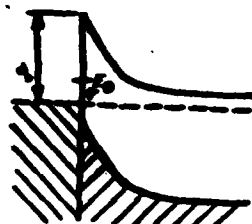
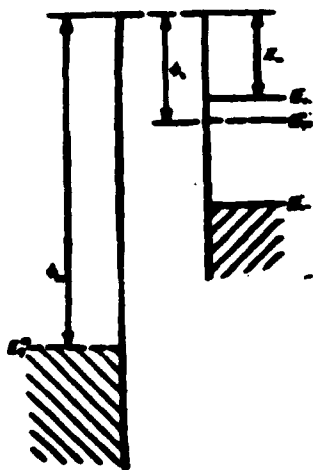
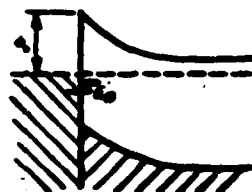
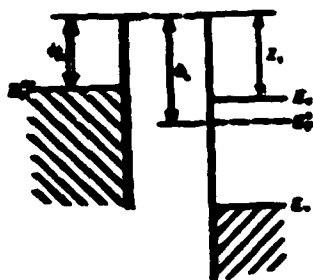
**Stanford University**

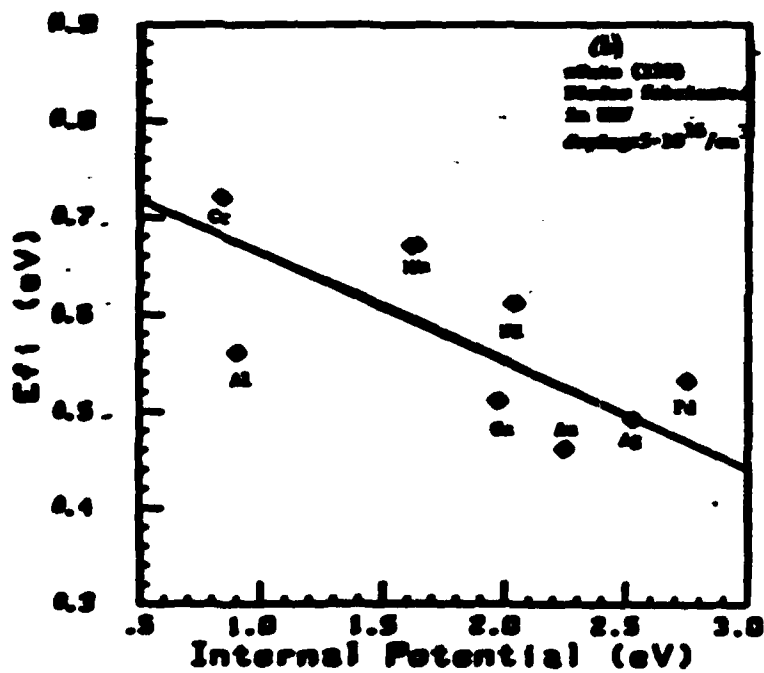
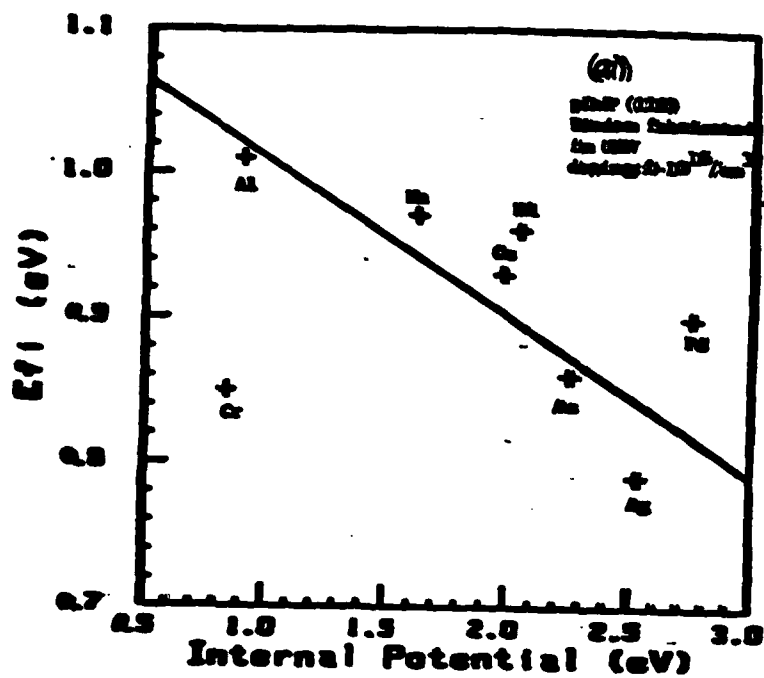
**Z. Liliental-Weber and E. R. Weber**

**U.C. Berkeley**











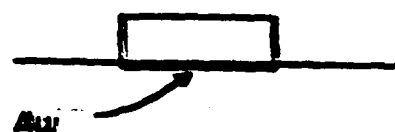
20

Room  
Temp.



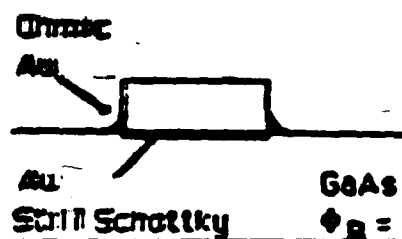
AuGaAs  
 $\Phi_B = 0.91 \text{ eV}$

Anneal  
to 290°C



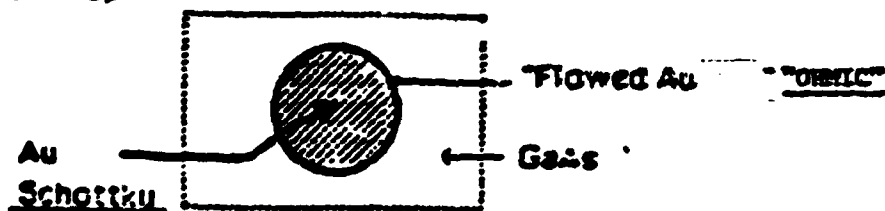
AuGa<sub>2</sub>G<sub>2</sub>As  
 $\Phi_B = 0.8 \text{ eV}$

Anneal  
to >360°C  
(Au-Ga  
eutectic  
temperature)

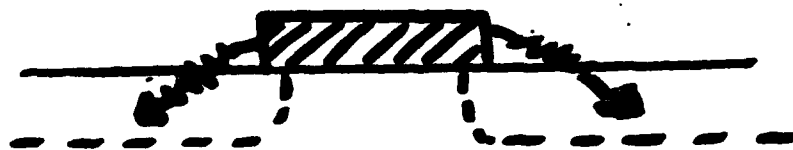
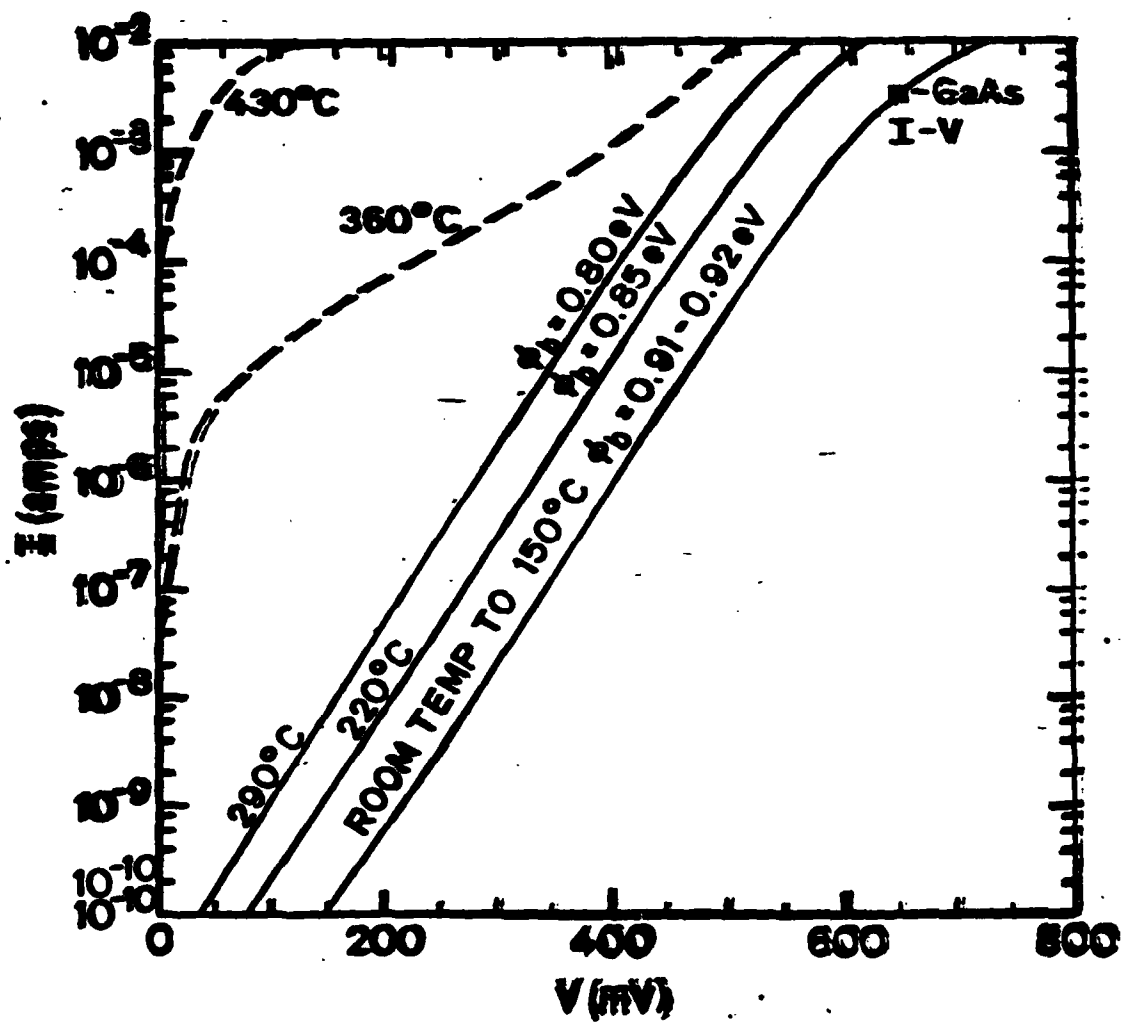


$\Phi_B = 0.8 \text{ eV}$

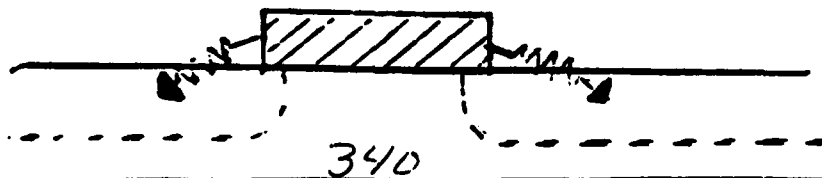
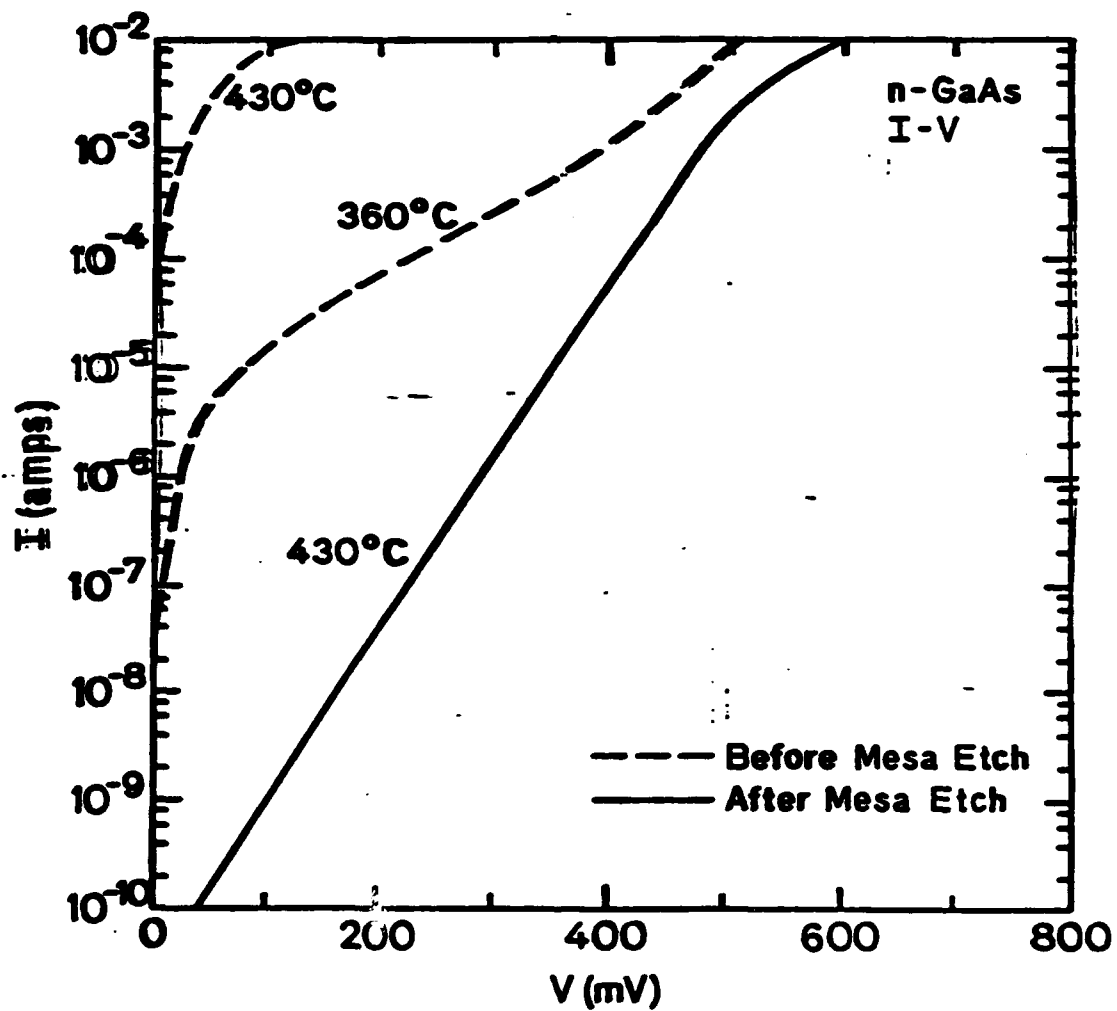
From Top

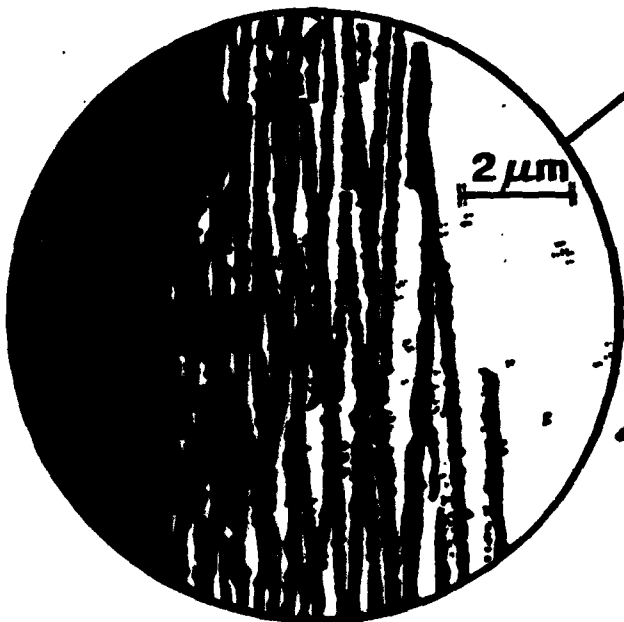
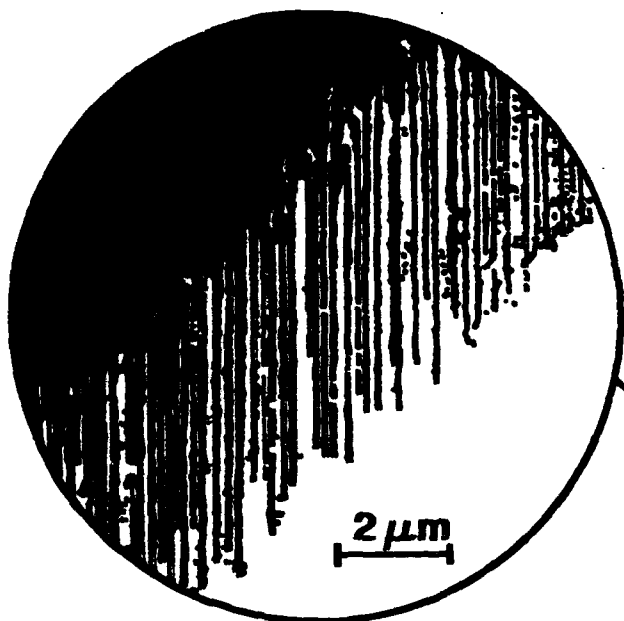


# AU-GaAs HEAT TREATMENT

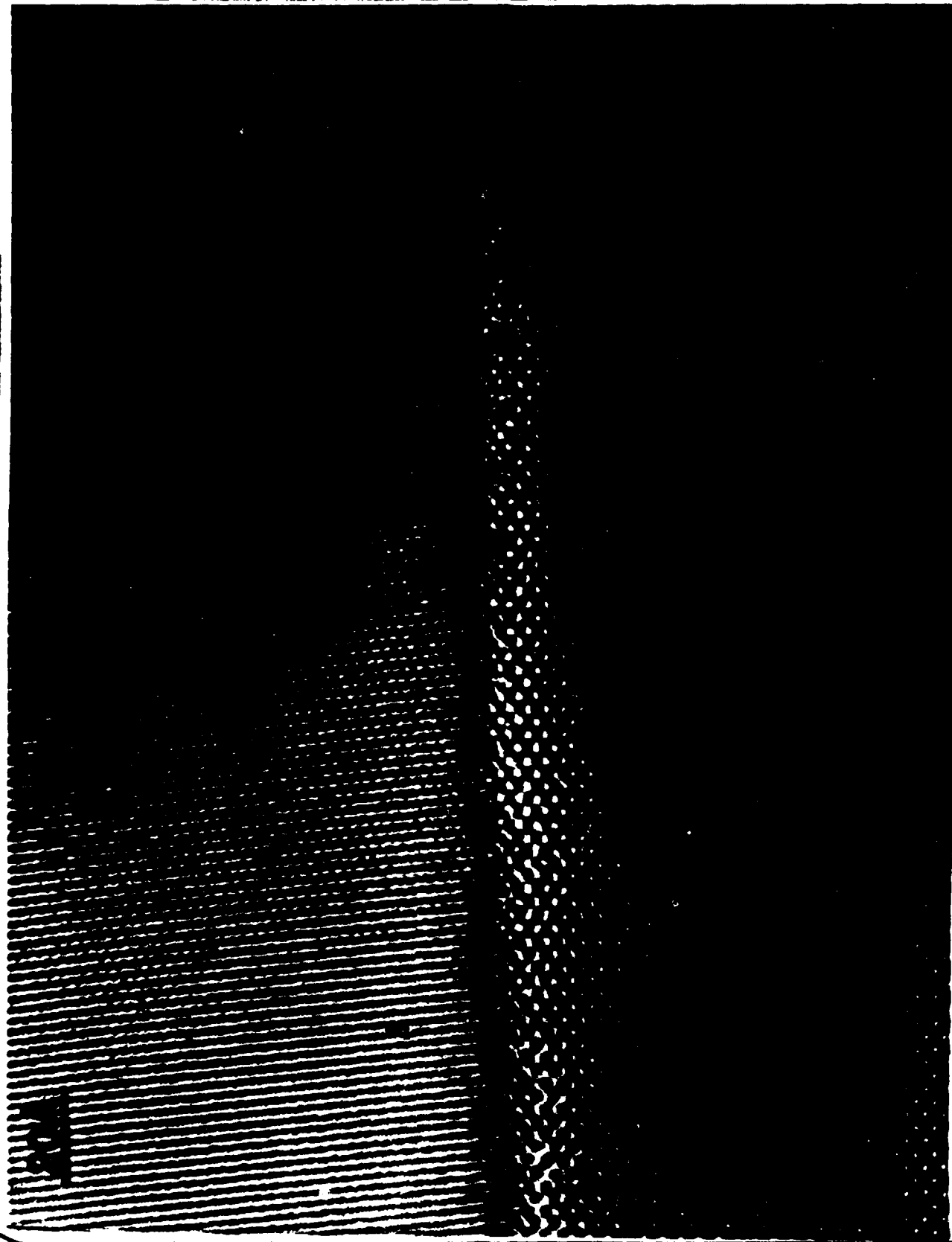


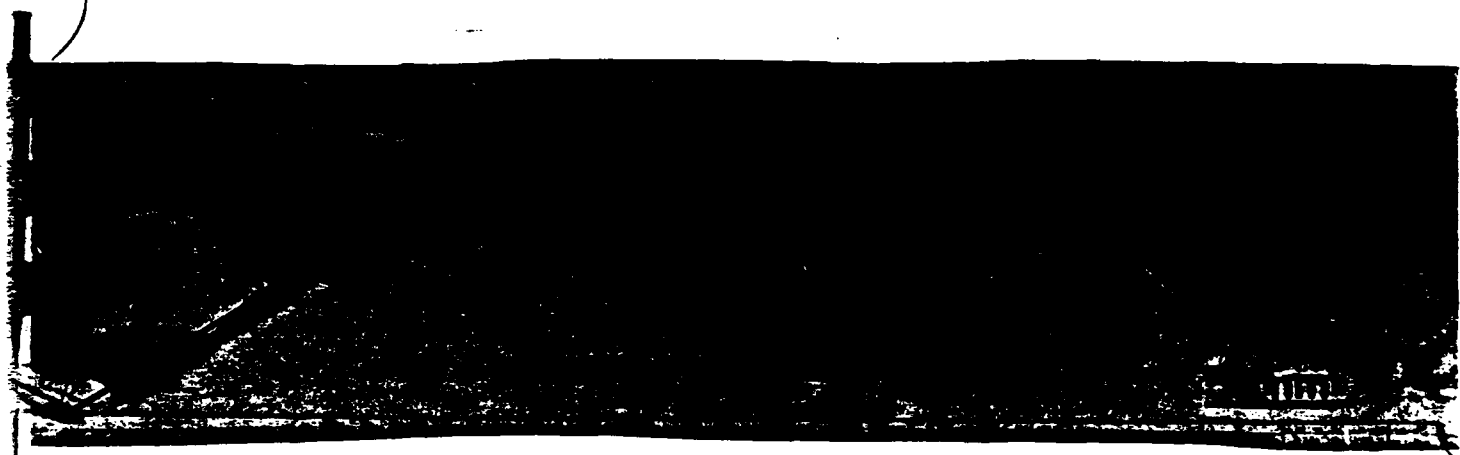
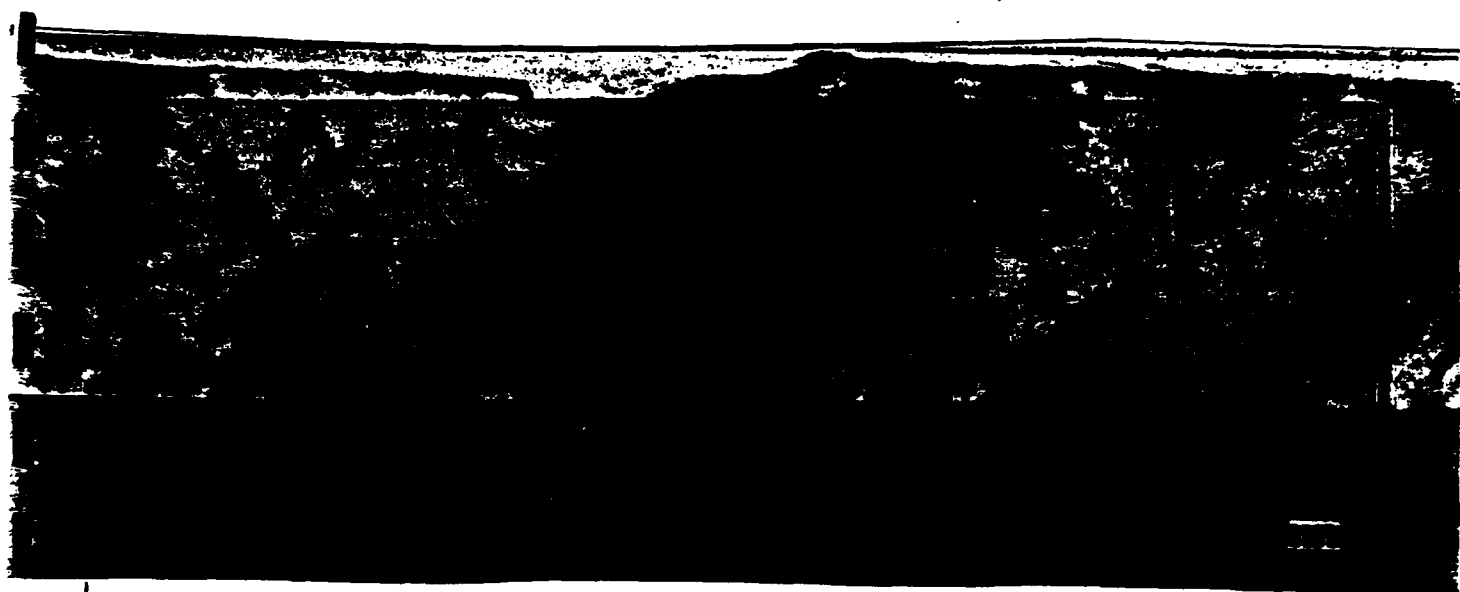
# Au - n GaAs ANNEALING STUDY



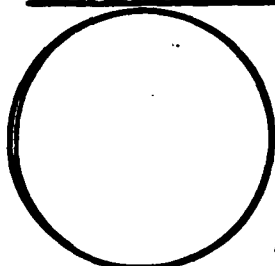


GaAs  $\langle 110 \rangle$

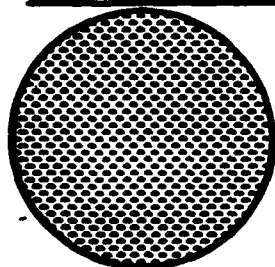




100 Å of Au deposited - unannealed

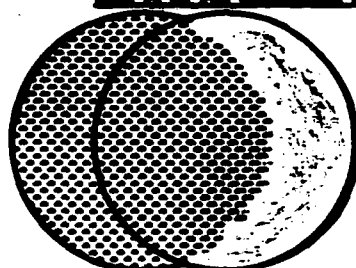


100 Å of Au Annealed at 325°C

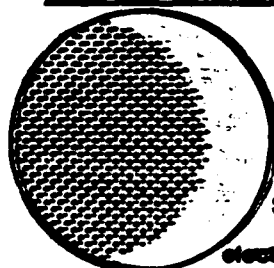


Forms separated islands  
of Au-Sn alloy

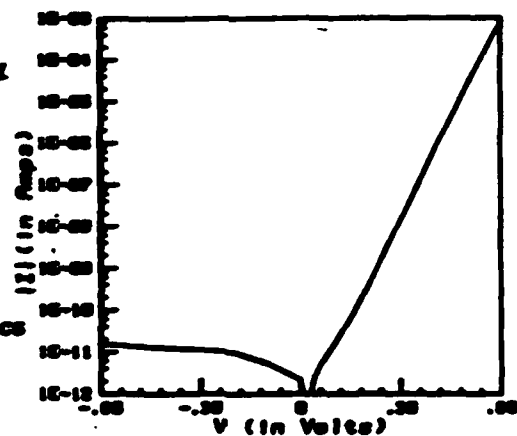
200 Å of Au deposited on top

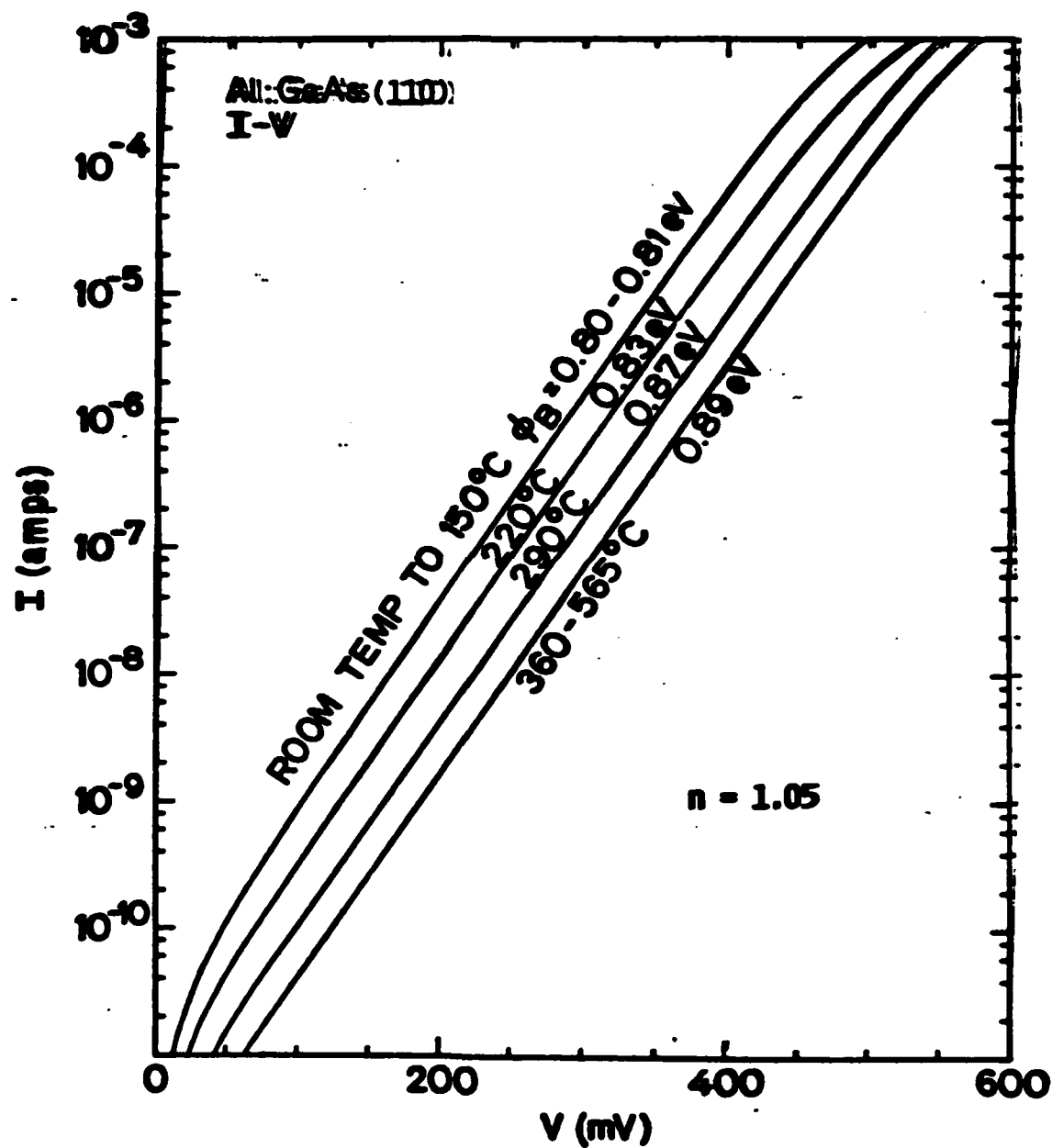


Mass shift to surface effect of majority



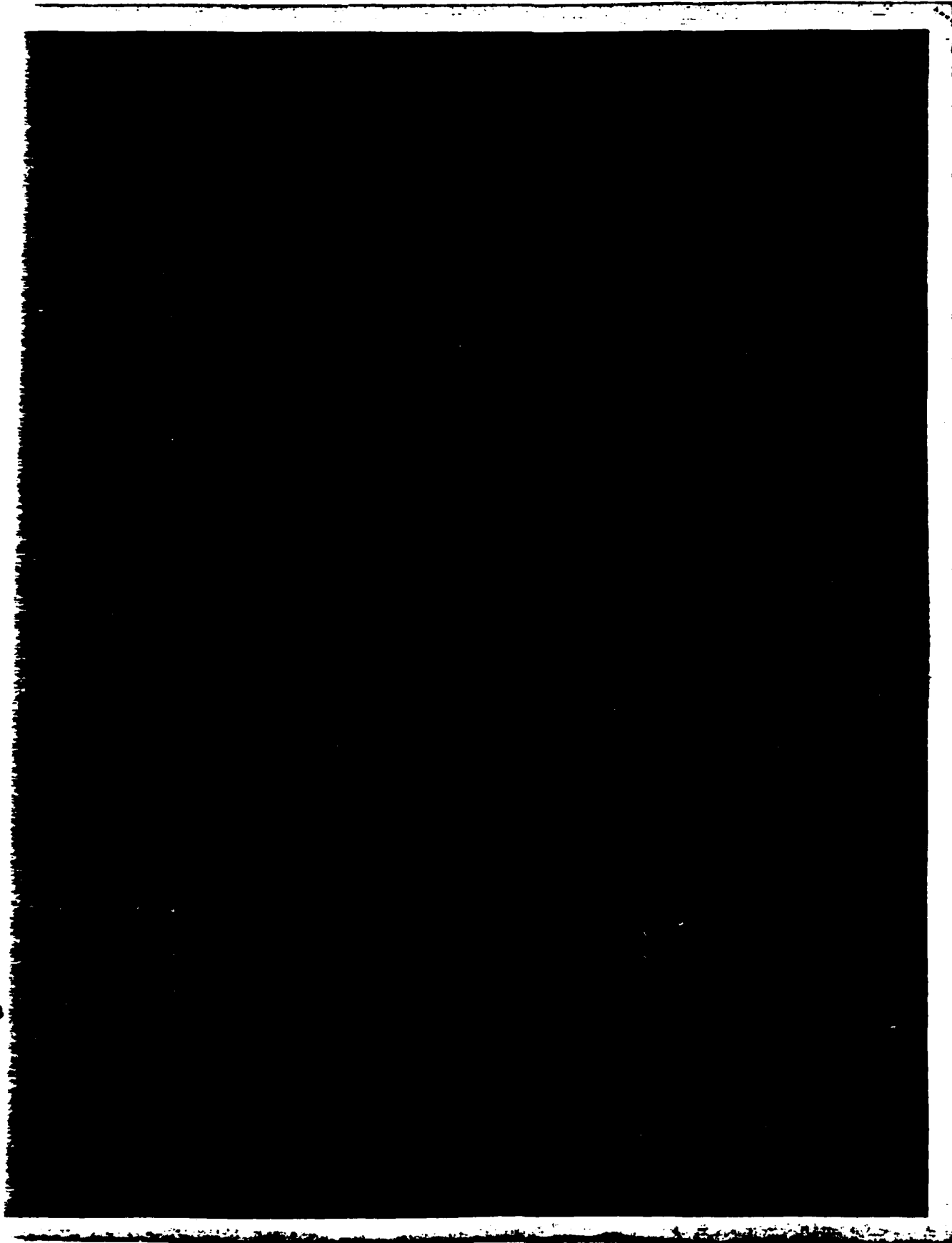
Strong rectifying  
electrical characteristics





345





346

**THE STRUCTURE OF Au/GaAs AND Al/GaAs  
INTERFACES**

**Zuzanna Liliental-Weber**

**Materials and Molecular Research Division  
Lawrence Berkeley Laboratory  
Berkeley, CA 94720**

# **THE STRUCTURE OF Au/GaAs AND Al/GaAs INTERFACES**

- **INTRODUCTION**
- **Au AND Al CONTACTS ON CLEAVED GaAs (110)**
  - UHV-deposited structures
  - annealed structures (UHV-deposited)
  - annealed structures (air-exposed)
- **Au CONTACTS ON CHEMICALLY PREPARED GaAs (100)**
  - annealed structures
- **Al CONTACTS DEPOSITED BY MBE ON GaAs (100)**
  - as-deposited structures
- **CONCLUSIONS**

**This work was done in cooperation with:**

**Nathan Newman, W.E. Spicer (cleaved structures)**

**R. Ludeke (MBE-deposited structures)**

**T. Sands (chemically prepared structures)**

**Funding was provided by:**

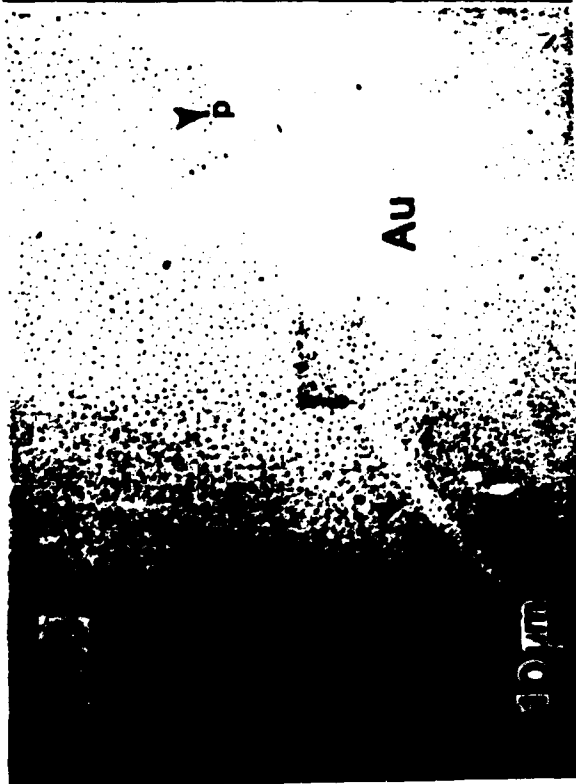
**Department of Energy**

**Office of Naval Research/IST**

**Electron microscopy was carried out at the**

**National Center for Electron Microscopy, LBL, Berkeley**

as-deposited

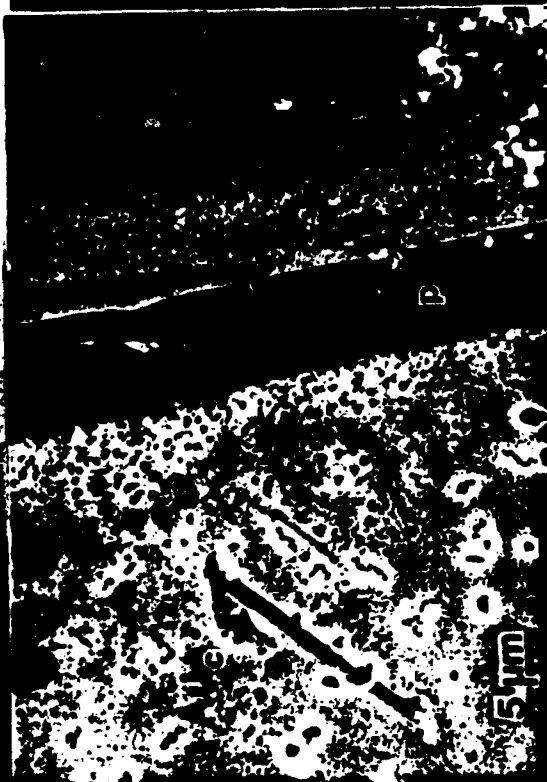


annealed at 400°C



part  
control  
sample

350

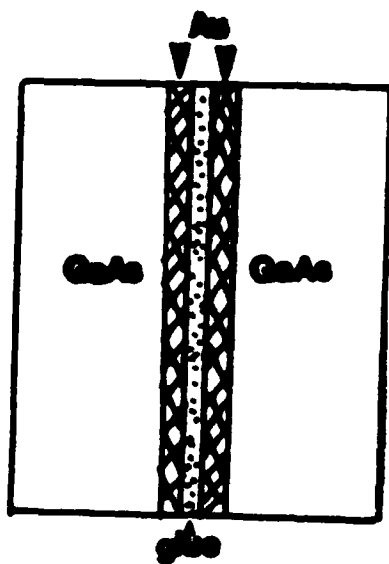
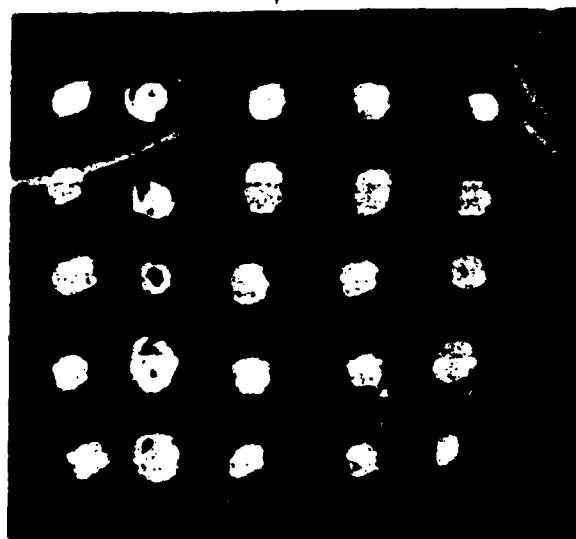


after mesa etching



after mesa etching  
preferential etching  
beneath the  
crystallites

Au dots



cross-section  
sample



plan view sample

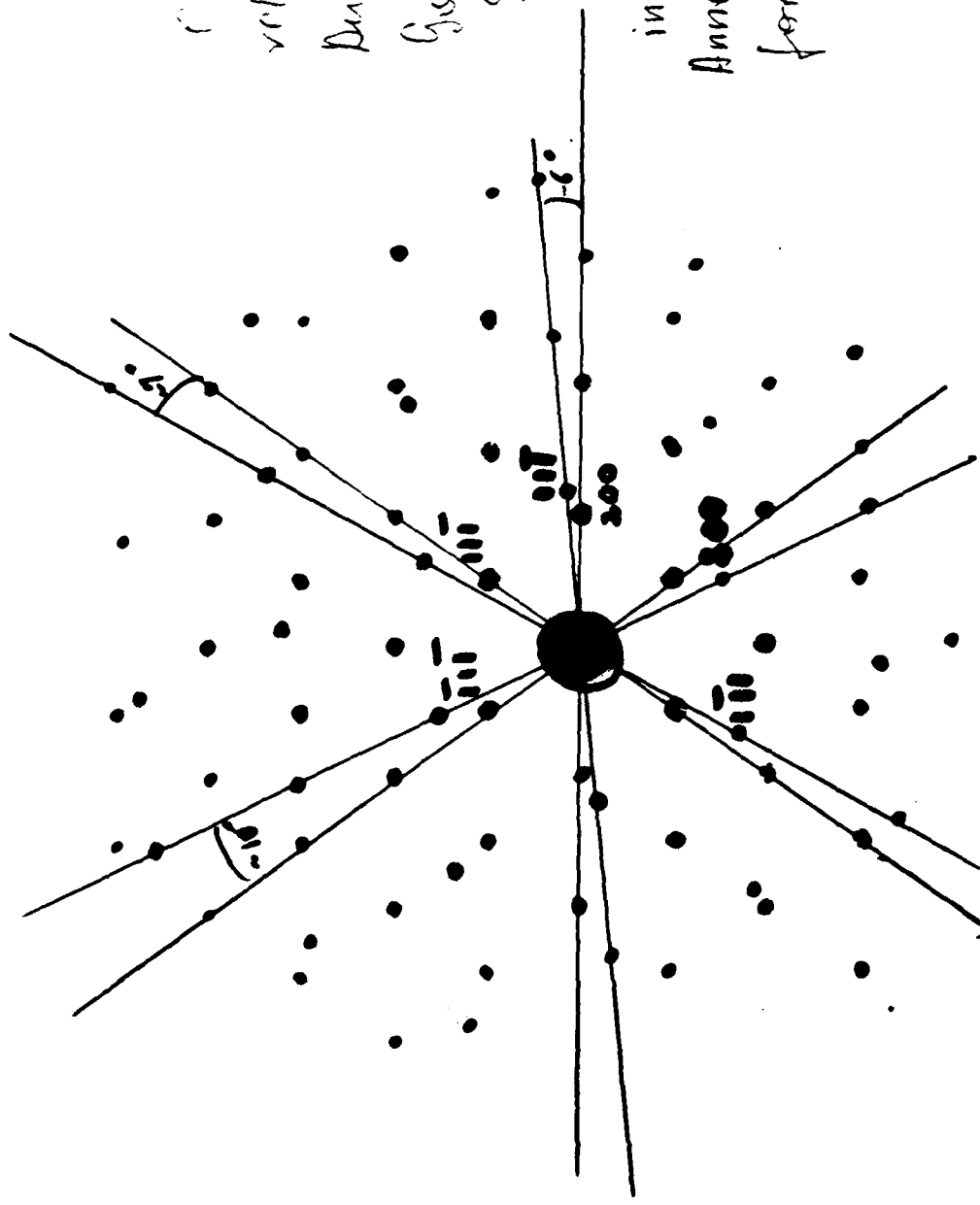
UHV cleaved  
40°C annealing

20A

40A

35A

50As



Preparation  
 relationship of  
 Au planes with  
 GaAs planes.  
 Sample cleaved  
 in UHV with  
 in situ Au deposition.  
 Annealing in  $N_2$   
 for 10 min at 400°C

353

$$\begin{aligned}
 (111)_{GaAs} &= 3.26 \text{ \AA} \\
 (111)_{Au} &= 2.355 \text{ \AA}
 \end{aligned}$$

$$(200)_{Au} = 2.826 \text{ \AA}$$

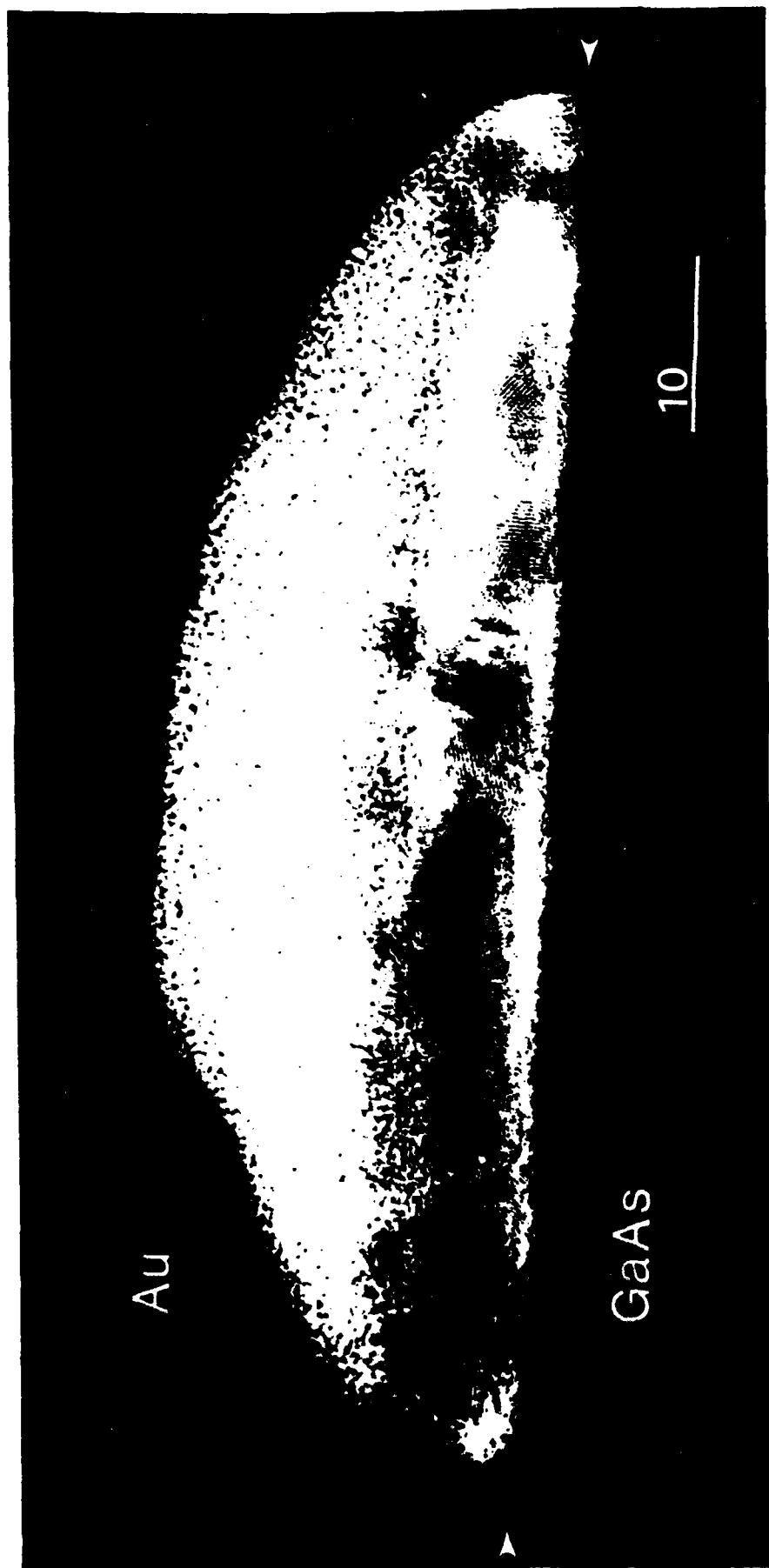
$$(111)_{Au} = 2.355$$

$$5 \times 2.826 = 6 \times 2.355 = 14.13 \text{ \AA}$$

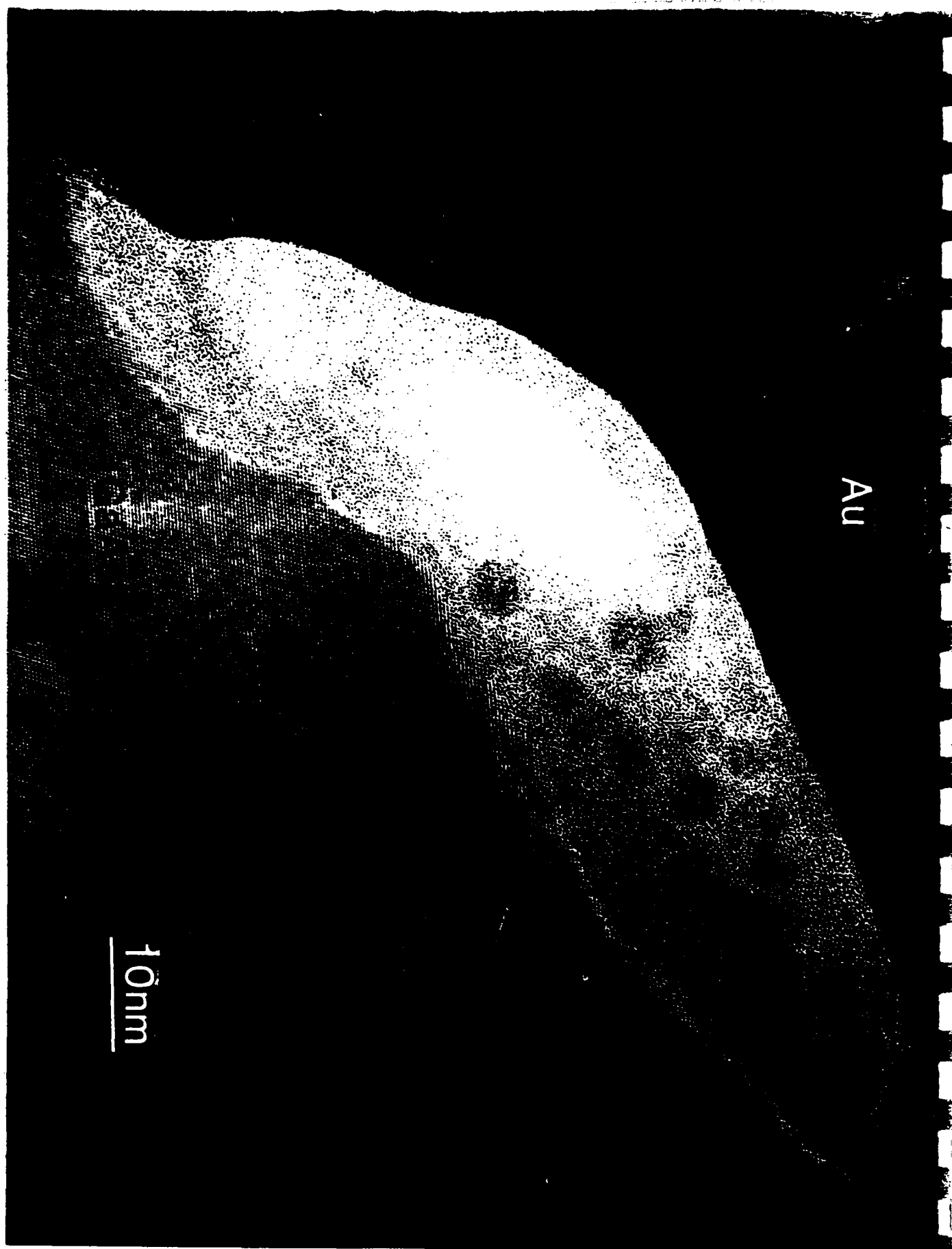




Trington formed in the Ru layer after  
consolidating at 4050p



355 Polycrystalline Au particles present inside triangular formed  
in Au after annealing at 400°C.



356  
Tegafur - mixed in the Au layer on the surface of  
- Gel. Polymethylsiloxane particles are imbedded in the surface

U-AUUHV2

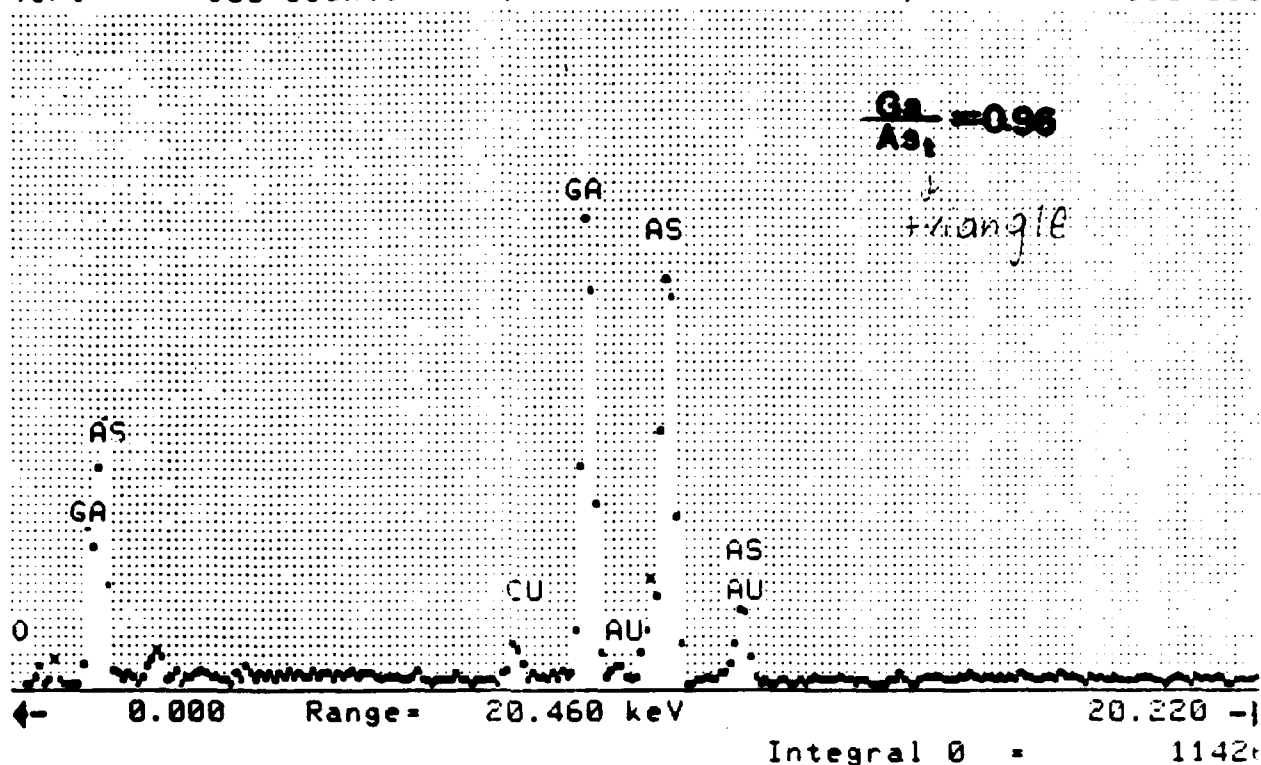
Vert = 500 counts Disp = 1

Preset =

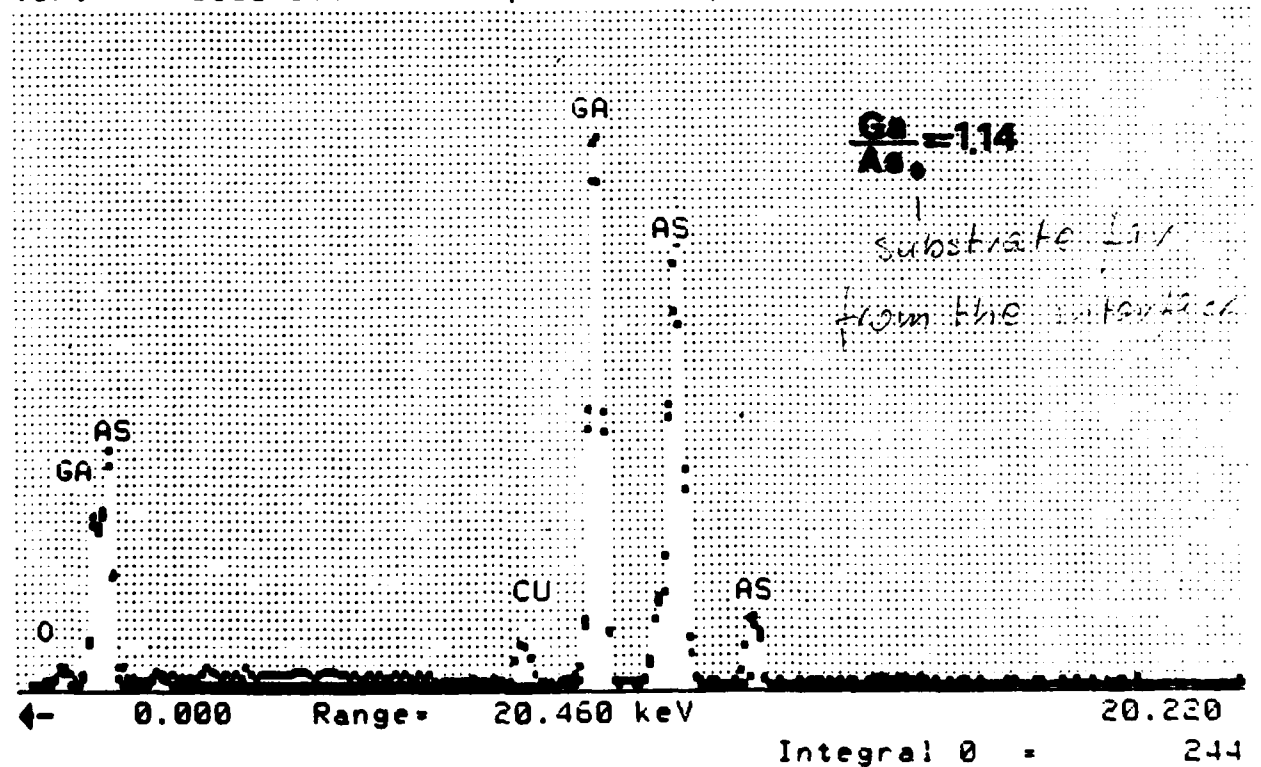
300 sec

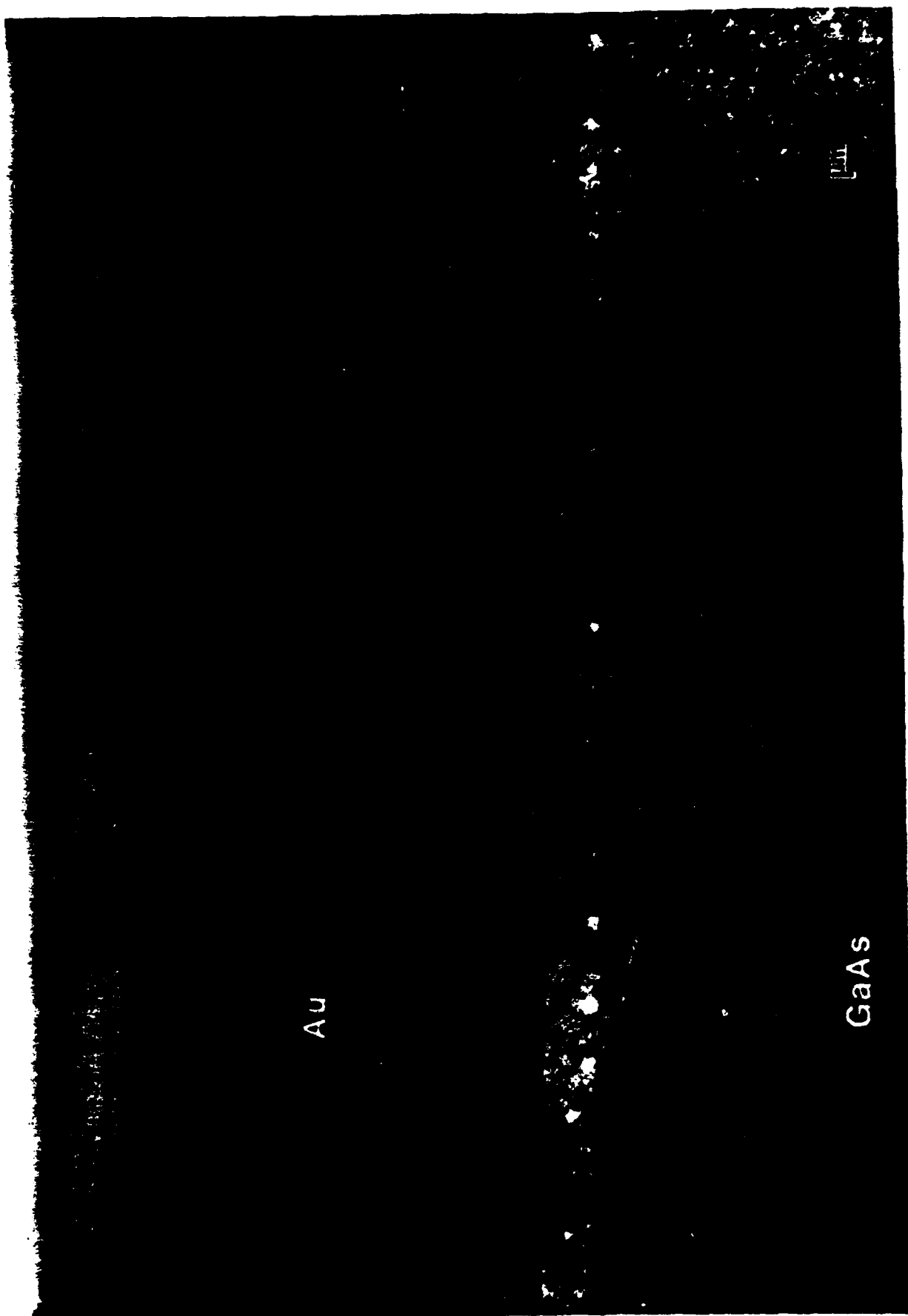
Elapsed =

500 sec



Vert = 1000 counts Disp = 1 Comp = 3 Preset = 300 se  
Elapsed = 500 se





Au

GaAs

100 nm

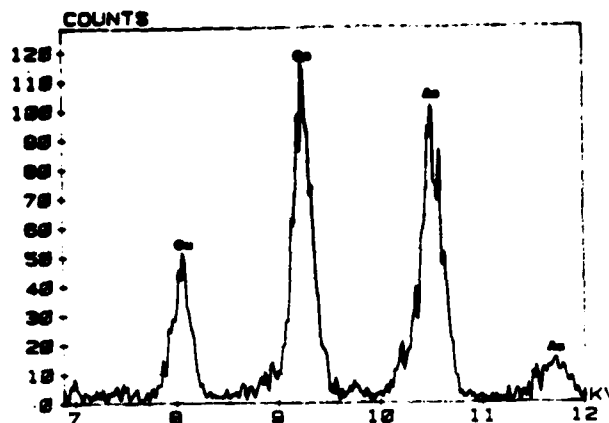
358

Clusters of As distributed below the Au/GaAs interface

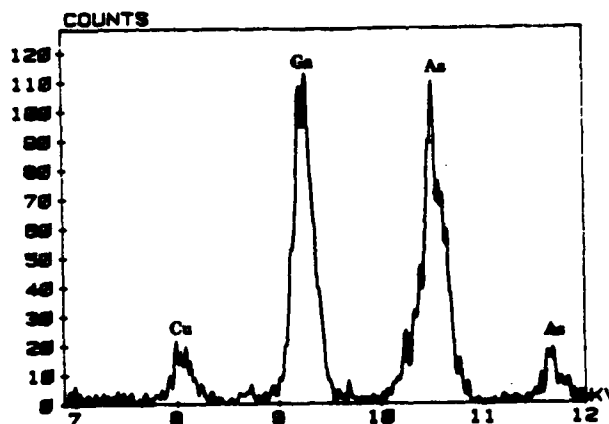
00857-5115A

Voids formed on the interface on the cleavage  
steps

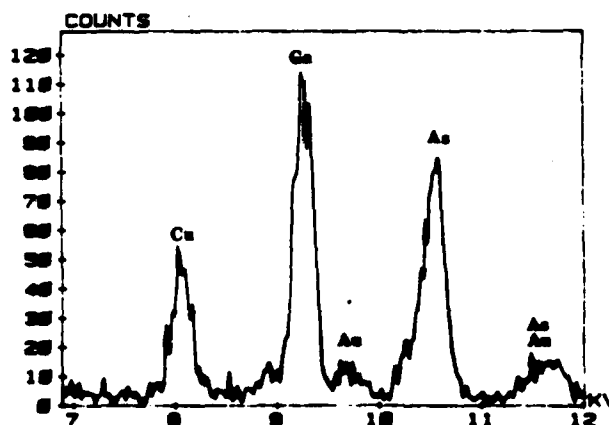
XAB857-5111



on Se  
1.50 A  
1.50 A



on Se  
1.50 A  
1.50 A



on Se  
1.50 A  
1.50 A

XBL 8510-4315

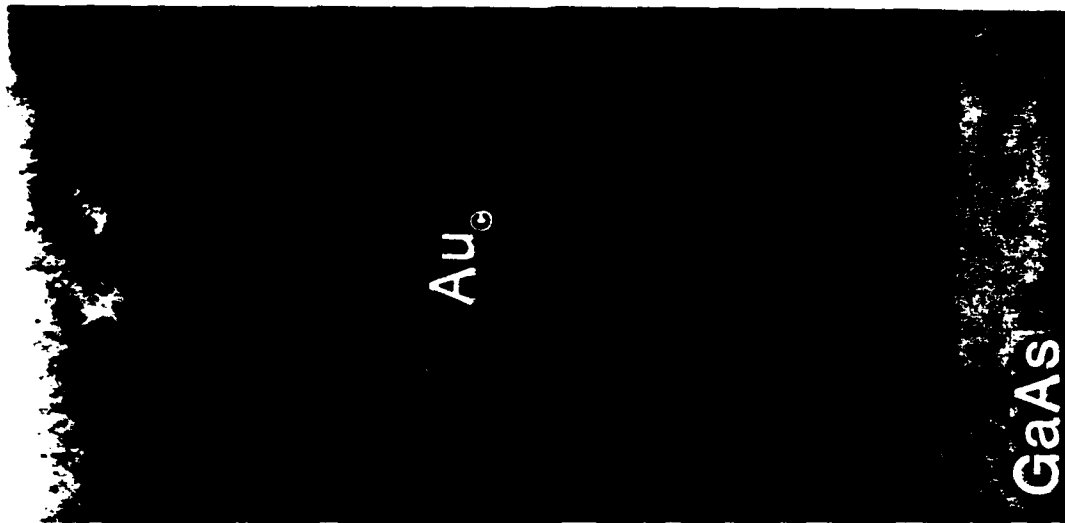
Line for H<sub>2</sub>O<sub>2</sub> analysis  
- 1.50 A for

e beam parallel to  $(100)$

cross-section of Au/GaAs  
interface on the periphery  
of Au dot



cross section  
of the Au/GaAs  
interface  
from the central  
part of the Au  
dot



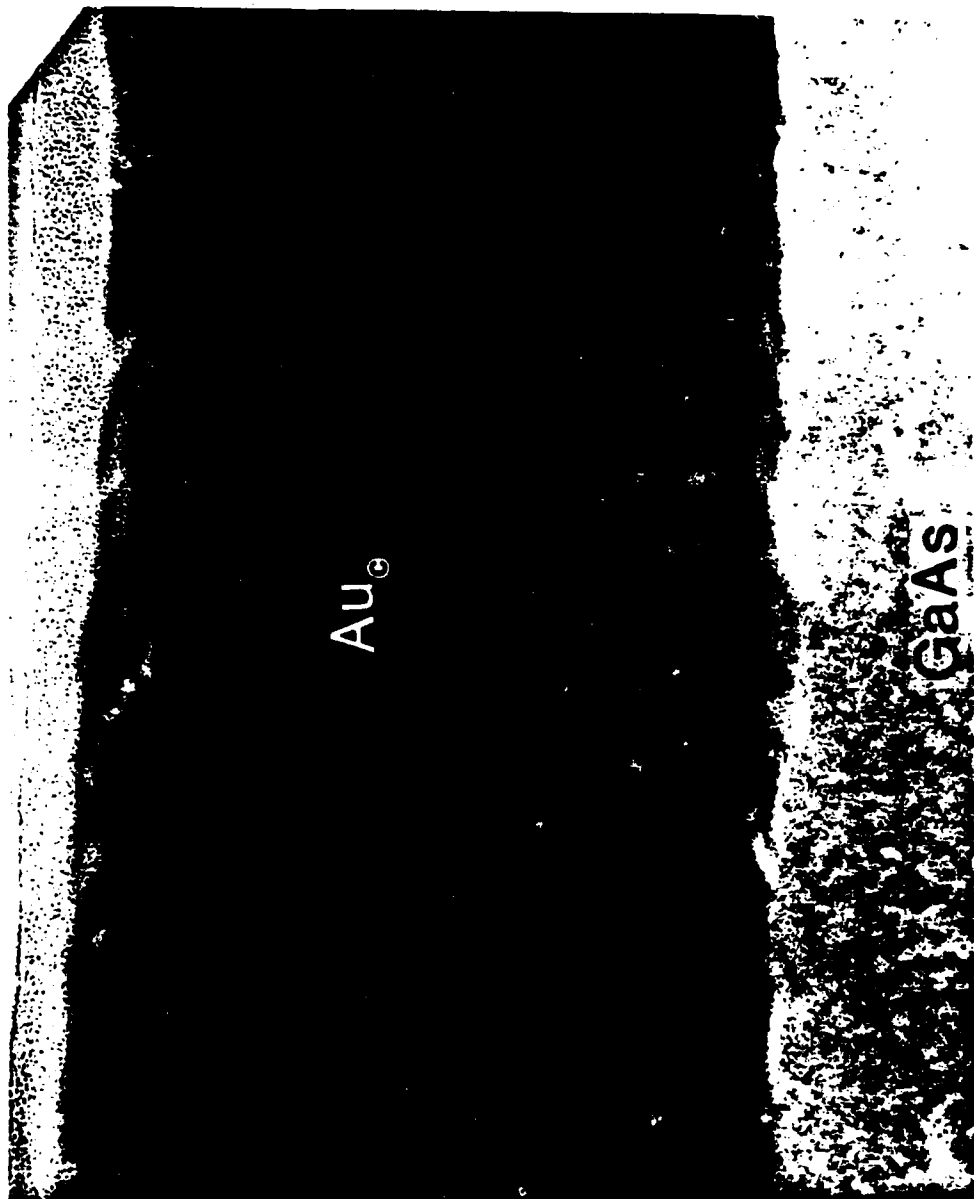
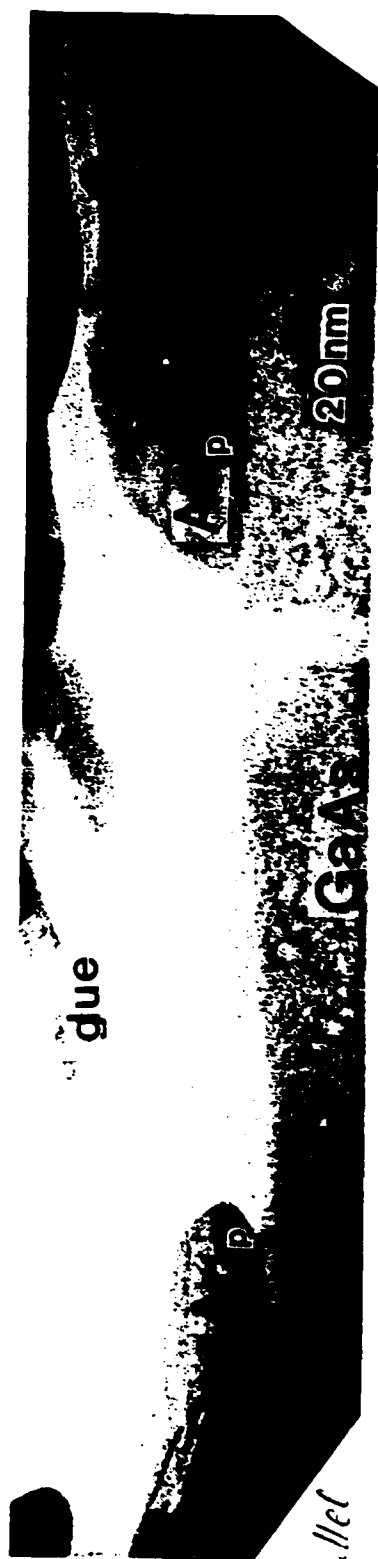


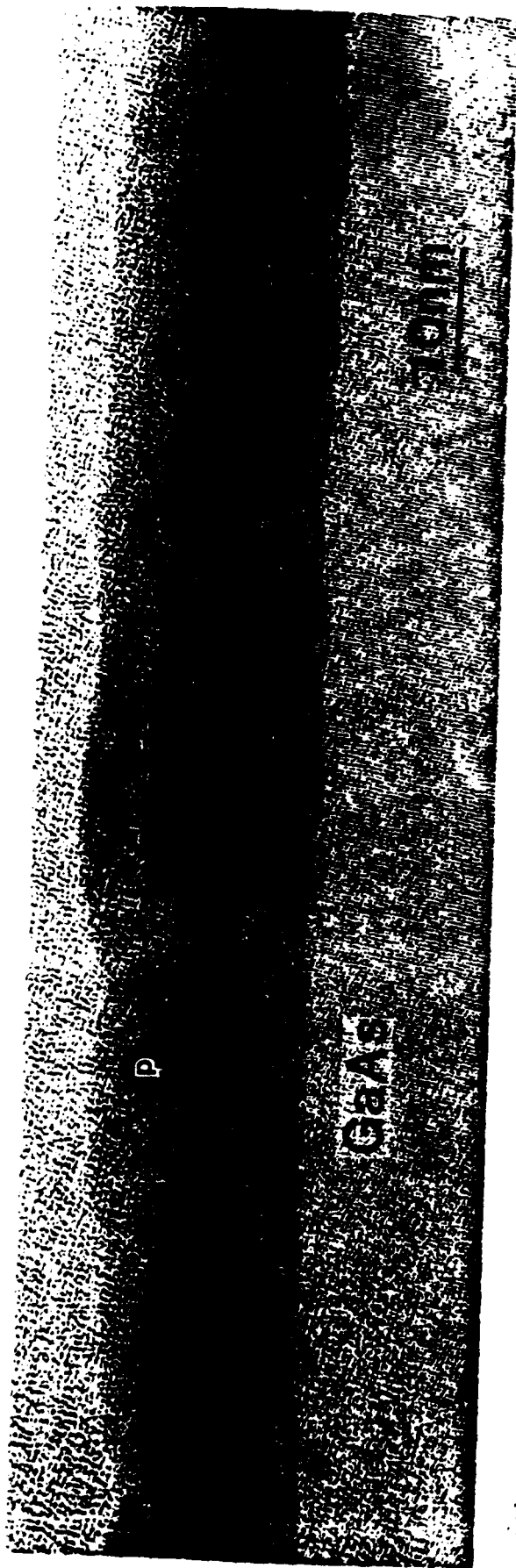
cross section  
of the area  
between two  
crystallites on  
the periphery  
of annealed  
Au dot  
(beam parallel  
to (011))



cross-section  
of the interface  
in the central  
part of Au dot

362





$$(200)_{\text{GaAs}} = 2.826 \text{ \AA}$$

$$\{011\} \parallel \{011\}_{\gamma\text{Ga}_2\text{O}_3} \quad 17$$

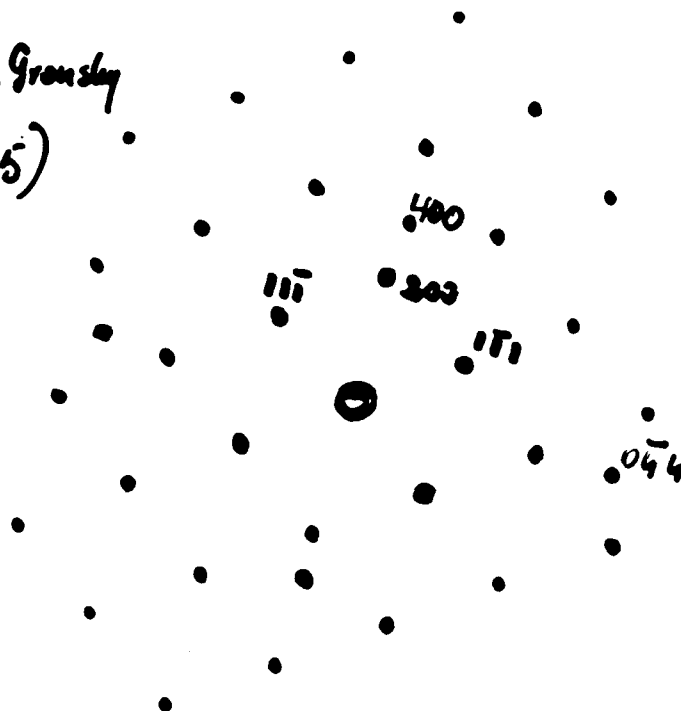
$$400_{\gamma\text{Ga}_2\text{O}_3} = 2.05 \text{ \AA} \approx (200)_{\text{Au}} = 2.039 \text{ \AA}$$

$$\text{Al} = 2.024 \text{ \AA}$$

$$\text{Ag} = 2.044 \text{ \AA}$$

T. Sands, J. Washburn and R. Gronsky

Met. Lett. vol 3, p. 247 (1985)



$$(220)_{\text{GaAs}} = 1.998 \text{ \AA}$$

$$\Rightarrow \frac{2}{3} \times 1.998 \text{ \AA} = 5.99 \text{ \AA}$$

$$(044)_{\gamma\text{Ga}_2\text{O}_3} = 1.45 \text{ \AA} \approx (022)_{\text{Au}} = 1.442 \text{ \AA} \quad 4 \times 1.45 \text{ \AA} = 5.8 \text{ \AA}$$

$$\sim 3\%$$

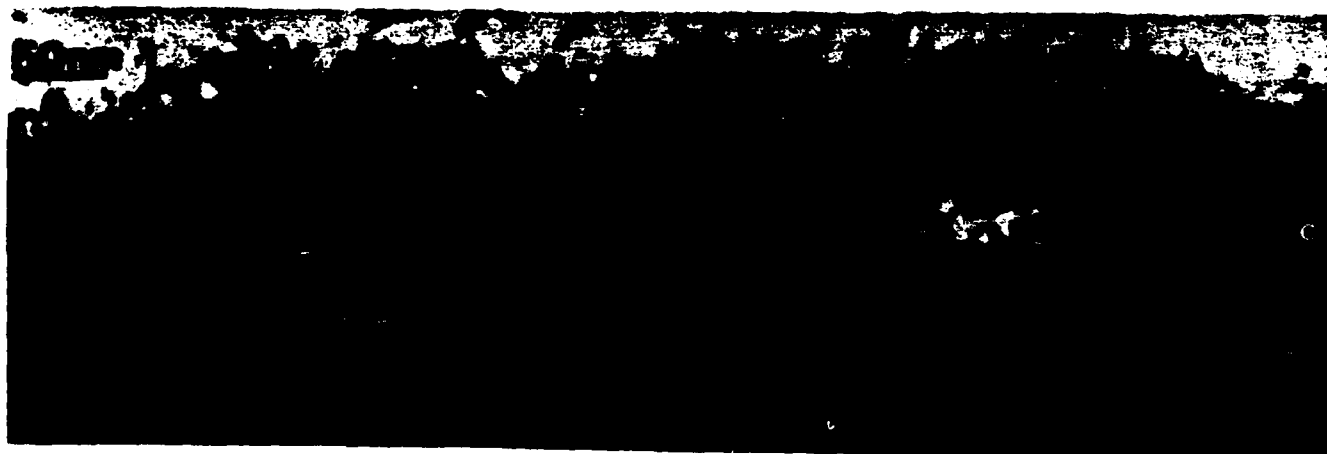
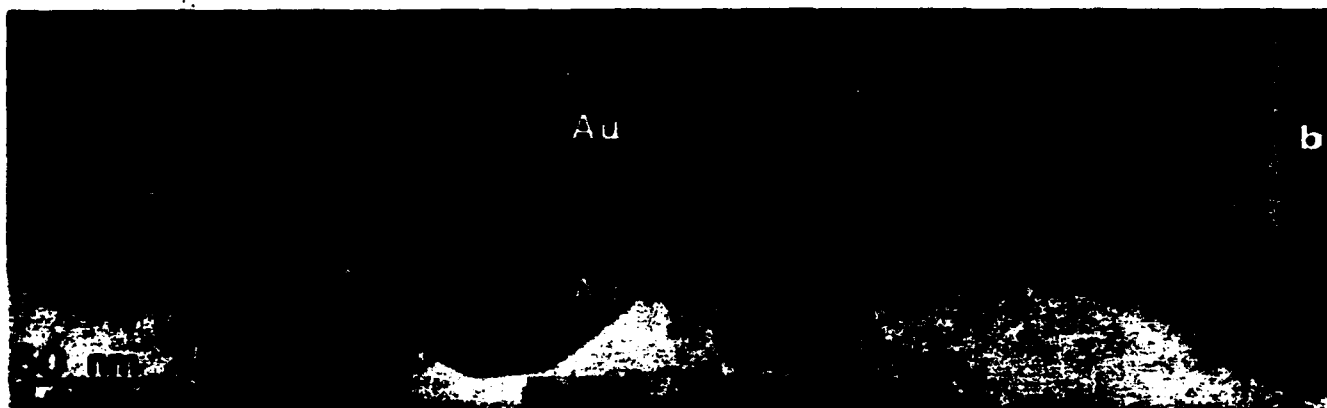
$$\text{Al} = 1.431$$

$$\text{Ag} = 1.445$$

J.W. Evans and O.R. Monteiro

GaAs exposed at 500°C to 30 Torr of oxygen

GaAs  $\rightarrow$  epitaxial  $\gamma\text{Ga}_2\text{O}_3 \rightarrow$  polycryst  $\gamma\text{Ga}_2\text{O}_3 \rightarrow$  polycryst  $\beta\text{Ga}_2\text{O}_3$



0X3882-1034

365

13-Jan-1966 20:12:56

U-AUTS7

Vert.

200 counts

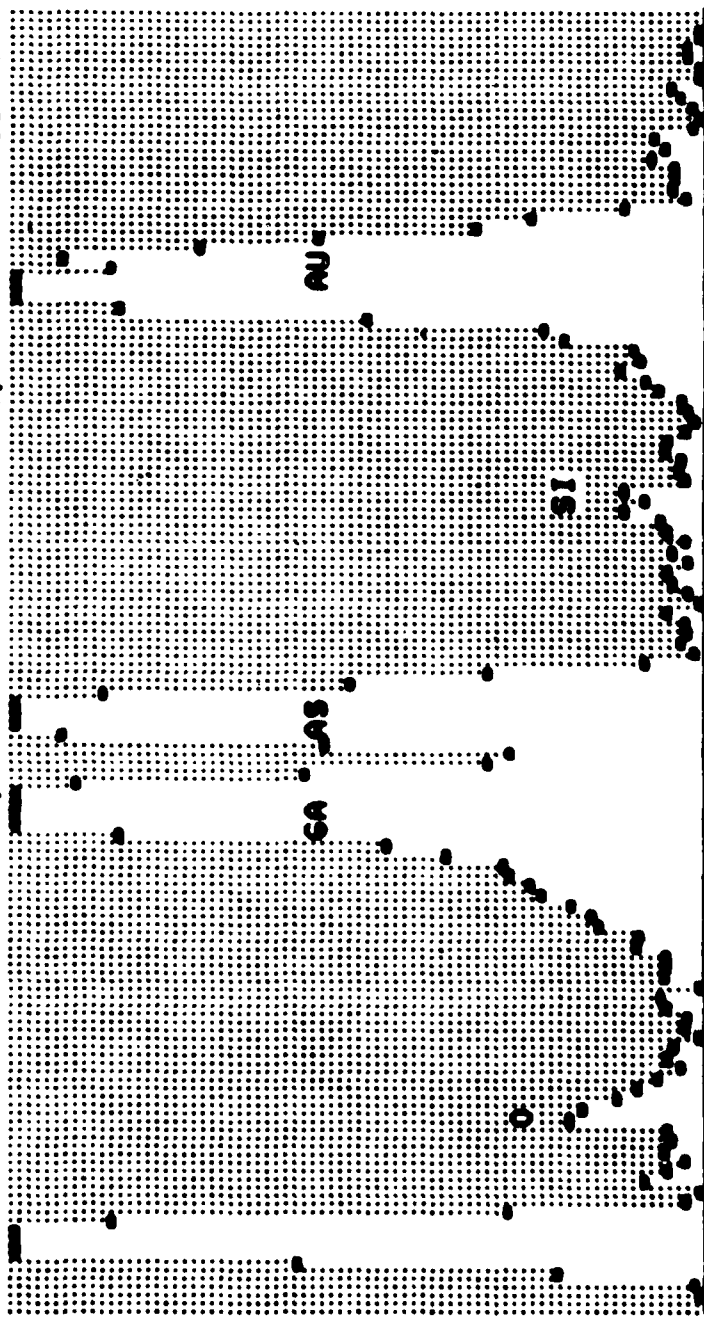
Disp. 1

Preset-

300 secs

Elapsed-

300 secs



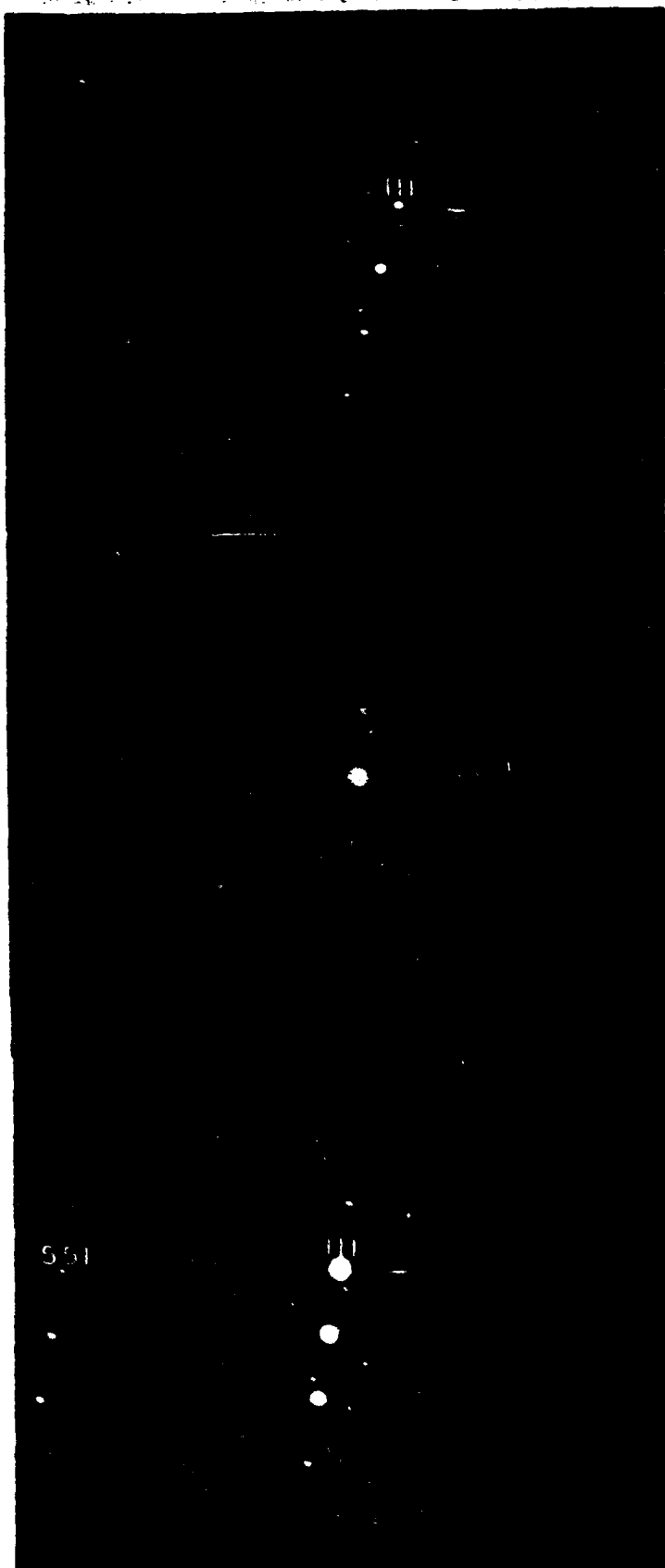
← 0.160 Range= 20.460 keV 2.600 →  
Integral 0 - 10770

XBL 861-165 A

366

367

21



{112}

551

{2}

368

•XBB 686-6220

TO THE

9219-89898X



## CONCLUSIONS

- **SURFACE PREPARATION (PRESENCE OF OXYGEN) DETERMINE**

- interface morphology
- metal grain orientation-relationship with GaAs
- formation of new phases

- **CONTACT FORMATION MECHANISM:**

- **Schottky contacts:**
  - \* Au, Al and  $\text{TiSi}_2$  Schottky contacts show increased As/Ga ratios in GaAs near the metal/semiconductor interface
  - \* evidence for interfacial defects
  - \* results support defect models of "Schottky" barrier formation
- **Ohmic contacts:**
  - \* elongated crystallites at the periphery of annealed Au contacts protrude into the GaAs and provide low-barrier current paths
  - \* protrusions at air-exposed interfaces do not provide current paths
  - \* results support field-enhanced tunneling as dominant Ohmic contact mechanism

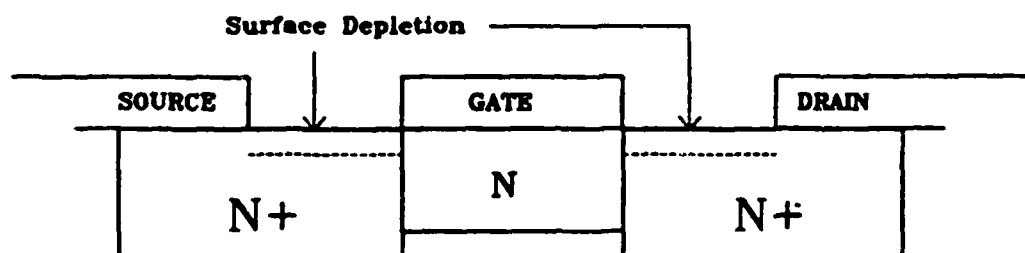
# **Refractory Silicide Contacts for Self-Aligned GaAs MESFETs**

**T. Jackson  
J. DeGelormo  
G. Pepper  
D. Basile (CMU)**

**IBM**

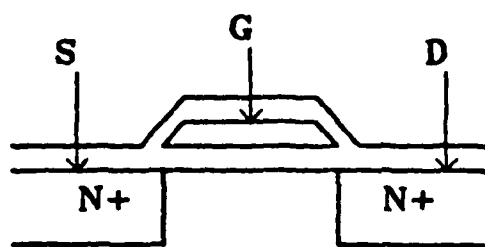
371

# SELF-ALIGNED ENHANCEMENT MODE GaAs MESFET



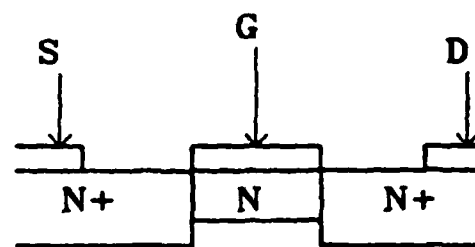
SI GaAs

# SILICON GATE NMOS



P-SILICON

# SELF-ALIGNED GaAs MESFET



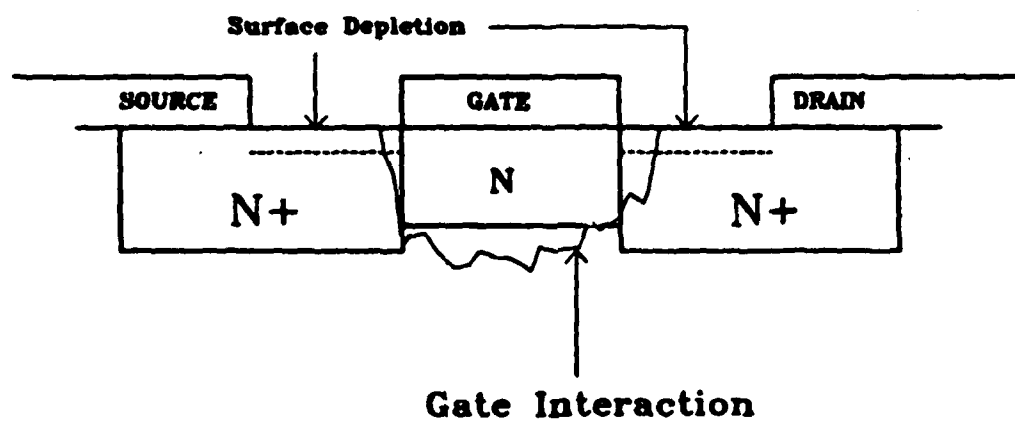
SI GaAs

Diagram showing seven downward-pointing arrows, representing forces, arranged horizontally.

GATE
N
SI GaAs

Diagram illustrating the structure of a GaAs HEMT (High Electron Mobility Transistor). The structure consists of a GaAs substrate (SI GaAs) with an N+ layer. A GATE region (N) is defined on top of the N+ layer, and an N+ region is shown to the right of the gate.

# SELF-ALIGNED ENHANCEMENT MODE GaAs MESFET



SI GaAs

## **Refractory Gate Self-Aligned MESFET**

**Need a gate material that:**

- **Can be patterned to small dimensions ( $< 1 \mu\text{m}$ ).**
- **Can serve as a mask for the N<sup>+</sup> self-aligning implant.**
- **Can survive the N<sup>+</sup> implant activation anneal (800 - 1000° C, 1 sec. - 1 hr.) with stable barrier height, ideality and carrier concentration under the gate.**
- **Can survive As-rich anneal environment.**

## **Candidate Materials**

- **Refractory Metals**
- **Silicides**
- **Nitrides**
- **Borides**
- **Carbides**
- **Et Ceterides**



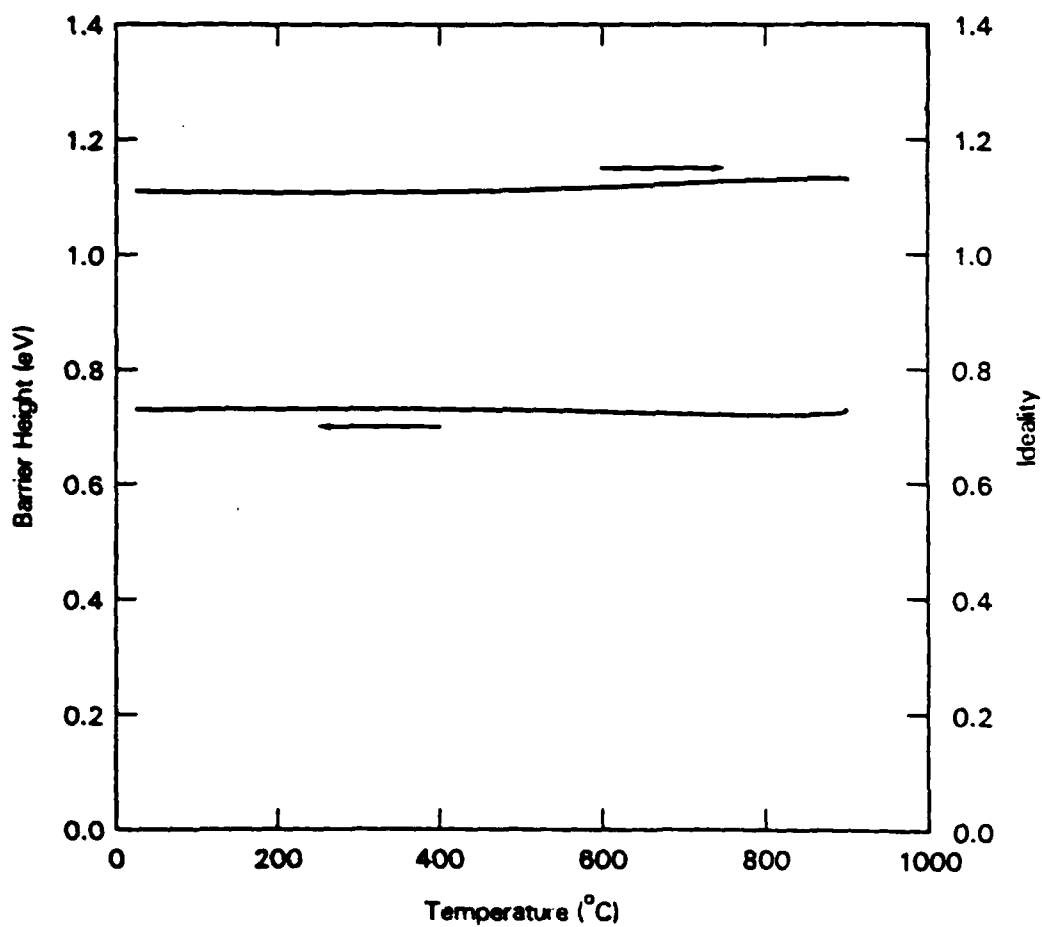
## W/Si

- Pure W has large, columnar grain structure either as deposited or after moderate anneal (grains size  $\sim$  film thickness). Interacts strongly with GaAs above  $\sim 600^{\circ}$  C although FETs can be made by RTA.
- Many intentional or unintentional impurities (e.g. Al, O<sub>2</sub>, N, Si). give drastically reduced grain size and reduce interaction between such films and GaAs.
- Use of Si as grain refiner also allows formation of stable refractory phases: W<sub>5</sub>Si<sub>3</sub>, W<sub>3</sub>Si.

## W/Si

- Easily etched to submicron dimensions (RIE).
- Dense film. Thin films useful as ion implant mask.
- "Good" films show amazing thermal stability on GaAs.
- Relatively stable in As-rich annealing environment (arsine atmosphere anneals okay).
- Acceptable film resistivity.

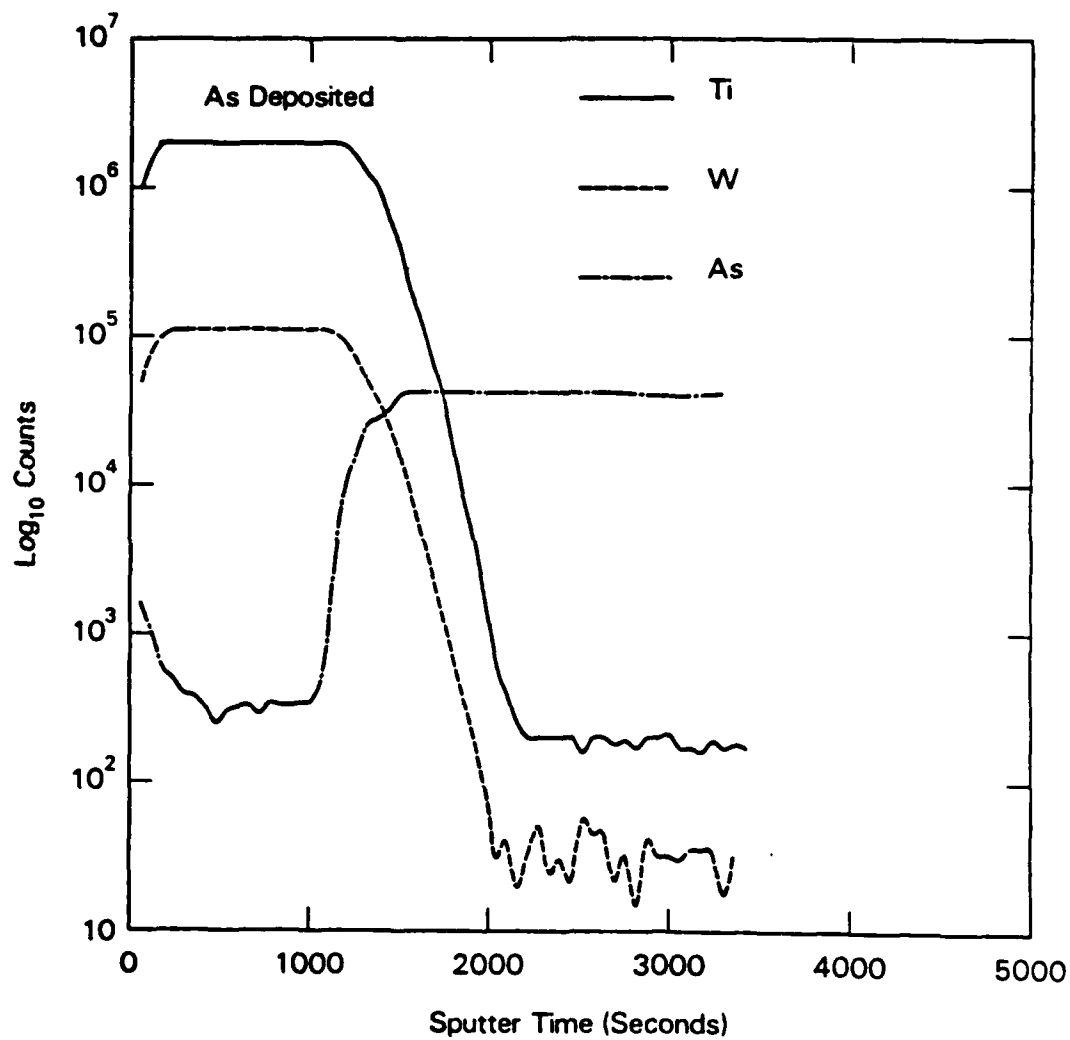
# I-V: Ti/W



380

10/88 (T. Jackson)

## SIMS: Ti/W Film

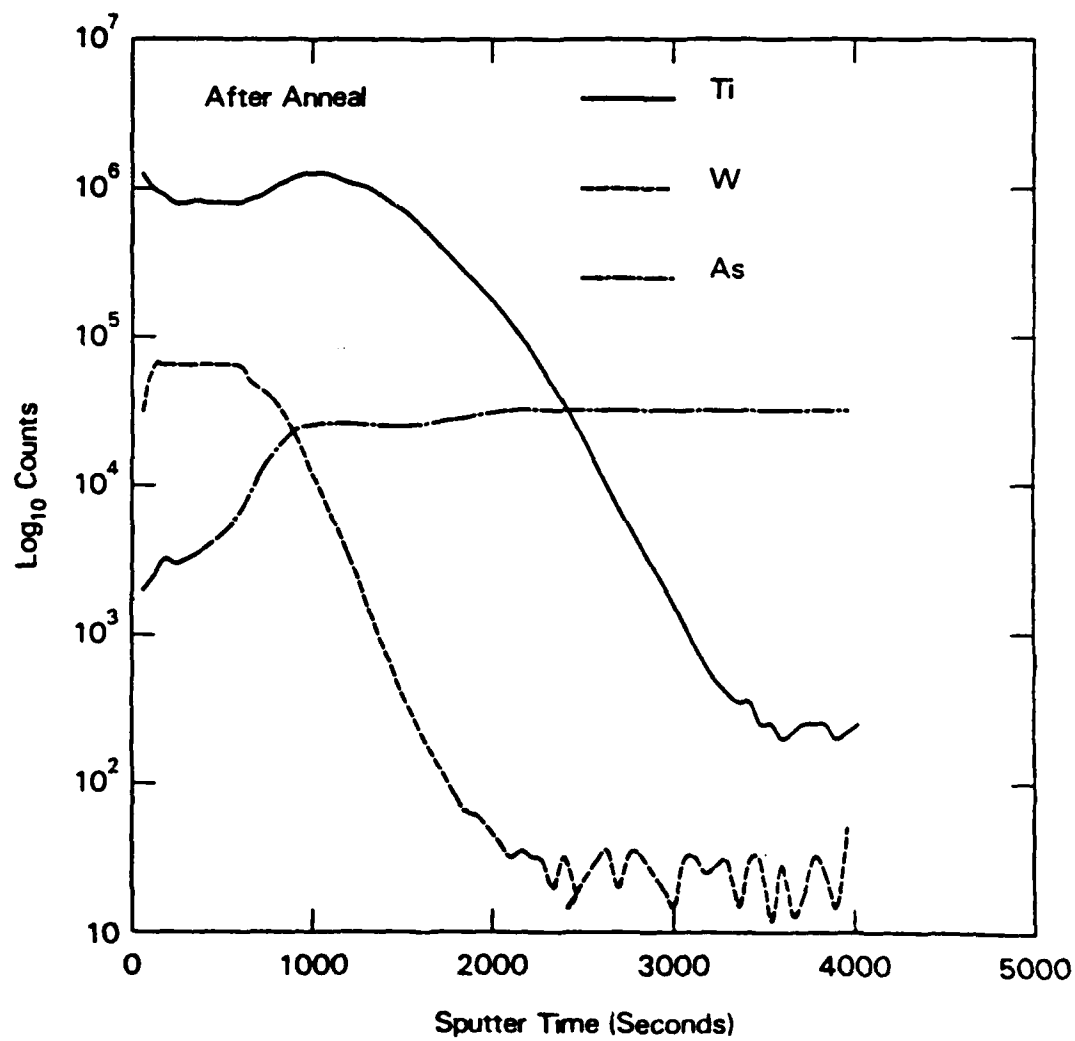


As Deposited

381

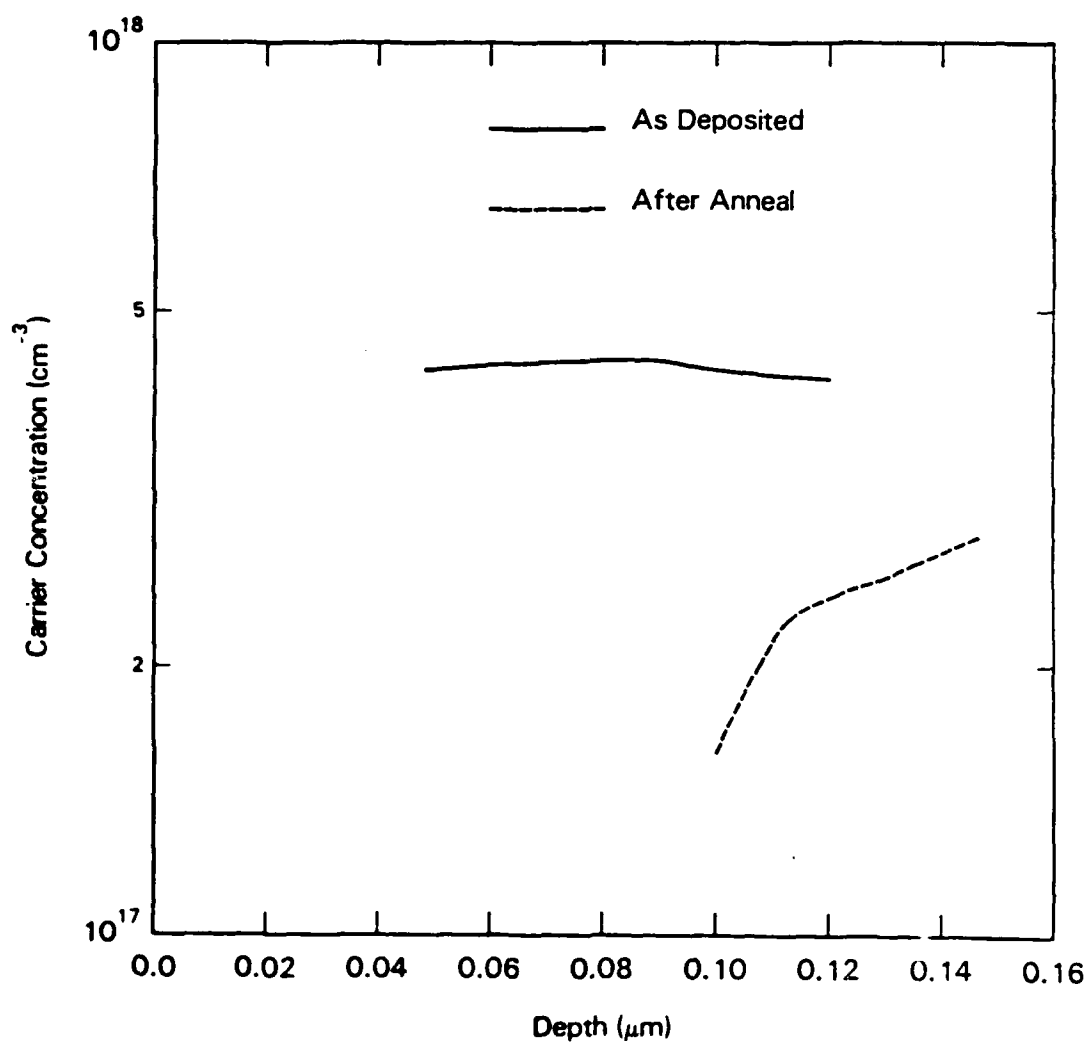
10/86 (T. Jackson)

## SIMS: Ti/W Film



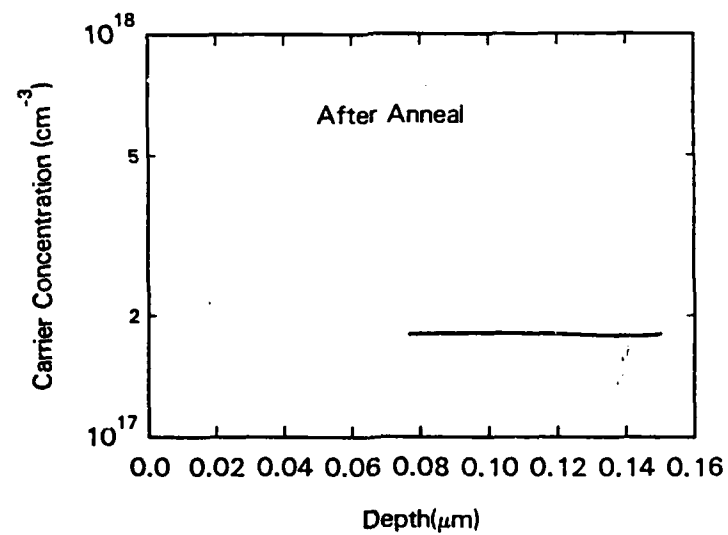
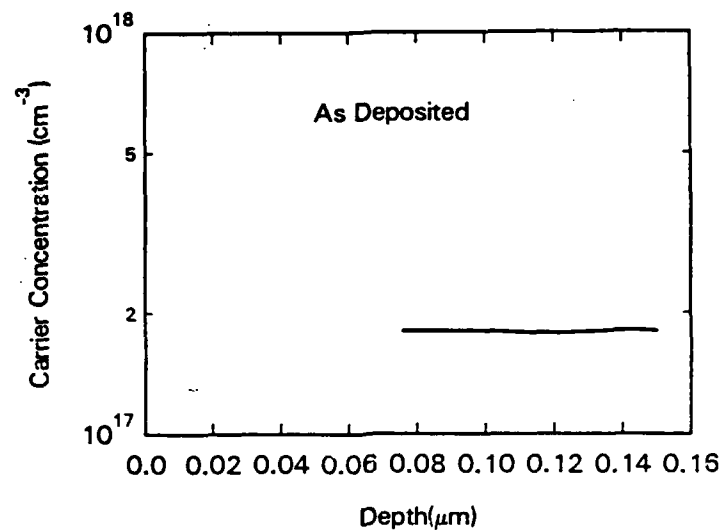
Annealed: 850° C, 15 min.

## C-V: Ti/W



As deposited and after 850° C, 15 min. anneal

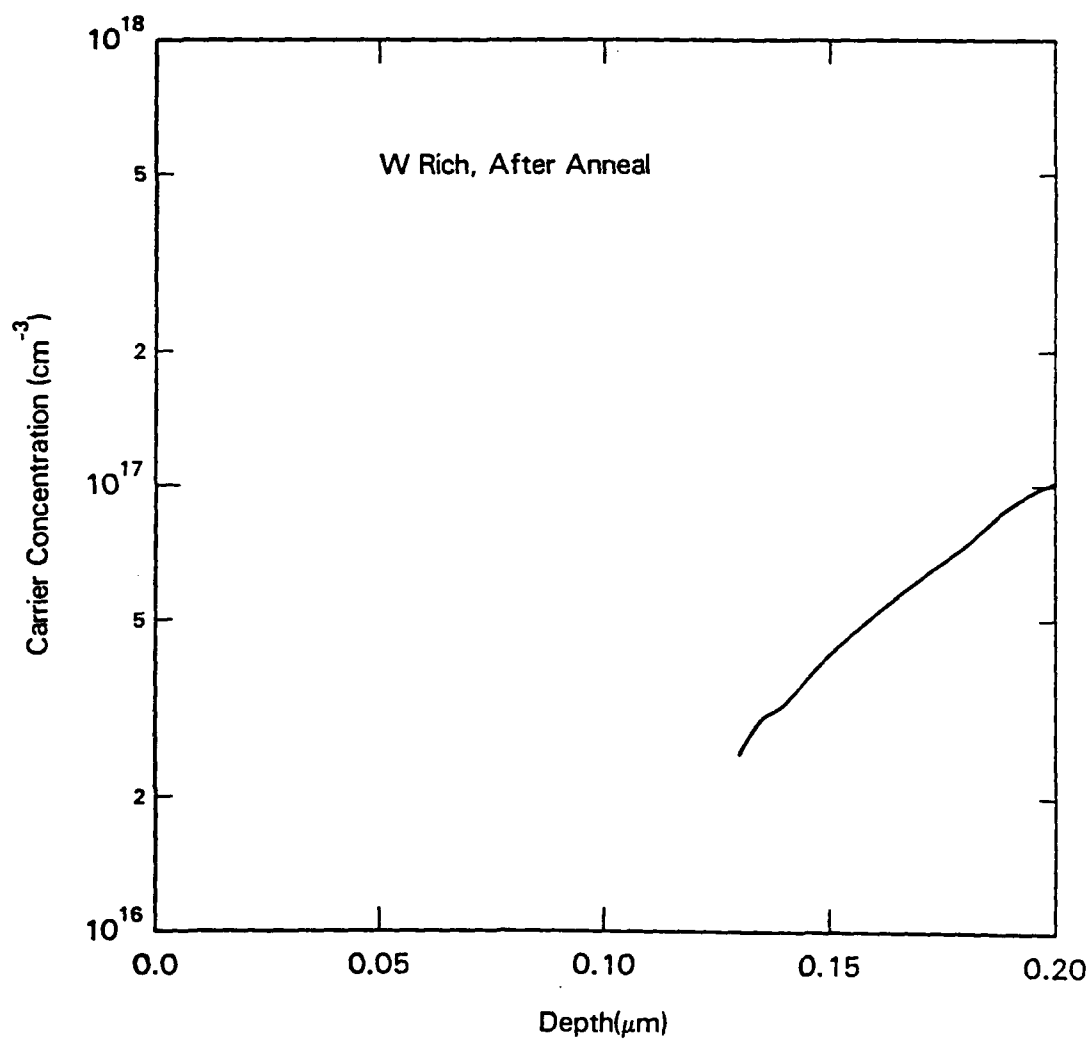
## C-V: "Good" W/Si



Annealed:  $850^{\circ}\text{C}$ , 20 min.

$\sim\text{W}_3\text{Si}$

# C-V: W Rich W/Si



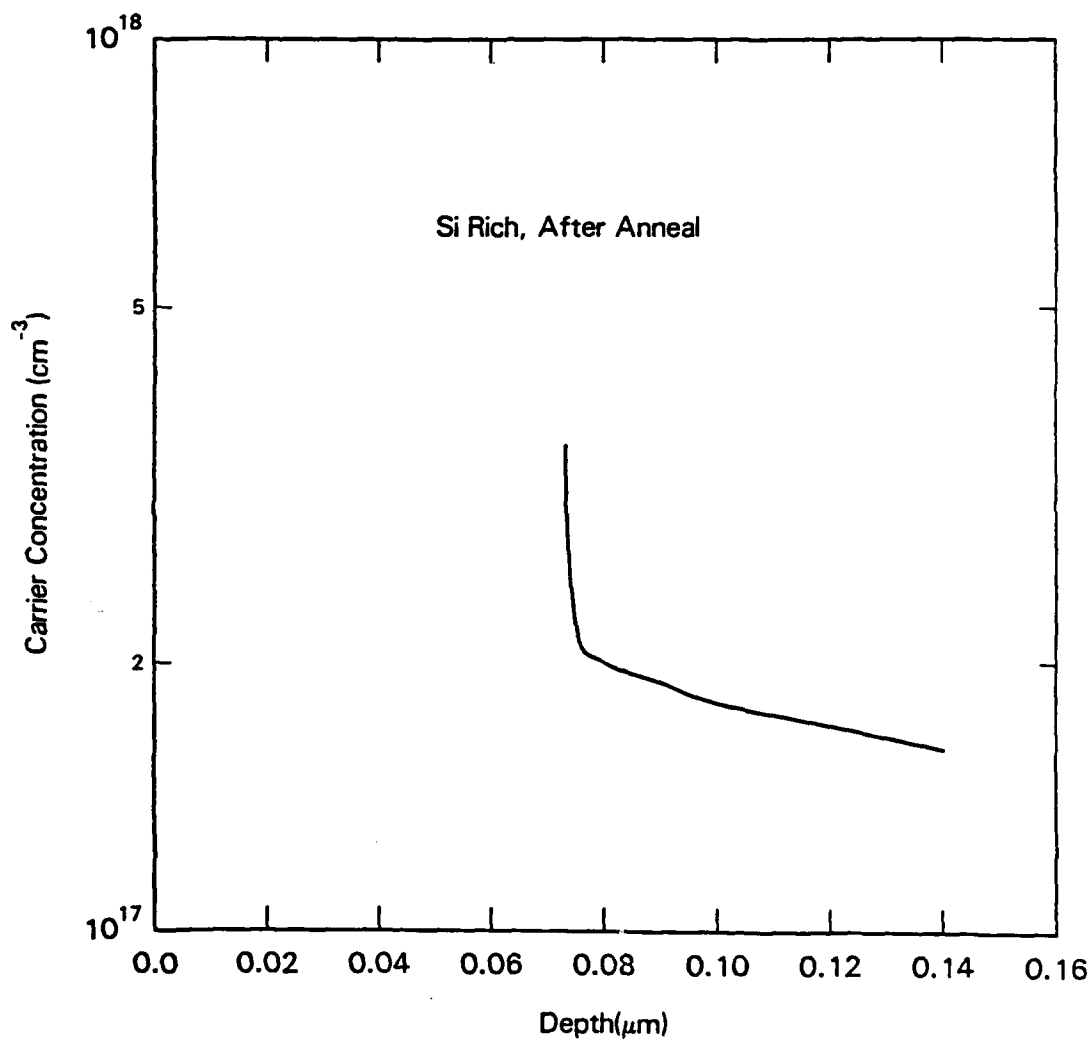
Annealed: 850° C, 20 min.

385

10/86 (T. Jackson)

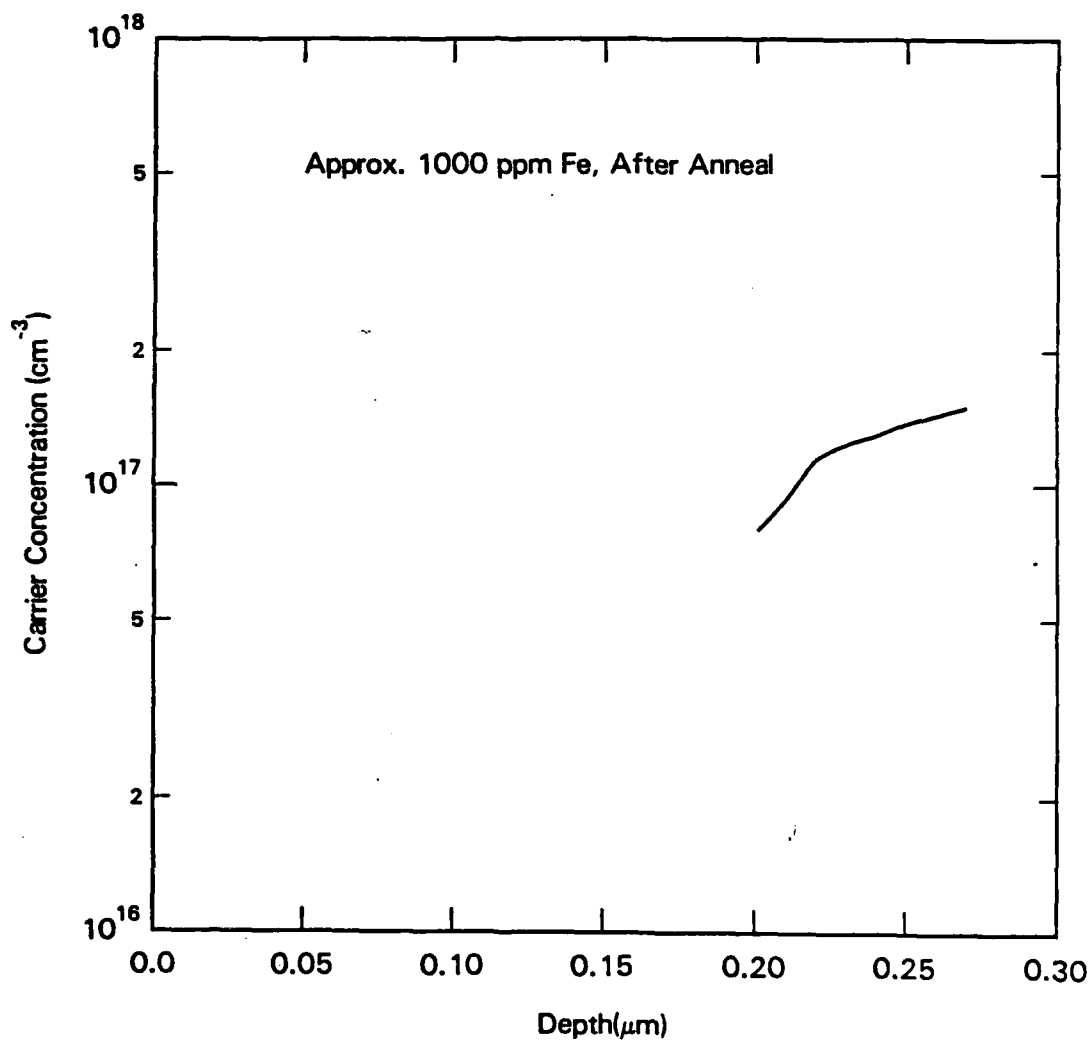


## C-V: Si Rich W/Si



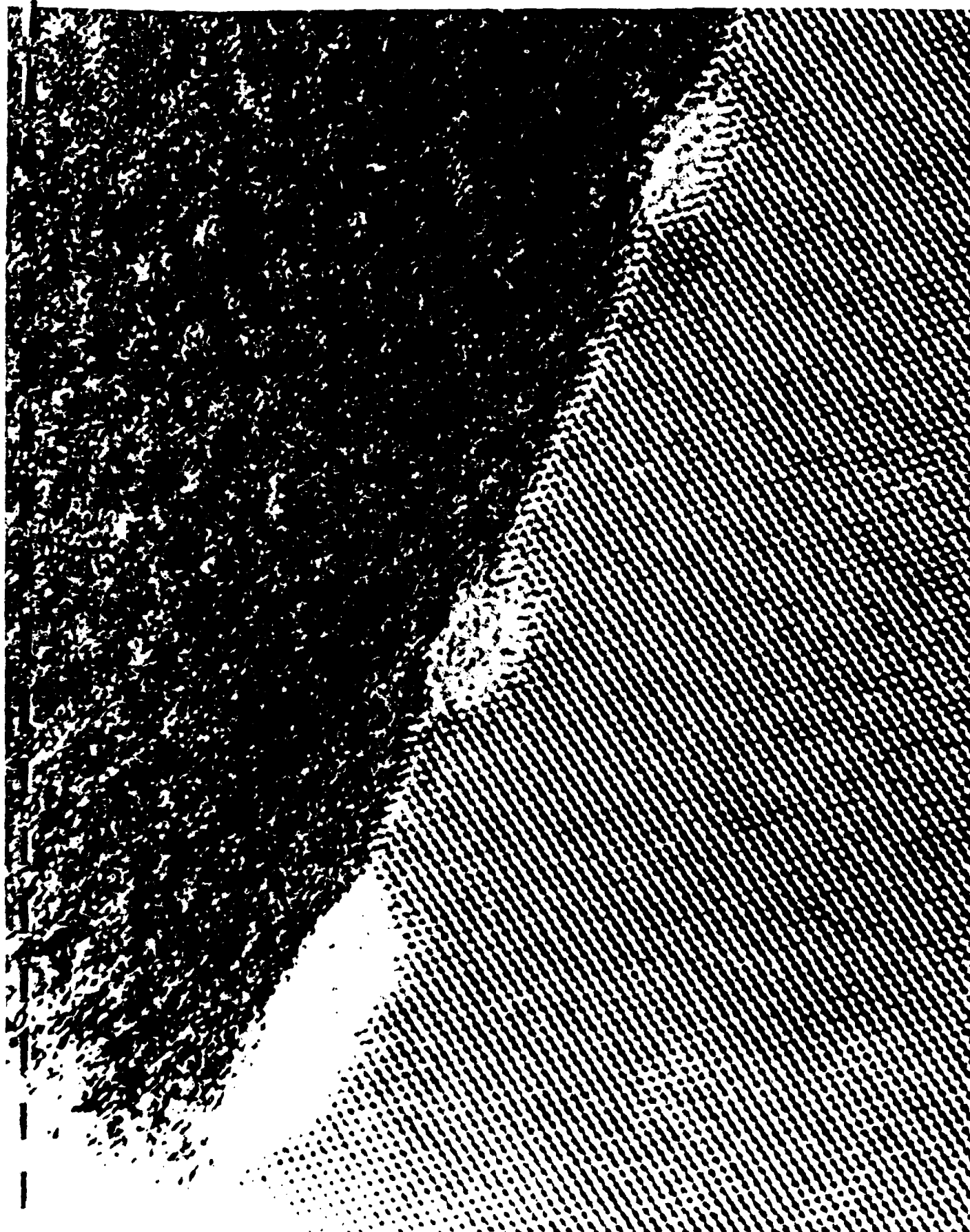
Annealed: 850° C, 20 min.

## C-V: Fe Contaminated W/Si



Annealed: 850° C, 20 min.

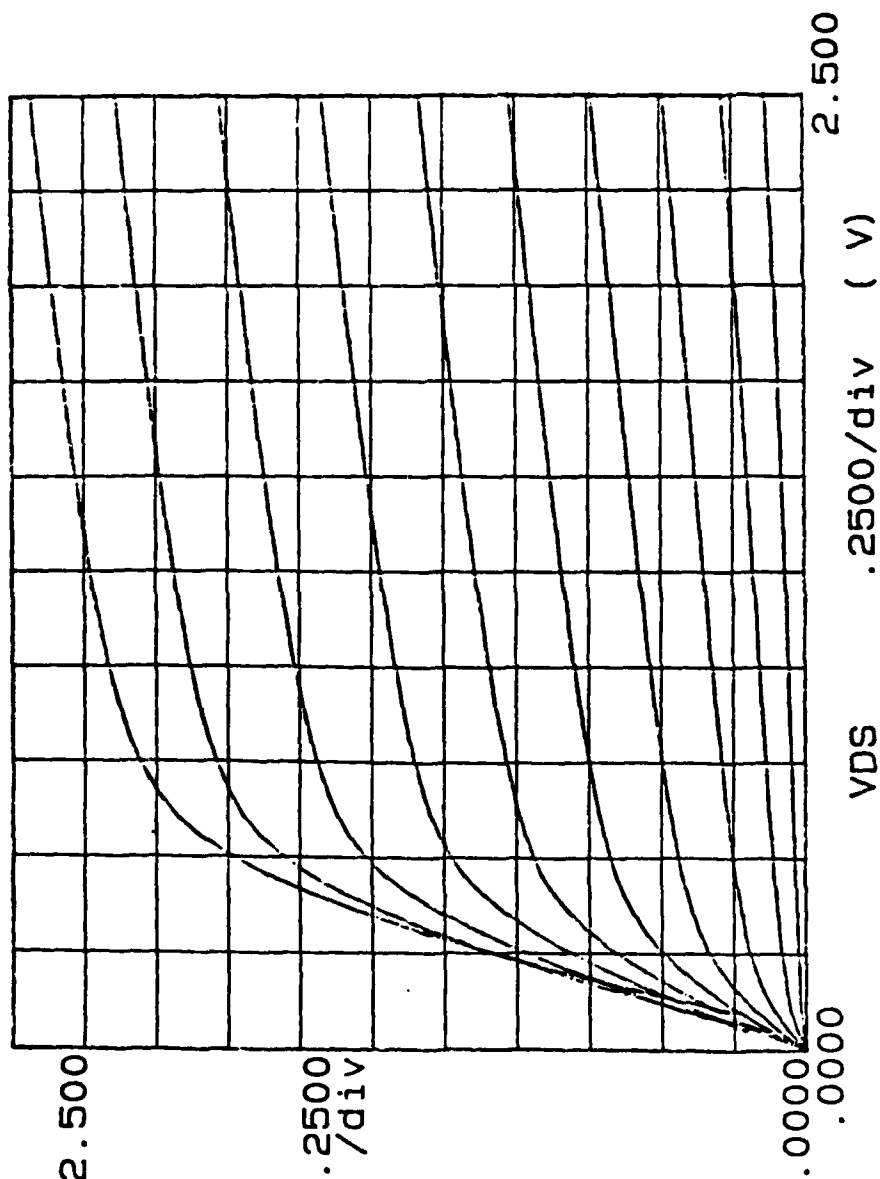




390

# \*\*\*\*\* GRAPHICS PLOT \*\*\*\*\*

ID (mA)

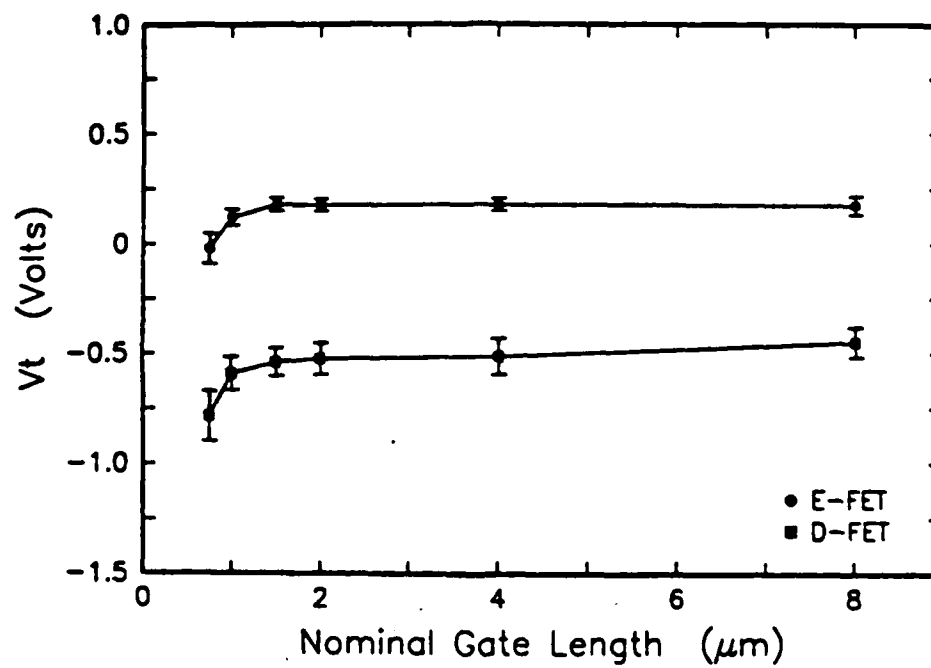


Variable1:  
VDS -Ch2  
Linear sweep  
Start .0000V  
Stop 2.5000V  
Step .0500V

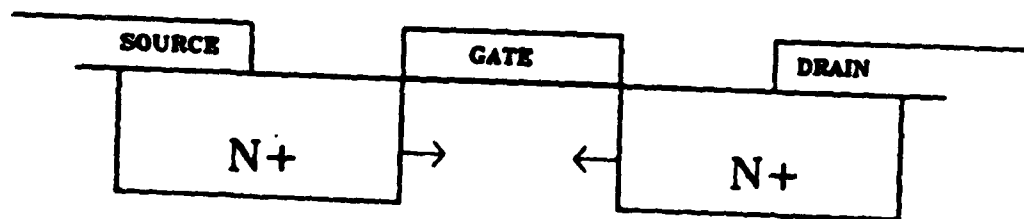
Variable2:  
VG -Ch3  
Start .0000V  
Stop .8990V  
Step .1000V

Constants:  
VS -Ch1 .0000V

## Short Channel Effects



**"No-Channel"  
FET**



**SI GaAs**

## Vt for "No-channel" MESFETs

0.4 micron thick W/Si gate MESFETs with no channel implant. N+ implant =  $5 \times 10^{13}/\text{cm}^2$ . Anneal 800° C, 10 min.

Gate Length	Threshold Voltage
-------------	-------------------

0.25 micron	-2.0 V
-------------	--------

0.5 micron	+0.5 V
------------	--------

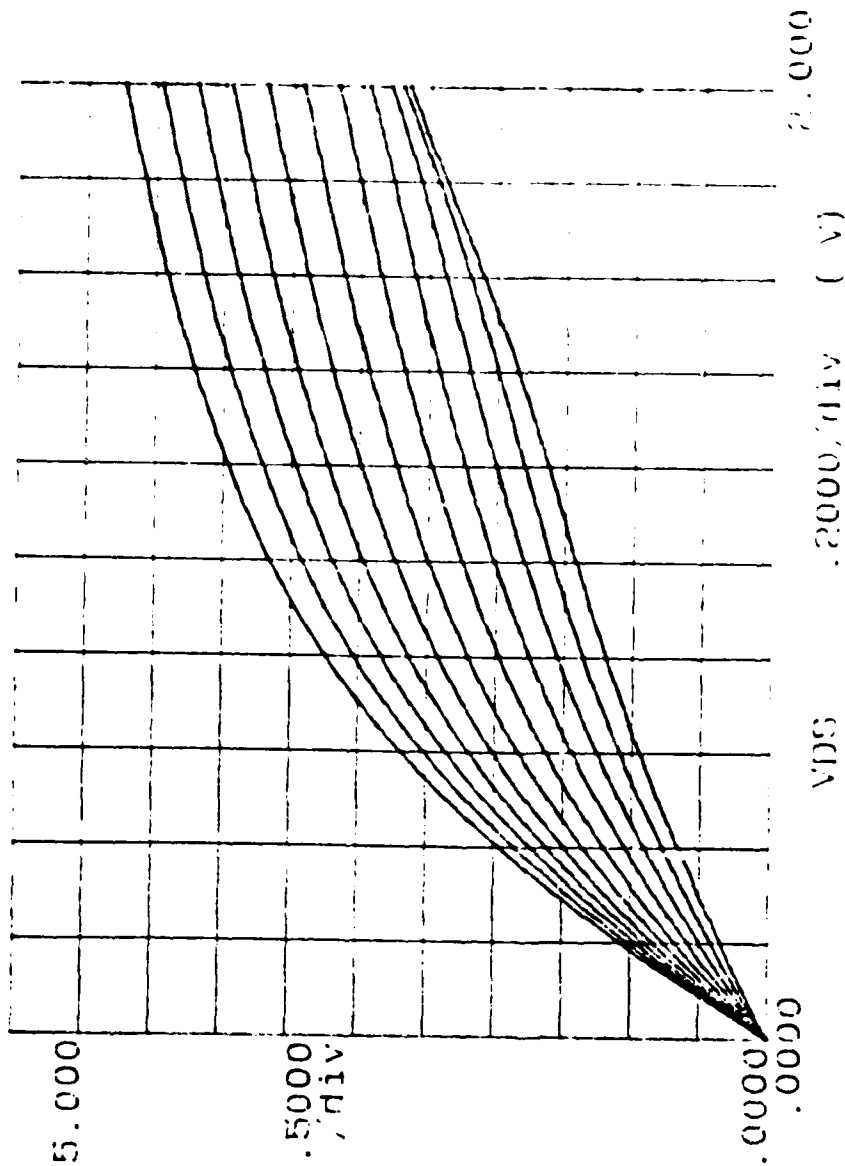
1.0 micron	+1.0 V
------------	--------

Companion structures with W/Si removed prior to anneal showed only small conduction even at 0.25 micron gate length.



\*\*\*\*\* GRAPHICS PLOT \*\*\*\*\*  
2.2 .2\*10 NO CHANNEL

ID (mA)



Variable1:  
VDS -Ch2  
Linear sweep  
Start .0000V  
Stop 2.0000V  
Step .0500V

Variable2:  
VG -Ch3  
Start .0000V  
Stop -2.0000V  
Step -2000V

Constants:  
VS -Ch1 .0000V

395

4000  $\Omega$  w/s:

## Stress Effects

- FETs with no channel implant.
- Short channel effects for convention MESFETs.
- Interacting silicide films show enhanced interaction at pattern edges.
- Samples annealed without capping dielectric and insufficient As overpressure show preferential As loss near gate edge.

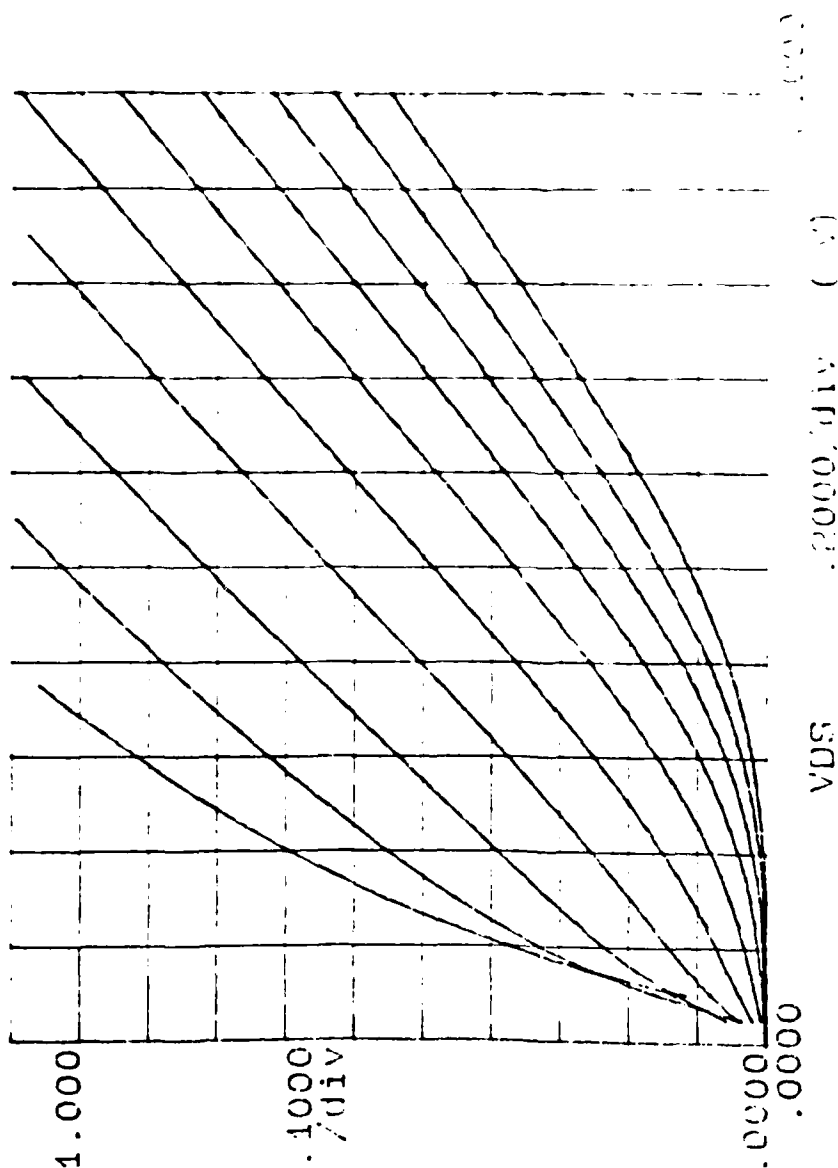
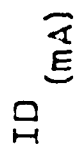
→ Flash Anneal

→ One step farther from equilibrium

\*\*\*\*\* GRAPHICS PLOT \*\*\*\*\*

$0.5 \times 10^{-4}$  800°C-10' Anneal

4000 A w/s;



```
Variable1:
VDS -Ch2
Linear sweep
```

Start	Stop
0.000V	2.000V
0.050V	2.000V

```
var10b102:
v6      -ch3
```

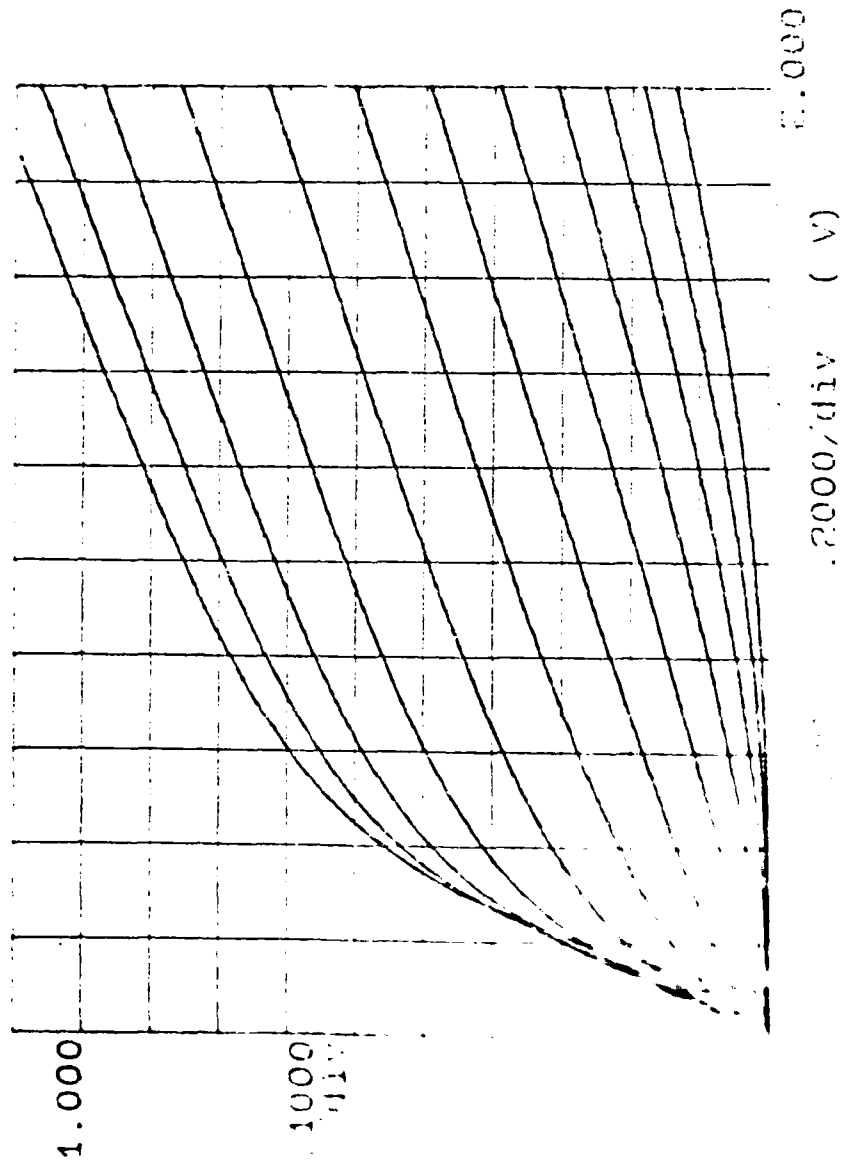
Start  
Stop  
Stop  
Stop

## Contents:

VS -CH1 .0000V

\*\*\*\*\* GRAPHICS PLOT \*\*\*\*\*  
 0.5x10<sub>um</sub> 850°C - 6" Flash (Arlene)  
 4000 Å w/s:

ID (mA)



Variable1:  
 VDS -Ch2  
 Linear sweep  
 Start .0000V  
 Stop 2.0000V  
 Step .0500V

Variable2:  
 VG -Ch3  
 Start .0000V  
 Stop 1.0990V  
 Step .1000V

Constants:  
 VS -Ch1  
 .0000V

AD-A183 158

A WORKSHOP ON 3-5 SEMICONDUCTOR: METAL INTERFACIAL  
CHEMISTRY AND ITS EFFECTS (U) STANFORD UNIV CA  
W E SPICER ET AL. 05 NOV 86 N00014-87-G-0038

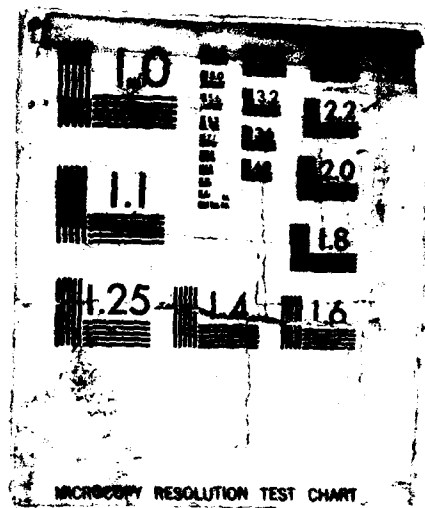
5/7

UNCLASSIFIED

F/G 20/12

NL

57



## Flash Anneal

- Reduces short channel effects.
- Makes "bad" silicide look better.
- Makes silicide phase formation and silicide-GaAs interaction even harder to understand.

10/86 (T. Jackson)

## Opinion

- Refractory gate materials exist that permit fabrication of self-aligned MESFET circuits at LSI level.
- Performance may be compromised by gate material limitations.
- Understanding of GaAs - refractory gate interface and interaction is rudimentary.
- "Realistic" problems difficult to attack; in general not being worked on much.
- Things will get tougher as channels become shorter and shallower.



# Capacitance-voltage characterization of silicide-GaAs Schottky contacts

T. N. Jackson and J. F. DeGelormo

IBM, T. J. Watson Research Center, Yorktown Heights, New York 10598

(Received 5 June 1985; accepted 25 July 1985)

Capacitance-voltage carrier concentration profiling has been used to investigate the high temperature stability of refractory metal silicide films on GaAs. This technique is more sensitive to silicide-semiconductor interactions than is forward  $I$ - $V$  characterization since tenacious surface Fermi level pinning of GaAs can yield stable diode barrier height and ideality factor measurements even for some cases of gross silicide-semiconductor interaction. Using  $C$ - $V$  characterization we have found tungsten silicide film compositions that exhibit excellent high temperature stability on GaAs and have suggested failure mechanisms for other less stable film compositions.

## INTRODUCTION

High-performance GaAs MESFET circuits fabricated using refractory gates to allow self-alignment offer attractive process simplicity. However, such processes require excellent stability of the refractory gate material on GaAs after high temperature ( $\sim 800$ – $1000^\circ\text{C}$ ) anneals. To date, silicide films, particularly W-Si films, have been used most successfully for this purpose. However, in contrast to the silicide films used in silicon technology, the films used for GaAs technology have usually had compositions near  $\text{W}_3\text{Si}_3$ , not  $\text{WSi}_2$ . Also, the films used for GaAs technology are deposited at the desired composition since there is neither opportunity nor desire to react with the substrate. Because of this only a small fraction of the knowledge gained from the study of silicide films on silicon is applicable to the study of silicide films on GaAs.

## EXPERIMENTAL

Previous workers<sup>1,2</sup> have concentrated on diode  $I$ - $V$  characteristics as a means for evaluating the stability of silicide films on GaAs. This is somewhat surprising since the device of interest, the MESFET, uses the depletion layer characteristics of the diode, and since it is well known that the GaAs surface Fermi level position is tenaciously pinned near the middle of the forbidden region for a wide variety of surface interactions and anneals.<sup>3,4</sup> It is suggested that  $C$ - $V$  is a more useful tool for evaluating the electrical stability of silicide (and other) films on GaAs. To illustrate this, Fig. 1 shows the apparent stability of a Ti-W-Si film deposited on Si-doped GaAs ( $n \sim 4 \times 10^{17}/\text{cm}^3$ ) by magnetron sputtering from Ti-W and Si targets. As can be seen, there is no significant change in barrier height or ideality as determined by diode forward  $I$ - $V$  characteristics, even for anneals at temperatures as high as  $900^\circ\text{C}$ . The urge to call this a stable film and claim no interaction with the GaAs is strong. However,  $C$ - $V$  measurements show that this film is not stable, at least in the sense required for successful use as a self-aligned MESFET gate. Figure 2 shows the results of  $C$ - $V$  carrier concentration profiling for the films of Fig. 1 before and after an  $850^\circ\text{C}$ , 20 min anneal. The  $C$ - $V$  measurements were done using a 1 MHz capacitance meter and a computer-controlled data acquisition system. For each measurement the capacitance

was measured in reverse bias only, and the value of carrier concentration found nearest the sample GaAs-silicide interface is for zero bias. Before anneal the results show a carrier concentration near the surface of about  $4 \times 10^{17}/\text{cm}^3$  and a zero bias depletion depth of about 50 nm. After the  $850^\circ\text{C}$  anneal the sample shows a marked reduction in carrier concentration near the surface and the zero-bias depletion depth has increased to about 100 nm. Since a typical channel thickness for self-aligned MESFET's is 50–200 nm, this amount of interaction is not negligible.

The results of SIMS measurements on the Ti-W-Si films of Figs. 1 and 2 are shown in Figs. 3(a) and 3(b). Figure 3(a) shows the composition profile for the as-deposited film. Figure 3(b) shows the SIMS composition profile for the film after an  $850^\circ\text{C}$ , 15 min anneal. There is obviously substantive movement of Ti into the GaAs from the deposited film, and of As out of the GaAs and into the film. Although Figs. 2 and 3 show that the interaction of this Ti-W-Si film with GaAs is gross, the  $I$ - $V$  results by contrast suggest film stability.

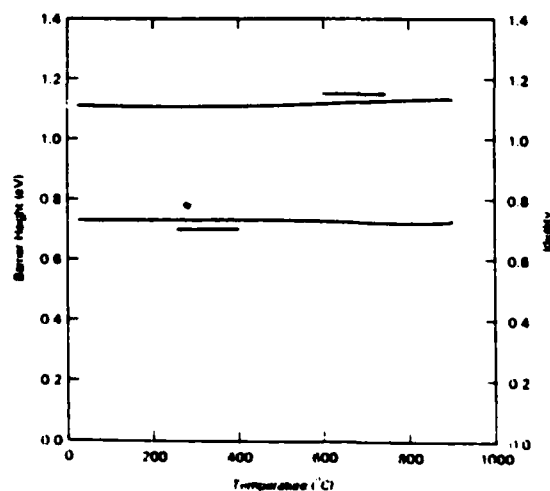


FIG. 1. Barrier height and ideality factor as a function of anneal temperature for Ti-W-Si diodes on bulk-doped GaAs ( $n \sim 4 \times 10^{17}/\text{cm}^3$ , 15 min anneal).

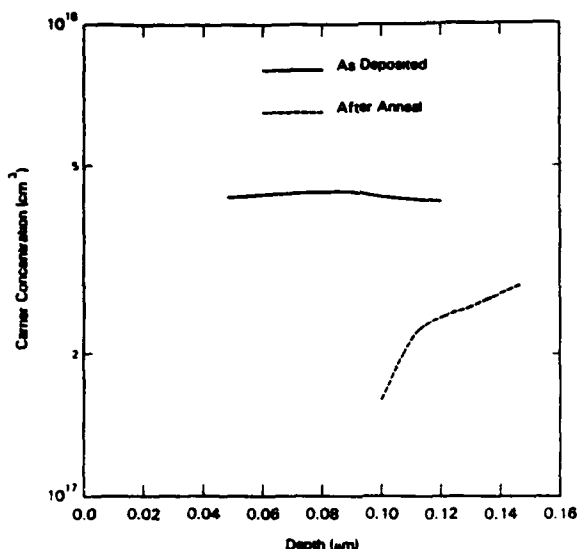


FIG. 2. C-V carrier concentration profiling results for Ti-W-Si diodes on bulk-doped GaAs before and after an 850 °C, 15 min anneal ( $n \sim 4 \times 10^{17} / \text{cm}^3$ ).

Using C-V profiling as a sensitive measure of silicide-GaAs interaction we have characterized co-sputtered W-Si films as a function of composition. The films were sputter deposited from planar magnetron elemental sources with both sources depositing simultaneously onto a rotating substrate holder. The substrates were Si-doped GaAs with  $n \sim 2 \times 10^{17} / \text{cm}^3$ . Some previous workers<sup>1</sup> have had difficulty depositing a wide range of W-Si compositions because of stress (film failure) at some compositions. By using the

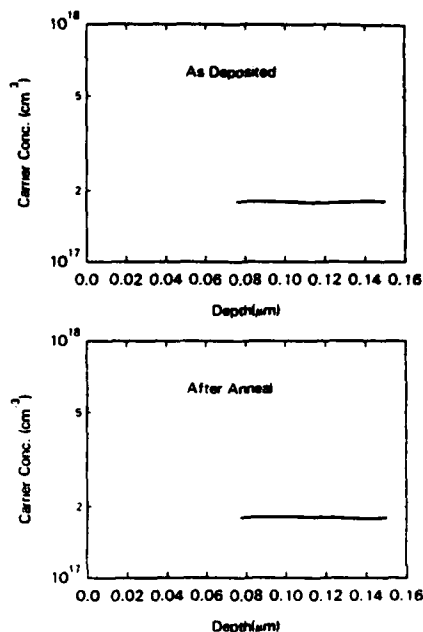


FIG. 4. C-V carrier concentration profiling results for a W-Si film with composition near W<sub>3</sub>Si on bulk-doped GaAs ( $n \sim 2 \times 10^{17} / \text{cm}^3$ ) before and after an 850 °C, 20 min anneal.

results of Ref. 5 (an "atomic peening" stress control model) we have had no difficulty in depositing films across the entire compositional range from pure W to pure Si with approximately constant film stress. After deposition, the films were patterned into diodes for C-V analysis by reactive ion etching with  $\text{CF}_4 + \text{O}_2$  and then annealed in an anneal system that provides an arsenic overpressure to prevent GaAs decomposition.

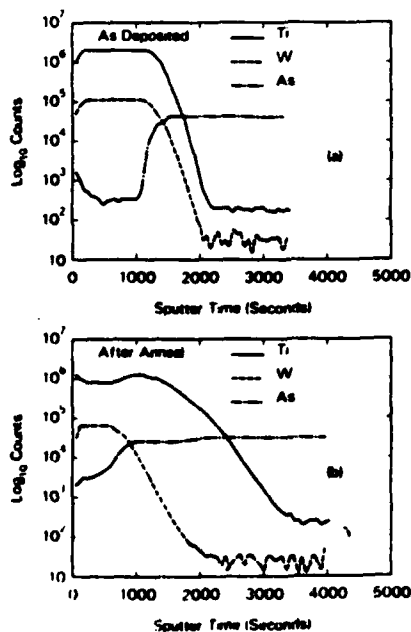


FIG. 3. SIMS profiles for a Ti-W-Si film on GaAs before and after an 850 °C, 15 min anneal.

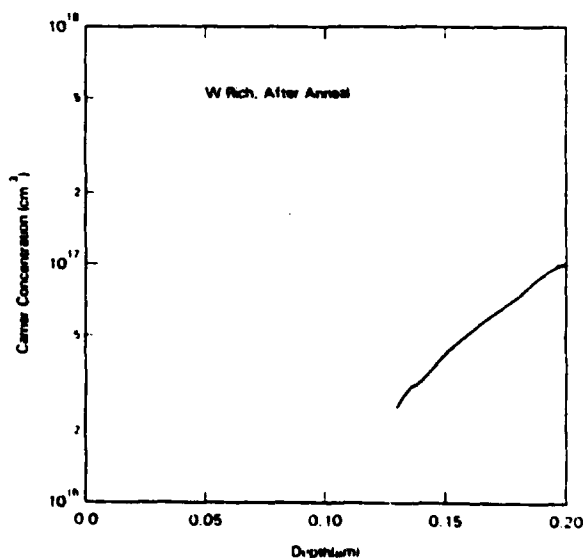


FIG. 5. C-V carrier concentration profiling results for a W-Si film with ~40 at. % W on bulk-doped GaAs ( $n \sim 2 \times 10^{17} / \text{cm}^3$ ) after an 850 °C, 20 min anneal.

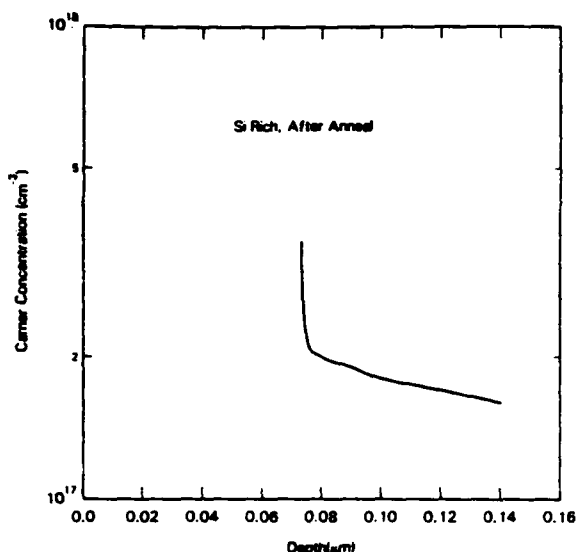


FIG. 6.  $C$ - $V$  carrier concentration profiling results for a W-Si film with  $\sim 45$  at. % Si on bulk-doped GaAs ( $n \sim 2 \times 10^{17} / \text{cm}^3$ ) after an  $850^\circ\text{C}$ , 20 min anneal.

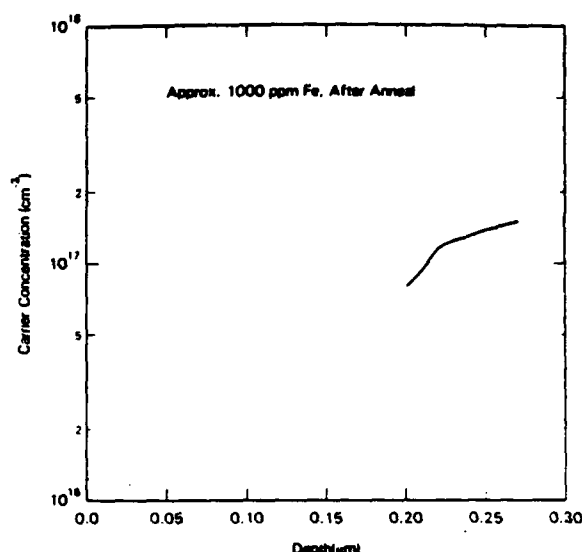


FIG. 7.  $C$ - $V$  carrier concentration profiling results for a W-Si film with composition near  $\text{W}_3\text{Si}$  containing  $\sim 1000$  ppm Fe on bulk-doped GaAs ( $n \sim 2 \times 10^{17} / \text{cm}^3$ ) after an  $850^\circ\text{C}$ , 20 min anneal.

Figure 4 shows that W-Si films with excellent  $C$ - $V$  stability can be obtained as described above. The results shown are for a film composition of approximately  $\text{W}_3\text{Si}$ . Such films also show excellent  $I$ - $V$  characteristic stability, as expected. Other workers<sup>1</sup> have found stable W-Si films with about 37.5–39 at. % Si ( $\text{W}_3\text{Si}_2$ ). While we also find that films of these compositions can be stable, the scatter in the  $C$ - $V$  results is greater than for films near  $\text{W}_3\text{Si}$ . We have used W-Si films with compositions near  $\text{W}_3\text{Si}$  to fabricate GaAs MES-FET devices and circuits with excellent characteristics.

Figure 5 shows the  $C$ - $V$  profile results for a film with large W content ( $\sim 90$  at. %) before and after an anneal at  $850^\circ\text{C}$  for 20 min. As can be seen, there is a large increase in zero-bias depletion width and significant carrier concentration decrease near the surface.  $I$ - $V$  measurements showed only small changes in barrier height and ideality (0.02 eV and 0.1) after such anneals. Also, SIMS could not resolve any interaction between the deposited film and the doped GaAs. This is not wholly surprising, since the required interaction need only be of the order of the GaAs doping concentration ( $\sim 2 \times 10^{17}$ ) and this level of interaction between a W-Si film and the GaAs substrate is difficult to probe by SIMS due to dynamic range difficulties.

Figure 6 shows  $C$ - $V$  profiling results for a film with large Si content ( $\sim 45$  at. % Si) before and after an  $850^\circ\text{C}$ , 20 min anneal. Note that the zero-bias depletion depth for the annealed film is now decreased compared to the unannealed film and there is a significant enhancement of the carrier concentration near the surface. In this case, the  $I$ - $V$  characteristics for the diode also showed large changes after anneal ( $\sim 0.3$  eV decrease in barrier height) and the diodes became "leaky" in reverse bias. These results are similar to those obtained for  $\text{WSi}_2$  films and may indicate that Si diffuses into GaAs from W-Si films under some conditions.

## DISCUSSION

The above results show some trends for interaction between W-Si and GaAs. There are three main regions of interest: a high Si content regime that exhibits  $C$ - $V$  characteristics consistent with Si diffusion into GaAs, a high W regime that shows doping concentration reduction near the silicide-GaAs interface perhaps due to W diffusion, and an intermediate region of relative film stability. It is expected that the boundaries between these regions will be soft, with fine variations for small composition changes. This is expected due to the nature of the film formation process. Consider: The silicide films as-deposited are nearly amorphous (x-ray diffraction analysis shows only slight coordination). The films are then annealed and react to form polycrystalline W-Si of varying phase or phases depending at least on composition and anneal. It is likely that the interaction phenomena for such films are strong functions of the kinetics of the silicide formation which is in turn a function of many variables such as the details of the anneal conditions and impurities in the deposited films. Also, it is known that the diffusion of Si into GaAs is a strong function of the arsenic pressure in the anneal system.<sup>6</sup>

It is also quite possible to have impurities present in W-Si films whose presence can have as large an effect on film stability as major changes in film composition. For example, Fig. 7 shows the  $C$ - $V$  profiling results before and after an  $850^\circ\text{C}$ , 20 min anneal for a film with the same W-Si composition as that of Fig. 4, but with about 1000 ppm Fe added to the film. It can be seen that this small addition of Fe has caused a change in zero-bias depletion width of almost 100 nm! This is particularly alarming since it is known that silicide sputtering targets may contain several impurities in amounts as high as 100 ppm.<sup>7</sup>

## CONCLUSION

Stable refractory metal silicide films are important components of some high-performance self-aligned GaAs MES-FET fabrication processes. While film formation technology has been adequate to date to allow progress with these processes, the details of film stability are poorly understood. Improvements in characterization and analysis of silicide films with compositions far from  $\text{WSi}_2$  should be fruitful.

<sup>1</sup>T. Ohnishi, N. Yokoyama, H. Onodera, S. Suzuki, and A. Shibatomi, Appl. Phys. Lett. 43, 601 (1983).

<sup>2</sup>W. F. Tseng and A. Christou, IEDM Tech. Dig. 1982, 174.

<sup>3</sup>J. M. Woodall and J. L. Freeouf, J. Vac. Sci. Technol. 19, 794 (1981).

<sup>4</sup>W. E. Spicer, P. W. Chye, P. R. Skeath, C. Y. Su, and I. Lindau, J. Vac. Sci. Technol. 16, 1422 (1979).

<sup>5</sup>D. W. Hoffman and J. A. Thornton, J. Vac. Sci. Technol. 20, 355 (1982).

<sup>6</sup>G. R. Antell, Solid-State Electron. 8, 943 (1965).

<sup>7</sup>S. C. Liang, J. Vac. Sci. Technol. B 2, 714 (1984).

404

# **MOVPE GROWTH OF III-V MATERIALS AND INTERFACES**

**T.F. Kuech  
IBM T.J. Watson Research Center  
Yorktown Heights, N.Y.**

- I. Introduction - MOVPE Growth**
- II. Bulk Growth of GaAs**
- III. Growth of V-V' Alloys**
- IV. Doping**
- V. Summary**

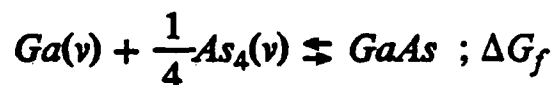
**IBM**

10/86 (T.F. Kuech)

405

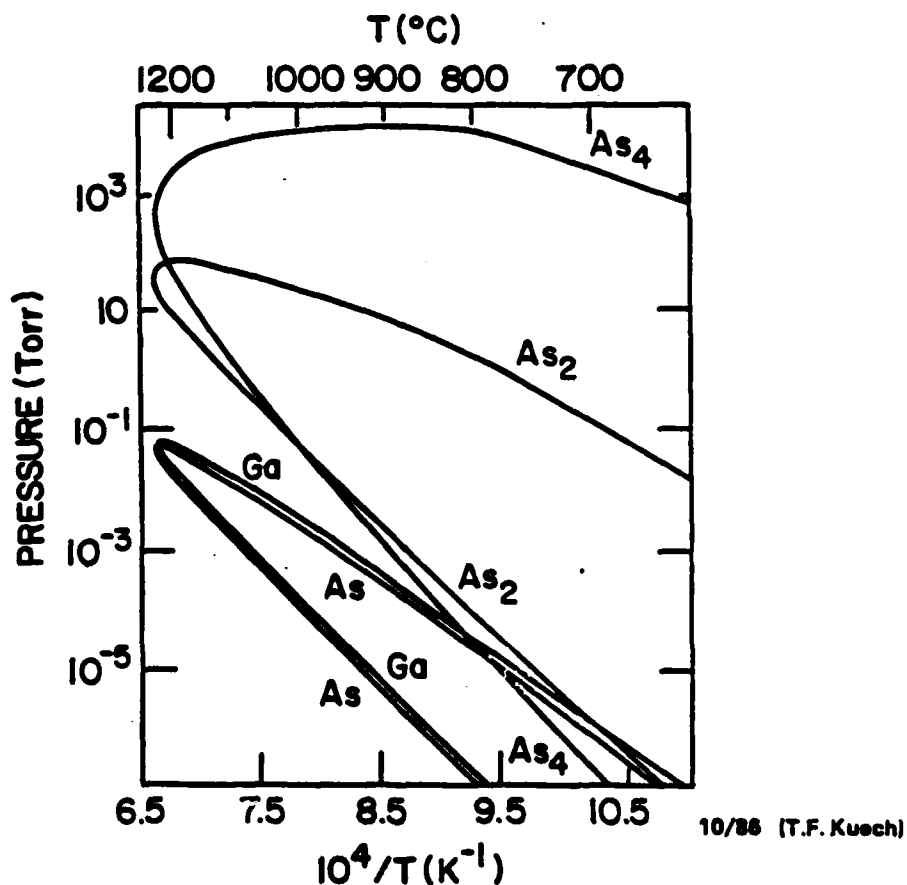
## GaAs and Crystal Growth

At Thermal Equilibrium



$$K_{eq}^{-1} = P_{Ga}^o P_{As_4}^o{}^{\frac{1}{4}}$$

- The Ga and As activities (pressures) are interdependent and can assume a range of values.



## Crystal Growth and Thermodynamic Equilibrium

For crystal growth to occur, a supersaturation must be present in the growth ambient.

$$P_{Ga} P_{As_4}^{\frac{1}{4}} > P_{Ga}^o P_{As_4}^{o\frac{1}{4}}$$

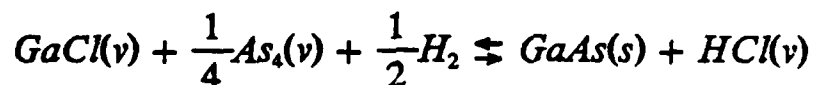
In CVD this supersaturation is due to the decomposition of reactive chemical precursors.

- Near Equilibrium
  - small supersaturation
  - fast reaction kinetics

- Liquid Phase Epitaxy



- Halide Growth



- Growth chemistry far from chemical equilibrium

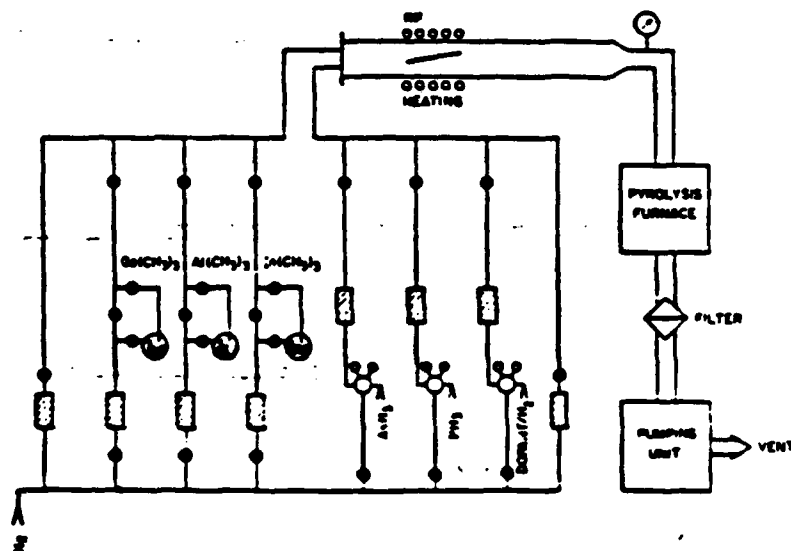
Metal-organic Vapor Phase Epitaxy

**IBM**

10/86 (T.F. Kuech)

## MOVPE Growth

An open tube, cold wall epitaxial growth Technique which utilizes metal-organic and hydride growth precursors in a  $H_2$  or  $N_2$  carrier gas.



### Growth Conditions

Growth Rate	$= 0.5 - 6.0 \mu\text{m/hr}$
Growth Rate	$\propto X_{MO}$
Gas Composition:	
Metal-Organic	$X_{MO} \approx 10^{-3} - 10^{-6}$
Hydride	$X_{Hydride} \approx 5 - 100 X_{MO}$
$P_{\text{Reactor}}$	$= 0.01 - 1 \text{ atm.}$
Growth Temperature	$= 550 - 800^\circ\text{C}$
Carrier Gas	$H_2, N_2, \dots$

**IBM**

10/86 (T.F. Knecht)



## MOVPE Growth Precursors

A wide variety of growth precursors are available increasing the versatility of this growth technique.

An ideal vapor source should possess:

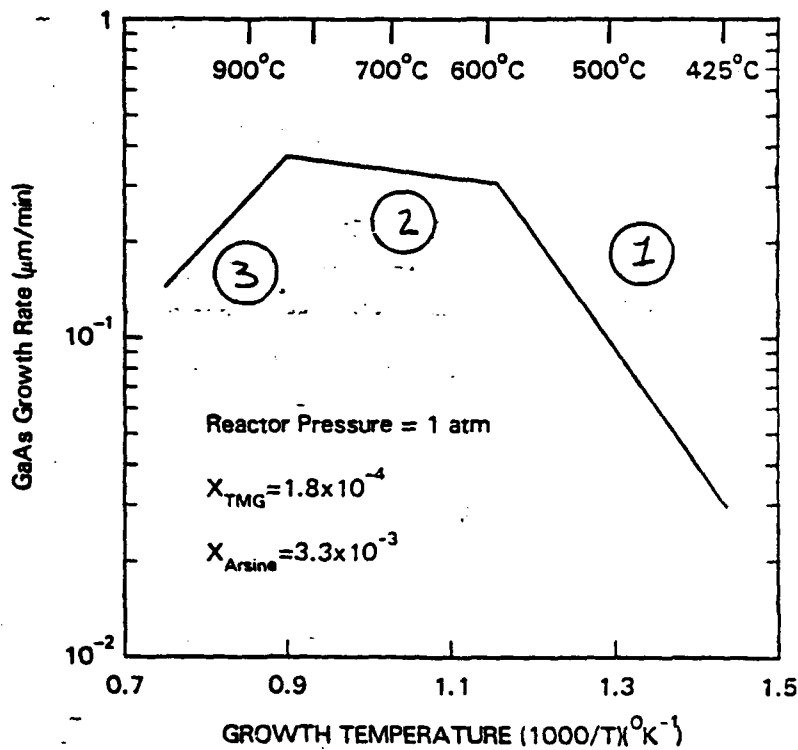
- Adequate vapor pressure
- Suitable purification routes
- Suitable pyrolysis temperatures (RT stability)
- No interaction with growth apparatus  
(Stainless steel, ..)
- Appropriate reaction routes during growth

<u>Cation Source</u>	<u>Anion Source</u>	<u>Compound Semiconductor</u>
$\text{Ga}(\text{CH}_3)_3$	$\text{AsH}_3$	$\left\{ \begin{array}{l} \text{GaAs} \\ \text{Al}_x\text{Ga}_{1-x}\text{As} \\ \text{GaAs}_y\text{P}_{1-y} \\ \text{Al}_x\text{Ga}_{1-x}\text{P} \\ \text{In}_x\text{Ga}_{1-x}\text{Sb} \end{array} \right.$
$\text{Ga}(\text{C}_2\text{H}_5)_3$	$\text{AsH}(\text{C}_2\text{H}_5)_2$	
$\text{Al}(\text{CH}_3)_3$	+ $\text{PH}_3$	
$\text{Al}(\text{C}_2\text{H}_5)_3$	$(\text{CH}_3)_3\text{PH}_2$	
$\text{In}(\text{CH}_3)_3$	$\text{Sb}(\text{CH}_3)_3$	

**IBM**

10/88 (T.F. Kuech)

## Temperature Dependence



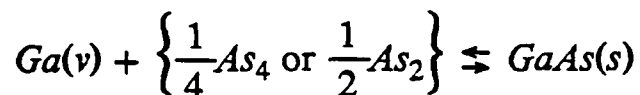
1. Chemical Kinetic Limitation
2. Gas Phase Mass Transport
3. Ga Desorption (?) with  $P_{Ga} \approx P_{TMG}$

IBM

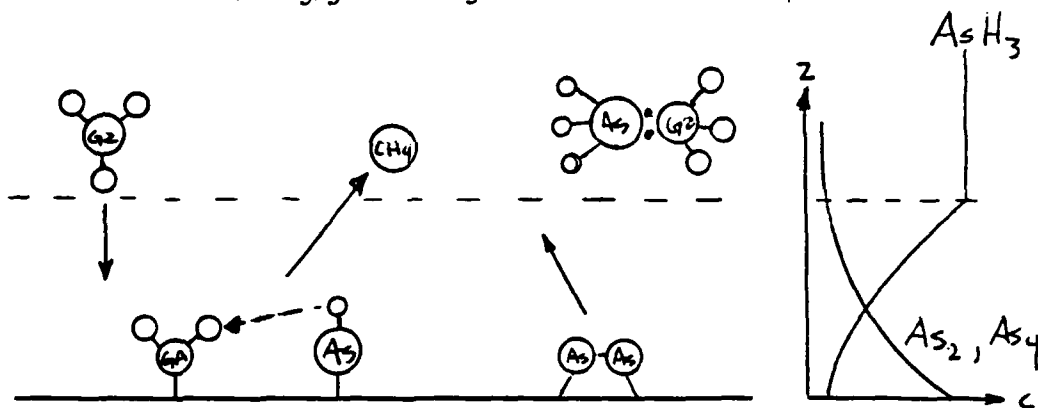
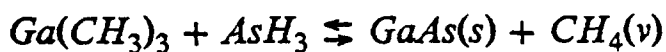
10/86 (T.F. Kuech)

## Near the Growth Surface

### Phase Equilibrium

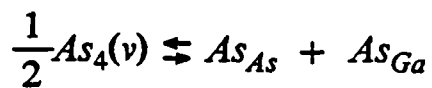
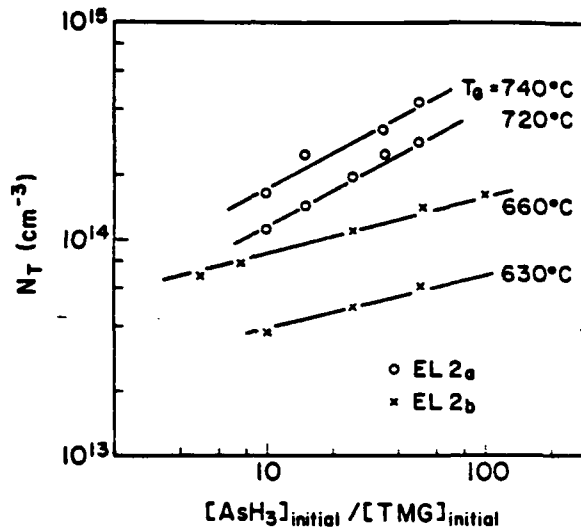


### Chemical Equilibrium



- Gas Phase Reactions
- Metal-organics react to completion at or near surface
- As Activity determined by the generation of As(v) at the surface and diffusion of As(v) away from the surface.

## Stoichiometric Defects



$$K_{eq} = [\text{As}_{\text{Ga}}] P_{\text{As}_4}^{-\frac{1}{2}}$$

$$[\text{EL2}] = [\text{As}_{\text{Ga}}] \propto P_{\text{As}_4}^{\frac{1}{2}}$$

M.O.Watanabe, A.Tanaka, T.Udagawa, T.Nakainsi, and Y.Zohta, Jap.J.Appl.Phys. Vol.22, (1983) 923.

**IBM**

10/86 (T.F. Kuech)

## Growth Environment Interactions

### Hetero-interfaces

III-III'

- residence time
- lattice matching
- large V partial pressures

V-V'

- kinetics of hydride decomposition
- thermodynamics
- residence time
- lattice matching

IBM

06/86 (T.F. Kuech)

## III-III' Interfaces

### Interface Structure:

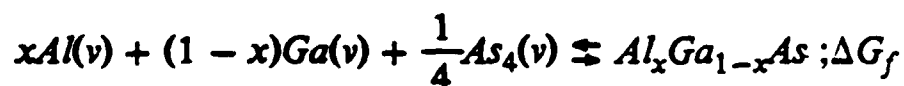
- Large  $P_v$ ,  $(\frac{V}{III}) > > 1$
- Growth rate limited by the mass transport of metal alkyl to the surface
- Interface abruptness
  - limited by the residence time,  $\tau$ , of the reactants in the reactor
  - interface width,  $\Delta w$   
 $\Delta w \approx GR * \tau$
  - growth interruption; impurity accumulation at the interface
- Lattice mis-matched systems
  - 3-D or island nucleation
  - dislocations

**IBM**

10/86 (T.F. Kuech)

## Al<sub>x</sub>Ga<sub>1-x</sub>As-GaAs Interfaces

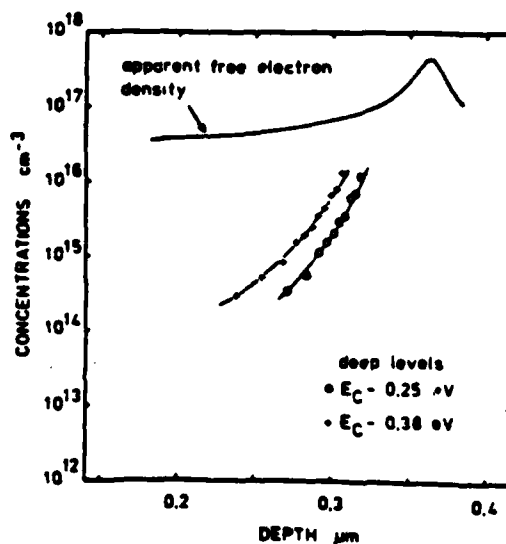
### Deep Level and Defects



$$|\Delta G_f^o(AlAs)| > |\Delta G_f^o(GaAs)|$$

$$P_{Al}^o P_{As_4}^{o \frac{1}{4}} < P_{Ga}^o P_{As_4}^{o \frac{1}{4}}$$

- Changes in stoichiometry at fixed As activity
- Defect concentrations may change at interfaces
- Misfit dislocations in lattice mismatched materials



D.Allsop, A.R.Peaker, E.J.Thrush, and G.Wale-Evans, J.Crystal Growth Vol.68, (1984) 295.

## V-V' Hetero-interfaces

### Growth Environment

- Large  $P_{V,V'}$  pressures
- Growth rate limited by mass transport of metal alkyl

### Heterojunction Formation

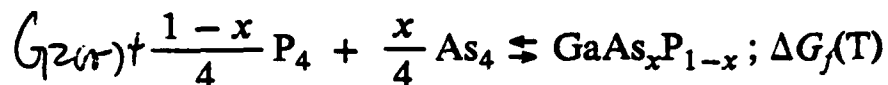
- Rapid switching of all components
- Interface width,  $\Delta w$ , is determined by the residence time of reactants:

$$\Delta w \approx GR * \tau$$

- Interface structure may reflect changes in the local activity of the group V components.

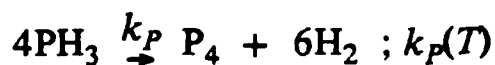
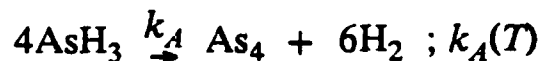


## Thermodynamics



$$\frac{P_{G_2} P_{As_4}^{\frac{x}{4}} P_{P_4}^{\frac{1-x}{4}}}{a_{GaAs_xP_{1-x}}} = K_f(T)$$

## Kinetics at the Growth Surface

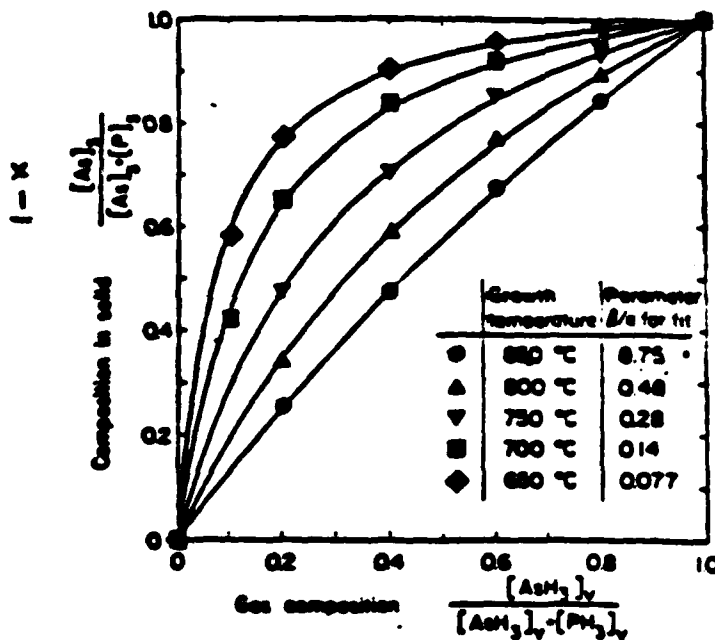


Composition is a function of growth temperature and may vary over the surface due to local variations in As/P in the gas phase.

08/88 (T.F. Kuech)

IBM

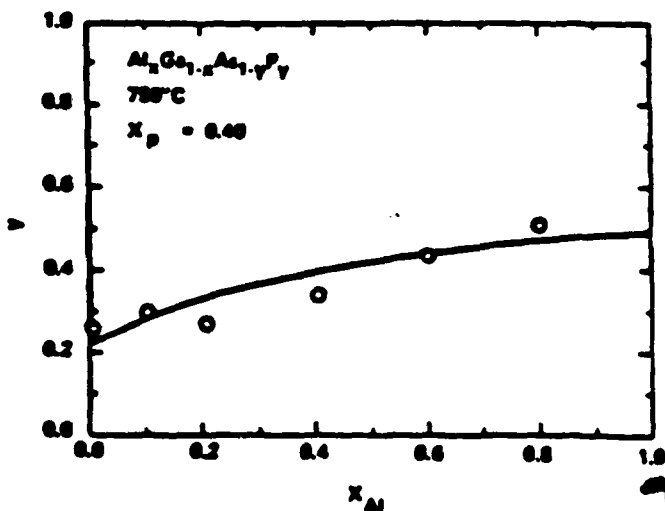
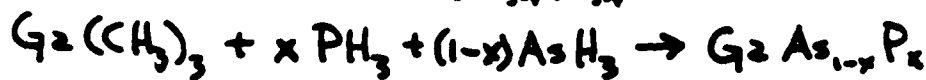
## GaAs<sub>1-x</sub>P<sub>x</sub>



### Incorporation Rate

$$x = \frac{1}{1 + \frac{\beta}{\alpha} \frac{P_{PH_3}}{P_{AsH_3}}}$$

- Kinetics of Decomposition
- Adsorption Rate



### Influence of Alloy Composition

- Influences Decomposition Rate
- Thermodynamic Influences

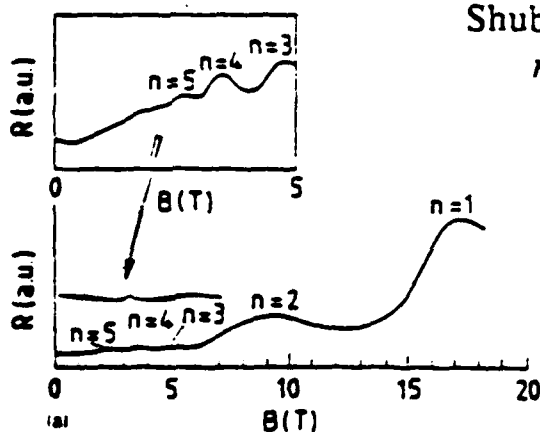
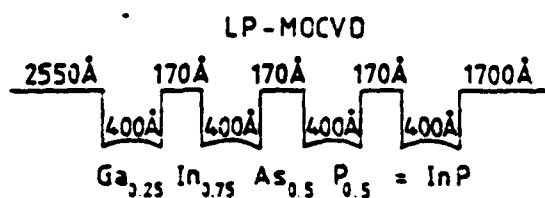
IBM

08/88 (T.F. Kuehn)

# $\text{In}_x\text{Ga}_{1-x}\text{As}_y\text{P}_{1-y}\text{-InP}$ Heterostructures

## Multi-Quantum Wells

M. Razeghi, J.P. Duchemin, J.C. Portal  
Appl. Phys. Lett. V26 (1985) 46.



## Growth Conditions

Low Growth Rate  $\sim 3 \text{ Å/sec}$

High Gas Velocity

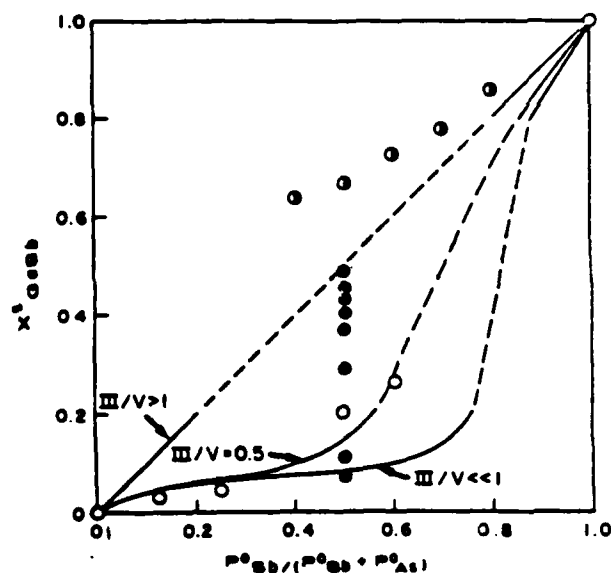
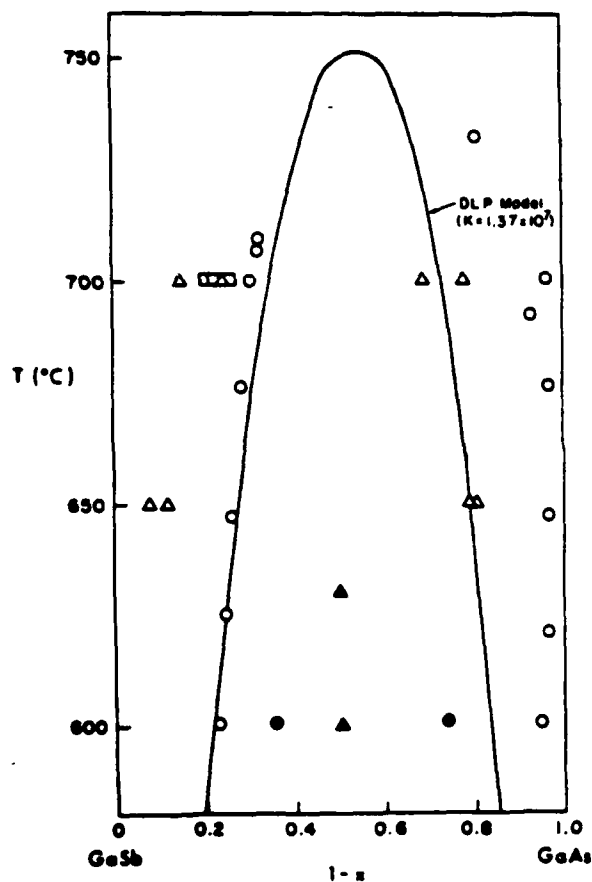
Continuous Growth

- residence time of gases  $\sim 1 \text{ sec}$

IBM

08/86 (T.F. Kuech)

## GaAs<sub>y</sub>Sb<sub>1-y</sub> - Metastable Compositions



G.B.Stringfellow and M.J.Cherng, J.Crystal Growth Vol.64, (1983) 413.  
 M.J.Cherng, G.B.Stringfellow, and R.M.Cohen, Appl.Phys.Lett. Vol.44, (1984) 677.

**IBM**

10/86 (T.F. Kuech)

## Growth of $\text{GaAs}_y\text{Sb}_{1-y}$

Input Reactants Decomposed at the Growth Front

$$P_{\text{Ga}(\text{C}_2\text{H}_5)_3} \cong P_{\text{Ga}}, P_{\text{As}(\text{CH}_3)_3} \cong P_{\text{As}_4}, P_{\text{Sb}(\text{CH}_3)_3} \cong P_{\text{Sb}_4},$$

GaAs in  $\text{GaAs}_y\text{Sb}_{1-y}$ :

$$\frac{a_{\text{GaAs}}^s}{P_{\text{Ga}}^o P_{\text{As}_4}^{o \frac{1}{4}}} = K_{\text{GaAs}}$$

GaSb in  $\text{GaAs}_y\text{Sb}_{1-y}$ :

$$\frac{a_{\text{GaSb}}^s}{P_{\text{Ga}}^o P_{\text{Sb}_4}^{o \frac{1}{4}}} = K_{\text{GaSb}}$$

Composition:

$$y = \frac{P_{\text{As}_4} - P_{\text{As}_4}^o}{(P_{\text{As}_4} - P_{\text{As}_4}^o) + (P_{\text{Sb}_4} - P_{\text{Sb}_4}^o)}$$

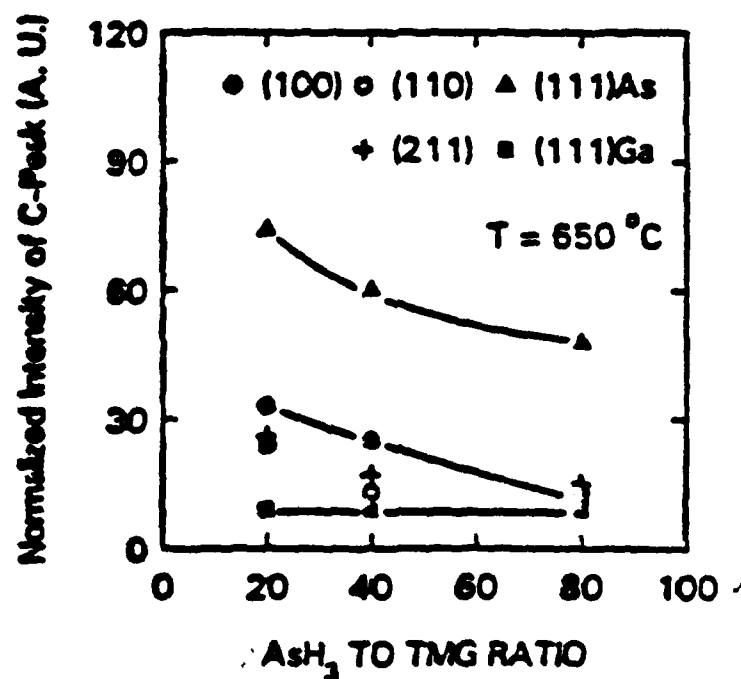
Stoichiometry:

$$(P_{\text{Ga}} - P_{\text{Ga}}^o) = 4(P_{\text{As}_4} - P_{\text{As}_4}^o) + 4(P_{\text{Sb}_4}^o - P_{\text{Sb}_4})$$

**IBM**

10/88 (T.F. Kuech)

## Growth of GaAs from $\text{Ga}(\text{CH}_3)_3$ and $\text{AsH}_3$



- $N_{\text{carbon}}$  ⇒ increases with  $T_{\text{growth}}$
- ⇒ decreases with  $P_{\text{arsine}}$
- ⇒ increases with As surface site density

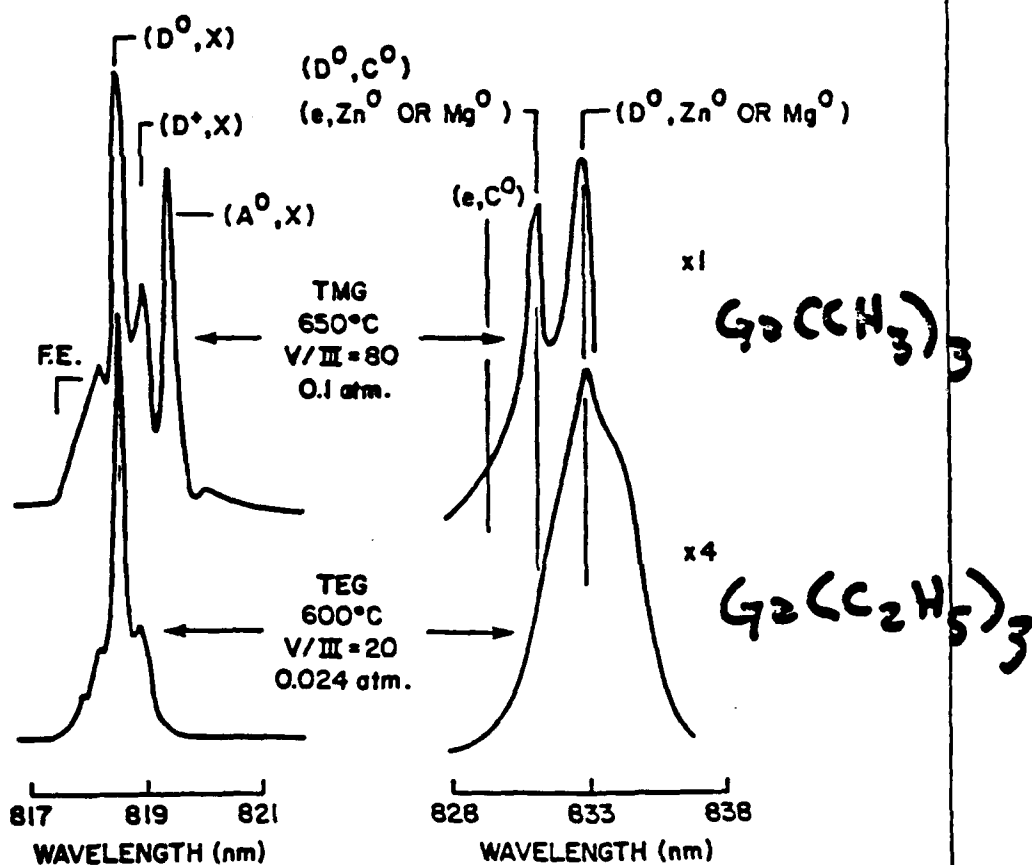
T.F.Kuech and E.Veuhoff, J. Crystal Growth, 68, 148(1984).

**IBM**

# Carbon Reduction with the Ethyl Based Chemistry

## Low Temperature (2K) Edge Luminescence

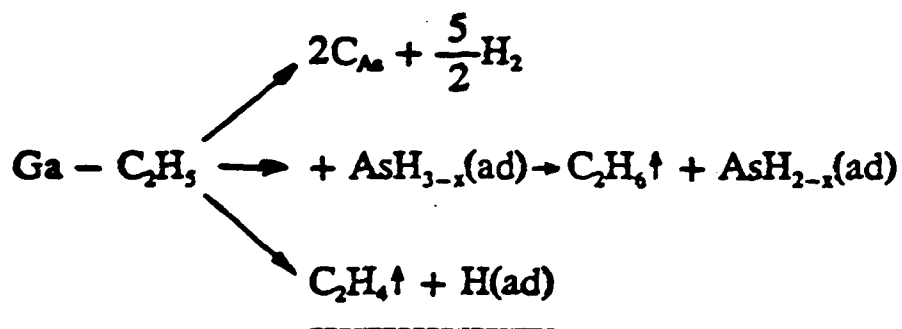
Low carbon content films are possible with the ethyl based chemistry. Zinc is then the dominant residual acceptor with these materials.



IBM

## Ethyl Based MOVPE Growth

### Possible Reaction Paths:



The use of larger hydrocarbon radicals:

1. weakens the metal-carbon bond
2. introduces new reaction paths for decomposition and carbon elimination.

IBM-THORNTON

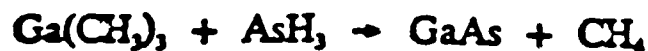
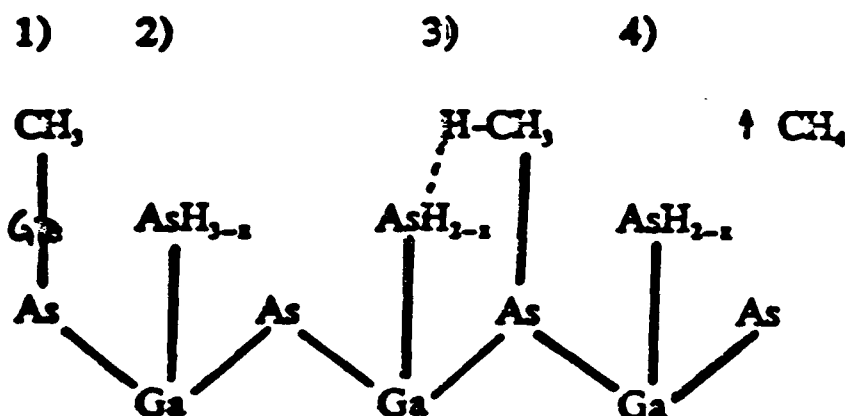
**IBM**

12/85 (T.F. Kuech)



## Model of Carbon Incorporation for Methyl Based Growth of GaAs

1. Adsorption of  $\text{CH}_3$  on As atoms
2. Adsorption of  $\text{AsH}_{2-x}$  on Ga atoms
3. Hydrogen Transfer Reaction  
 $\text{CH}_3(\text{ad}) + \text{AsH}_{2-x} \rightarrow \text{CH}_4(\text{ad}) + \text{AsH}_{2-x}(\text{ad})$
4. Desorption of  $\text{CH}_4$   
 $\text{CH}_4(\text{ad}) \rightarrow \text{CH}_4(\text{g})$

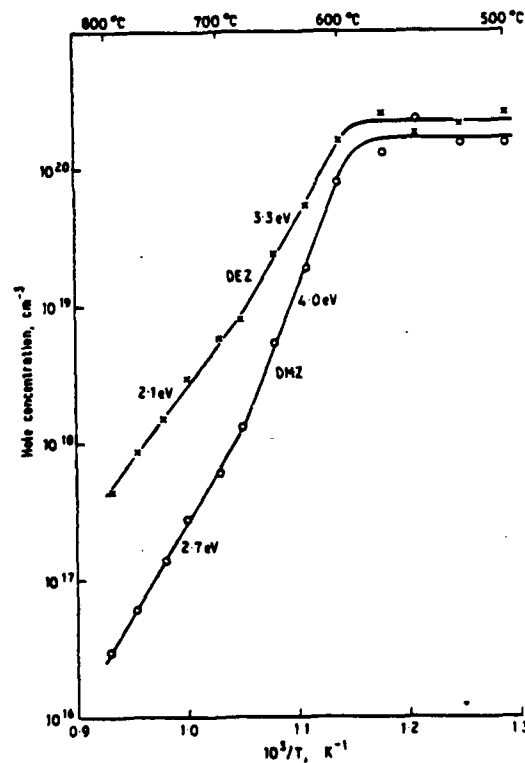


**IBM**

12/85 (T.F. Kuech)

## Zinc Incorporation

Zinc has a high elemental vapor pressure at temperatures encountered in MOVPE growth. The Zn can interact with the growth environment with the subsequent Zn concentration in the solid being dictated by the Zn partial pressure above the growth surface.



R.W.Glew, J.Crystal Growth Vol.68, (1984) 44.

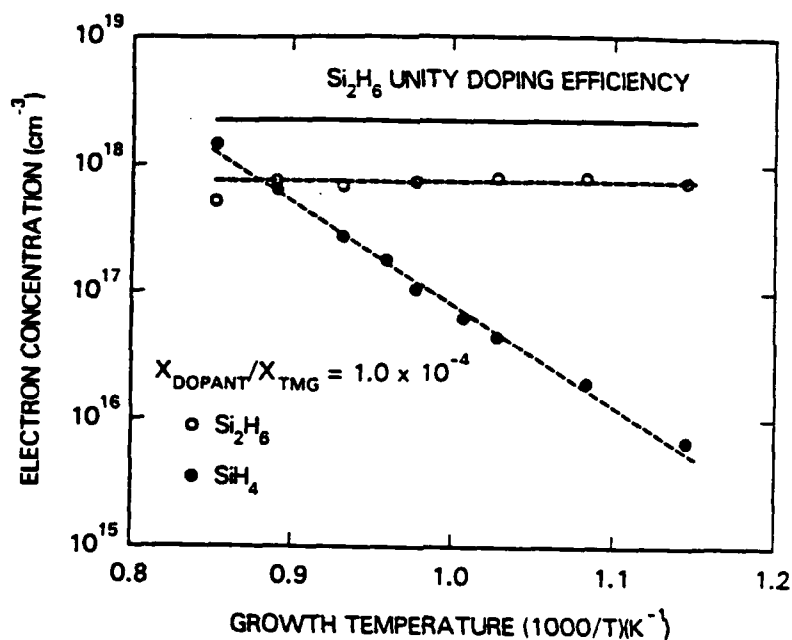
IBM

10/86 (T.F. Kuech)

## SiH<sub>4</sub> versus Si<sub>2</sub>H<sub>6</sub>

SiH<sub>4</sub> - Surface Reaction Limited

Si<sub>2</sub>H<sub>6</sub> - Mass Transport Limited



For a high degree of doping uniformity, the dopant incorporation must be mass transport limited in its behavior:

such that at the growth front,

$$J_{\text{dopant}} \propto J_{\text{Ga}} \rightarrow \Delta n \propto \Delta \left[ \frac{J_{\text{dopant}}}{J_{\text{Ga}}} \right]$$

**IBM**

## Summary

Little is known about the actual growth reactions taking place during the MOVPE process. There is substantial evidence that during the MOVPE growth of a III-V materials the growth front is in near thermal equilibrium.

- Stoichiometric Defects
- Alloy Composition in V-V' Materials

The growth environment can affect the electrical properties of interfaces due to changes in the defect structure of the materials as the composition is altered across an interface. The change in the chemical composition near the growth front dictates, in part, the structure of the interface.

**IBM**

10/86 (T.F. Kuech)

# **Studies of Buried Interfaces**

**using**

**Total External Reflection  
of X-Rays**

**and**

**Extended X-Ray Absorption  
Fine Structure**

**EXAFS**

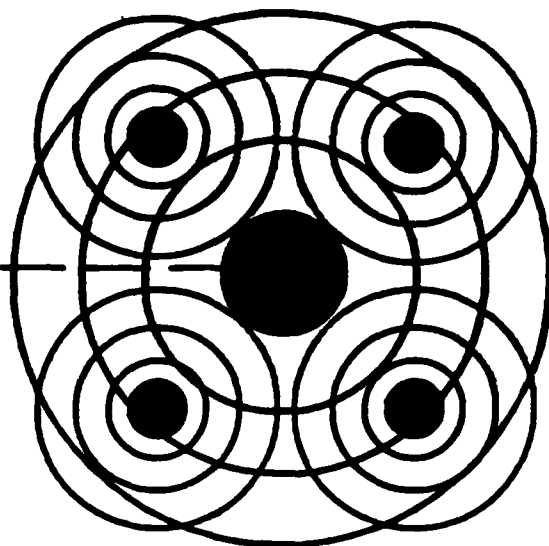
**Bruce A. Bunker  
Notre Dame**

# E X A F S

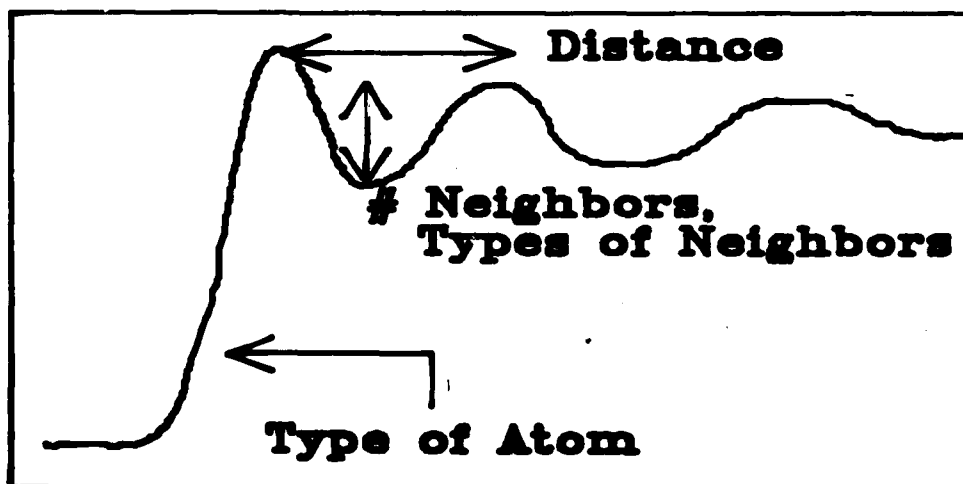
**Extended X-Ray Absorption Fine Structure**

**Incident X Ray**

**Interference  
Modulates  
X-Ray Absorption  
Coefficient**



**Absorption Coefficient**

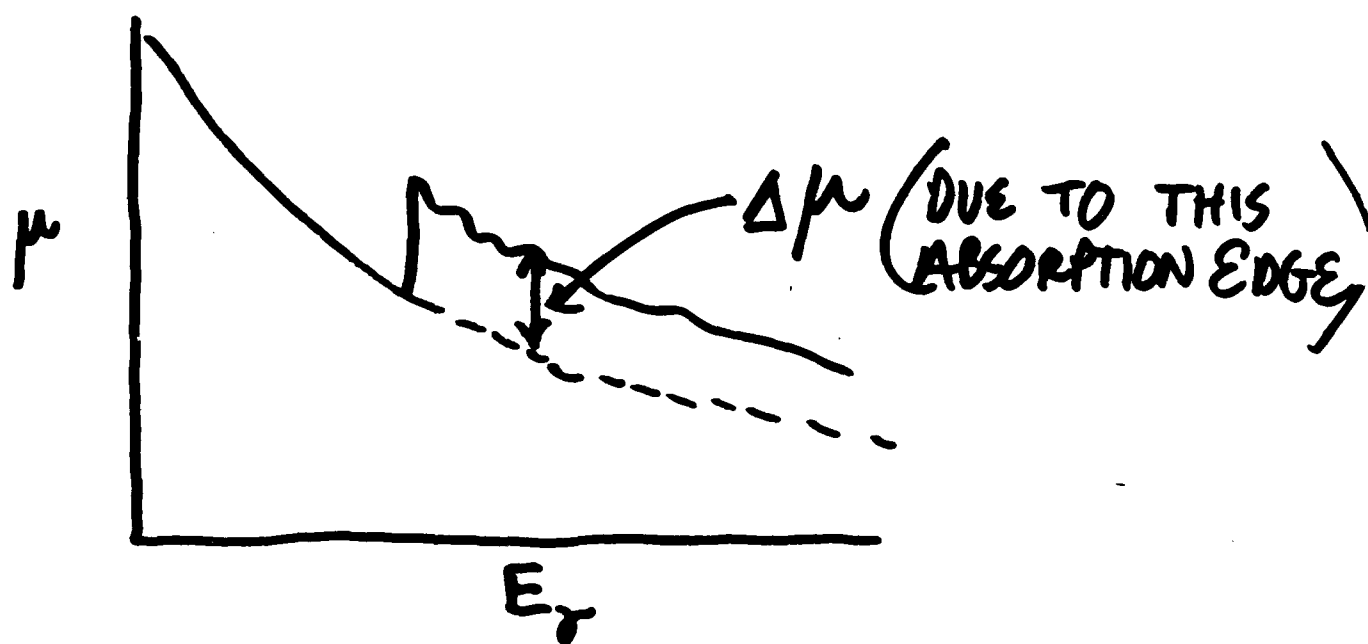
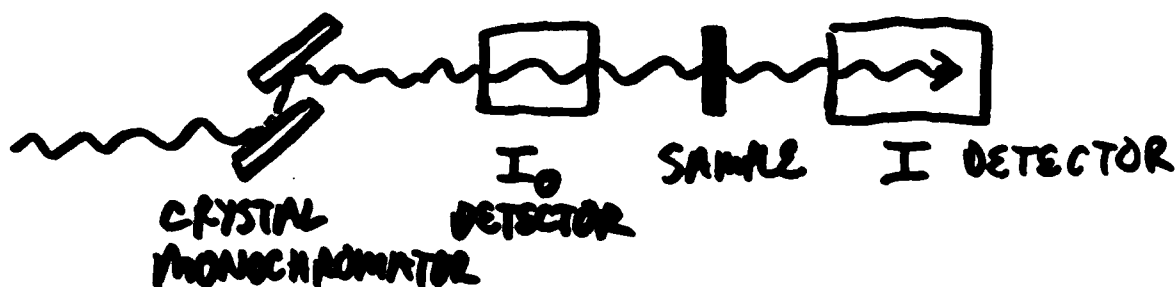


**X-Ray Energy**

- o Atom-Specific
- o Local Environment
- o 1st, 2nd, sometimes 3rd shells

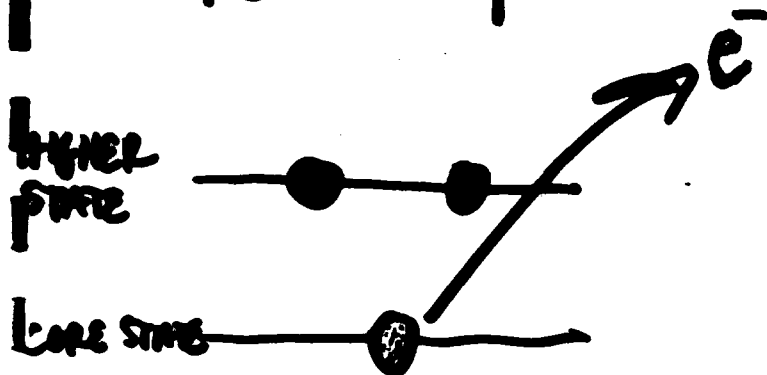
# EXPERIMENTAL METHODS

## (1) TRANSMISSION



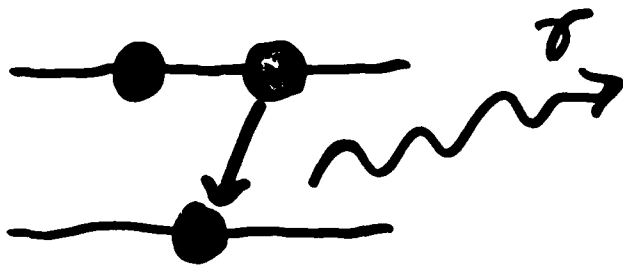
$\Delta\mu \sim \# \text{CORE HOLES PRODUCED}$   
AS A FUNCTION OF X-RAY  
ENERGY

# CREATION & DECAY OF CORE HOLES

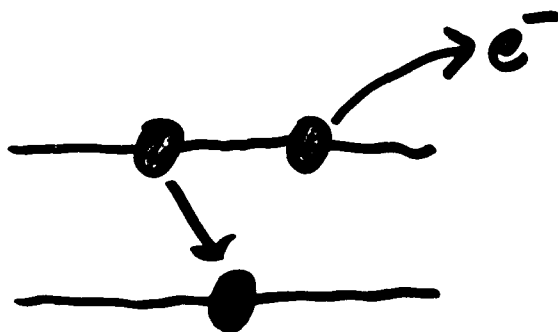


ABSORPTION

CREATION OF CORE HOLE



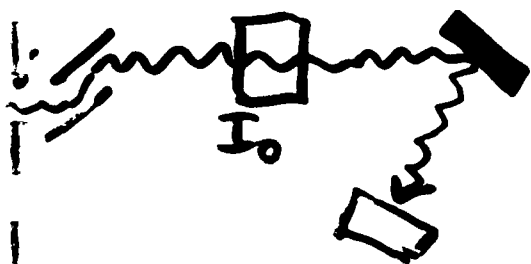
X-RAY FLUORESCENCE  
DECAY OF CORE HOLE,  
EMISSION OF X-RAY  
PHOTON



AUGER ELECTRON  
EMISSION

DECAY OF CORE HOLE,  
EMISSION OF SECOND  
ELECTRON

FLUORESCENT X-RAYS EMITTED AT  
CONSTANT ENERGY (DIFFERENCE BETWEEN  
ATOMIC LEVELS)





# **Major Strength of EXAFS:**

## **LOCAL PROBE**

---

**Extreme Example:**  
**Impurity in Semiconductor**

---

**Focus on Impurity Atom,  
determine:**

- \* Types of Neighbors**
- \* Number of Neighbors**
- \* Distance to surrounding  
1st and 2nd shell atoms**
- \* Vibrational Properties**
- \* Site Symmetry**  
**(from Near-Edge Structure)**

# **Local Environment About Impurities in Semiconductors:**

## **The Fe Site in Fe-Implanted Si**

**with: P. Bandyopadhyay**

### **Determine:**

- impurity site**
- lattice relaxation**
- impurity complex formation**

---

### **Experimental Technique:**

- Grazing Incidence  
(Impurities near surface)**
- Fluorescence Detection  
(dilute impurities)**
- Sample Rotating During Data  
Acquisition  
(suppress Laue diffraction lines  
contaminating data)**

## Results: Fe Site in Fe-Implanted Si

- o Tetrahedral Interstitial Site
- o First Shell Expands  $0.10+0.05\text{\AA}$
- o Second Shell Contracts  $0.07+.06!$

**Precision measurement:**

**Beats in EXAFS Amplitude yield**

**Distance Difference  $R_2 - R_1$**

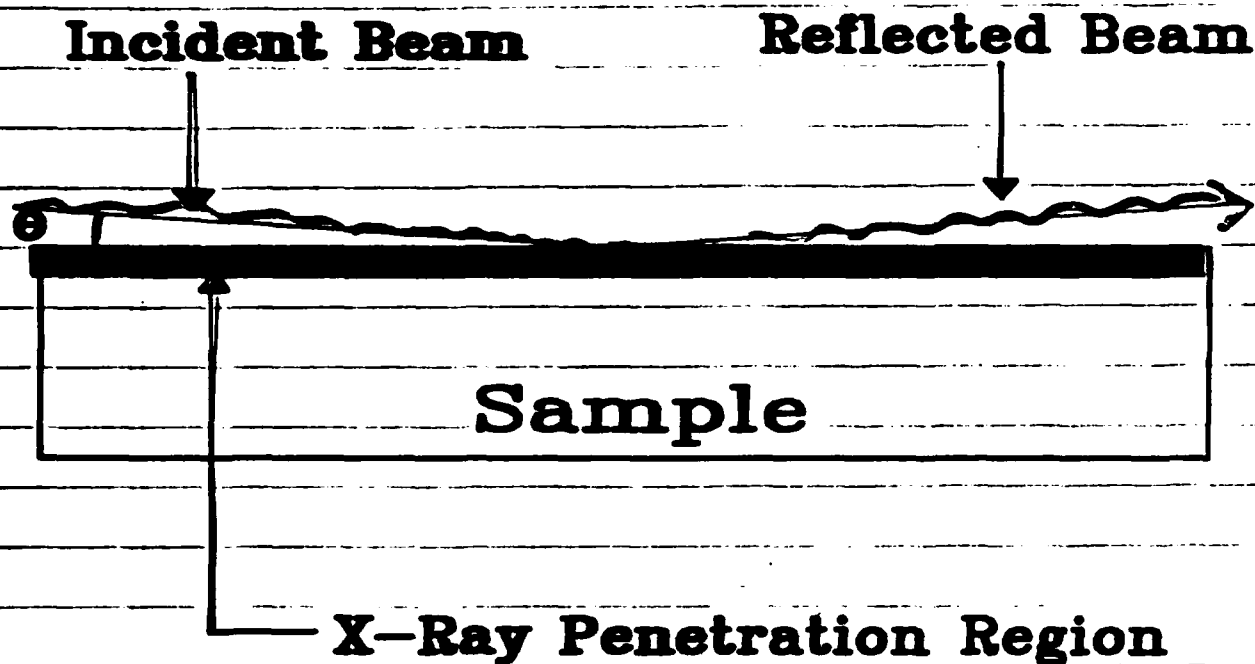
**If Undistorted:  $0.35\text{\AA}$**

**We Find:  $0.18 \pm 0.03\text{\AA}$**

**Excellent Agreement With Theory:  
Zunger, et al.:  $0.17\text{\AA}$**

**--- agreement within  $0.01\text{\AA}!$**

# Total External Reflection of X Rays...



For  $\theta > \theta_c$ ,  $d = \sim 1000\text{\AA} - 20\mu$   
 $\theta_c \approx 0.5^\circ$

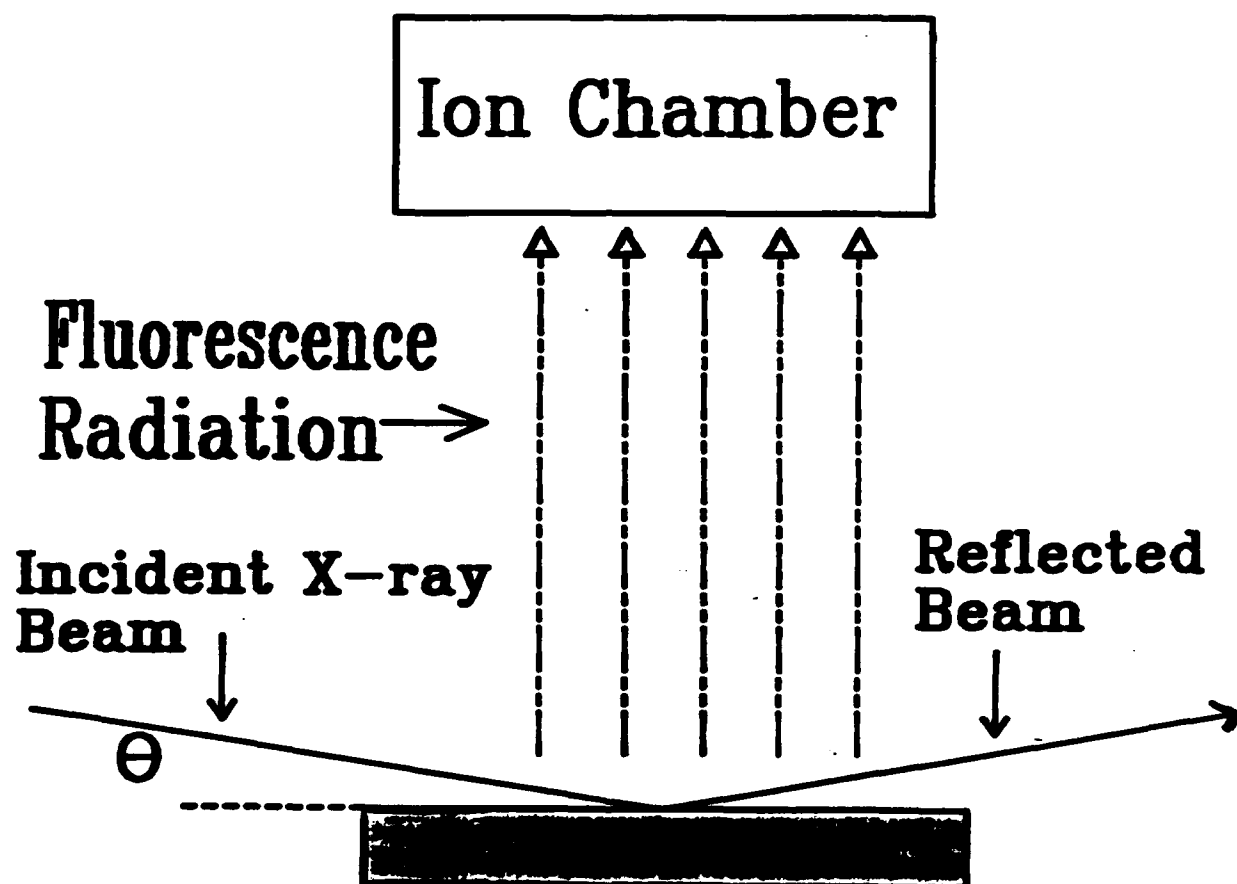
in x-ray region, index of refraction  $n < 1$

---> total external reflection possible  
 for grazing incidence

For  $\theta < \theta_c$ ,  $d = \sim 10 - 30\text{\AA}$

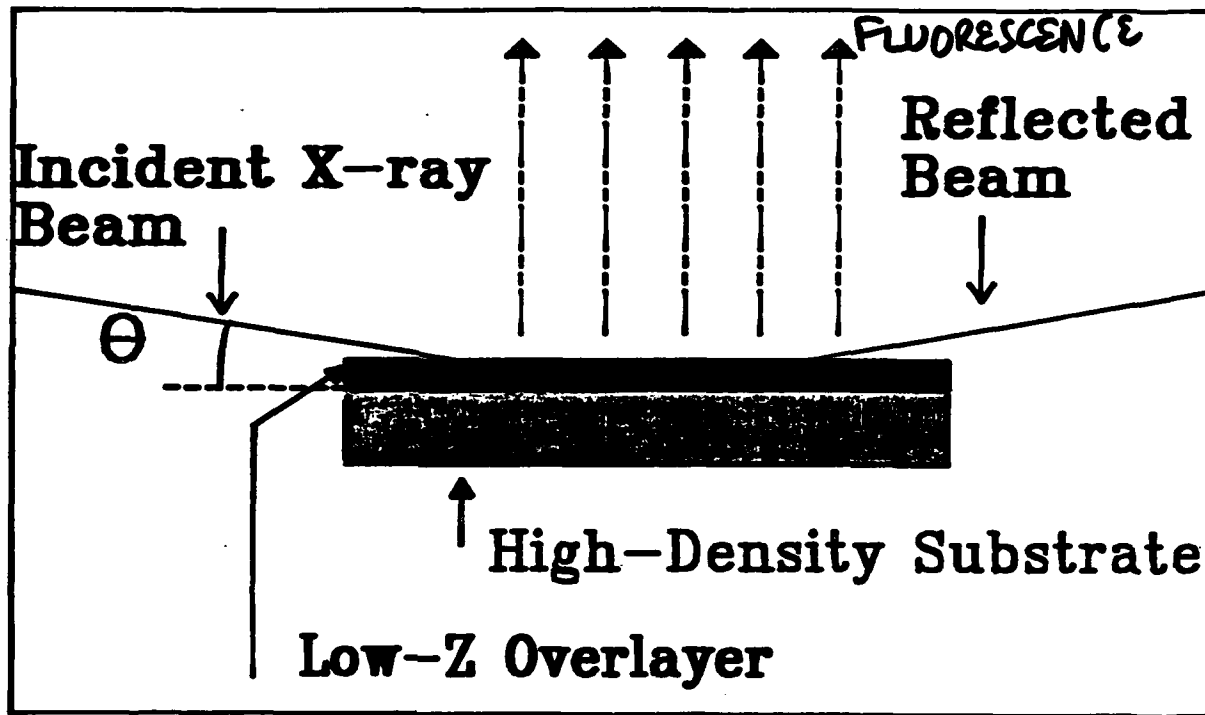
--- Surface Sensitivity

Total External Reflection  
+ Fluorescence Detection  
= Surface Sensitivity



Probe Local Environment  
within  $\sim 10$  Å of Surface  
MUCH MORE SENSITIVE THAN "SEXAFS"  
→ .01-.001 MONOLAYER DETECTABLE

# Low-Z Overlayers e.g. Al on GaAs



Tune  $\theta$  :  $\theta_{\text{Al}} < \theta < \theta_{\text{GaAs}}$

-- Sensitive to As atoms within  
 $\sim 10\text{\AA}$  of Buried Interface

Study: Diffusion  
Compound Formation  
Defect Complex Formation  
Schottky Barriers (?)

## SAMPLES

GAS, MBE GROWN

500 Å AL DEPOSITED IN-SITU

(1) 500°C DEPOSITION TEMP.

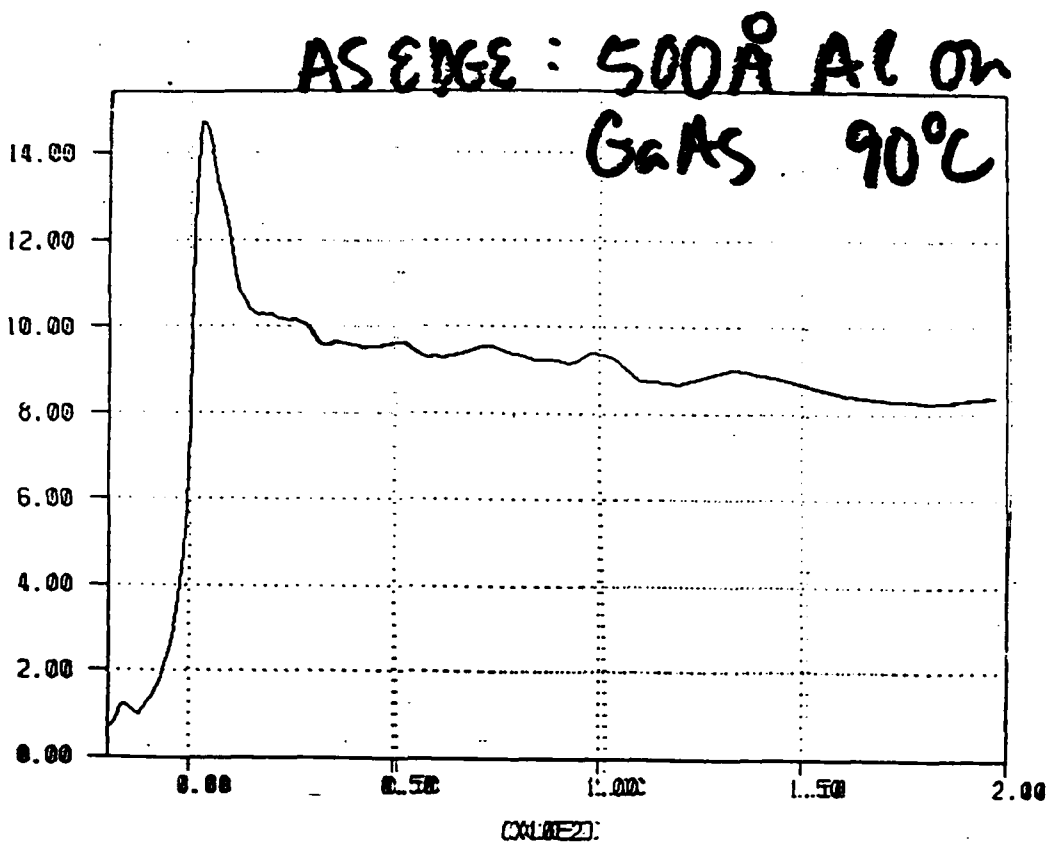
(2) 90°C " "

FRANK CHAMBERS

AMOCO RESEARCH LABS

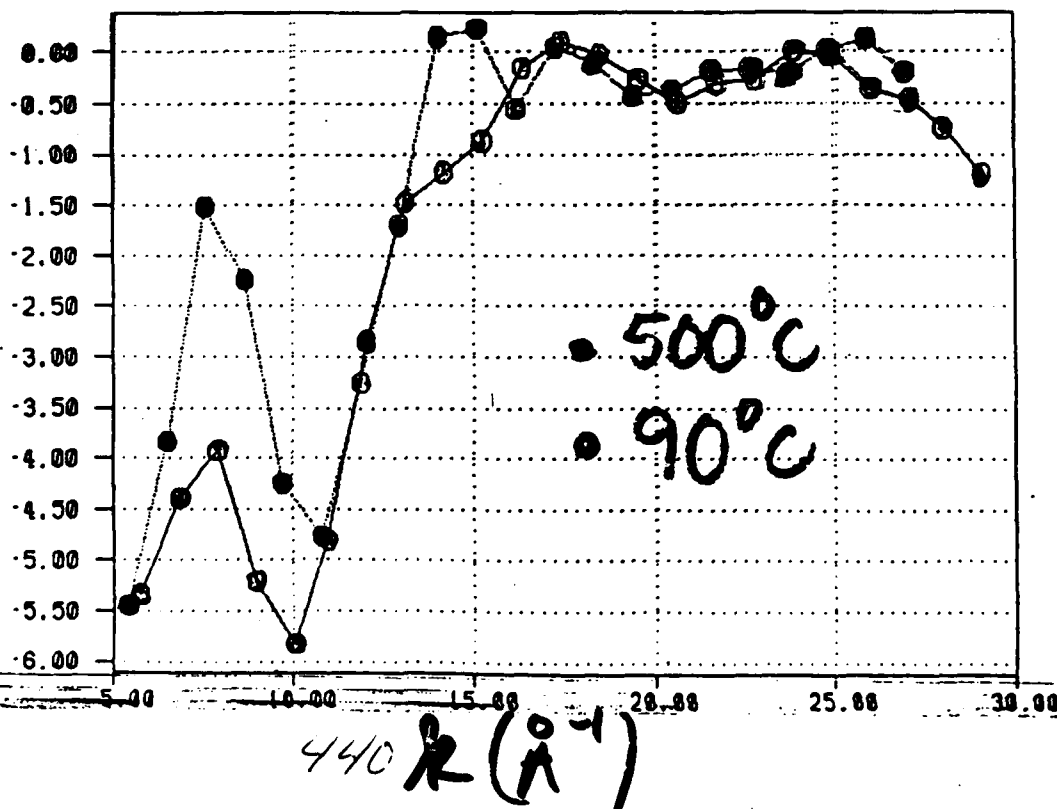
NAPERVILLE, IL

FLUORESCENCE  
SIGNAL (X10E-1)



X-RAY ENERGY - EDGE ENERGY

$d(\text{Fluor})/dE$   
(X10E-4)





## FUTURE WORK

- MORE CAREFUL DEPTH PROFILING  
BY SWEEPING ANGLE
- IN-SITU ANNEAL DURING MEASUREMENT
- STUDY OF DOPANT ATOMS  
MIGRATION TO INTERFACE?

## Summary

### Reflection - Mode EXAFS

- Probe Adsorbed Species

$\sim 1$  monolayer

- Probe Buried Interfaces

Study Atomic Environment For

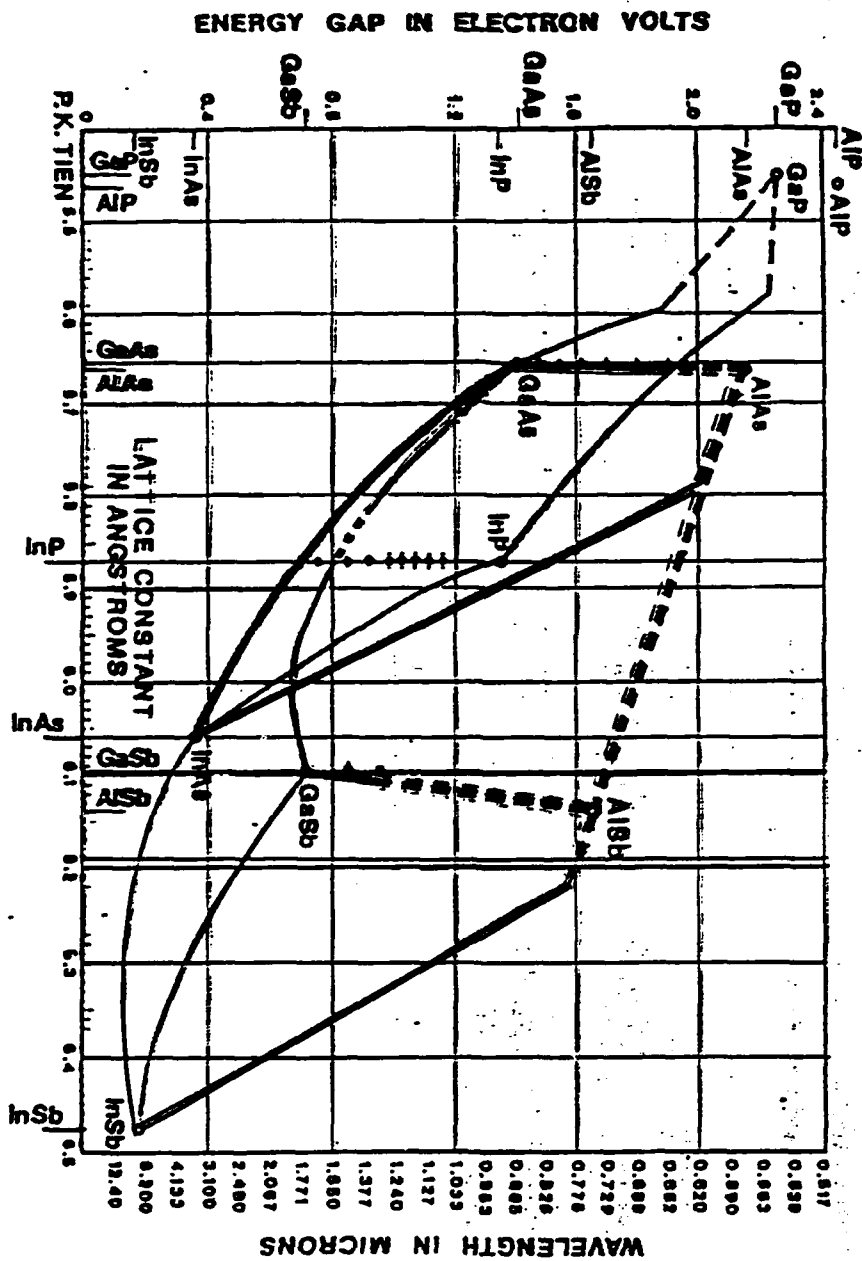
Atoms Within  $\sim 10 \text{ \AA}$  of Interface

### Around Each Species

- Types of Neighbors
- Number of Neighbors
- Bond Lengths

Composition Dependence of Metal In  $\text{Al}_x\text{Al}_{1-x}$   
Barrier Height and Its Application

Harry Wieder  
University of California - San Diego



$\text{In}_x\text{Al}_{1-x}\text{As} / \text{InP}$

lattice matched,  $x=0.52$

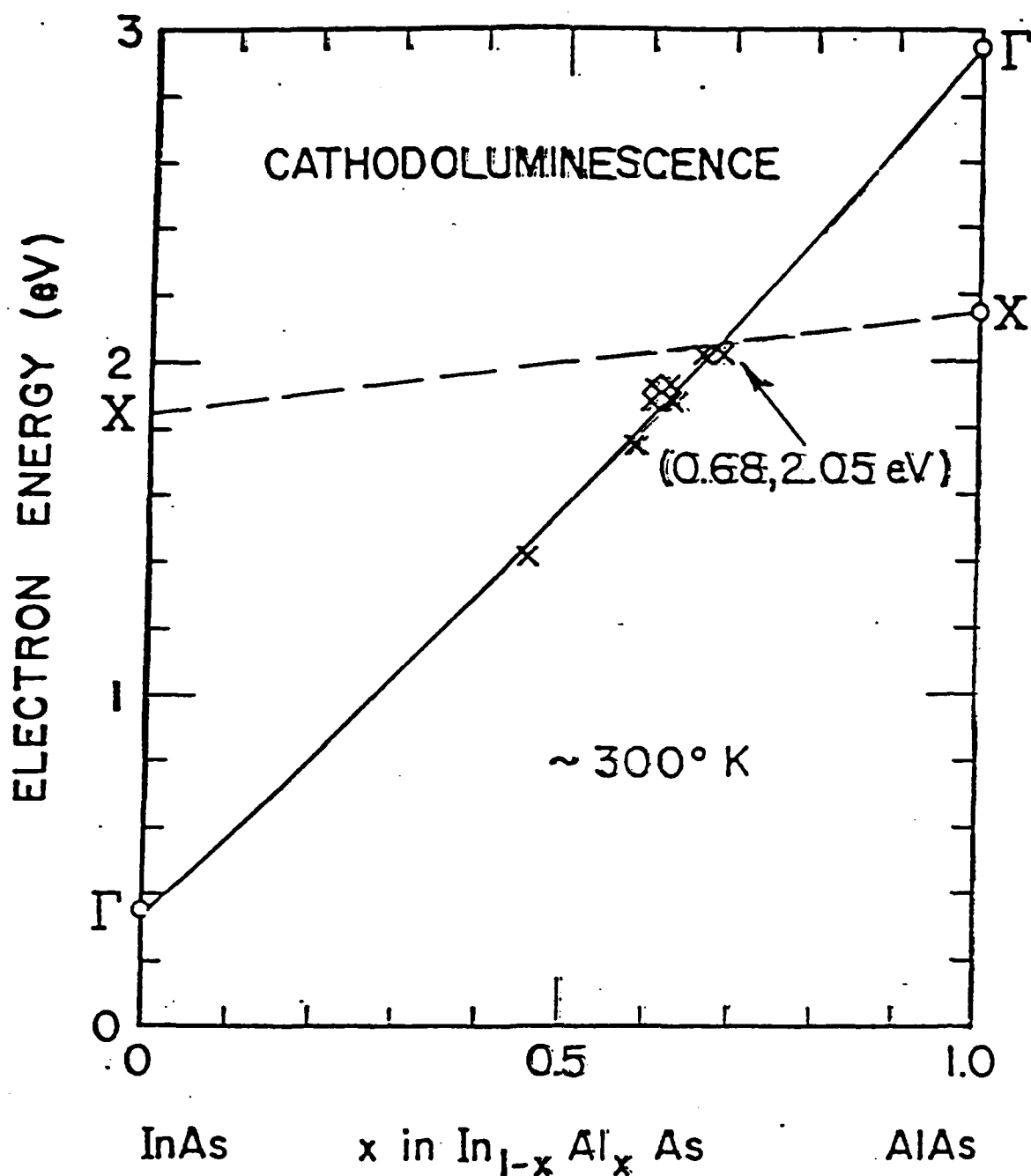
staggered band line-up

$$\Delta E_c = 0.52 \text{ eV}$$

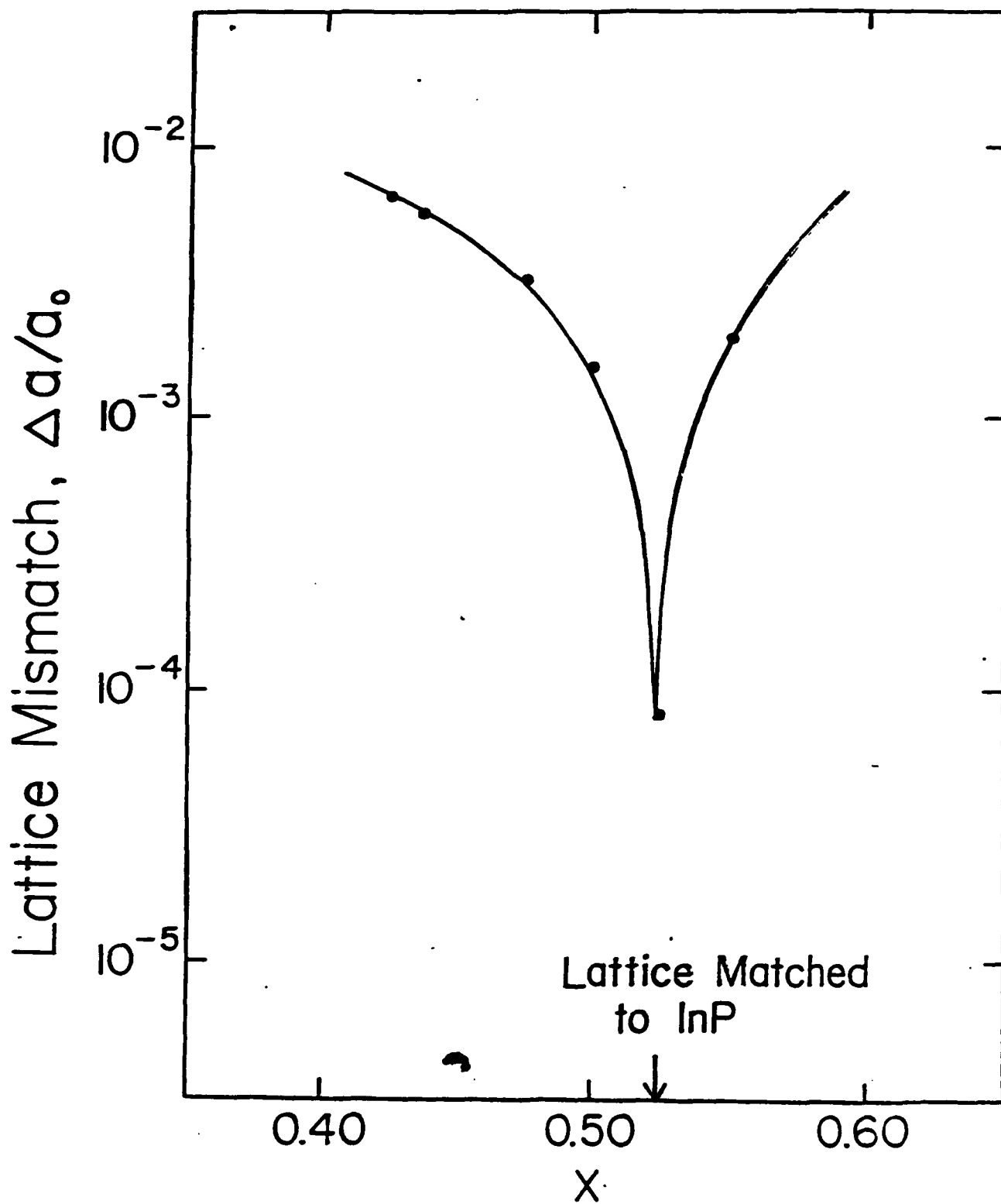
$$\phi_{\text{Bn}} = 0.8 \text{ eV}, \text{ C-V}$$

$$\phi_{\text{Bn}} = 0.6 \text{ eV}, \text{ internal photoemission}$$

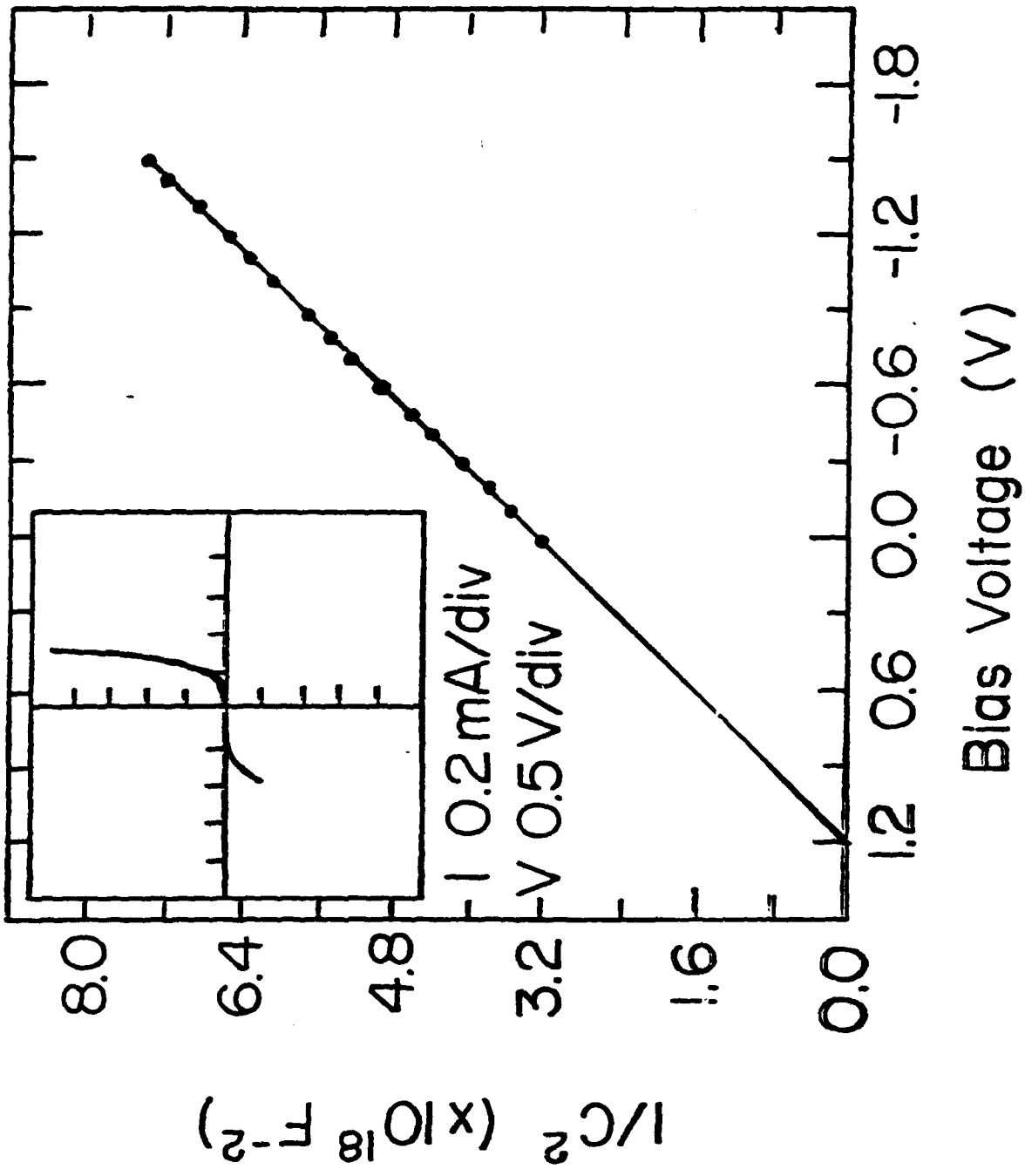
MBE grown,  $T_s < 530^\circ\text{C}$  ~SEMI-INSULATING



CL peak energies as a function of  $\text{In}_{1-x}\text{Al}_x\text{As}$  alloy composition at 300°K. The X conduction band has been extrapolated to InAs on the basis of the conduction band cross overpoint and the X point in AlAs. 446

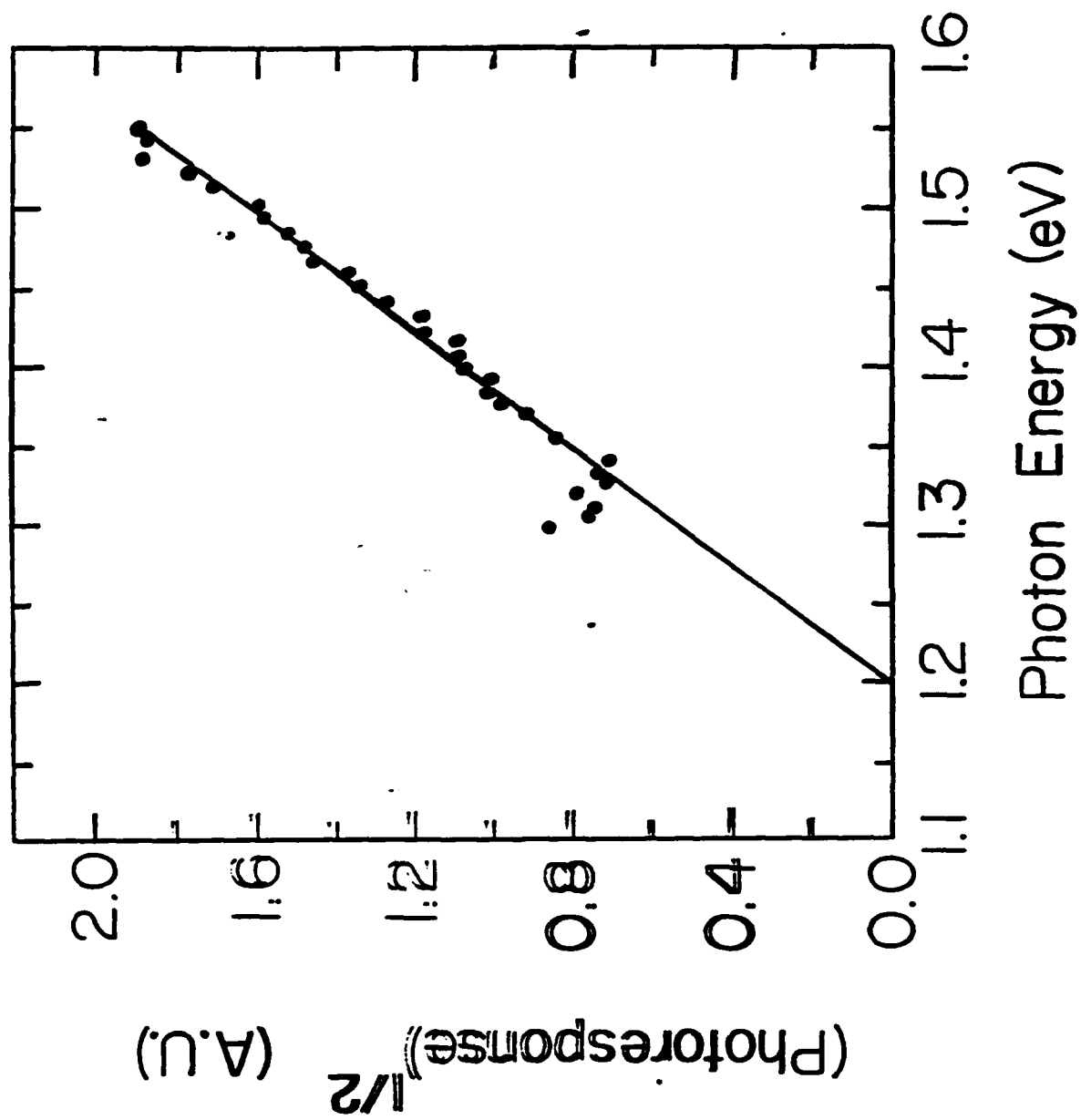


8th

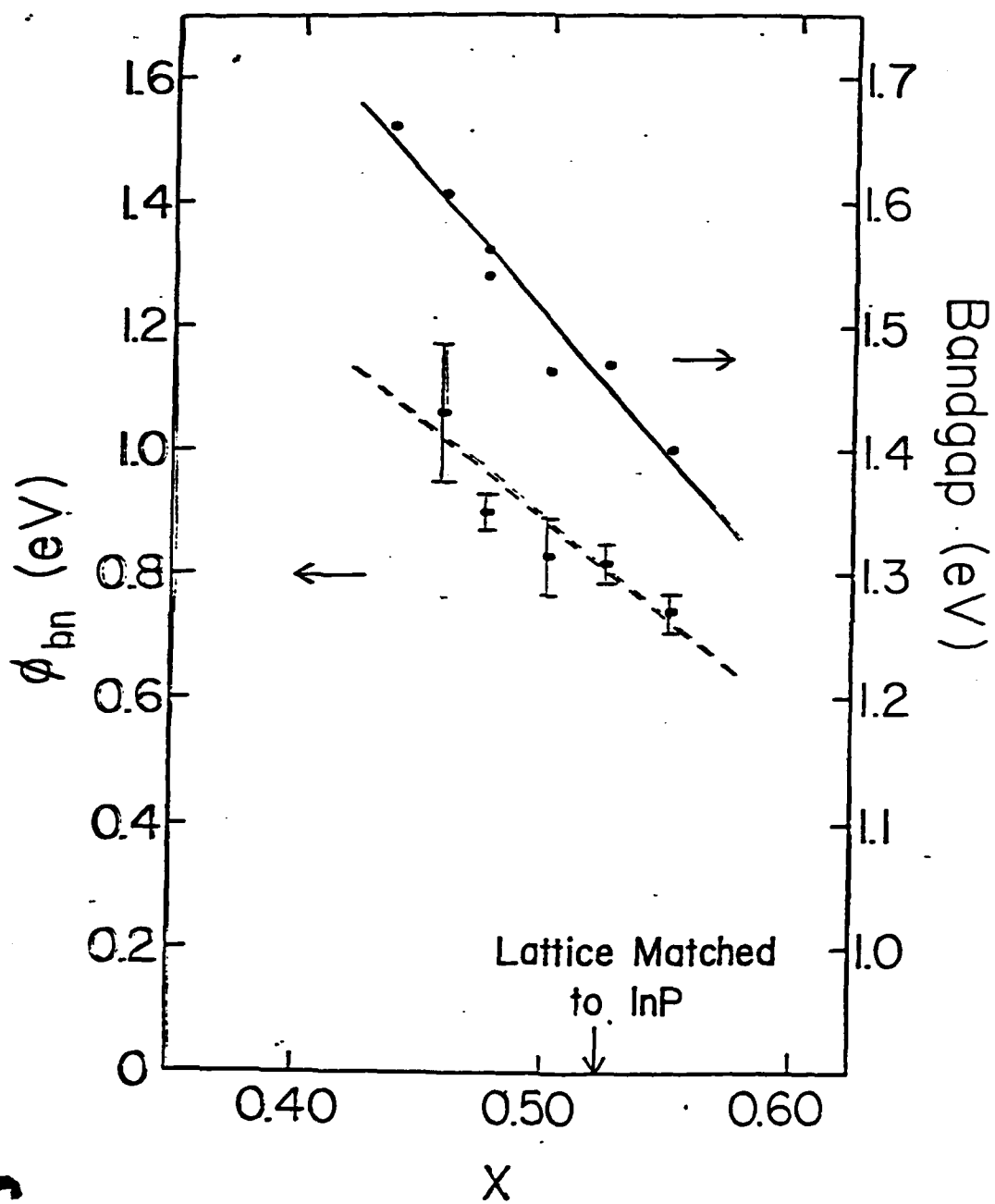


0.43 10<sup>-5</sup> 5.7

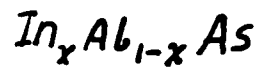




InGaAs



450



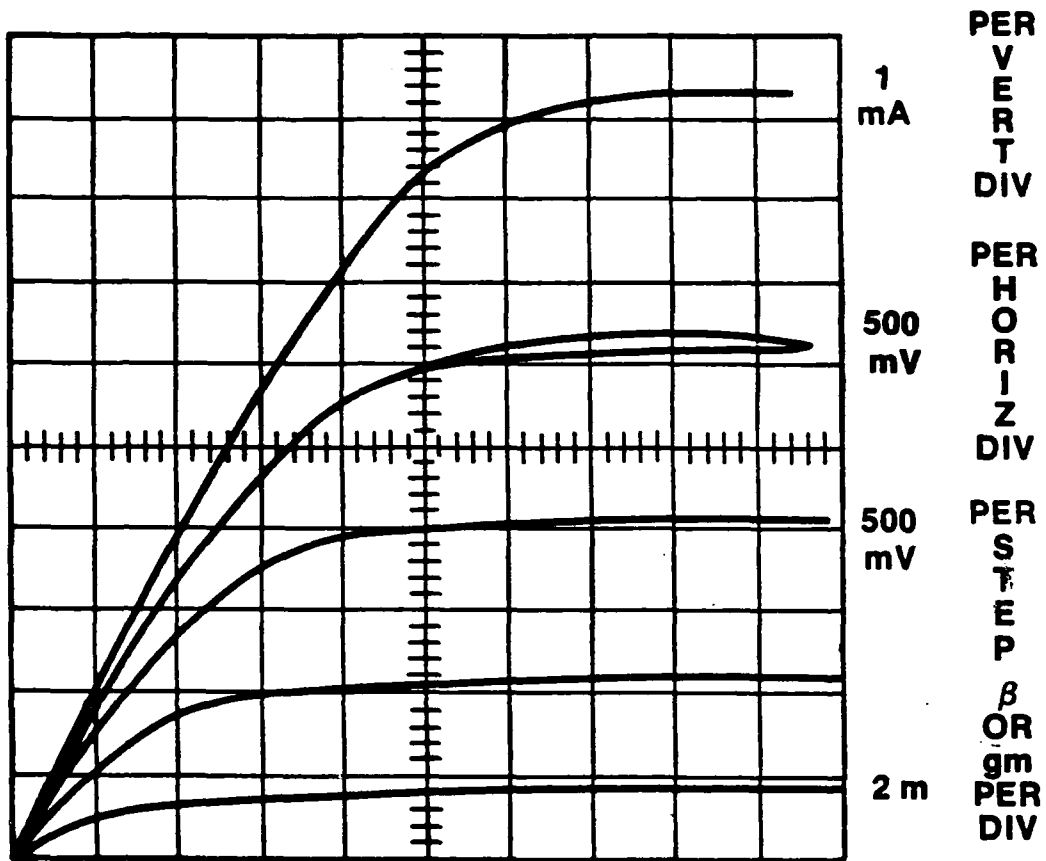
$$\phi_{\text{sn}} = 2.46 - 3.16 x \quad (x > 0.42)$$

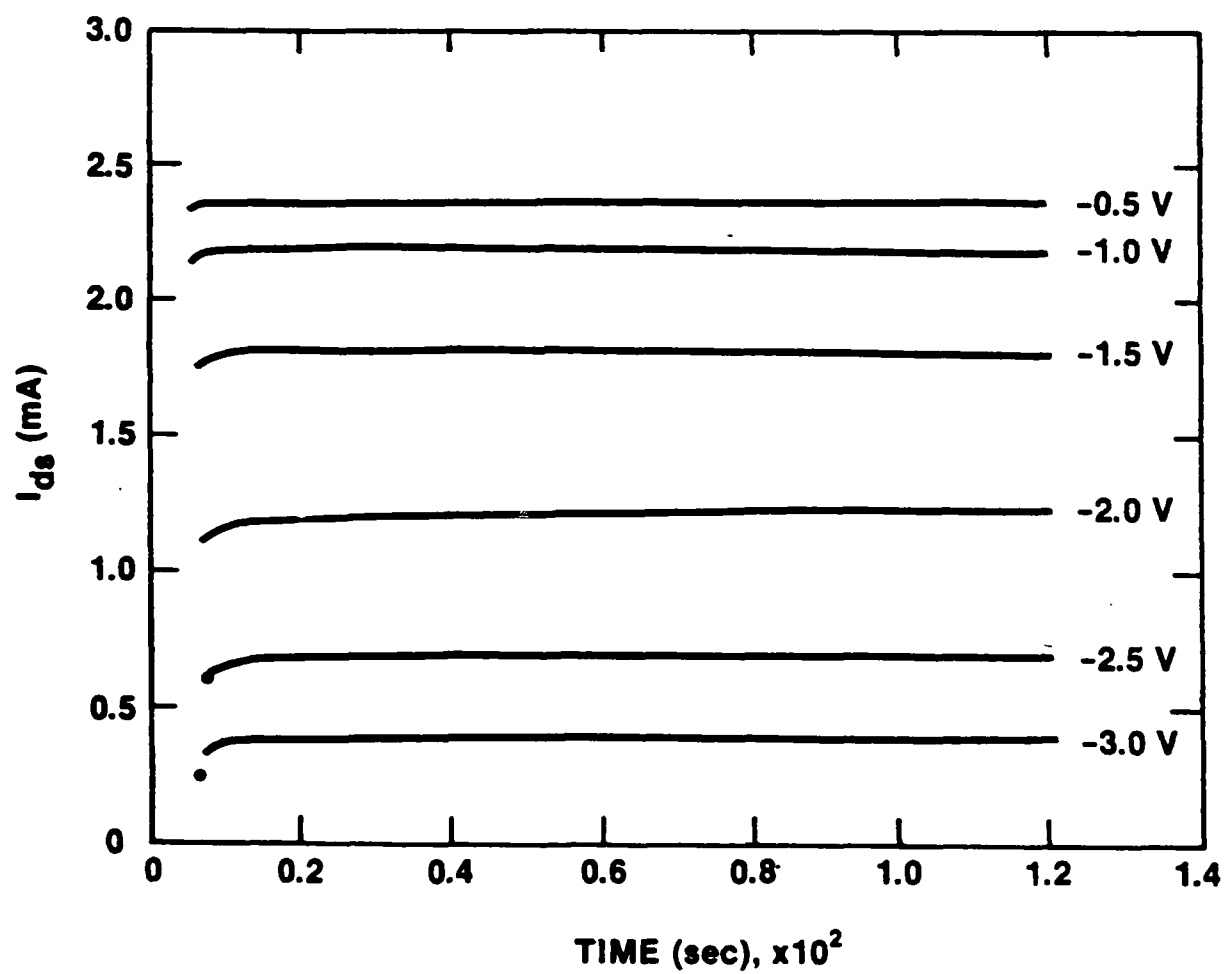
$$\phi_{\text{sn}}(\text{AlAs}) = 1.2 \text{ eV} \quad (\text{measured})$$

$$\phi_{\text{sn}}(x = 0.32) = 1.45 \text{ eV} \quad (\text{extrapolated})$$

$$\phi_{\text{sn}}(x = 0.78) = 0 \quad "$$

$$\phi_{\text{sn}}(x > 0.78) = \text{inverted surface} \quad "$$





453

# **(In-Situ) contacts to GaAs based on InAs**

S.L. Wright  
E.D. Marshall (summer student)  
R.F. Marks  
T.N. Jackson  
S. Tiwari  
H. Baratte

IBM Watson Research Center  
Yorktown Heights, NY.

**IBM**

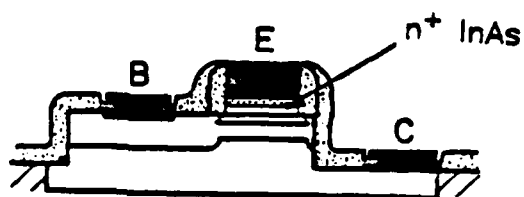
455

## In-Situ Epitaxial Contacts: Device Motivation

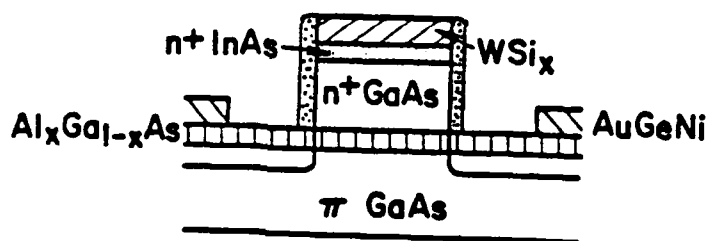
- Bandgap Engineering: improved understanding of ohmic contacts
- superior to Au/Ge/Ni:
  - very uniform and shallow
  - good temperature stability
  - potentially lower contact resistance ?
- compatible with refractory metallization
- good for self-alignment schemes involving small area contacts
- advantages for stop/regrowth applications

## Heterostructure Devices with In-Situ Contacts

HBT



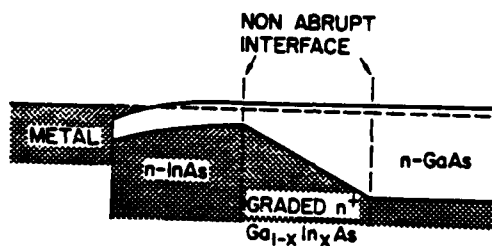
SISFET



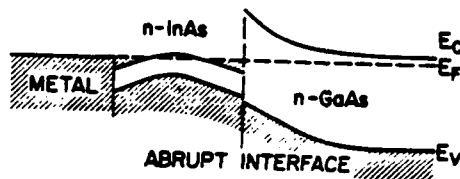


## In-Situ Contacts based on (In,Ga)As

graded bandgap contact: (In,Ga)As/GaAs (Woodall et al. 1981)

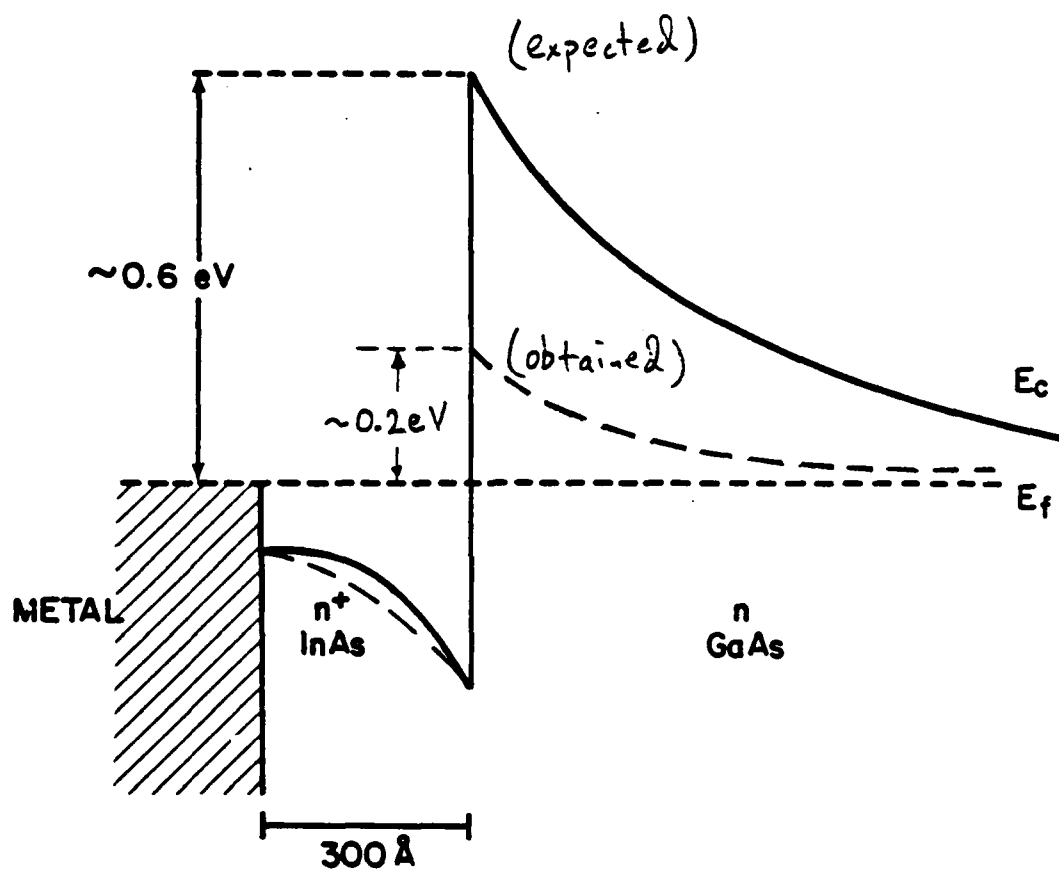


abrupt junction: InAs/GaAs



- Reproducible growth and processing
- May require less material than "graded" contact
- May require heat treatment

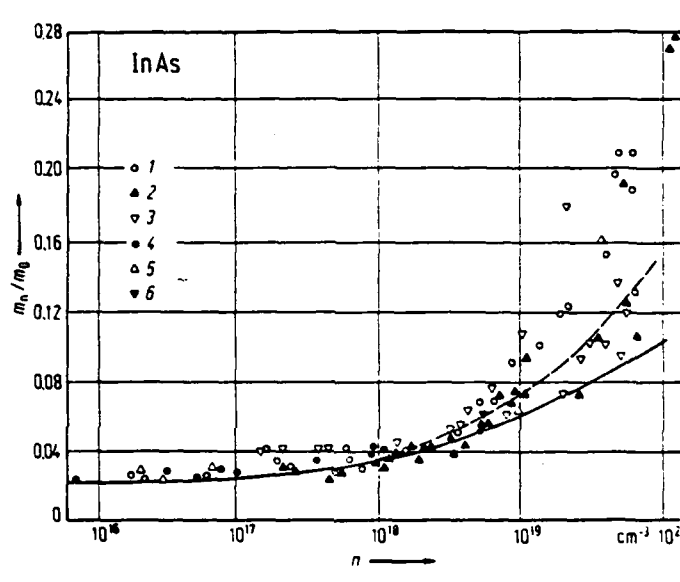
## InAs/GaAs Band Diagram



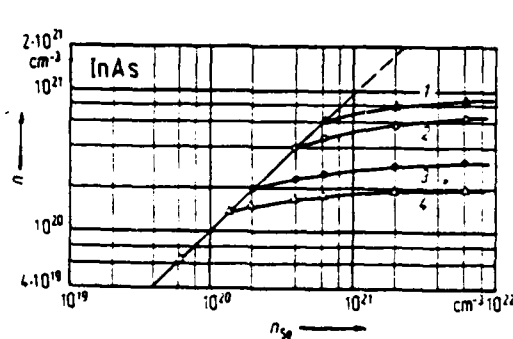
- Fermi level pinning
- Bulk InAs and GaAs Fermi level (doping)
- Conduction band discontinuity
- Strain and dislocations?

## GOOD news and BAD news

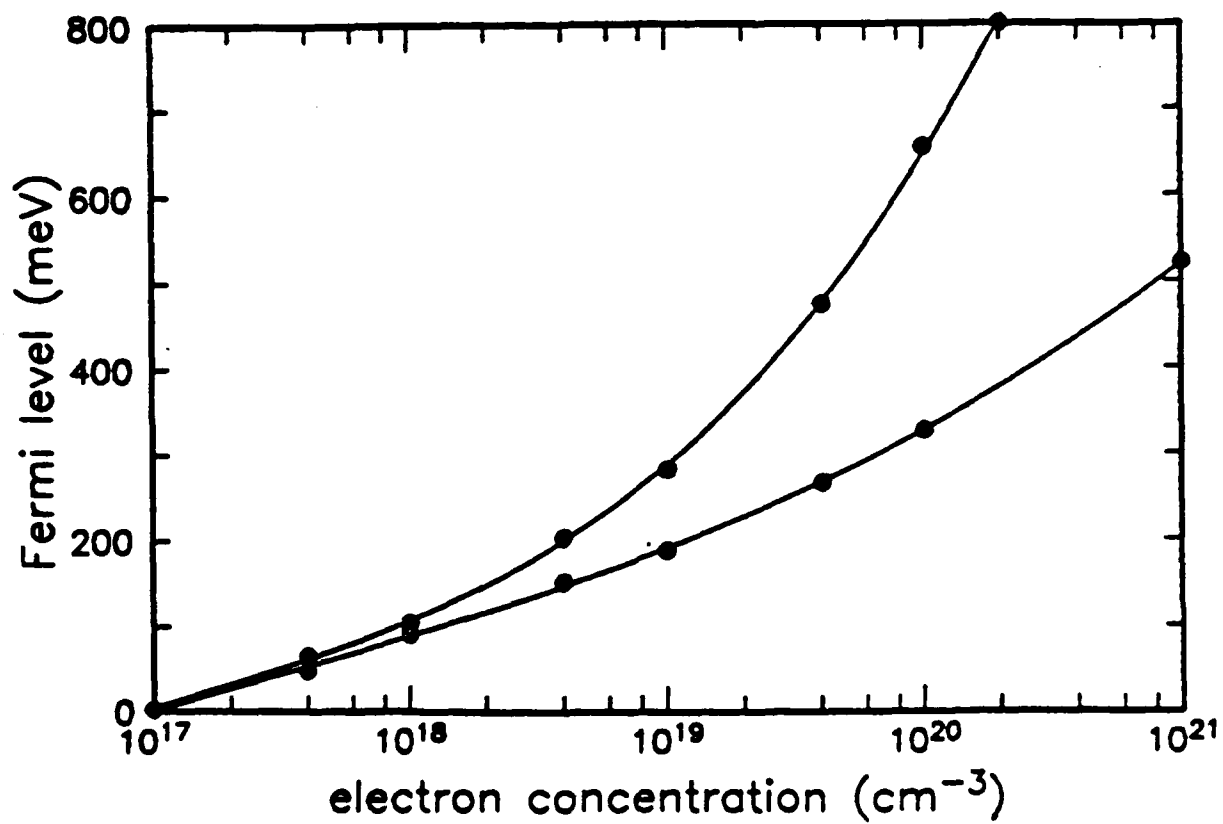
- $m^*$  increases sharply with doping (and fermi level)



- InAs can be doped with electrically active concentrations approaching 10<sup>21</sup> cm<sup>-3</sup>



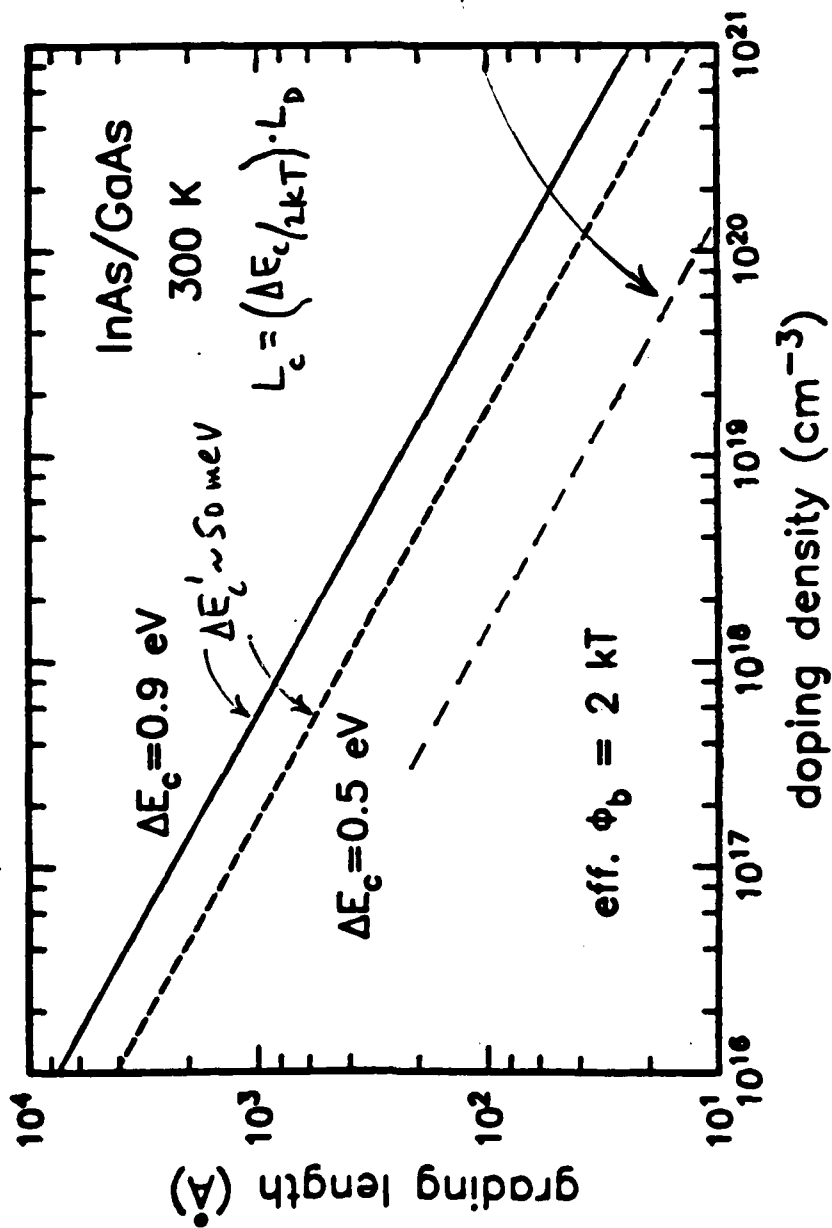
# InAs bulk Fermi level



09/86 (S.L. Wright)

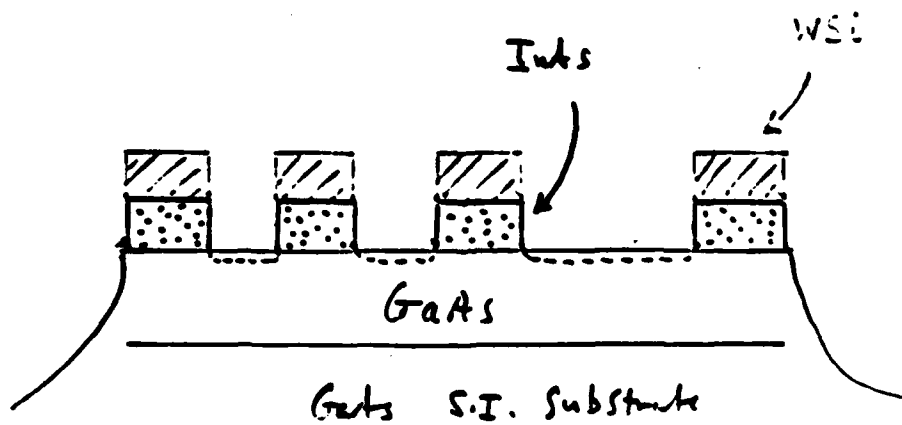
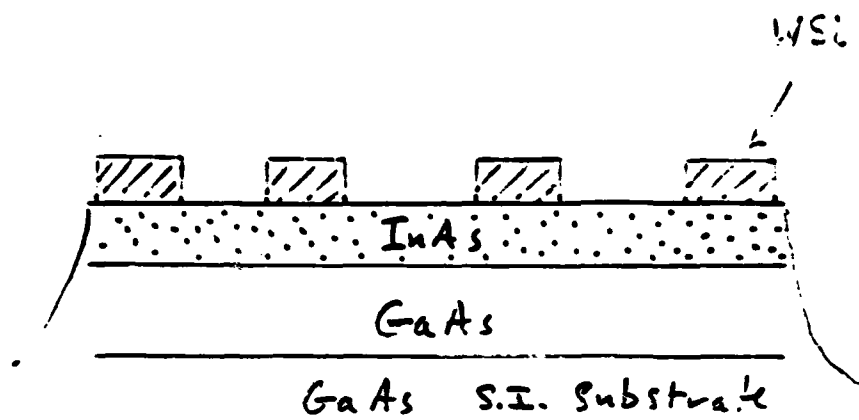
IBM

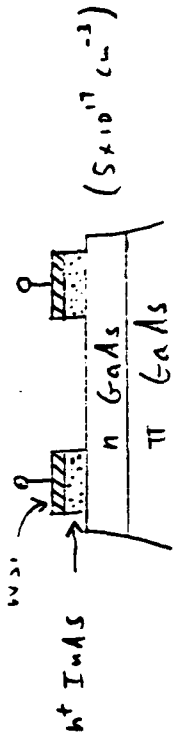
461



4/6 2

## Transmission Line Structures



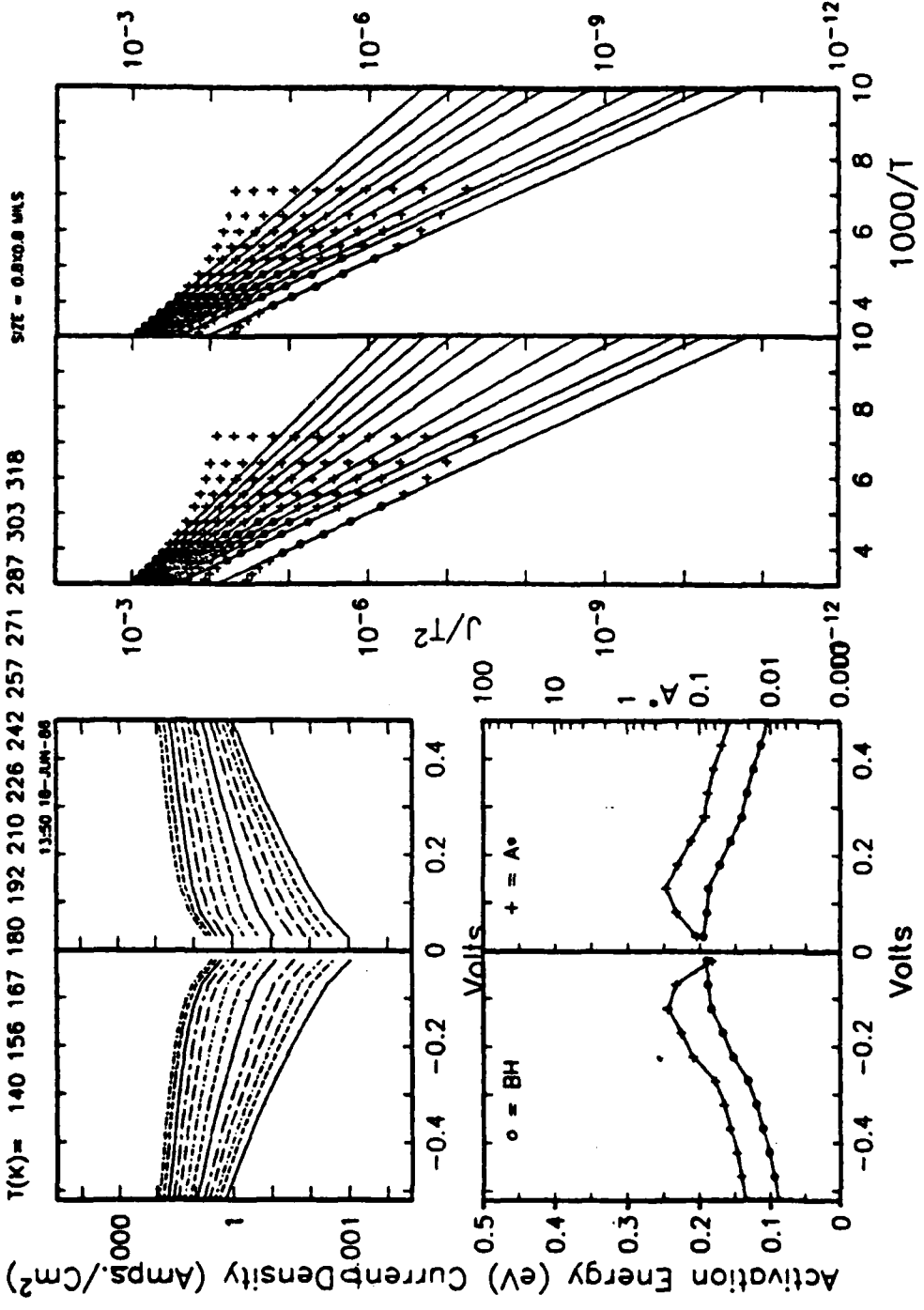


V844A16 INAS/GAAS TLM NON ANNEALED

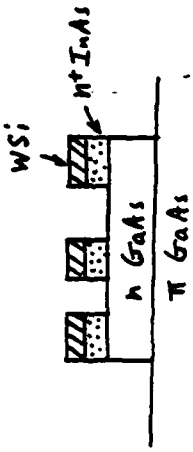
T(K) = 140 156 167 180 192 210 226 242 257 271 287 303 318

MANUAL DATA SELECTION

SIZE = 0.010.0 UMS

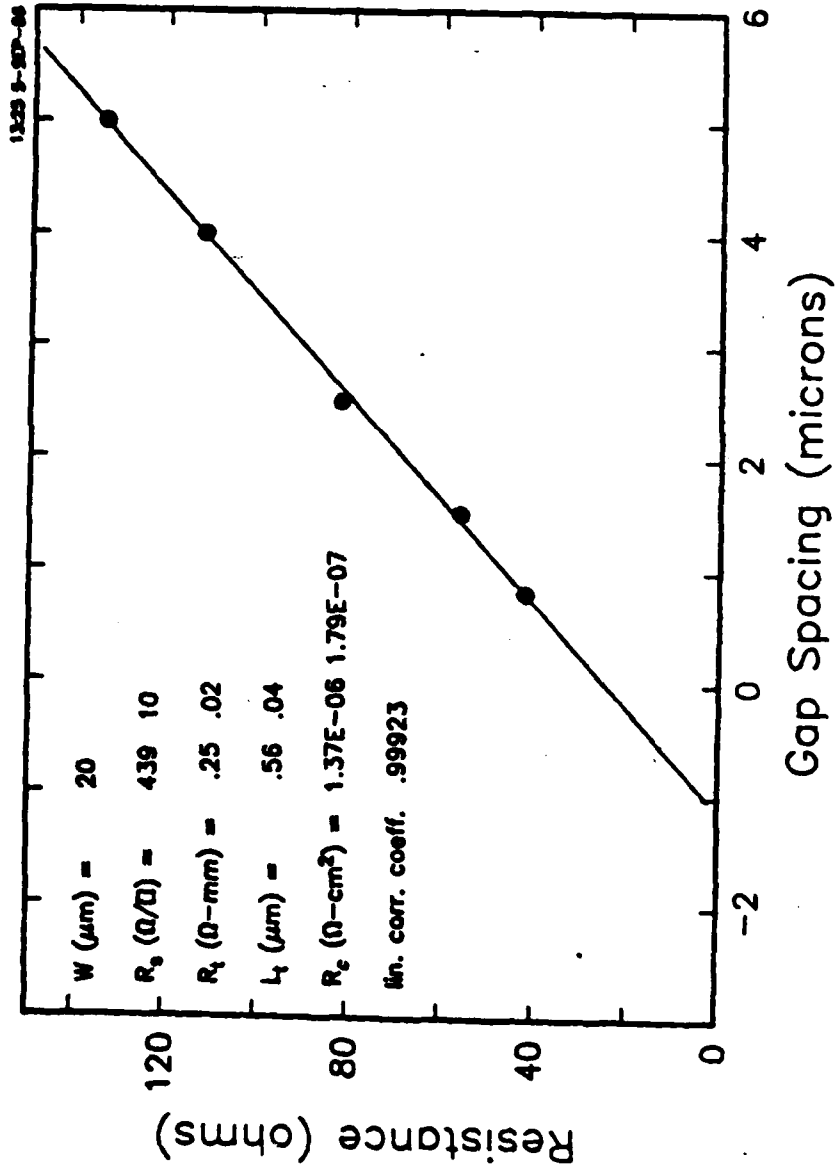


h 2/h



VB44 200A etch  
 abrupt, Se17 GaAs  
 1s 880 C anneal

gop	.8	1.5	2.5	4.0	5.0	11	.0
R	42.0	56.0	82.0	112.0	134.0	11	.0



465

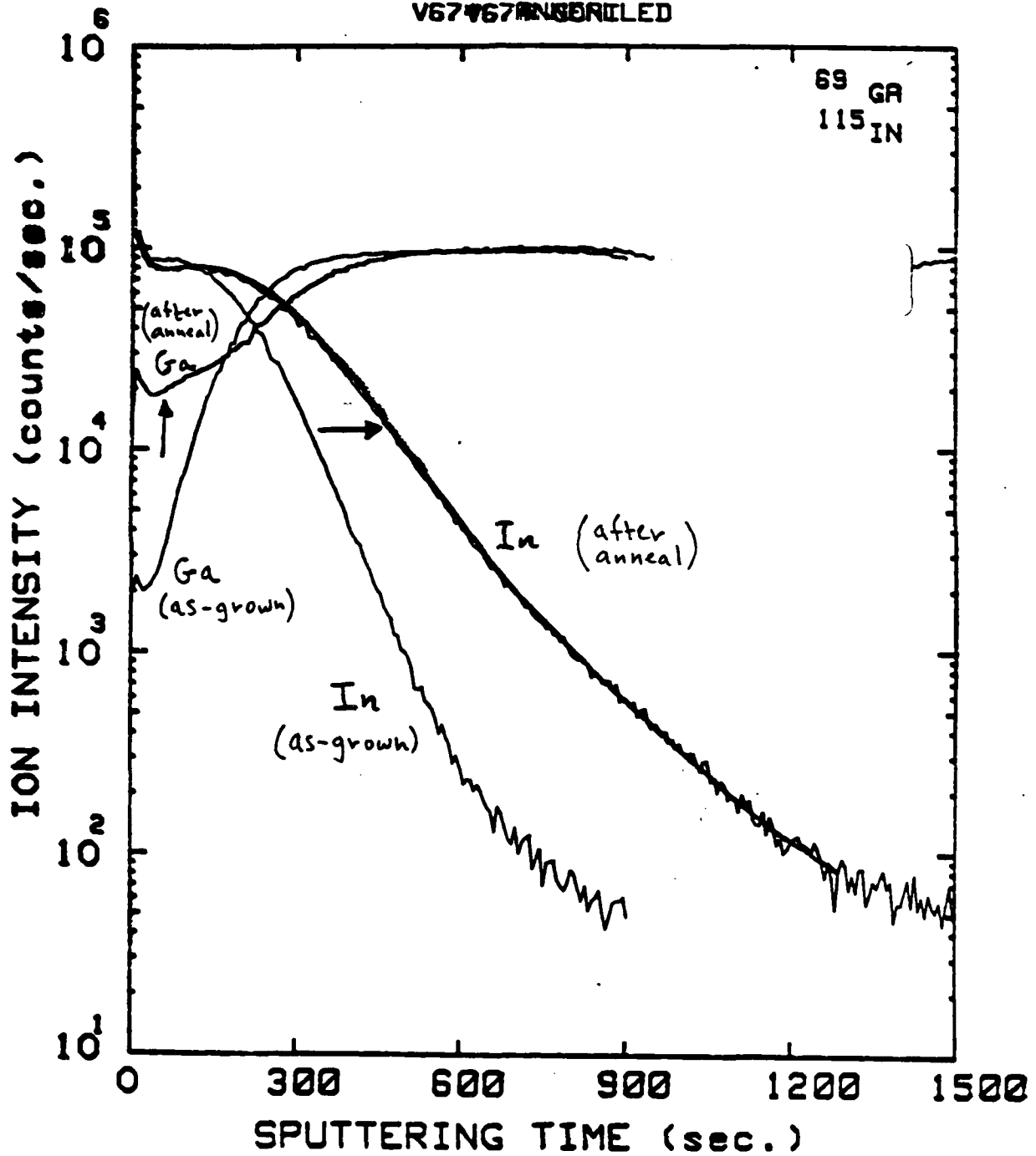




# SIMS DEPTH PROFILE 08-13-86

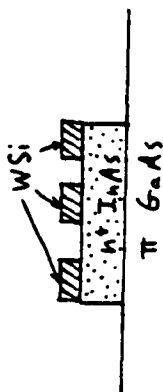
62258

V67 V67 INSERTE

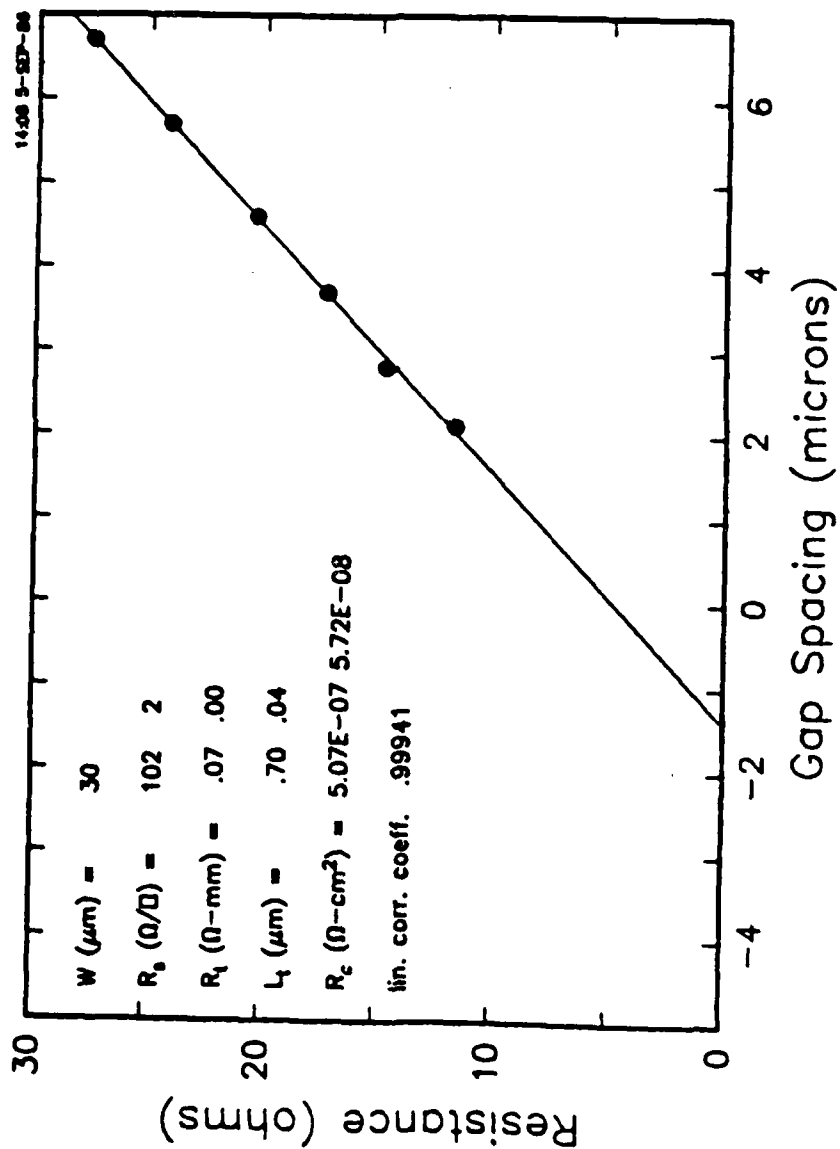


## Abrupt Structures: typical results

sample	GaAs doping ( $\text{cm}^{-3}$ )	$R_s(\Omega\text{-mm})$	$\rho_c(\Omega\text{-cm}^2)$
V671 300Å n+InAs 850°C, 3 sec	$2 \times 10^{17}$	0.47	$9 \times 10^{-6}$
V844 200Å n+InAs 880°C, 1 sec	$5 \times 10^{17}$	0.3	$1 \times 10^{-6}$
V917 300Å n+InAs 750°C, 5 min	$1 \times 10^{18}$	0.17	$2.6 \times 10^{-6}$
850°C, 18 sec		0.23	$2.2 \times 10^{-6}$



V903 1B3 gap 2.1 2.6 3.7 4.6 5.7 6.7 11 .0  
 n+ InAs on pl R 11.7 14.7 17.3 20.4 24.2 27.6 11 .0  
 18s 850 C anneal



## Metal/InAs interfacial contact resistance

ex) V903: 500Å n+ InAs/ $\pi$  GaAs buffer

Hall (300K):  $n_s \sim 2.6 \times 10^{14} \text{ cm}^{-2}$   
 $\mu \sim 300 \text{ cm}^2/\text{V-s}$   
 $R_s \sim 80 \Omega/\square$

heat treatment	$R_t(\Omega\text{-mm})$	$\rho_c(\Omega\text{-cm}^2)$
as-grown	0.07	$3\text{-}5 \times 10^{-7}$
650°C, 5 min	0.06	$3.6 \times 10^{-7}$
750°C, 5 min	0.06	$3.3 \times 10^{-7}$
850°C, 5 min	0.09	$2.3 \times 10^{-7}$
850°C, 18 sec	0.07	$4.0 \times 10^{-7}$

- finite WSi/InAs interface resistance  
 $\rho_c \leq 5 \times 10^{-7} \Omega\text{-cm}^2$
- NOT a limiting factor in most cases

## Graded Structures: typical results

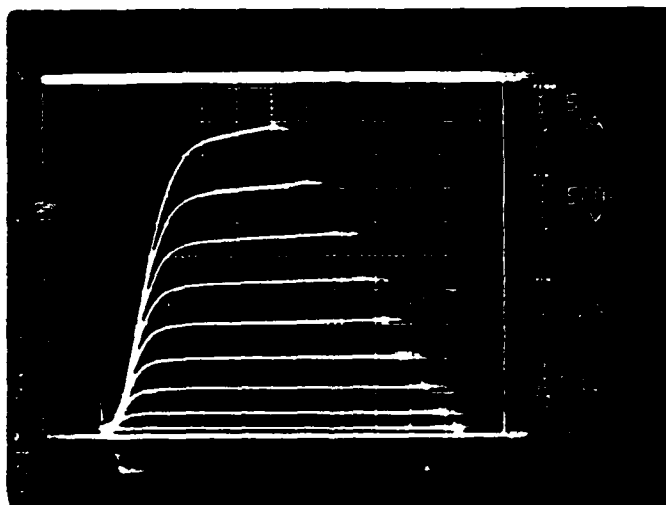
0.2 $\mu$ m  $1 \times 10^{18}$  GaAs channel/ graded layer/ 200 Å n+ InAs

contact layer etched down to channel in gap regions.

5 min. 750 °C arsine anneal

sample	$R_s(\Omega/\square)$	$R_t(\Omega\text{-mm})$	$\rho_c(\Omega\text{-cm}^2)$
V914 as-grown	213	0.09	$4 \times 10^{-7}$
600Å grade			
V914 annealed	458	1.0	$2 \times 10^{-5}$
V907 as-grown	192	0.08	$3.5 \times 10^{-7}$
320Å grade			
V907 annealed	209	0.19	$1.7 \times 10^{-6}$
V905 as-grown	207	0.09	$4 \times 10^{-7}$
180Å grade			
V905 annealed	176	0.07	$3 \times 10^{-7}$

## HBT characteristics



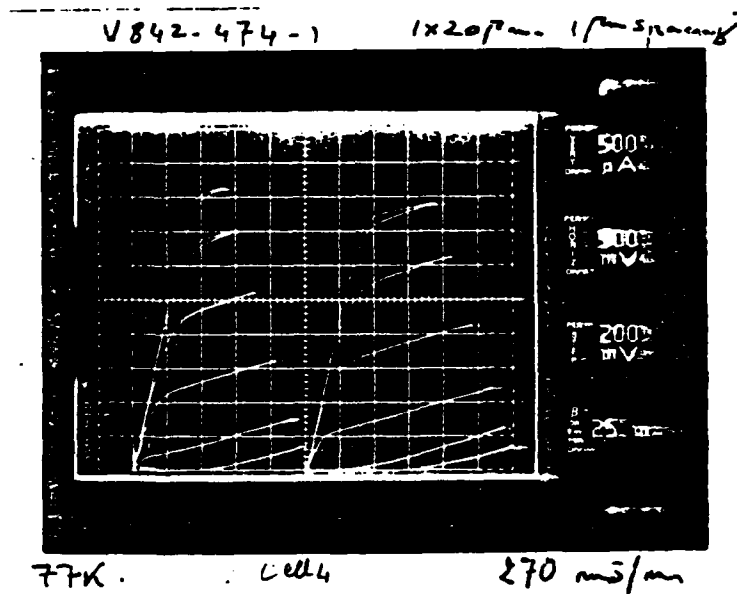
vertical npn structure on n+ substrate  
25  $\mu\text{m}$  diameter emitter  
WSi/InAs self-aligned ohmic contact  
p+ implant; 850  $^{\circ}\text{C}$ , 2-3 s anneal

06/86 (S.L. Wright)

IBM

471

# GaAs Gate FET with In-Situ contact



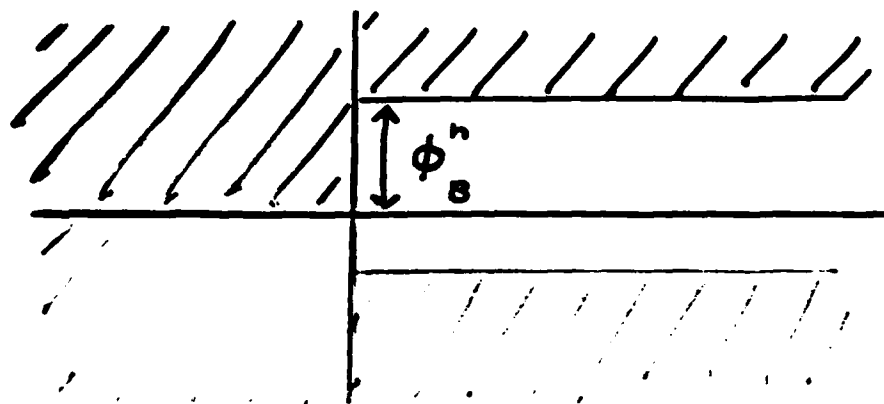
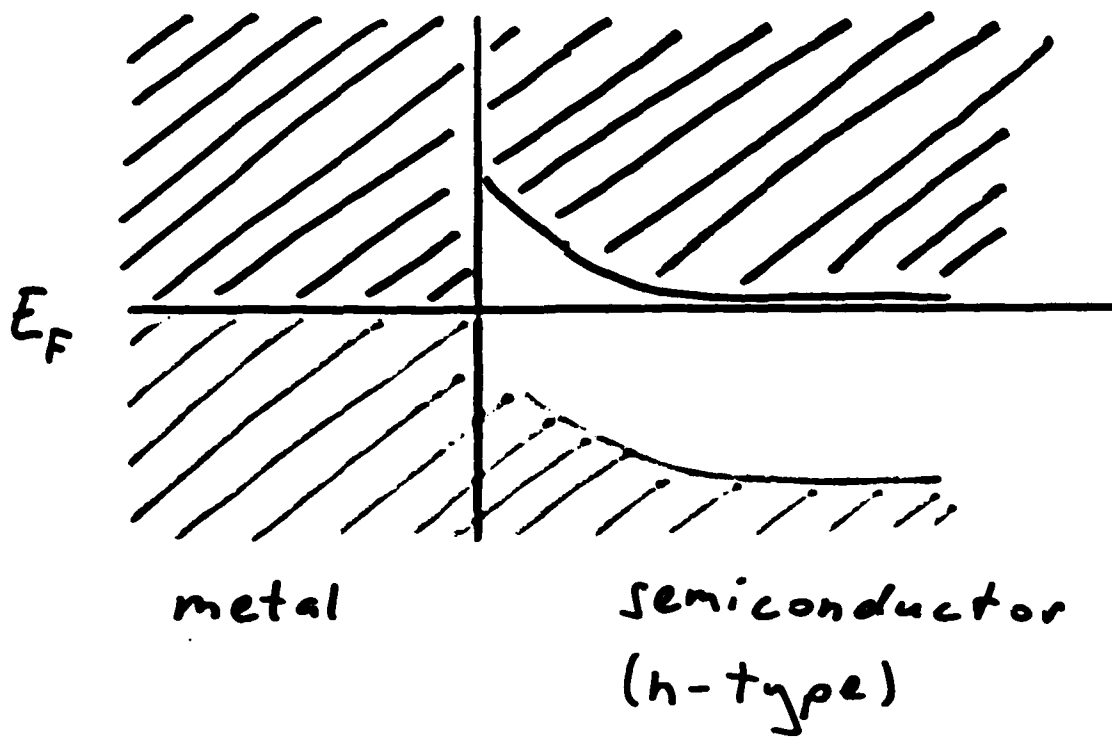
## Summary

- In-Situ Contacts: solution for self-aligned SISFET and HBT structures.
- Good morphology and electronic properties at small InAs thicknesses
- Transport data:  $\Delta E_c(\text{InAs/GaAs}) \sim 0.5\text{-}0.6\text{ eV}$   
HJ Fermi level NOT pinned near mid-gap.
- Abrupt structures which are capped are compatible with implant activation anneals. For  $10^{18}\text{ cm}^{-3}$  GaAs:  
as-grown:  $\rho_c \sim 1\text{-}5 \times 10^{-5}\ \Omega\text{-cm}^2$  (non-linear)  
annealed:  $\rho_c \sim 1 \times 10^{-6}\ \Omega\text{-cm}^2$ , ( $R_t \leq 0.3\ \Omega\text{-mm}$ )
- WSi/InAs interfacial resistance:  $\rho_c \leq 5 \times 10^{-7}\ \Omega\text{-cm}^2$
- as-grown graded structures have low contact resistance  
 $\rho_c \leq 4 \times 10^{-7}\ \Omega\text{-cm}^2$ ,  $R_t \leq 0.1\ \Omega\text{-mm}$
- tendency for graded structure contact resistance to degrade with heat treatment. spinodal decomposition?
- improvements are anticipated with optimal growth conditions and more heavily doped layers.

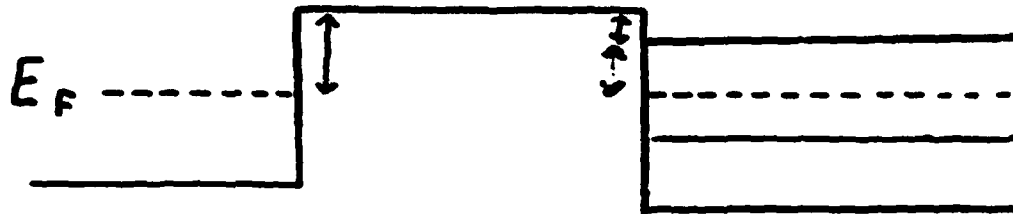


INTRINSIC MECHANISMS  
FOR  
FERMI-LEVEL PINNING  
AT  
SURFACES AND INTERFACES

JERRY TERSOFF  
IBM WATSON CENTE.



Schottky (1940)

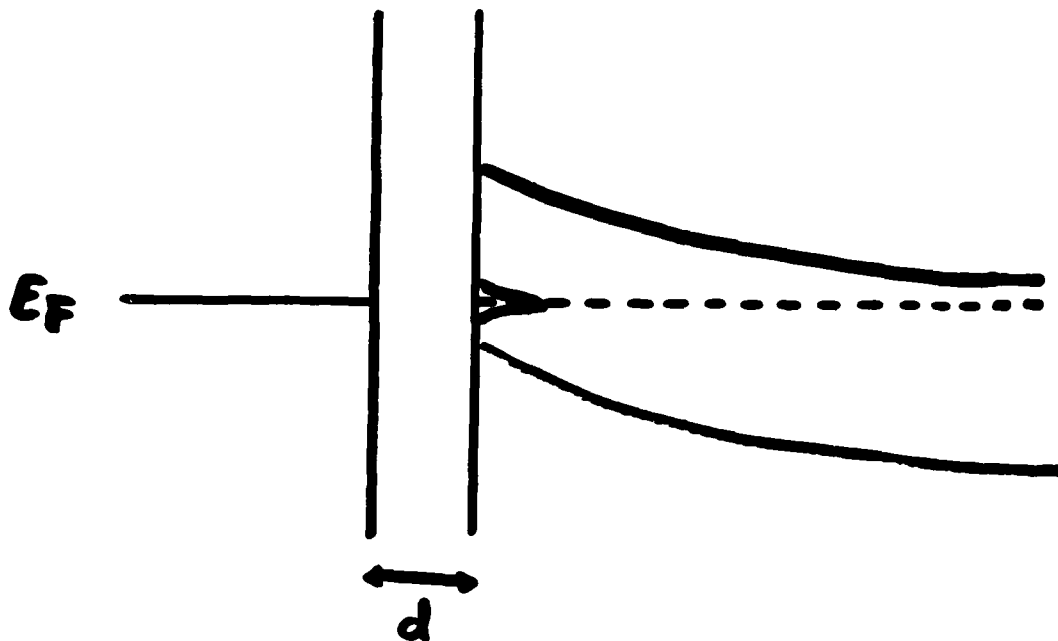


$\phi_b$  = metal work function  
- semiconductor  $e$  affinity

Terrible

Fermi level "pinned"

BARDEEN (1947)



$d \rightarrow \infty$        $10^{12}$  states/cm<sup>2</sup> with  $\mu$  at  $E_F$   
 $d \rightarrow 0$       need  $10^{14}$

Cf. true interface: "MIGS" etc.

HEINE (1965)

LOUIS et al. (1976)

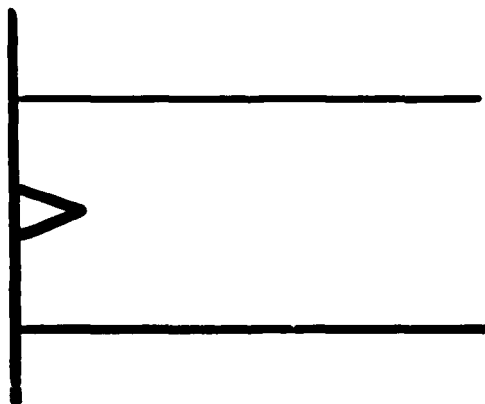
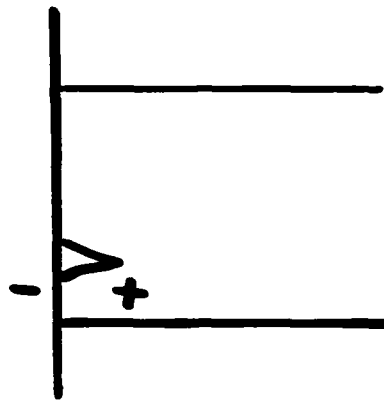
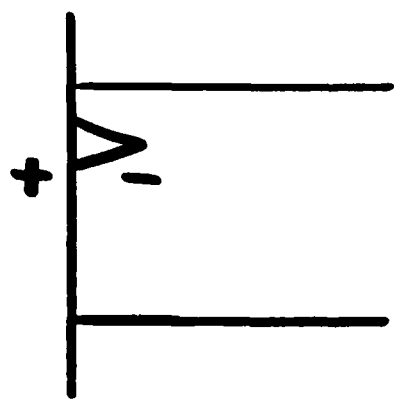
TEJEDOR et al. (1977)

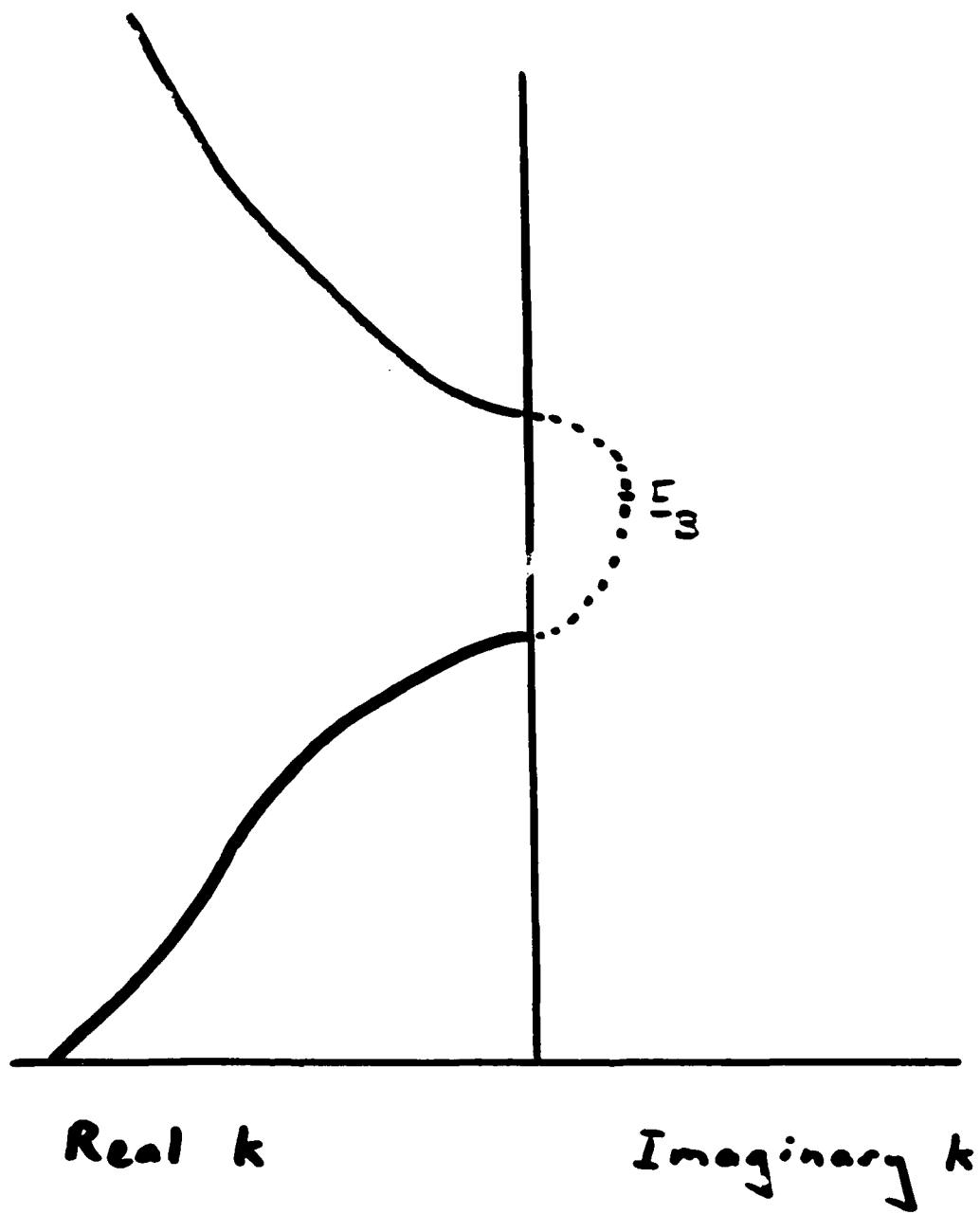
TERSOFF (1984)

WHAT IS  $\phi_b$ ?  $\Rightarrow$  WHAT IS  $E_{ss}$ ?

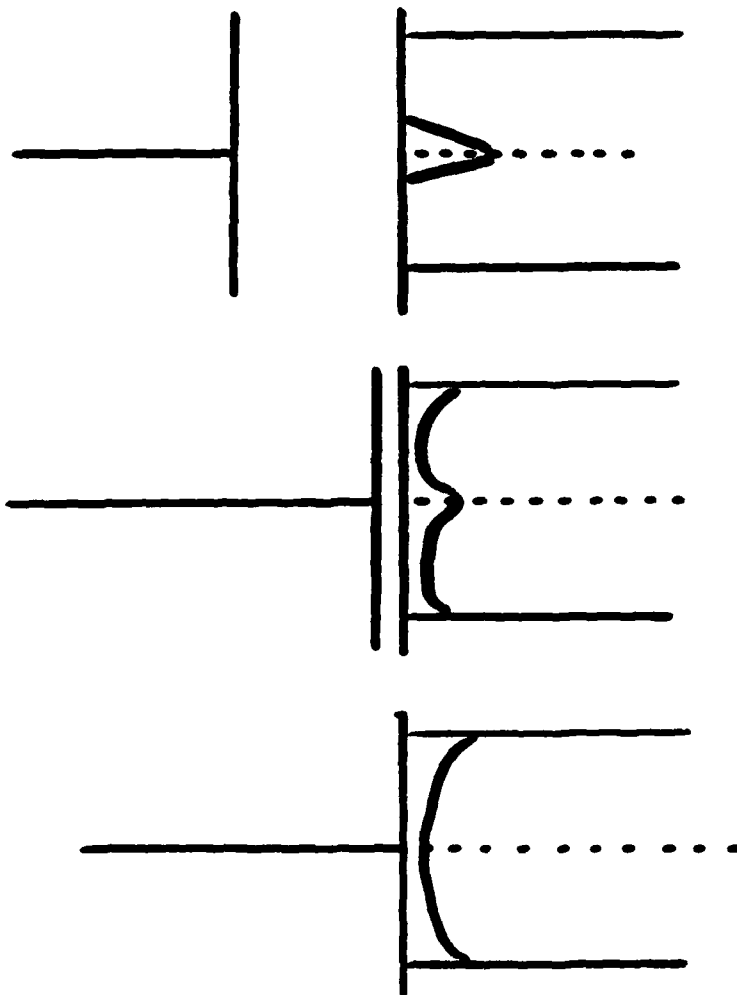
APPELBAUM + HAMANN (1974):

ROLE OF SELF-CONSISTENT DIPOLE





# SURFACE VS. INTERFACE



TEJEDOR + FLORES (1978)

SURFACE STATES AND INTERFACE STATES (MIGS) BOTH PIN  $E_F$  AT  $E_B$

GENERALIZE TO 3-D, HETEROPOLAR



FOR BARE SURFACE,

$$\phi_{lp} + \phi_{ln} = E_g - E_g^s.$$

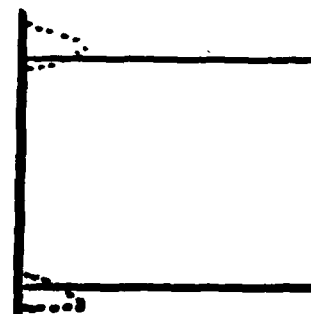
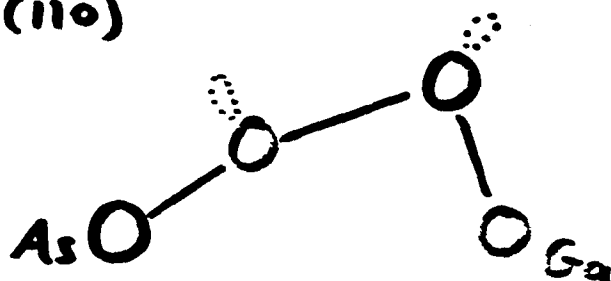
ADDING METAL BROADENS  
STATES ( $\rightarrow$  MIGS).

THEN  $E_g^s \rightarrow 0$ ,  $E_F$  PINNED MIDWAY,  
 $E_F \rightarrow E_g$

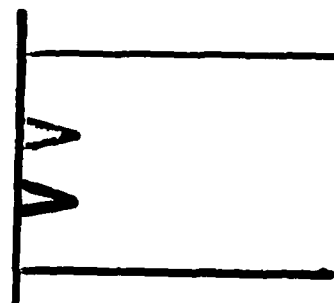
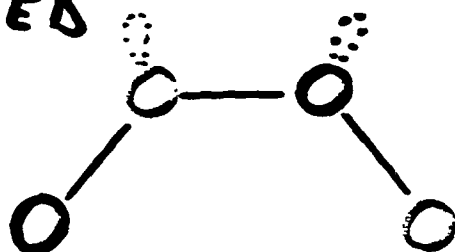


# POSSIBLE INTERPRETATION OF STANFORD EXPERIMENTS

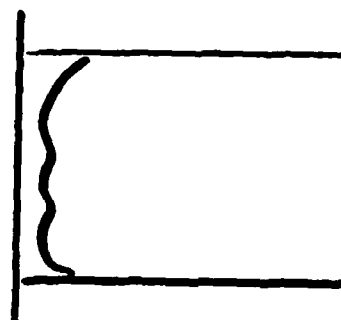
GaAs (110)



UNBUCKLED



METALLIZED



## PREDICTING SCHOTTKY BARRIERS

- AT BARE SURFACE, SURFACE STATES PIN  $E_F$  AROUND EFFECTIVE GAP CENTER  $E_B$   
(BARDEEN, APPELBAUM & HAMANN)
- AT METAL-SEMICONDUCTOR INTERFACE, SURFACE STATES HYBRIDIZE WITH METAL STATES, BECOME "MIGS";  
 $E_F$  STILL PINNED NEAR  $E_B$
- CALCULATE  $E_B$

Generalize to three dimensions

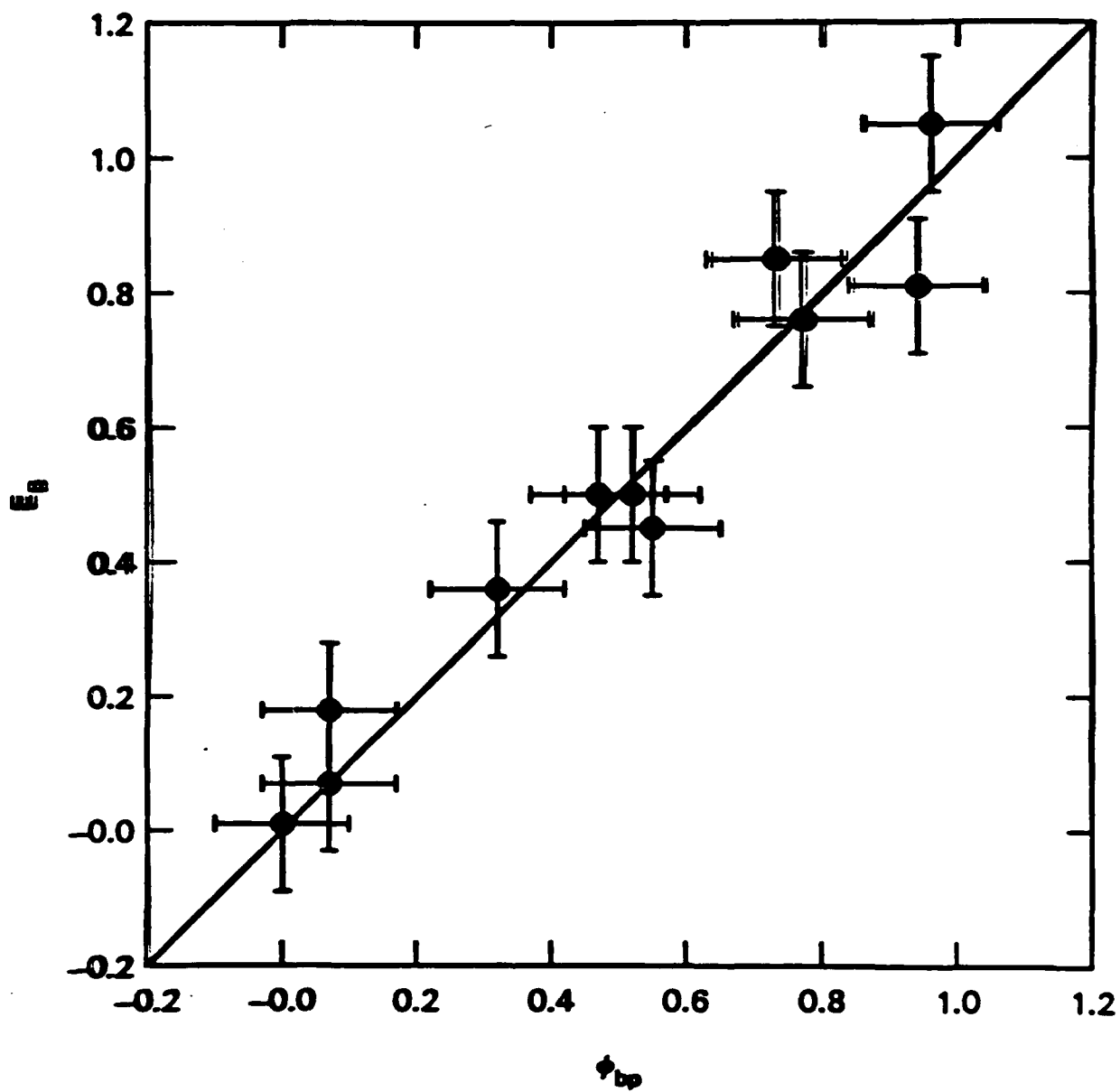
$$G(\vec{R}, E) \equiv \int d\vec{r} \sum_{nk} \frac{\psi^*(\vec{r}) \psi(\vec{r} + \vec{R})}{E - E_{nk}}$$
$$= \sum_{nk} \frac{e^{i\vec{k} \cdot \vec{R}}}{E - E_{nk}}$$

Locate  $E_B$  where valence + conduction  
bands contribute equally to  $G(\vec{R}, E)$

Reduces to branch point in 1-dimension

Calculation:

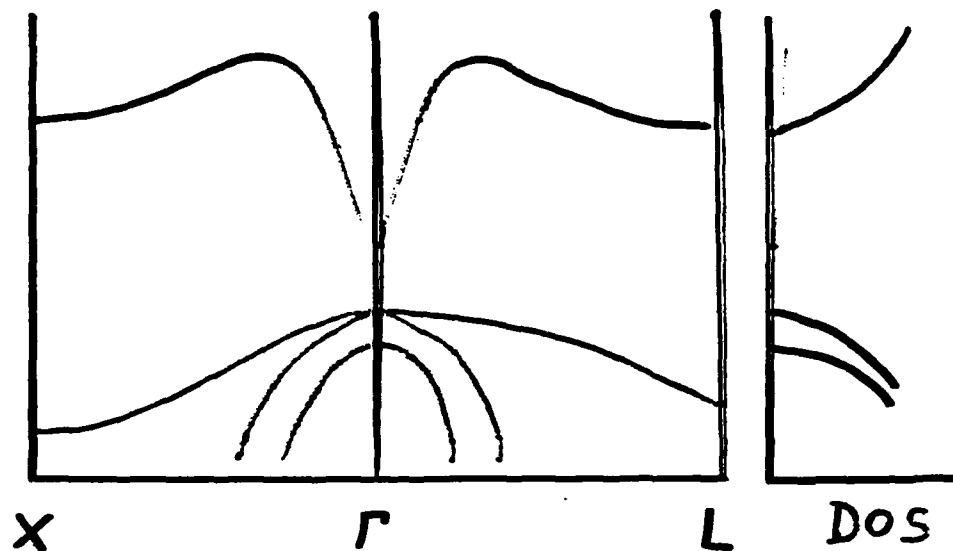
Input only  $E_{nk}$   
LAPW method  
band gap problem  
strain



485

# REAL SEMICONDUCTOR

LINE UP "CENTER" OF GAP



WHERE IS CENTER?

Effective gap center

$$E_o = (\bar{E}_v + \bar{E}_c) / 2$$

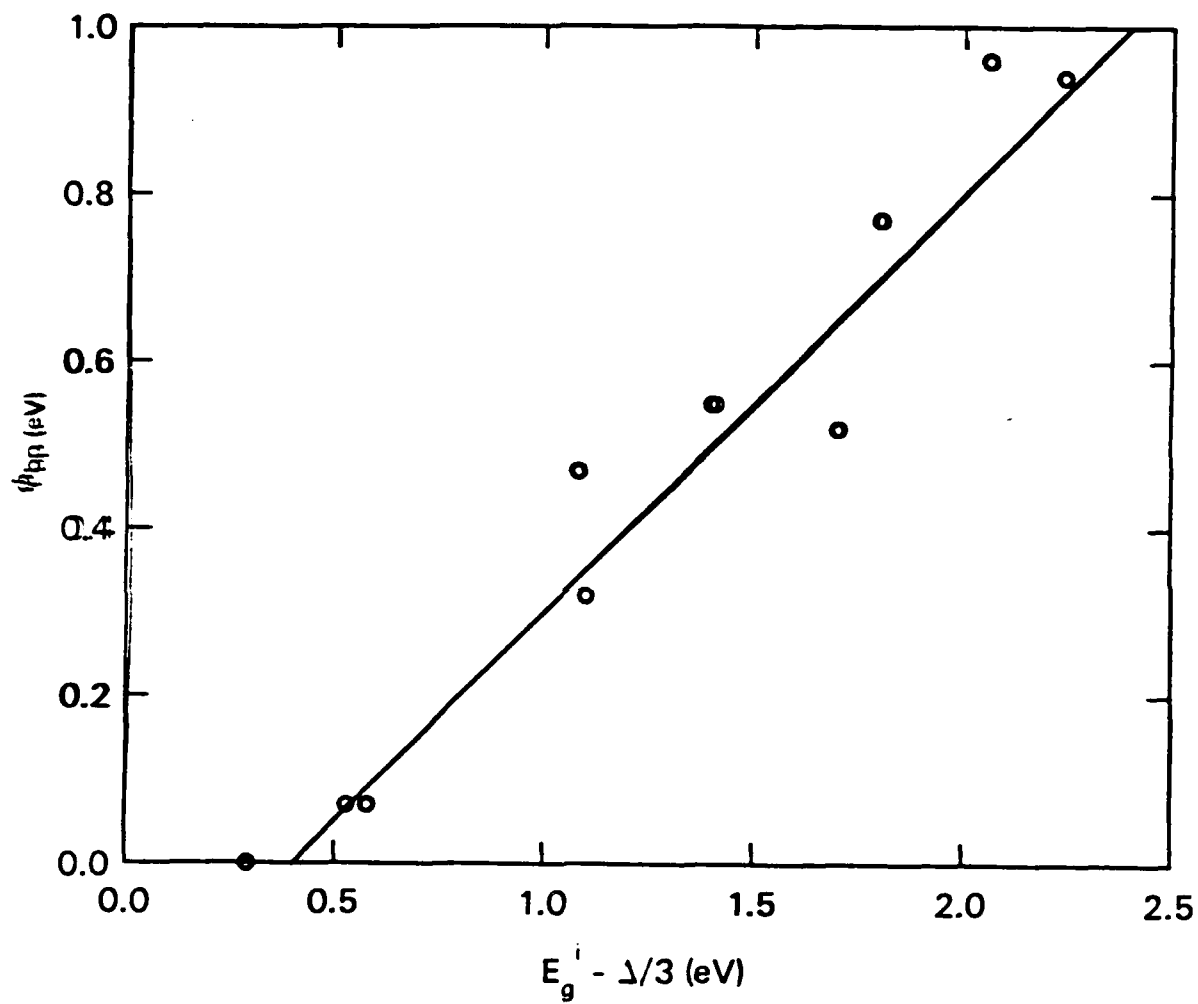
$$\bar{E}_v = E_v - \Delta / 3$$

$$\bar{E}_c = E_v + E_g^i$$

$$\begin{aligned}\bar{E}_B &= E_o - E_v = \frac{1}{2}(E_v - \frac{\Delta}{3} + E_v + E_g^i) - E_v \\ &= \frac{1}{2}(E_g^i - \frac{\Delta}{3})\end{aligned}$$

need some adjustable parameter

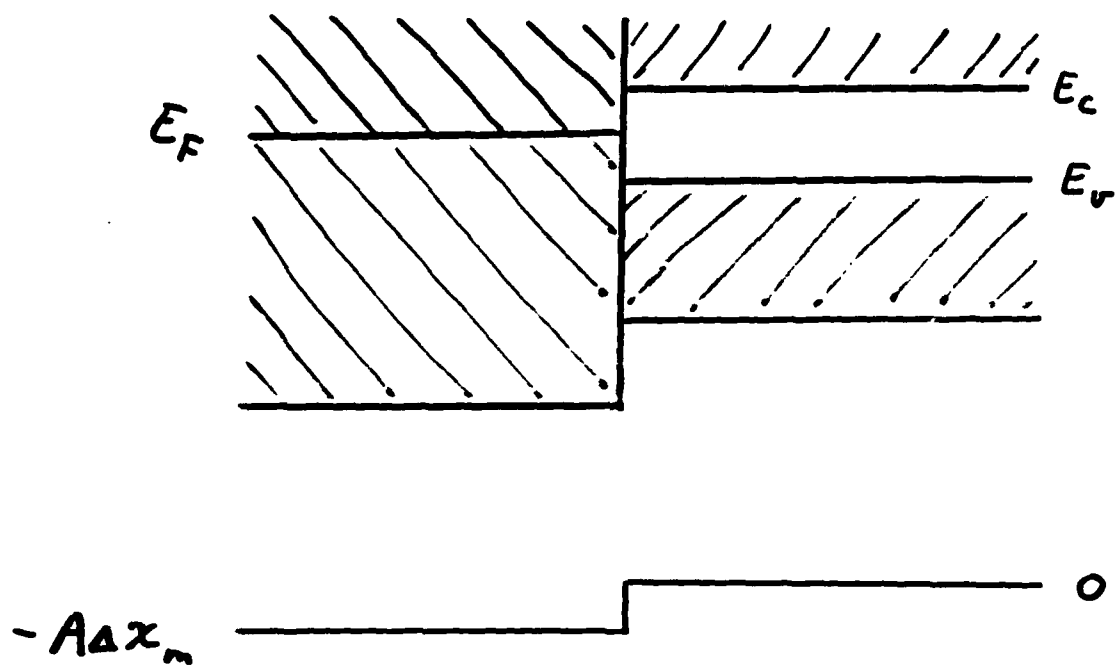
$$\Rightarrow E_B = \frac{1}{2}(E_g^i - \frac{\Delta}{3}) + \delta_m$$



$$\delta_m = -0.20 \text{ eV}$$

$$rms = 0.07 \text{ eV}$$

$$max = 0.13 \text{ eV}$$



$$S = \frac{d\phi_{bn}}{d\chi_m}$$

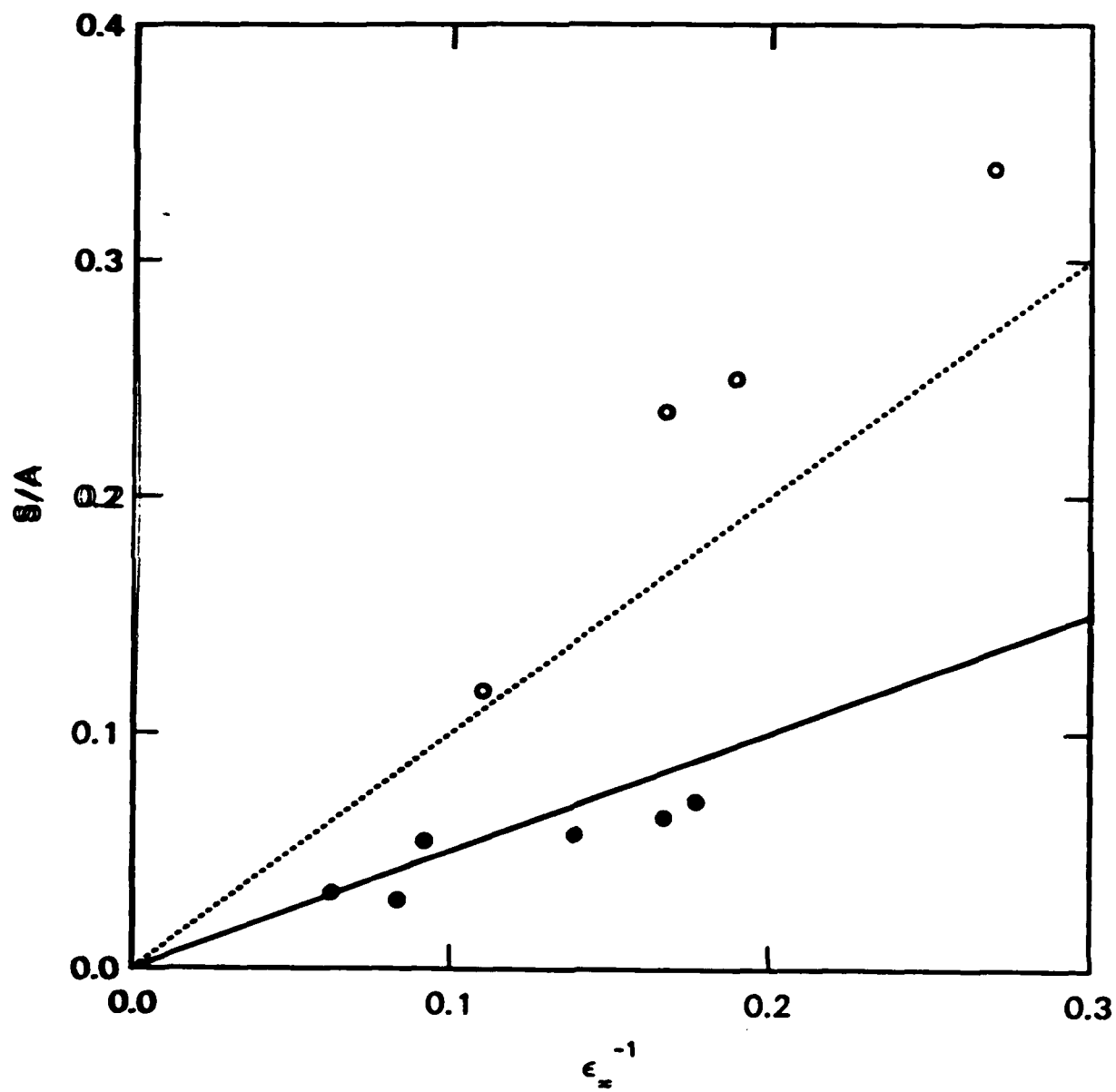
$$\bar{S} = S/A \quad A \approx 2.8 \text{ eV}$$

$$\Delta\phi_{bn} = S \Delta\chi_m = A \Delta\chi_m / E_{eff}$$

$$\Rightarrow \bar{S} = 1/E_{eff}$$

$$0 \leq \bar{S} \leq 1/E_{eff} \quad \text{guess} \quad \bar{S} \approx 1/2E_{eff}$$





## ROLE OF INTERFACE IDEALITY

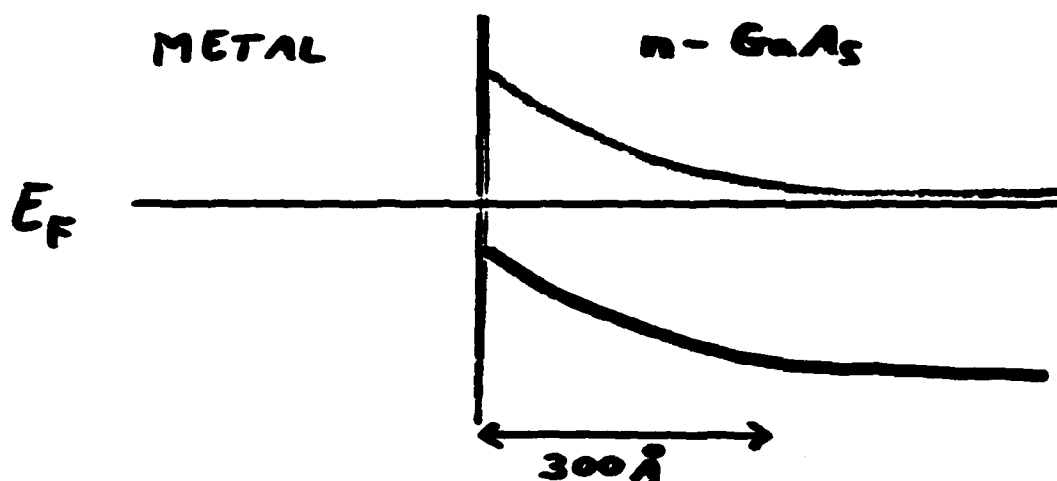
THEORY ONLY VALID FOR "IDEAL"  
SURFACE, INTERFACE?

- $E_F$  PINNED BY GAP STATES
- STATES DETERMINED BY BOTH SEMICONDUCTOR BULK AND INTERFACE.  
[SCHRÖDINGER EQ. AND BOUNDARY COND.]
- WHEN INCLUDE DIPOLE SELF-CONSISTENTLY, FIND STATES DISTRIBUTED SO  $E_F$  FALLS AT  $E_B$ .

EXPECT  $E_F$  PINNED NEAR  $E_B$   
FOR WIDE VARIETY OF STRUCTURES

# IMPORTANCE OF INTERFACE CHEMISTRY, STRUCTURE

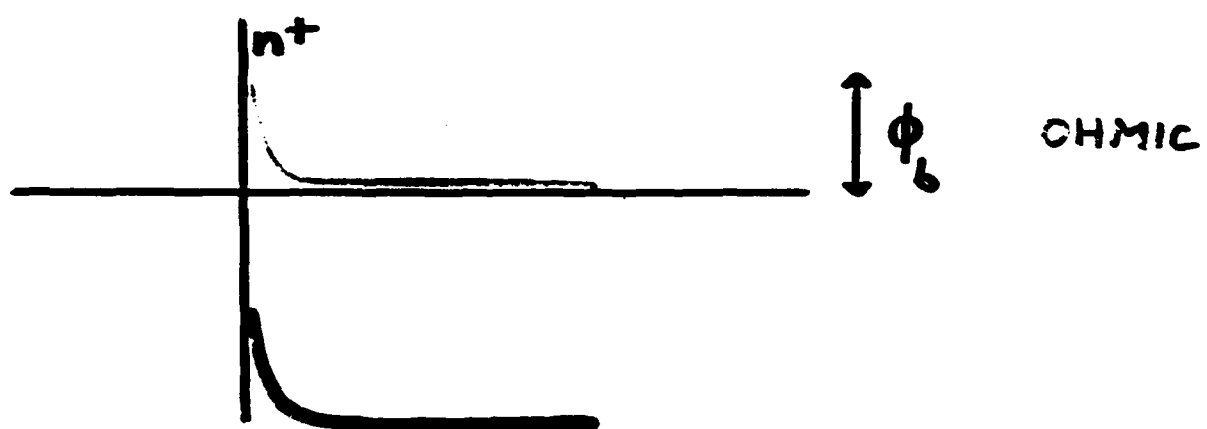
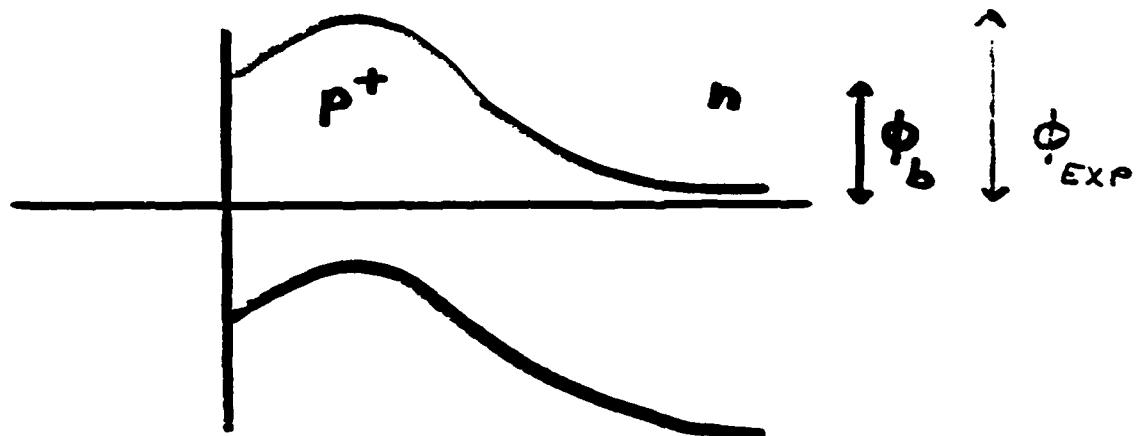
SCHOTTKY BARRIER NOT IMPORTANT!  
TRANSPORT IS IMPORTANT!



IDEAL INTERFACE:  $\phi_b \rightarrow$  TRANSPORT

OTHER POSSIBILITIES.

# SIMPLE EXAMPLES



MORE COMPLEX POSSIBILITIES

LATERAL INHOMOGENEITY

RESONANT TUNNELING, HOPPING

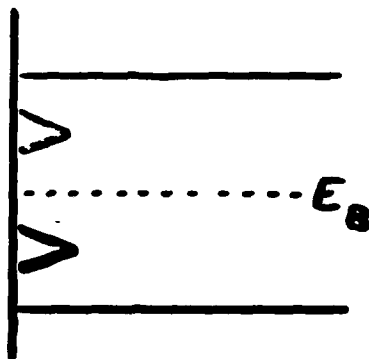
EXCHANGE REACTION ( $\text{Al-GaAs}$ )

IMPORTANCE OF EXPERIMENTALLY  
CHARACTERIZING TRANSPORT

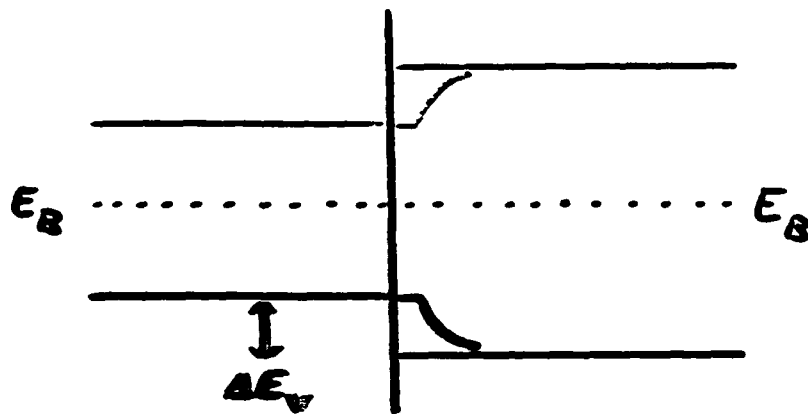
I-V vs. T; IDEALITY

C-V vs. V

CONNECTION WITH HETEROJUNCTIONS  
HAD GAP STATES SYMMETRIC ABOUT  $E_B$



SIMILARLY, AT HETEROJUNCTION,  
ALIGN TWO  $E_B$ 'S.



$$\Delta E_V = \Delta E_B = 1.1 \text{ eV}$$

AD-A183 158

A WORKSHOP ON 3-5 SEMICONDUCTOR: METAL INTERFACIAL  
CHEMISTRY AND ITS EFFECTS (U) STANFORD UNIV CA  
W E SPICER ET AL. 05 NOV 86 N00014-87-G-0038

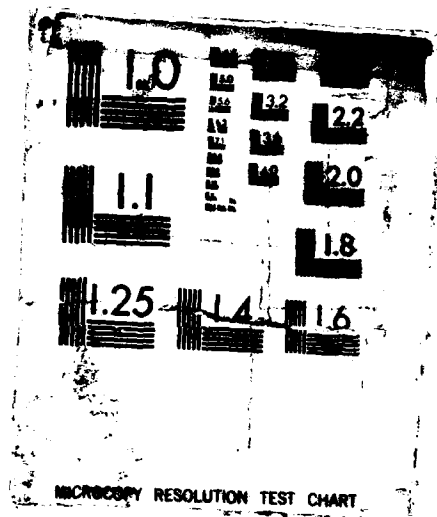
6/7

UNCLASSIFIED

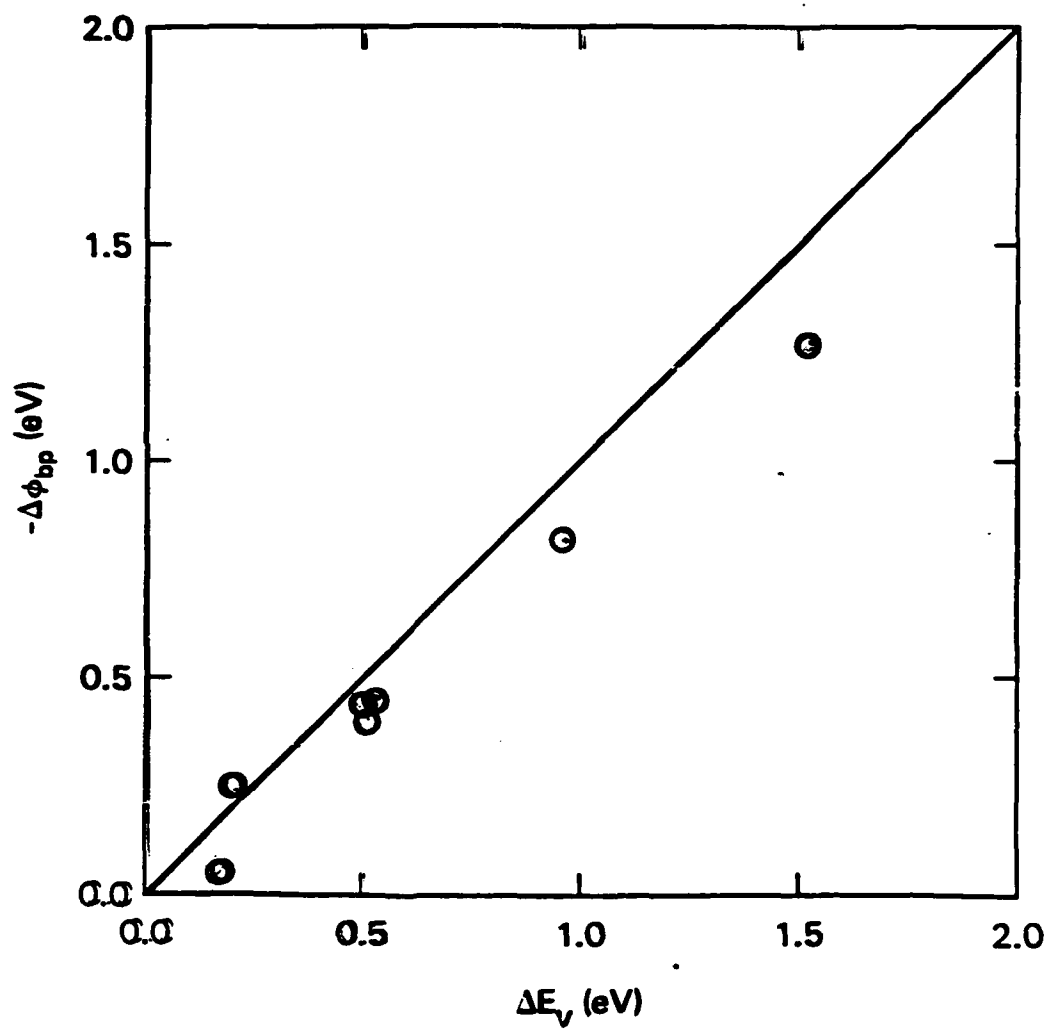
F/G 20/12

NL

ST







496

## SUMMARY

- INTRINSIC SURFACE OR INTERFACE STATES PIN  $E_F$  NEAR  $E_B$
- EXCELLENT AGREEMENT WITH EXP
- $E_B \sim \frac{1}{2} E_g^2$
- METAL DEPENDENCE:  $S \sim 1/\epsilon_\infty$
- DIRECT CONNECTION WITH BAND LINEUPS
- EVIDENCE AGAINST EXTRINSIC MECHANISM

**Recent Photoemission and Cathodoluminescence  
Spectroscopy Studies of III-V  
Semiconductor-Metal Interfaces**

**Leonard J. Brillson**

**Xerox Corporation**

**RECENT PHOTOEMISSION AND**  
**CATHODOLUMINESCENCE SPECTROSCOPY STUDIES OF**  
**III-V SEMICONDUCTOR-METAL INTERFACES**

- **CHEMISTRY OF CLEAN  $\text{In}_x\text{Ga}_{1-x}\text{As}$  METAL INTERFACES**
- **CHEMICAL DEPENDENCE OF  $\text{In}_x\text{Ga}_{1-x}\text{As}$   $E_F$  MOVEMENTS**
- **DIRECT OBSERVATIONS OF III-V/METAL INTERFACE STATES**
- **SPECTRAL CORRELATION WITH ELECTRONIC AND CHEMICAL STRUCTURE**

Supported in Part by the Office of  
Naval Research

## COLLABORATORS

**Enrique Viturro**  
**Michael Slade**

**Xerox Webster Research Center**  
**Xerox Webster Research Center**

**Michael Kelly**  
**Lila Tache**  
**Douglas Kilday**  
**G. Margaritondo**

**University of Wisconsin-Madison**  
**University of Wisconsin-Madison**  
**University of Wisconsin-Madison**  
**University of Wisconsin-Madison**

**Peter Kirchner**  
**Dave Pettit**

**IBM Yorktown**  
**IBM Yorktown**

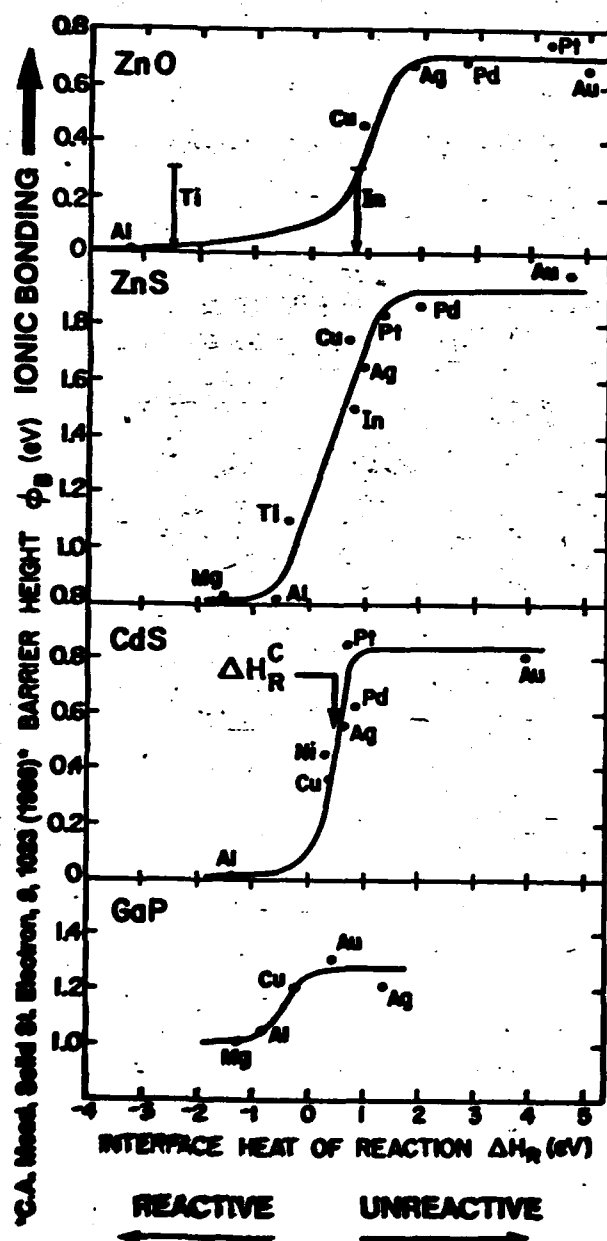
**Jerry Woodall**  
**Steve Wright**

**IBM Yorktown**  
**IBM Yorktown**

**Piero Chiaradia**

**Istituto Struttura Materia, Frascati**

# TRANSITION IN SCHOTTKY BARRIER FORMATION WITH CHEMICAL REACTIVITY

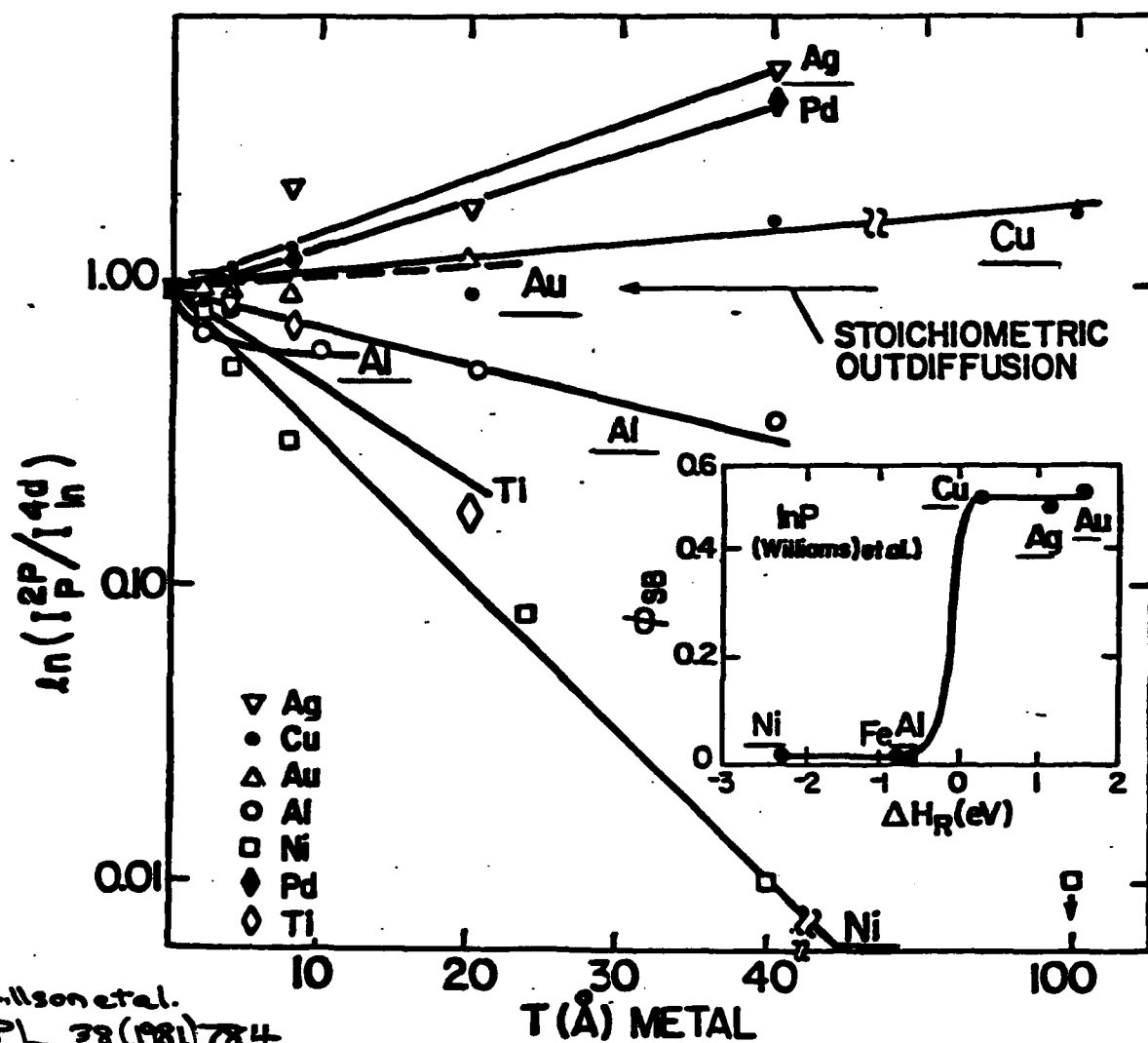


SAME TRANSITION FOR  
IONIC AND COVALENT  
SEMICONDUCTORS

TRANSITION AT  
EXPERIMENTALLY  
DETERMINED  $\Delta H_R$

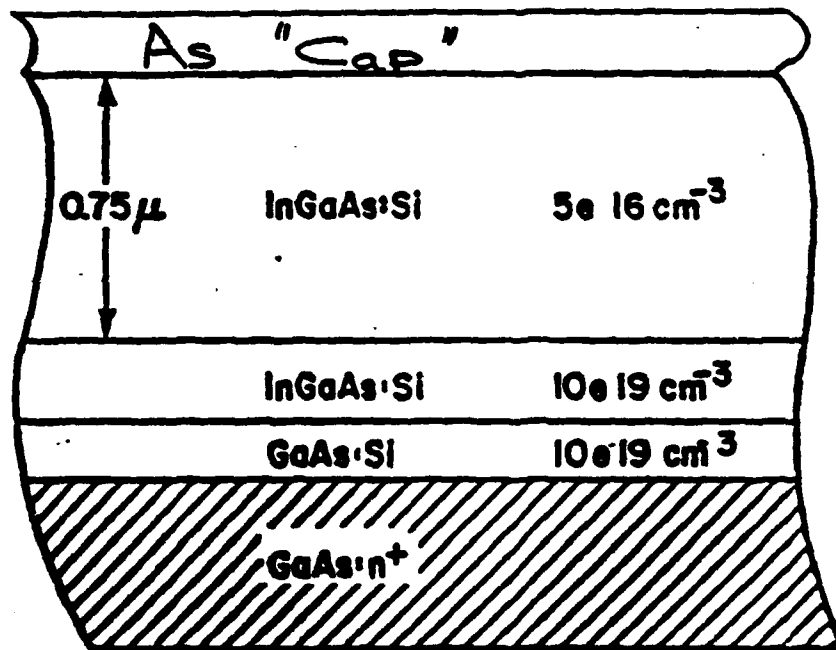
L.J. Brillson  
Phys. Rev. Lett. 40, 280 (1978)

# STOICHIOMETRY OF OUTDIFFUSION VS SCHOTTKY BARRIER HEIGHT



STRENGTH OF INTERFACE CHEMICAL BONDING  
DETERMINES ELECTRICITY - ACTIVE SITES (III-V's)

# Thermal Cleaning of As- "Capped" $\text{In}_x\text{Ga}_{1-x}\text{As}(100)$

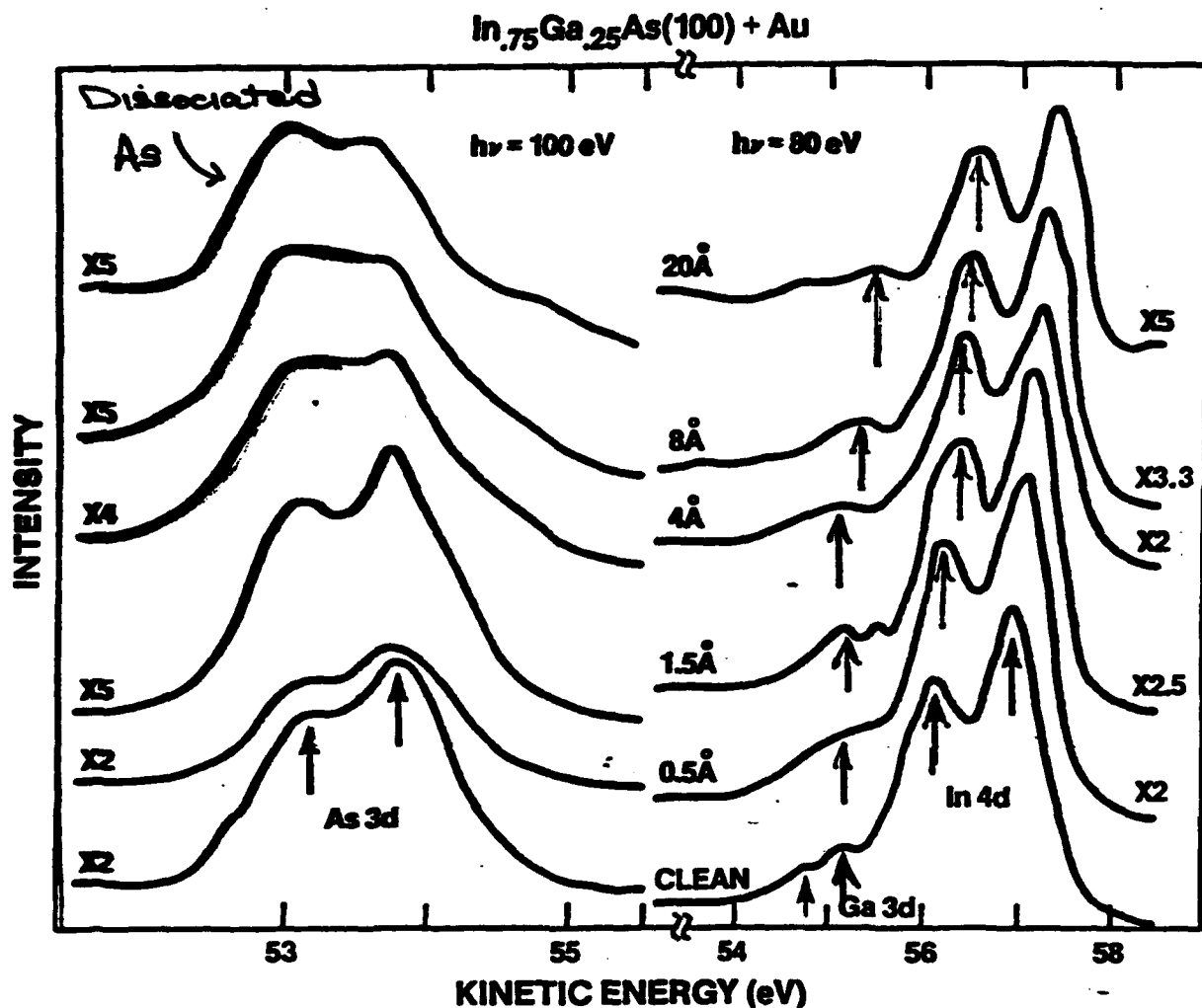


Woodell, Pettit, Kitchner, & Wright

- Clean, Ordered  $\text{In}_x\text{Ga}_{1-x}\text{As}$  Grown By MBE
- "Ohmic" Back Contacts
- De-"capping" of As Protective Layer in JHV



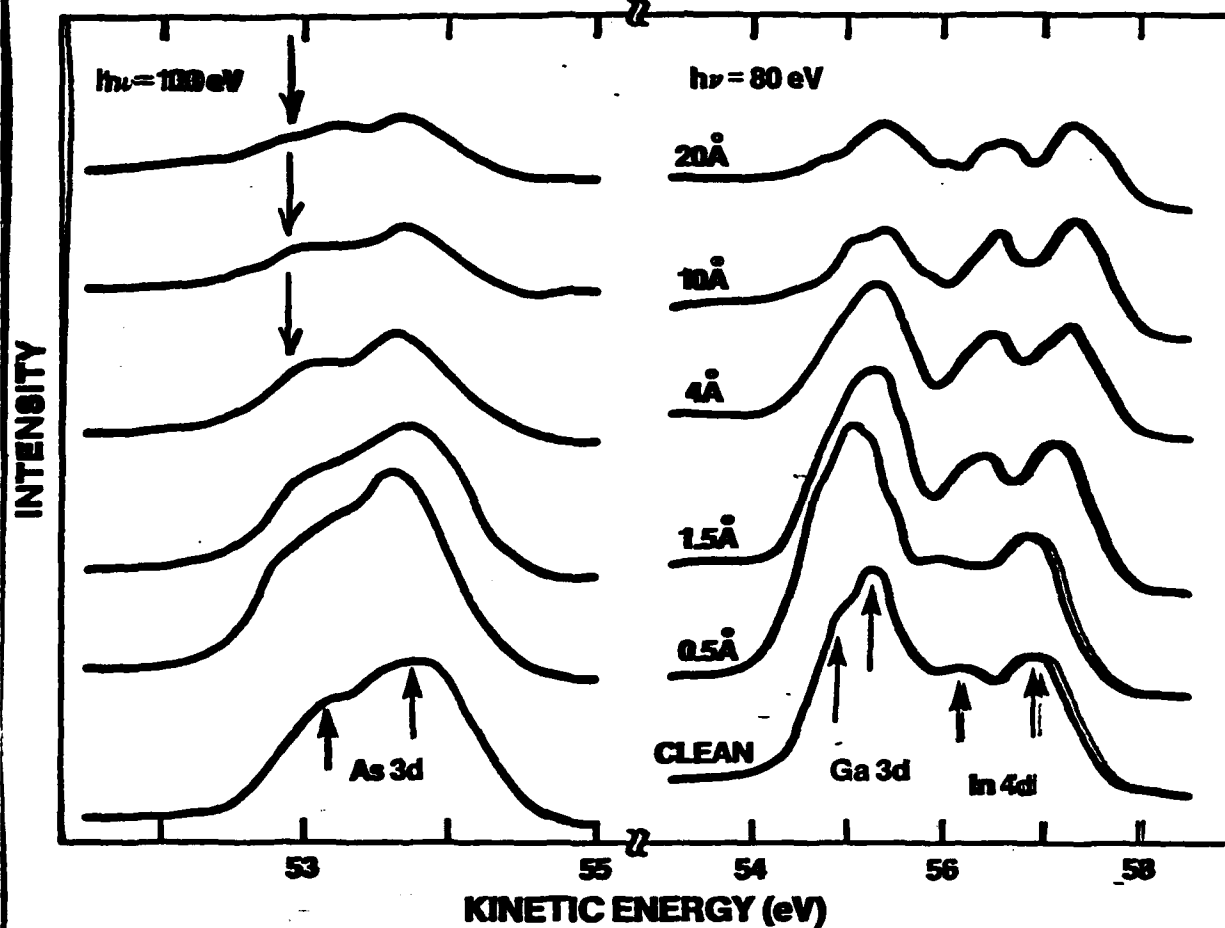
# Interface Dissociation



- As - Rich Outdiffusion
- No Strongly Dissociated In or Ga
- $E_F$  Shift: Lower Binding Energies

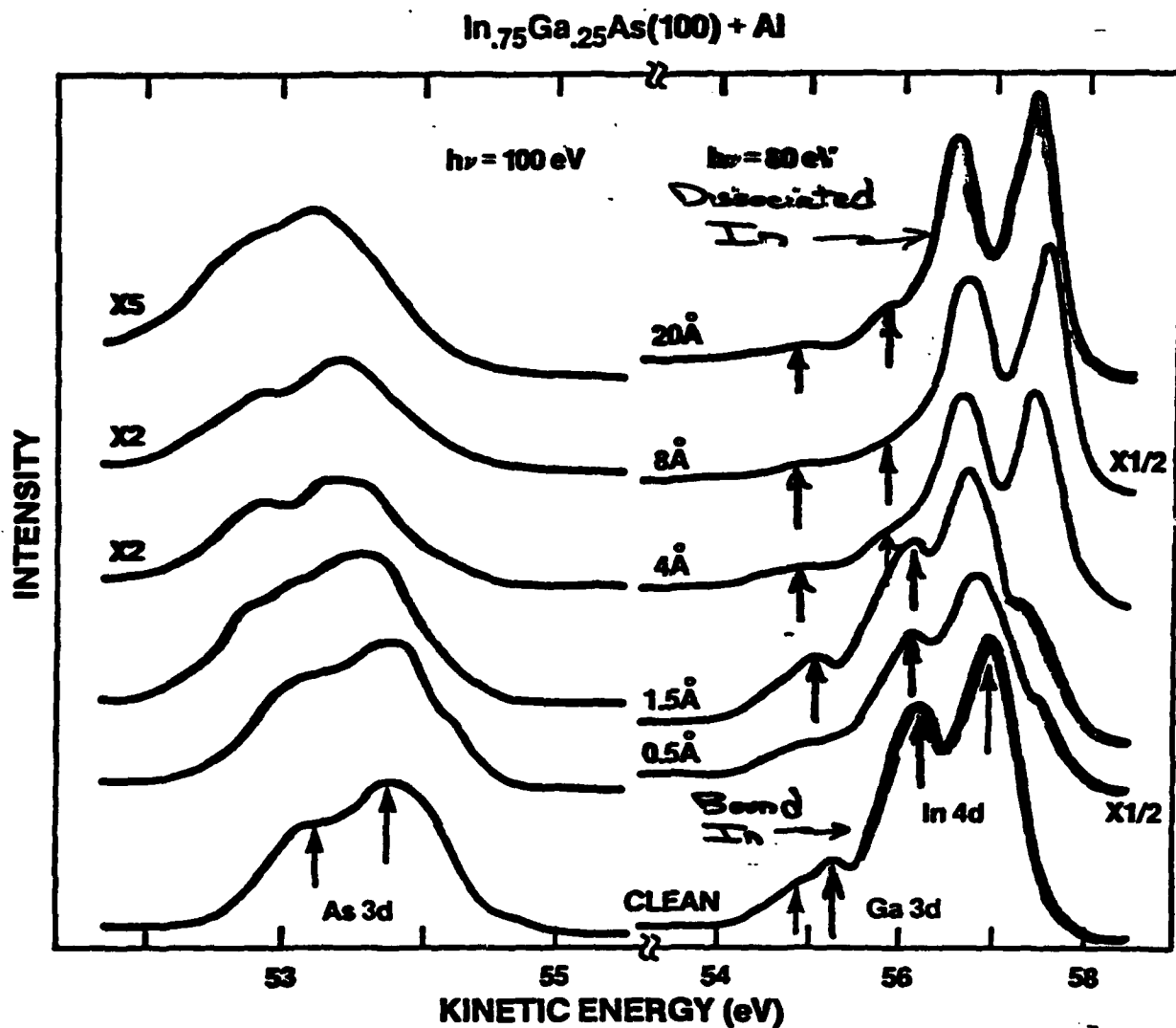
# Interface Dissociation: Low In Alloy

$\text{In}_{25}\text{Ga}_{75}\text{As}(100) + \text{Au}$



- Little if Any Dissociated As
- No As-Rich Outdiffusion
- Contrast with High In Alloy

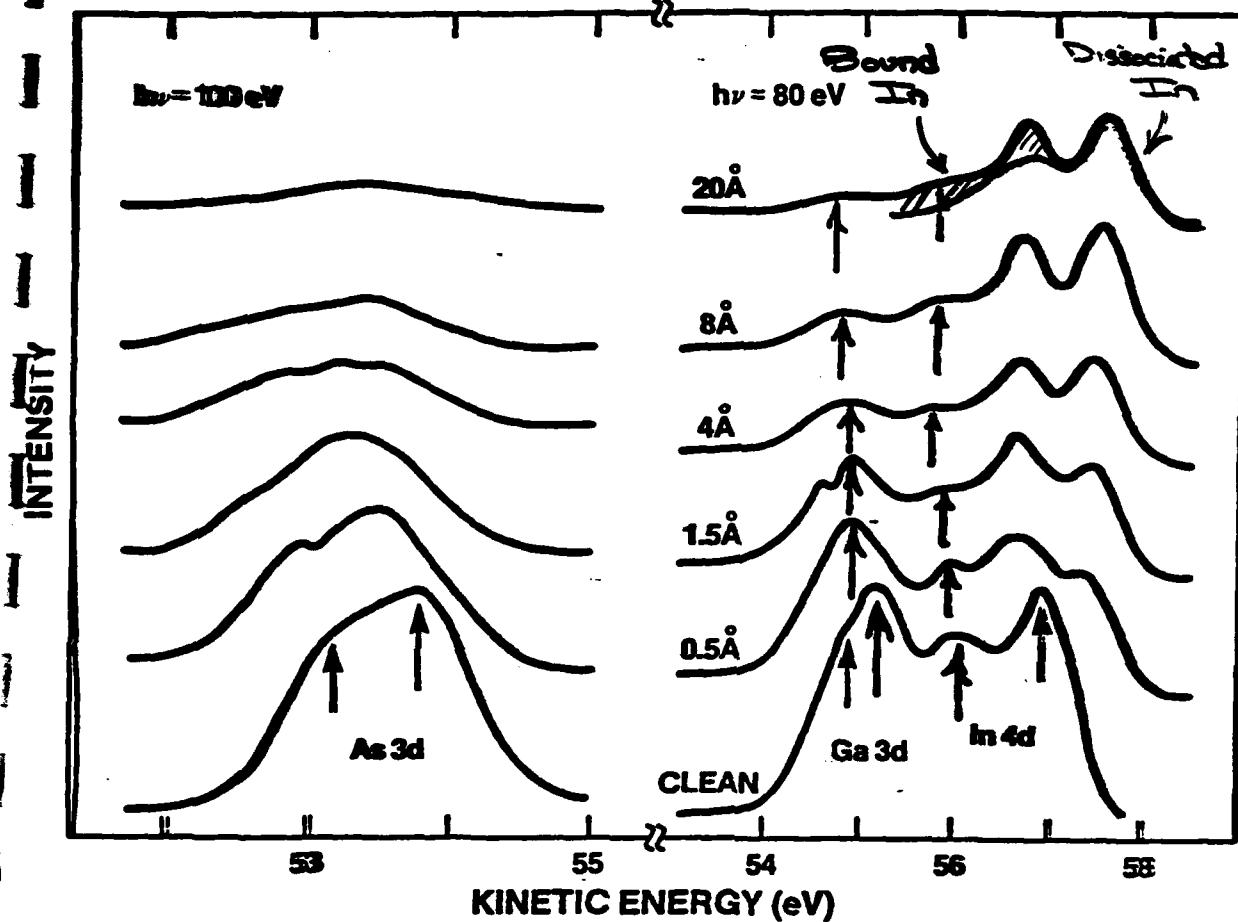
# Interface Exchange Reaction



- Al Replaces In in InGaAs Lattice  
— Low  $\text{Bound In} / \text{Bound Ga}$
- No Ga Dissociation
- $E_F$  Shift: Higher Binding Energies
- Little As Outdiffusion

# Interface Exchange Reaction

$\text{In}_{25}\text{Ga}_{75}\text{As}(100) + \text{Al}$



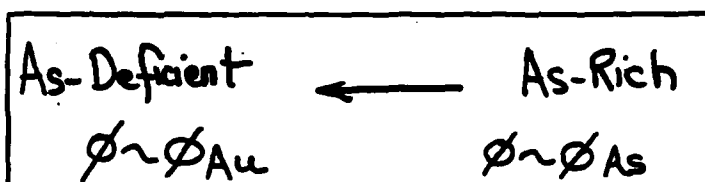
- Lower Proportion of Dissociated/Bound In
- Higher Proportion of Bound In/Bound Ga

⇒ KINETIC LIMITATION TO REPLACEMENT REACTION

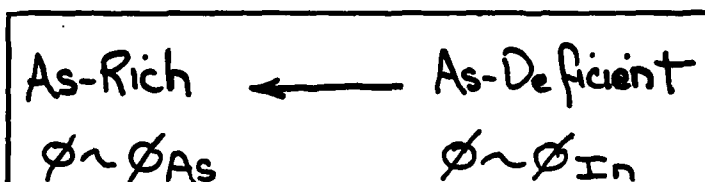
- Higher Proportion of Surface As

# Metal-Semiconductor Interface Composition

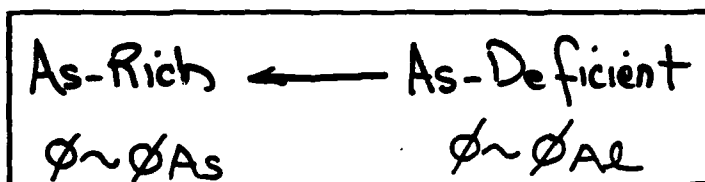
Au



In

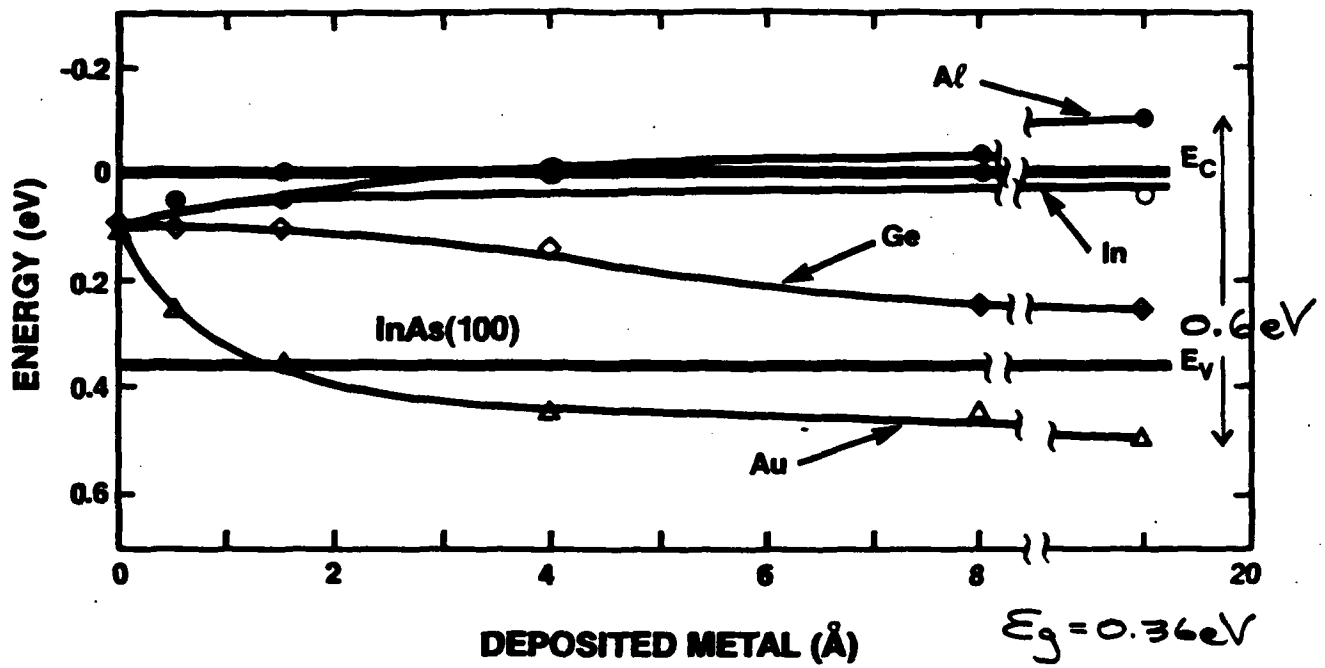


Al



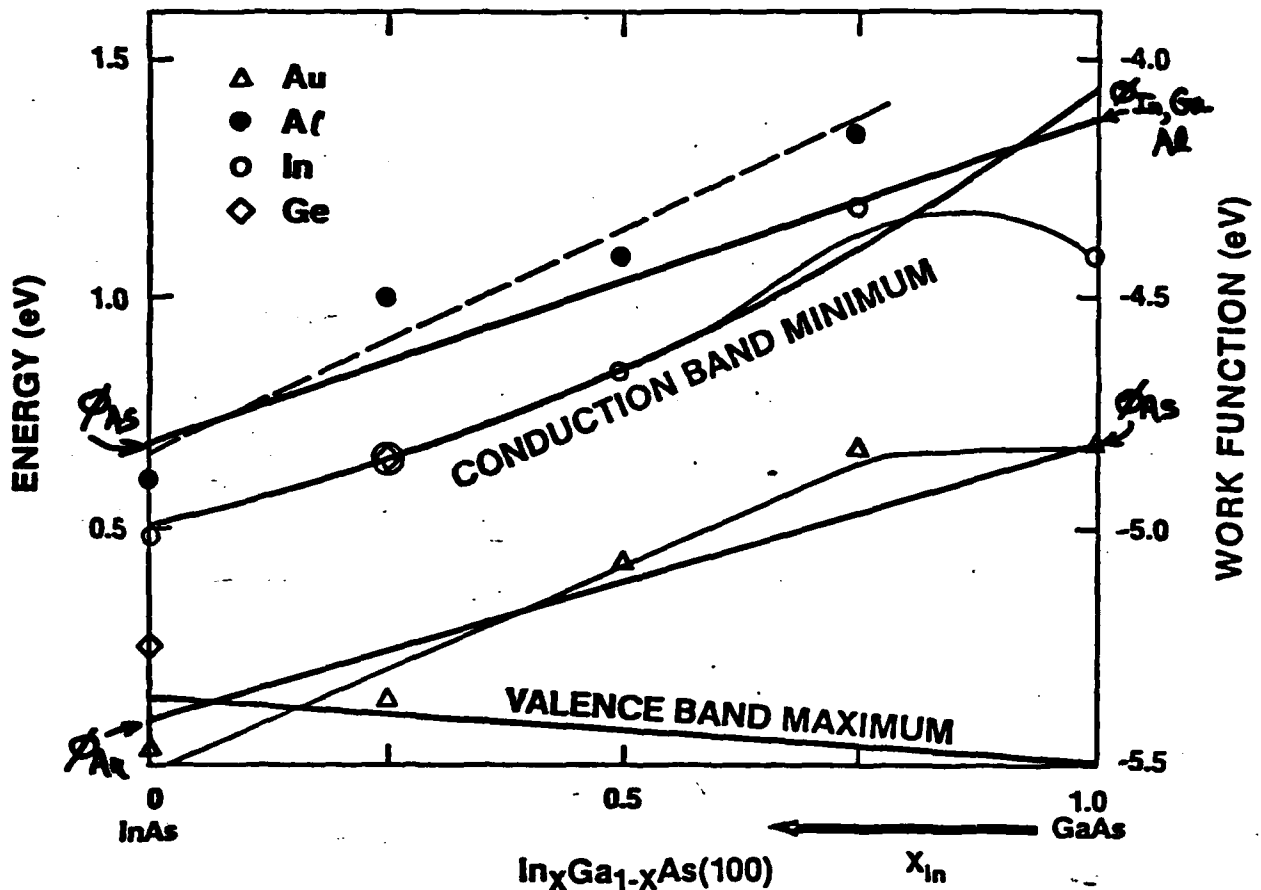
InAs     $In_xGa_{1-x}As$     GaAs

## Fermi Level Movement With Metal Deposition - InAs(100)



- Wide Range of  $E_F$  Stabilization
- $E_F$  Movement Above Monolayer Coverage

# $E_F$ Stabilization Energies For Metals on $\text{In}_x\text{Ga}_{1-x}\text{As}$ (100)

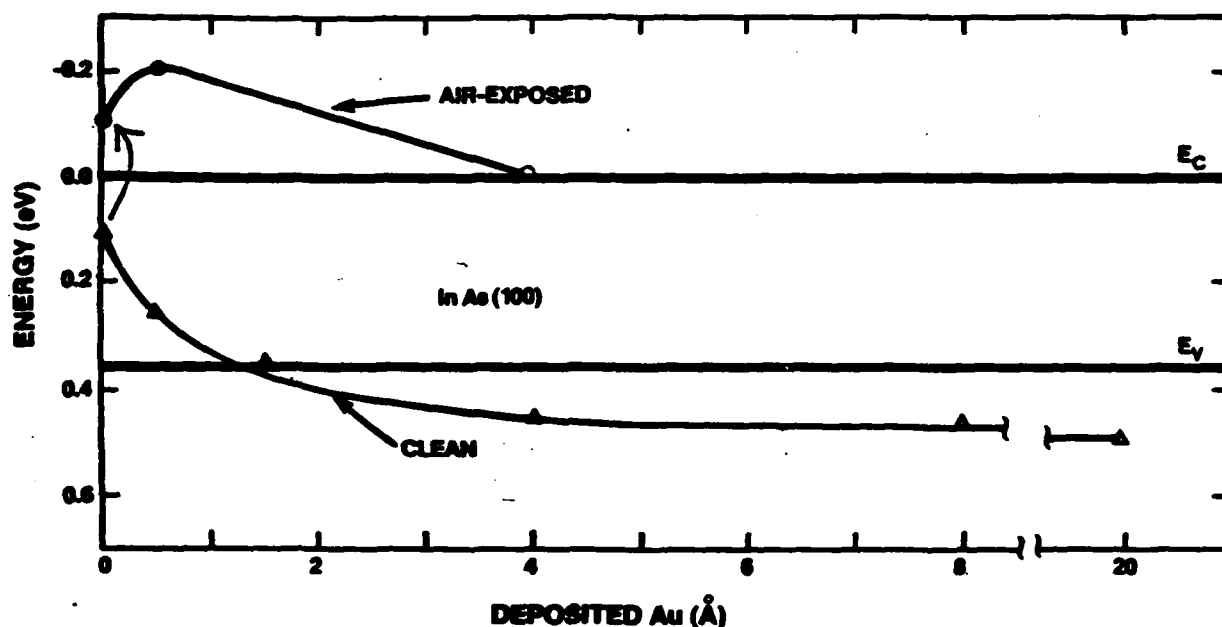


- $E_F$  Not "Pinned"
- Regular Trends Across Alloy Series
- Tracking With Conduction Band
- Air - Exposed Surfaces: Different

Appl. Phys. Lett.,  
in press  
48, 1458 (1986)

## Influence of Air Exposure - In As(100)

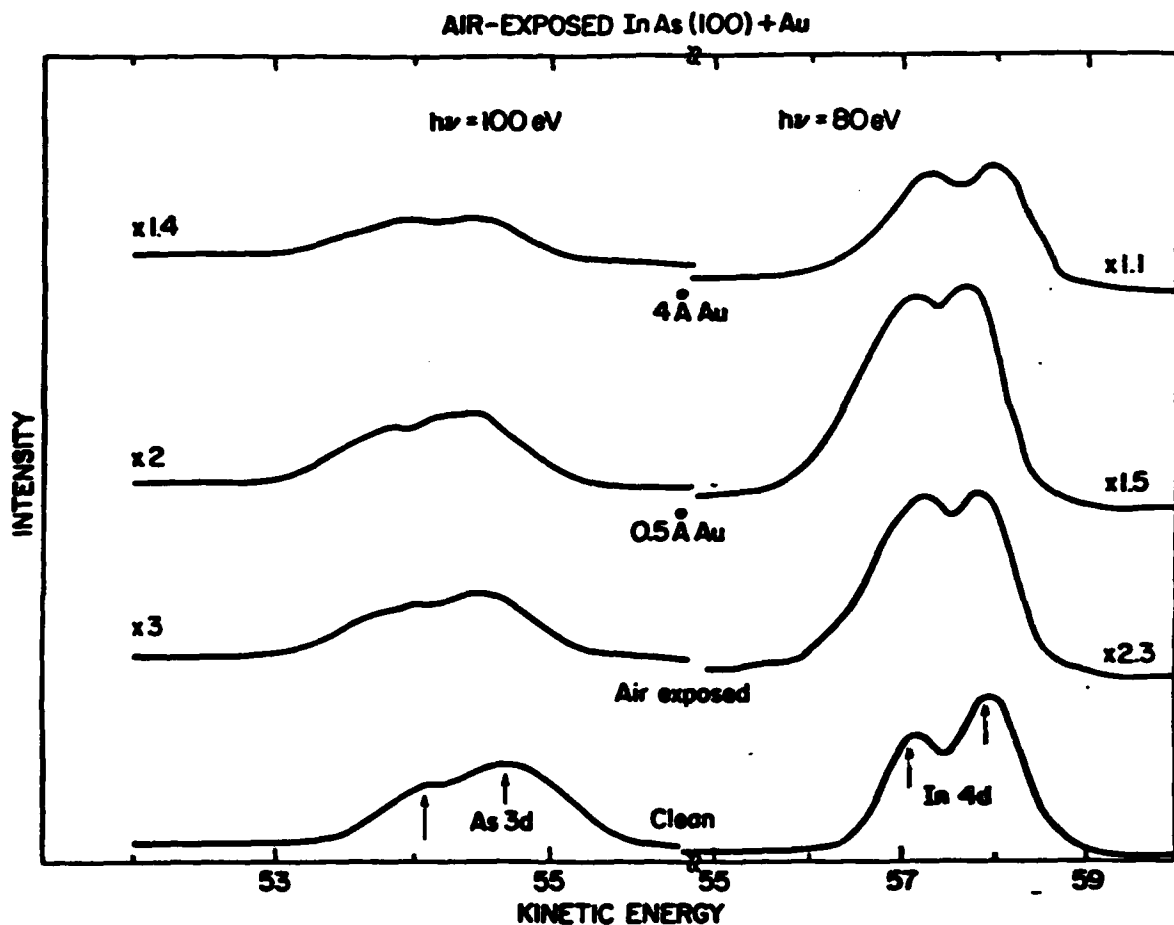
All Initial Surfaces: Clean, Ordered



- Major Changes With Air Exposure
- Accounts For Previous Electrical Data

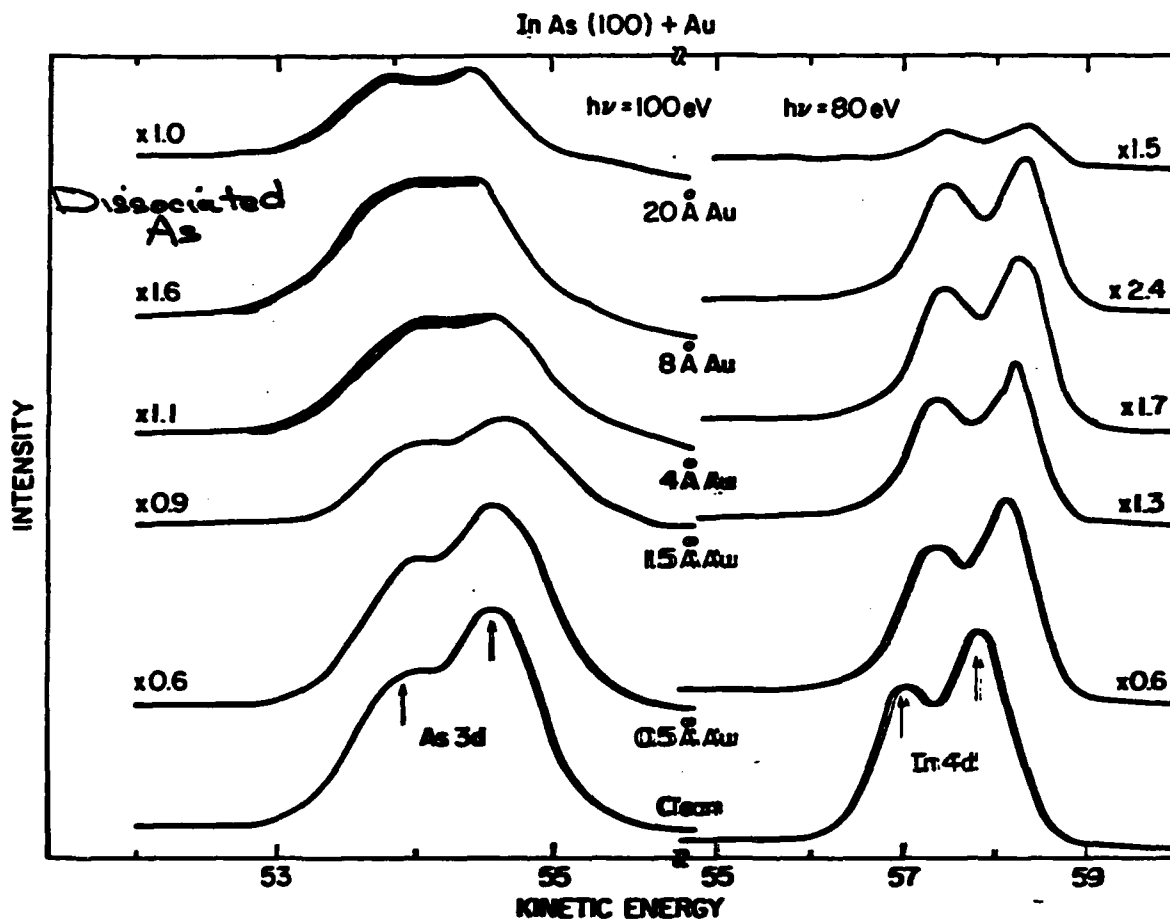


# Effect of Air Exposure on Au-InAs Interface Dissociation



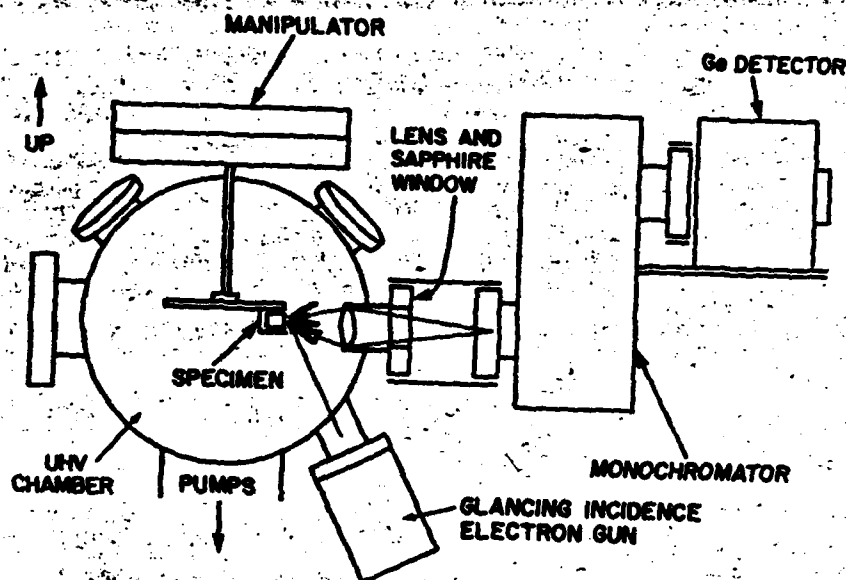
- Little Dissociated. As
- As/In Decreases with Au Coverage
- As outdiffusion Twice as Large for Clean InAs

# Au-InAs Interface Dissociation



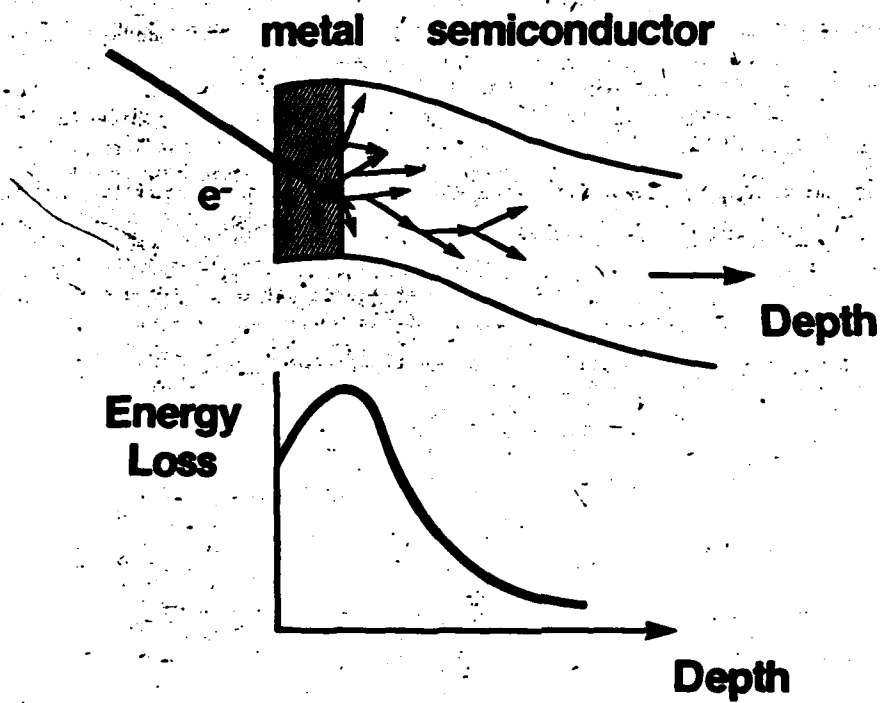
- Significant Dissociated As
- As / In Increases with Au Coverage

# Cathodoluminescence Spectroscopy



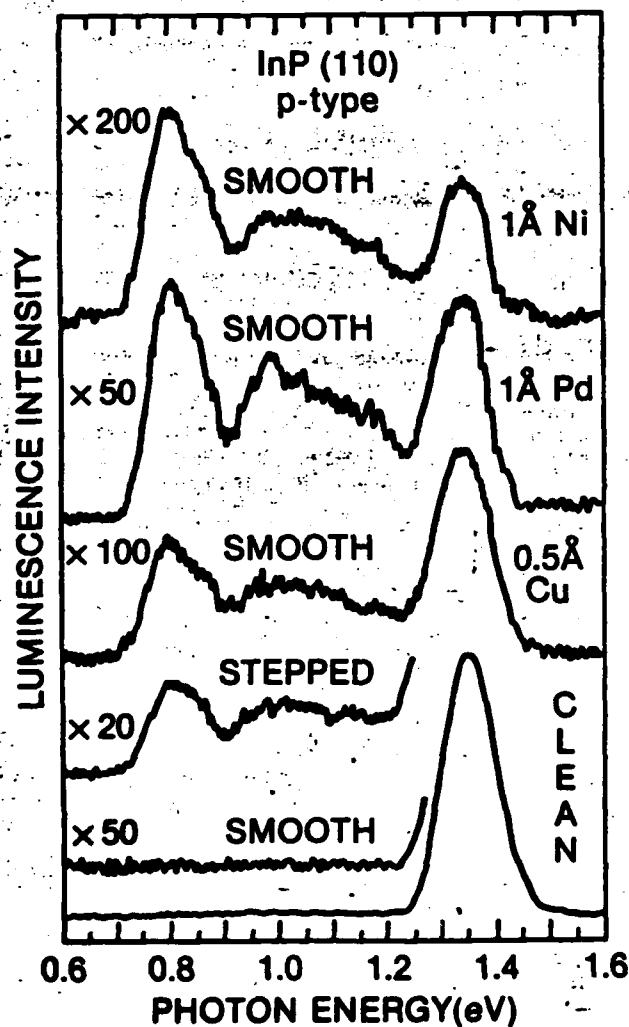
- UHV Surface Preparation
- Low Electron Energy & Glancing Incidence
- IR Sensitivity ( $h\nu > 0.6\text{eV}$ )

## Spatial Range of Interaction



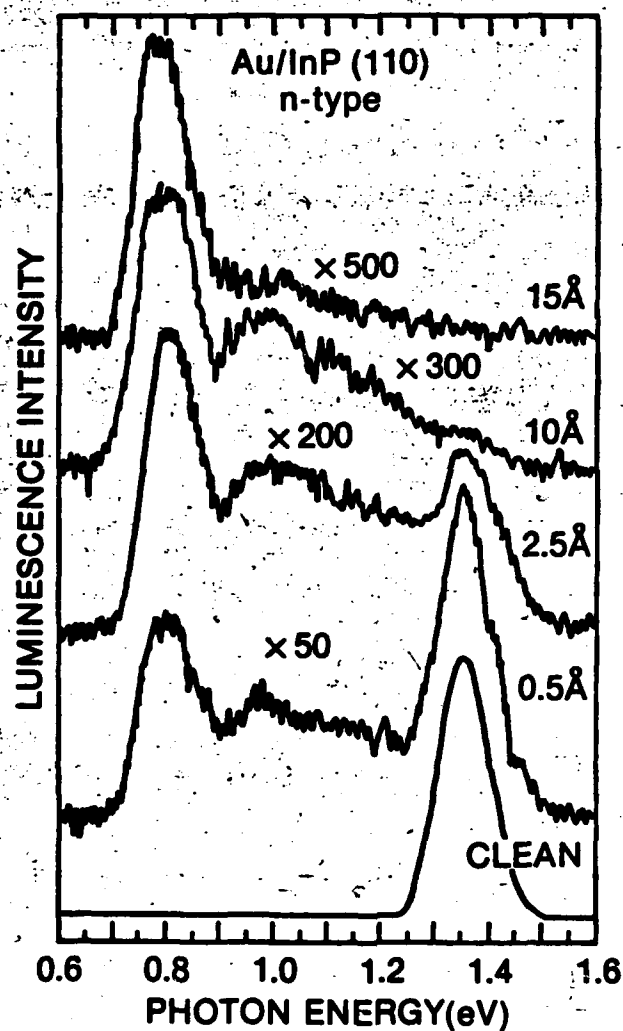
- Near Surface Excitations
- Depth Resolution

## Extrinsic Interface States: InP (110)



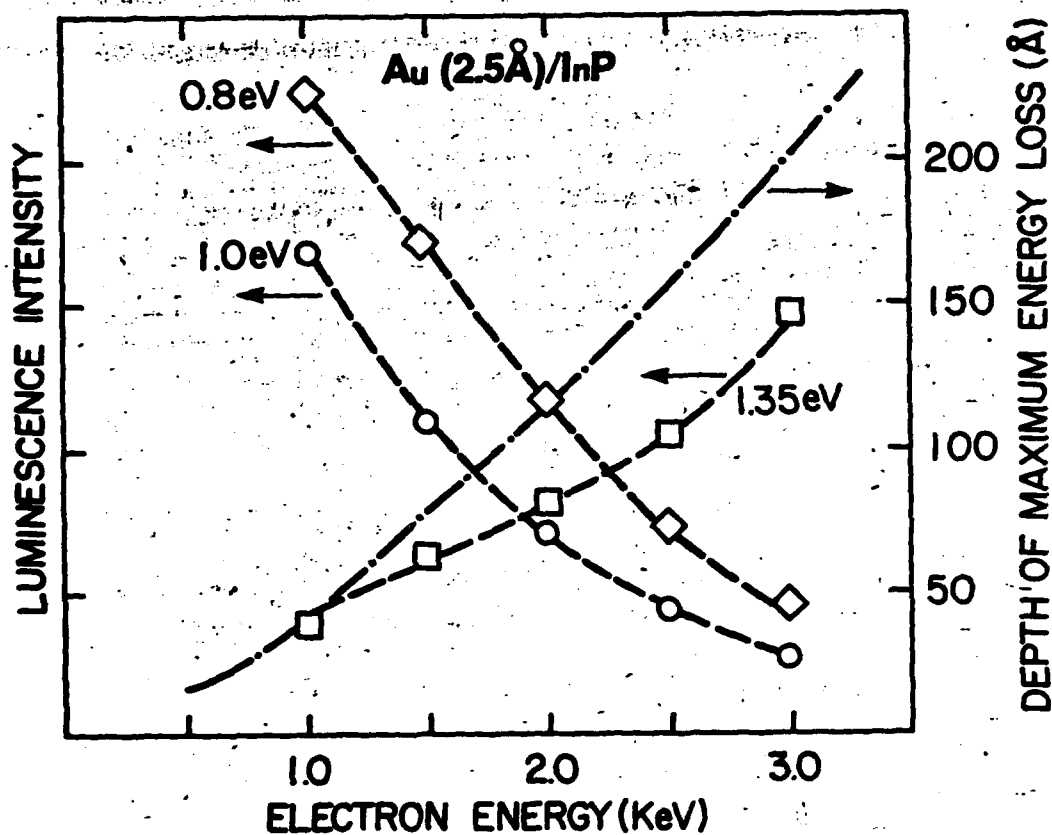
**Submonolayer Metal Deposition & Cleavage Steps  
Produce Broken Bonds**

## Spectral Shape vs Multilayer Metal Deposition: Au/InP



**0.78 eV Peak Dominates  
at Multilayer Coverage**

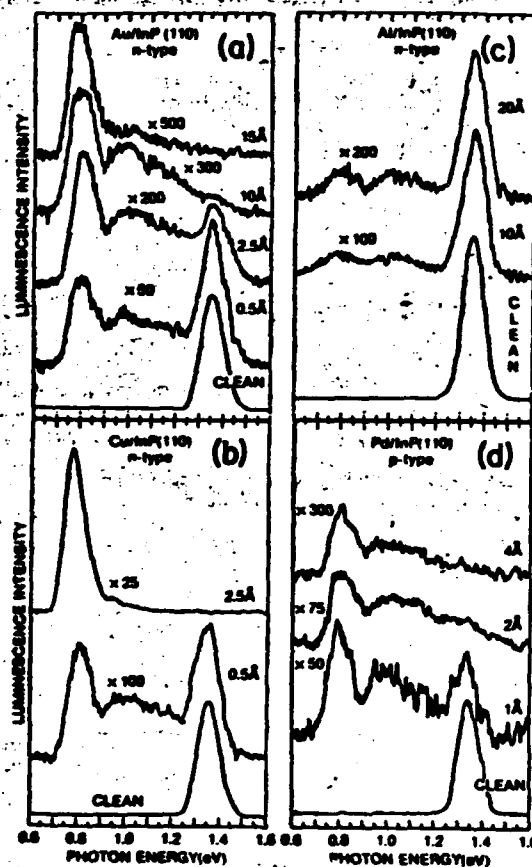
## Depth Resolved CLS



- Near Surface Localization of Recombination Centers

- "Buried" Interfaces

# Optical Emission from Metal-Induced States

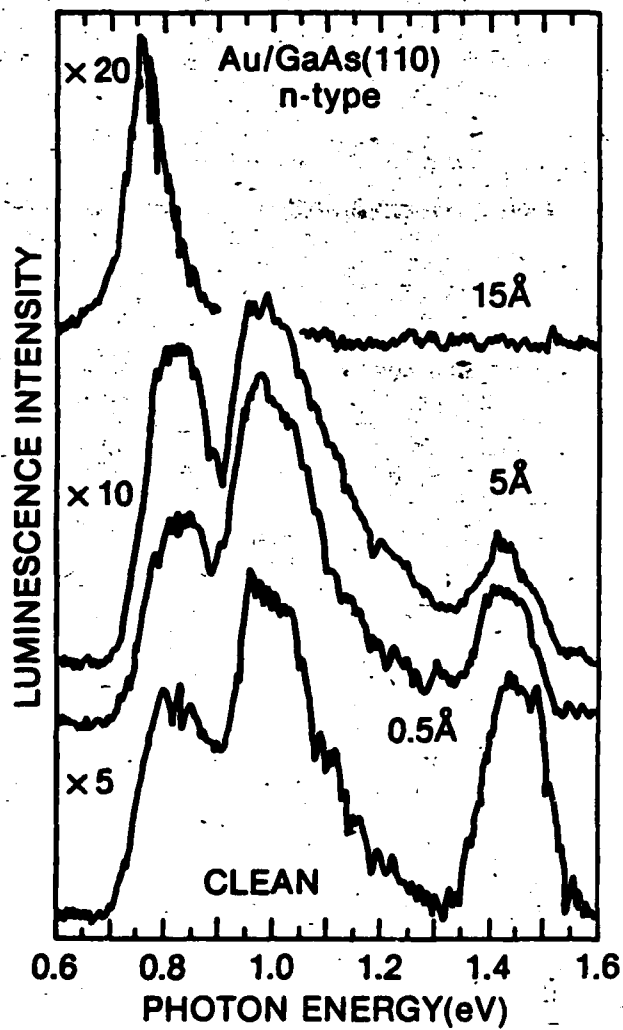


C. Viturro et al.,  
Phys. Rev. Lett.  
57, 487 (1986)

- Deep Level Interface States
- Multilayer Coverage Evolution
- Band Bending Correlation

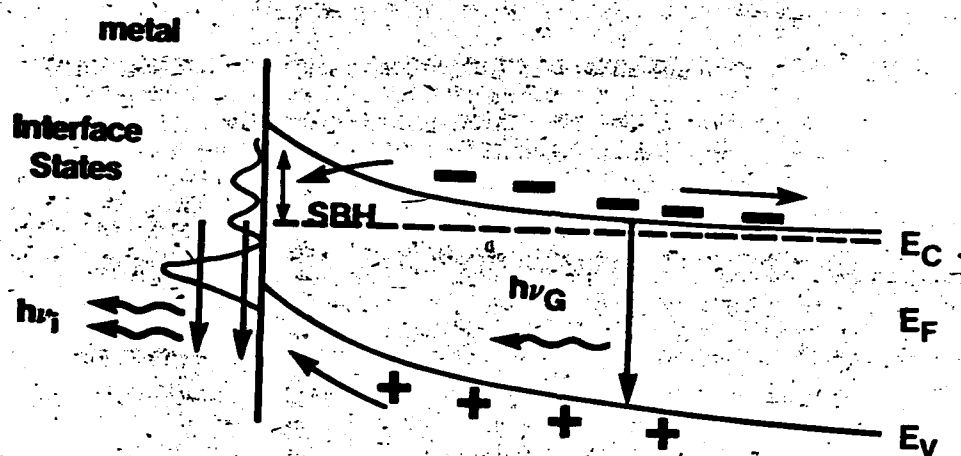


## Metal-Induced vs Bulk Trap States



- Metal-Induced States Dominate at Multilayer Coverage

## Correlation with Schottky Barrier Heights



InP (110) n-type

Metal

Schottky Barrier

$E_G - h\nu_i$

Au, Cu  
Al

~ 0.5eV  
0-0.25eV

0.57 eV  
0, 0.2-0.5 eV

GaAs (110) n-type

Au

0.8-0.9eV

0.7 eV

## CONCLUSIONS

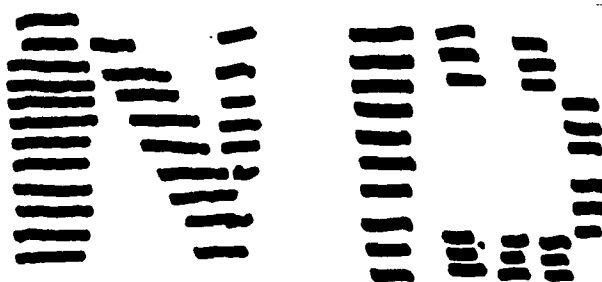
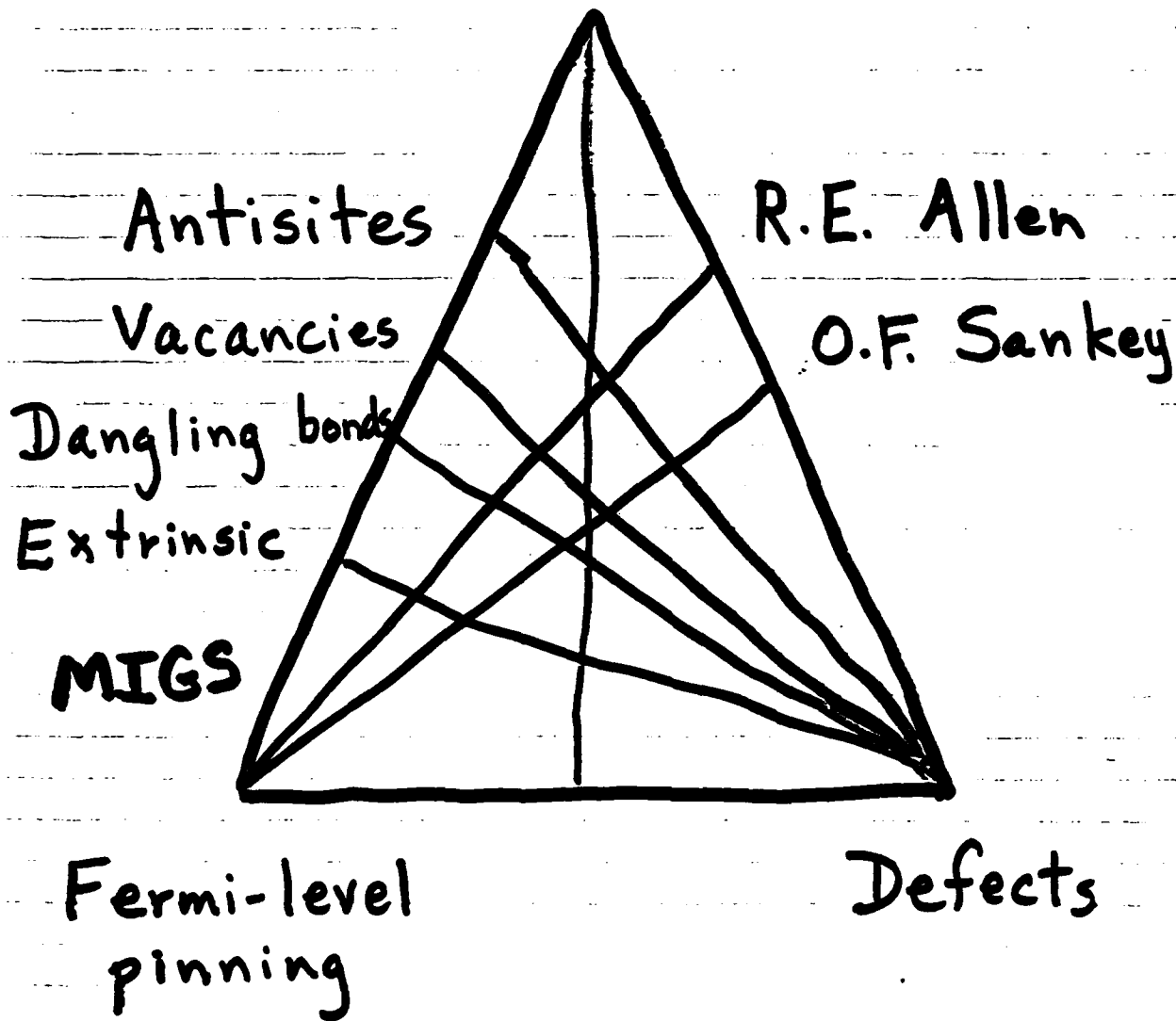
- METAL DEPENDENT CHEMICAL TRENDS ACROSS  $\text{In}_x\text{Ga}_{1-x}\text{As}$  ALLOY SERIES
  - CHEMICALLY-MODIFIED WORK FUNCTION MODEL
  - EFFECTS OF AIR EXPOSURE
- 
- DIRECT OPTICAL EMISSION FROM INTERFACE STATES
  - METAL, MORPHOLOGY, MONOLAYER AND MATERIAL DEPENDENCES
  - SPECTRAL CORRELATION WITH ELECTRONIC AND CHEMICAL STRUCTURE

Antisite Defects and Schottky Barriers

Jack Dow

Notre Dame University

# Schottky barriers



# OUTLINE

① Schottky barriers are due to Fermi-level pinning by surface deep levels (Bardeen)

② Native defects (formed during deposition of metal contact) provide the pinning levels (Spicer).

③ Chemical reactions can determine which defects are dominant (Brillson)

④ In III-V's, normally  
antisites  
vacancies  
extrinsic

Co-authors:

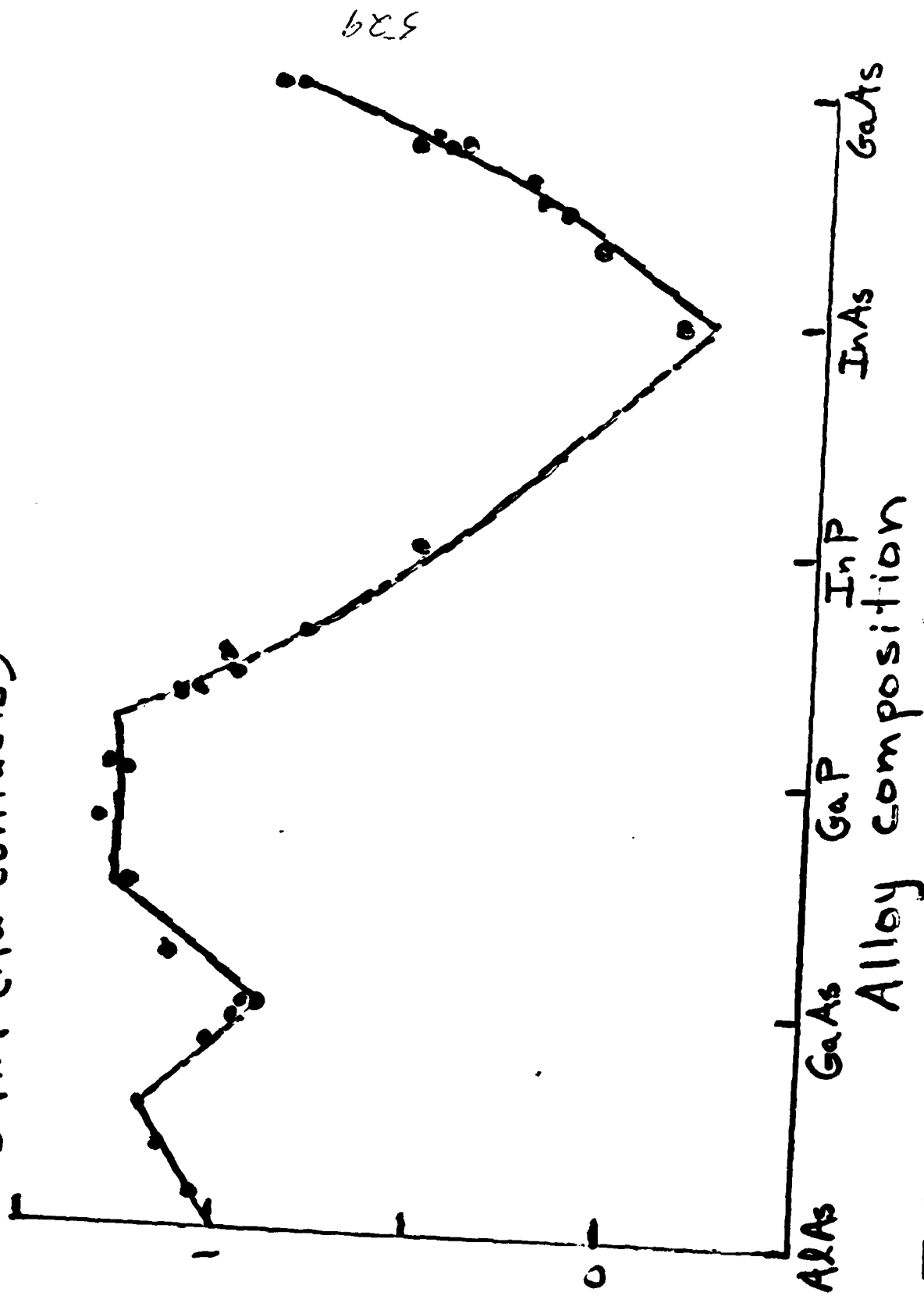
R.E. Allen

527

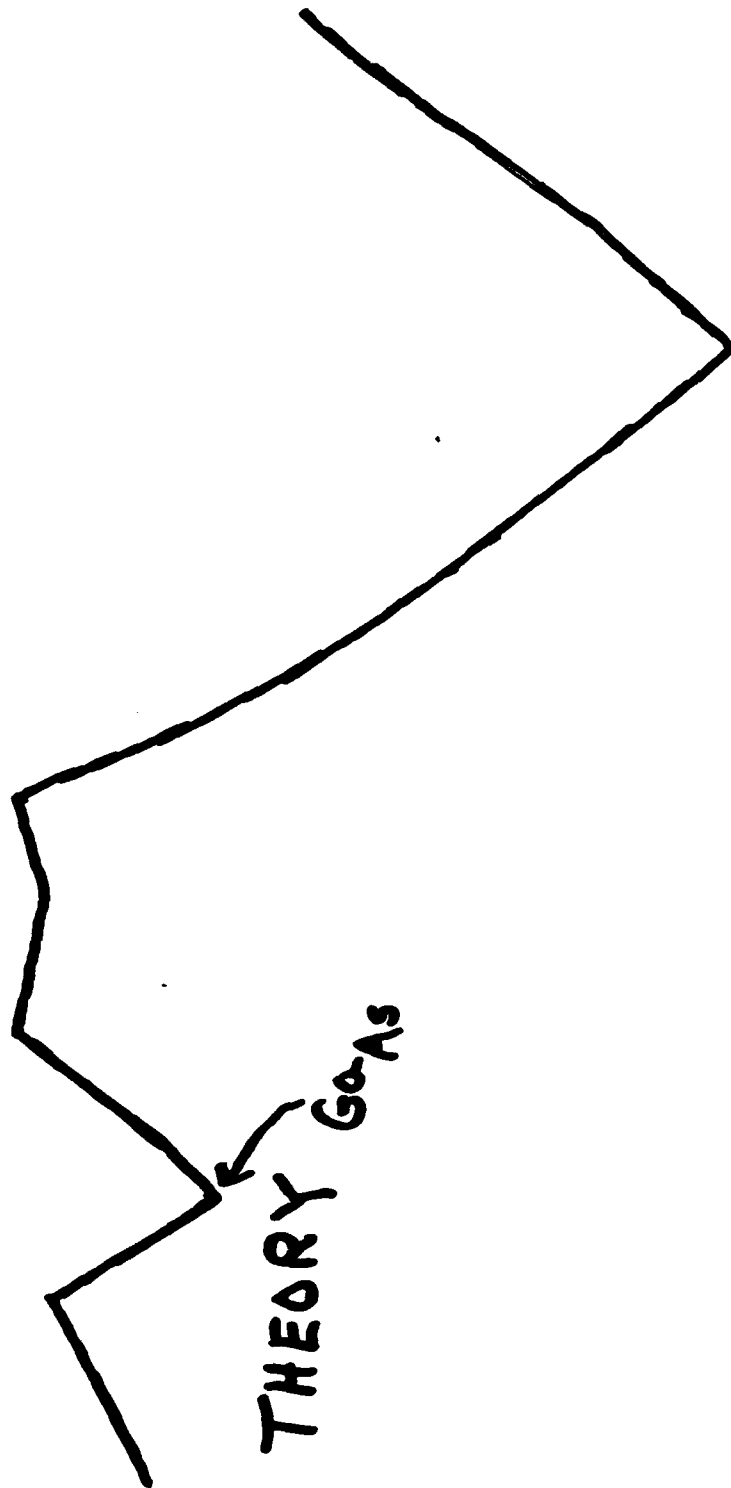
O.F. Sankey

Schottky Barrier Height (eV)

DATA (Au contacts)



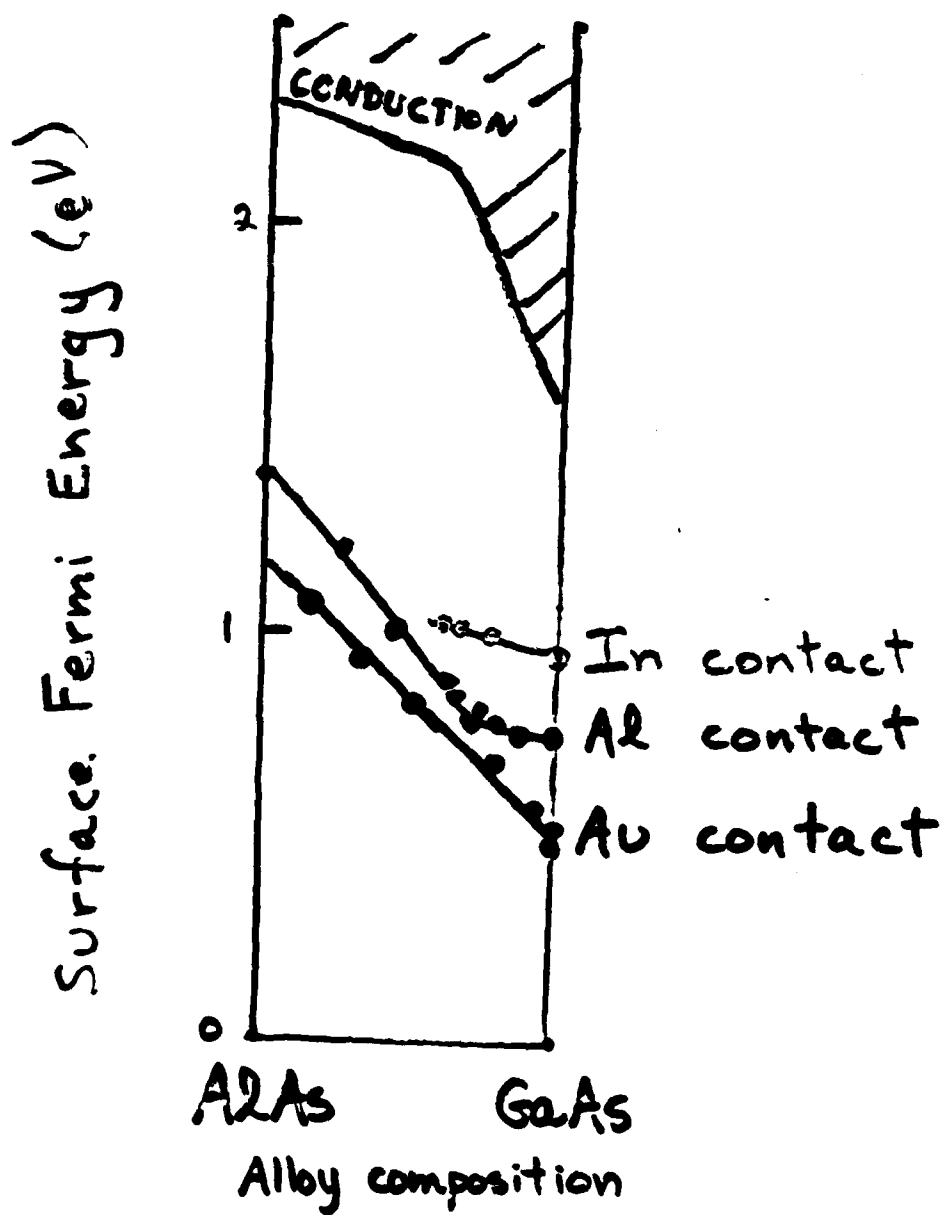
530



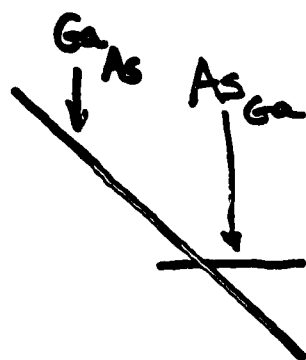
THEORY GO-As



Dependence  
on contact



THEORY



Ga As

---

—

Ga<sub>As</sub>

—

—●—●—

As<sub>Ga</sub>

—

—●—●—

DATA

---

Explains:

① # Donors  $\approx$  # Acceptors (Mönch)

$$\begin{array}{ccc} \text{---} & = & \text{---} \\ \text{or} & & \\ \# \text{Ga}_{\text{As}} & \approx & \# \text{As}_{\text{Ga}} \end{array}$$

② Chemisorption defect  $\neq$  cleavage defect  
 $\text{Ga}_{\text{As}} \neq \text{As}_{\text{Ga}}$  (Mönch)

③ Abrupt change of barrier  
at  $T_{\text{anneal}}$  (antisite); (Mönch)

a) p-barrier ---  $\text{As}_{\text{Ga}}$

b) n-barrier remains ---  $\text{Ga}_{\text{As}}$

④ Surface levels  $\neq$  bulk levels

All impurities produce

a)  $\infty$  shallow levels if  $\Delta z \neq 0$

b) 4 deep levels if s. p-bonded

Deep:  $V_{\text{central-cell}}$

Shallow:  $-\frac{\Delta z e^2}{\epsilon r}$

SHALLOW  
IMPURITY

————  $T_2(p)$   
————  $A_1(s)$

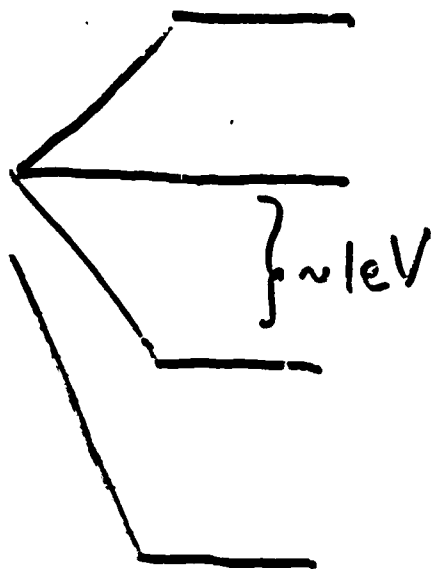
DEEP  
IMPURITY

————  $T_2(p)$

$E_{gap}$  ————— CONDUCTION  
Shallow

————  $A_1(s)$   
deep

○ ————— VALENCE

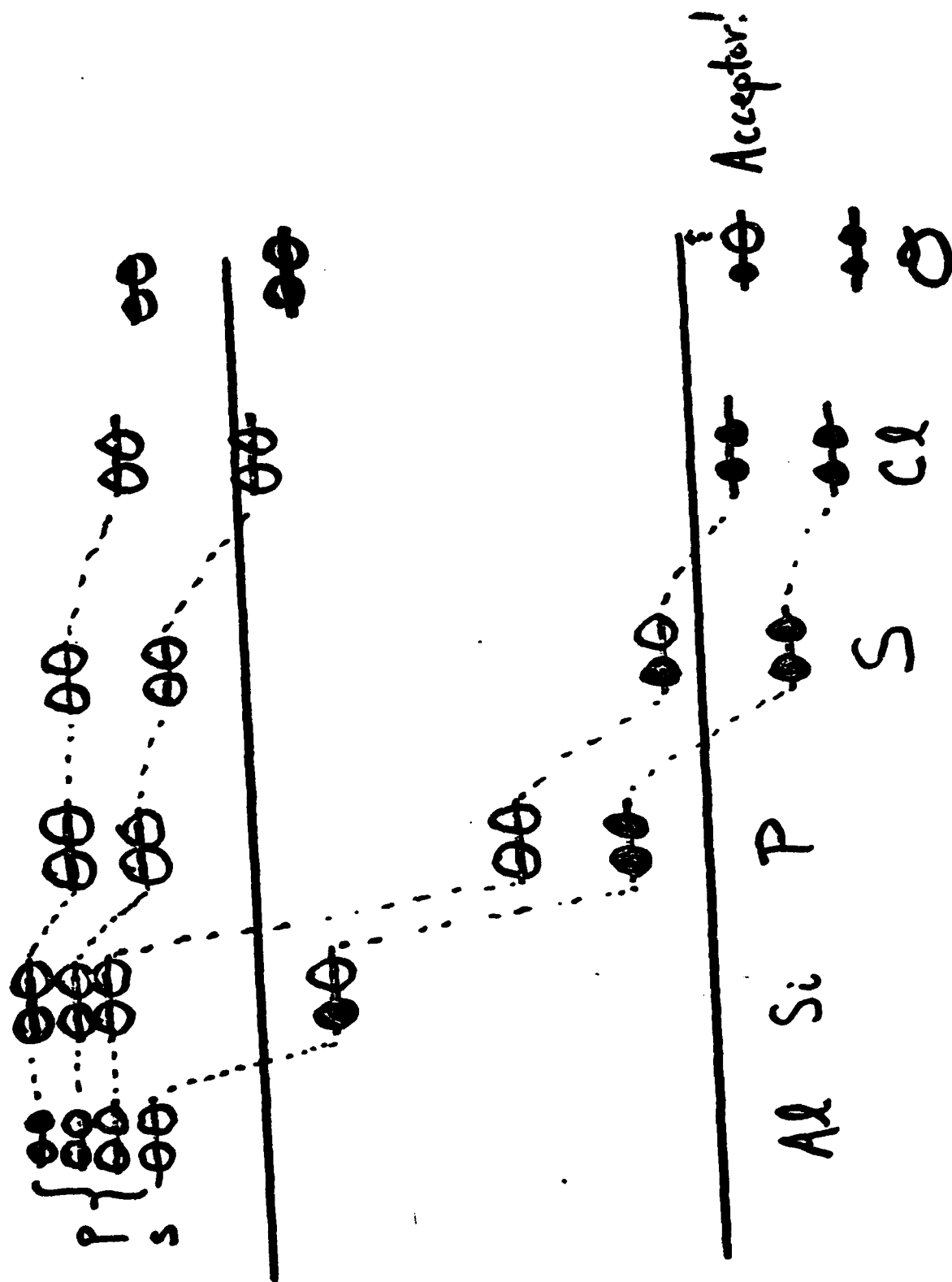


SURFACE  
or other  
non- $T_d$

Surface levels  $\neq$  bulk levels



# Surface Ga site: Doping anomaly



## PART II:

Si/Transition-metal silicide

Schottky barriers

O.F. Sankey, R.E. Allen, + J.D. Dow  
Solid State Commun. 49, 1 (1984).

### FACTS:

(A) On  $\sim 1\text{eV}$  scale, barrier is independent of

- i) transition metal ( $\text{Ni}$ ,  $\text{Pt}$ ,  $\text{Pd}$ )
- ii) crystal structure ( $\text{NiSi}$ ,  $\text{NiSi}_2$ ,  $\text{Ni}_2\text{Si}$ )
- iii) Si surface
- iv) stoichiometry

(B) On  $\sim 0.1\text{eV}$  scale barrier depends on

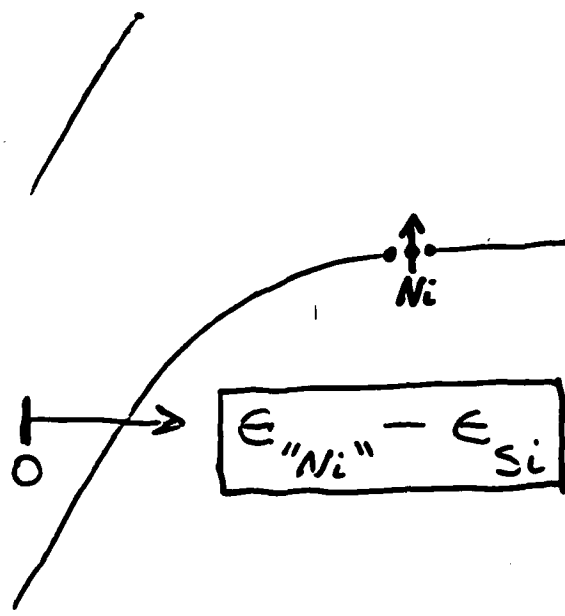
- i) transition metal ( $\sim \epsilon_{\text{atomic}}$ )
- ii) crystal structure

(C) Barrier forms with  $< 1$  monolayer of transition metal

(D)  $\phi_n + \phi_p \approx E_{\text{gap}}$

(E) Si is similar to III-V's

$Ni$   
 $- \epsilon_{s,p}$



No crossing  
 makes level  
 independent  
 of  $Ni$ , etc

$Ni$   
 $- \epsilon_d$

CONDUCTION

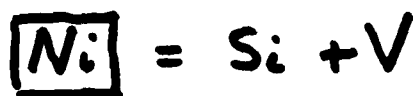
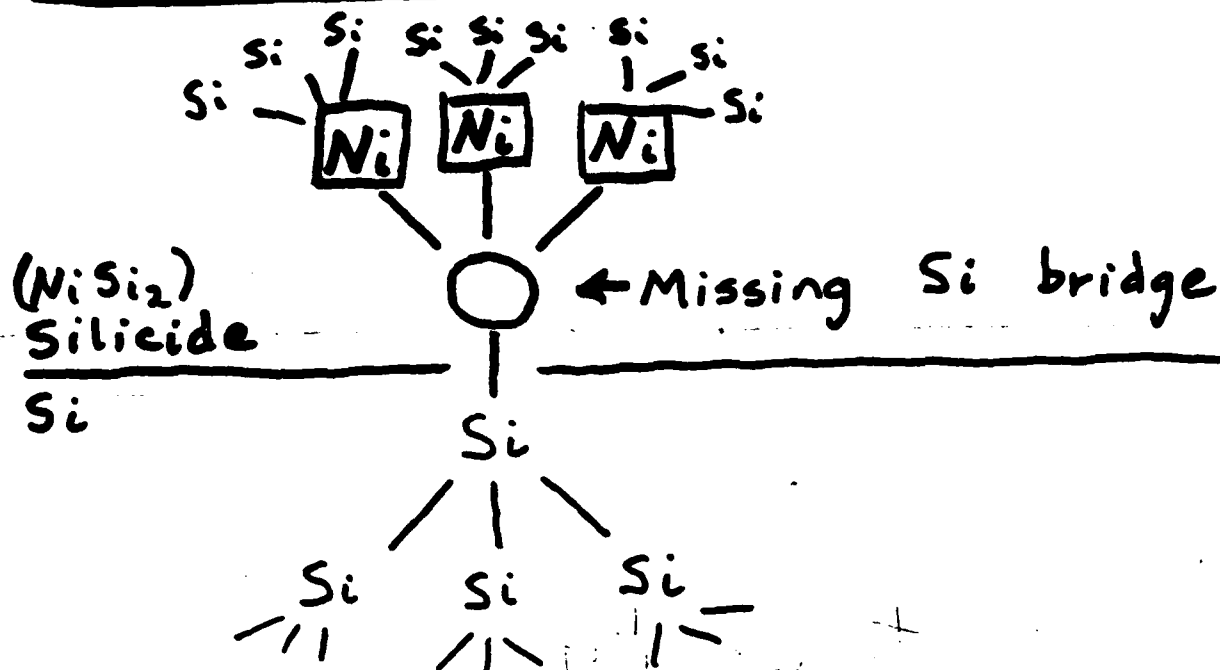
$V_{Si}(T_2)$  —

VALENCE

$V_{Si}(A_1)$  —

# Schottky barriers in silicides

---



Si/T-metal silicide

$\frac{CB}{\frac{\phi}{VB}}$

Schottky barriers  $\phi$

- ①  $\phi$  independent of T-metal on 1eV scale (Ni, Pt, Pd)
- ②  $\phi$ : chemical trends with T-metal on 0.1eV scale
- ③  $< 1$  monolayer of T-metal gives  $\phi$
- ④  $\phi$ : independent of crystal structure (on  $> 0.1$  eV scale):  $NiSi$ ,  $NiSi_2$ ,  $Ni_2Si$ .
- ⑤  $\phi$ : independent of stoichiometry, Si surface (on  $> 0.1$  eV scale)
- ⑥  $\phi_n + \phi_p \approx E_{gap}$
- ⑦ Si is similar to III-V's.

# Summary

- ① Fermi level pinning  
(Bardeen)
- ② By defects at interface
  - Antisites: III-V/non-reactive
  - Vacancies: III-V/reactive
  - Dangling bonds: Si/TM silicide
  - Extrinsic: n-InP: S, Sn(Spicer)
- ③ Chemical reactions  
produce various defects  
(Brillson)
- ④ New field: surface defect  
spectroscopy

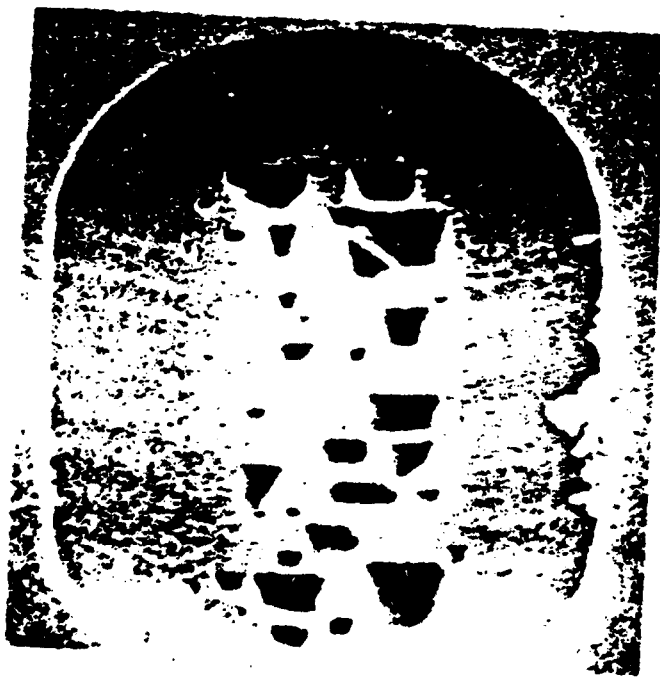
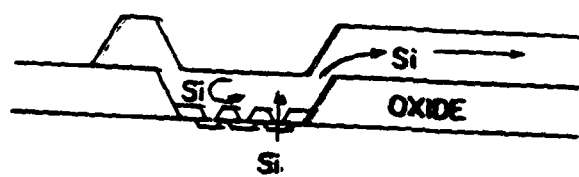
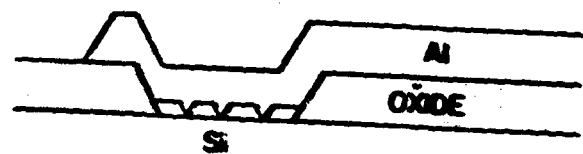
Scattering by barriers

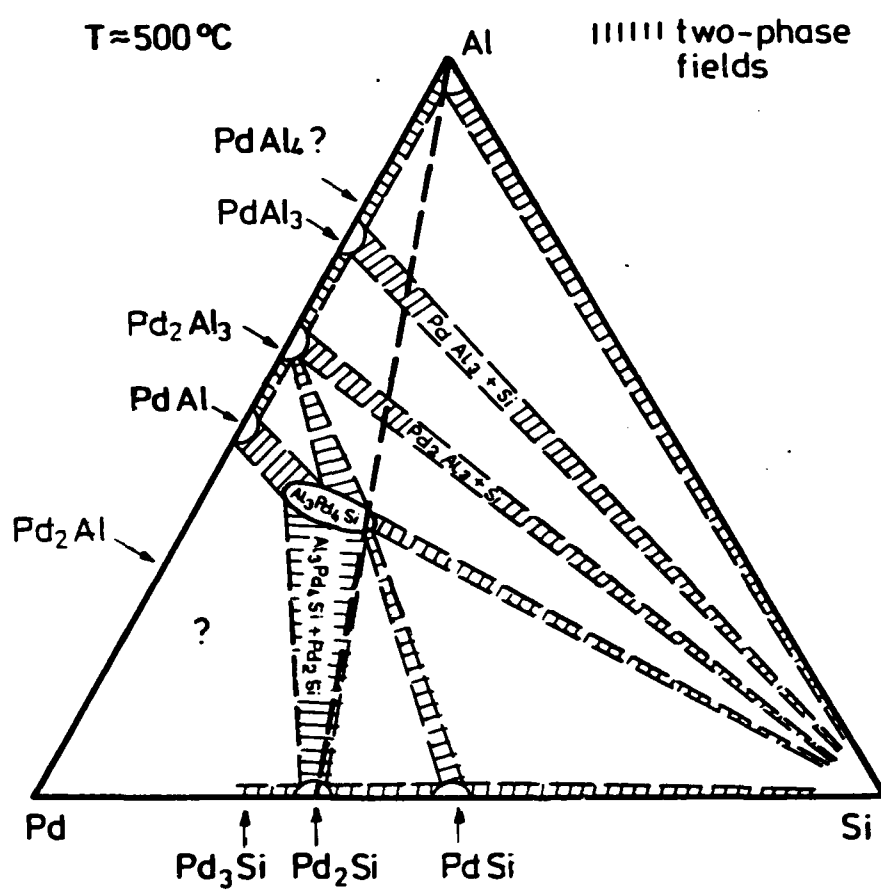
**Direct Measurements of Electronic States  
at Metal/GaAs Interfaces**

**Paul Ho**

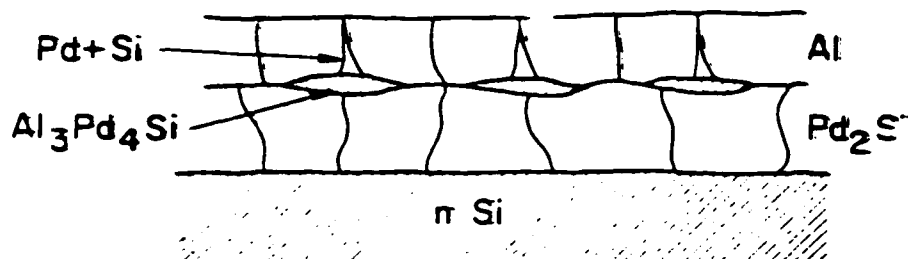
**IBM - Yorktown Heights**



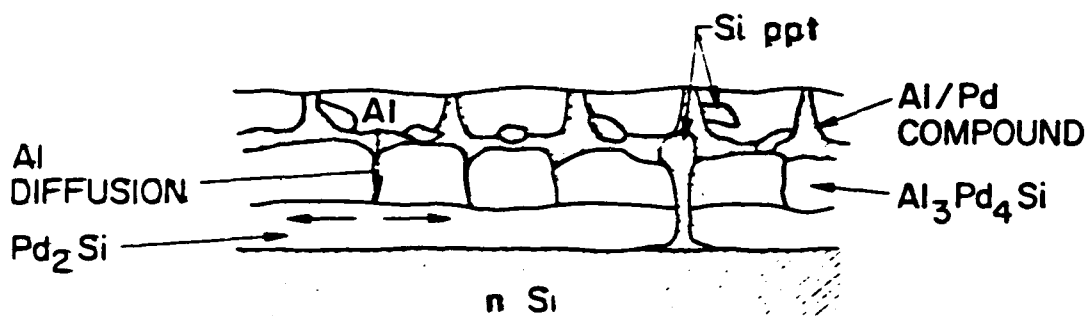




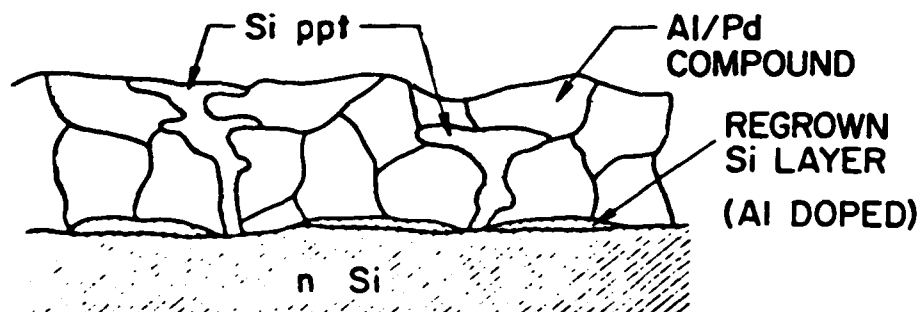
# SCHEMATIC PRESENTATION OF Al/Pd<sub>2</sub>Si/Si REACTION



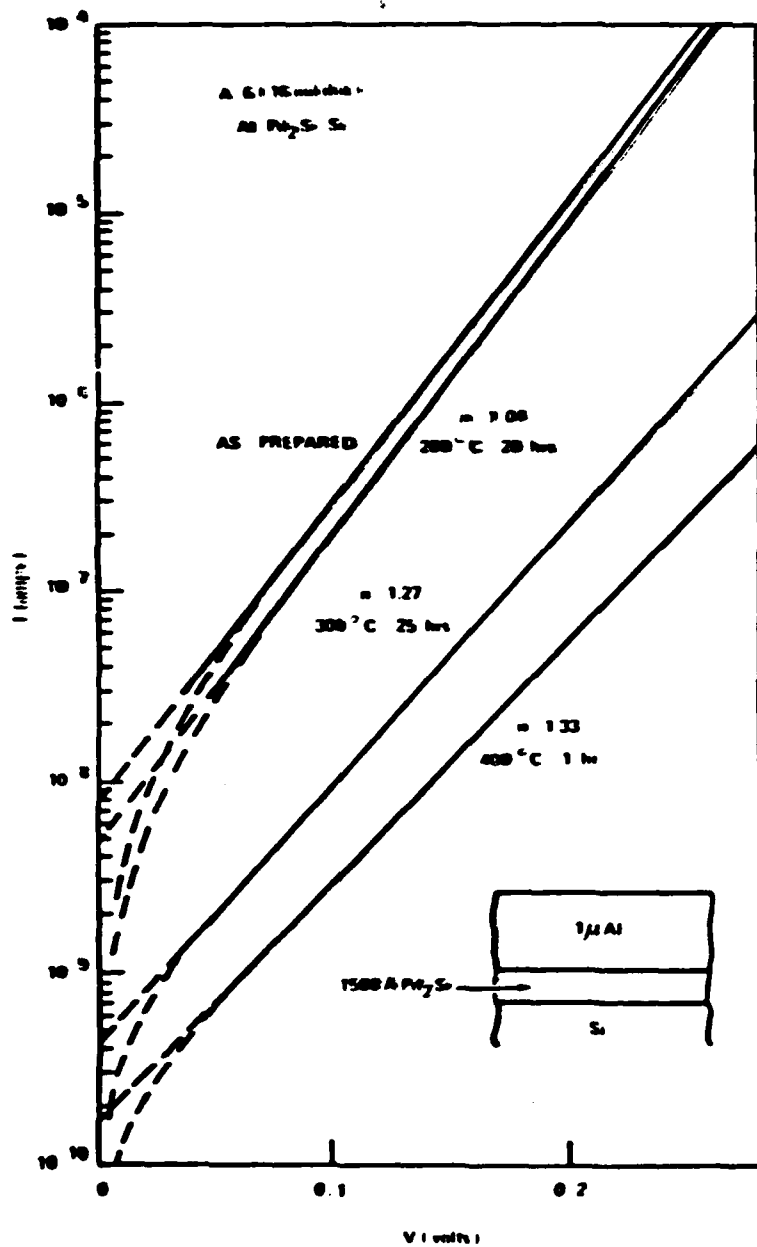
a) INITIAL STAGE



b) INTERMEDIATE STAGE



c) FINAL STAGE



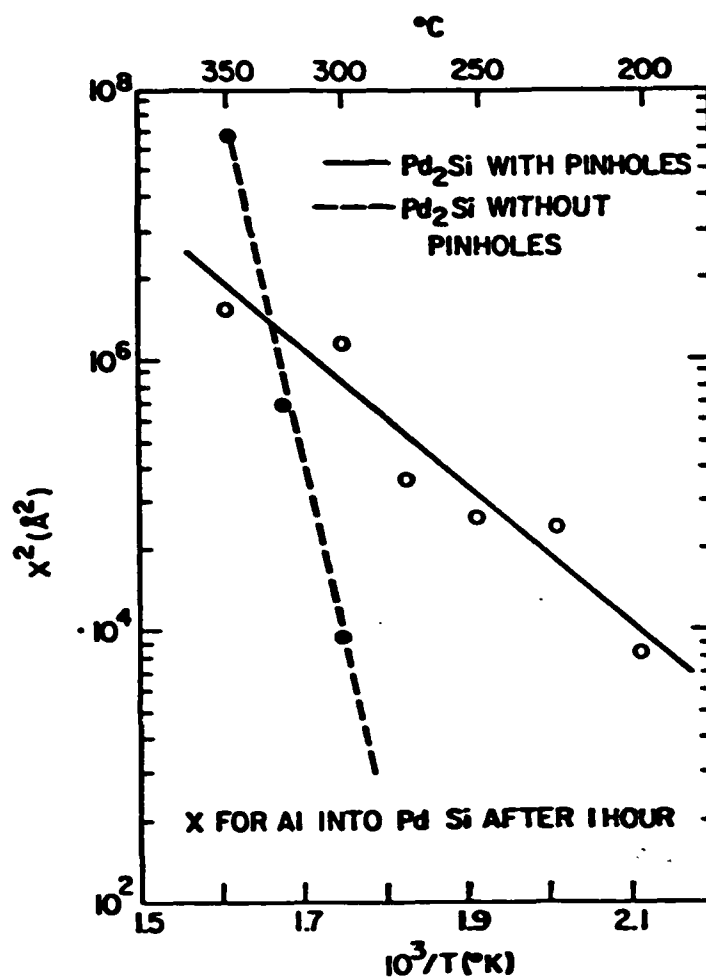


**Fig. 7.** Comparison of the rates of  $\text{Pd}_2\text{Si}$  dissociation in Al/ $\text{Pd}_2\text{Si}$ /Si contacts for polycrystalline  $\text{Pd}_2\text{Si}$  films containing pinholes on Si(111) and pinhole-free on Si(100). The rate of dissociation was measured from the distance  $X$  of Al penetration into  $\text{Pd}_2\text{Si}$ . Data are normalized to 1 hr and plotted vs.  $X^2$  because of the kinetics.

1. Microstructure, e.g. grain boundaries,  
Interface & Layer composition important

KINETICS FACTOR AND CONTROL

2. The thermodynamic tie line is  
a band reflecting the phase field.

$M_xGa_yAs$  particularly relevant to  
the stability.

3. Electrical properties can't be observed  
by TEM or spectroscopy techniques

4. Precipitates (particularly As) on  
the electrical interface important.

COOLING CYCLE !!!

# DIRECT OBSERVATION OF INTERFACE STATES

R. Haight, N. Amer, E. Yang & P. Ho

## GOAL

To study the characteristics of the interface  
states

Energy distribution

In-depth distribution

Dynamic behavior

TRANSPORT PROPERTIES AT JUNCTIONS

SCHOTTKY BARRIER FORMATION

## TECHNIQUES

Laser transient spectroscopy

Time-resolved photoemission

Thin interfaces

High energy resolution. Polarization  
Photothermal spectroscopy

Defect characterization

In-depth sensitivity

Spatial - lateral sensitivity

Transport measurement

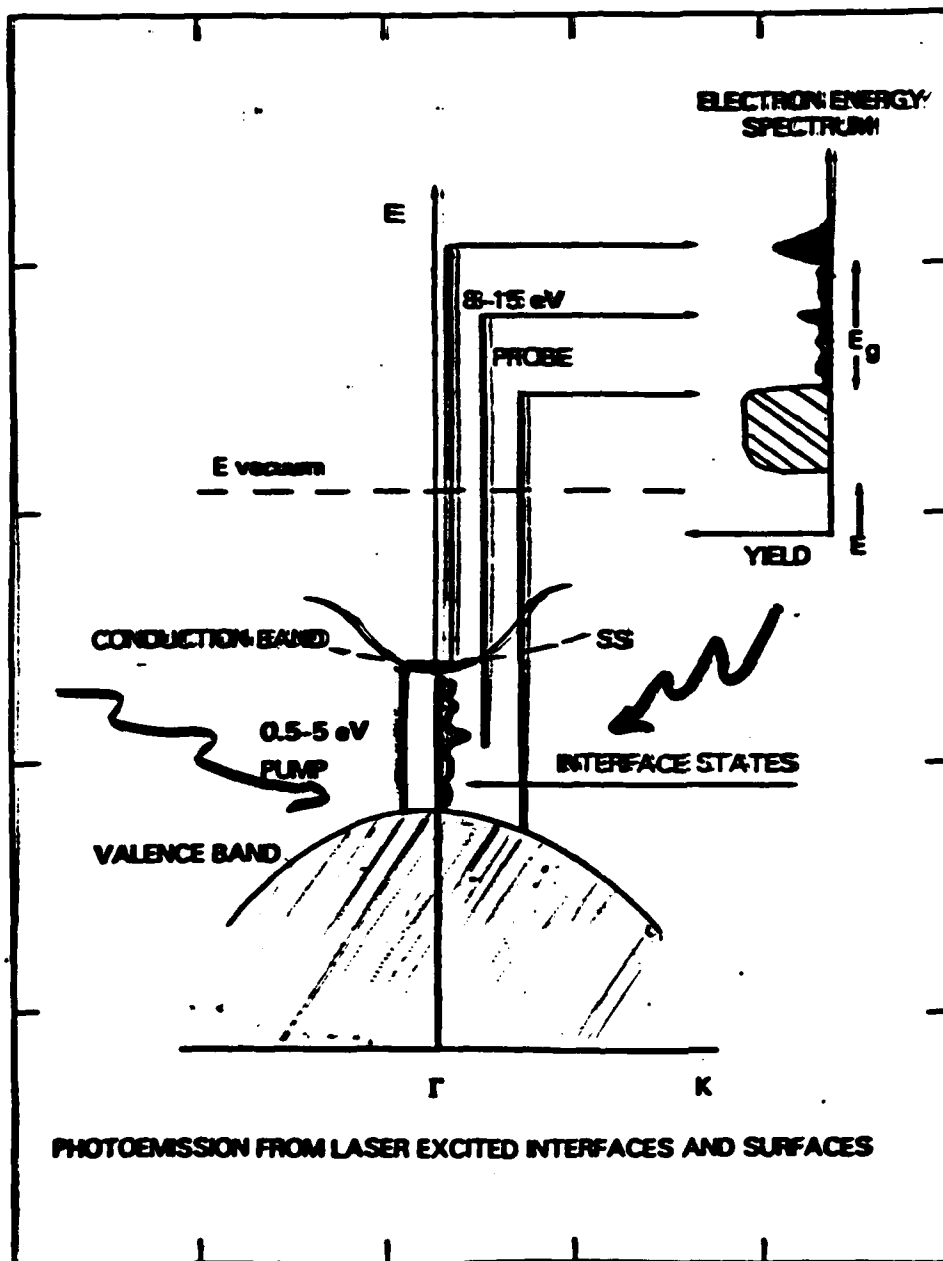
Accurate phase capacitance spectroscopy

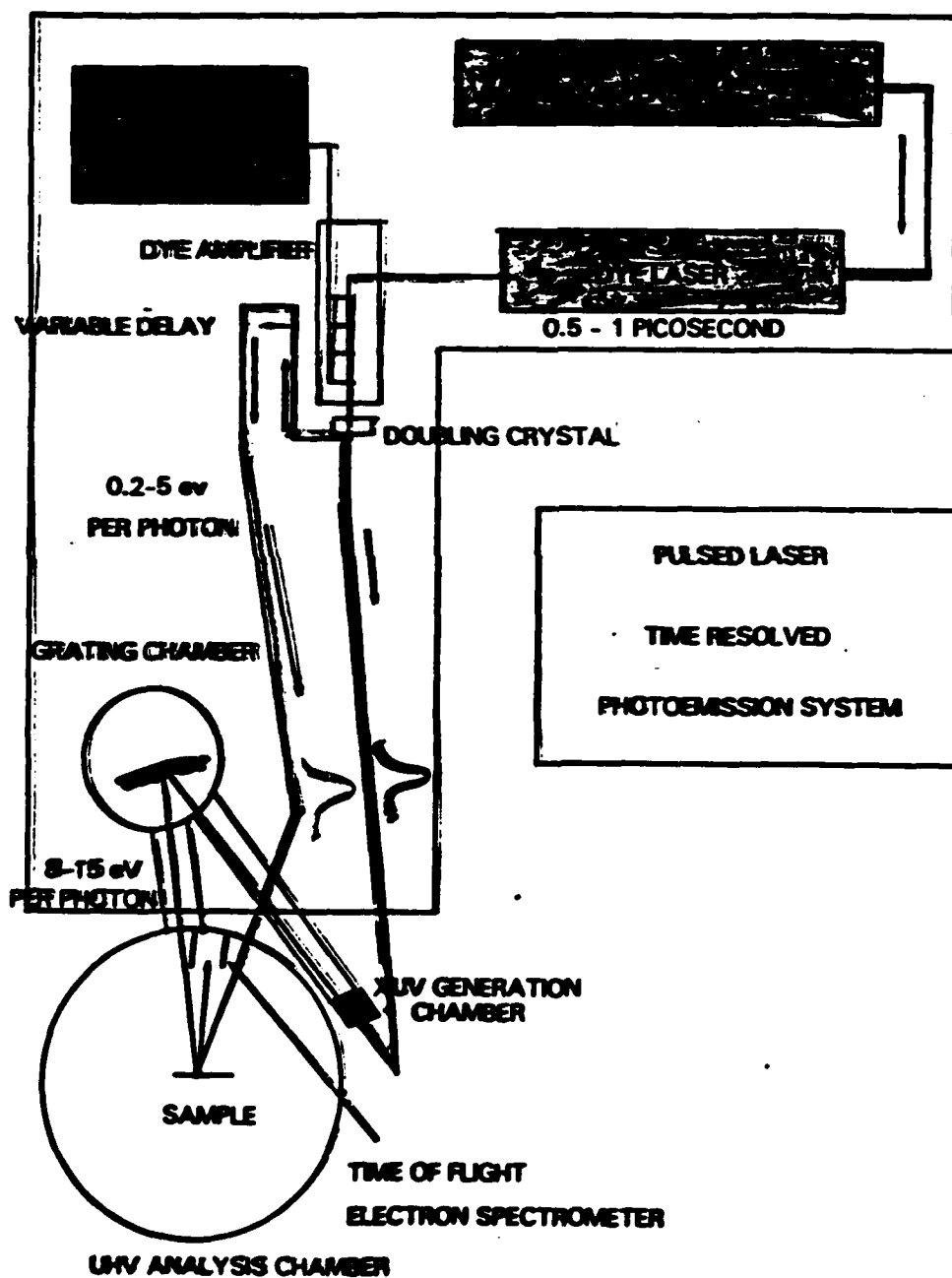
Buried interface

Charge transport at interface.

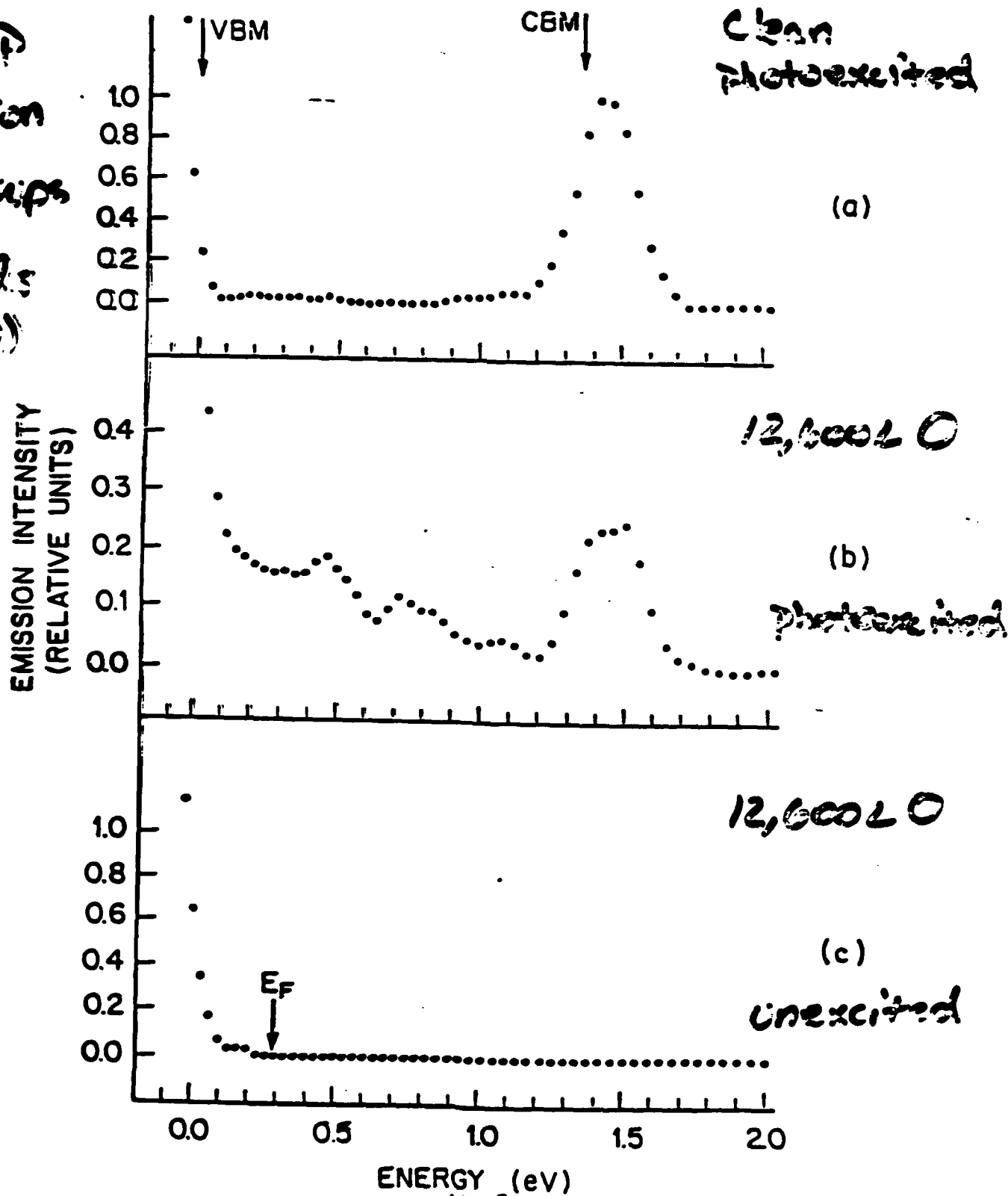
ALL ARE DYNAMIC TECHNIQUES 555







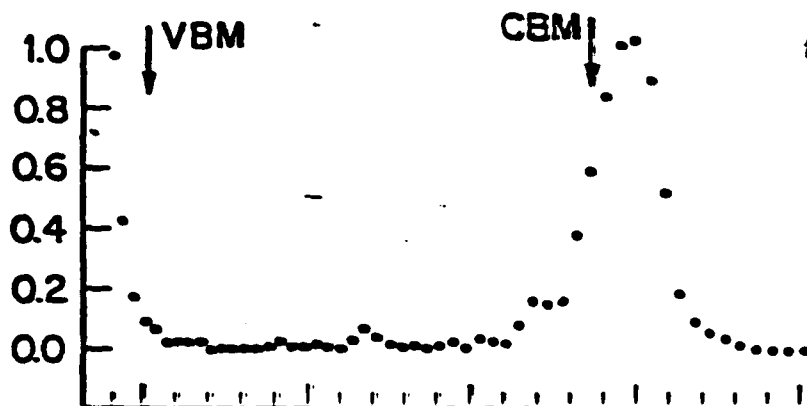
gap  
region  
occupies  
7.25  
(110)



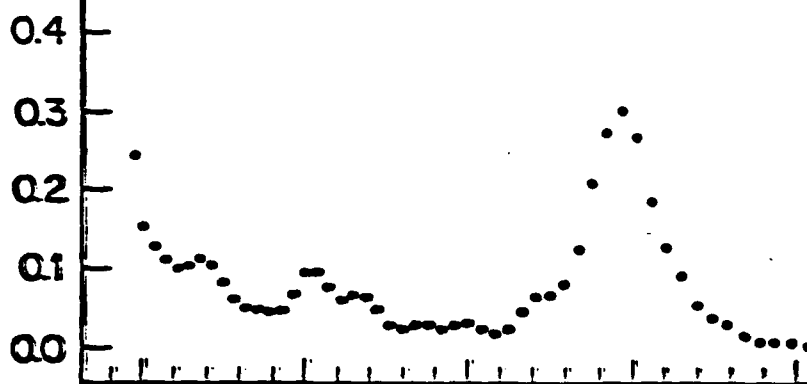
gap  
region  
fluctuations

gaps  
(110)

EMISSION INTENSITY  
(RELATIVE UNITS)

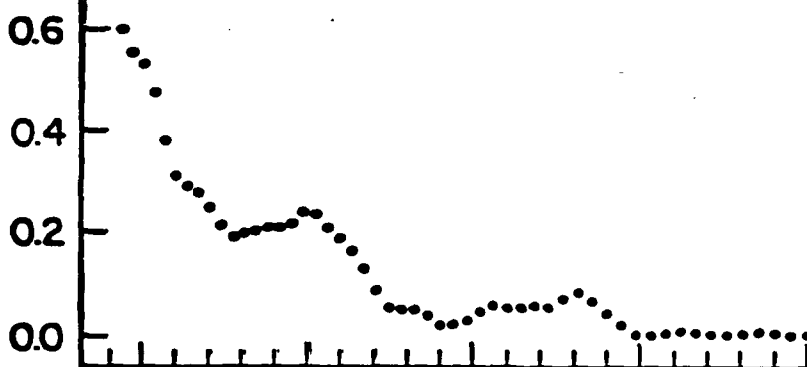


Clean  
photoexcited



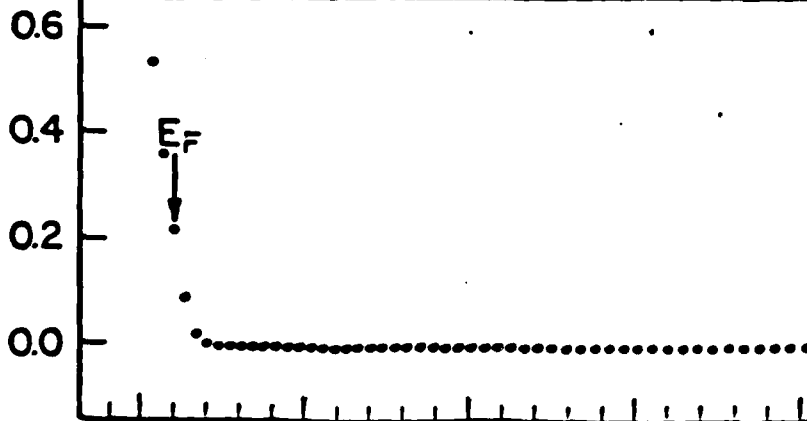
0.1 ml Au

photoexcited



0.35 ml Au

photoexcited



0.1 ml Au

unexcited

ENERGY (eV)

559

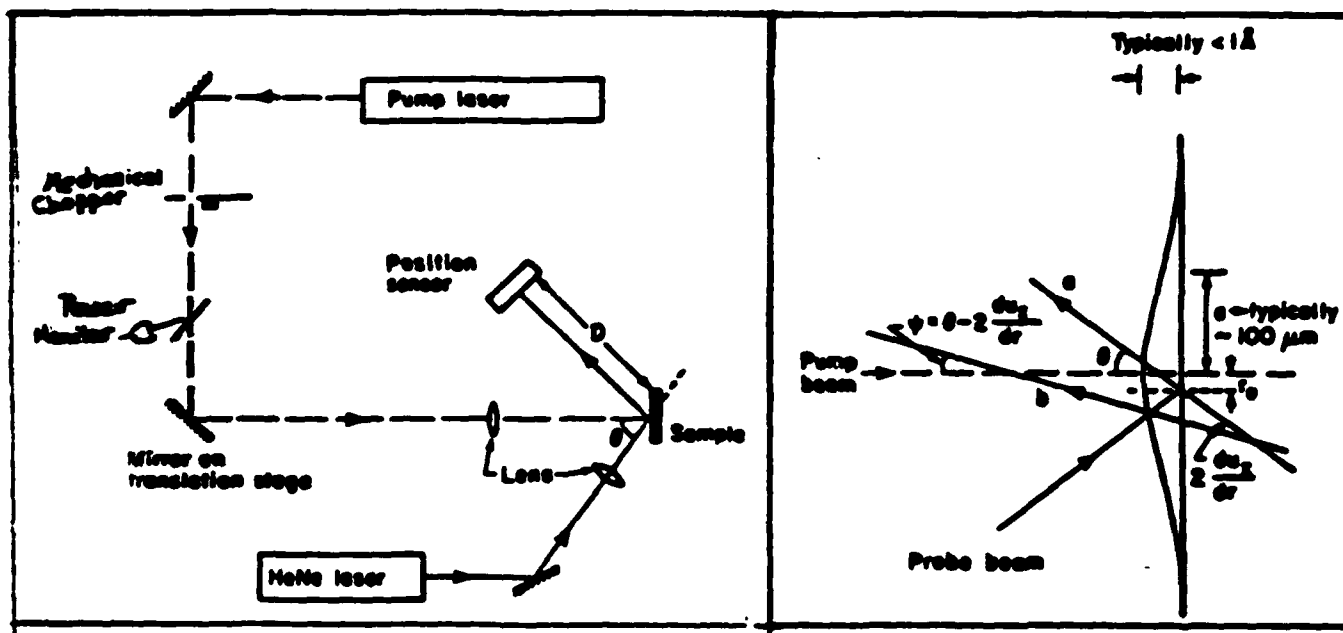
R. Hain

J. G. G. G.

P. R. L.

SL 2846 (1986)

In depth distrib. — freq.  
 Interface — optical discontinuity.



Experimental Arrangement and Physical Principle  
 of Photothermal Displacement Spectroscopy

## **Sources of Optical Heating**

### **Non-Radiative Processes:**

- **Carrier thermalization  $\implies$  lattice heating  
 $\implies$  Employed to measure minute optical  
absorption ( $\alpha l \sim 10^{-7} - 10^{-8}$ )**
- **Non-radiative carrier recombination  
yields carrier mobility and lifetime; dynamics**

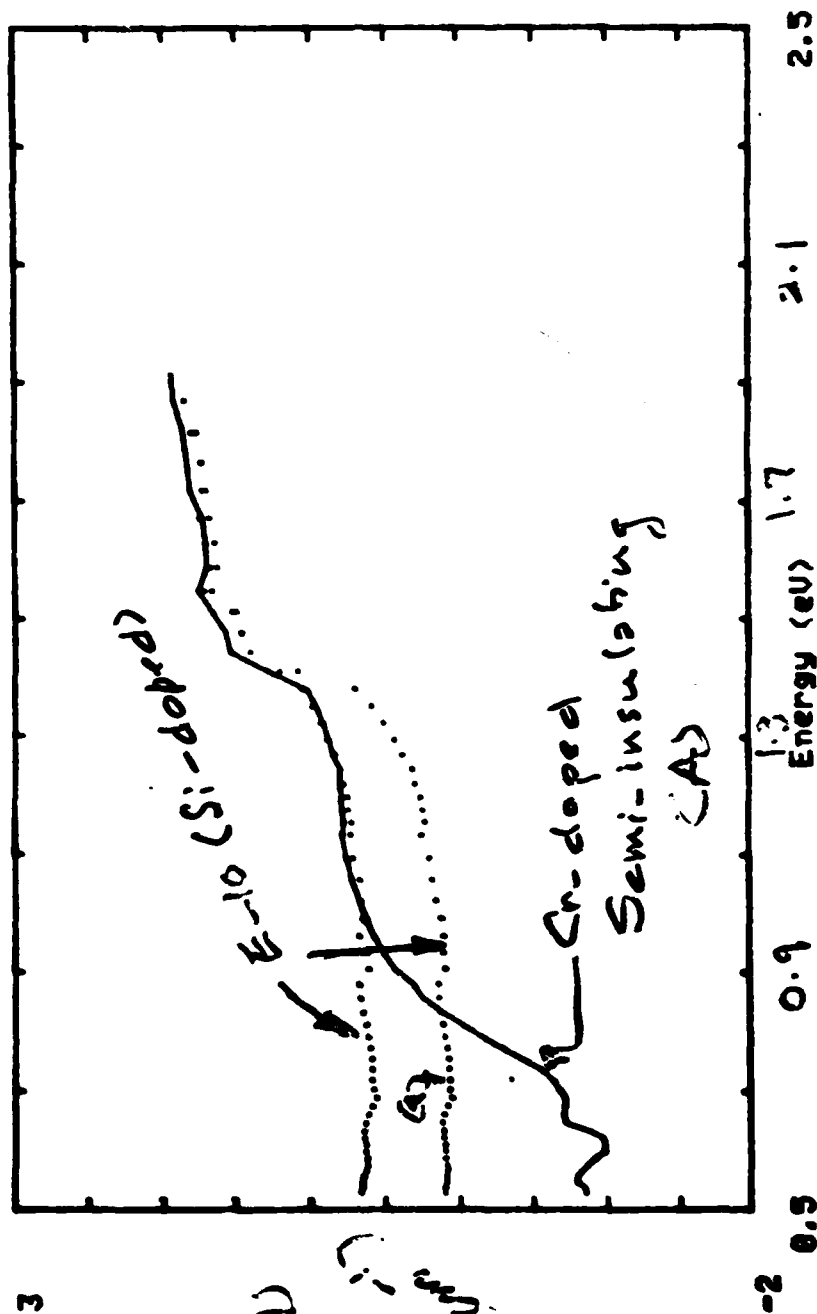
The diagram illustrates a pump-probe experiment setup. A rectangular sample of length  $l$  is shown. A "Modulated Pump Beam" (represented by three wavy arrows) is incident on the top surface of the sample. A "Probe Beam" (represented by a straight arrow) is incident on the right side of the sample at a depth  $x$  from the top surface. The probe beam is scattered at an angle  $\theta(x)$  from the surface. The sample is labeled "Sample".

**Can measure minority carrier lifetime and diffusion length (on the  $\mu\text{m}$  scale)**

**GaAs**

LINE GRAPH: A (T=0.045 cm)  
 DOT GRAPH: top E10 (t set at 0.05 cm (t=0.08 cm))  
 btm G (t=0.05 cm)

GaAs : A,G,E 10



$h\nu$  (eV)

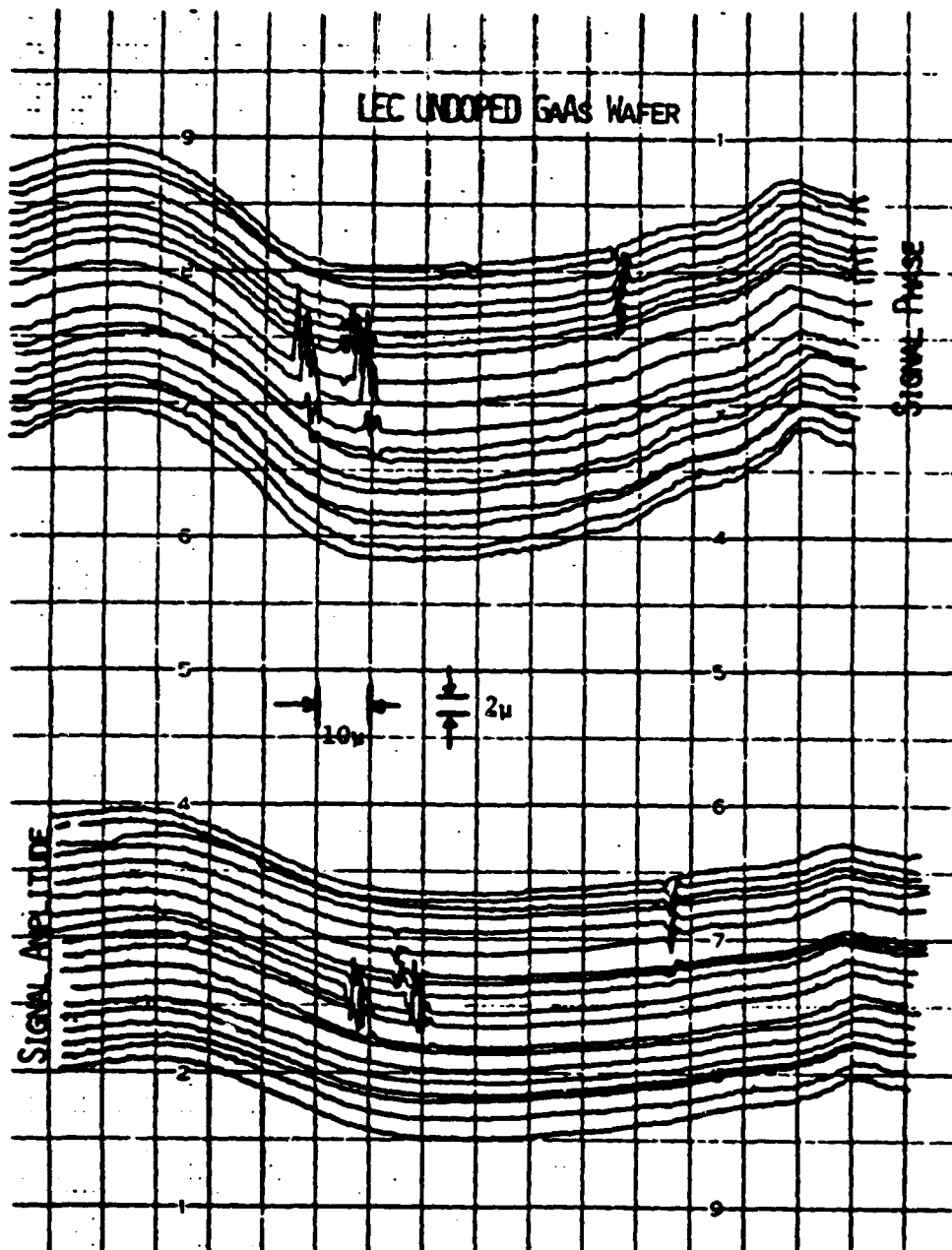
563



HENLETT-PACKARD

PHASE

AMPLITUDE



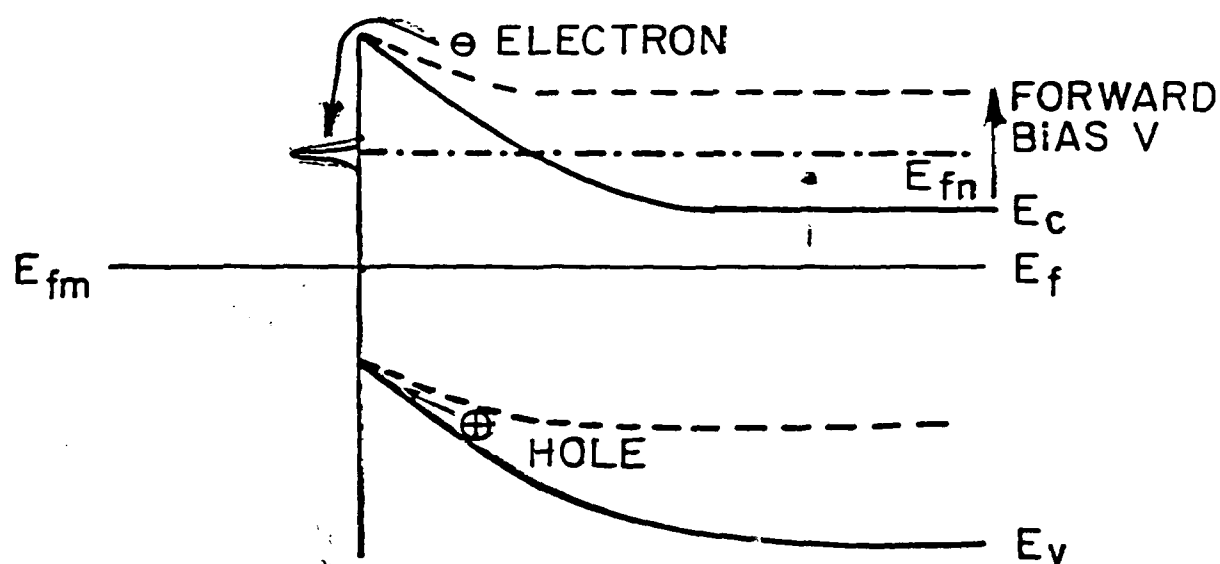
XBL 645-1701

X

Photothermal Scans of GaAs Wafer  
Showing Arsenic Inclusions

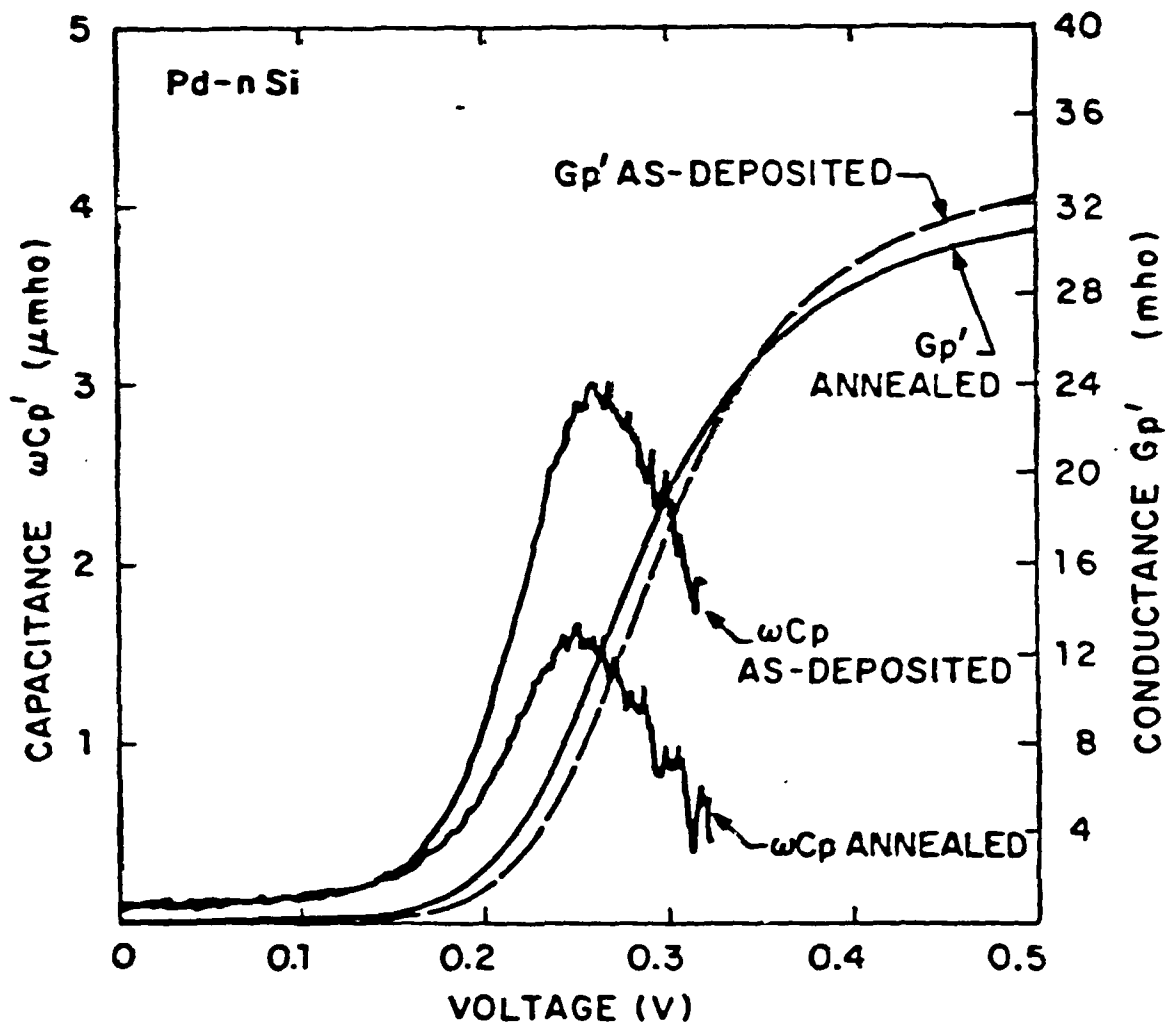
SILICIDE

n-SILICON



INTERFACE STATE CAPACITANCE SPECTROSCOPY

Temp, Freq. Dependence

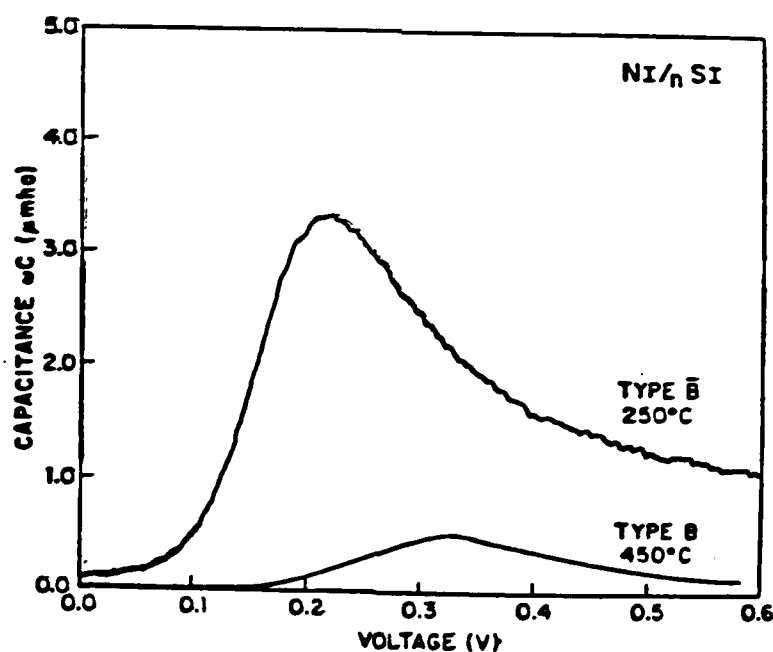


## Interface states measurements

- Measures empty interface states in forward bias

Results:

- Low density of states for nearly perfect interfaces
- Ten times higher density for mixed-phase interfaces
- High and low barrier diodes show an energetic separation of their corresponding interface states by about 0.12 eV.



TYPE B vs. TYPE B  $\text{NiSi}_2/\text{n-Si}$  DIODES

**THE ROLE OF TRANSITION METAL  
IMPURITIES IN SCHOTTKY BARRIER  
FORMATION**

**R. Ludeke**

**In Collaboration with:**

**W. Drube**

**F.J. Himpsel**

**G. Hughes**

**G. Landgren**

**D. Rieger**

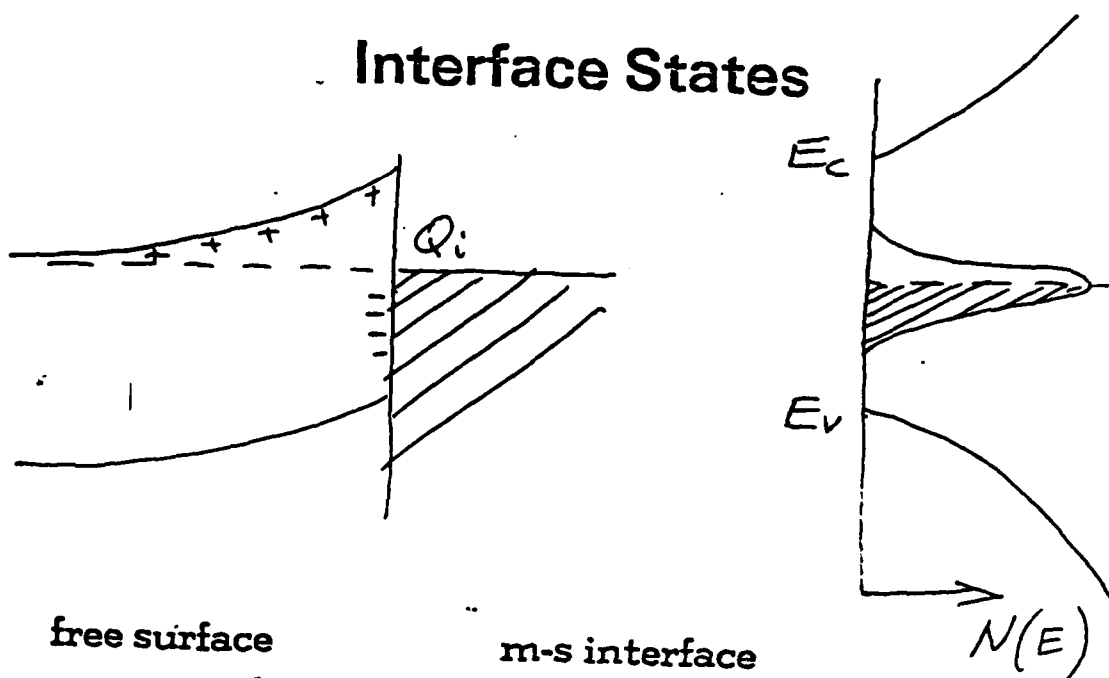
**F. Schaffler**

**D. Straub**

## OUTLINE

- Limitations of present Schottky models
- "Anamalous" behavior of transition metals
  - range of barrier height values
  - evidence for interface states in gap
- Model for transition metal Schottky barrier:
  - characteristics of substitutional impurities
  - experimental evidence
- Conclusions
  - limitations of model
  - remaining issues

## Interface States



free surface

$$(2q\epsilon N_D V)^{1/2} \lesssim Q_i \lesssim$$

m-s interface

$$\frac{\epsilon V}{4\pi d}$$

$$10^{12}$$

$$\lesssim Q_i \lesssim$$

$$10^{14} \text{ e cm}^{-2}$$

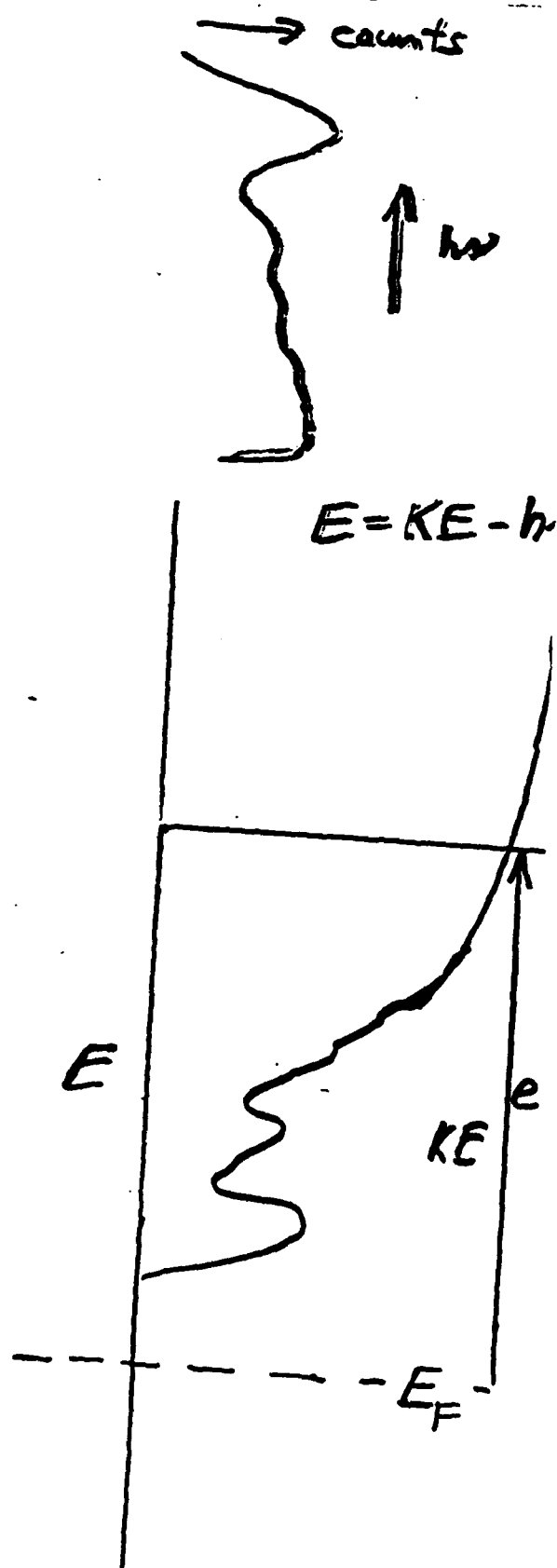
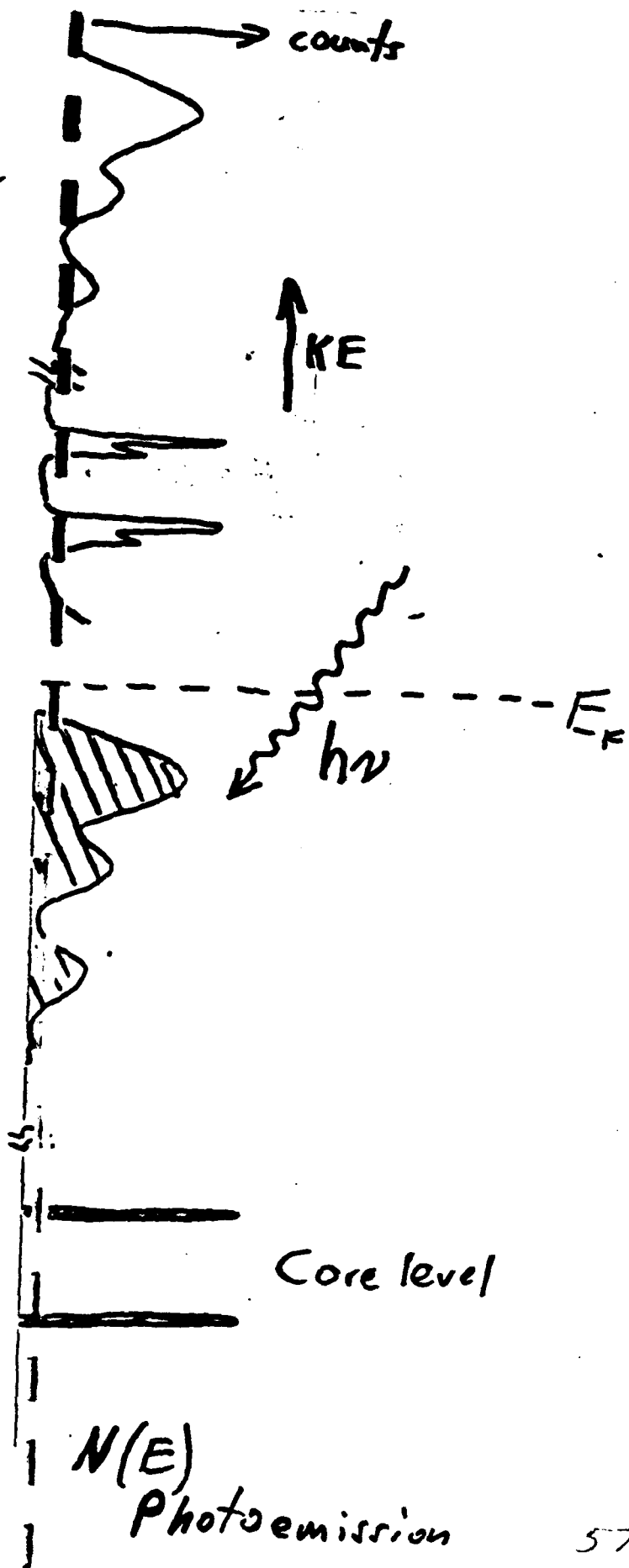
## Origin and properties

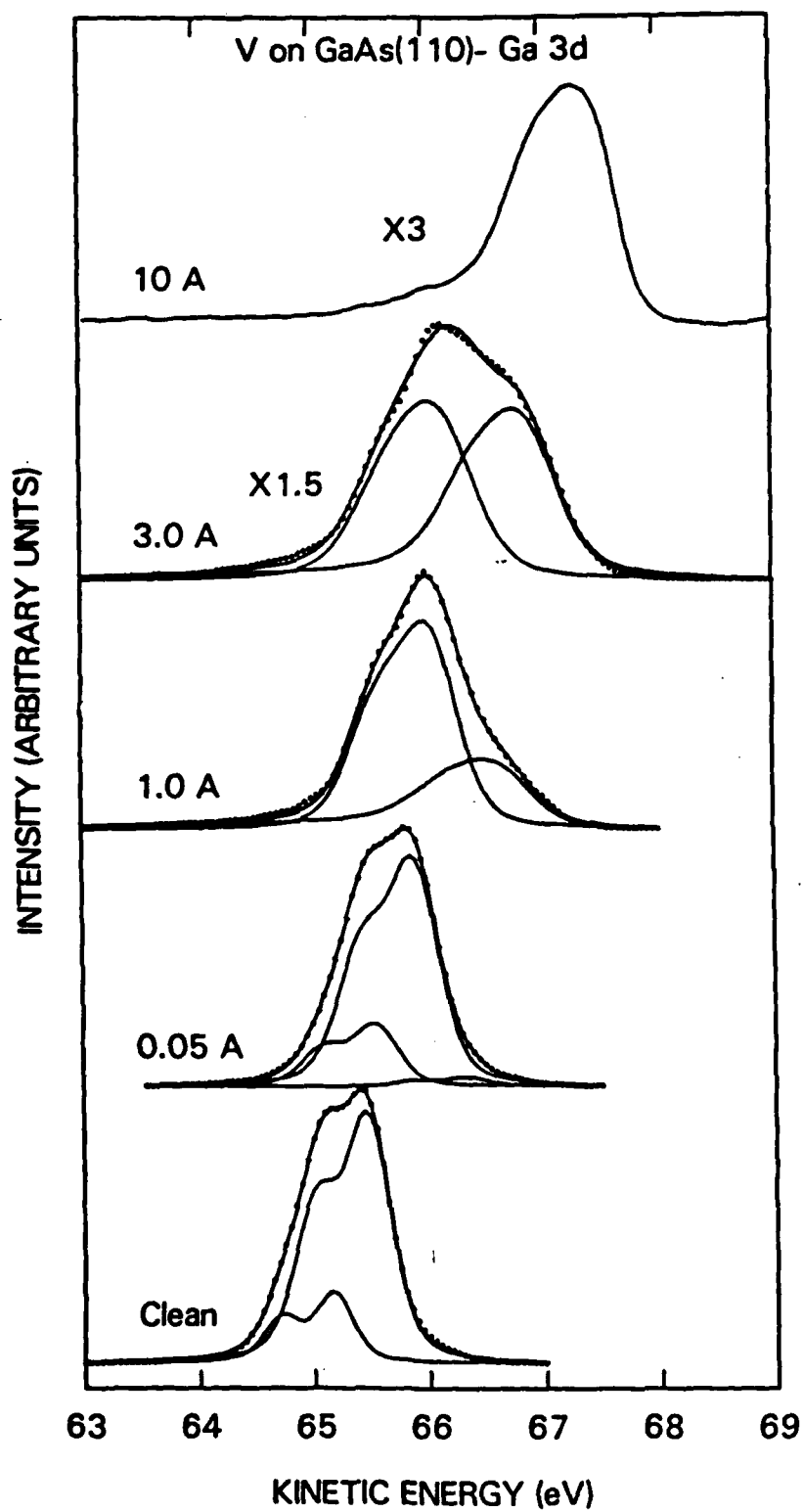
- "intrinsic" defects
- "extrinsic" interface states
- all:
  - sufficient density
  - acceptor + donor properties
  - $E(\text{donor}) \approx E(\text{acceptor})$
- up to now no definitive identification

## **CHARACTERISTICS OF SOME SCHOTTKY MODELS**

- **Unified defect model**
  - metal independent
  - separate pinning for n & p-type material
  - interface states intrinsic to semiconductor
  - energetically separated acceptor and donor states
- **Effective work function model**
  - metal dependent
  - $\phi$  (anion) is relevant parameter
  - presence of anion clusters at interface
- **Metal Induced Gapstates**
  - metal independent
  - requires delocalized states (metal)

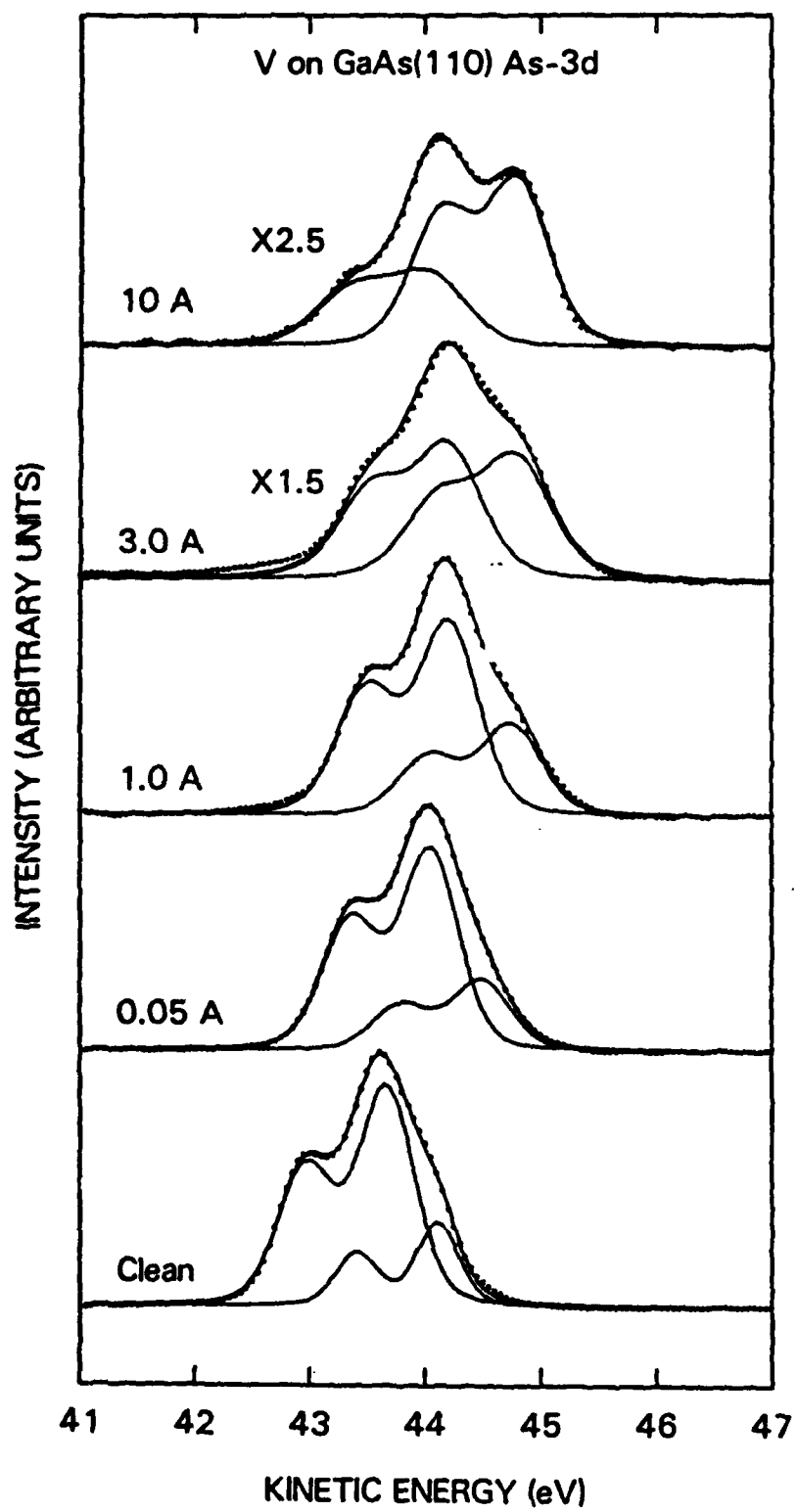






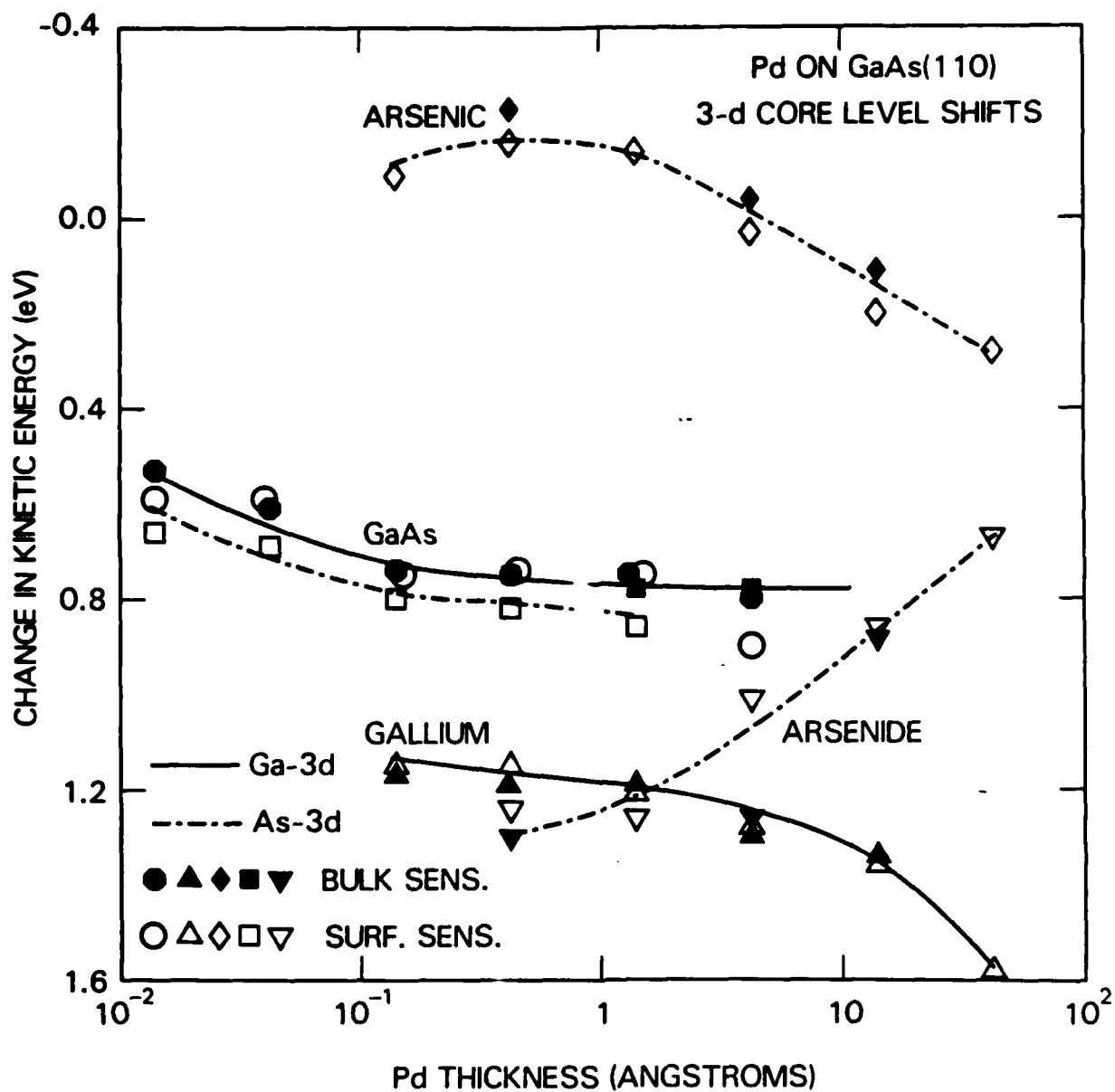
574

- 25 8

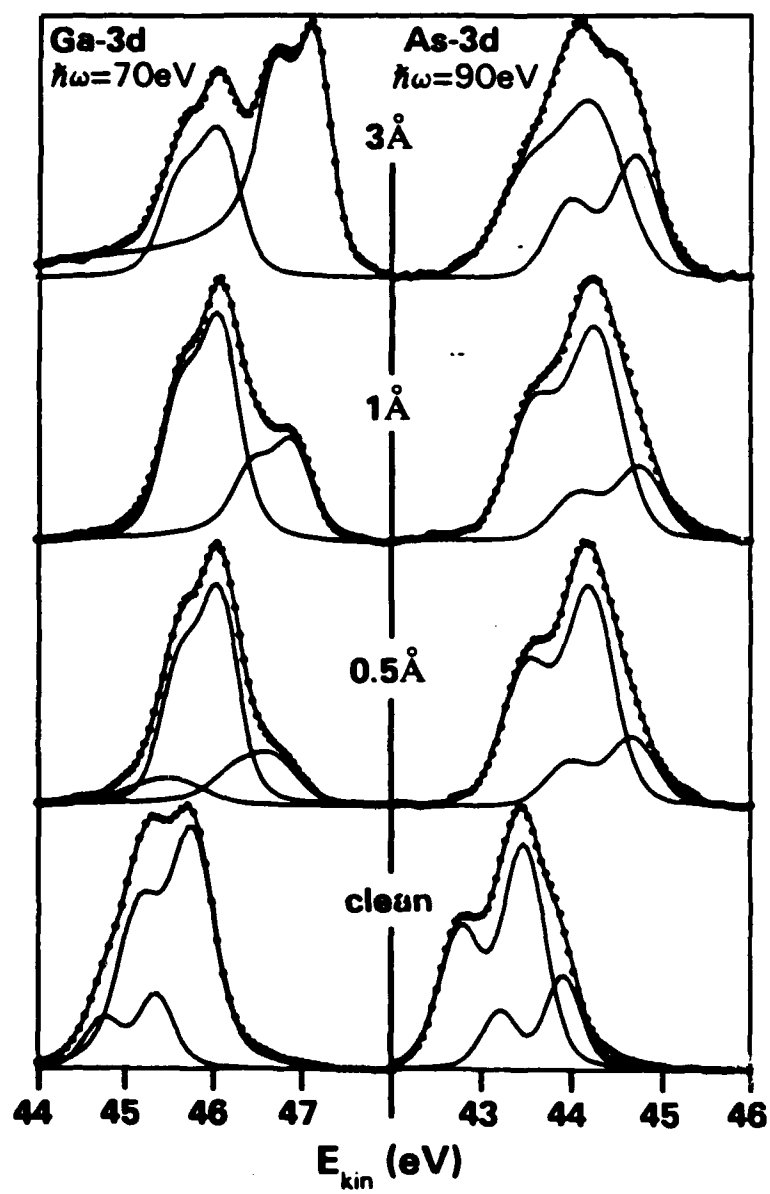


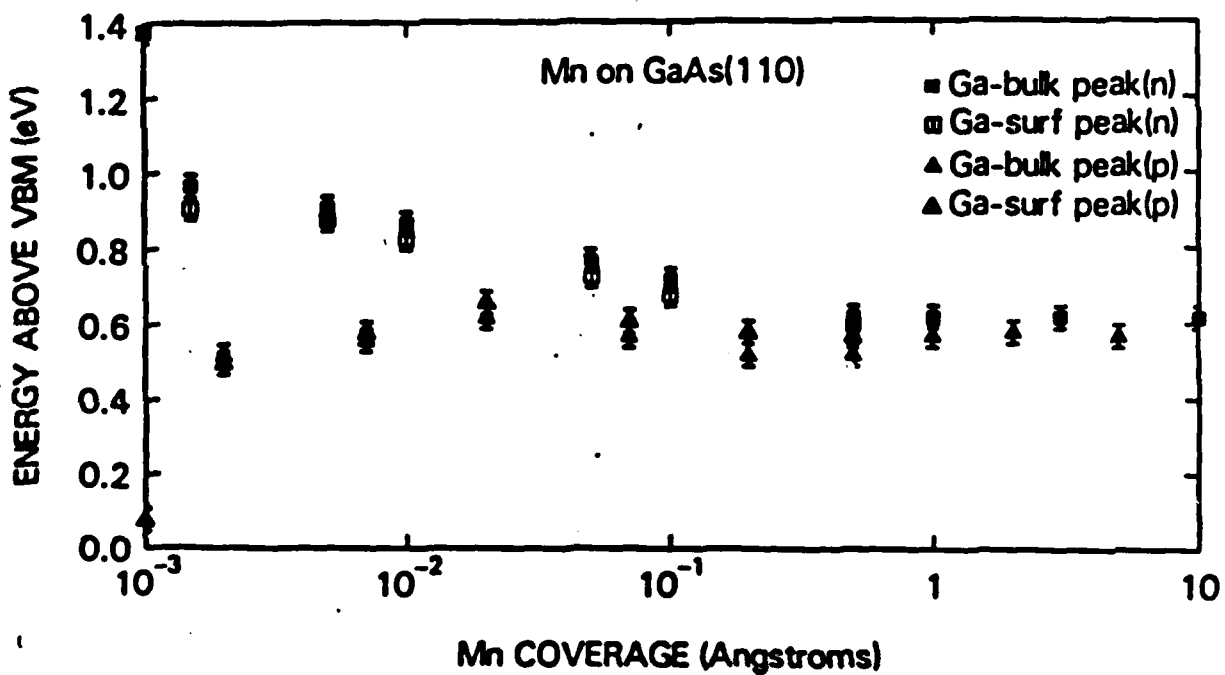
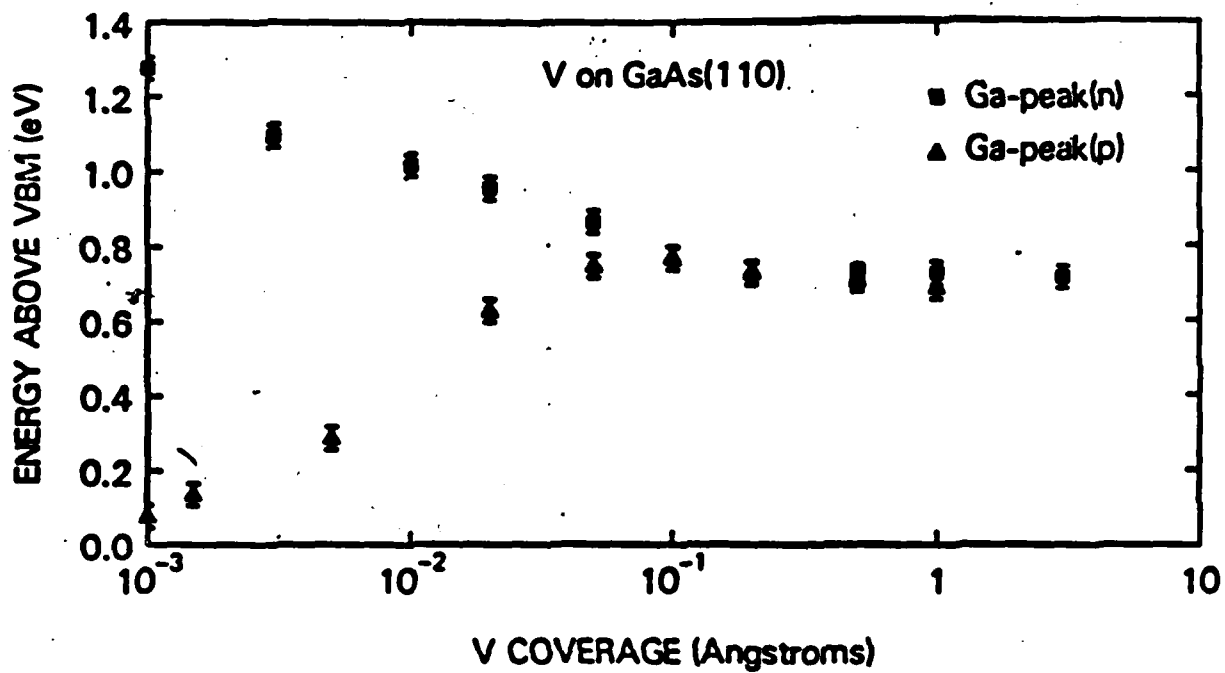
575

F 26 9

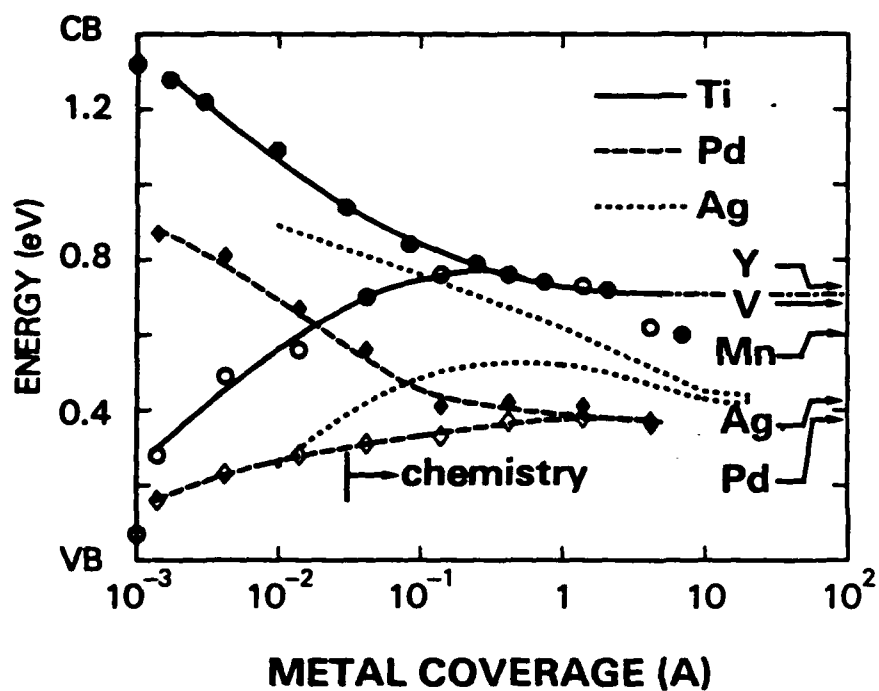


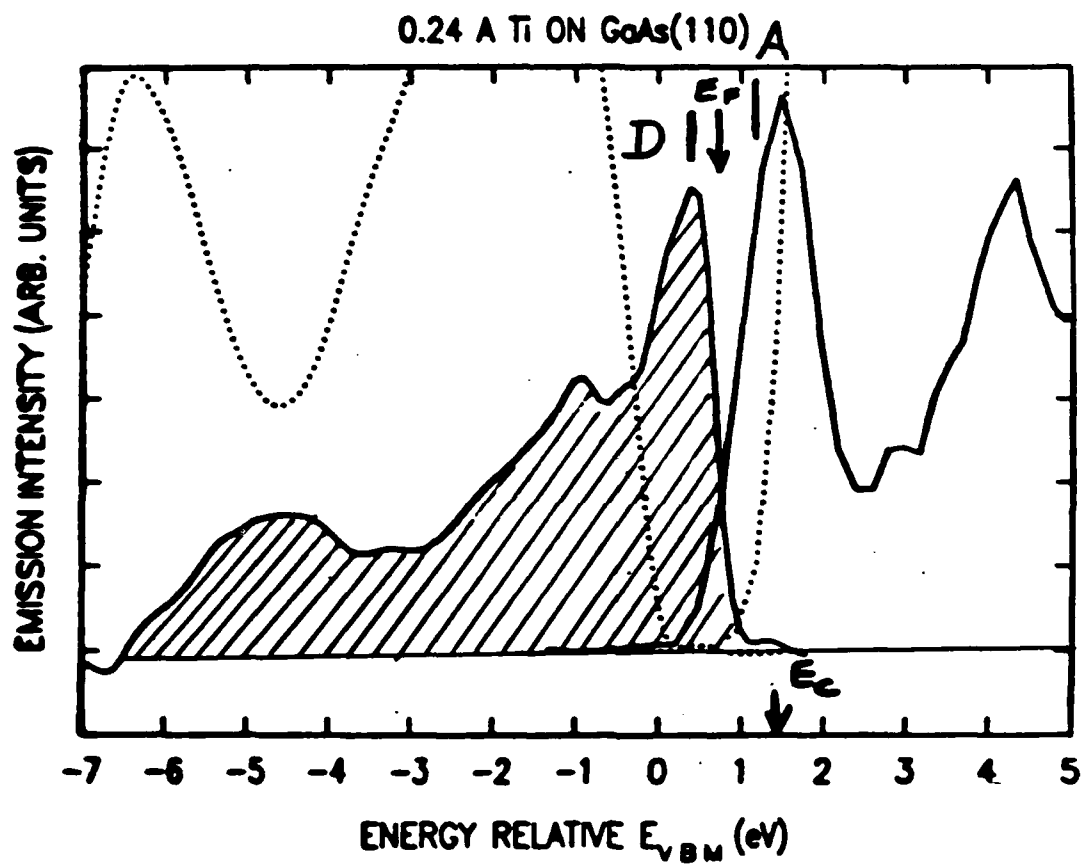
# Mn on n-GaAs(110)





# FERMI LEVEL AT GaAs(110) INTERFACE



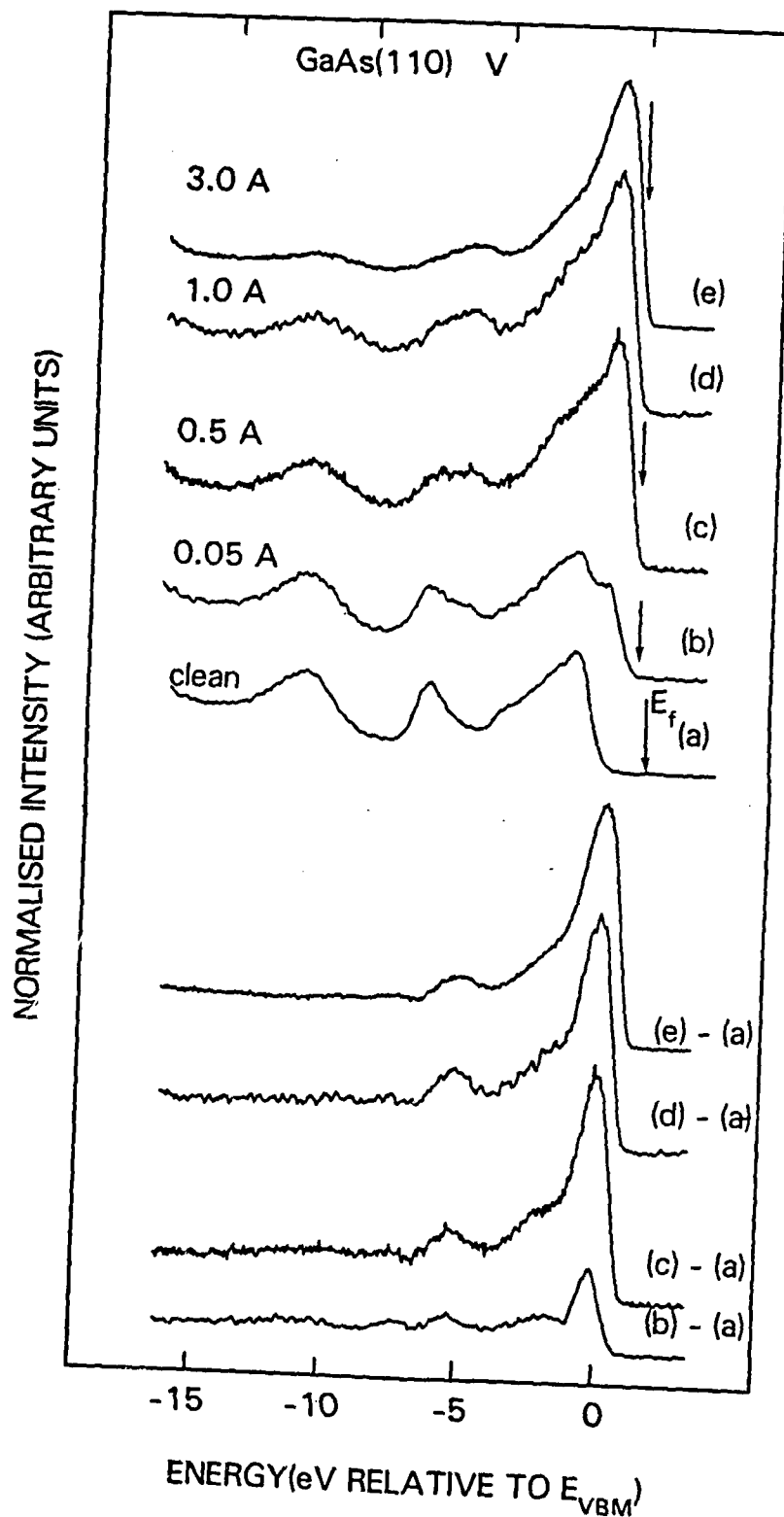


bonding

non-bonding

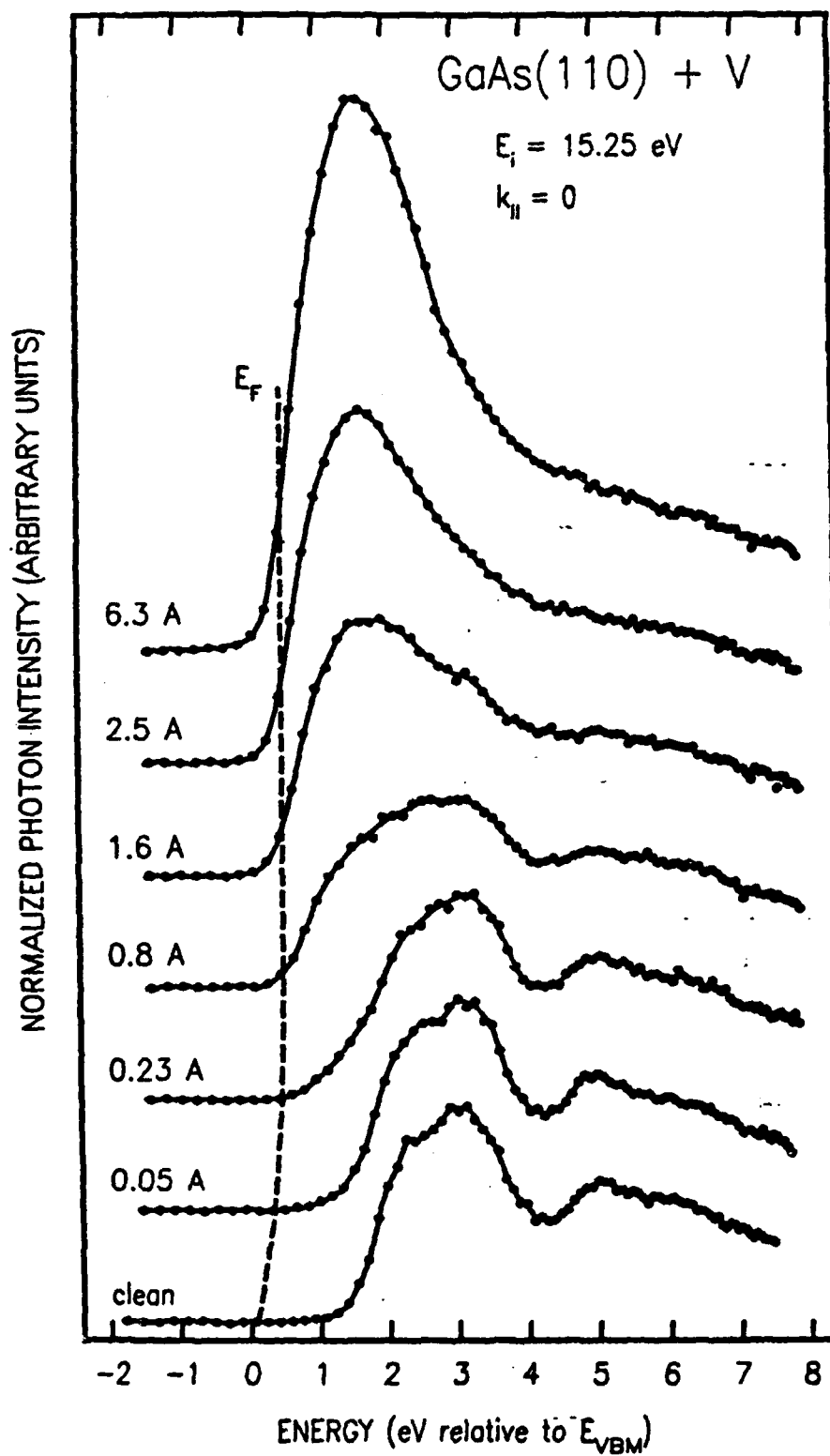
anti-bonding

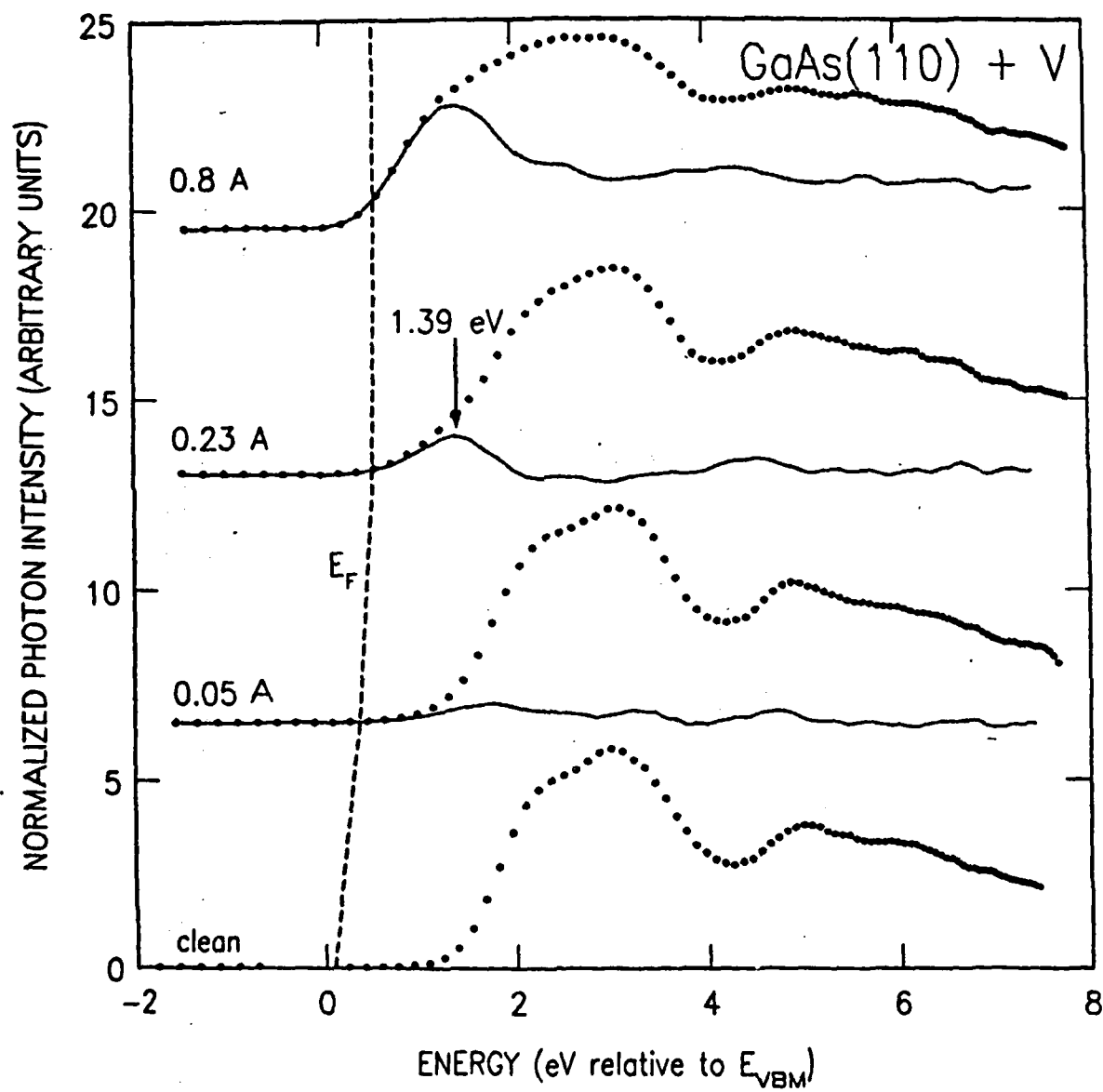


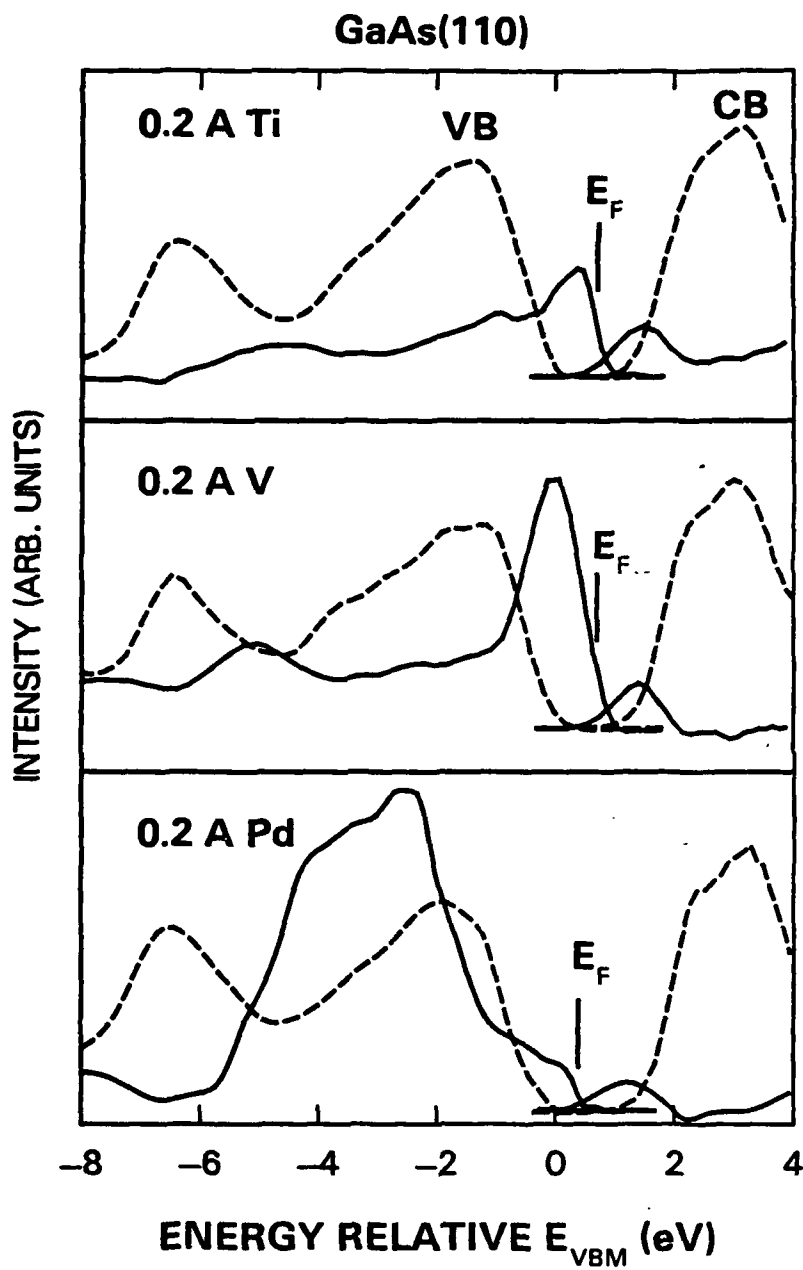


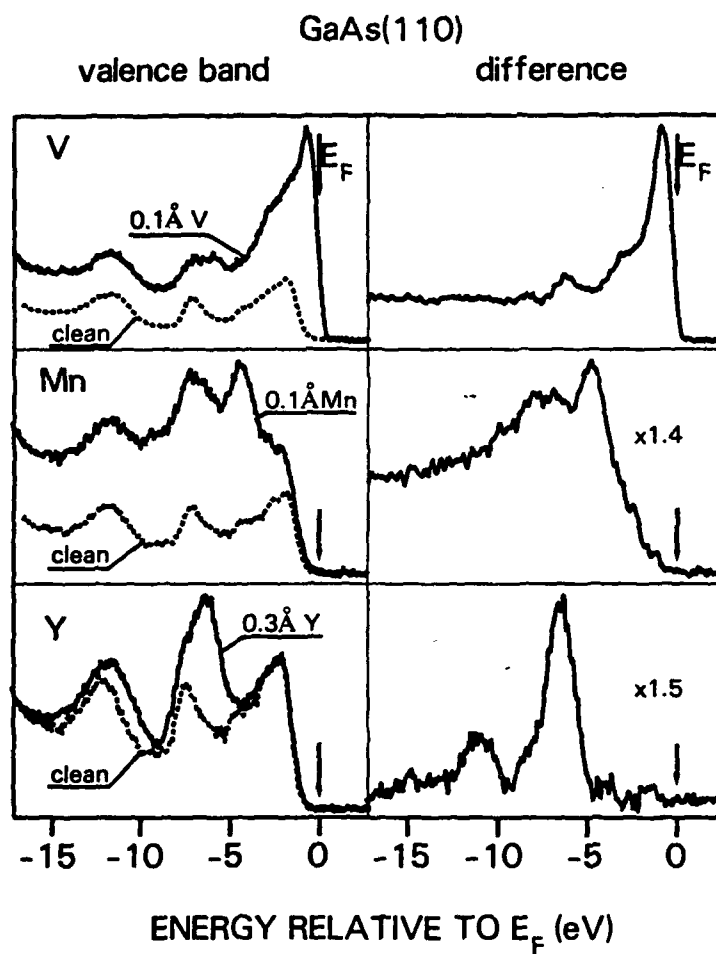
581

F. J. A. B.





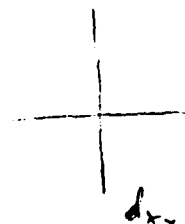
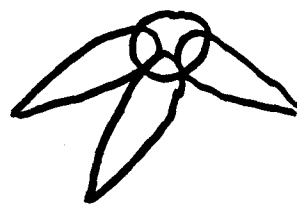
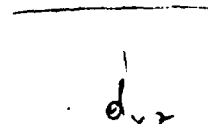
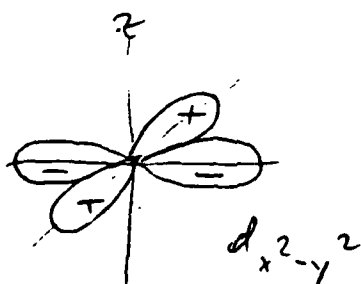
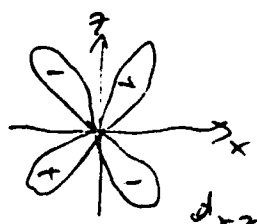
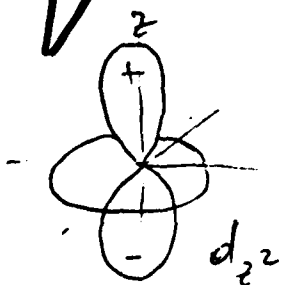
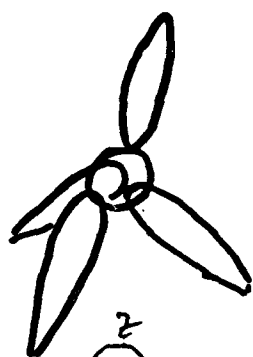
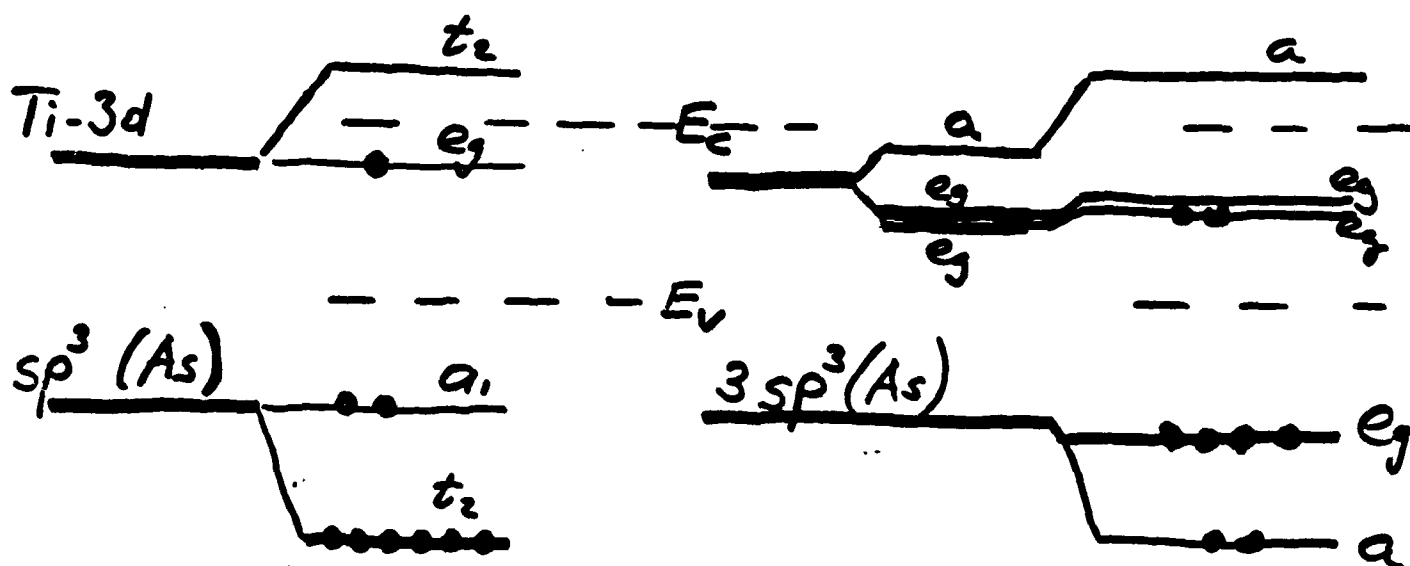




Bulk  
 $T_d$

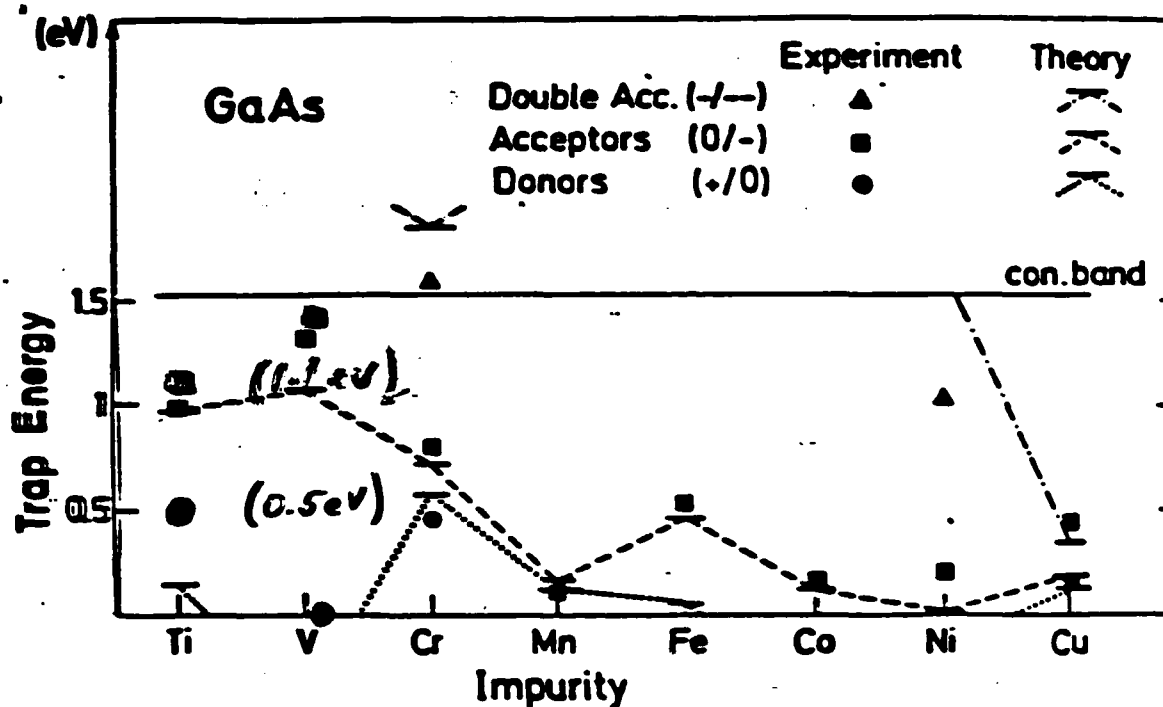
GaAs

Surface  
 $\sim C_{3v}$



586

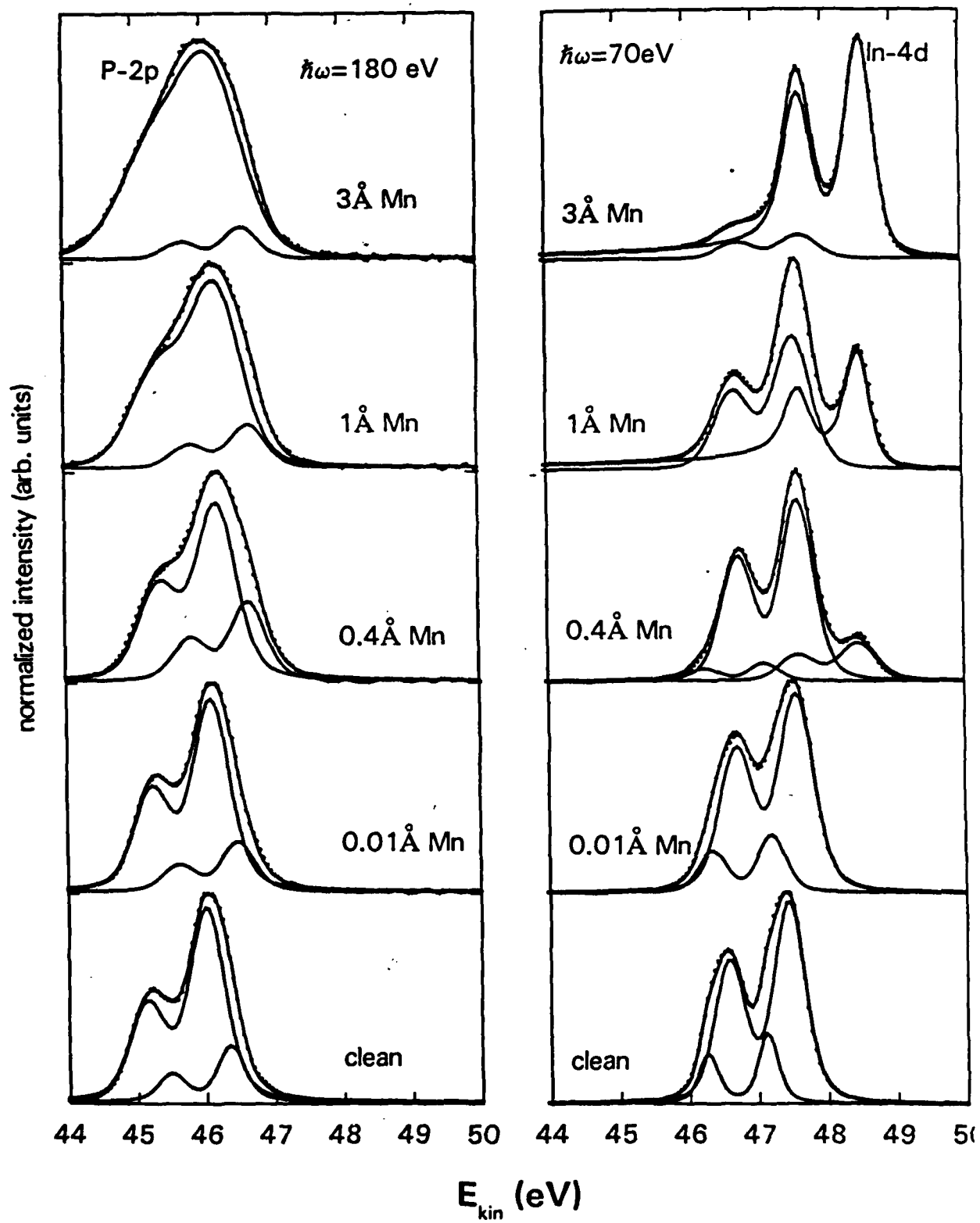
40 15



● (A. Hennel, unpublished)

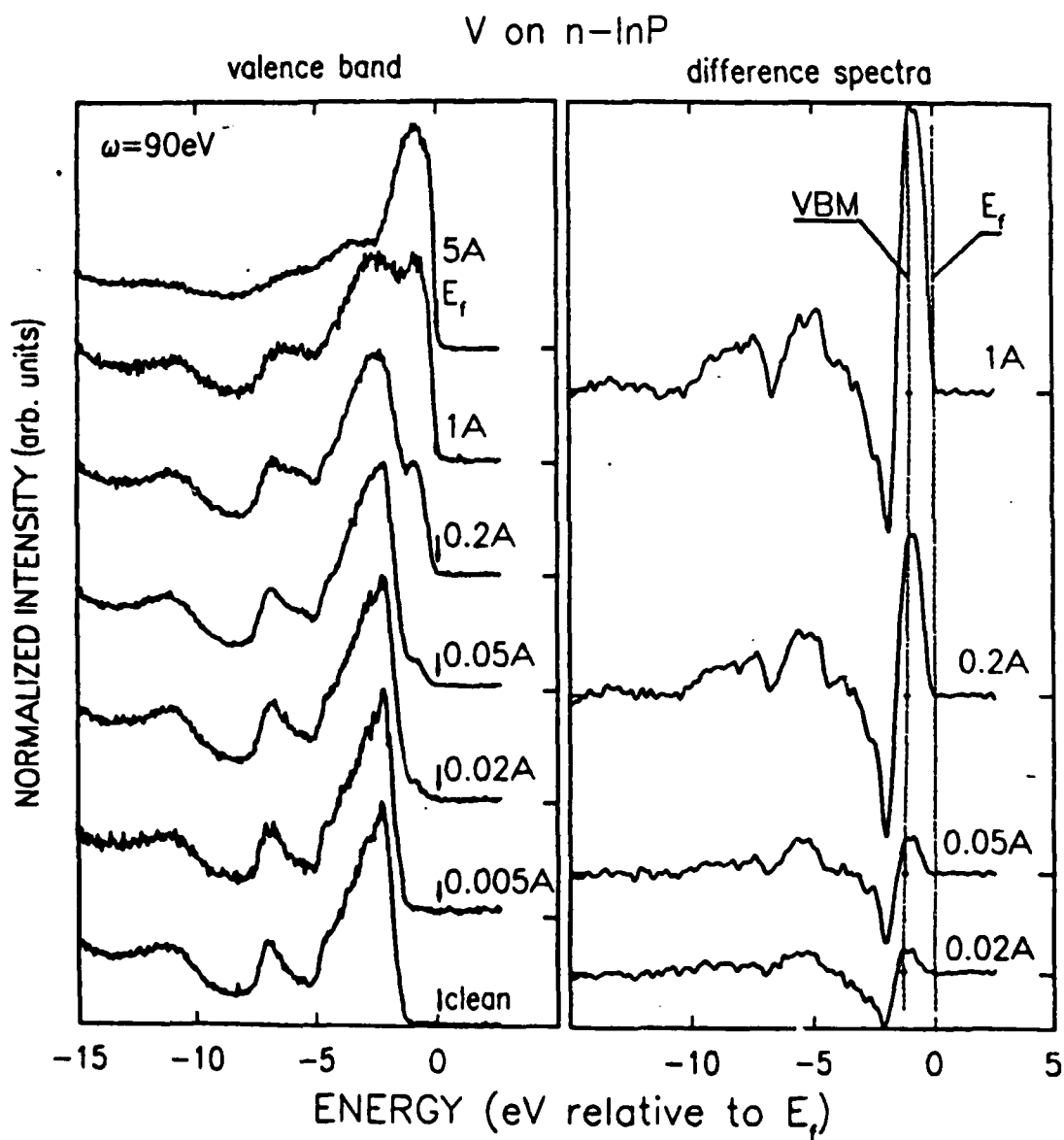
Energy levels of transition-metal impurities in GaAs as calculated by Vogl and Baranowski compared with experimental data. From Ref. 87.

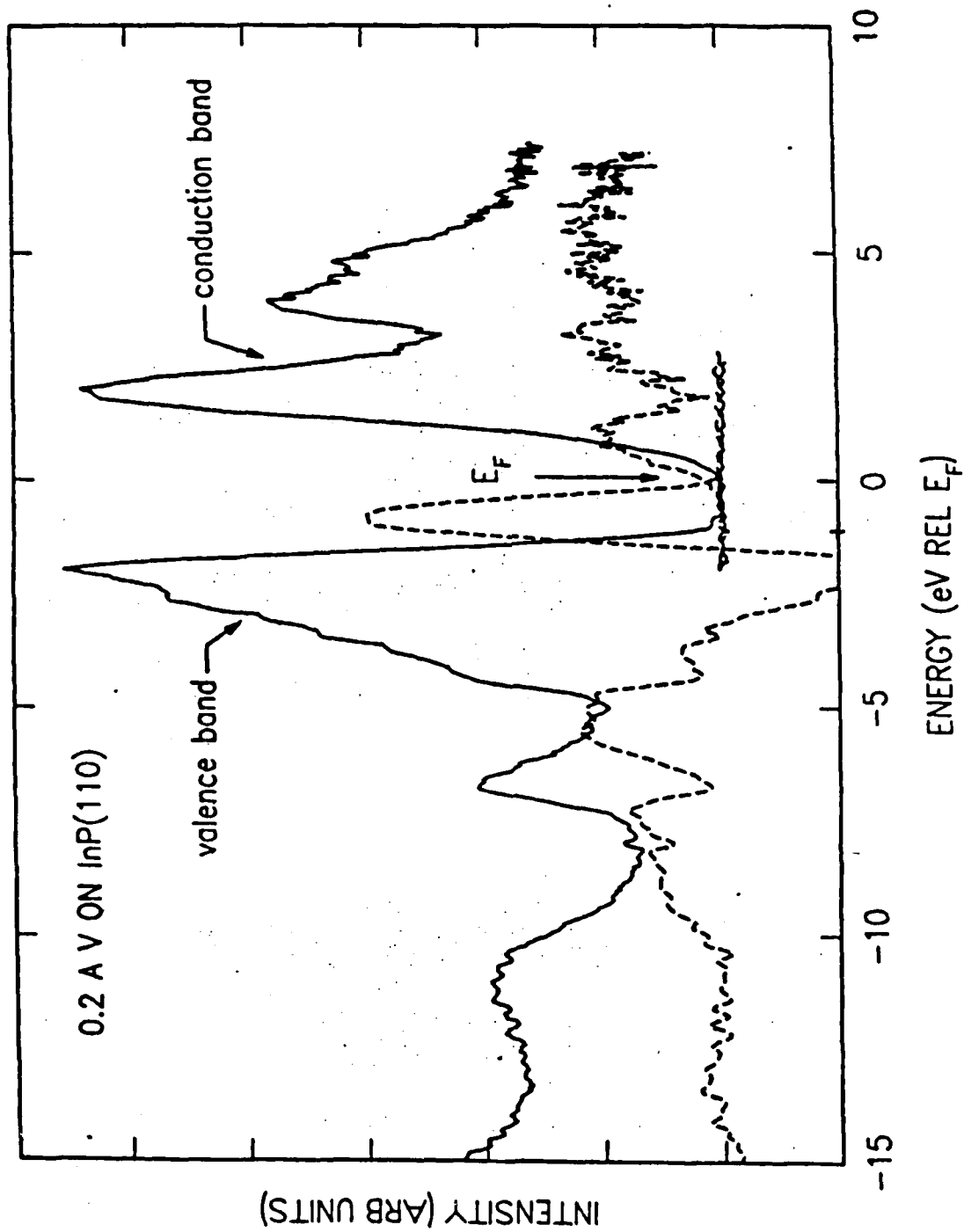
# Mn on n-InP



588







540

Fig. 22

#82

# Comparison of spectral peaks + substitutional impurity levels

		<u>Present data</u>			
		bulk impurity levels			
		GaAs		InP	
Ti	A	1.30 *	<u>1.40</u>		
	D	0.50	<u>0.45</u>		
V	A	1.30	<u>1.39</u>	in CB	
	D	0	<u>0</u>	0.21	<u>0.20</u>
Mn	A	-	-		
	D	(-1)	<u>-4</u>		

\* energies referred to VBM

## CONCLUSIONS AND SUMMARY

- Observation of interface states:
  - filled and empty states in bandgap
  - states determine Fermi level
  - derived from d-electrons of transition metal
- Chemical evidence and spectroscopic signature suggests a substitutional impurity
- Limitations and issues
  - not applicable to all transition metals
  - single defect oversimplified
  - independent corroboration required
  - role of chemistry at interface
  - relevance to thick coverage not known

Effects of Coverages, Relaxation, and  
Screening at Interfaces

Walter Harrison  
Stanford University

WALT HARRISON

# TIGHT-BINDING THEORY

Every thing understandable

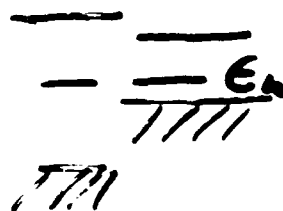
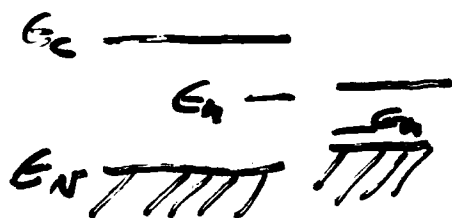
Sometimes predictable

Background: heterojunctions

$$E_N = \frac{E_P^+ + E_P^-}{2} - \sqrt{\left(\frac{E_P^+ - E_P^-}{2}\right)^2 + \left(\frac{1.28 \hbar^2}{2m d^2}\right)^2}$$

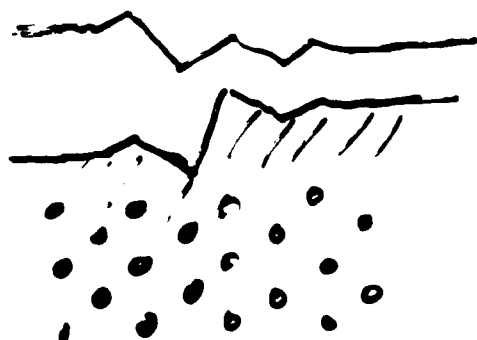
Natural band lineups

Neutral point



Really  $\Delta E_v + \Delta E_c$  is

Dipole from 1st planes cross section



Direction of dipole

Not seen

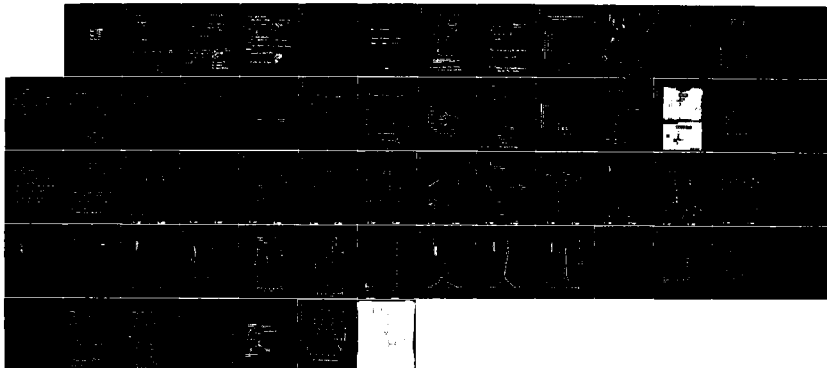
AD-A183 158

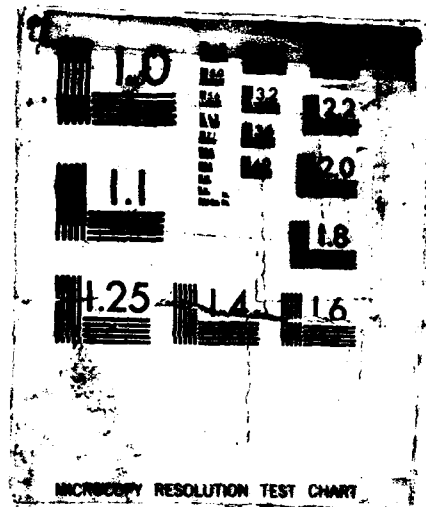
A WORKSHOP ON 3-5 SEMICONDUCTOR: METAL INTERFACIAL  
CHEMISTRY AND ITS EFFECTS (U) STANFORD UNIV CA  
W E SPICER ET AL. 05 NOV 86 N00014-87-G-0038

7/7

UNCLASSIFIED

F/G 20/12 NL







# Alternate views:

van-de-Walle-Martin, Andersen

no dipole

Tight-binding: True if measure  $\epsilon_r$  from  $\bar{\epsilon}_h$

They found  $\bar{\epsilon}_h$

Approximates  $\epsilon(0) \approx \infty$ . Ignores local effect

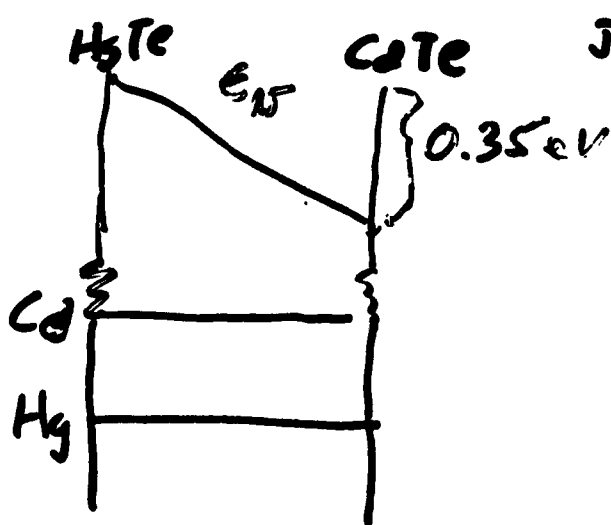
Launoo:

no charge: requires  $\Delta \bar{\epsilon}_h = 0$

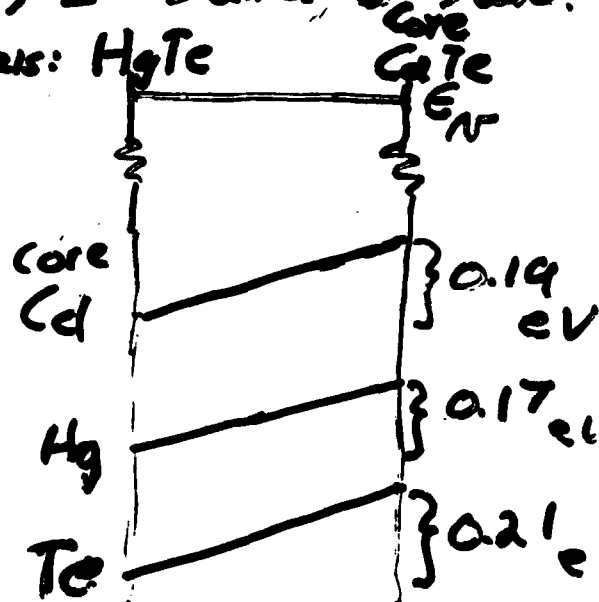
## Core-shifts

Shift: Hg cores in Hg-Cd-Te

All HgTe bonds,  $Z^*$  same,  $\epsilon$  same?

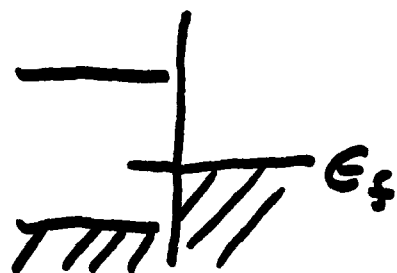


$$\Delta \epsilon_r = 0.35 \text{ eV} \quad 595$$



$$\Delta \epsilon_r = 0.28 \text{ eV}$$

# SCHOTTKY BARRIERS

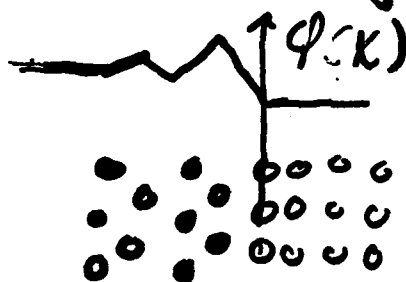


Reasonable accord

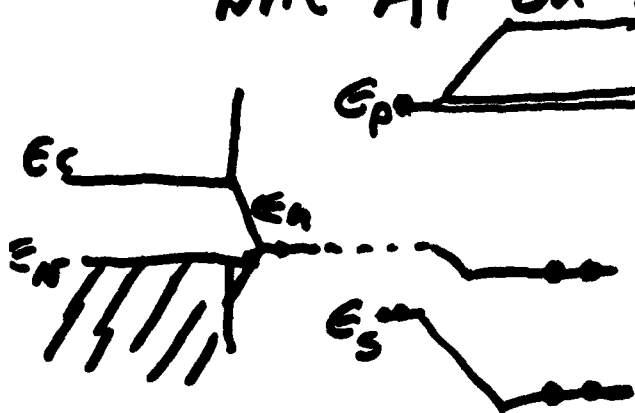
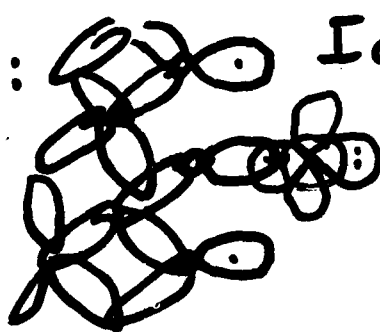
Really  $\rightarrow \frac{E_h - E_f}{E(0)} \in \text{semi.}$

$S = 1/E(0)$

Should fluctuate



Partial coverage: Ideal geometry  
One Al on Si:




In this geometry  
No charge  
No band bending

Multiple atoms

No local charge till bands cross

$E_F$

$E_F$   Width  $\approx 2\sqrt{n \frac{V_{ppr}^2 + V_{pr}^2}{2}}$

$\pi$    $\approx \pi$  3eV

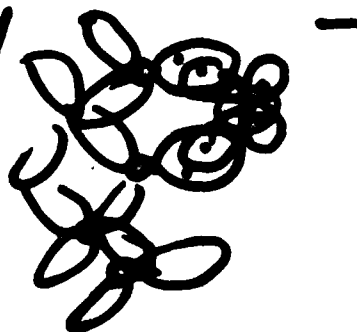
No band bending

But dipoles arise to shift metallic levels.

Once bands cross  $E_F$ , band-bending begins.

Depends on geometry

Favored for n-type.



**Unpinned GaAs Surfaces by  
Photochemistry**

**Jerry M. Woodall**

**IBM - Yorktown Heights**

**OXIDE/III-V INTERFACES**

P. Kirchner, A. Warren, S. Offsey,  
J. Baker, J. Tsang, S. Wright

**IBM**

*T.E. Kazior et al. J Appl. Phys. 54 2533 (1983)*

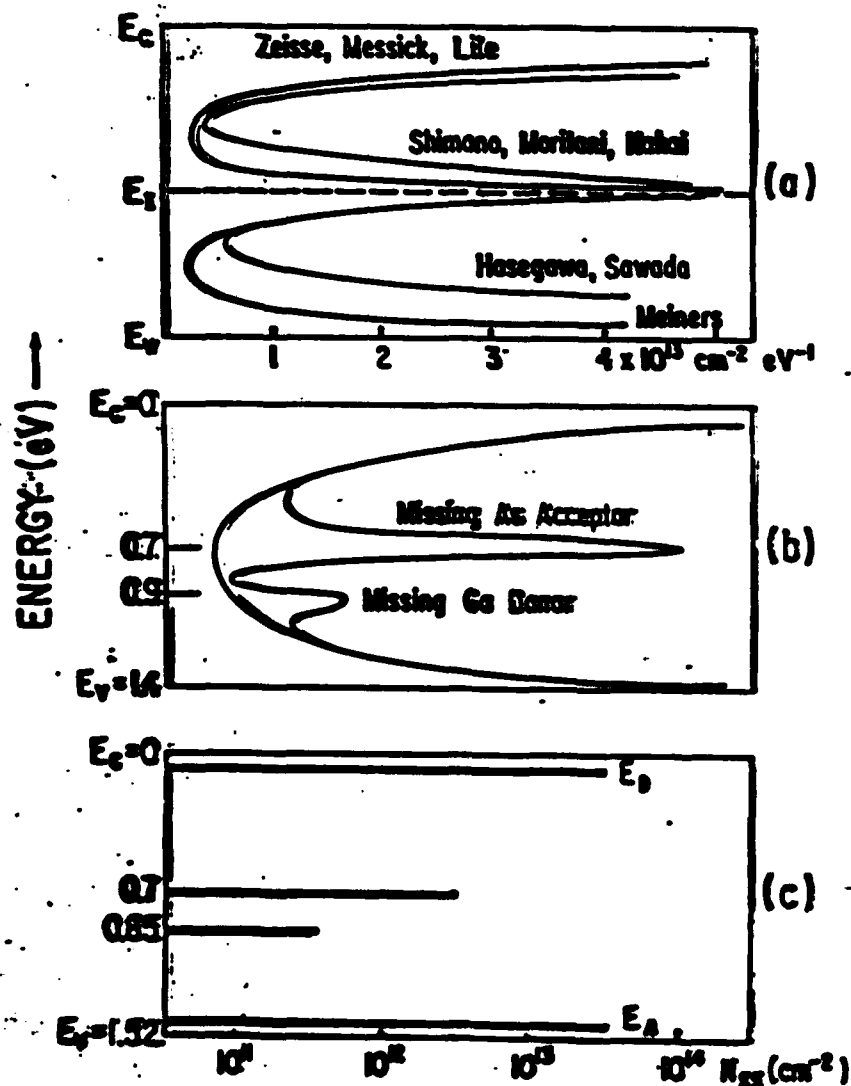
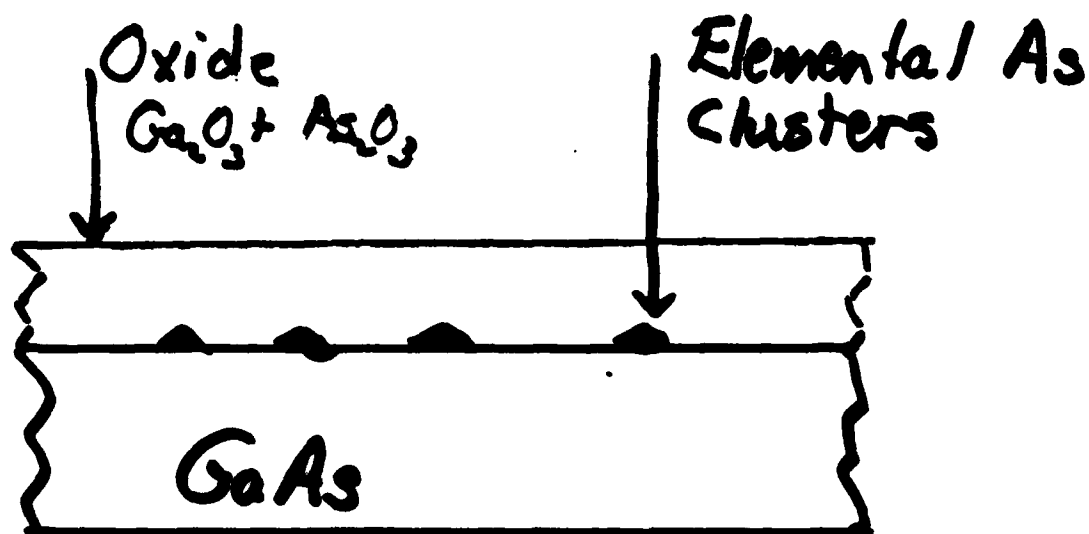
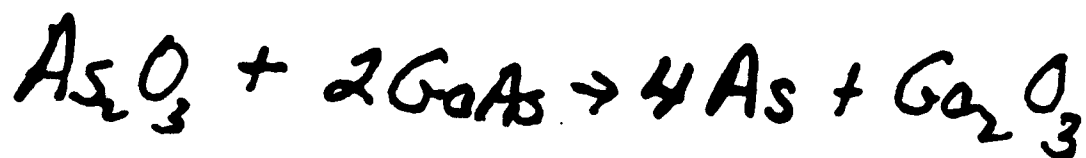


FIG. 1. GaAs interface state models: (a) U-shaped distributions obtained from capacitance measurements (Ref. 1-4); (b) unified defect model (Ref. 10); (c) our model derived from photoionization discharge current analysis (Ref. 15-21).

*Evidence for Fermi Level Pinning  
at GaAs/Oxide Interfaces*



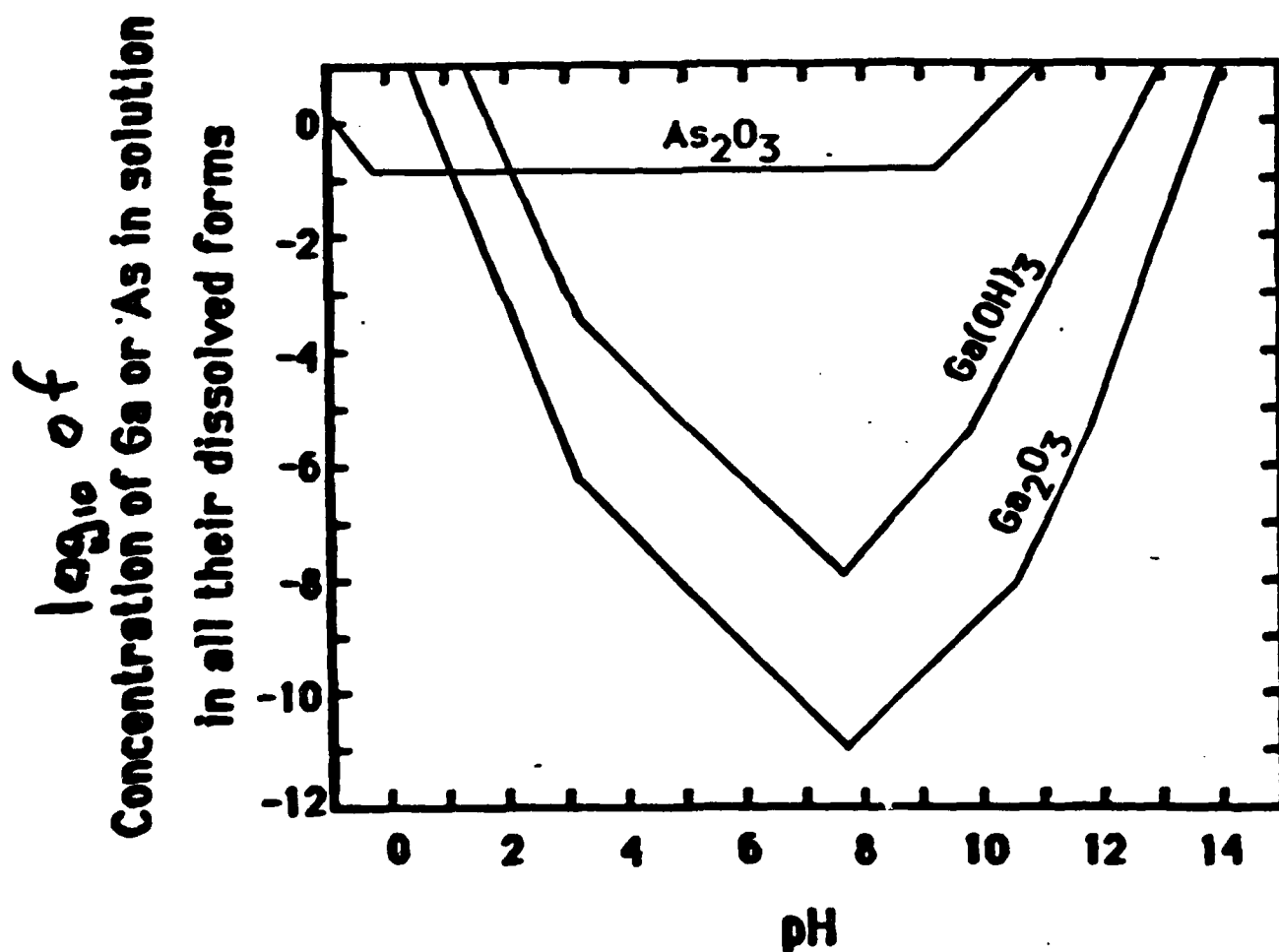
The Oxidized GaAs Surface



$$\Delta F < 0$$

" $E_F$  Pinning" (i.e. Schottky Barrier)  
Due to As Clusters

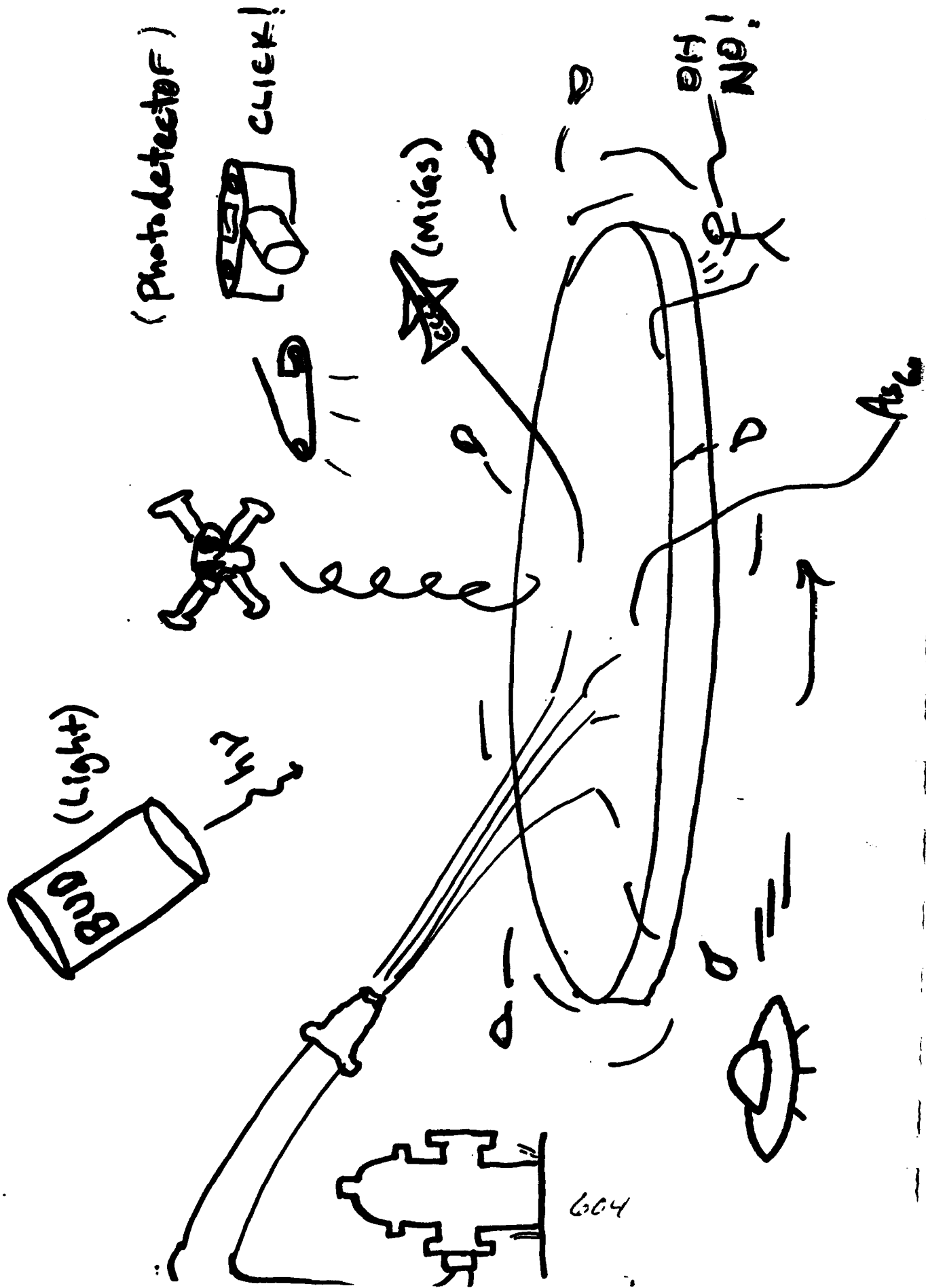
## Influence of pH on the solubility of Ga and As oxidation products

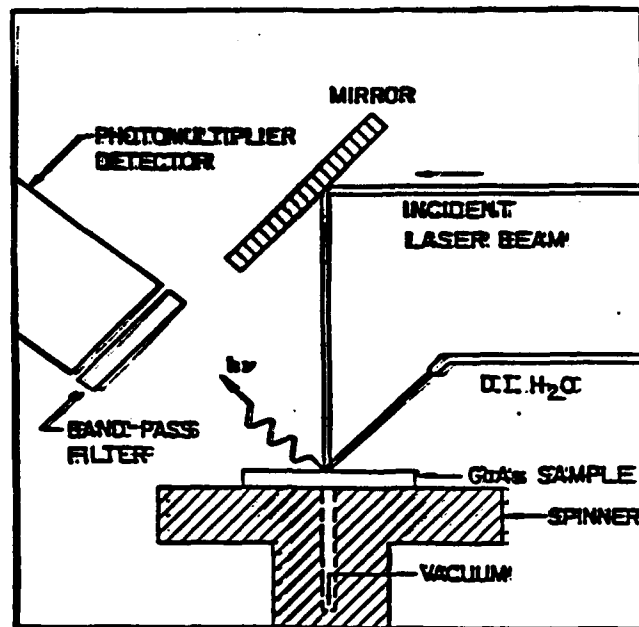


After M. Pourbaix, Atlas of Equilibria in Aqueous Solutions

Courtesy of D. Podlesnik, Columbia U.



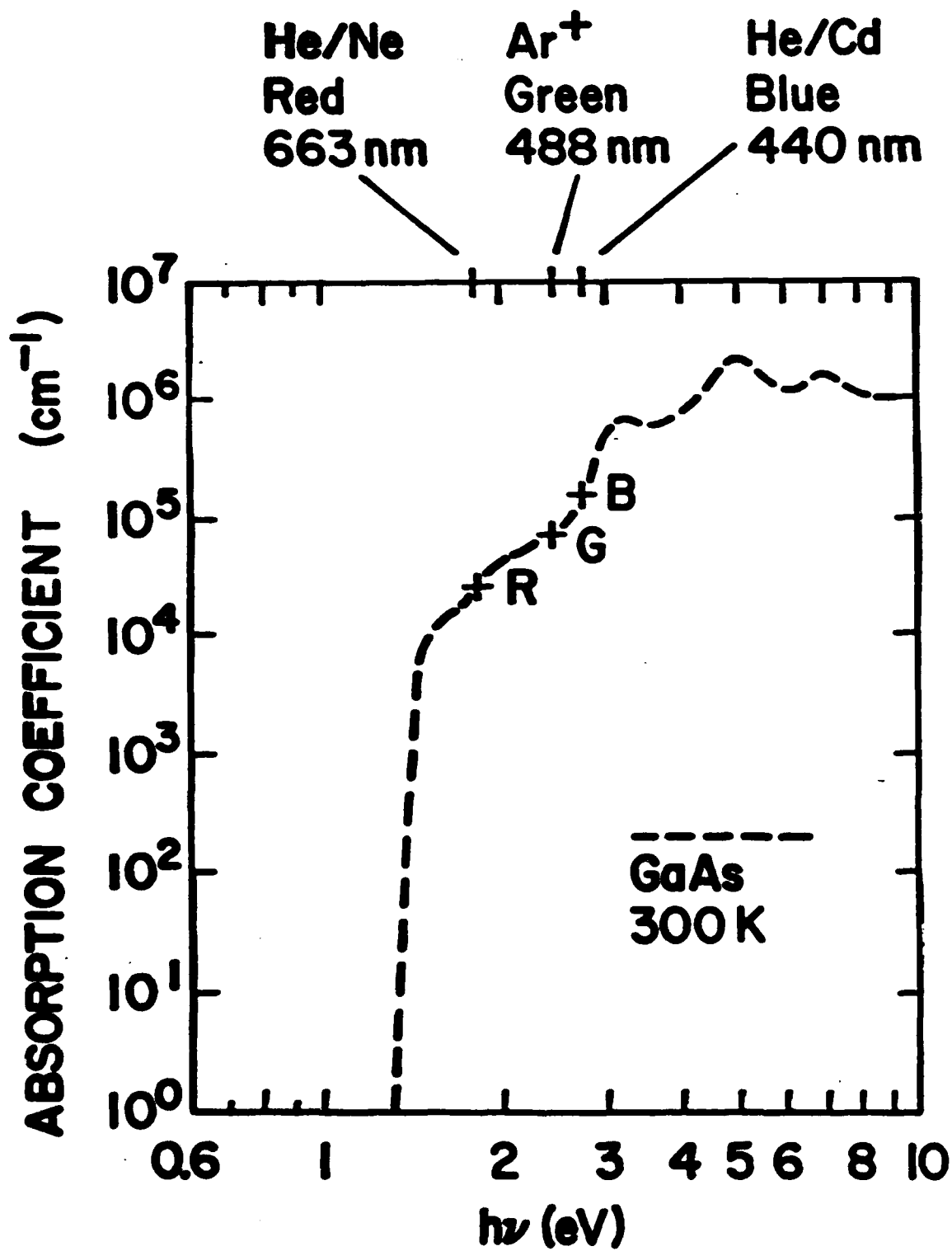




### Experimental Setup

#### Verification of the Unpinned Surface

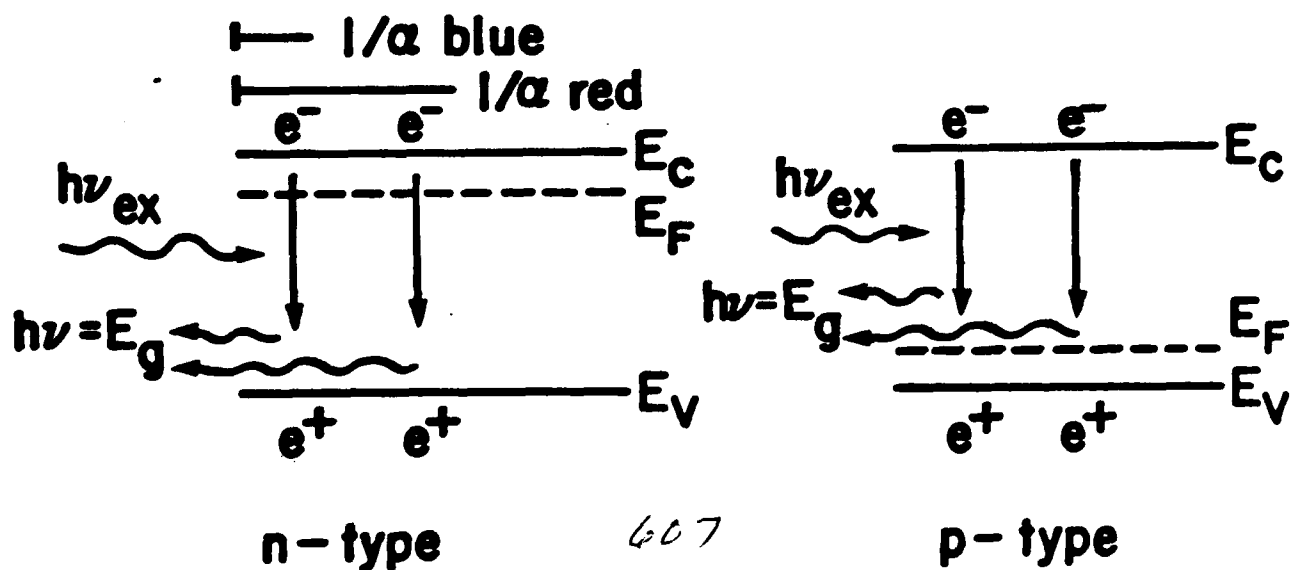
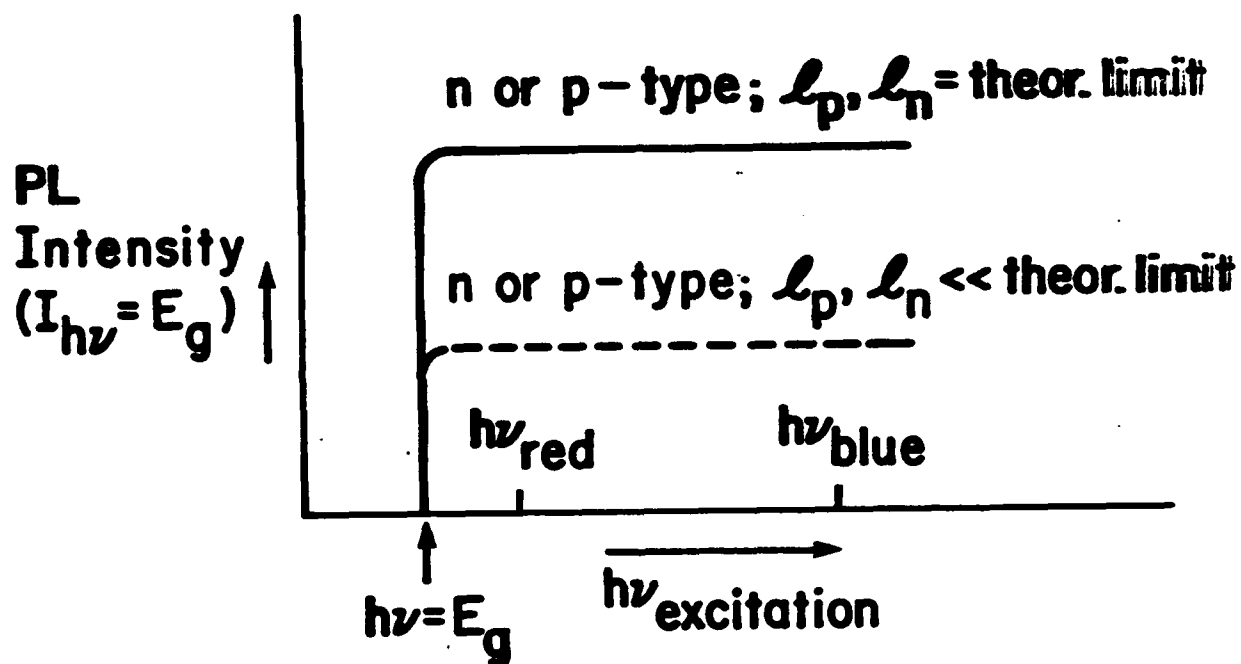
- Band edge photoluminescence of n and p-type GaAs versus excitation energy shows a nearly flat response indicating substantial decrease in both surface band bending and surface recombination velocity
- Raman Spectroscopy shows a reduced LO phonon intensity and an enhanced plasmon intensity indicating a reduced surface depletion region
- C-V measurements of Hg/PMMA/GaAs MOS capacitors are consistent with low interface state density



606

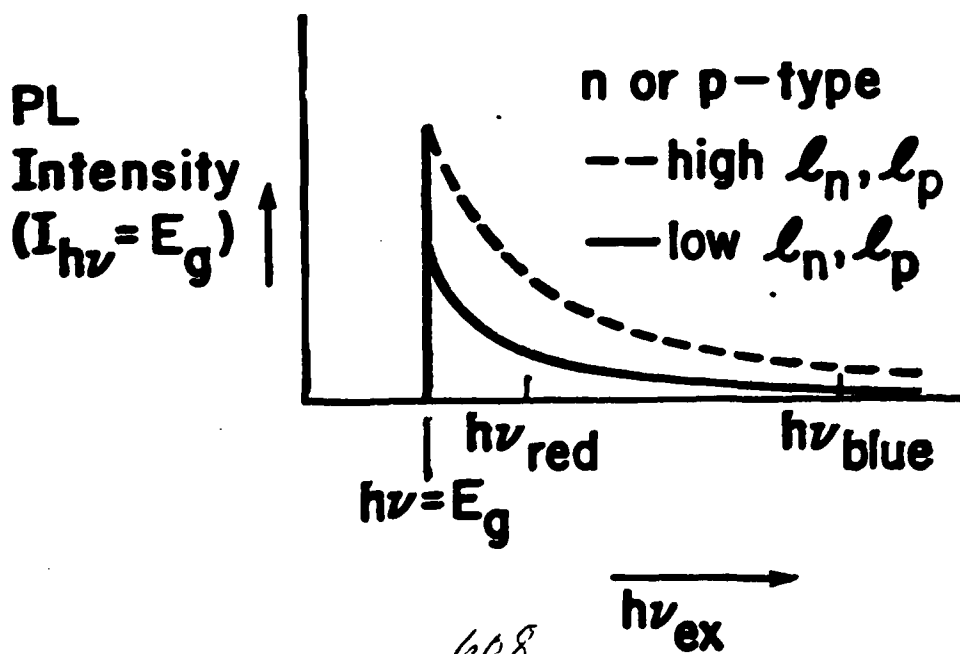
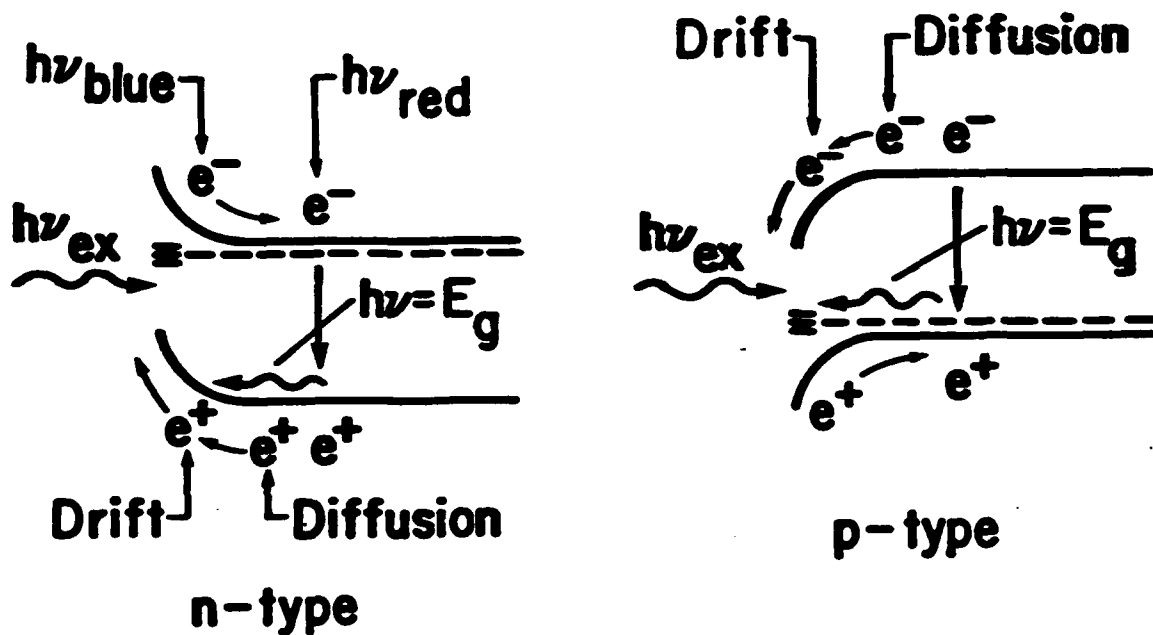
# PHOTOLUMINESCENCE (PL) SPECTROSCOPY

## CASE I: NO PINNING, i.e. flat band



# PHOTOLUMINESCENCE SPECTROSCOPY

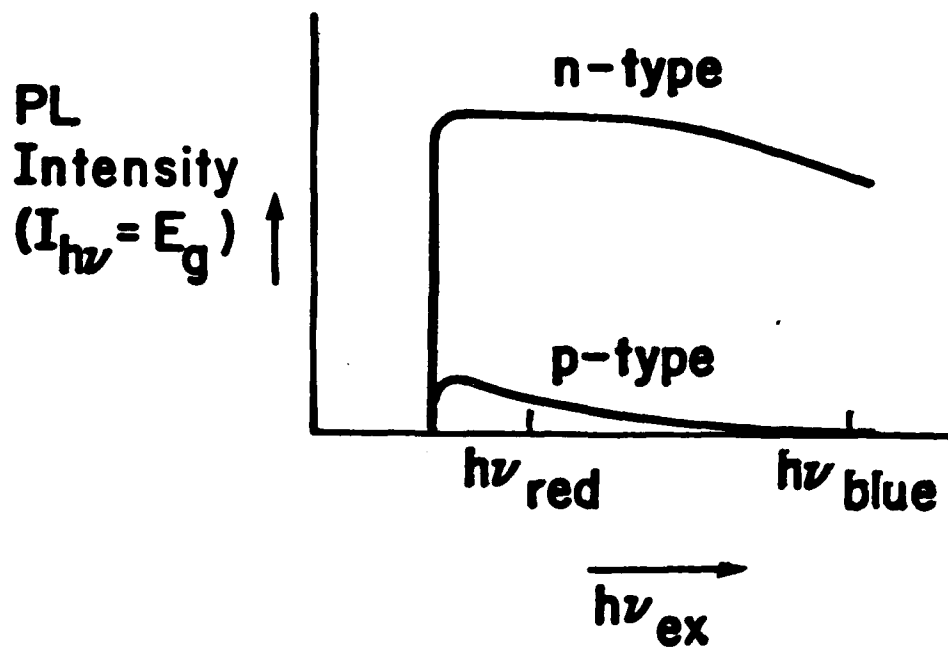
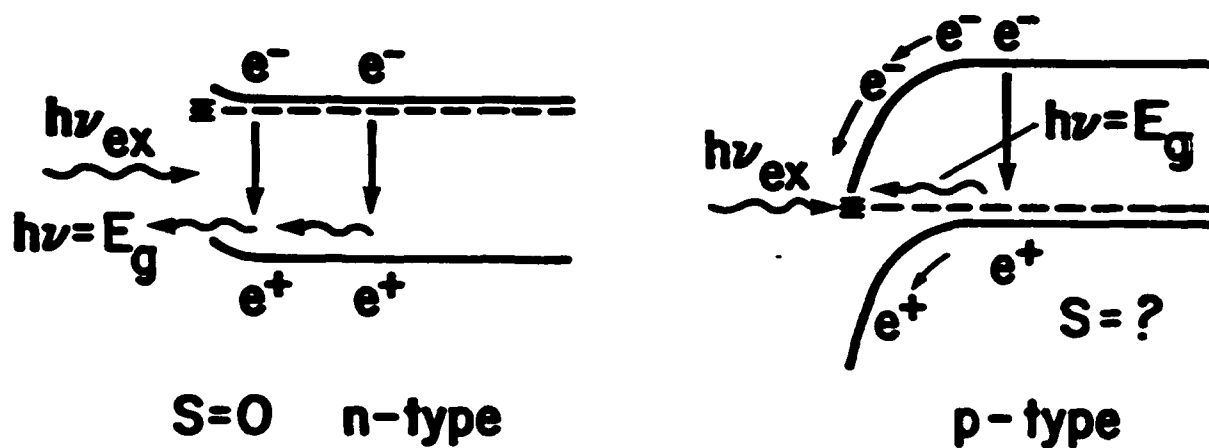
## CASE II: MID-GAP PINNING



# PHOTOLUMINESCENCE SPECTROSCOPY

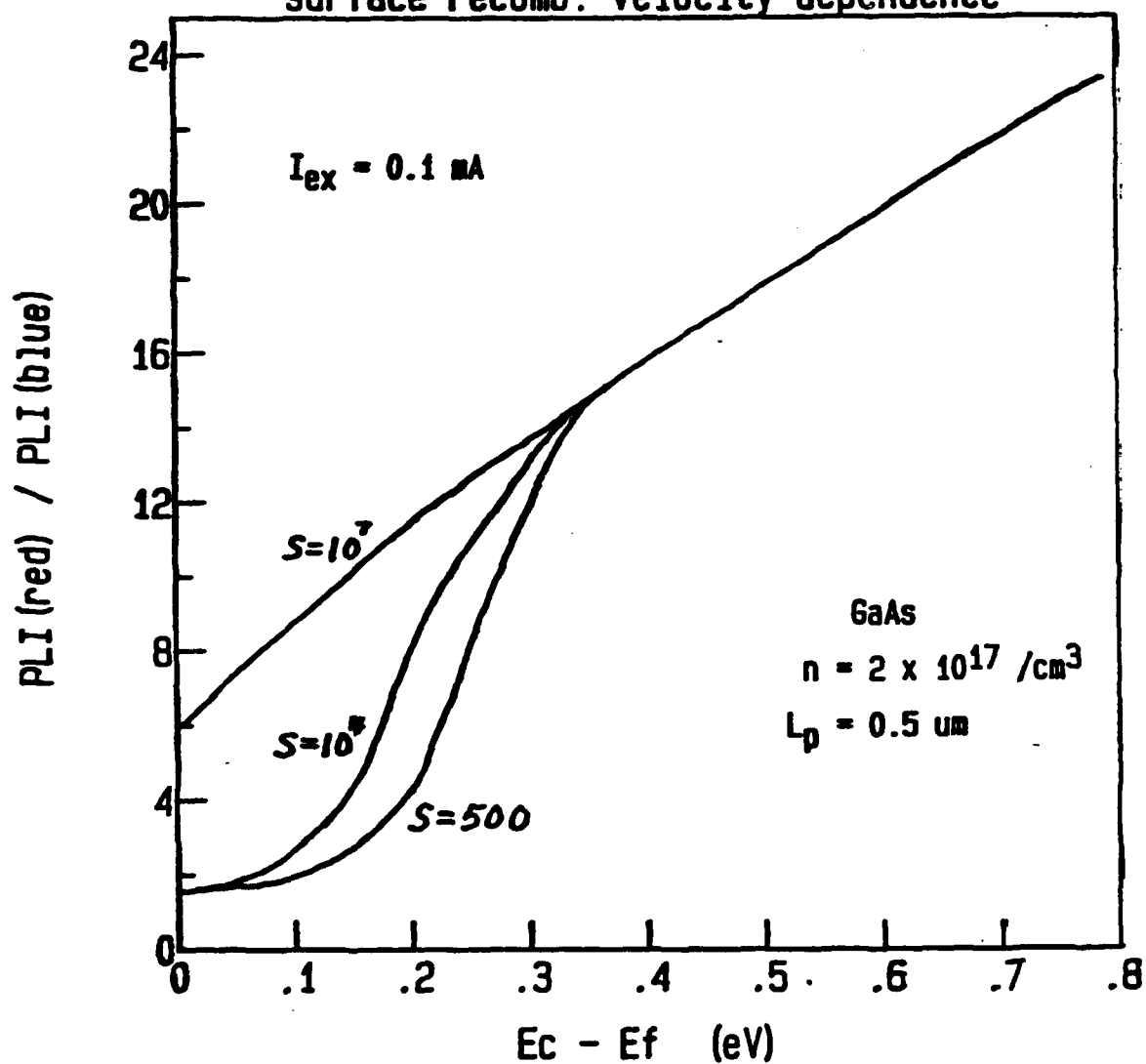
## CASE III: PINNING NEAR A BAND EDGE

e.g. InP

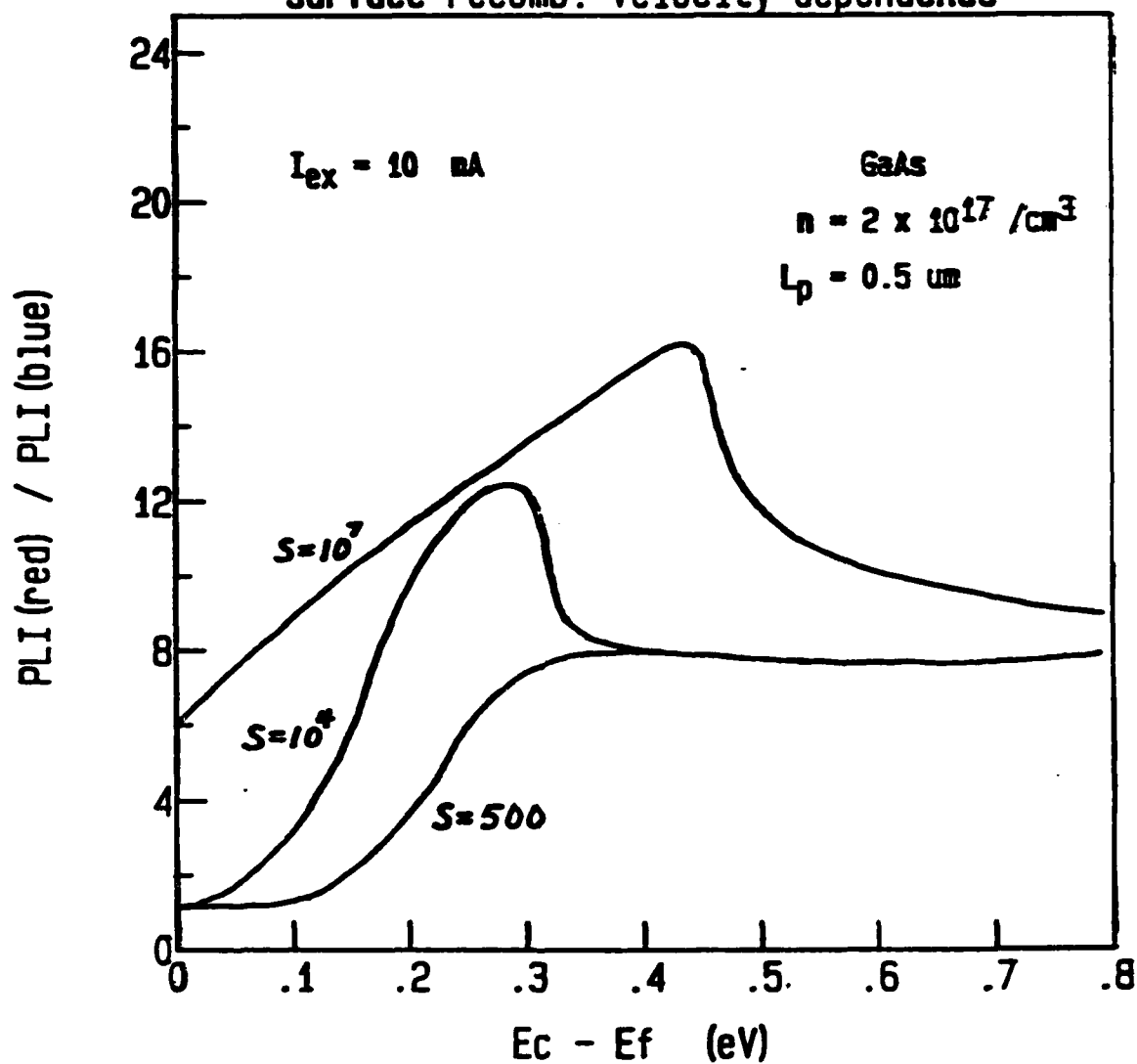


609

# PL Quantum Yield vs. Band Bending surface recomb. velocity dependence



# PL Quantum Yield vs. Band Bending surface recomb. velocity dependence





# Photoluminescence Results

## PL Intensity:

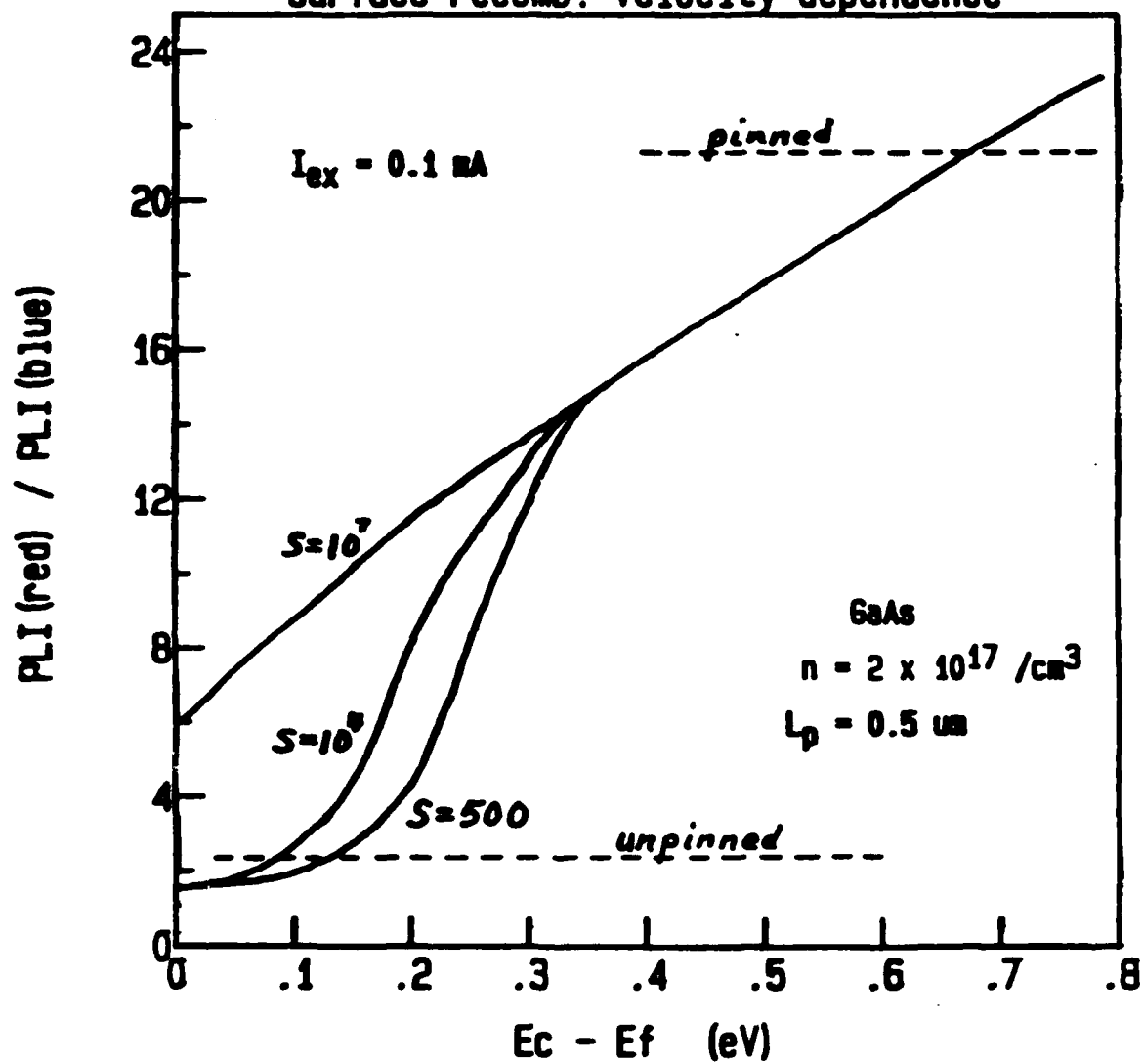
	<u>Before</u>		<u>After</u>	
	blue	red/blue	blue	red/blue
n-type	1	20	15	-2
p-type	10	4	80	~2

Analysis: Woodall et al. JVST 16(5)1389  
(1979)  
n-type GaAs  
 $N_D = 2 \times 10^{17} / \text{cm}^3$   
 $L_p = 0.5 \mu\text{m}$  from EBIC

$$\text{red/blue} = 20 \Rightarrow \begin{aligned} V_B &= 0.8 \text{ volts} \\ v_s &= 10^7 \text{ cm/sec} \end{aligned}$$

$$\text{red/blue} = 2 \Rightarrow \begin{aligned} V_B &= 0.1 \text{ volts} \\ v_s &= 10^4 \text{ cm/sec} \end{aligned}$$

# PL Quantum Yield vs. Band Bending surface recomb. velocity dependence



# Plasmon - Phonon Coupling

Courtesy F. Pollak, Brooklyn College

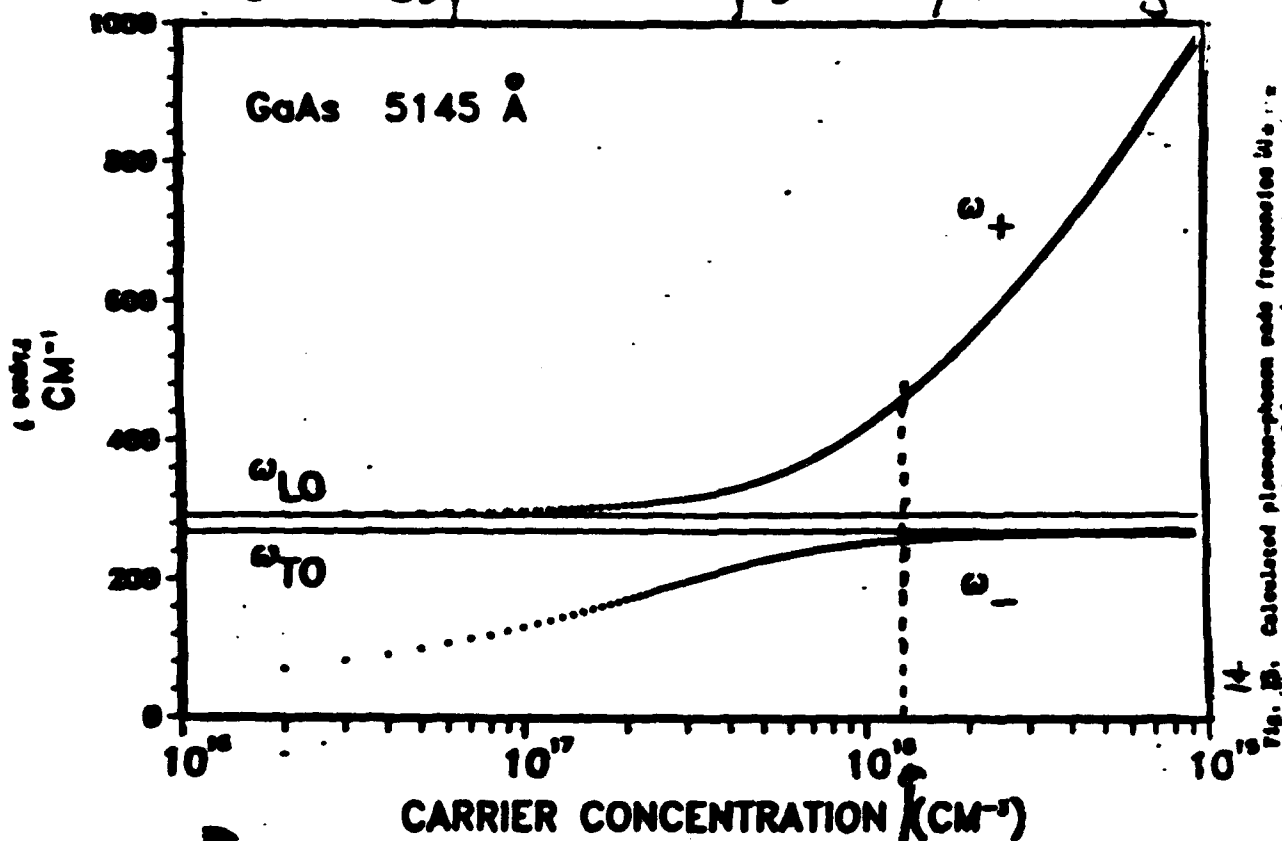
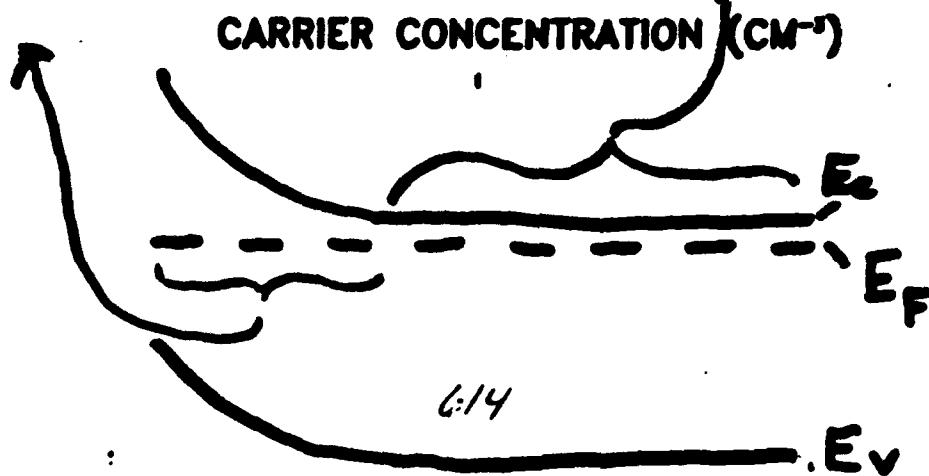
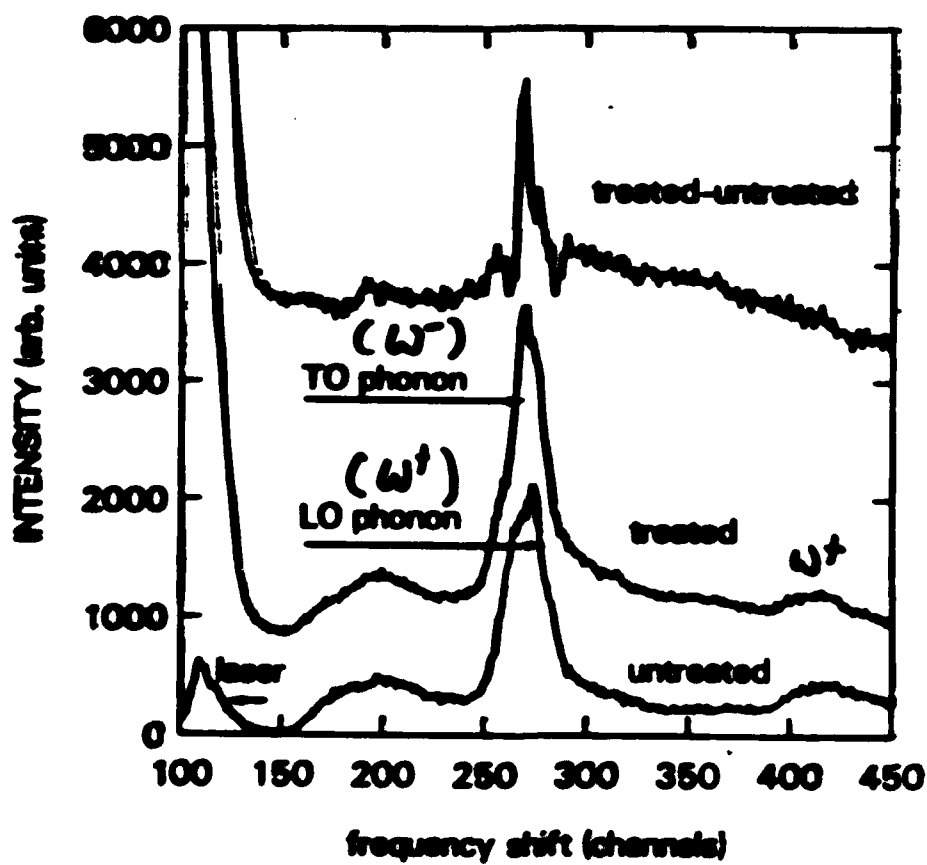
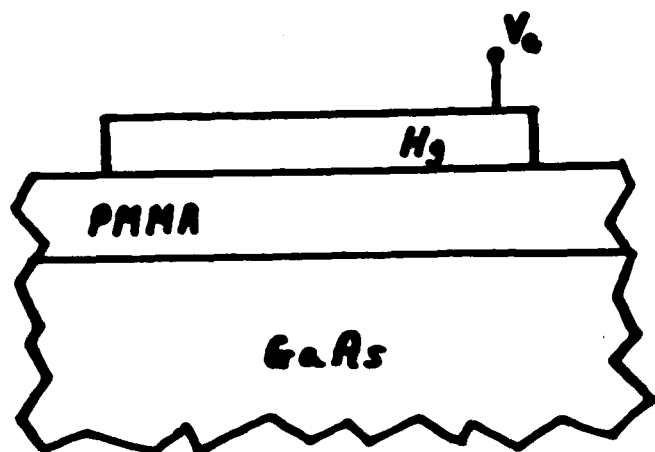


Fig. 14. Calculated plasmon-phonon mode frequencies  $\omega_{\pm}$  as a function of free carrier concentration for GaAs. The solid lines correspond to the bulk LO and TO modes. The calculations have been corrected for finite carrier concentration effects.

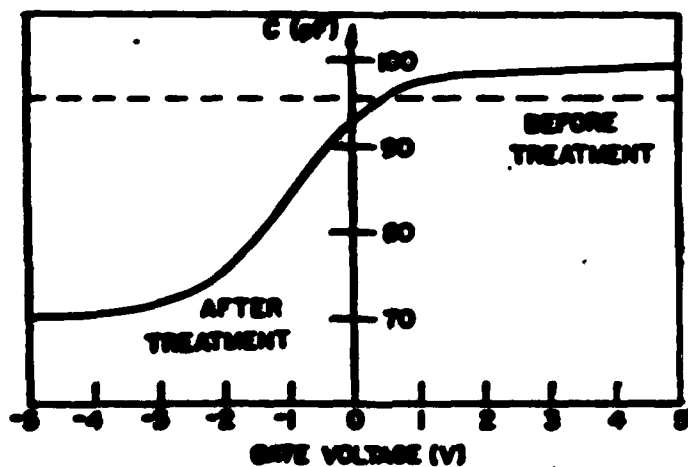




# Capacitor Structures

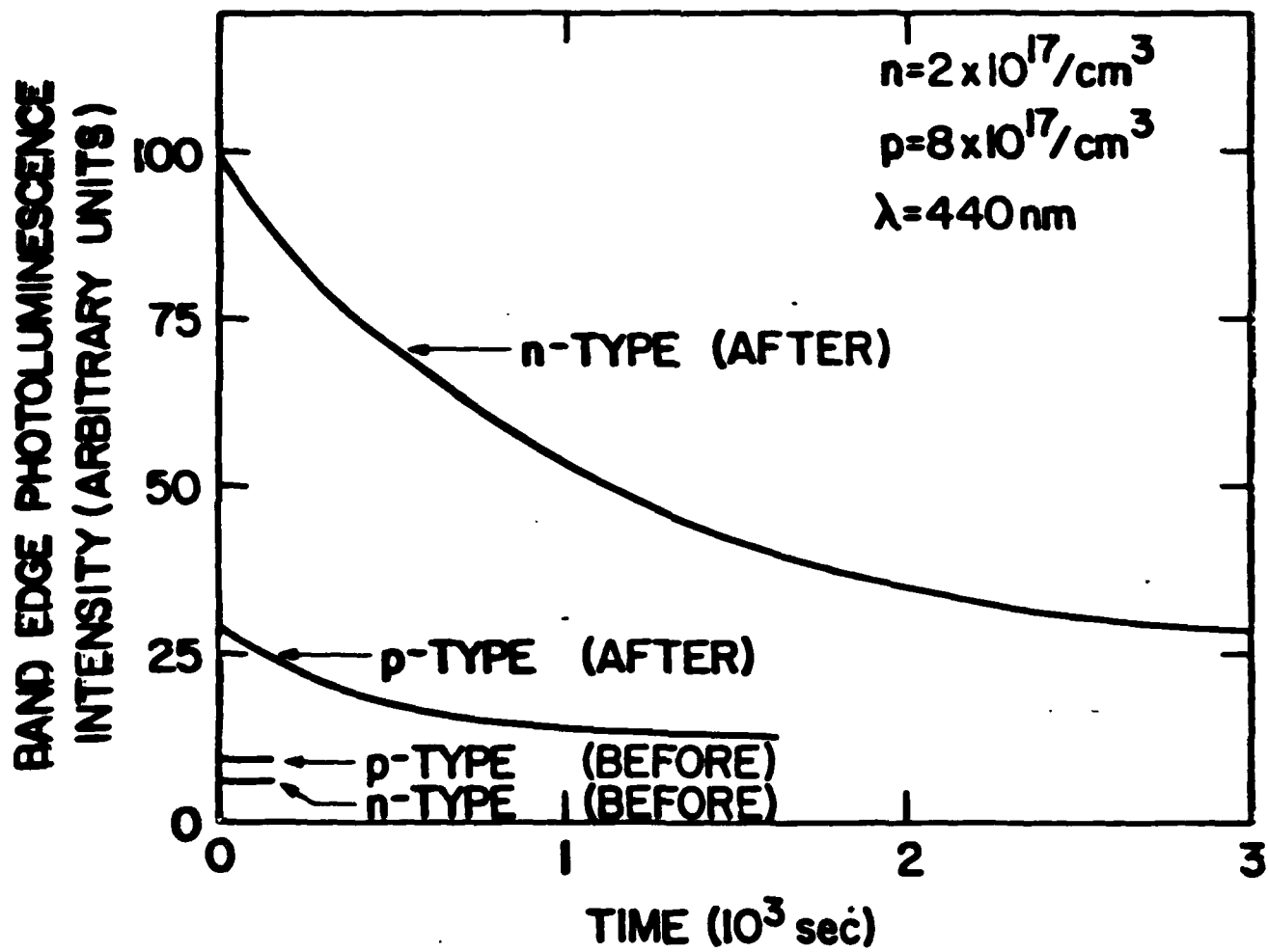


0.1  $\mu\text{m}$  of PMMA on treated or untreated GaAs

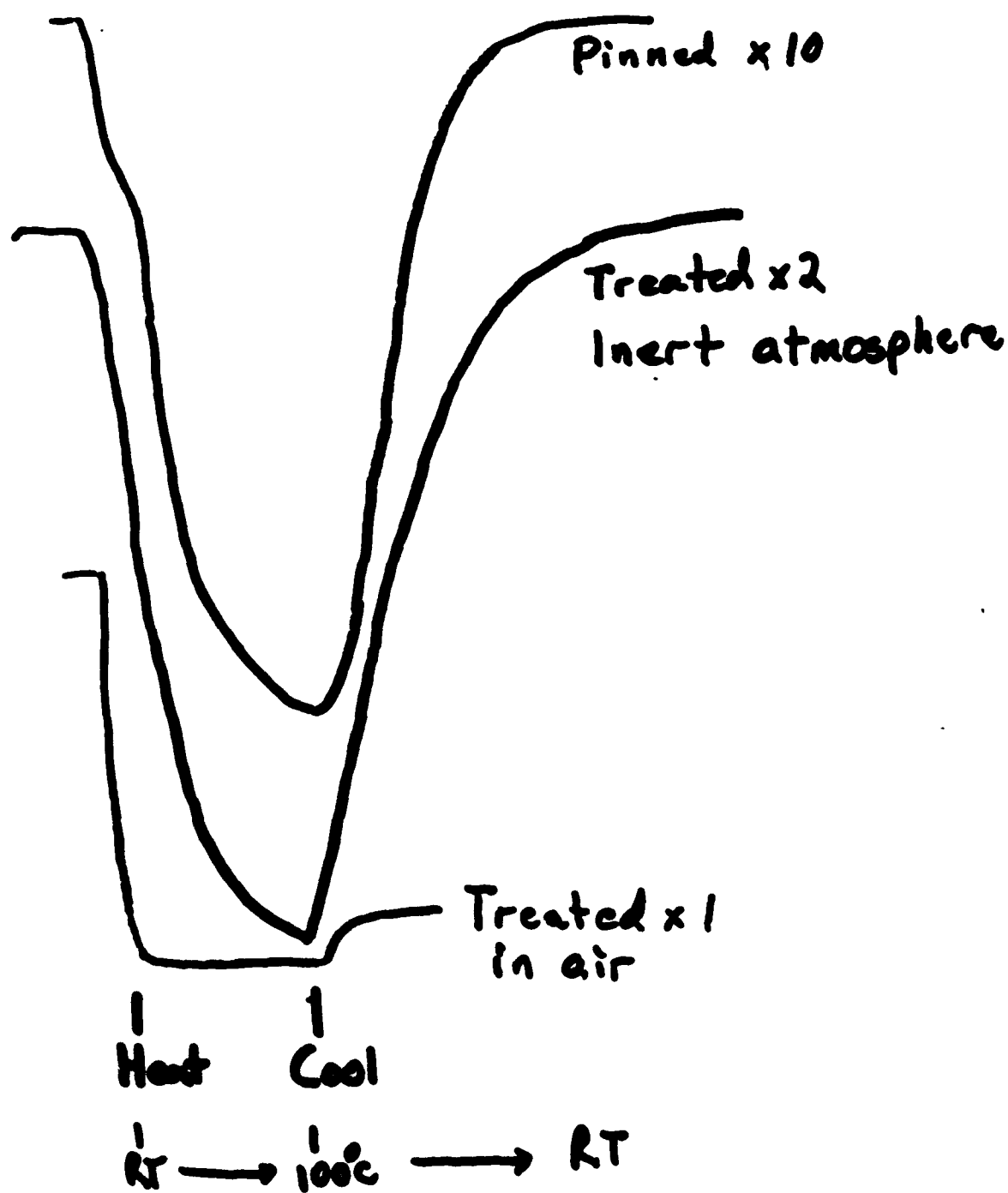


(20 KHz)

High frequency C-V, n-type GaAs  
 from Offsey, et al., APL 48(7) 475 (1986)  
 616



# PL vs Time



# Auger Data

Photo-Rinsed

Etched, Rinsed, Air Exposed

C

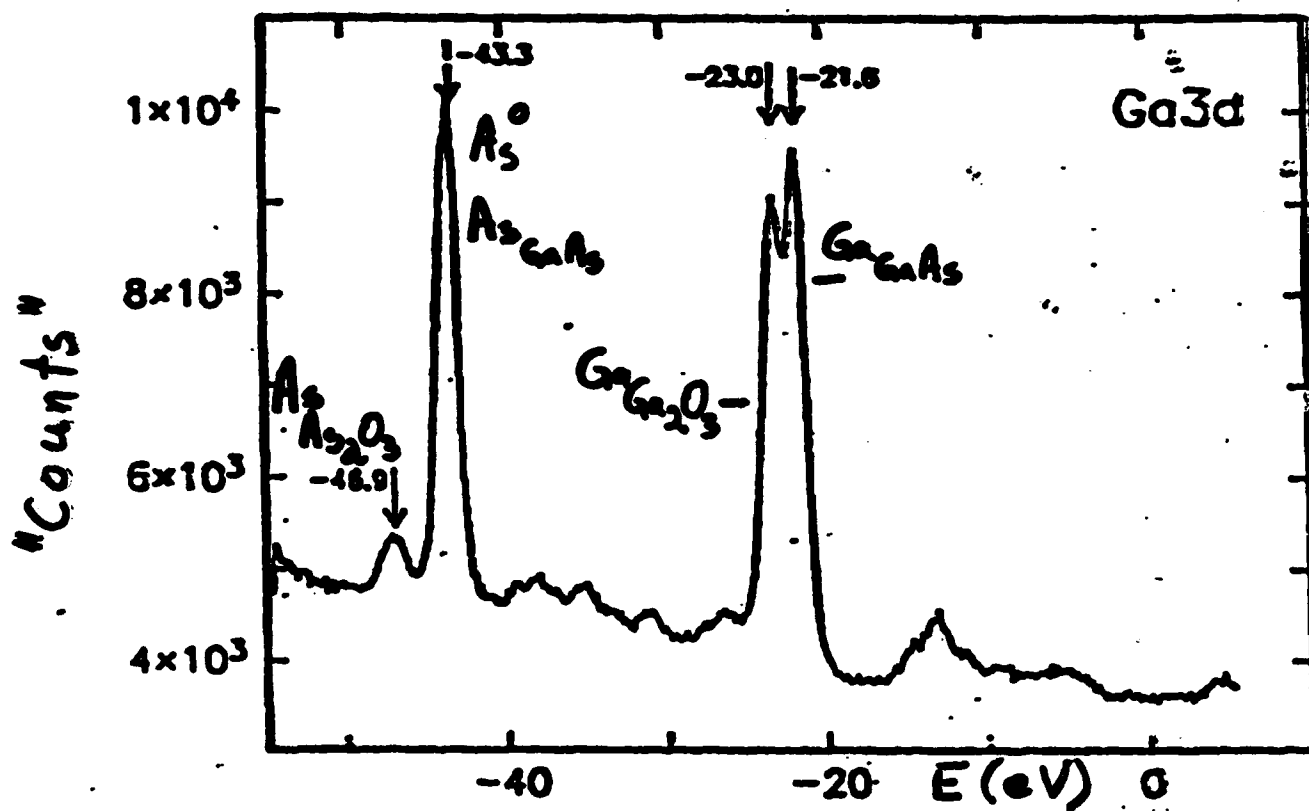
O

Ga. As

619



# XPS Data - J. Baker



$\Rightarrow 13 \text{ \AA } Ga_2O_3 (90\%)$

### **Characteristics of the Treated (Unpinned) Surface**

- Repins in air ( $\tau \cong 1$  h) and on heating in air ( $\tau < 1$  m,  $T \cong 100^\circ\text{C}$ )
- Repins in acid and base solutions and vapors ( $\tau \cong 1$  s)
- Stable in vacuum and inert ambients even on heating ( $T \cong 100^\circ\text{C}$ )
- Stable in desiccated air at room temperature
- Auger electron spectroscopy of thick oxide layers shows oxide consists of  $> 98\%$  Ga oxide and  $< 2\%$  As oxide (detection limit). Untreated surface shows about equal parts of Ga and As oxides
- XPS of thinner oxides shows oxide species to be predominantly  $\text{Ga}_2\text{O}_3$

# Chemistry

1. Band-bending sweeps  $h\nu$ -generated minority carriers to surface, speeding oxidation
2.  $\text{GaAs} \rightarrow \text{Ga}_2\text{O}_3, \text{As}_2\text{O}_3, \dots, \text{As}^\circ$
3.  $\text{H}_2\text{O}$  removes  $\text{As}_2\text{O}_3$  &  $\text{As}^\circ$   
(Massies & Contour JAP 58 (1985) 806)
4.  $\text{Ga}_2\text{O}_3$  passivates GaAs surface
5. residual band-bending drives further oxidation

## Conclusions

- Unpinned GaAs in air
- Detection by CV, PL, Raman
- $\text{Ga}_2\text{O}_3$  layer
  - OK passivation
  - Lousy insulator
- Behavior supports EWF model where  $\text{As}^\circ$  is culprit
- Simple, inexpensive process

⇒ STILL A LONG WAY  
FROM GaAs MOSFETs

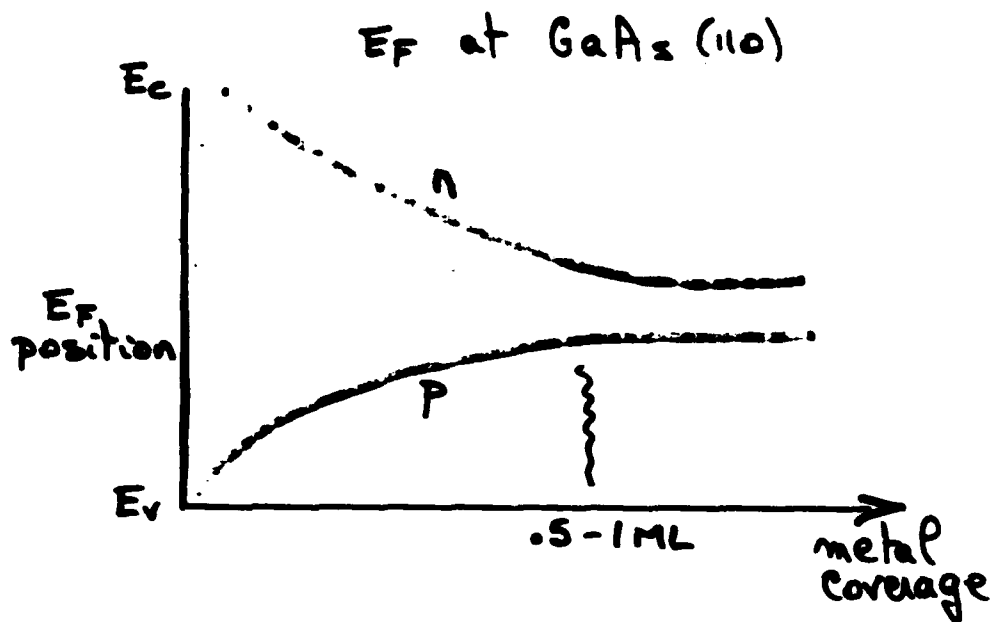
# Kinetics of Initial Stages of Schottky Barrier Formation\*

K. Stiles and A. Kahn  
Dept. of EE, Princeton Univ.

D. Kilday and J. Margaritondo  
SRC, Univ. of Wisconsin

\* Partially supported by NSF (DMR-84-06820)

1. Motivation for low temperature (LT) experiments.
2. Experiments (LEED, AES, EELS, SXPS).
3. Morphology of interfaces formed at LT Al, In and Au on GaAs(110).
4. Effect of temperature on initial pinning at GaAs interfaces with Al, Au, In, Ag and Sn : multi-mechanism picture?
5. Conclusions.



### Metal-induced defects

- Origin of defects?
- Nature of defects?
- homogeneity of pinning?
- role of structure?

### Metal-induced gap states

- pinning at ultra-low coverage? (metal?)
- homogeneity of pinning

Rapid and quasi-symmetric initial pinning on n- and p- substrates at RT could result from simultaneity of various "interface phenomena"

## Experiment

Soft X-ray Photoemission Spectroscopy:  
band bending measured from Ga-3d and As-3d  
core level shifts.

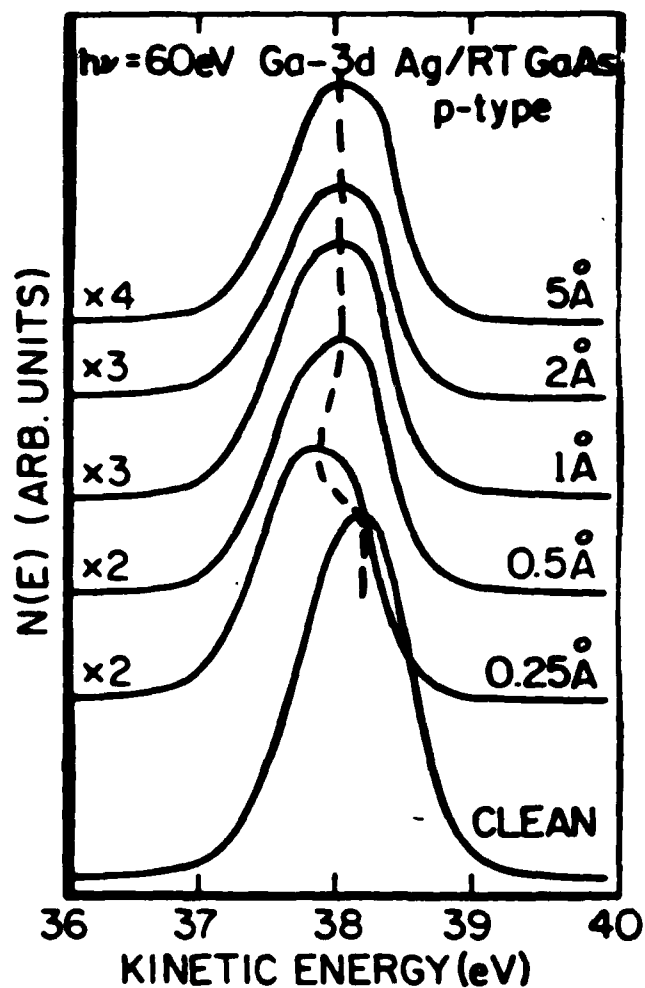
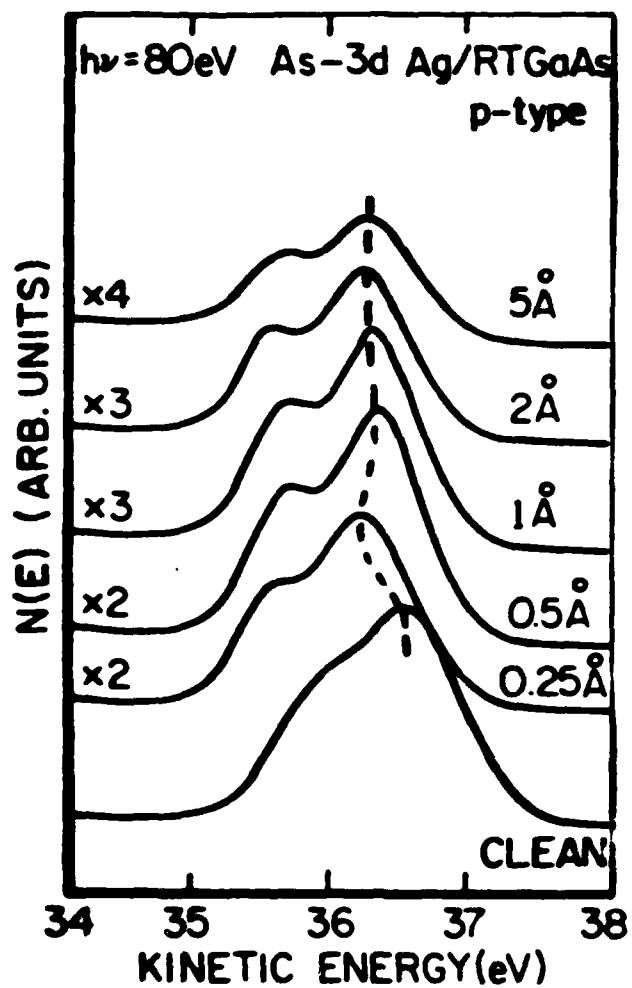
n-type ( $4-7 \times 10^{17} \text{ cm}^{-3}$ ) and p-type ( $1 \times 10^{18} \text{ cm}^{-3}$ )  
GaAs substrates.

metal deposited on room temperature (RT) and  
 $80^\circ \text{ K}$  (LT) surfaces.

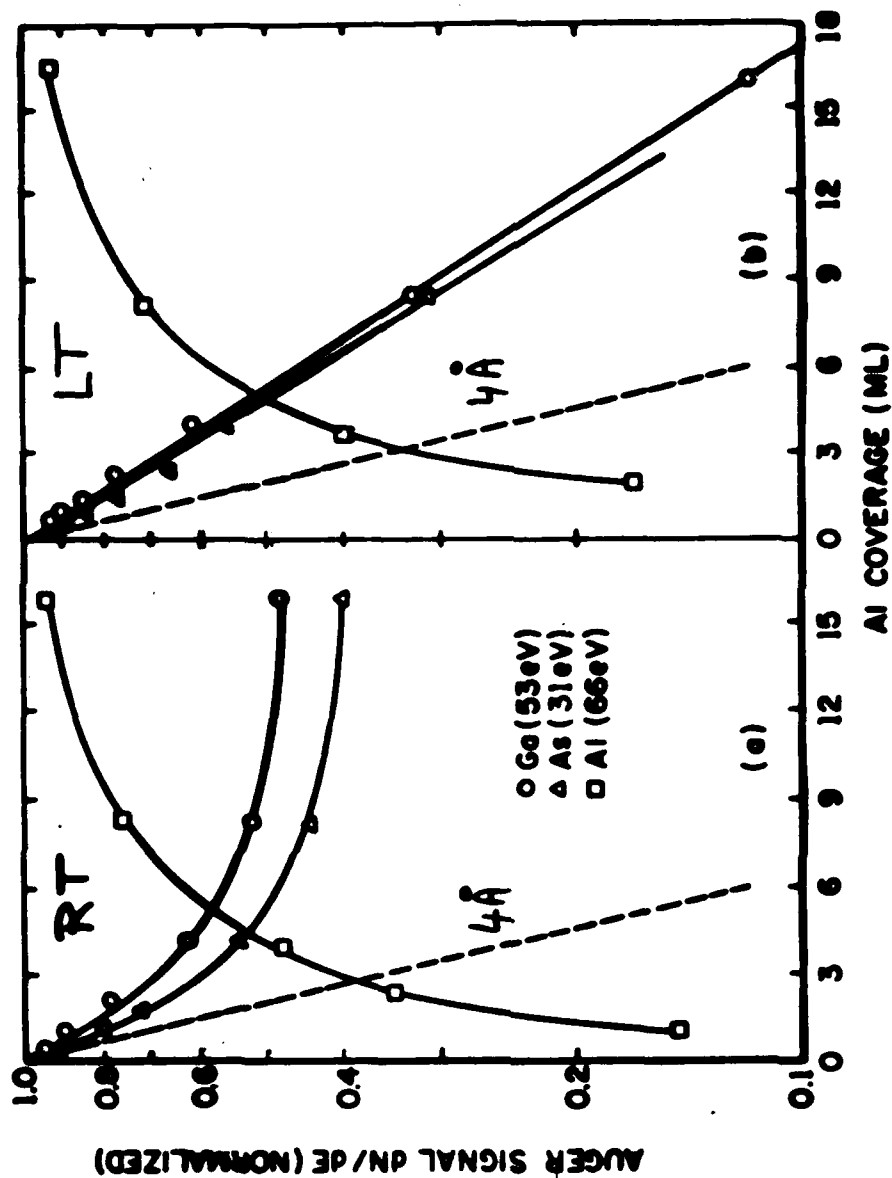
coverage ranges :  $0.05 - 20 \text{ \AA}$

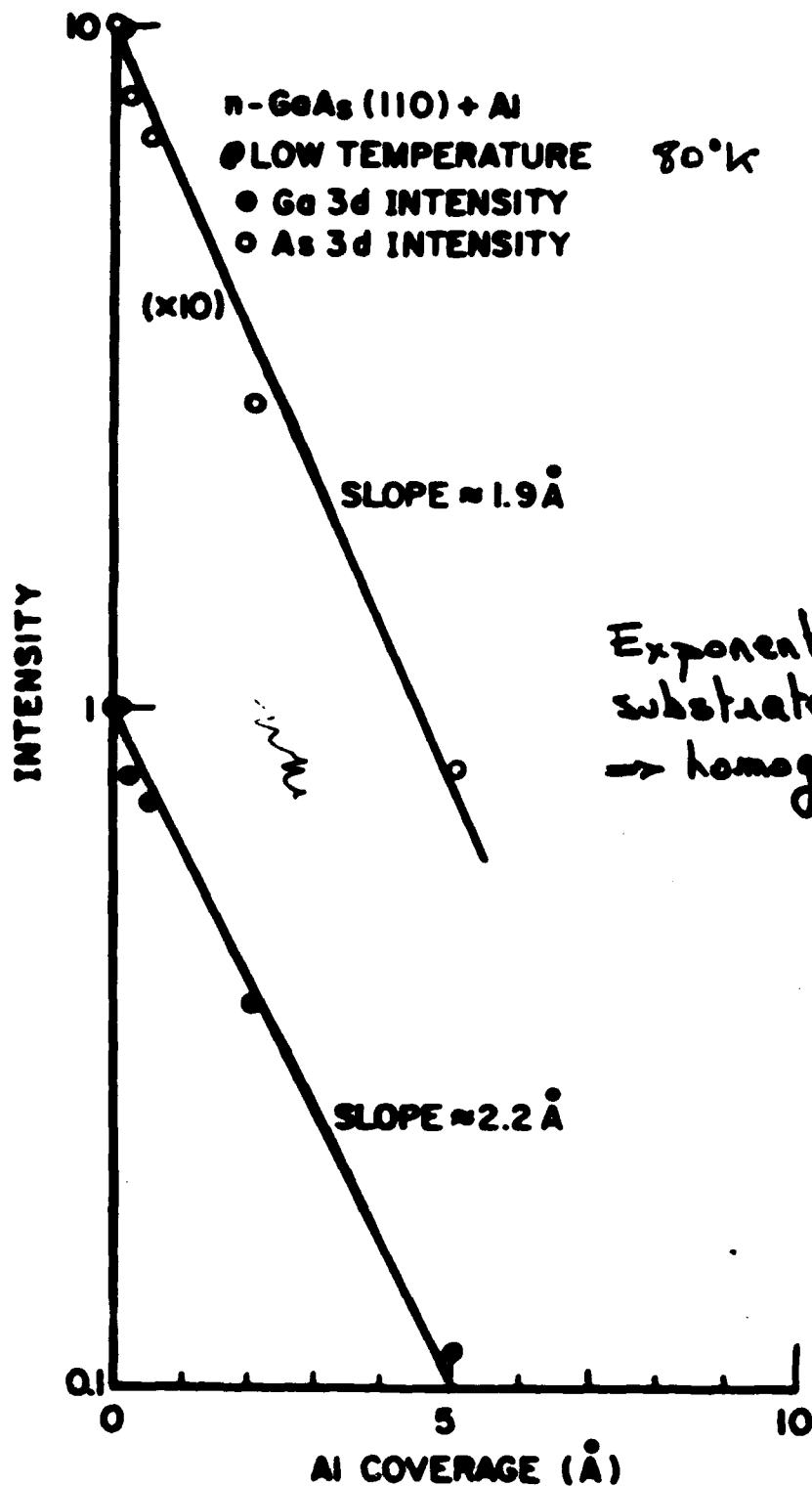
Other measurements :	LEED	Al, In / GaAs
	AES	Al, In, Au / GaAs
	EELS	Al, In, Au / GaAs
	CPD	Al,





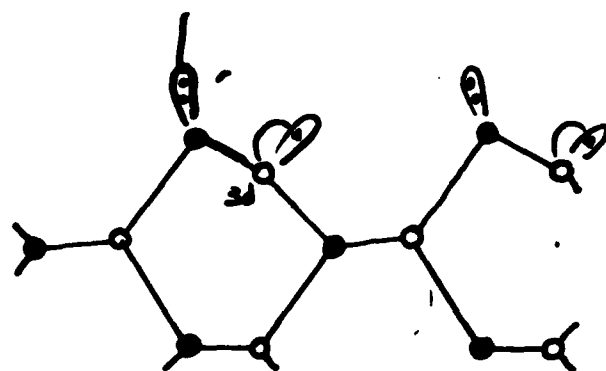
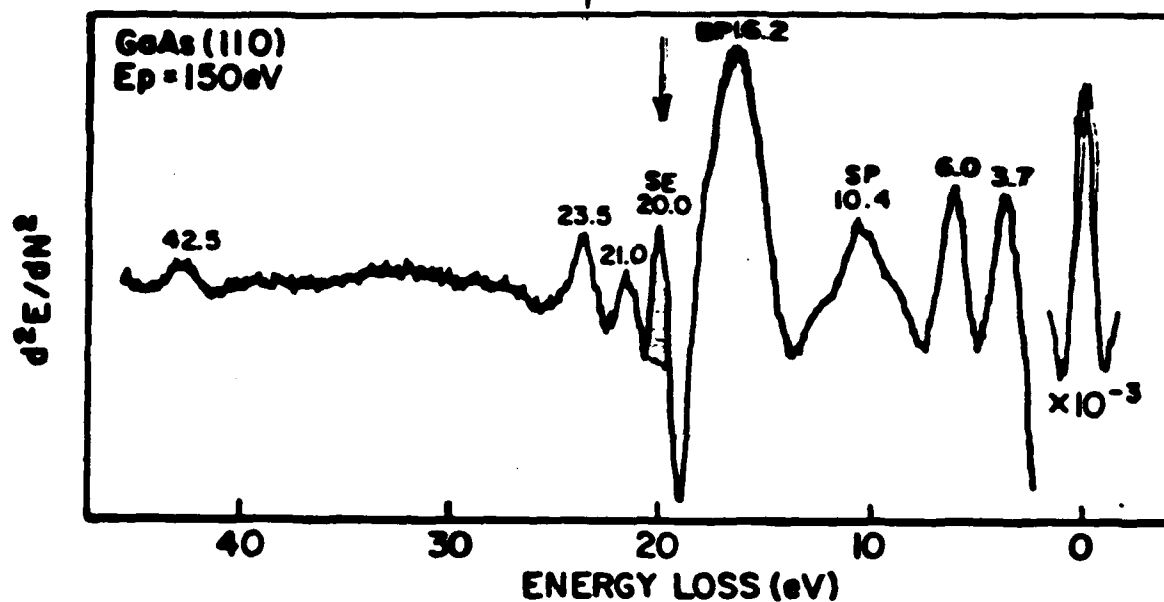
# Al on GaAs(110) (110°K)





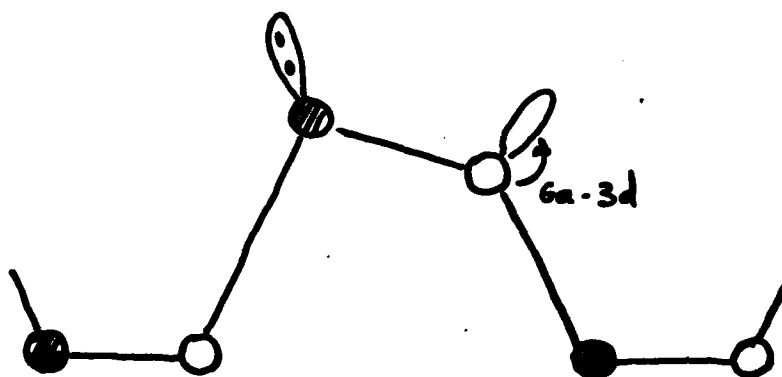
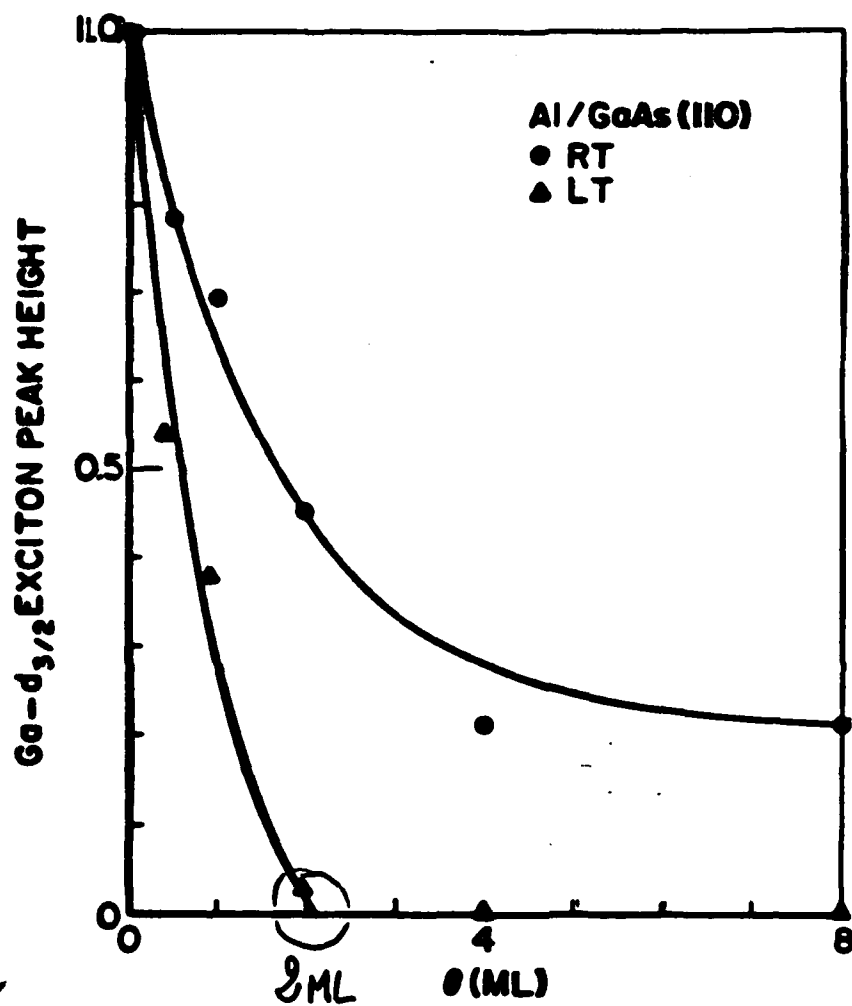
# EELS SPECTRUM FROM GaAs(110)

surface Exciton

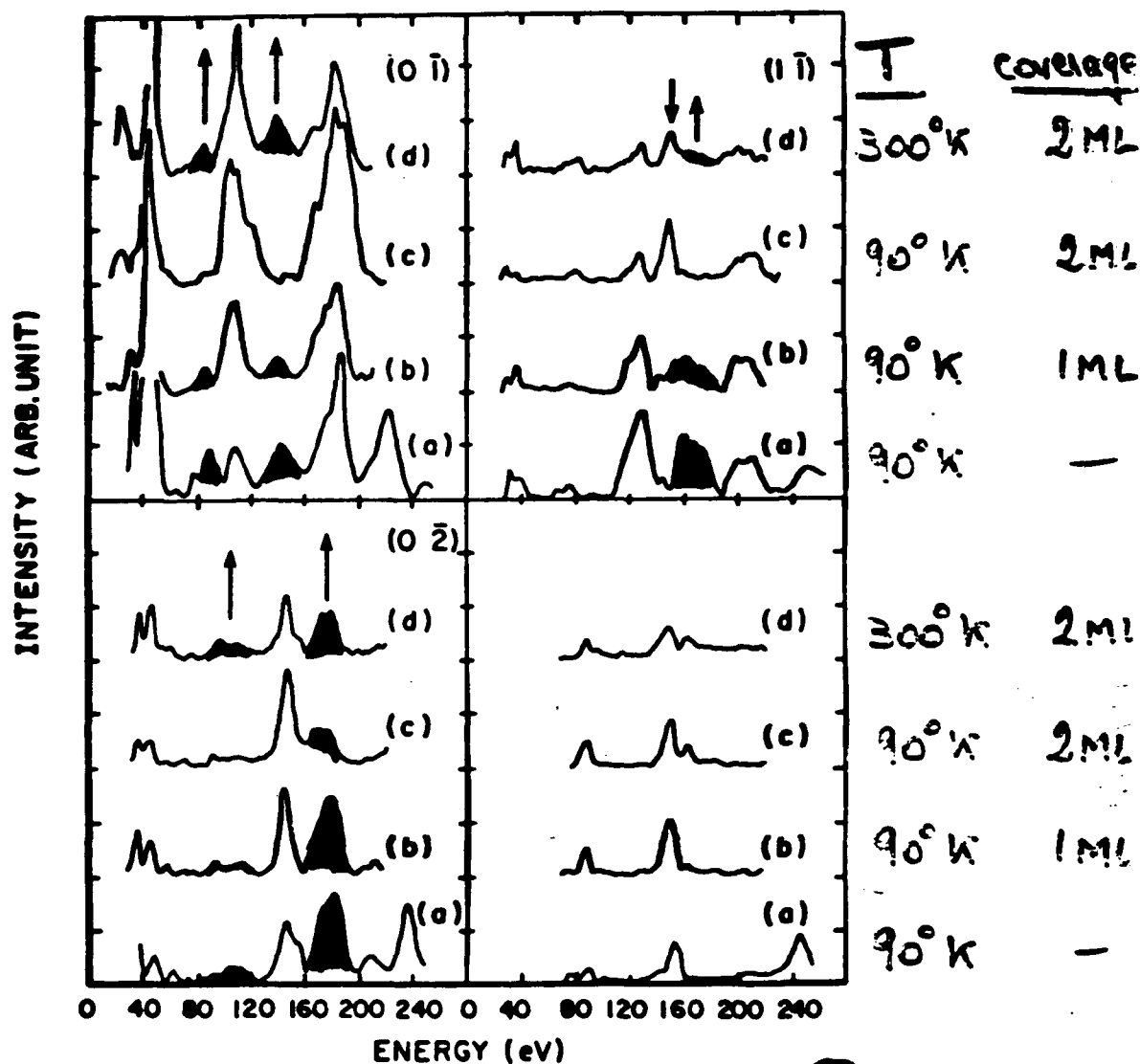


● As  
 ○ Ga

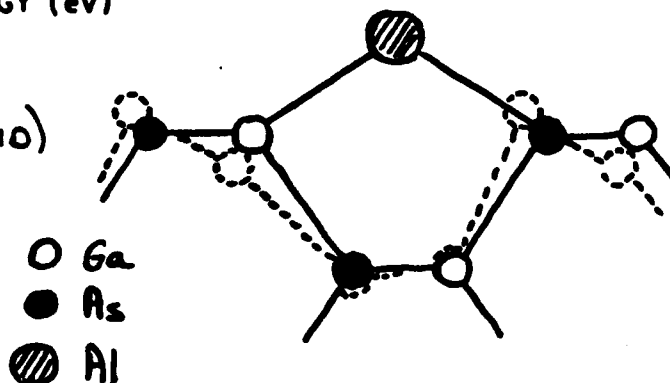
20 eV SE peak characteristic of  $sp^2$  like Ga



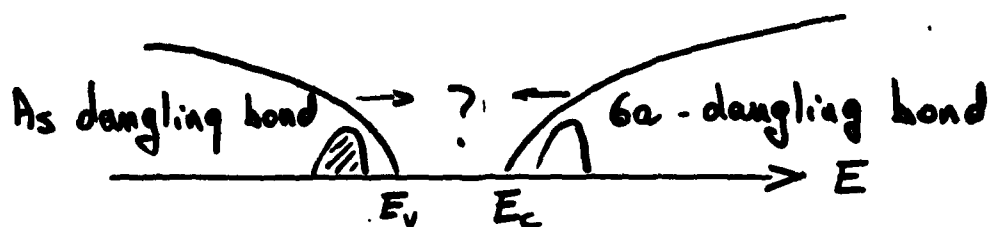
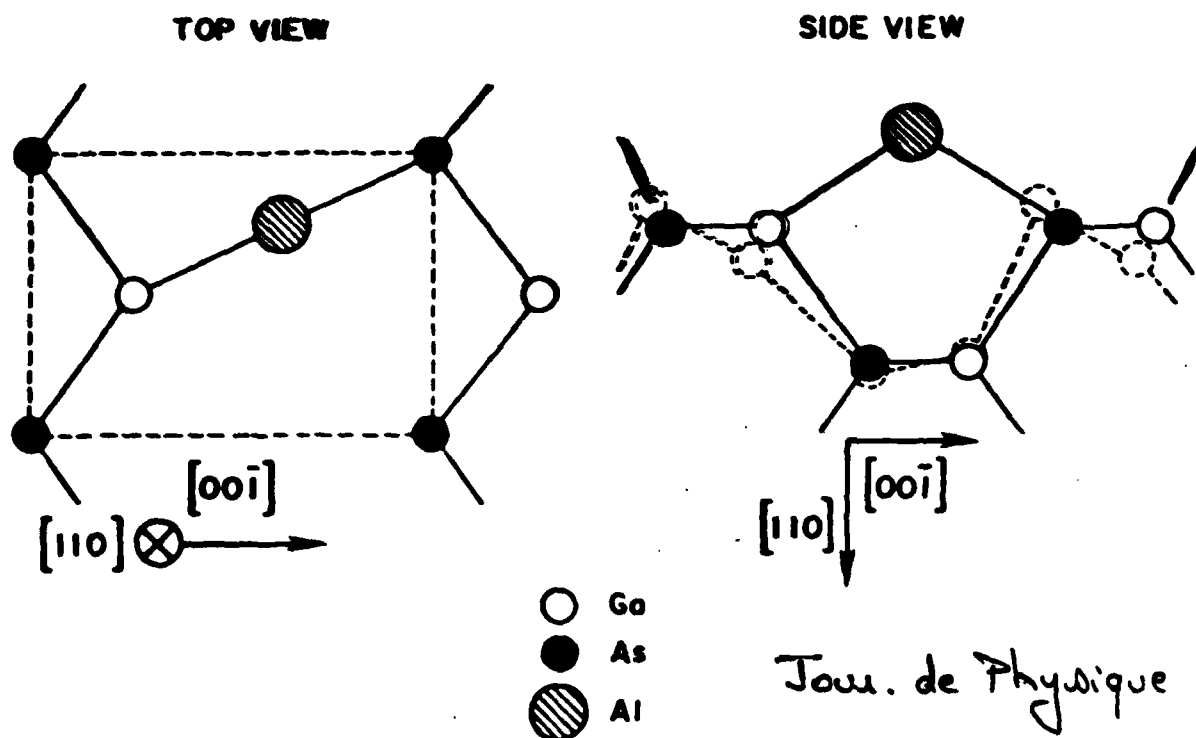
# GaAs LEED intensities for Al deposited at LT

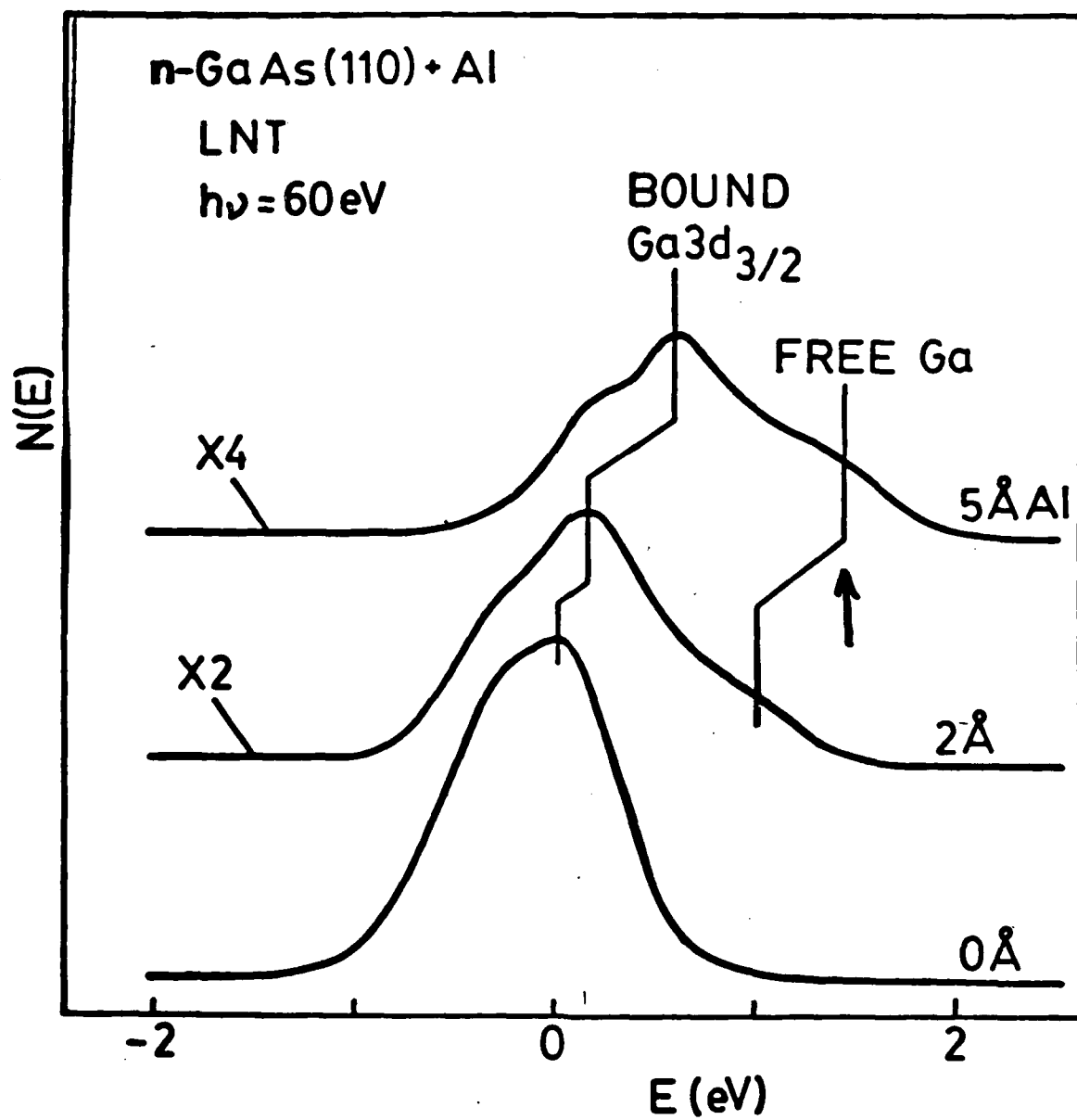


Reversible Al-induced  
cancellation of the GaAs (110)  
surface relaxation  
(detected at LT)



# Reversible Al-induced cancellation of the GaAs (110) surface relaxation (detected at LT)





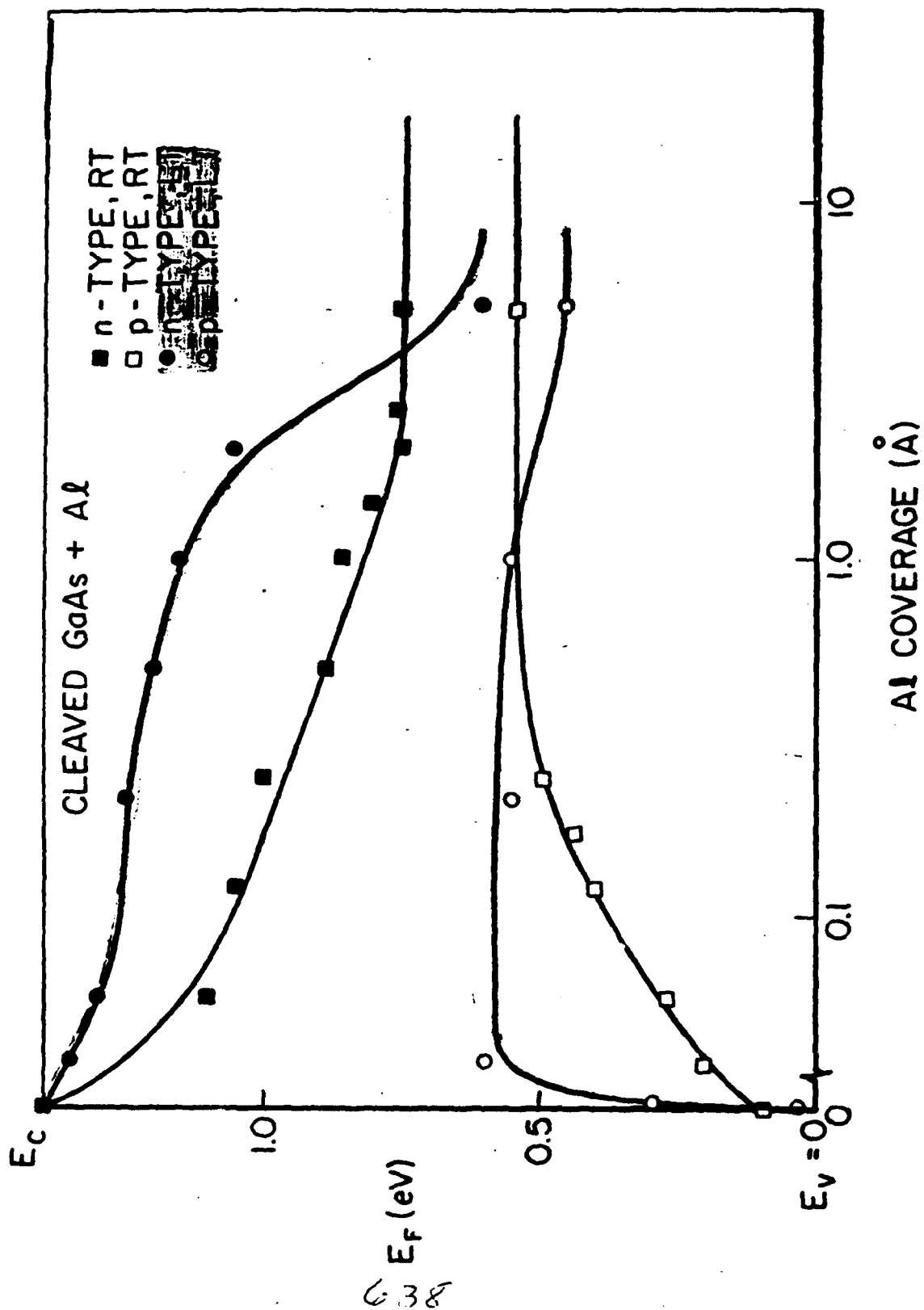
Reduced Al - Ga exchange reaction

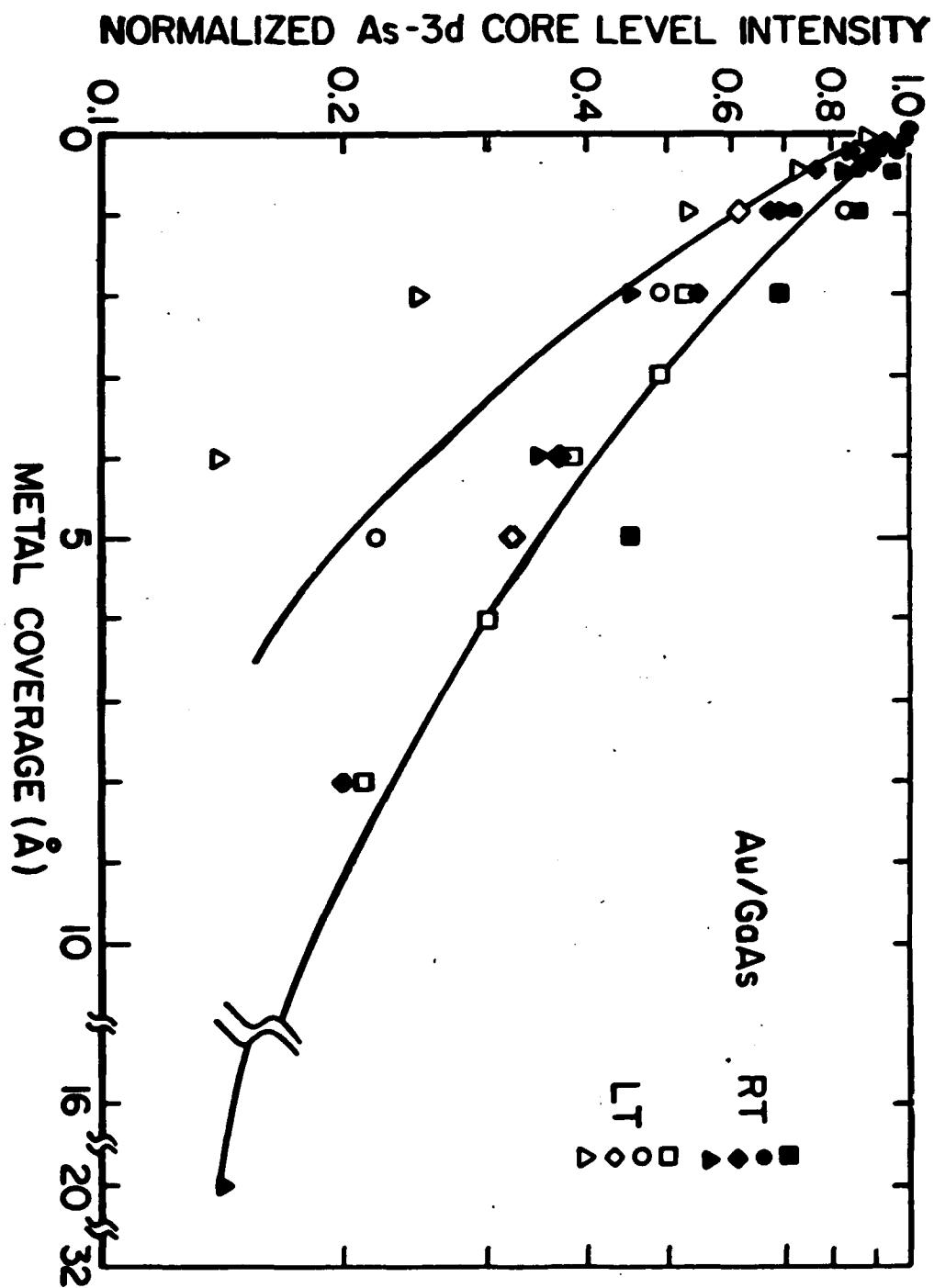
Solid State Communications

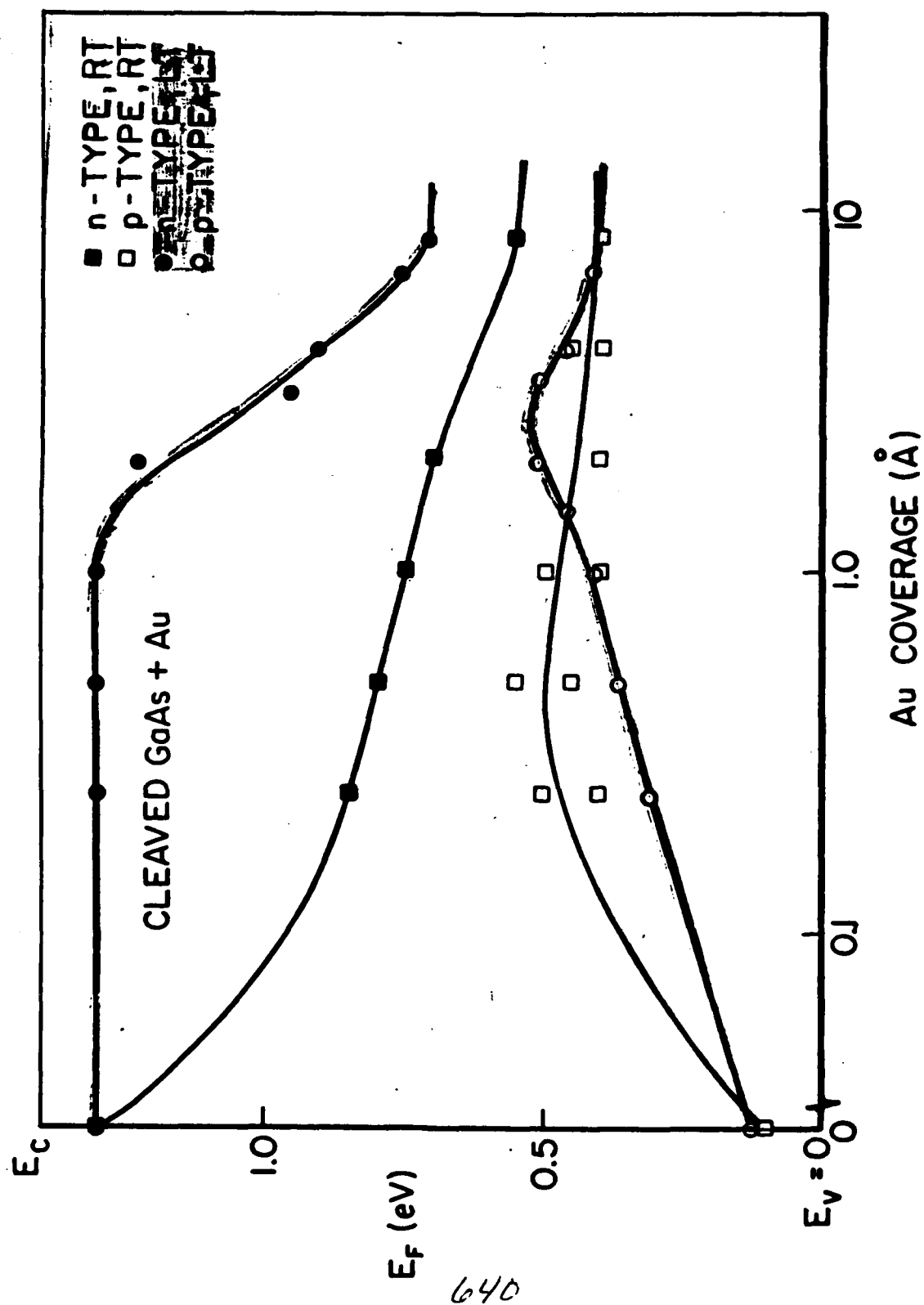
637

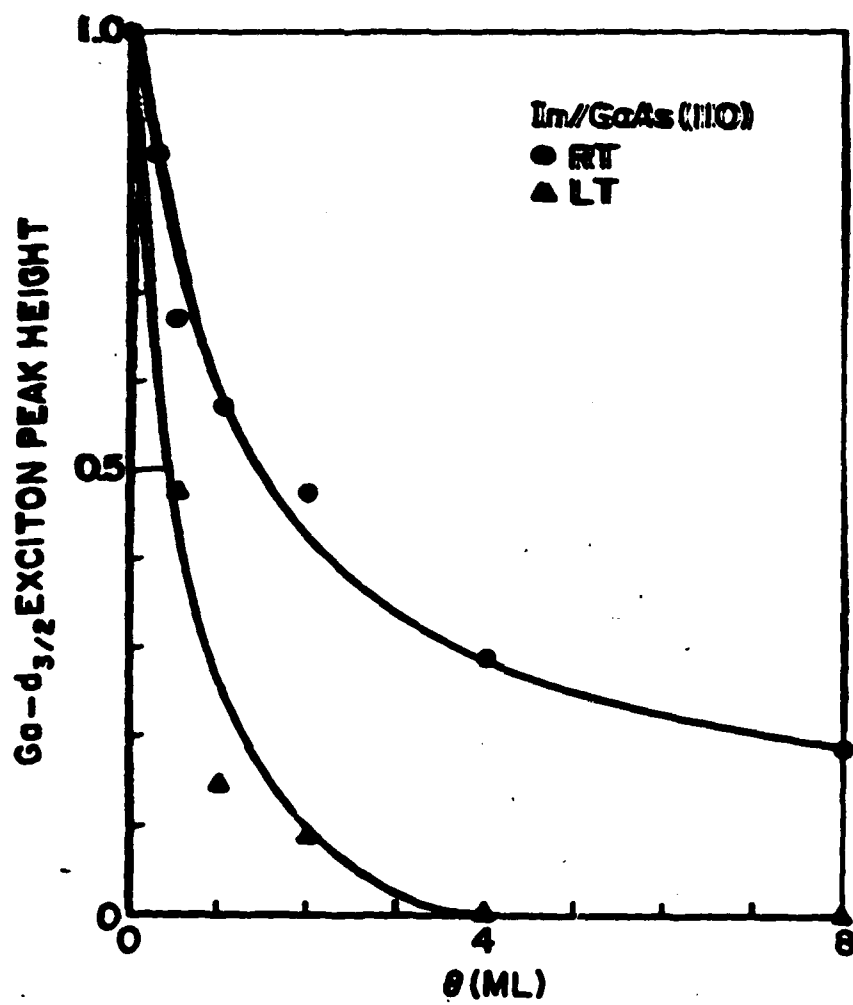
1986

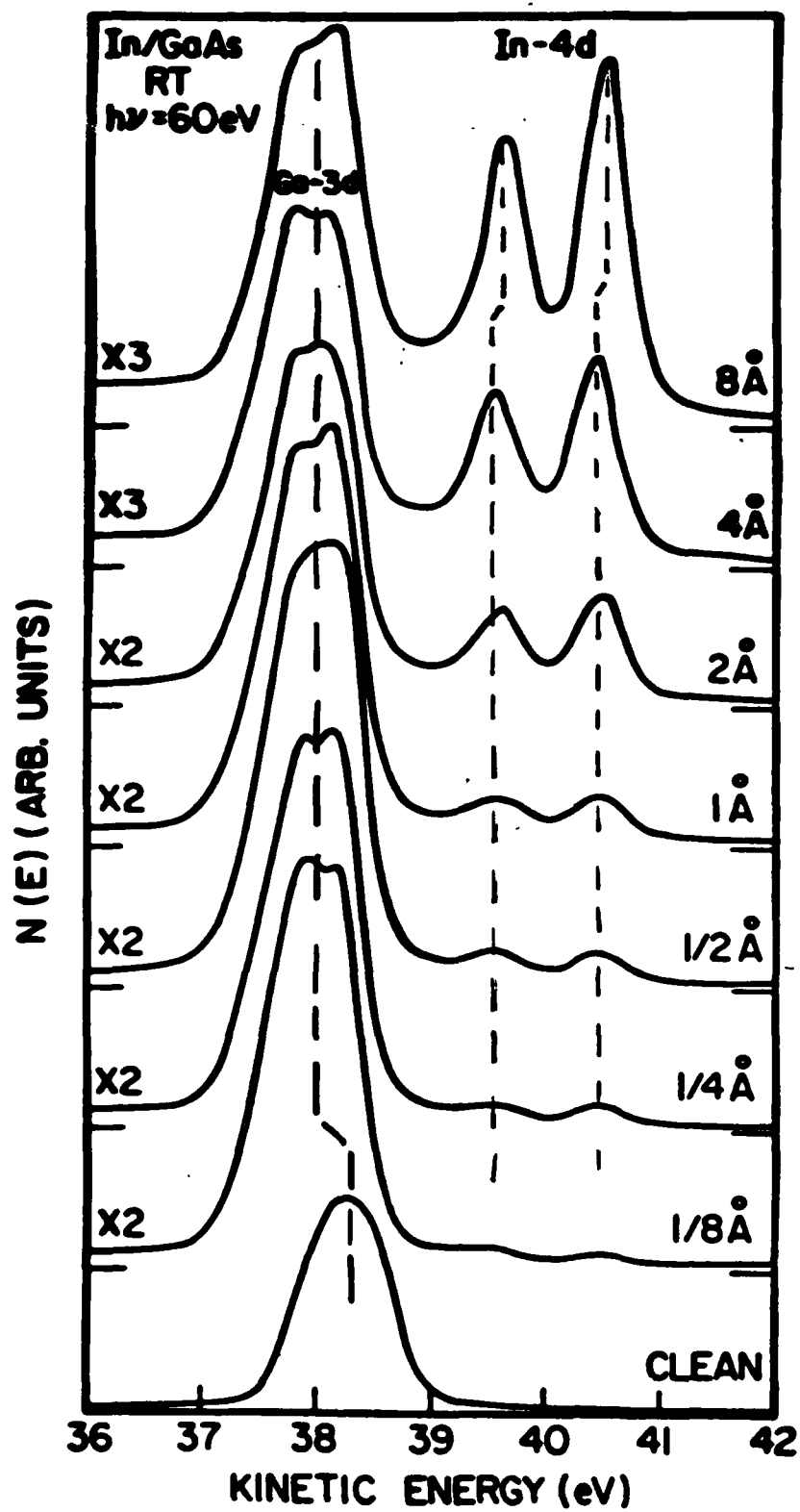


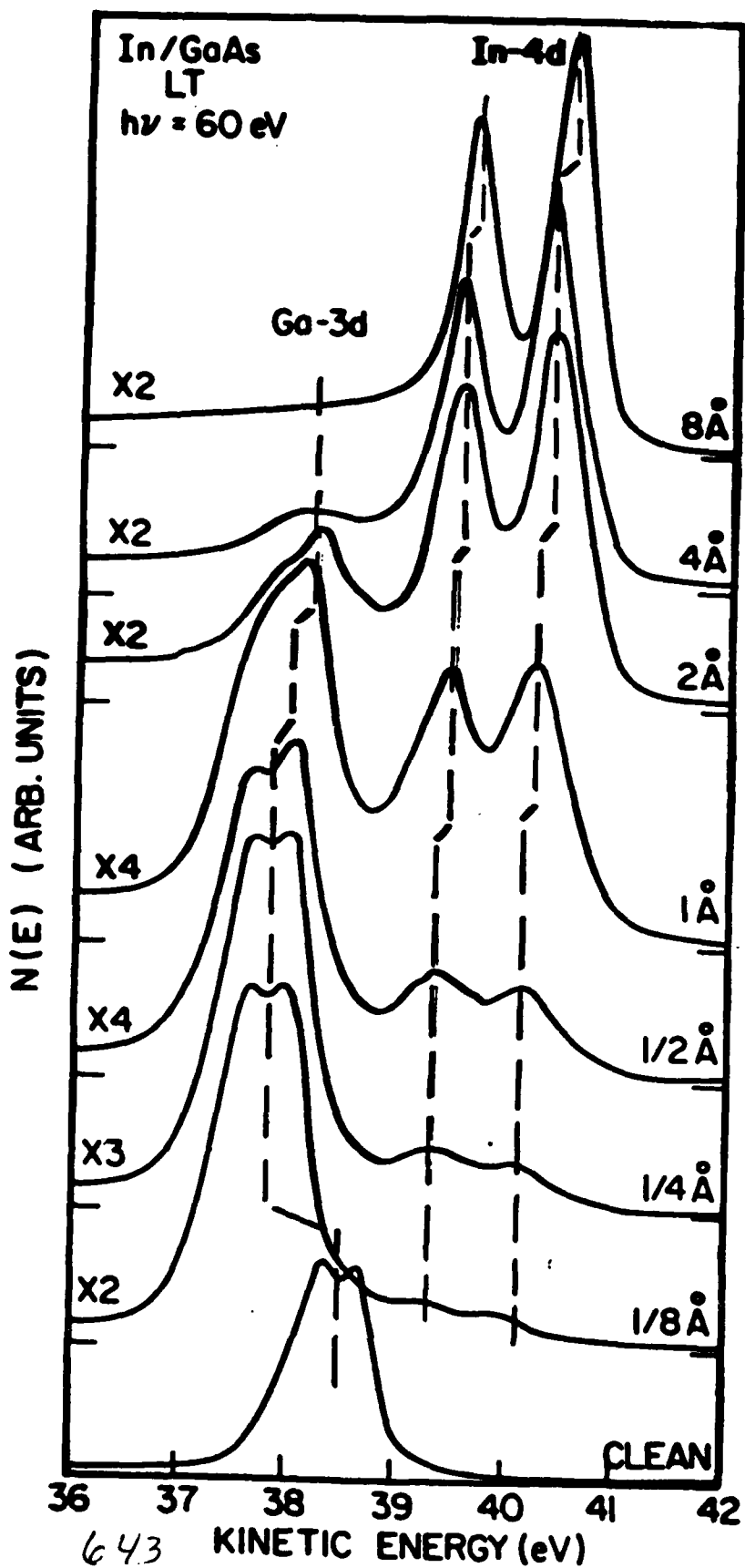


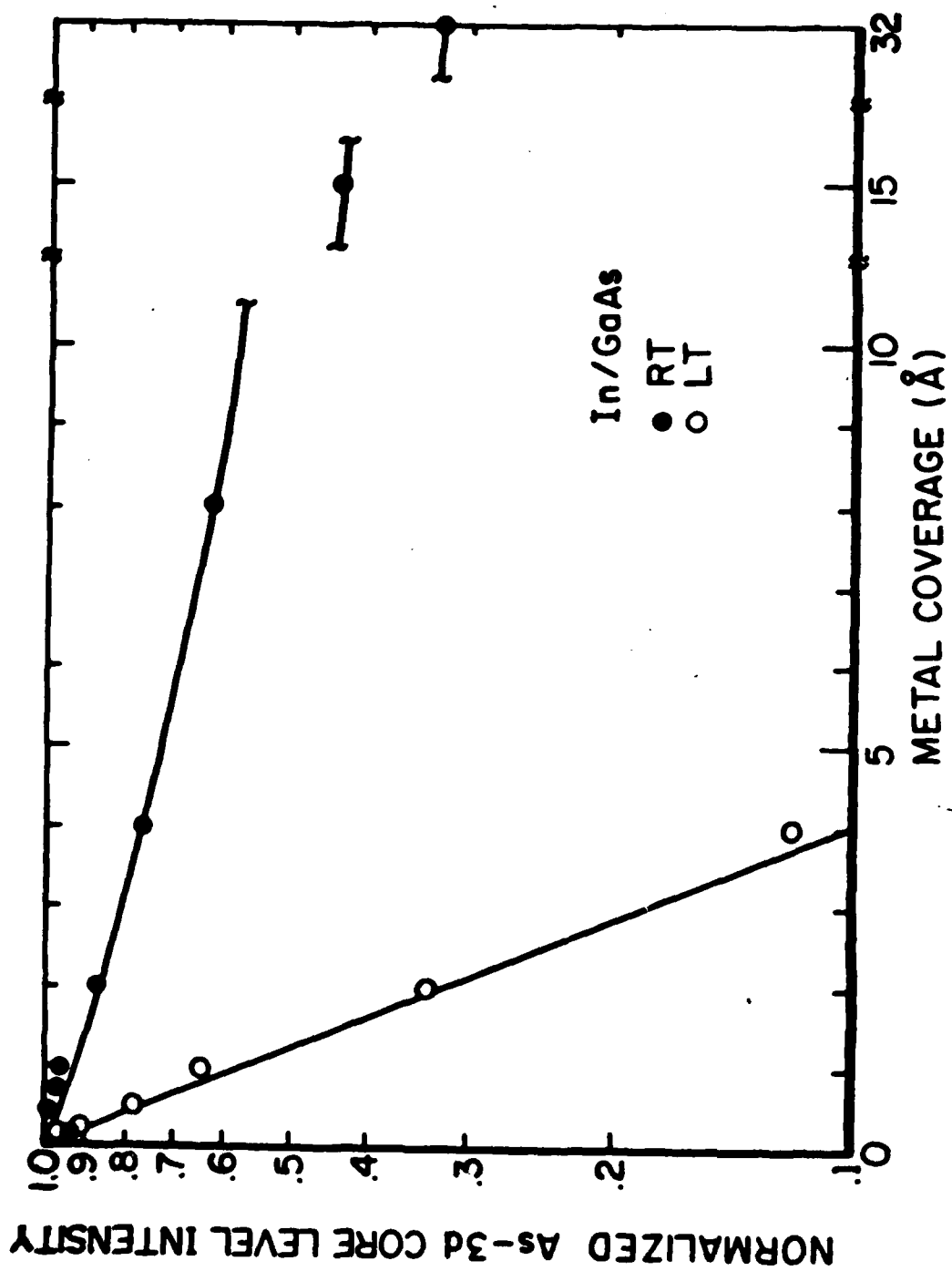


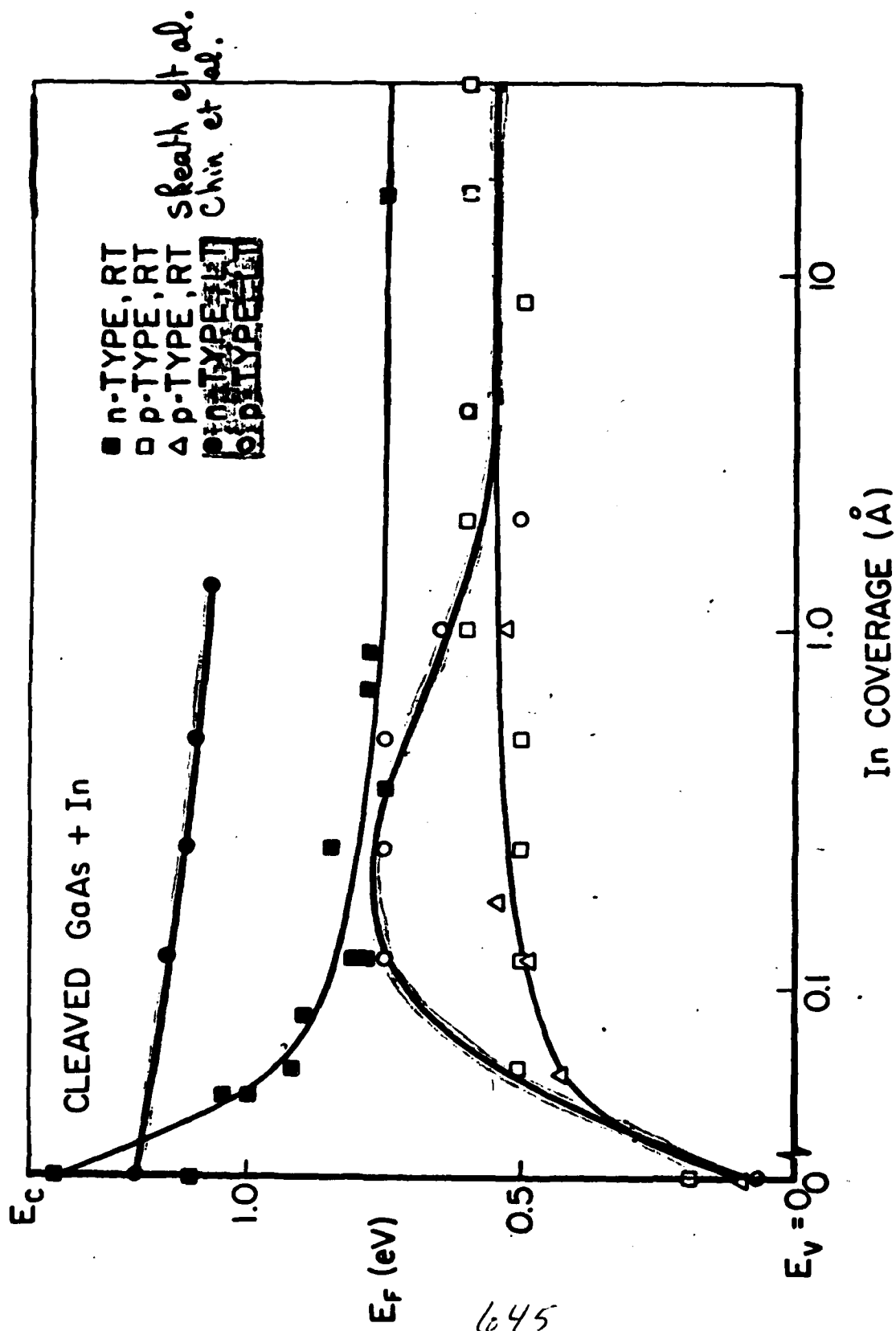




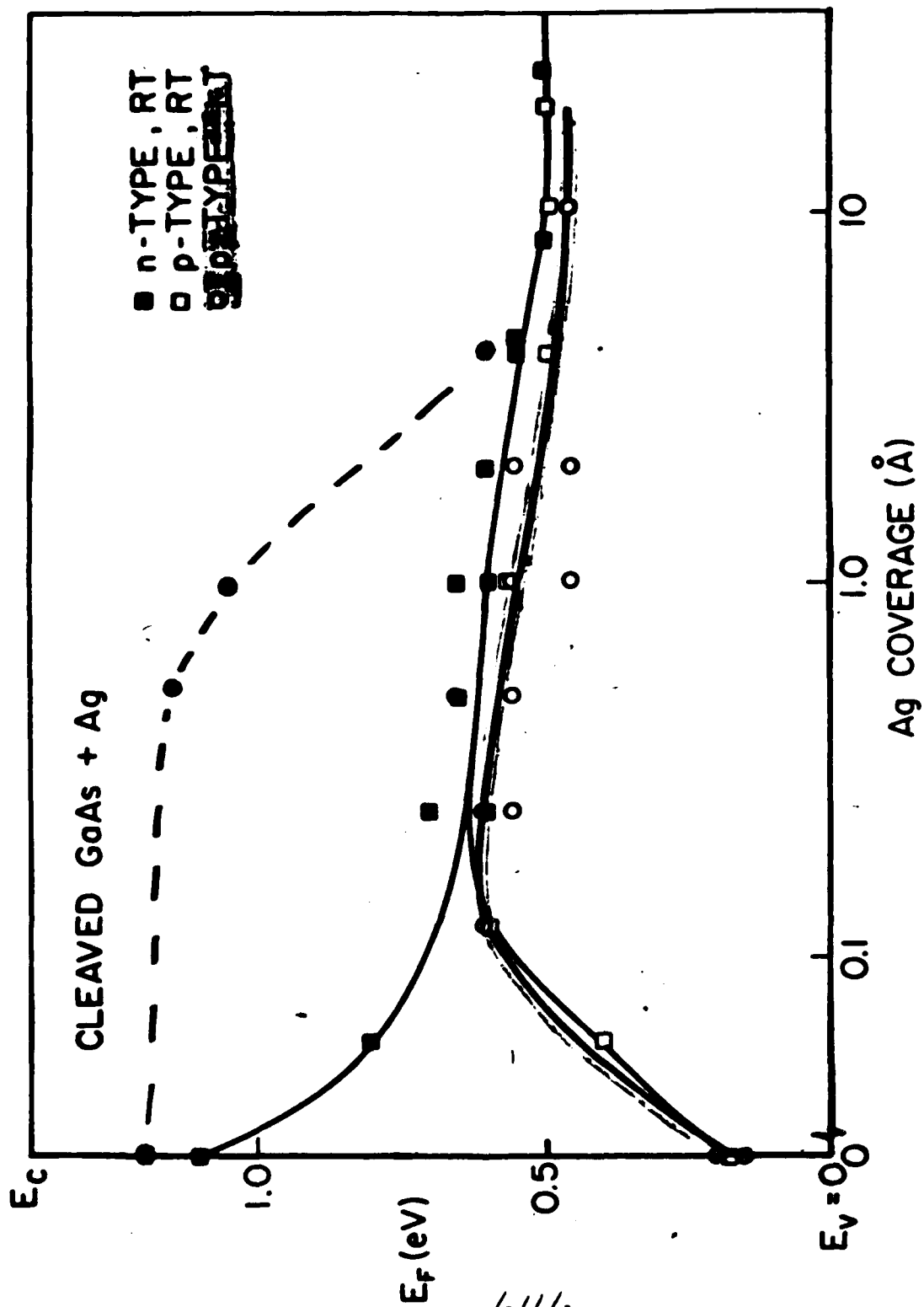


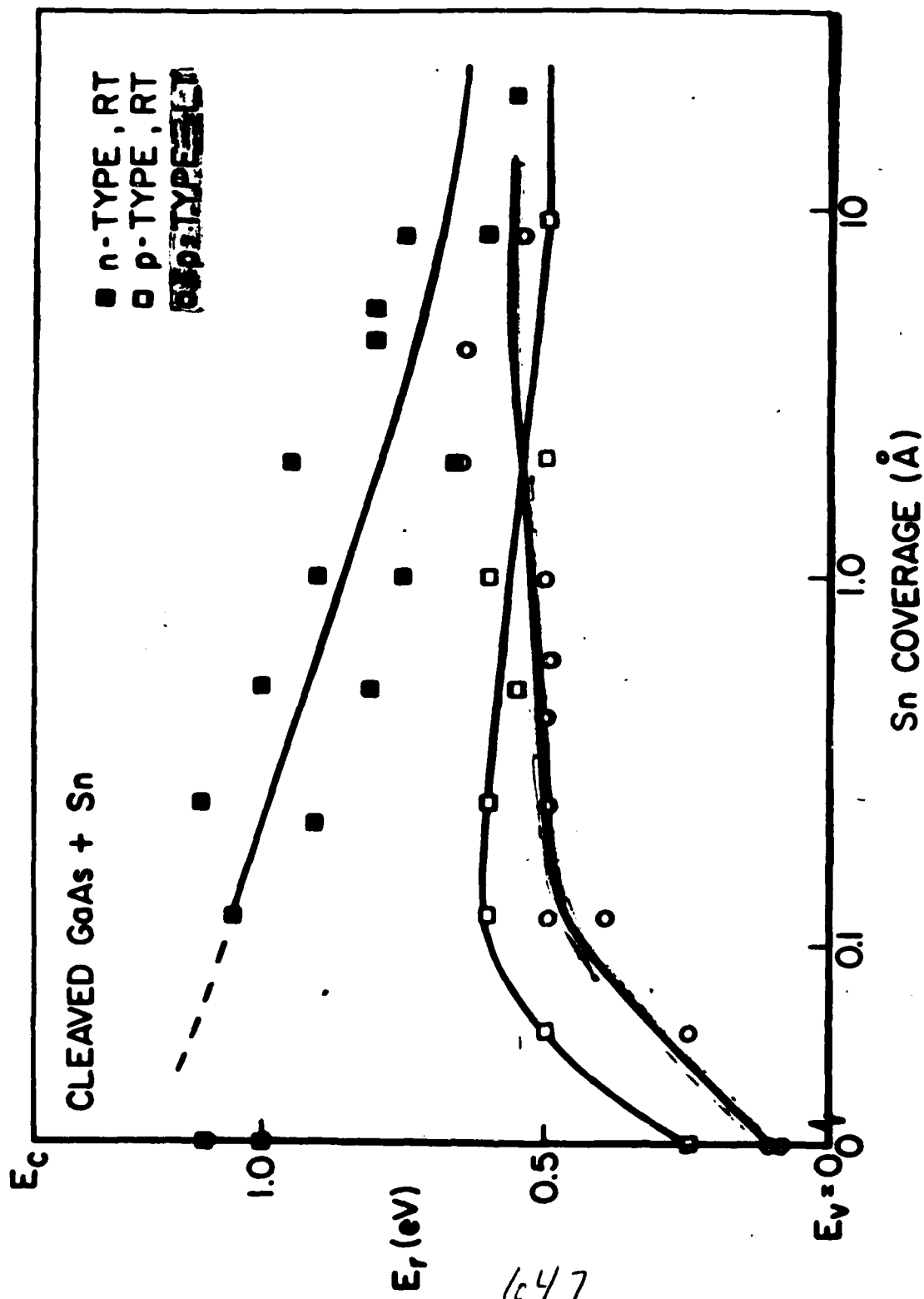












## Overlayer Morphology

- ① Deposition at AT generally involves substantial clustering, chemical reaction or interdiffusion
- ② Deposition at LT enhances overlayer homogeneity: lower surface mobility and reduced clustering. (residual clustering with thermal evaporation)

Interdiffusion and reactions are slowed down.

Atomic reconstruction induced by the metal at the SC surface can be detected (Al / GaAs)

## Initial $E_F$ pinning rates at RT and LT.

Metal	n- GaAs		p- GaAs	
	RT	LT	RT	LT
Al	fast	slow	fast	fast
Au	fast	slow	fast	fast
In	fast	slow	fast	fast
Ag	fast	(slow)	fast	fast
Sn			fast	fast

Slow pinning at LT on n- GaAs consistent with reduced clustering, defect formation, chemical reaction.

Fast pinning at LT on p- GaAs requires a different mechanism.

## Initial pinning rates

- \* The deposition temperature affects the kinetics of Schottky barrier formation: rate of EF pinning different at 80°K.
  - \* The strong asymmetry in pinning rates on LT n- and p-GaAs results from the partial inhibition of some interface phenomena. It makes it impossible to explain the Schottky formation process with a single mechanism.
  - \* From the point of view of defects:
    - need a substantial complication of model:
      - ex  $\text{As}_{\text{Ga}}$  (double donor) + compensating defect
- ← different kinetics →
- Or
- entirely different model
    - ex acceptors activated by formation of clusters or chemical reaction
    - + donors linked to reconstruction or interface bonds.

## Conclusions.

1. LT deposition simplifies the overlayer system by reducing interactions (except structural) with the semiconductor.
2. It reveals fundamental differences in the initial pinning on n- and p- substrates, marked by fast interactions at RT
3. If 2. holds true, it requires re-thinking of initial pinning mechanisms.

**Microscopic Metal Clusters and Schottky  
Barrier Formation**

**S. Doniach**

**Applied Physics  
Stanford University**

# Effect of clustering on Surface Fermi level pinning

Single defect model:

$$\phi_b = - \frac{Q^2}{2 n_d e}$$

← charge transferred  
 $\propto$  number of defects/area  
 ← donor density  
 → band bending

Saturates when

$$\mu_{\text{defect}} = \mu_{\text{semicond}} + \phi_b$$

→ defect electron affinity  
 ← bulk semiconductor Fermi level

Cluster charging model:

$$\mu_{\text{cluster-complex}} = \frac{\partial E_{\text{complex}}}{\partial n}$$

← electron affinity  
 ← Coulomb's energy  
 $E_{\text{complex}} = n \epsilon_c + n^2 \frac{U}{C(R)}$   
 → # of electrons transferred  
 ← effective capacitance (6.54)



## Clustering model assumptions

$$C(R) \propto R \propto N^{1/3}$$

effective capacitance

$$\text{Coverage} = N_c \cdot N$$

number of clusters ← held Fixed

number of atoms per cluster varying

## Equilibrium condition :

$$\epsilon_c + n \frac{U}{C(R)} = -n^2 \left( \frac{N_c}{N_{\text{sat}}} \right)^2 (\epsilon_c - \epsilon_s) + \epsilon_s$$

average electron number per cluster

cluster density

single defect saturation density

Fit data in terms of parameters

$$\epsilon_c - \epsilon_s, \quad \alpha = \frac{U/C_1}{\epsilon_c - \epsilon_s}, \quad \beta = \left( \frac{N_c}{N_{\text{sat}}} \right)^2$$

$$\text{empirically } \beta = \beta_0 \alpha^{3.3 \pm 0.55}$$

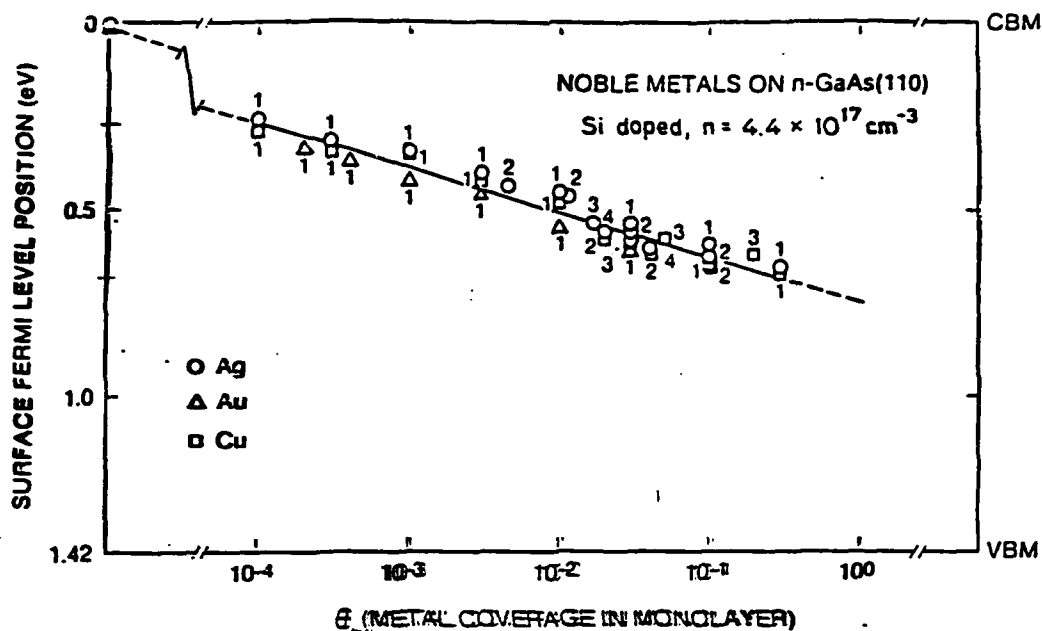
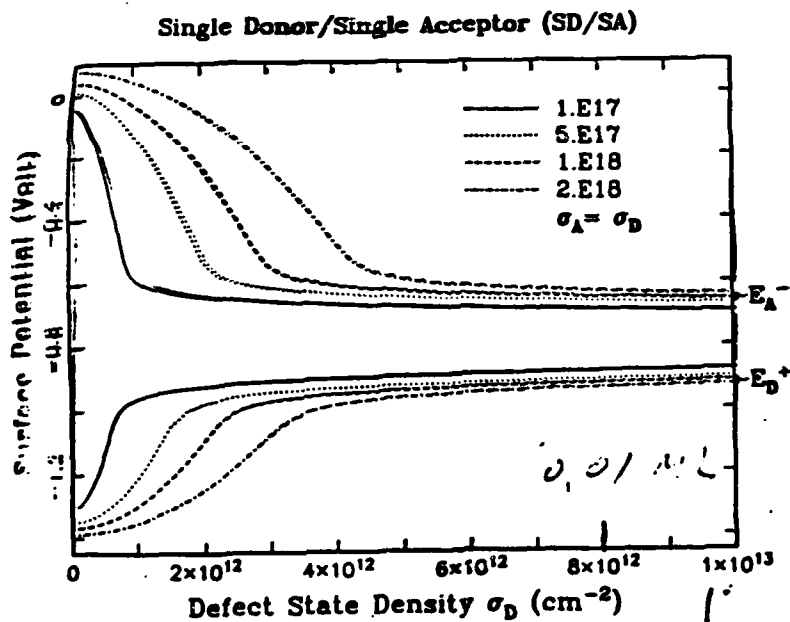


Fig. 3. The n-GaAs (110) surface band bending as the function of the effective noble metal coverage or the ideally cleaved n-GaAs (110) surface band bending as the function of the noble metal coverage. The numbers in the mark refer to the sample numbers as shown in Fig. 2.

K.K.Chin, R.Cao, K.Hiyang, C.E. McCants, I.Lindan + W.E Spicer

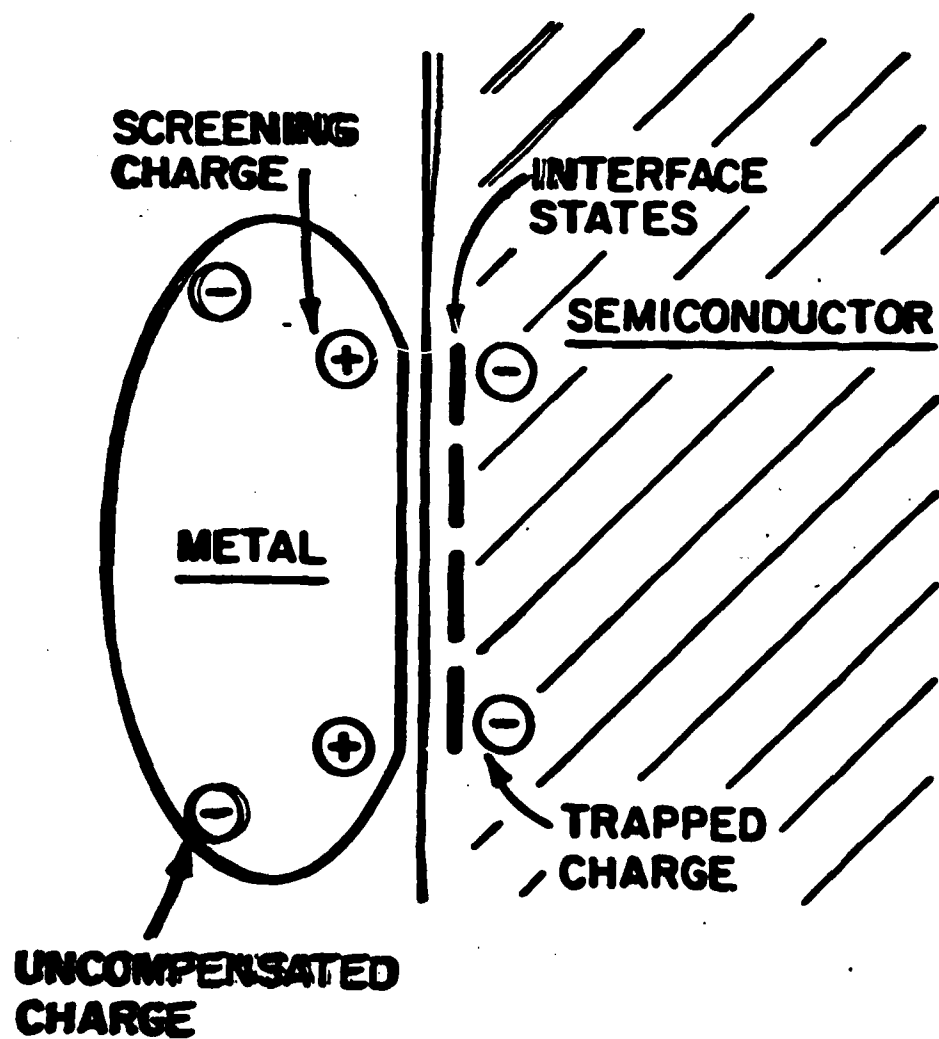


Tang + Freeouf

654

J Vac Sci Tech

B2 459 (84)



data: Kuau Kén Chin

